

REPORT DOCUMENTATION PAGE			Form Approved OMB No. 0704-0188	
Public reporting burden for this collection of information is estimated to average 1 hour per response, including the time for reviewing instructions, searching existing data sources, gathering and maintaining the data needed, and completing and reviewing the collection of information. Send comments regarding this burden estimate or any other aspect of this collection of information, including suggestions for reducing this burden, to Washington Headquarters Services, Directorate for Information Operations and Reports, 1215 Jefferson Davis Highway, Suite 1204, Arlington, VA 22202-4302, and to the Office of Management and Budget, Paperwork Reduction Project (0704-0188), Washington, DC 20503.				
1. Agency Use Only (Leave blank).	2. Report Date. December 1992	3. Report Type and Dates Covered. Final, 1/89 to 6/91		
4. Title and Subtitle. Navy Tactical Applications Guide, Volume 8 Part 2 Arctic — East Siberian/Chukchi/Beaufort Seas Weather Analysis and Forecast Applications		5. Funding Numbers. Program Element No. 63704N/O&M,N Project No. X1596/CNOC Task No. Accession No. DN658753/ DN656794		
6. Author(s). Robert W. Fett <sup>1</sup> Contributor: Thomas L. Kozo <sup>2</sup>		8. Performing Organization Report Number. NRL/PU/7541--92-0005		
7. Performing Organization Name(s) and Address(es). Naval Research Laboratory, Marine Meteorology Division, Monterey, CA 93943-5006 (Formerly Naval Environmental Prediction Research Facility, Monterey, CA)		10. Sponsoring/Monitoring Agency Report Number.		
9. Sponsoring/Monitoring Agency Name(s) and Address(es). Space and Naval Warfare Systems Command (PMW-141) Washington DC 20361-5100 Commander Naval Oceanography Command Stennis Space Center, MS 39529-5000		11. Supplementary Notes. <sup>1</sup> Formerly head of NEPRF Tactical Applications Department; now a consultant in satellite meteorology. <sup>2</sup> Presently NRL Marine Meteorology Division, Monterey, CA.		
12a. Distribution/Availability Statement.  Approved for public release; distribution is unlimited.		12b. Distribution Code.		
13. Abstract (Maximum 200 words).  Environmentally, the north polar region is one of the most active regions on Earth, and for ships and seamen, one of the most dangerous due to the combined effects of wind, sea state, and structural icing. It is also the region most neglected and difficult to analyze or forecast because of the sparsity of surface, upper air, and ocean observations, and less than adequate numerical models. This volume illustrates, with high resolution satellite data and supplementary conventional surface and upper air analyses, some of the significant recurring patterns of weather and oceanographic phenomena in the Arctic. This volume is dedicated to weather and oceanographic phenomena in the regions surrounding northern Alaska and northern Siberia (Part 1 covered the Norwegian Sea, Barents Sea and Greenland). Its purpose is to document Arctic weather phenomena as observed by satellite, and in doing so, assist meteorologists in the development of satellite interpretation skills.				
14. Subject Terms.  DMSP, AVHRR, ice, polar lows, floebergs, polynyi		15. Number of Pages. 388 16. Price Code.		
17. Security Classification of Report. UNCLASSIFIED	18. Security Classification of This Page. UNCLASSIFIED	19. Security Classification of Abstract. UNCLASSIFIED	20. Limitation of Abstract. Same as Report	

AN (1) AD-A265 585  
 FG (2) 040200  
 FG (2) 081200  
 FG (2) 080300  
 CI (3) (U)  
 CA (5) NAVAL RESEARCH LAB MONTEREY CA  
 TI (6) Navy Tactical Applications Guide, Volume 8 Part 2:  
 Arctic - East Siberian/Chukchi/Beaufort Seas. Weather  
 Analysis and Forecast Applications.  
 TC (8) (U)  
 DN (9) Final rept. Jan 89-Jun 91.  
 AU (10) Fett, Robert W.  
 AU (10) Kozo, Thomas L.  
 RD (11) Dec 1992  
 PG (12) 389  
 RS (14) NRL/PU/7541-92-0005  
 PJ (16) X1596  
 RN (18) XB-SPAWAR  
 RC (20) Unclassified report  
 ND (21) Original contains color plates: All DTIC/NTIS  
 reproductions will be in black and white. See also  
 Volume 8, Part 1, AD-A230 720.  
 DE (23) \*WEATHER FORECASTING, \*SEA ICE, \*ARCTIC REGIONS, \*  
 METEOROLOGICAL SATELLITES, \*AIR WATER INTERACTIONS, \*  
 ICE MECHANICS, \*SEA STATES, \*WEATHER, \*WIND, ALASKA,  
 ARTIFICIAL SATELLITES, BARENTS SEA, GREENLAND, HIGH  
 RESOLUTION, ICE, ICE FORMATION, CHUKCHI SEA,  
 METEOROLOGICAL PHENOMENA, CASE STUDIES, MATHEMATICAL  
 MODELS, STORMS, CLOUDS, FRONTS (METEOROLOGY), FRONTS (OCEANOGRAPHY), OCEANOGRAPHIC DATA, ICEBERGS,  
 RADIOMETERS, SEASONAL VARIATIONS, ATMOSPHERIC MOTION,  
 BEAUFORT SEA, MODELS, NORWEGIAN SEA, OBSERVATION,  
 OCEANS, PATTERNS, POLAR REGIONS, SHIPS, SIBERIA,  
 SURFACES.  
 DC (24) (U)  
 ID (25) PE63704N, WUDN658753, WUDN656794, DMSF (Defense  
 Meteorological Satellite Program), AVHRR (Advanced Very  
 High Resolution Radiometer), East Siberian Sea.  
 IC (26) (U)  
 AB (27) Environmentally, the north polar region is one of the  
 most active regions on Earth, and for ships and seamen,  
 one of the most dangerous due to the combined effects  
 of wind, sea state, and structural icing. It is also  
 the region most neglected and difficult to analyze or  
 forecast because of the sparsity of surface, upper air,  
 and ocean observations, and less than adequate  
 numerical models. This volume illustrates, with high  
 resolution satellite data and supplementary  
 conventional surface and upper air analyses, some of  
 the significant recurring patterns of weather and  
 oceanographic phenomena in the Arctic. This volume is  
 dedicated to weather and oceanographic phenomena in the

Page 2

\*\* MAY CONTAIN EXPORT CONTROL DATA \*\*

ADAXXXXXX MICROFICHE ARE HOUSED IN THE GENERAL MICROFORMS RM

regions surrounding northern Alaska and northern  
 Siberia (Part 1 covered the Norwegian Sea, Barents Sea  
 and Greenland). Its purpose is to document Arctic  
 weather phenomena as observed by satellite, and in  
 doing so, assist meteorologists in the development of  
 satellite interpretation skills. DMSF, AVHRR, Ice,

Polar lows, Floeberg's, Polynvi

AC (28) (U)  
 DL (33) 01  
 SE (34) F  
 CC (35) 424779



APPROVED FOR PUBLIC RELEASE  
DISTRIBUTION IS UNLIMITED

NRL/PU/7541--92-0005

## NAVY TACTICAL APPLICATIONS GUIDE

LIBRARY  
RESEARCH REPORTS DIVISION  
NAVAL POSTGRADUATE SCHOOL  
MONTEREY, CA 93943-5002

# VOLUME 8 PART 2 ARCTIC

East Siberian/Chukchi/Beaufort Seas

## WEATHER ANALYSIS and FORECAST APPLICATIONS

METEOROLOGICAL  
SATELLITE  
SYSTEMS



NAVAL RESEARCH LABORATORY  
MARINE METEOROLOGY DIVISION  
MONTEREY, CALIFORNIA 93943-5006

NAVY TACTICAL APPLICATIONS GUIDE

VOLUME 8  
PART 2

ARCTIC  
EAST SIBERIAN/CHUKCHI/BEAUFORT SEAS  
WEATHER ANALYSIS  
AND FORECAST APPLICATIONS

METEOROLOGICAL SATELLITE SYSTEMS

*Prepared under the direction of*

Robert W. Fett, Consultant,

for

NAVAL RESEARCH LABORATORY

// Marine Meteorology Division

Monterey, California 93943-5006



---

SCIENCE AND TECHNOLOGY CORPORATION

---

101 RESEARCH DRIVE  
HAMPTON, VIRGINIA 23666

## *Acknowledgments*

The support of the sponsors, Space and Naval Warfare Systems Command, Program Element 63704N, and Commander Naval Oceanography Command, Program Element O&M,N, is gratefully acknowledged.

This volume could not have been published without the devoted effort of the NEPRF\* Meteorological Laboratory personnel who obtained required documentation, and spent many hours on the computer terminal entering information for the analyses utilized in the studies. AG1 John Coleman, AG1 Joe Grinde, and AG3 Peter Hoffman did an outstanding job in supporting the work effort required for this volume.

PH2 Kathy Smith processed many of the original photos utilized. The correlative meteorological data were provided by the Fleet Numerical Oceanography Center, Monterey, California.

Additional satellite imagery were supplied by the NOAA National Snow and Ice Data Center, Boulder, Colorado, Air Force Global Weather Center, Offutt Air Force Base, Nebraska and the Air Force readout site at Elmendorf Air Force Base, Anchorage, Alaska.

A special thanks to Dennis Perryman, NRL, Monterey, who proofread many of the studies and offered excellent suggestions.

---

\* *The former Naval Environmental Prediction Research Facility, later the Atmospheric Directorate of the Naval Oceanographic and Atmospheric Research Laboratory, is now the Marine Meteorology Division of the Naval Research Laboratory.*





# Contents

<i>Acknowledgments</i> .....	iii
<i>Introduction</i> .....	vii

## Section 1

### *Large-Scale Atmospheric Phenomena and Effects*

1A Severe Storms of Large-Scale Magnitude .....	1A-1
1B Arctic Fronts, Highs and Lows .....	1B-1

## Section 2

### *Polar lows*

2A Introduction to Polar Lows .....	2A-1
2B Case Studies .....	2B-1

## Section 3

### *Local-Scale Atmospheric Phenomena and Effects*

3A Leads and Polynyi: Air/Sea Interaction Effects .....	3A-1
3B Mountain-Gap Winds .....	3B-1
3C Islands of Grounded Sea Ice: Their Use in Detecting Changes in Direction of Ice Motion and Their Role in Lead Formation .....	3C-1
3D Characteristic Structure and Seasonal Changes in Arctic Sea Ice .....	3D-1
3E Land and Sea Breezes .....	3E-1
3F Orographic Cloud Formations and Other Unique Cloud Effects .....	3F-1





## *Introduction*

Strategic interest in the Arctic has increased significantly over the past several years with the realization that more than 50% of the world's petroleum lies north of the Arctic Circle. U.S. Naval Forces are expanding their efforts to include operations further and further north so that, in the event of hostilities in Arctic waters, the Fleet has experience and competence to conduct operations safely and effectively in those areas.

Environmentally, the north polar region is one of the most active regions on the Earth and, for ships and seamen, one of the most dangerous in war or peacetime operations. Every year several vessels are lost in the Arctic due to combined effects of wind, sea state, and structural icing. It is also the region most neglected and difficult to analyze or forecast because of the sparsity of surface, upper air, and ocean observations, and the less than adequate numerical models. The models have often been found to fail to respond realistically to Arctic conditions. Hope for improvement lies in employing new high resolution numerical models with better planetary boundary layer (PBL) and ocean and ice parameterizations, and exploiting the full range of satellite sensors now available for use in the development of new analysis and forecast techniques, specifically adapted to this region.

This volume has been developed to illustrate, with high resolution satellite data and supplementary conventional surface and upper air analyses, some of the significant recurring patterns of weather and oceanographic phenomena in the Arctic. Volume 8, Part 1, is dedicated to weather and oceanographic phenomena in the region surrounding Greenland, and in the Norwegian and Barents Seas. Volume 8, Part 2, is dedicated to a depiction of similar phenomena in the regions of the East Siberian, Chukchi, and Beaufort Seas.

The meteorologist well-versed in the art of satellite interpretation can very rapidly become a confident analyst and forecaster, even in unfamiliar areas of the world. It is the purpose of this volume to assist in the development of such skills.



# Section 1

## *Large-Scale Atmospheric Phenomena and Effects*

### *1A Severe Storms of Large-Scale Magnitude*

Introduction .....	1A-1
--------------------	------

#### *Case Studies*

1 Beaufort Sea—North Slope 15–18 September 1985.....	1A-2
2 Extreme Ship Icing Event—Western Gulf of Alaska .....	1A-37
3 Meridional Trough Cyclogenesis—A Severe Summer Storm Development in the Beaufort Sea (26–28 July 1982) .....	1A-63

### *1B Arctic Fronts, Highs and Lows .....*

1B-1

#### *Case Studies*

1 Westward-Moving Low from the Chukchi to the East Siberian Sea .....	1B-1
2 The “Col Cloud” Frontal Interconnections .....	1B-27
3 Frontal Movement/Col Cloud Formation Over Alaska (19–21 February 1989) .....	1B-31
4 Col Cloud Effects—East Siberian Sea .....	1B-45
5 Arctic Fronts and the “Fleur-de-lis” Cloud Pattern (16–19 April 1989).....	1B-49





## *1A Severe Storms of Large-Scale Magnitude*

### *Introduction*

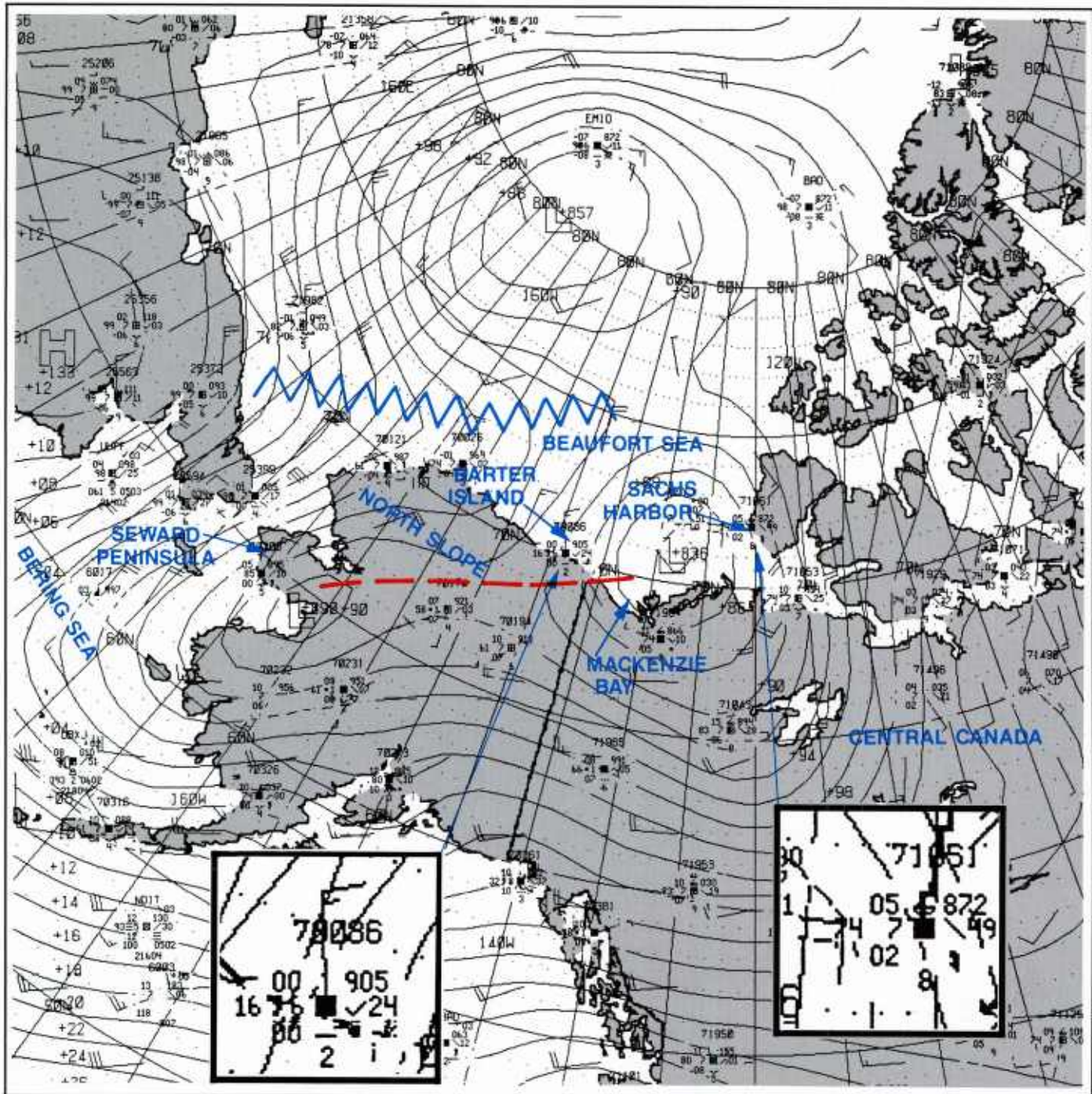
Severe storms of large-scale magnitude, having diameters of approximately 1000 km, occasionally develop over the central Arctic and can bring sustained winds of 50 kt or greater to coastal stations and offshore oil rigs off of the North Slope of Alaska. The fetch of the winds over open water of the southern Beaufort Sea can produce seas of 8 meters or more in height, posing significant hazards to ships and oil rigs in the region.

The storms form as the result of baroclinity or strong horizontal temperature gradient between cold, dry Arctic air and warmer, moist air that has been advected into polar latitudes from more southerly and often maritime regions.

Intensification of such storms occurs over a time interval of 1-10 days through conversion of the potential energy of the system to kinetic energy. This process involves lowering the center of gravity of the cold Arctic air as it sinks and moves southward, and lifting the warm air mass as it moves northward. The changes with time of the horizontal temperature gradient, produced by this process at level after level in the vertical, also result in a thermal wind shear in the vertical, causing jet stream formation at higher elevations.

Intensification of the system can be detected from existing 850-, 700-, or 500-mb analyses by noting the isotherm pattern about the storm. Concentric isotherm patterns imply no development (barotropic); but, when the isotherms are located nearly perpendicular to the isobars, so that cold air advection is implied west of the storm center, and warm air advection is implied east of the storm center, the system intensifies.

Moreover, soundings will reveal stable conditions over stations where warm air advection is occurring and more unstable conditions where cold air advection is occurring. Strong surface winds can be anticipated when the unstable air mass replaces the stable air mass, as violent mixing brings strong winds from aloft down to the surface.

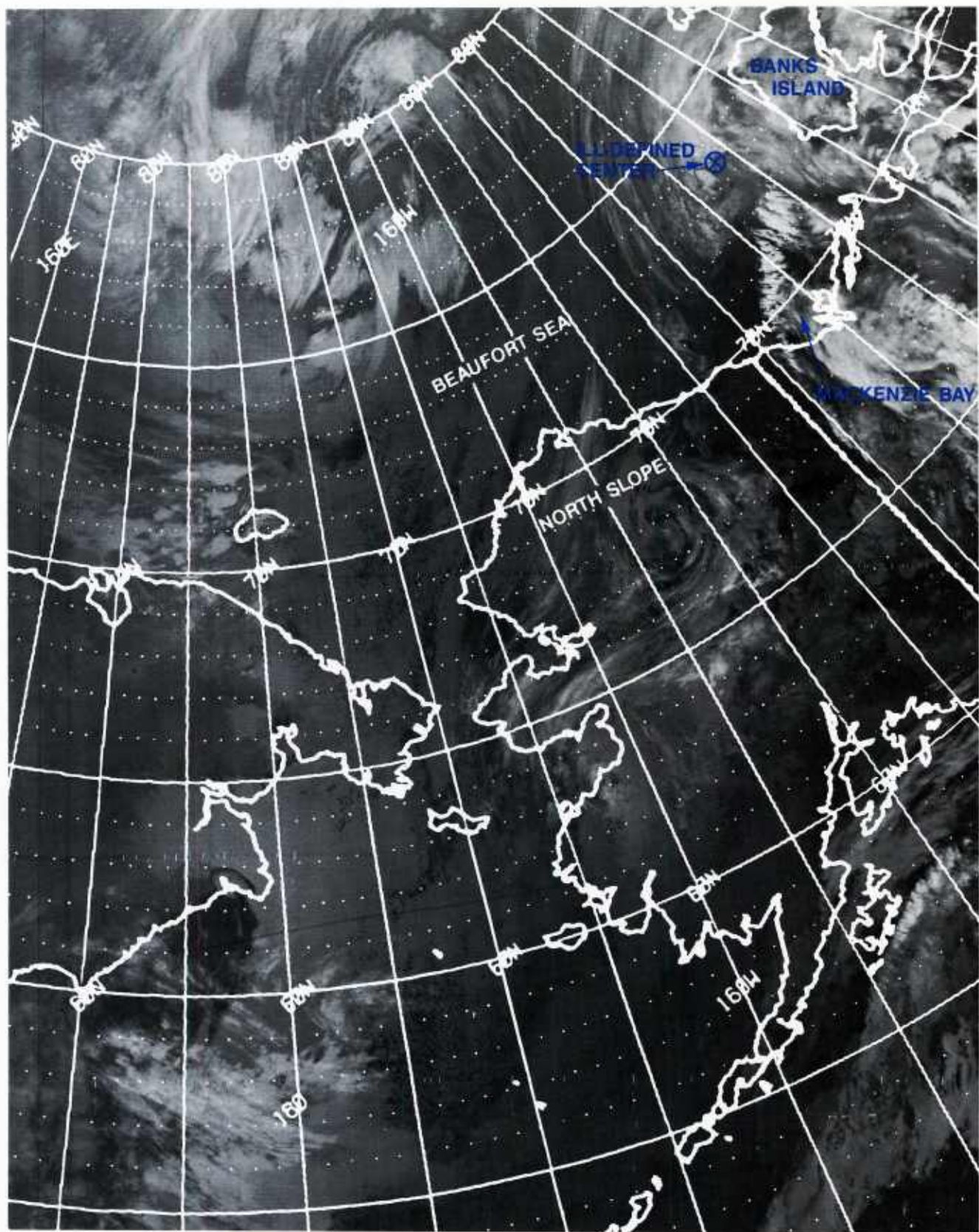


1A-2 FNOC surface analysis, 15 September 1985, 0600 GMT

### Case 1 Beaufort Sea—North Slope 15-18 September 1985

The FNOC surface analysis for 15 Sep 1985 at 0600 GMT (Fig. 1A-2) shows a 983.6 mb low centered near Mackenzie Bay, east of the North Slope. A trough extends from this low to another low (989.0 mb) centered near the Seward Peninsula of Alaska. Temperatures on the east side of the Mackenzie Bay low are warmer than on the west side of the low, with Sachs Harbor reporting 5°C while Barter Island, in northerly flow, reports a temperature of 0°C.





1A-3 DMSP infrared (TS) data. 15 September 1985, 0613 GMT.

A DMSP infrared image acquired at 0613 GMT (Fig. 1A-3) shows cloud features of the region. The Mackenzie Bay low shows no evident circulation centered over that location. However, an ill-defined center is suggested near 73.5N, 132W, just west of Banks Island.

Another DMSP infrared view at 0748 GMT (Fig. 1A-4) shows a better view of the region extending into central Canada. The first thing to note about this view is the marked change from the chaotic, cloudy, unstable western portion of the image to the nearly clear, stable condition of the eastern portion. From the surface analysis (Fig. 1A-2), it can be seen that this change separates a low pressure region over Alaska, NW Canada, and the Bering Sea from higher pressure over central Canada. The pattern implies advection of relatively warm, moist air in a southerly flow over much of the NW Canadian archipelago.

The long arc of clouds leading up to Mackenzie Bay from the Gulf of Alaska and crossing the North American coastline near 55N, 130W is interesting in that this flow pattern is not suggested at the surface level (Fig. 1A-2); however, it is shown on the NMC 850 mb analysis for 15 September at 0000 GMT (Fig. 1A-5a). The isobars do not show this type of flow direction, but the wind barbs do. The analysis suggests that the long arc of clouds immediately precedes a short wave trough at this level. Interestingly, this is not true at 500 mb (Fig. 1A-5b), where a ridge line is seen to extend through that area. It can be concluded that this effect is a lower tropospheric effect and points out the need to always consider such levels in Arctic analysis.

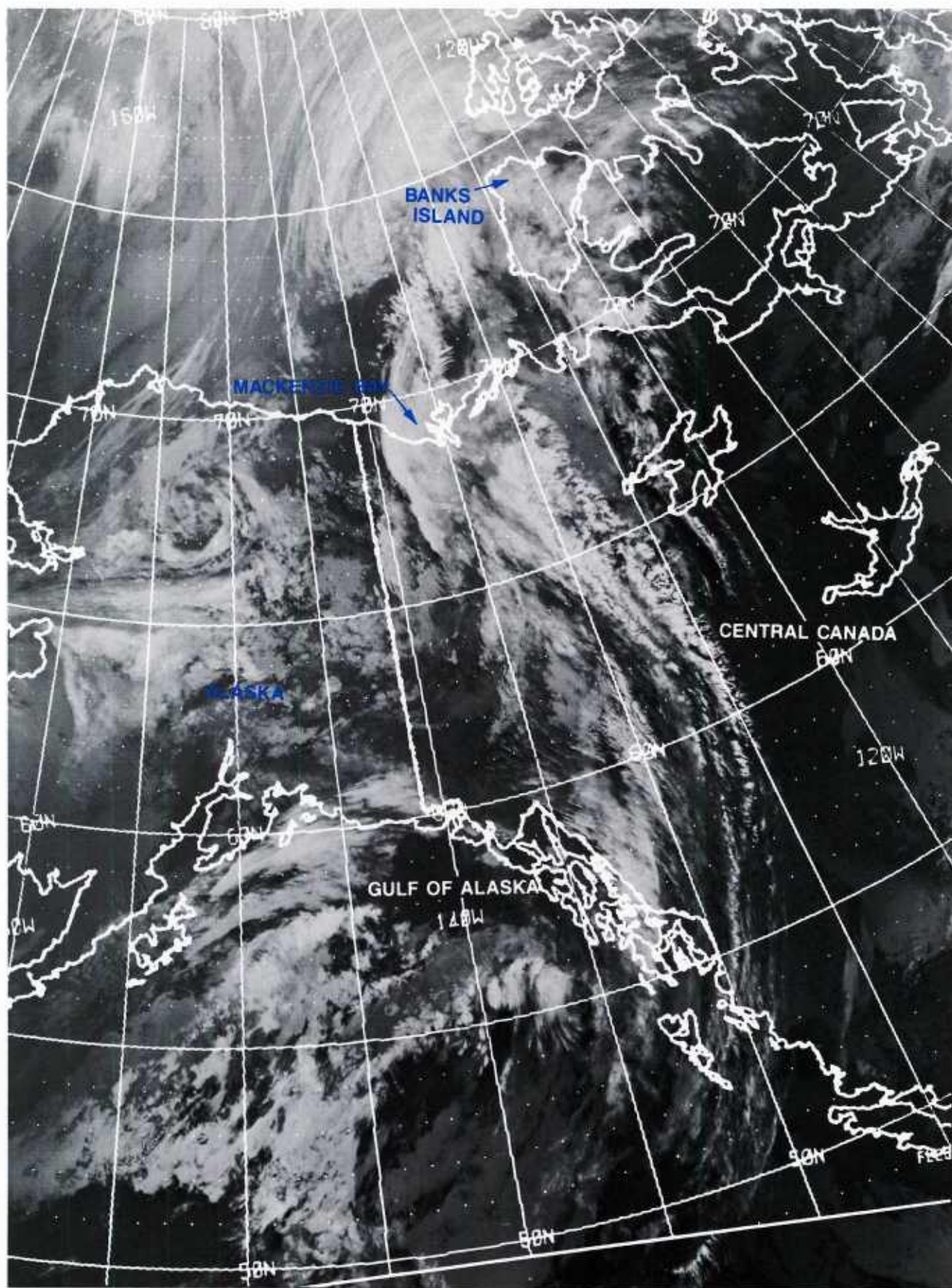
It does not appear, at this time, that the arc of clouds represents a frontal band. Temperatures on either side of the arc in the surface analysis (Fig. 1A-2) show little change, and the isotherm pattern on the 850 mb chart does not support a front at that location. Rather, the feature appears to be a dynamically induced effect caused by the short wave trough with which it is associated.

By 0000 GMT on 16 September, however, based on the 850 mb analysis (Fig. 1A-6a), one could argue that frontogenesis had indeed occurred in association with the band in the region just east of Banks Island. The isotherm pattern shows pronounced cold air advection west of the low, and warm air advection east of the low, with a packing of isotherms in the Banks Island vicinity.

The blue circles on the 16 September 0000 GMT surface analysis (Fig. 1A-6b) shows the indicated frontogenetic pattern. Note that the surface temperature at Sachs Harbor on Banks Island fell from 5°C in southerly flow (Fig. 1A-2) on 15 September to -2°C on 16 September as the low moved past the station, exposing it to northerly flow from off the ice.

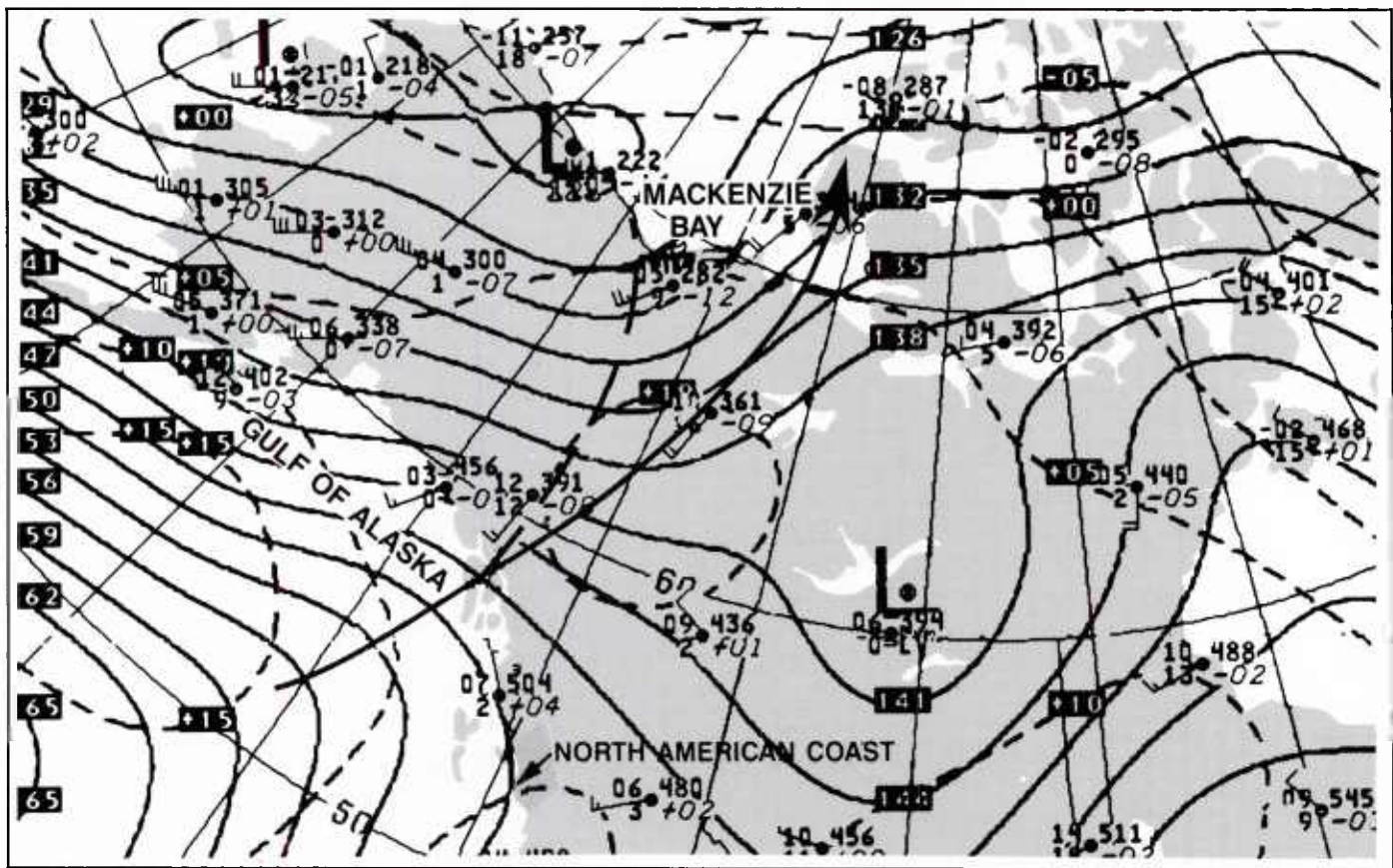
Fog reports are numerous east of the front as moist air, in southerly flow under stable conditions, is cooled to saturation. The further development and movement of this frontal feature, which is not followed by satellite data, are shown in surface analyses every 12 hours from 16 September at 1200 GMT through 17 September at 1200 GMT (Figs. 1A-7a through 1A-8). During this period, temperatures over western Canada fell markedly as flow changed from westerly (Fig. 1A-2) to strong northerly (Figs. 1A-6b through 1A-8).



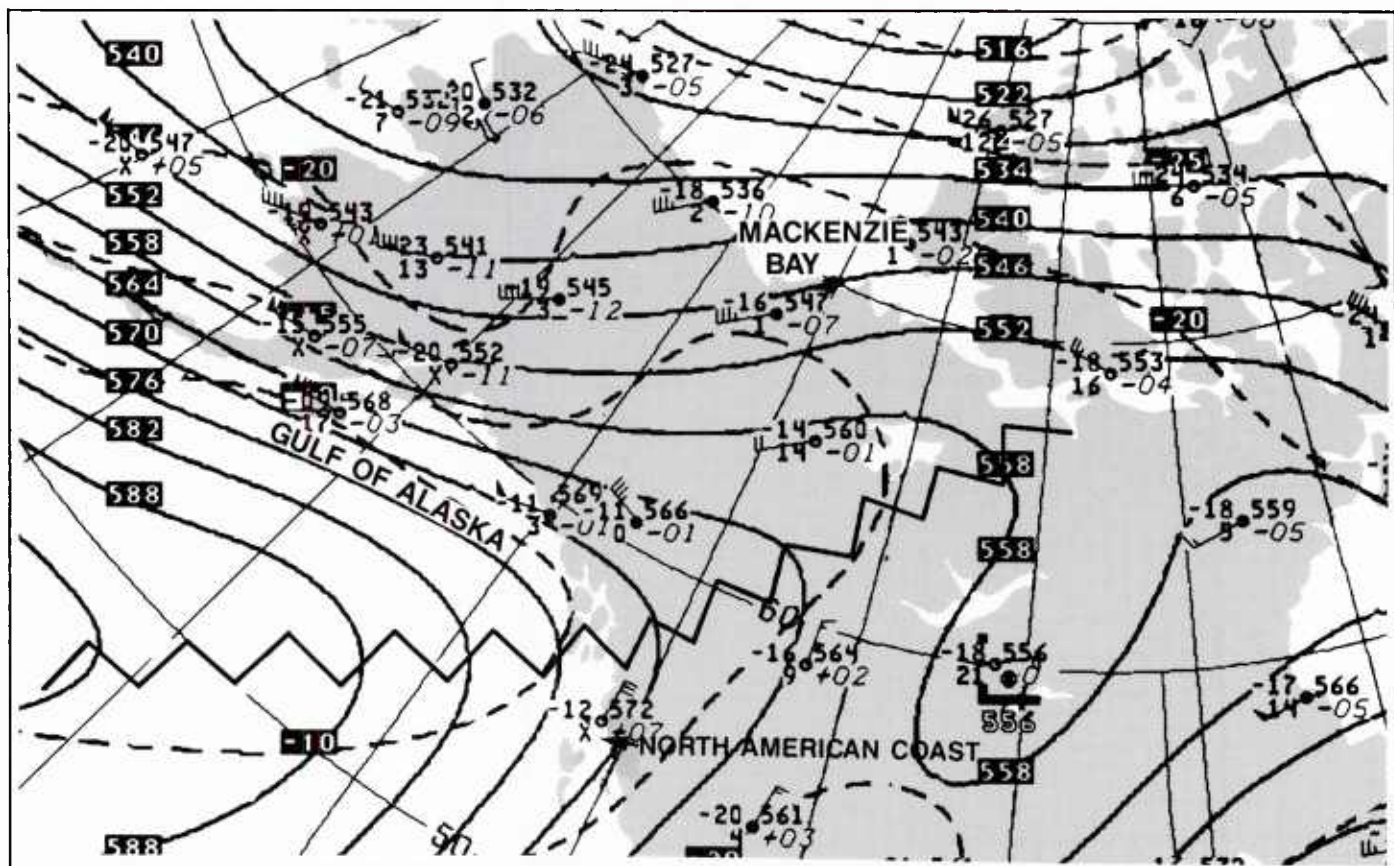


1A-4 DMSP infrared (TS) data. 15 September 1985, 0748 GMT.



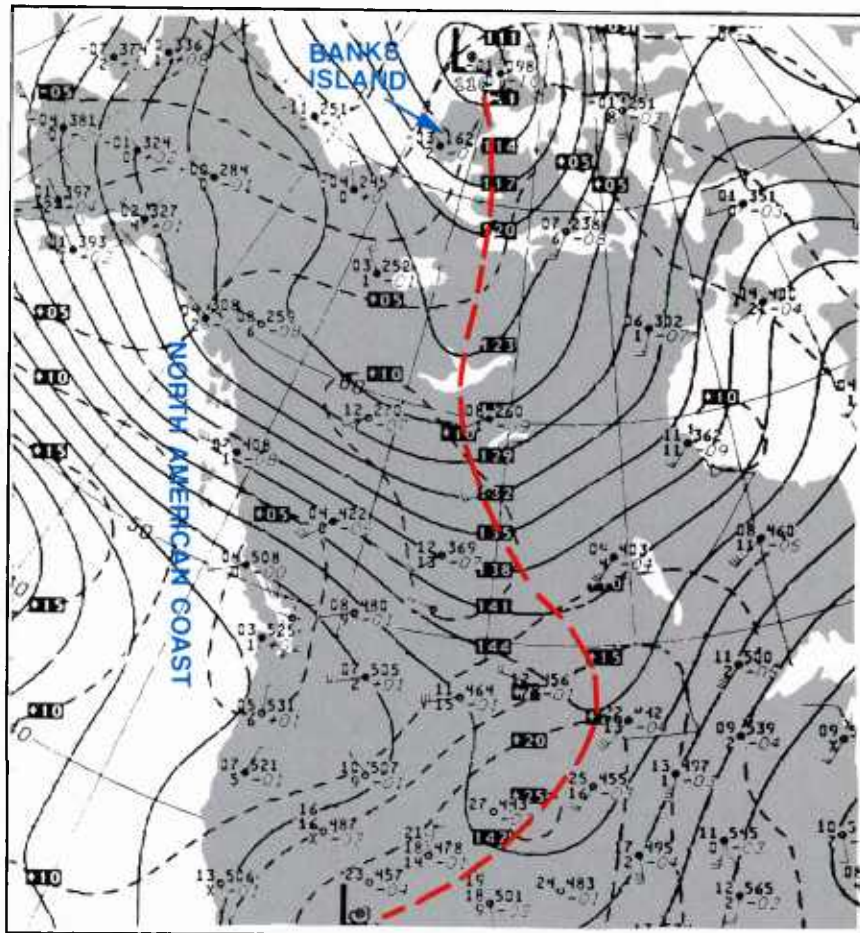


1A-5a NMC 850 mb analysis. 15 September 1985, 0000 GMT.

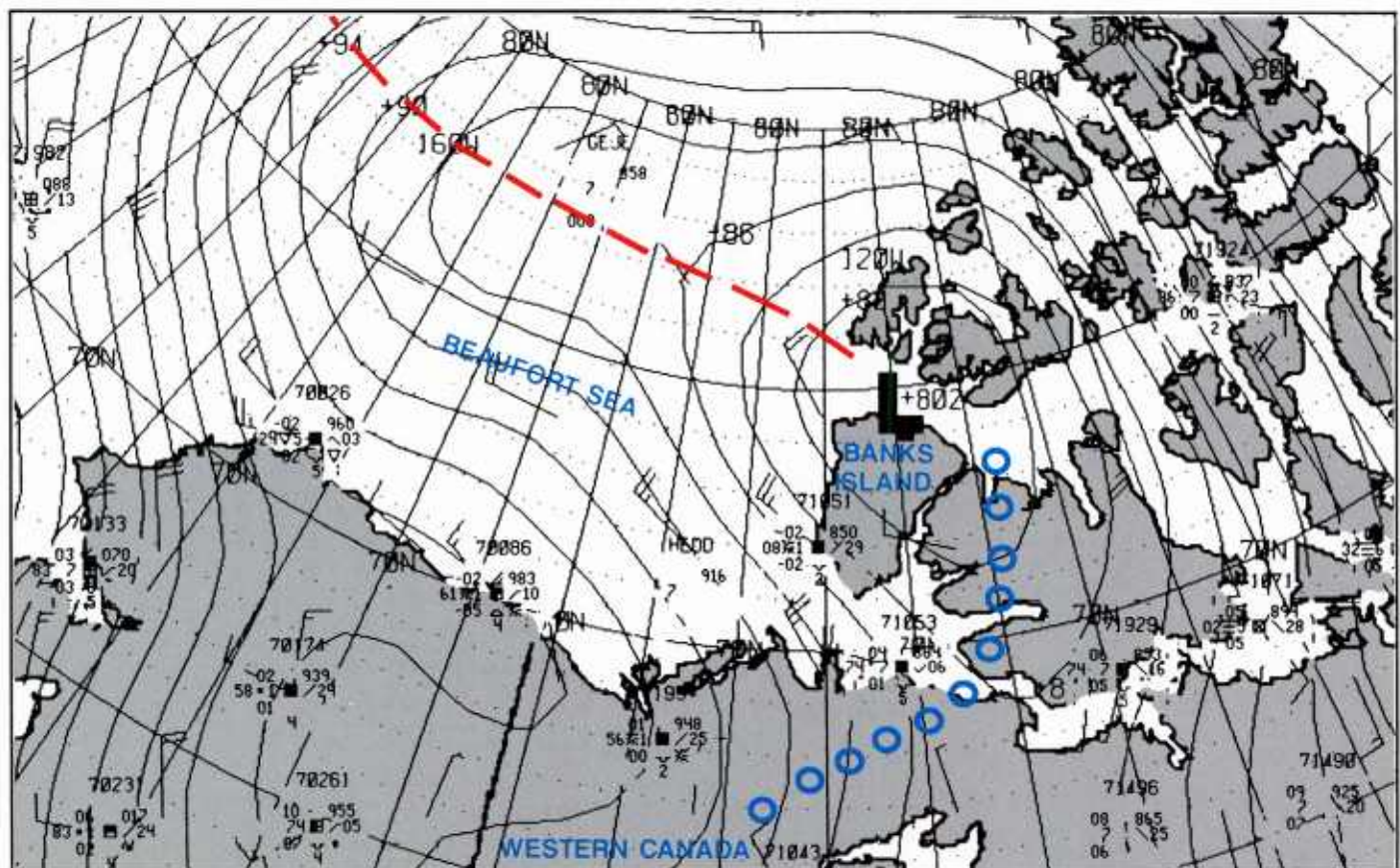


1A-5b NMC 500 mb analysis. 15 September 1985, 0000 GMT.



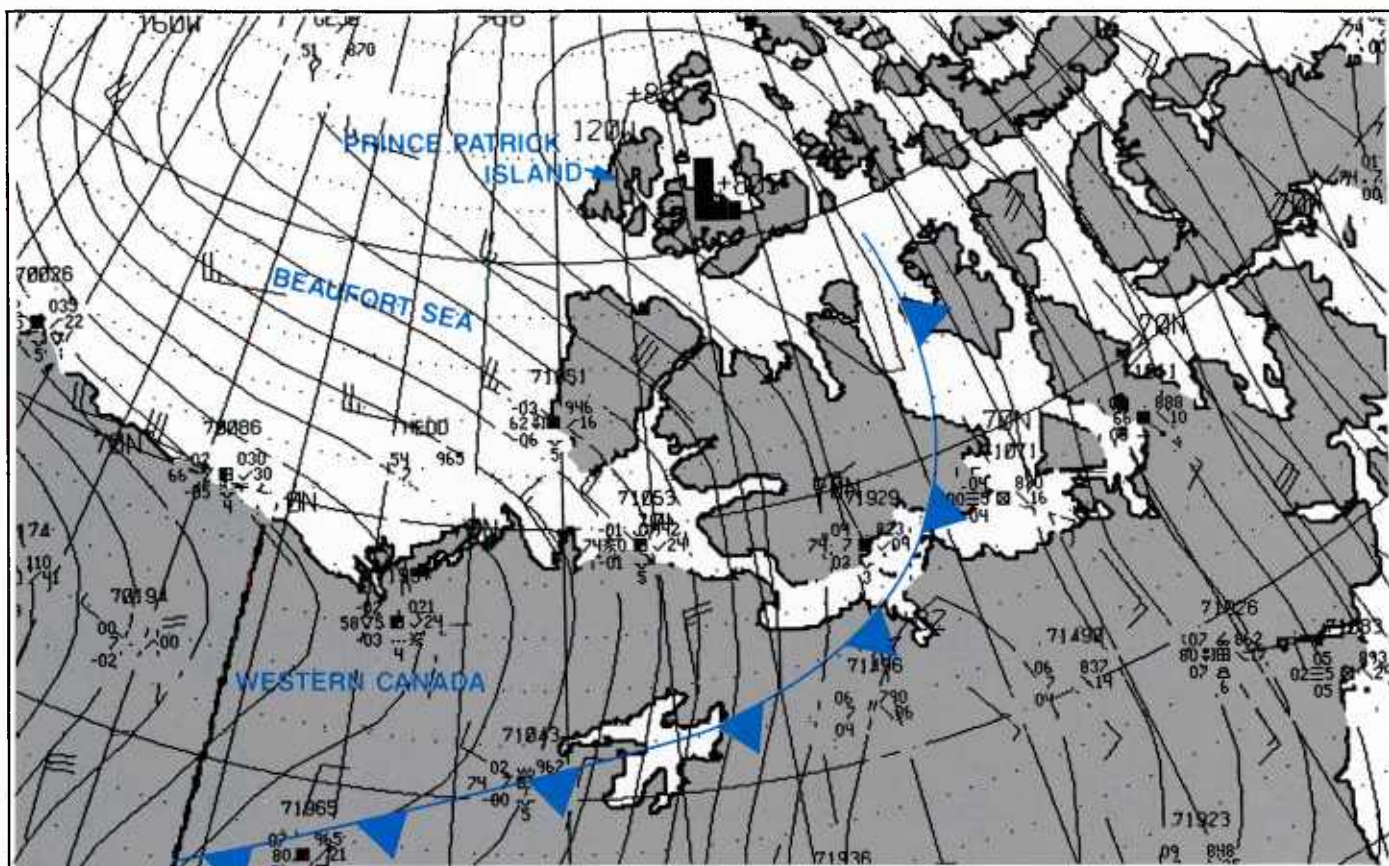


1A-6a 850 mb analysis. 16 September 1985, 0000 GMT.

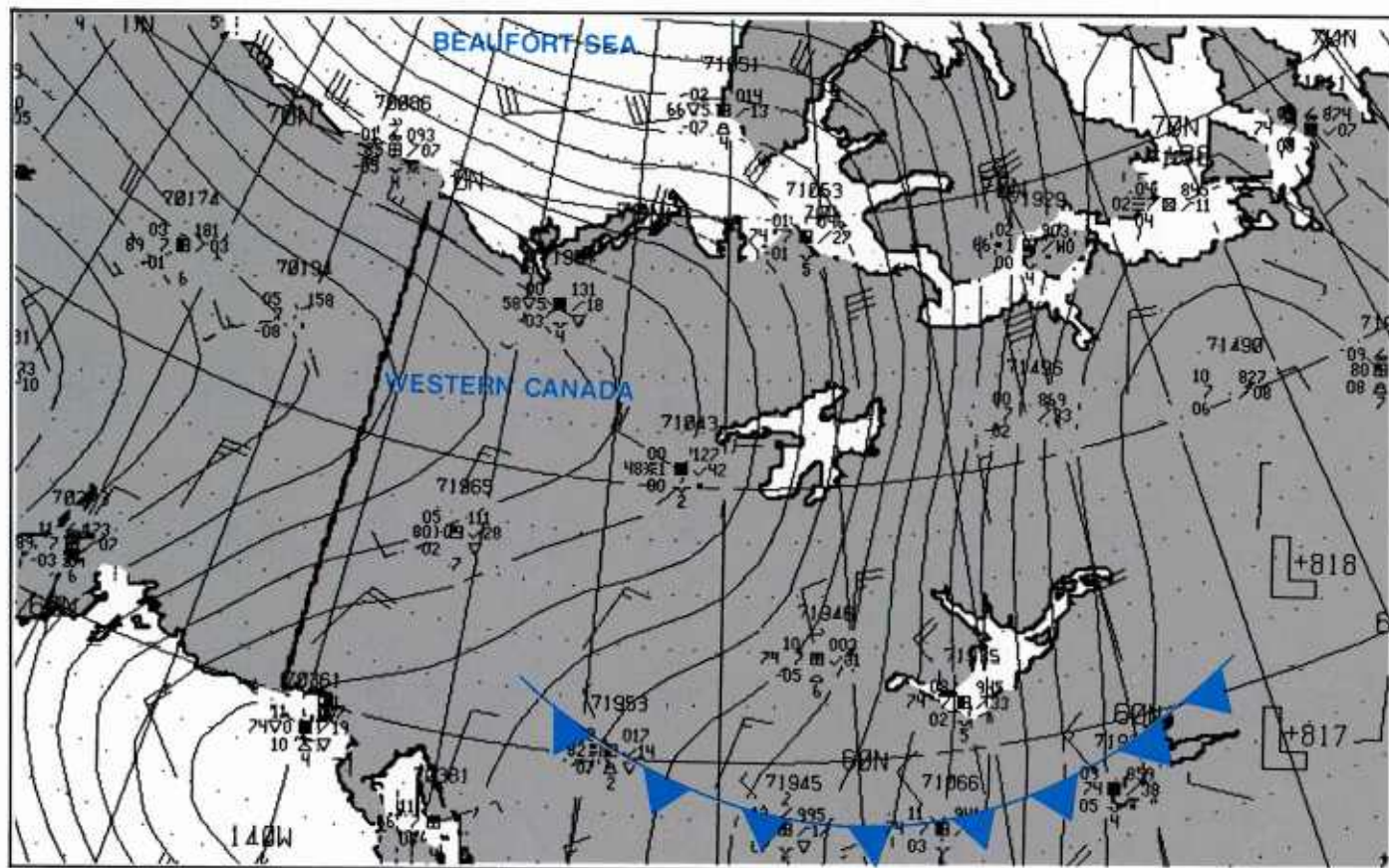


1A-6b FNOC surface analysis. 16 September 1985, 0000 GMT.



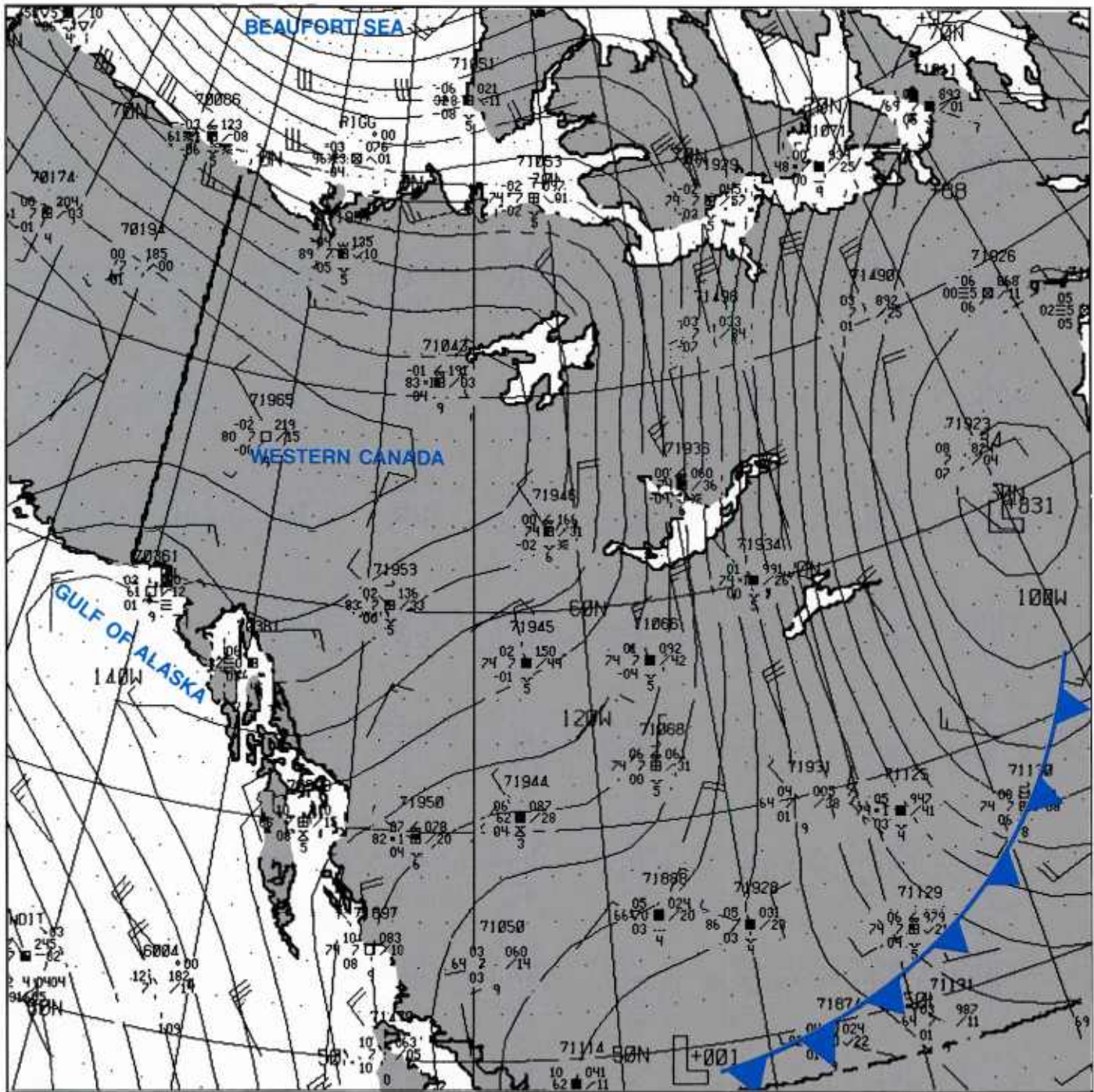


1A-7a FNOc surface analysis. 16 September 1985, 1200 GMT.



1A-7b FNOc surface analysis. 17 September 1985, 0000 GMT.

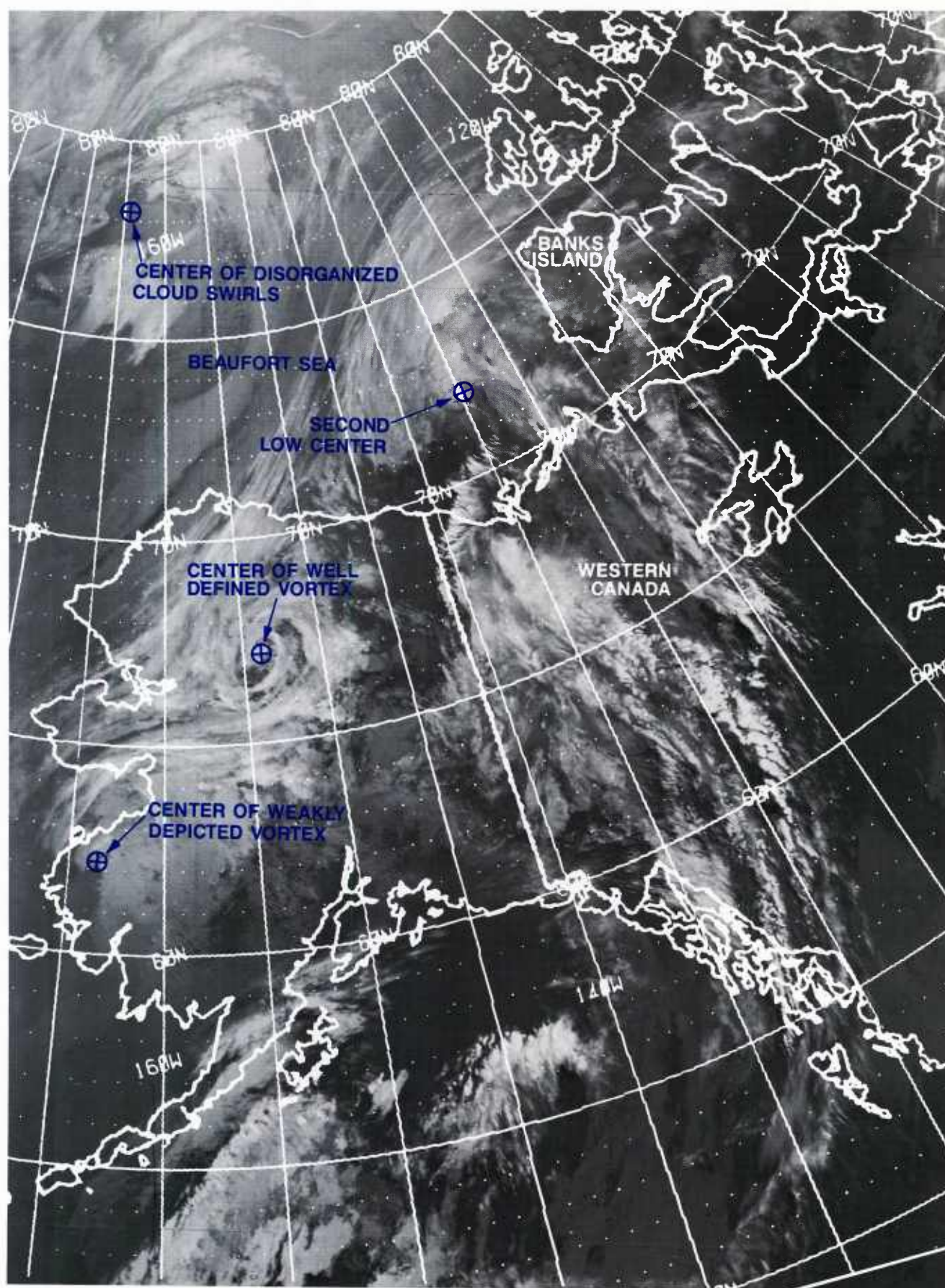




1A-8 FNOC surface analysis. 17 September 1985, 1200 GMT.

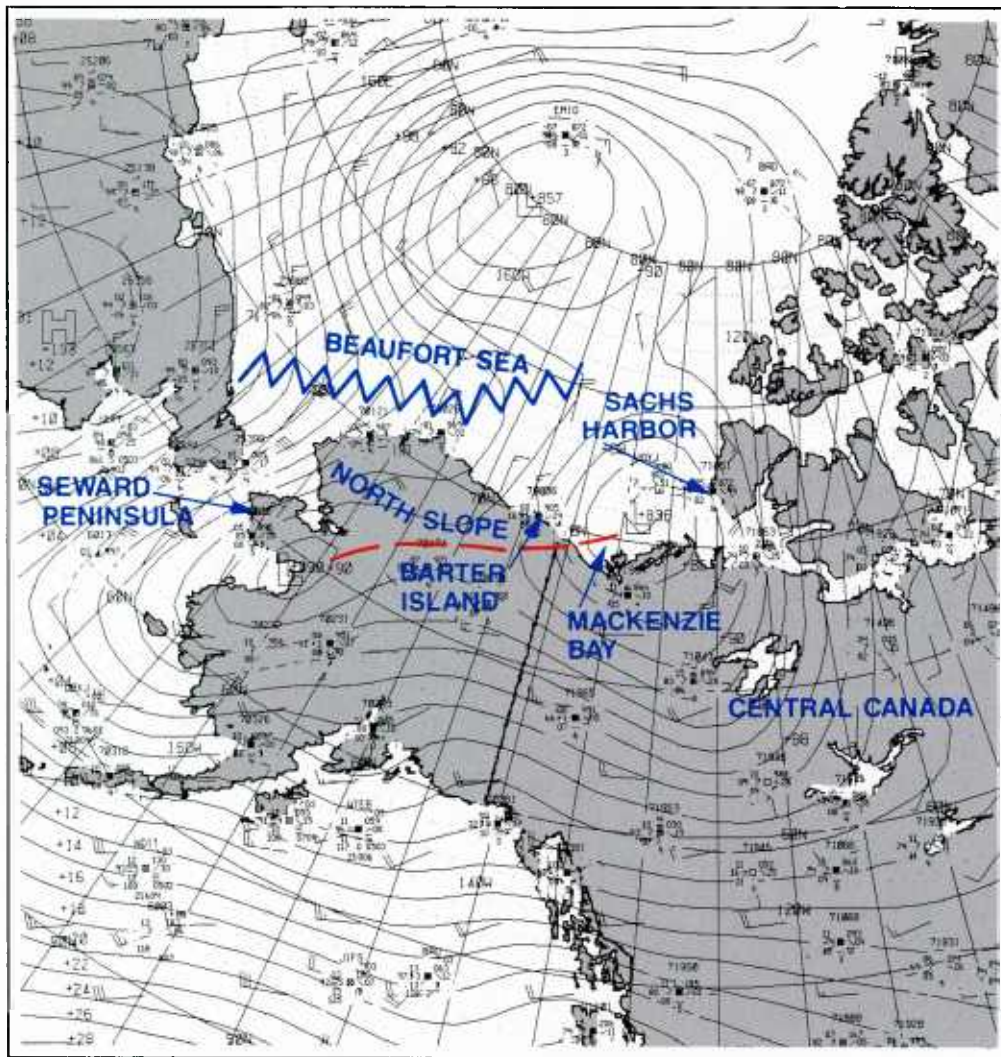
While the front moved south, a major storm evolved over the Beaufort Sea (see Figs. 1A-6b through 1A-8). The storm, which was extremely costly to oil interests in the region, lasted the longest and proved to be one of the most severe of the 1985 storm season. On September 16 and 17 ESSO resources was forced to evacuate Minutis I-53, "an artificial island situated 80 nm west-northwest of Tukoyaktuk. As the island eroded, a \$30 million derrick toppled and a damaged storage container released 2440 barrels of diesel oil into the Beaufort Sea" (Parker et al., 1985).





1A-9a DMSP infrared (TS) data. 15 September 1985, 0432 GMT.



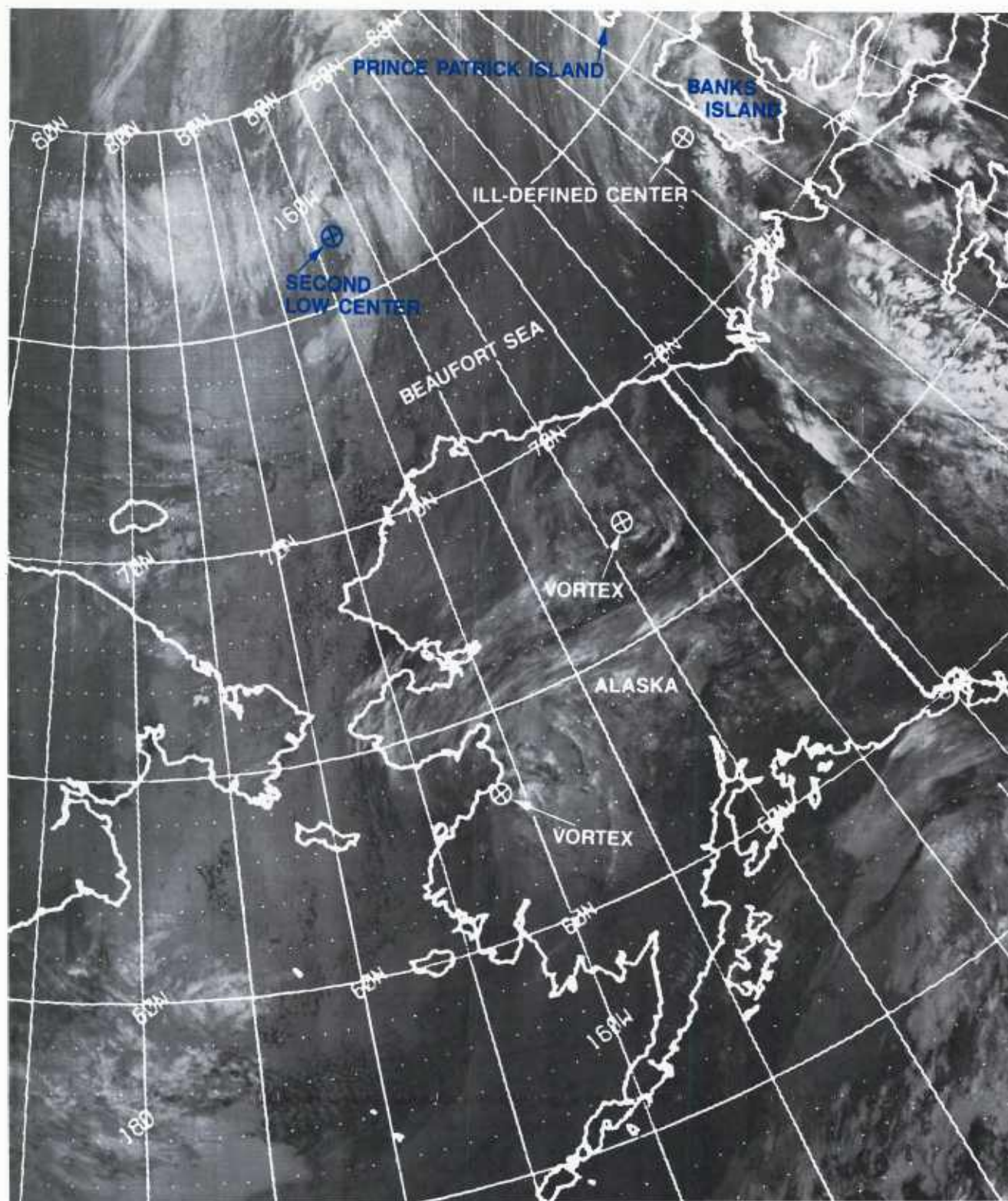


1A-9b FNOG surface analysis. 15 September 1985, 0600 GMT.

An early stage of storm development on 15 September at 0432 GMT (Fig. 1A-9a, storm centers indicated by a  $\oplus$ ) shows a rather disorganized region of cloud swirls centered in the general area of 78N, 165W. The surface analysis for 15 September at 0600 GMT (Fig. 1A-9b) shows a surface low in that area centered closer to 80N. Another low center north of Mackenzie Bay relates reasonably well to an ill-defined cloud center suggested west of Banks Island near 72N, 135W. Note from the satellite data (Fig. 1A-9a) that the two systems are quite distinct. A point is made of this because the AES Executive Summary of this storm referred to earlier (Parker et al., 1985) suggests that the Banks Island low became the major Beaufort Sea storm, whereas the results of this study indicate that it was the evolution of cloud features to the west that became the major storm.

The two vortices over Alaska are shown in Figure 1A-9a—one weakly depicted near 62N, 163W and the other well-defined with center at 67N, 154W—are only part of the storm. The southernmost vortex does not appear as a closed circulation in the surface analysis (Fig. 1A-9b) whereas the central Alaskan vortex seems slightly displaced to the northeast of the low center indicated over the southern portion of the Seward Peninsula.

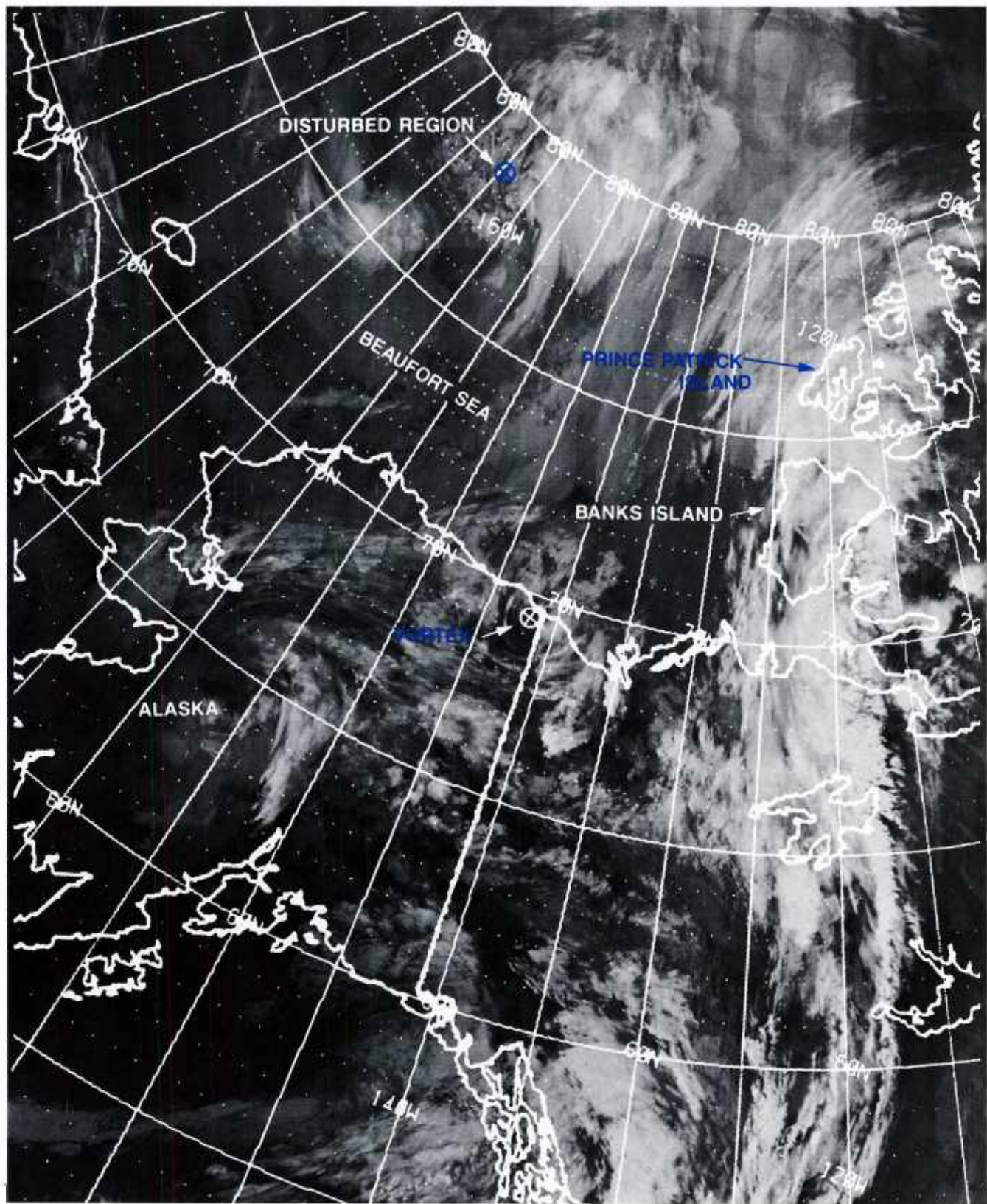




1A-10 DMSP infrared (IR) data: 15-September 1985; 0029 GMT.

A DMSP infrared view (Fig. 1A-10) of the systems about 5 hours after Figure 1A-9a shows further movement of these systems to the northeast. The approximate centers of the systems are indicated by a  $\oplus$ . In addition, the ill-defined center located near 73N, 127W west of Banks Island in Figure 1A-9a remains ill-defined and appears to be slipping northeastward toward Prince Patrick island. The low over the Beaufort Sea, meanwhile (center near 76.5N, 158W), is still apparent in a somewhat disorganized form, with several clusters showing signs of intensification.

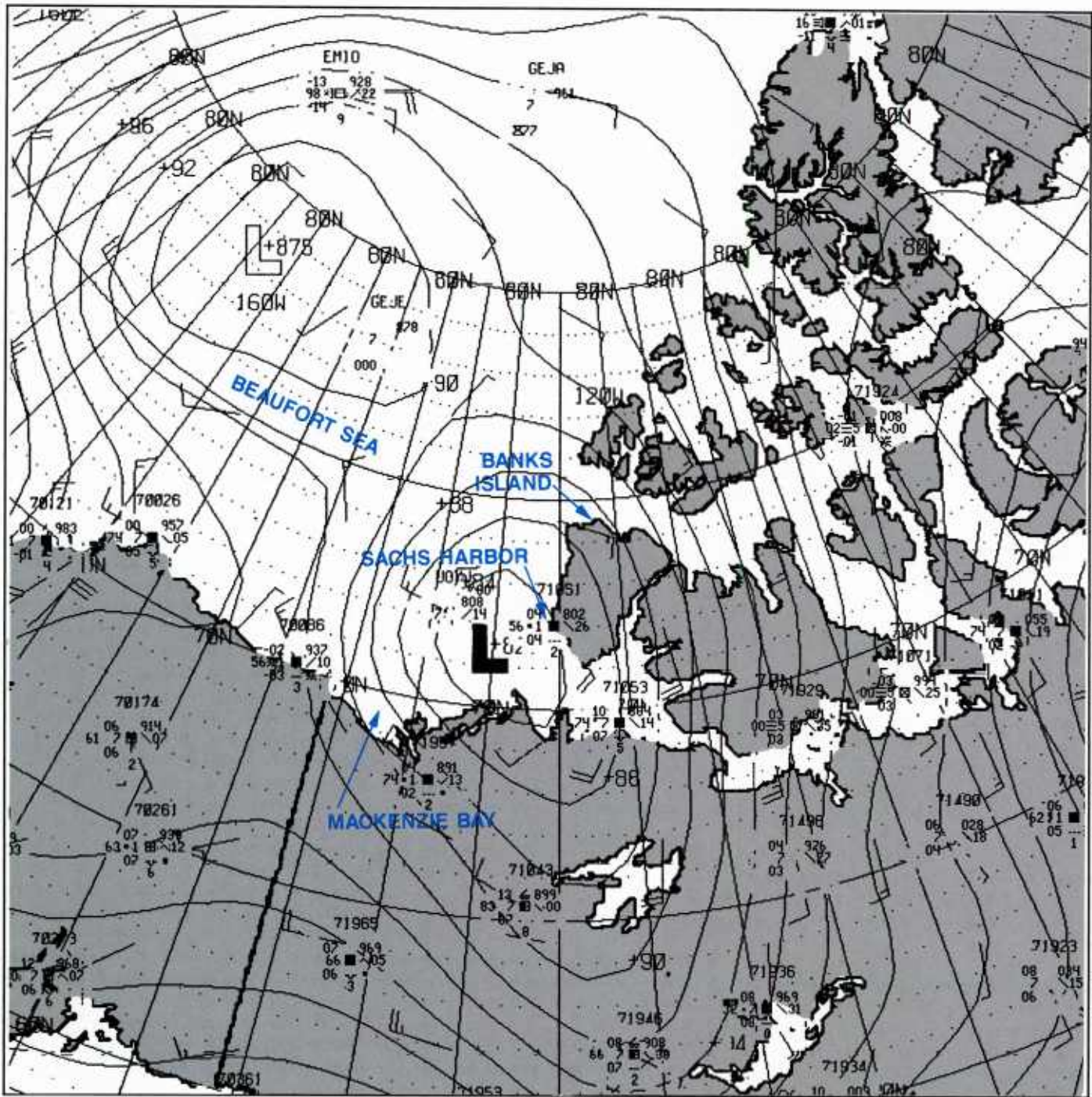




1A-11 DMSP infrared (TS) data. 15 September 1985, 1424 GMT.

Five hours later, at 1424 GMT (Fig. 1A-11), DMSP infrared data reveal that the central Alaska low has reached Mackenzie Bay (low center is indicated by a  $\otimes$ ), while the low originally west of Banks Island is no longer apparent, and its definition is lost in the frontogenetic structure extending north/south through Banks Island.





1A-12 FNOC surface analysis. 15 September 1985, 1200 GMT.

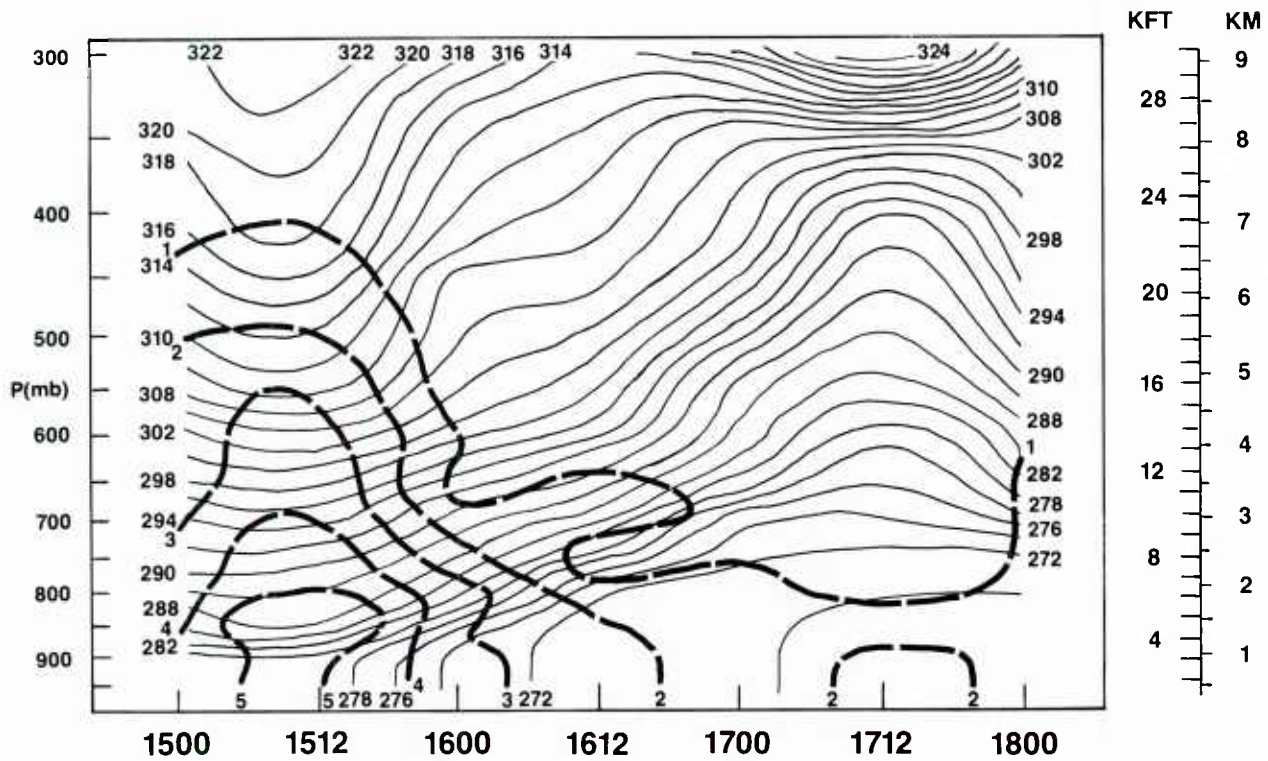
The FNOC surface analysis for 15 September at 1200 GMT (Fig. 1A-12) shows a low SW of Banks Island, but there is little support for this low as a viable entity judging from the satellite data (Fig. 1A-11) which show this region as clear except for the small vorticity center near 70N, 140W approaching Mackenzie Bay. Note that the low center (Fig. 1A-12) over the Beaufort, near 78.5N, 164W, coincides with the disturbed region appearing in the satellite data of Figure 1A-11.

A time-section for Sachs Harbor from 15 September 0000 GMT to 18 September 0000 GMT (Fig. 1A-13a) shows potential temperature and mixing ratio changes. The analysis suggests frontal passage at Sachs Harbor between 15 September 1200 GMT and 16 September 0000 GMT. Conditions were very moist and stable prior to frontal passage and became dry and unstable after the event. The upward bulging and spreading potential temperature lines on 17 September indicate instability.

A time-section of the wind field during the same period (Fig. 1A-13b) shows the shift from southwest flow near the surface on 15 September at 1200 GMT, to northwest flow on 16 September at 0000 GMT, as the front passed. The section is additionally interesting in showing the two separate jet streaks that passed over the region during the period of the Beaufort Sea storm development. The first jet is well-defined over Sachs Harbor on 15 September and the second on 17 September at 0000 GMT.



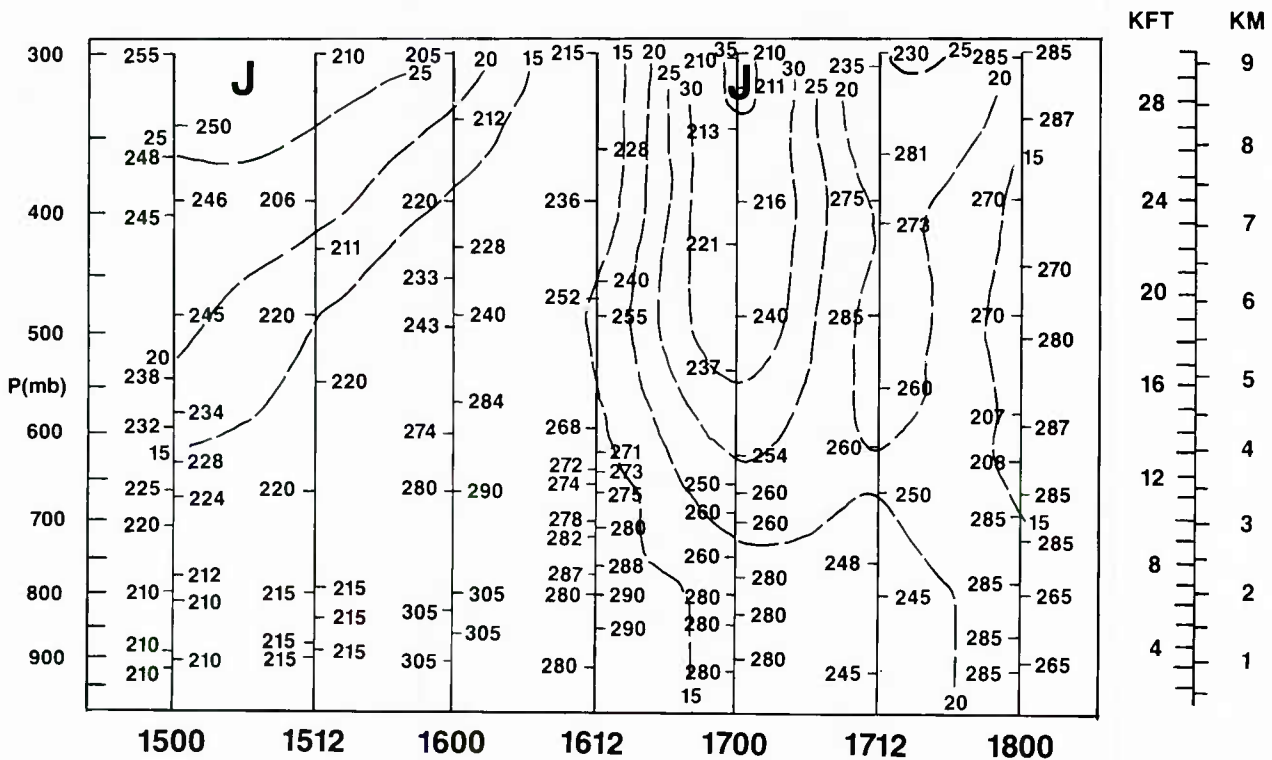
POTENTIAL TEMPERATURE IN KELVIN  
MIXING RATIO IN G/KG



station 71051

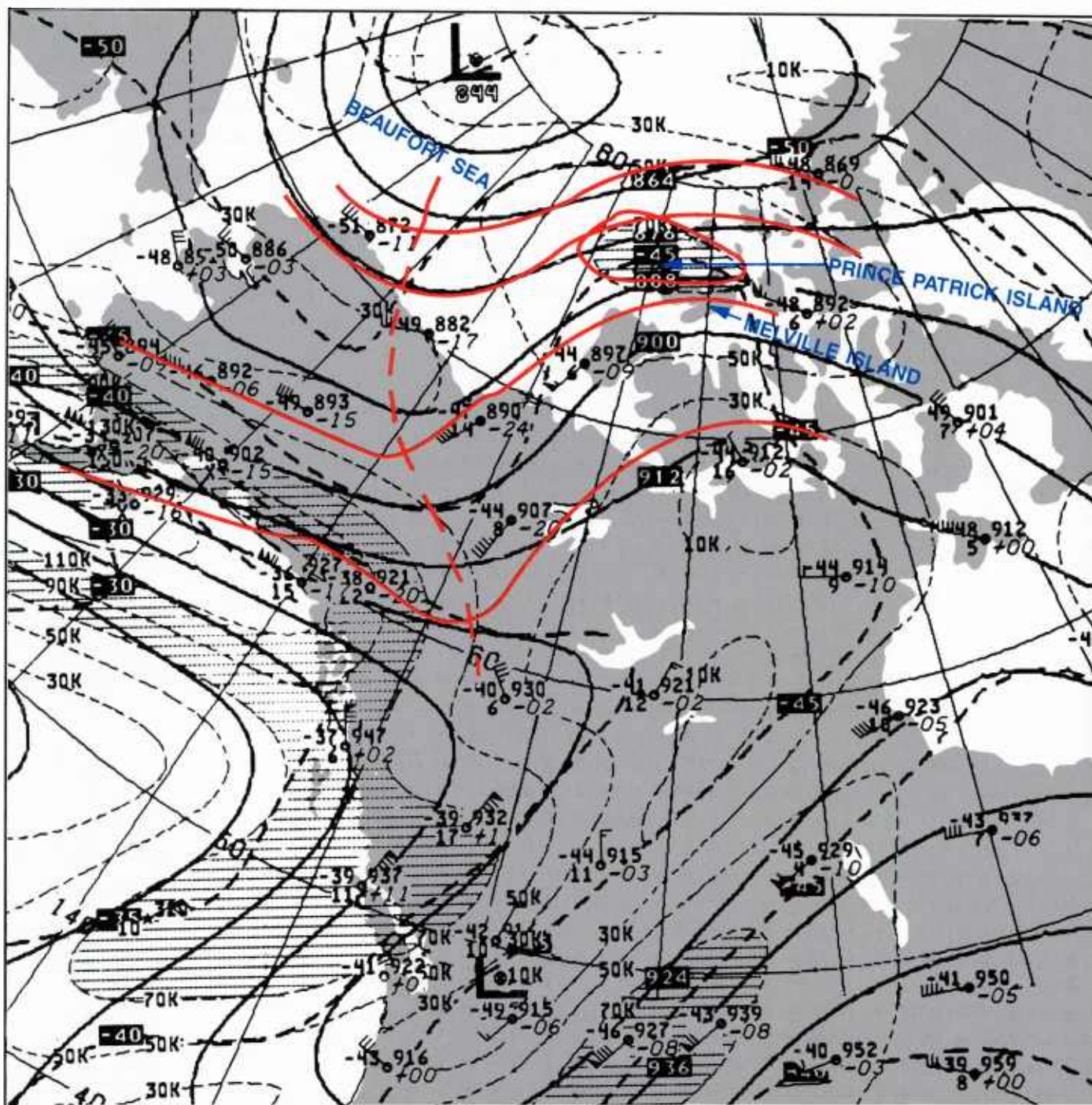
1A-13a A time-section for Sachs Harbor and Banks Island, Canada during the period 15-18 September 1985. Solid lines are potential temperatures contours; dashed lines represent mixing ratios.

WIND DIRECTION IN DEGREES CLOCKWISE FROM NORTH  
WIND SPEED IN M/S



station 71051

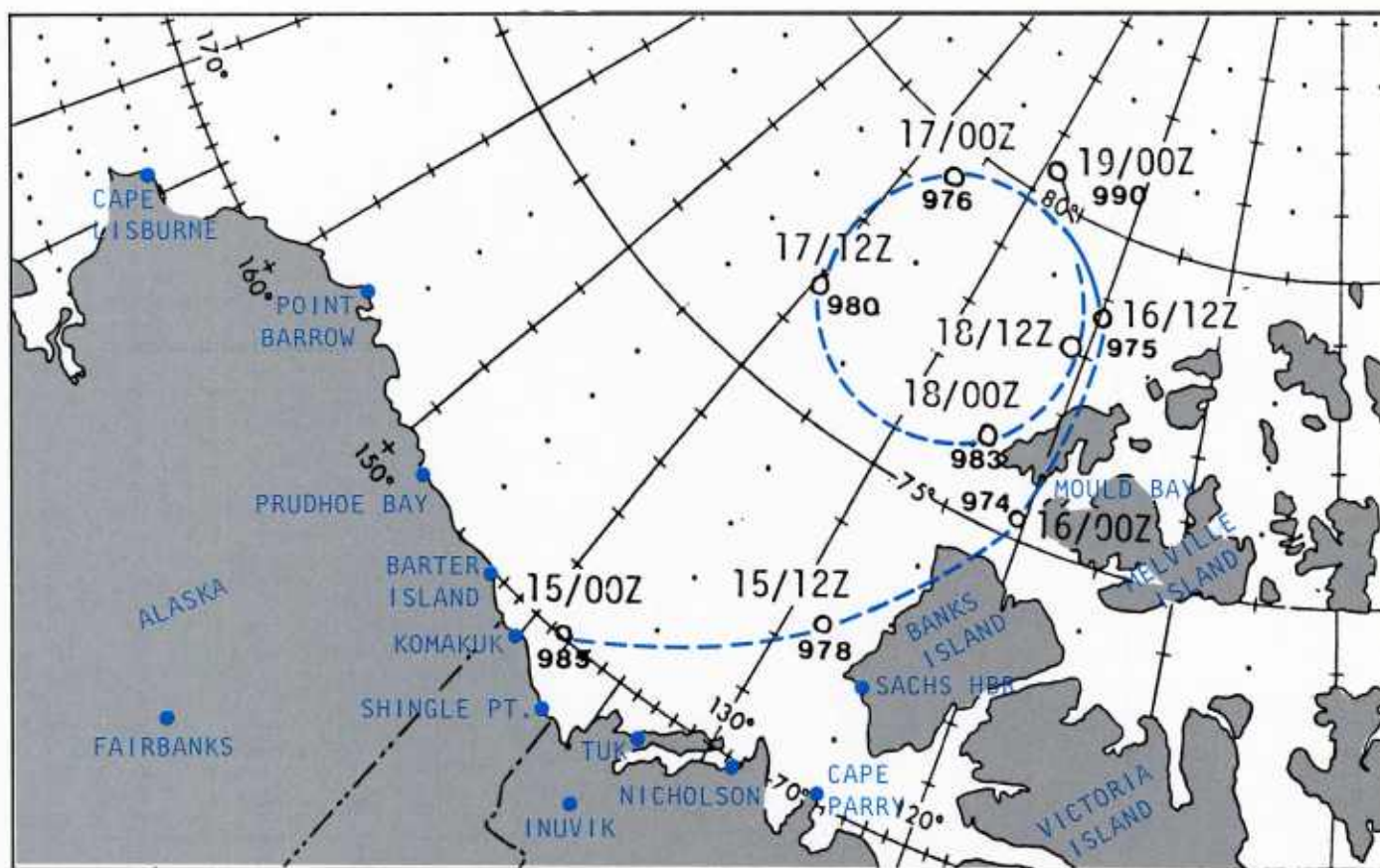
1A-13b A time-section for Sachs Harbor and Banks Island, Canada during the period 15-18 September 1985. Wind direction is shown on vertical lines; dashed lines represent isotachs.



1A-14 NMC 300 mb analysis. 15 September 1985. 1200 GMT.

The NMC 300 mb analysis for 15 September at 1200 GMT (Fig. 1A-14) shows the jet streak passing over Banks Island, which was reporting a southwest wind at 55 kt. The jet turned anticyclonically and increased speed as it moved eastward over Prince Patrick and Melville Island. The cirrus streaks associated with this jet are well revealed in the DMSP image of Fig. 1A-11.

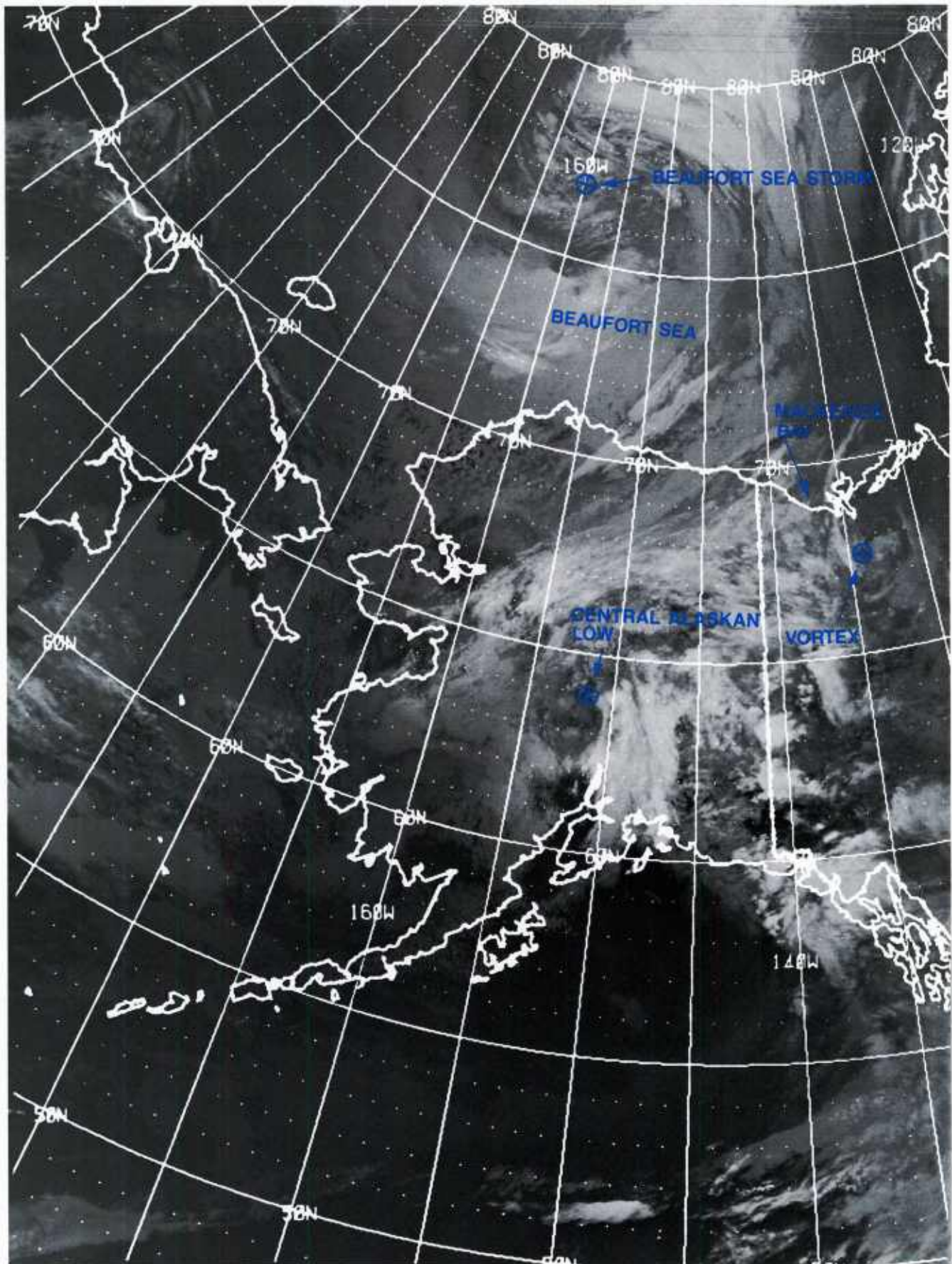




1A-15 Track of surface low center. 15-19 September 1985 (From Beaufort Weather Office 1985 Report).

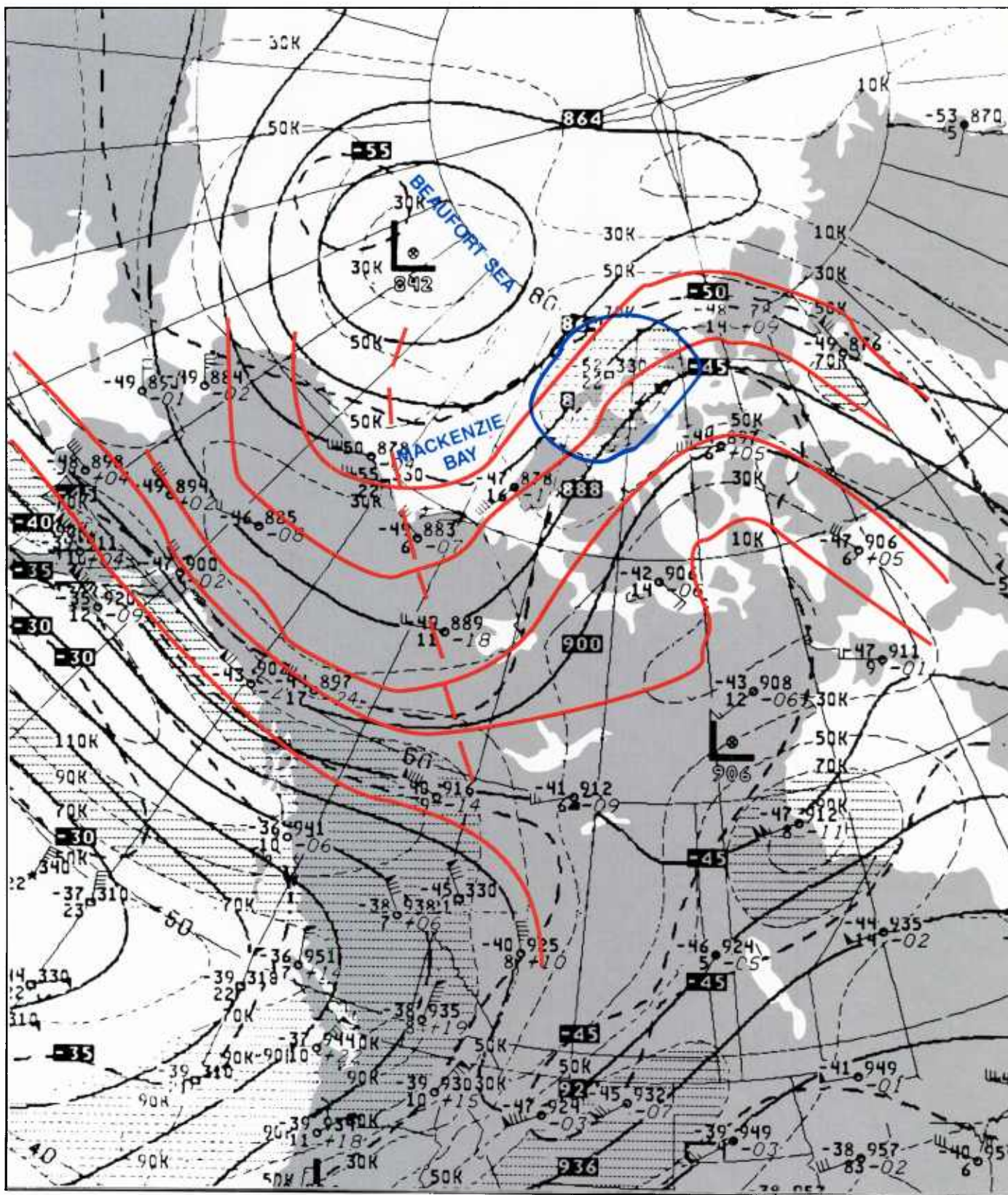
The Beaufort Sea storm in Figure 1A-11 is still disorganized with separate clusters of cloudiness circulating about the low pressure center. It is apparent from this image that the Beaufort Sea storm development was from a separate surface low pressure center than that analyzed just SW of Banks Island in Figure 1A-12. This suggests that the track of the low pressure center prepared by AES (Bullas, 1985) and shown as Figure 1A-15 in representing the surface low positions of the Beaufort Sea may be erroneous. Later in the period on 17 September, however, it is possible that the two surface lows merged into a single low near the positions shown in those data.

Figure 1A-16 is a DMSP infrared image taken 5 hours after Figure 1A-11. It shows further evolution of the Beaufort Sea storm at 1922 GMT. The system appears to be intensifying as low cloud bands over a wide distance are winding about the storm center, vaguely implied near 77N, 160W. At the same time, the central Alaskan center (near 64N, 151.5W) appears to have changed little from its rather weak condition, and the vortex that had been approaching Mackenzie Bay (center near 67.5N, 134W), is weakly defined, having moved southward along the Mackenzie River.



1A-16 DMSP infrared (TS) data, 15 September 1985, 1922 GMT.

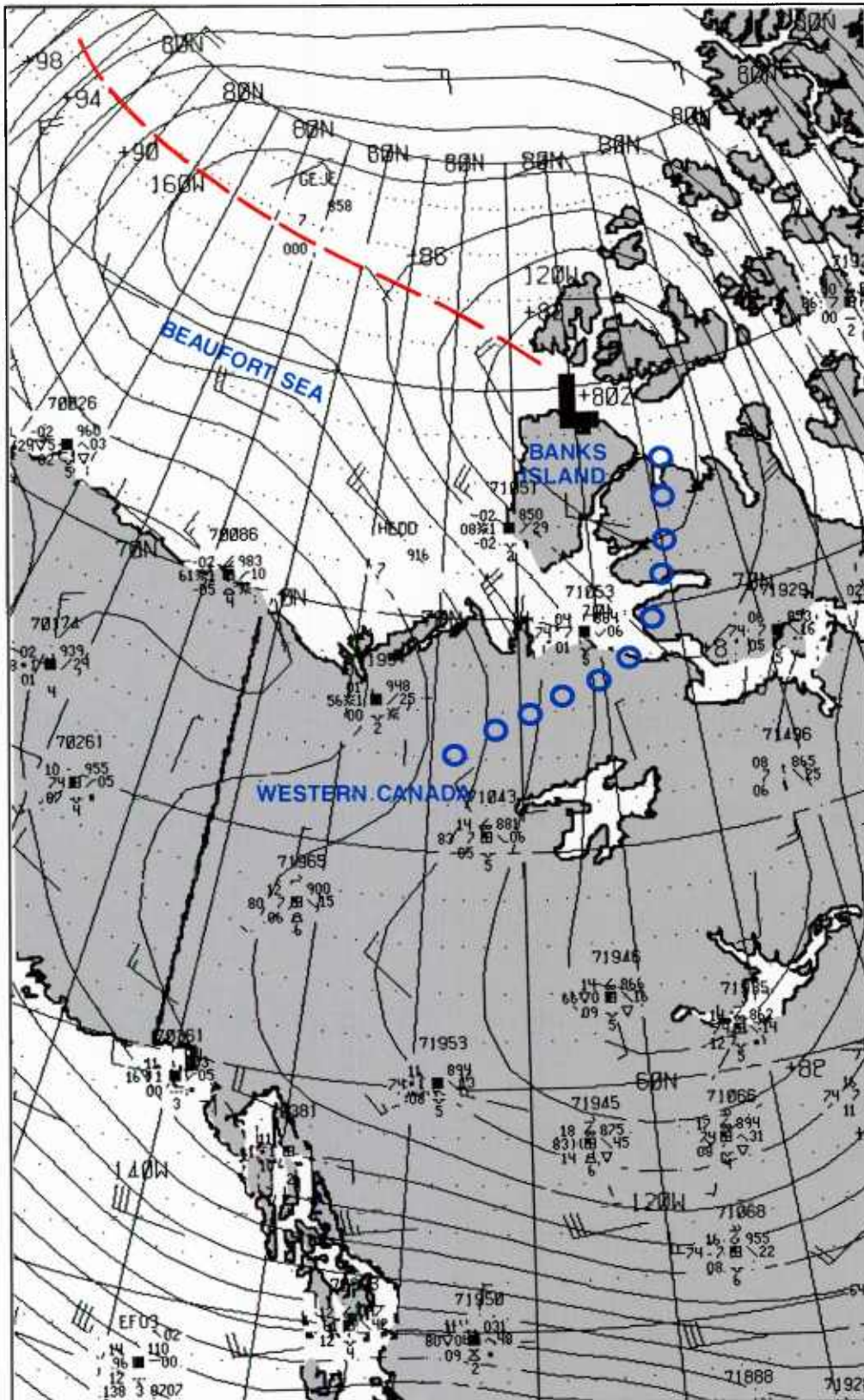




1A-17a NMC 300 mb analysis. 16 September 1985, 0000 GMT.

The jet streak shown aloft in the NMC 300 mb analysis on 16 September at 0000 GMT (Fig. 1A-17a) may have been a factor in the intensification of the Beaufort Sea storm. Strong positive vorticity was created in the region of the low because of this feature.

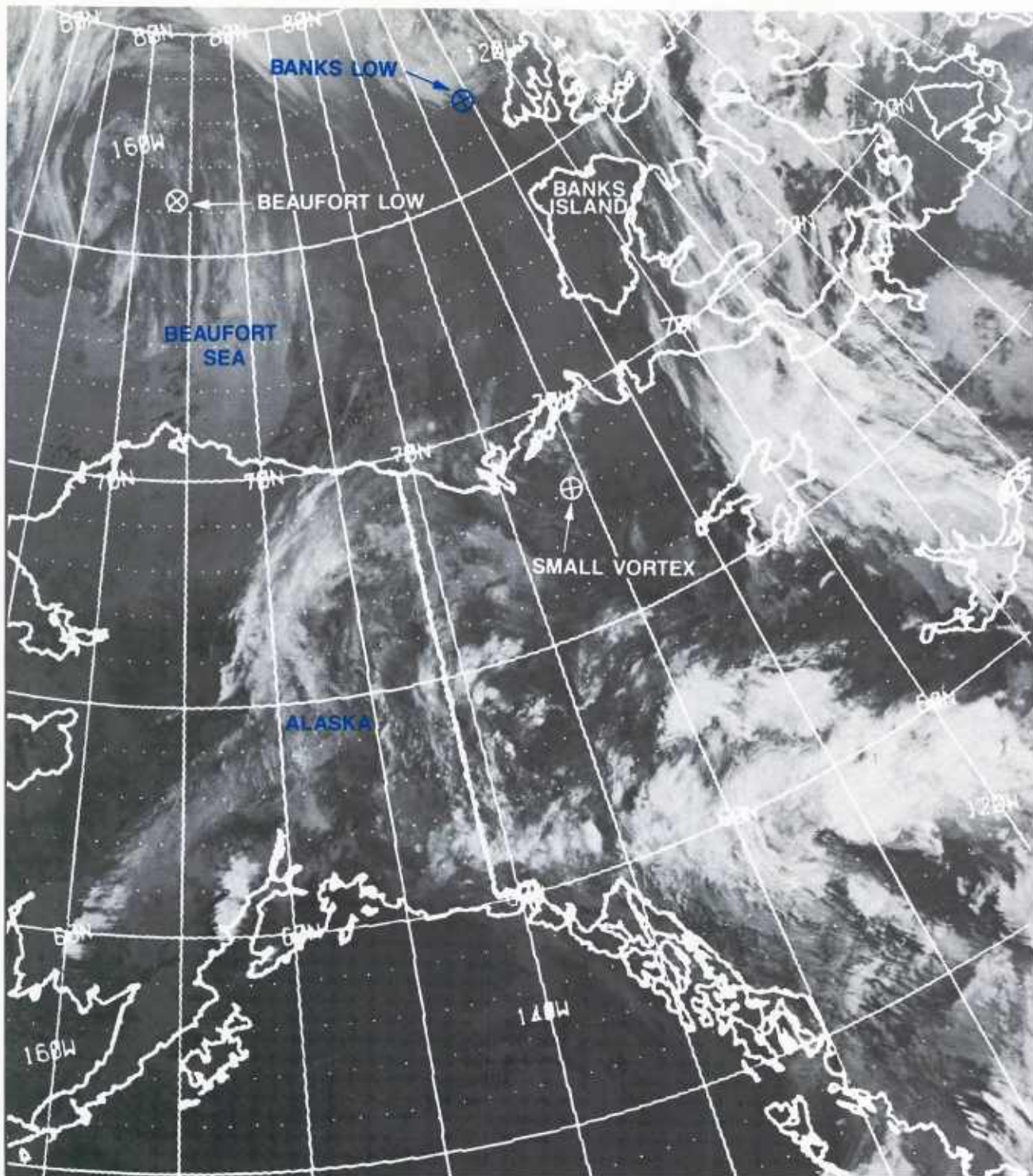




1A-17b FNOc surface analysis. 16 September 1985, 0000 GMT.

The FNOc surface analysis for 16 September at 0000 GMT (Fig. 1A-17b) does not show a developing system near 75N, 160W, but only a trough line through that position connected to a low on the north end of Banks Island.

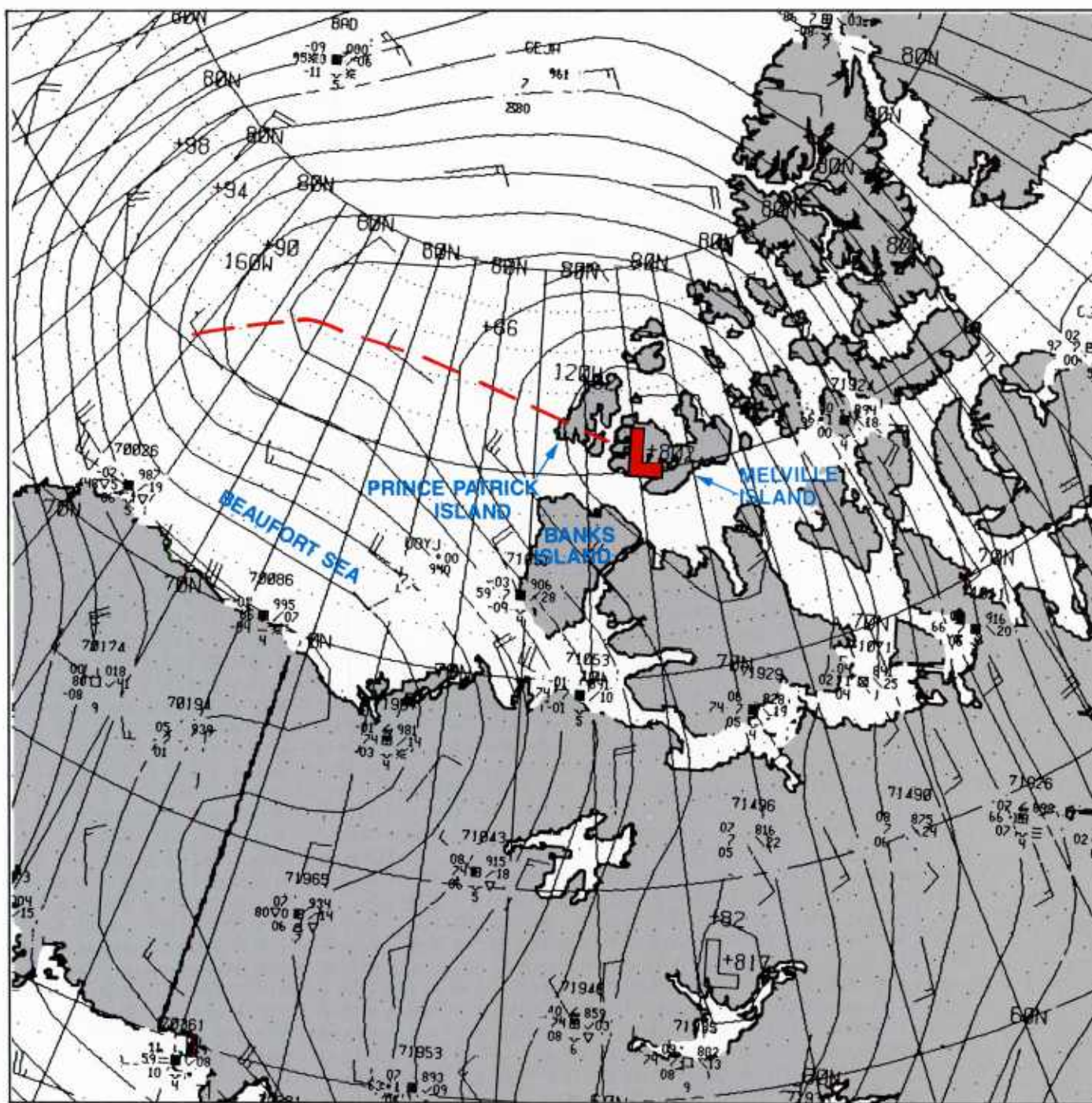




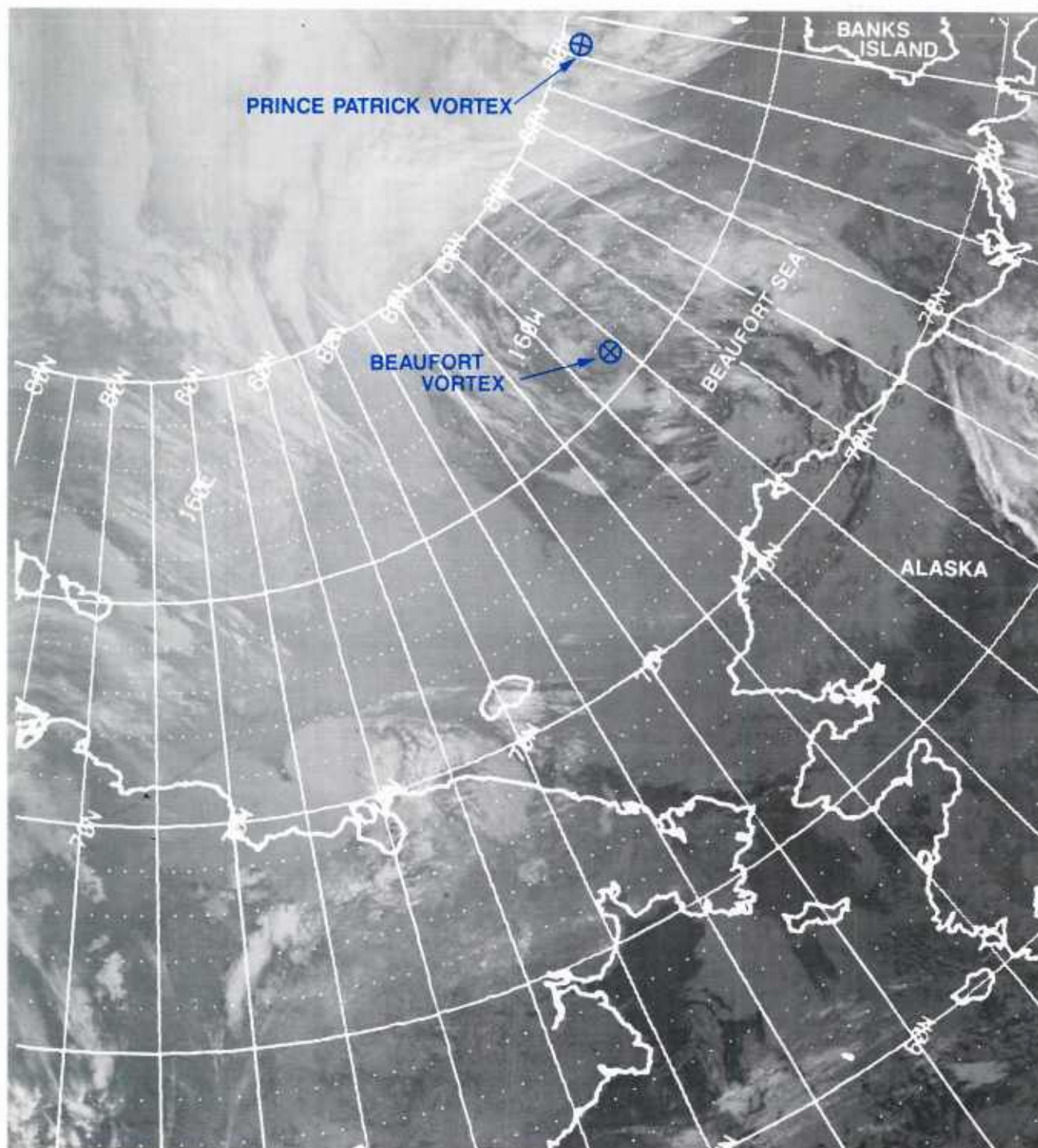
1A-18 DMSP infrared (TS) data. 16 September 1985, 0355 GMT.

A DMSP infrared view of the region on 16 September at 0355 GMT is shown in Figure 1A-18, and the FNOC surface analysis for 0600 GMT is shown in Figure 1A-19. The surface analysis shows the Banks low over Prince Patrick and Melville Island (center near 76N, 114W) with the Beaufort Sea low still in a trough region. A small vortex (center near 68N, 131W) is still faintly discernible east of the mouth of the Mackenzie River in the DMSP data (Fig. 1A-18) while the central Alaskan low has merged into a general trough area. A protrusion of cloudiness NW of Prince Patrick Island may mark the reappearance of the cloud vortex system associated with the Banks low over Prince Patrick Island. Note that this is hundreds of miles from the Beaufort low.





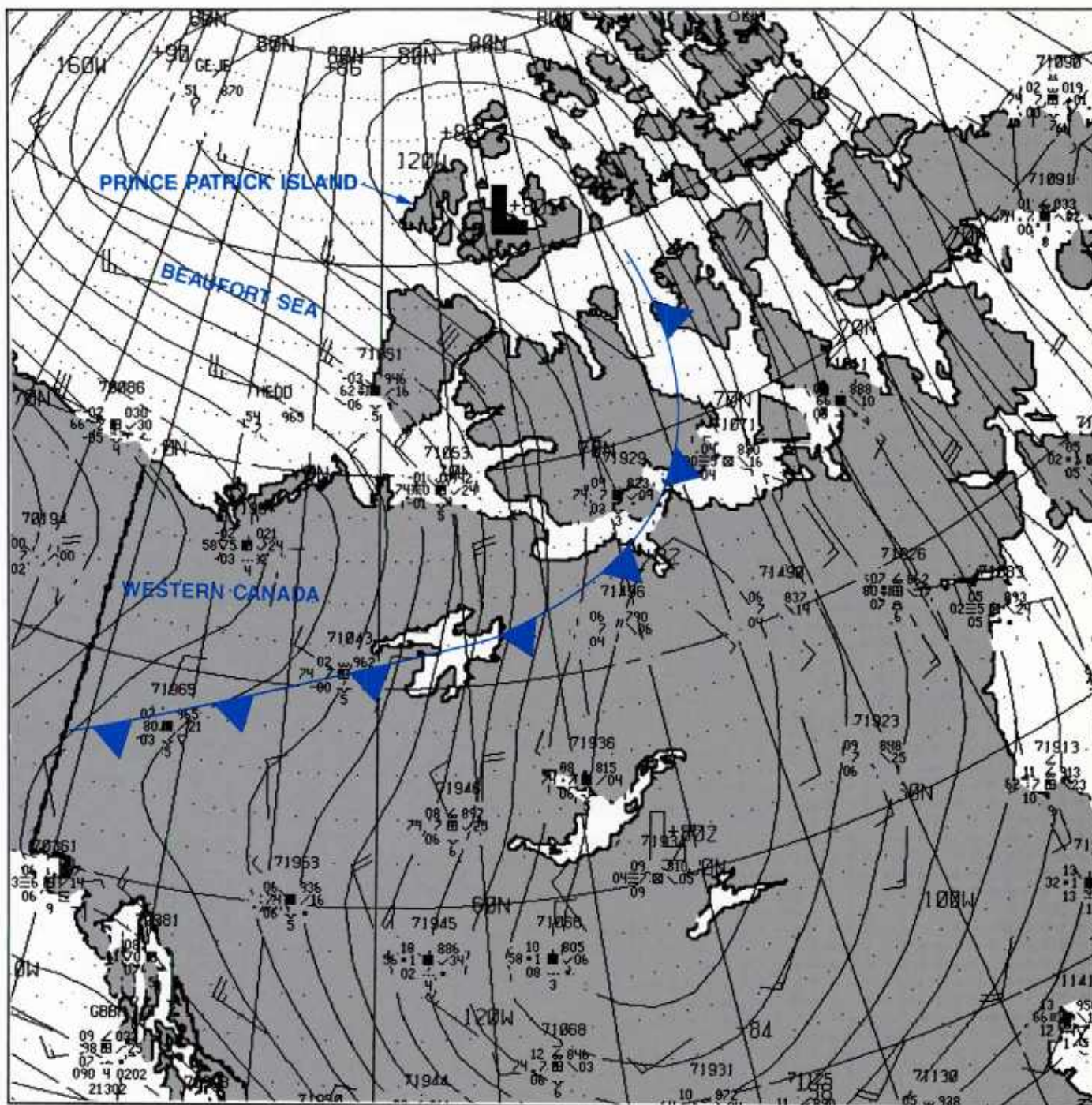
1A-19 FNOC surface analysis. 16 September 1985, 0600 GMT.



1A-20 DMSP infrared (TS) data. 16 September 1985, 0717 GMT.

A DMSP infrared view of the area on 16 September at 0717 GMT is shown in Figure 1A-20. The Beaufort vortex and Prince Patrick vortex (previously referred to as the "Banks low") are again evident in these data with little change in intensity.





1A-21 FNOc surface analysis, 16 September 1985, 1200 GMT

By 16 September at 1200 GMT, North Slope coastal stations started experiencing strong sustained surface winds at 25-30 kt. The FNOc surface analysis at this time is shown in Figure 1A-21.

As indicated in the report by Parker et al., 1985, "building 500 mb heights and low-level cold air advection were producing strong surface pressure rises over Alaska. These pressure rises contained and subsequently spread across the Yukon. The result was a tightening of the surface pressure gradient and a southward displacement . . ." of a protective ridge (see Fig. 1A-9b) that had been shielding the North Slope area. As the ridge was displaced southward, the North Slope was exposed to gale force winds.

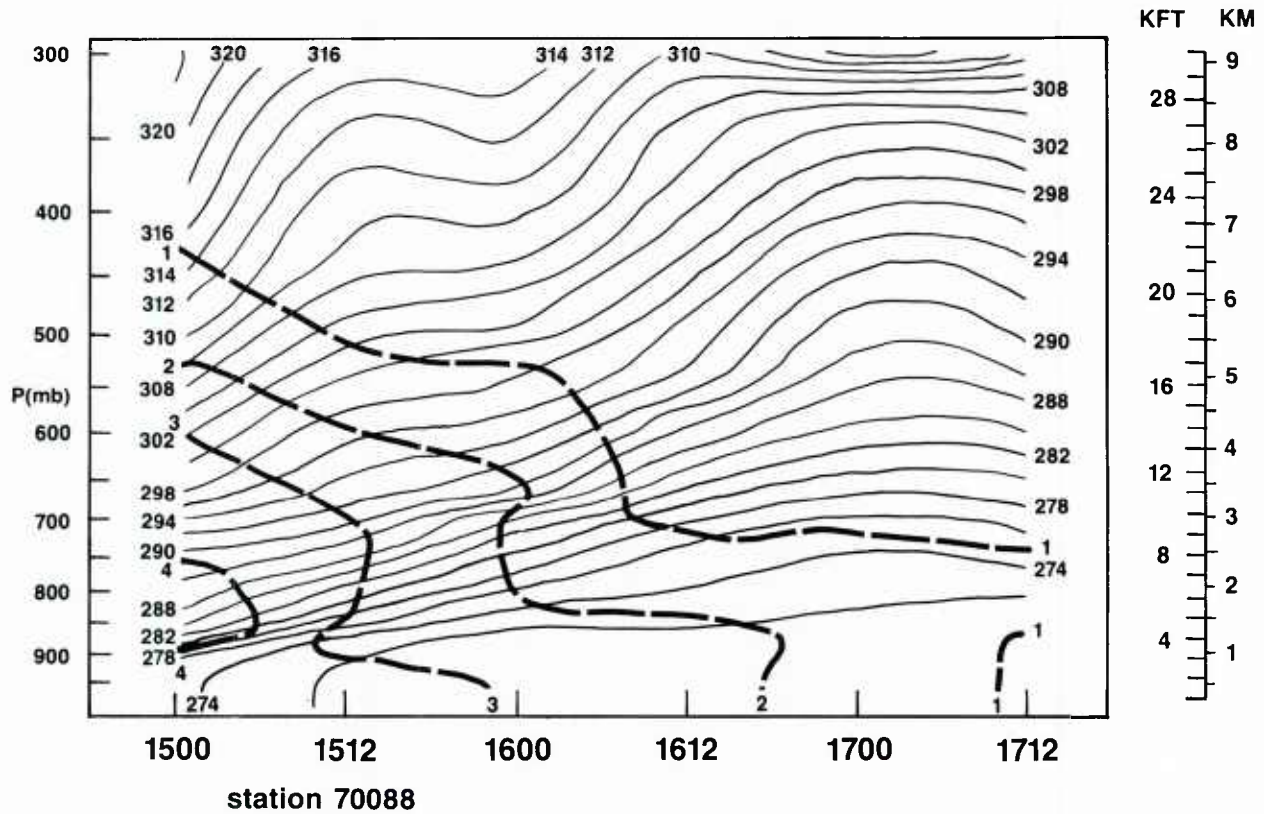


A time-section showing potential temperature and mixing ratio changes at Barter island is shown in Figure 1A-22a. On 15 September at 0000 GMT, stable conditions were associated with the warm, moist air which preceded frontal passage at Sachs Harbor (shown also in the time-section for the latter station, Fig. 1A-13a). Unstable conditions early on 17 September are again revealed by the upward-bulging and spreading potential temperature lines. The time-section for wind effects (Fig. 1A-22b) shows the dual jet systems over the region on 15 and 16 September.

It is noteworthy that unstable conditions on 17 September were associated with the approach of the second jet. The change from stable to unstable conditions appears, perhaps even more dramatically, in a comparison of Barter Island soundings on 15, 16, and 17 September 1985 at 0000 GMT (Fig. 1A-23, from Bullas, 1985). The figure vividly illustrates the pronounced advective cooling that took place during the period of Beaufort low development, as an initial stable lapse rate on 15 September changed to nearly dry adiabatic by 16 September.

# POTENTIAL TEMPERATURE IN KELVIN

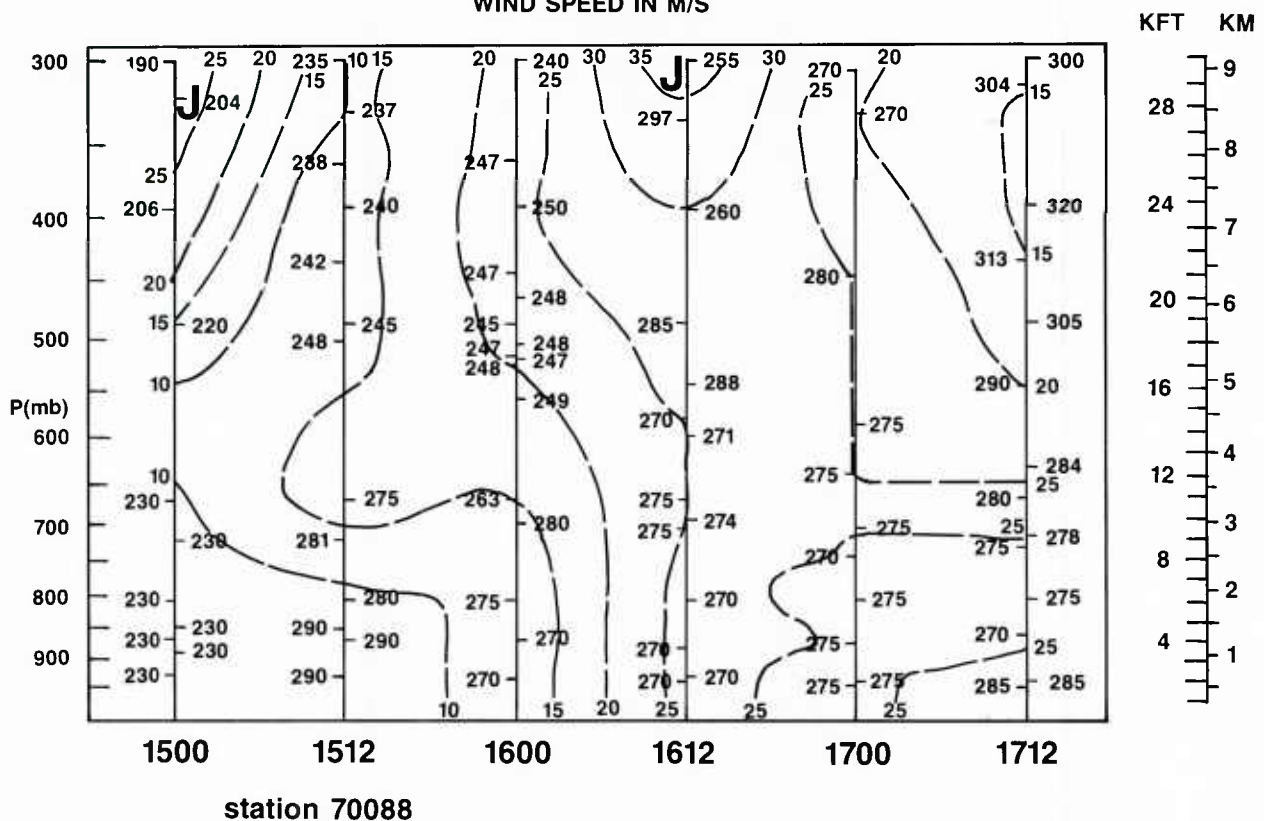
MIXING RATIO IN G/KG



1A-22a A time-section for Barter Island, Alaska, during the period 15-17 September 1985. Solid lines are potential temperature contours; dashed lines represent mixing ratio.

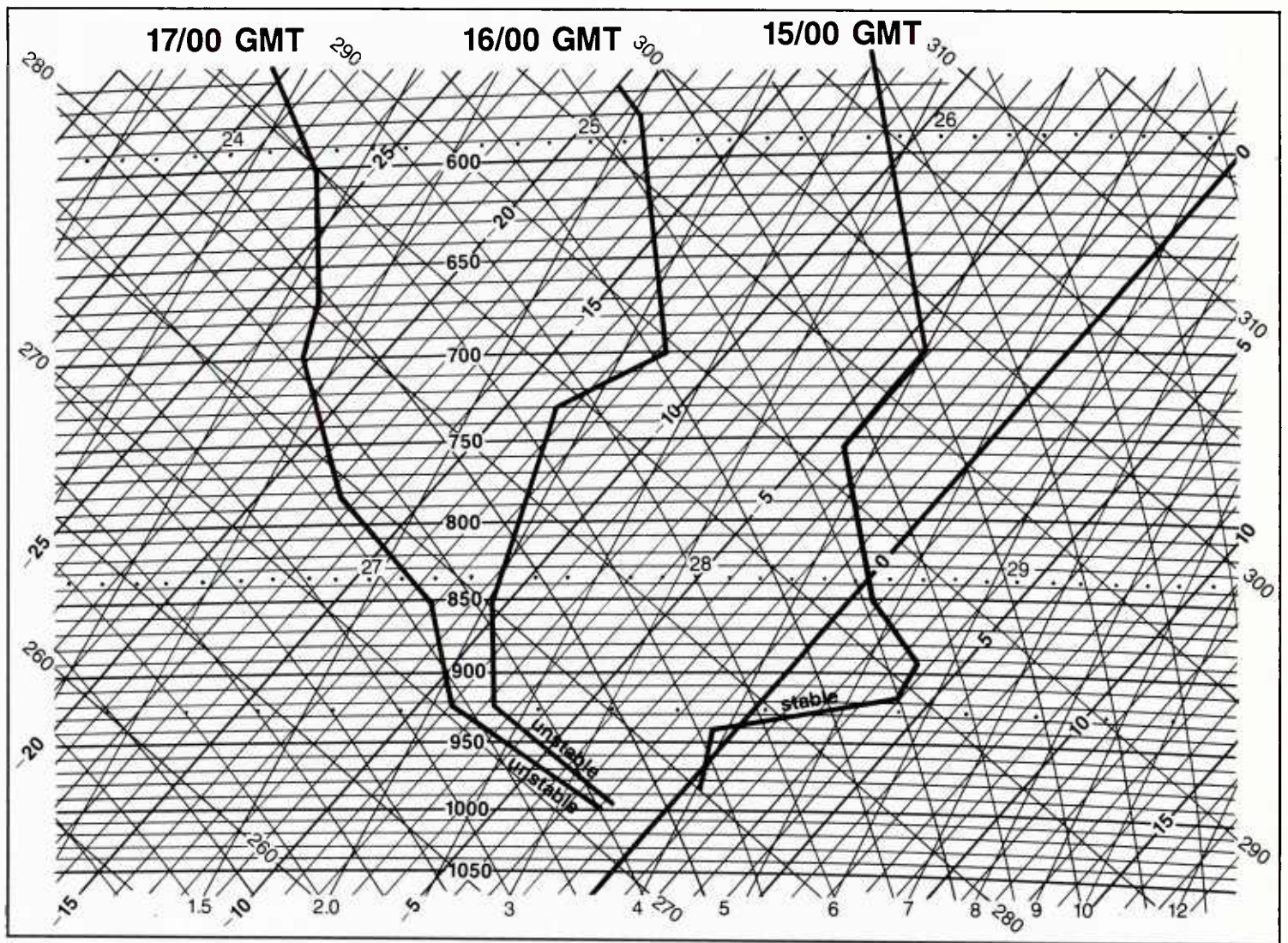
# WIND DIRECTION IN DEGREES CLOCKWISE FROM NORTH

WIND SPEED IN M/S



1A-22b A time-section for Barter Island, Alaska, during the period 15-17 September 1985. Wind direction is shown on vertical lines; dashed lines represent isotachs.





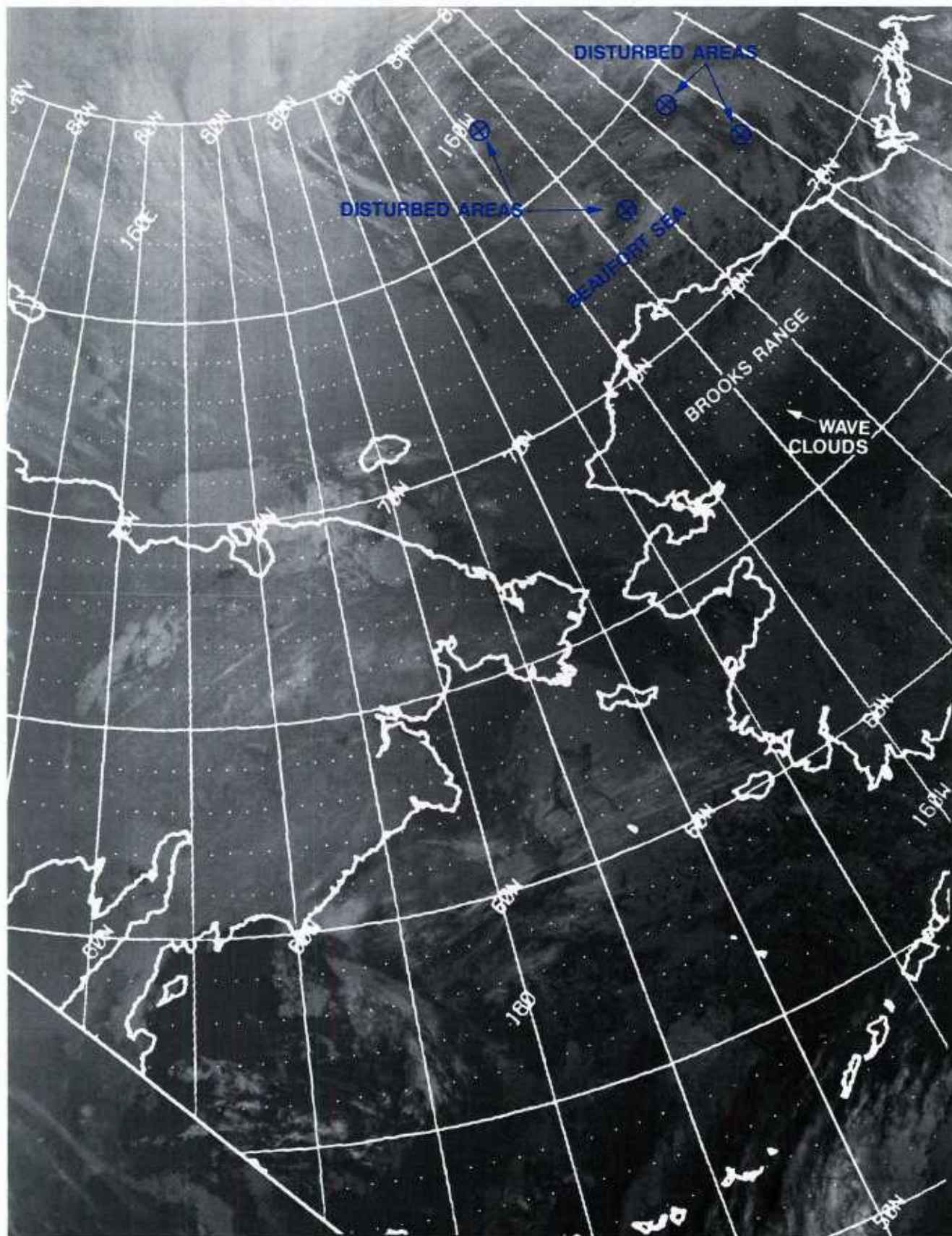
1A-23 Barter Island upper air soundings, 15-17 September 1985. (From Beaufort Weather Office 1985 Report).

At 1035 GMT on 16 September, DMSP data (Fig. 1A-24) reveal a large sprawling low with no well-defined center but having within the circulation several possible vorticity centers in cyclonic rotation. Possible centers are designated by red arrows ending with a  $\oplus$ . Wave clouds are faintly discernible over the Brooks  $\frac{1}{3}$  range indicating strong westerly flow aloft.

The surface analysis for 16 September at 1200 GMT (Fig. 1A-25a) still shows no closed low over the Beaufort, but only over Melville Island (center near 76.25N, 112W).

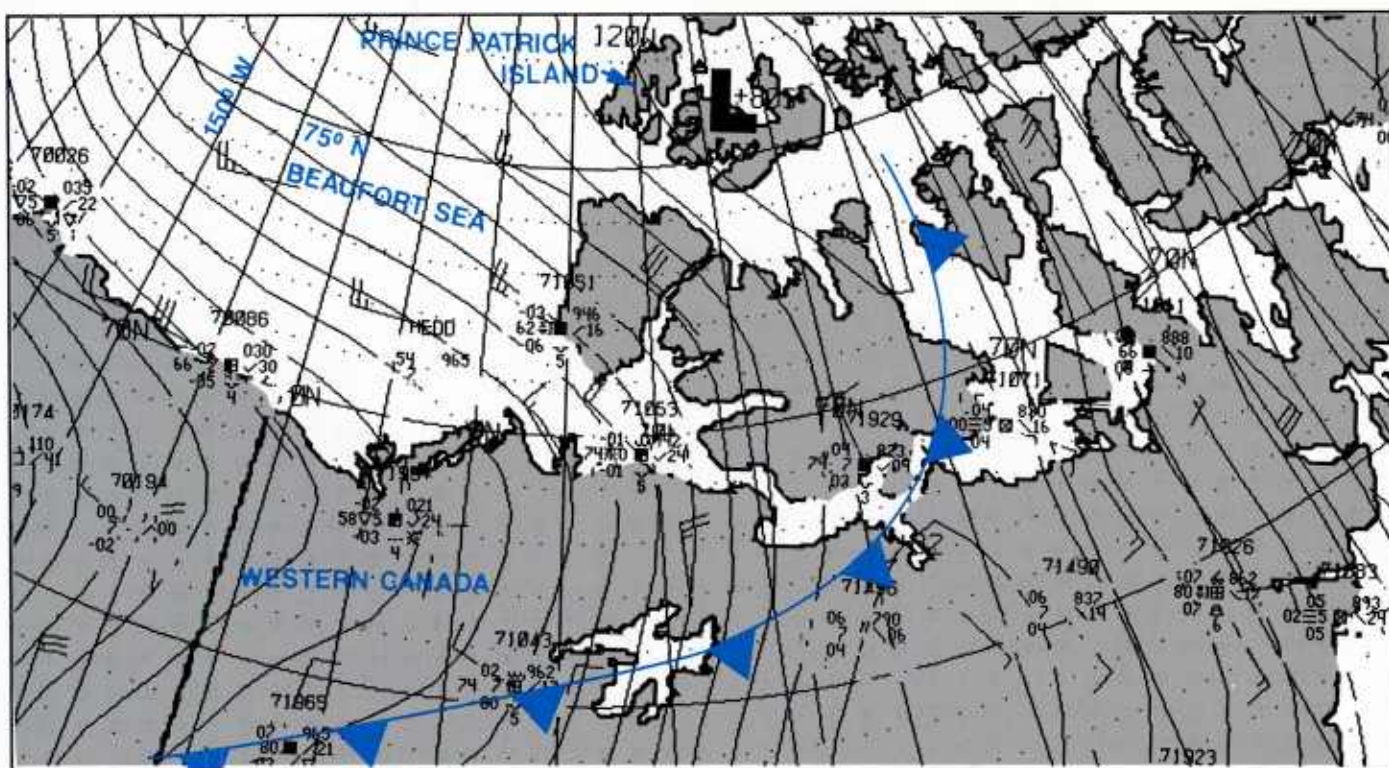
The 300 mb analysis for 16 September at 1200 GMT (Fig. 1A-25b) shows a 70 kt jet streak covering the region from west of Barrow to near Barter Island (see also Fig. 1A-22b). This places the Beaufort low in the left front exit region of the jet—a favorable position for intensification.



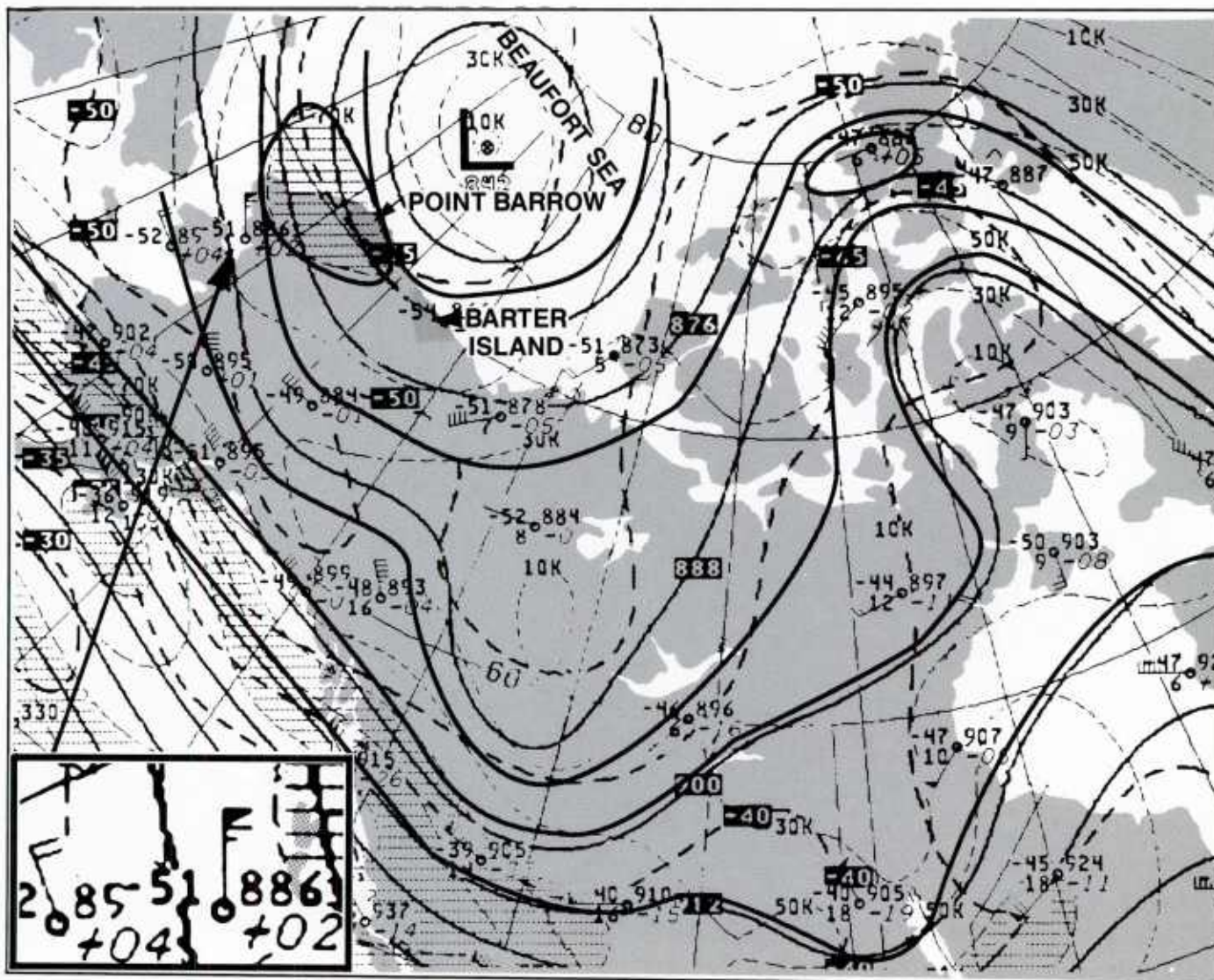


1A-24 DMSP infrared (TS) data. 16 September 1985, 1035 GMT.





1A-25a FNOc surface analysis. 16 September 1985, 1200 GMT.



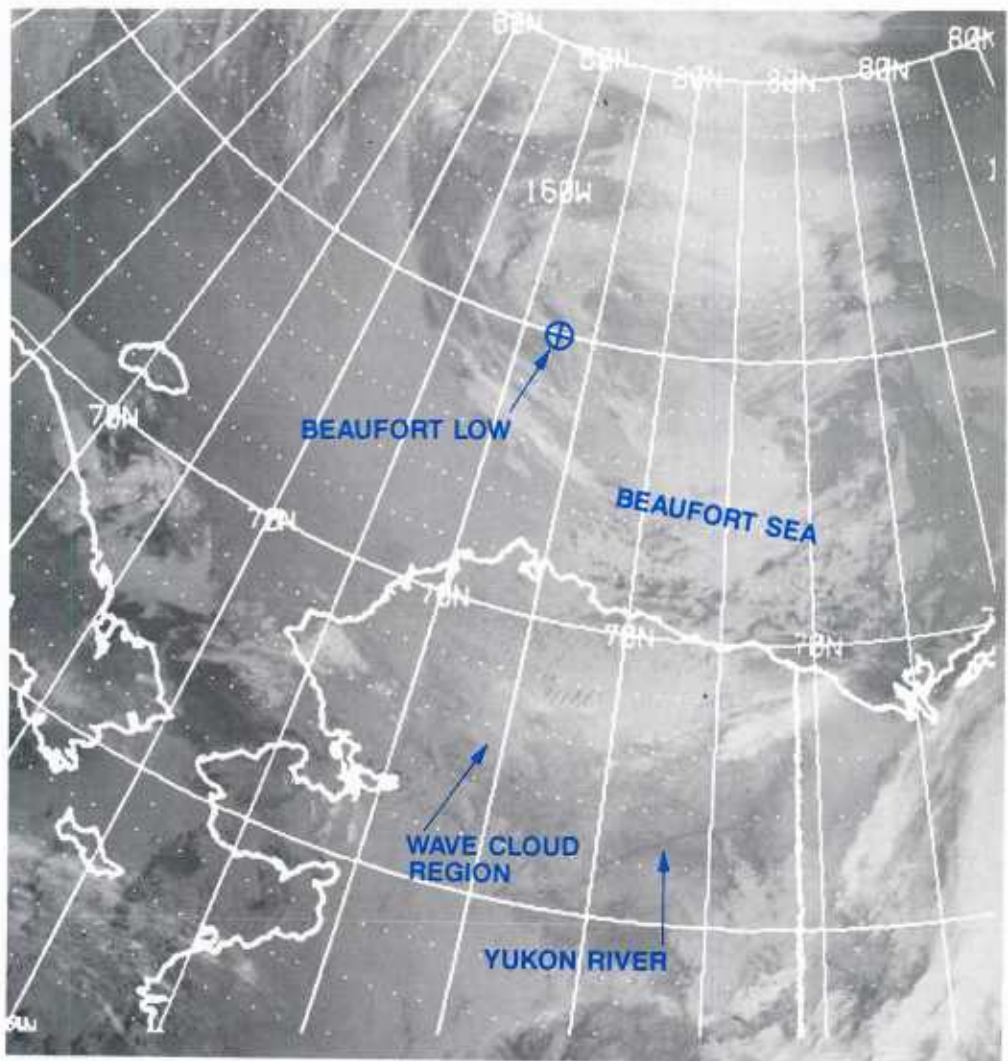
1A-25b NMC 300 mb analysis. 16 September 1985, 1200 GMT.



Five hours later, DMSP infrared data at 1541 GMT (Fig. 1A-26a) seem to indicate some coalescence of these centers near 75N, 157W. This is a long way from the FNOC 17 September 0000 GMT position shown on the surface analysis for that time (Fig. 1A-26b) which shows a center near 80N, 127W. (Note that this position differs by a few degrees from the Canadian-analyzed position shown in Fig. 1A-15.) Both positions, however, are far from the satellite-suggested center.

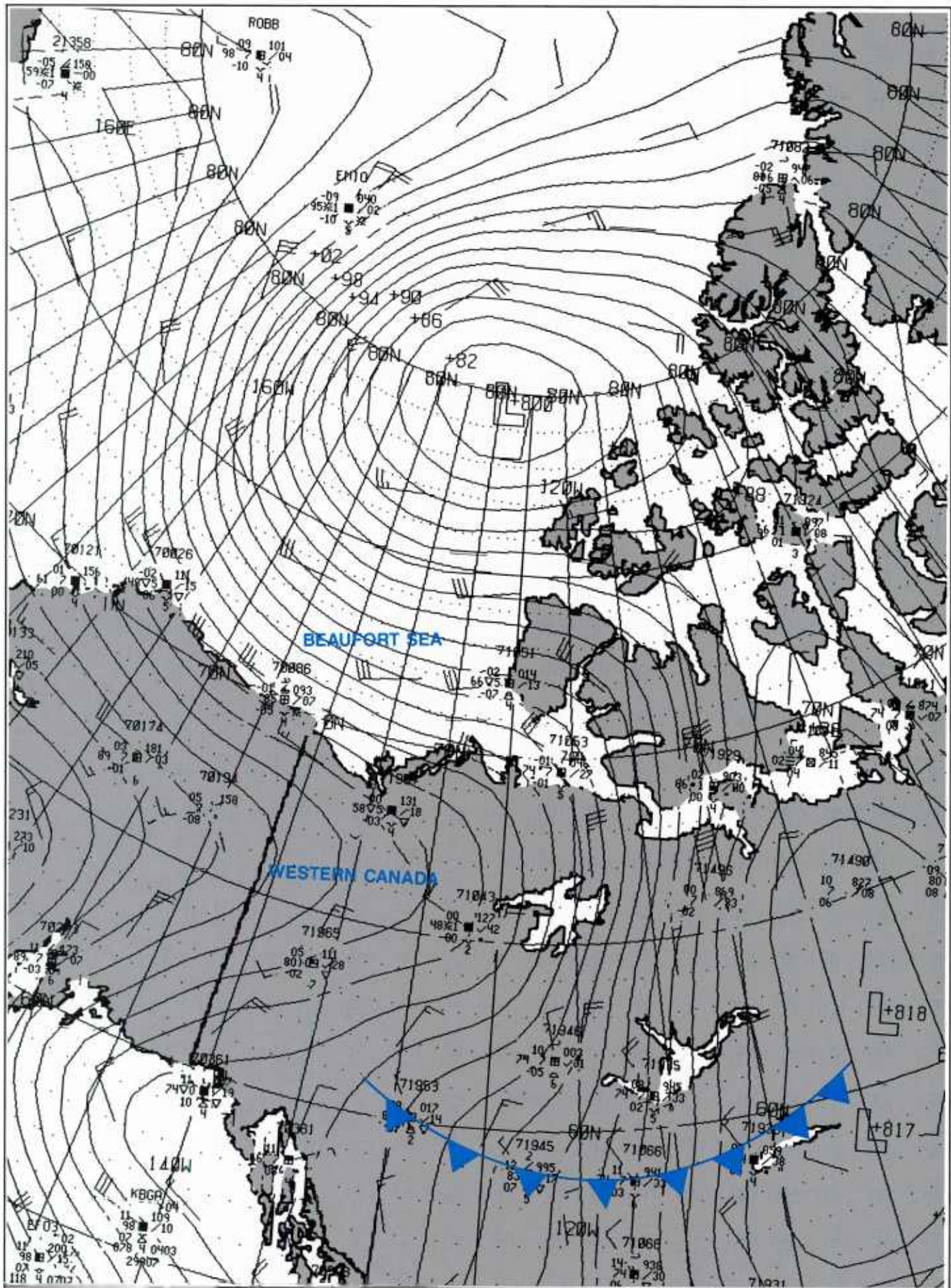
Additional views of the system were not available until 14 hours later, when DMSP infrared data on 17 September at 0515 GMT revealed a storm obviously undergoing rapid intensification (Fig. 1A-27). The center moved to a position near 78N, 137W, which is close to the 500 mb center (at 76N, 139W), shown in Figure 1A-28a, an NMC analysis for 17 September 0000 GMT. Wave clouds over and downstream from high terrain indicate jet force winds over Alaska, verified in the Barter Island time-section (Fig. 1A-22b) and also shown on the NMC 300 mb analysis for 17 September at 0000 GMT (Fig. 1A-28b).

The storm at this time (17 September 0515 GMT) is not far from analyzed surface low center positions suggested by the Canadians (Fig. 1A-15) and NMC (Fig. 1A-26b) on their 0000 GMT analyses. It might be argued that the low which they had been following coming up from Mackenzie Bay merged with the developing Beaufort low. On the other hand, it appears erroneous to suggest, as is shown in Figure 1A-15, that the Beaufort low had its origin near the north coast of Alaska on 15 September at 0000 GMT.



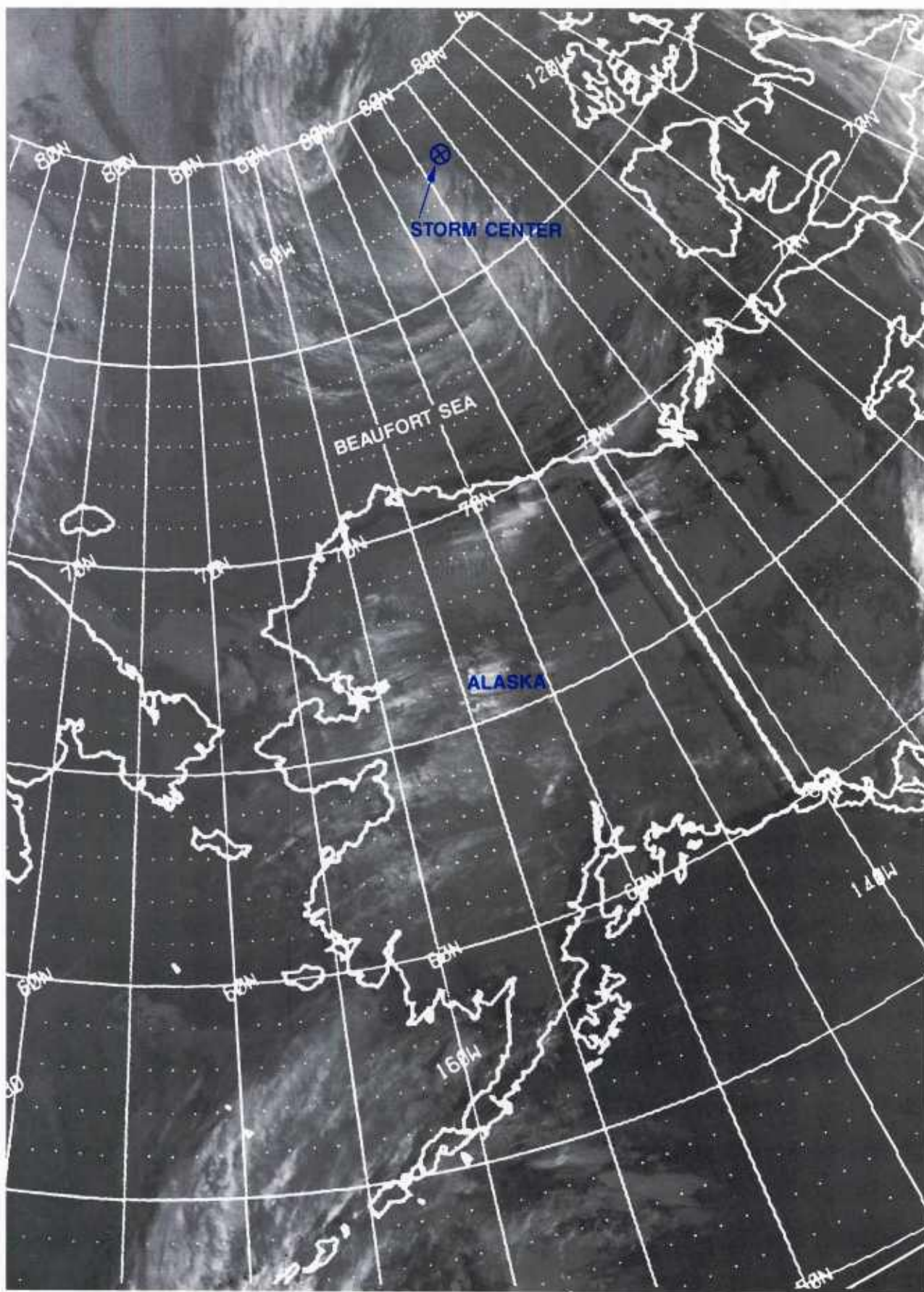
1A-26a DMSP infrared (TS) data. 16 September 1985, 1541 GMT.





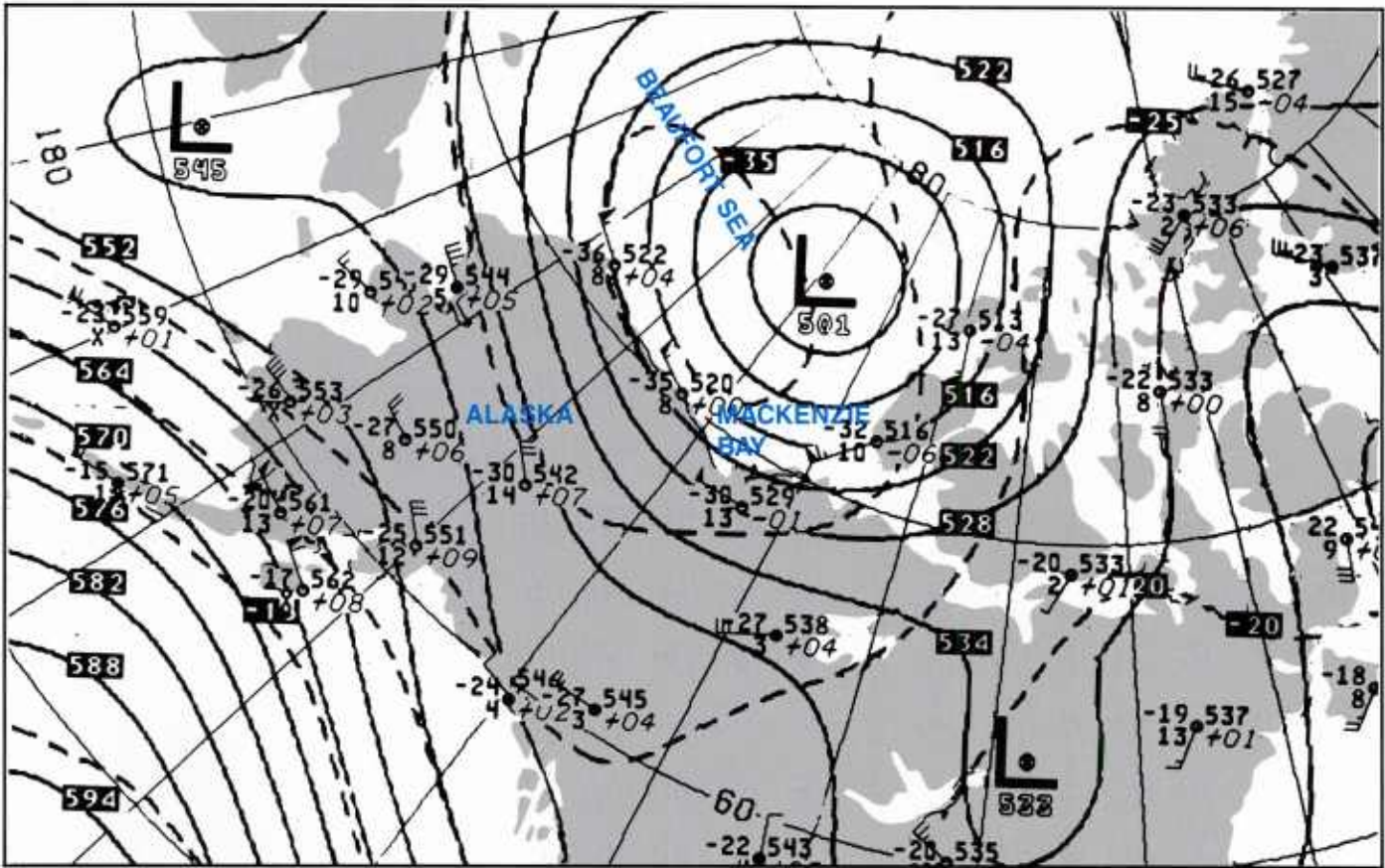
1A-26b FNOC surface analysis. 17 September 1985, 0000 GMT.



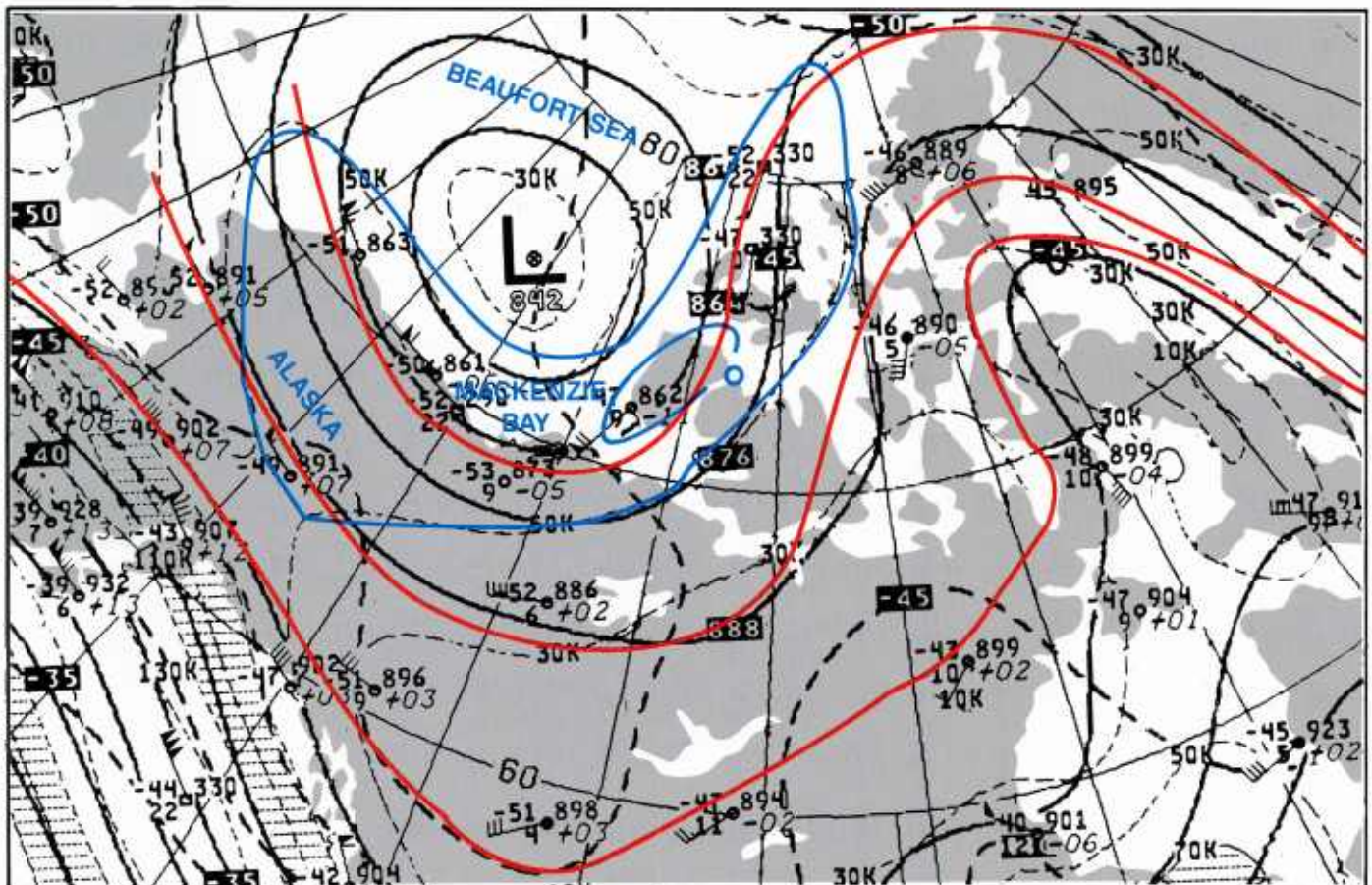


1A-27 DMSP infrared (TS) data, 17 September 1985, 0515 GMT.





1A-28a NMC 500 mb analysis. 17 September 1985, 0000 GMT.



1A-28b NMC 300 mb analysis. 17 September 1985, 0000 GMT.



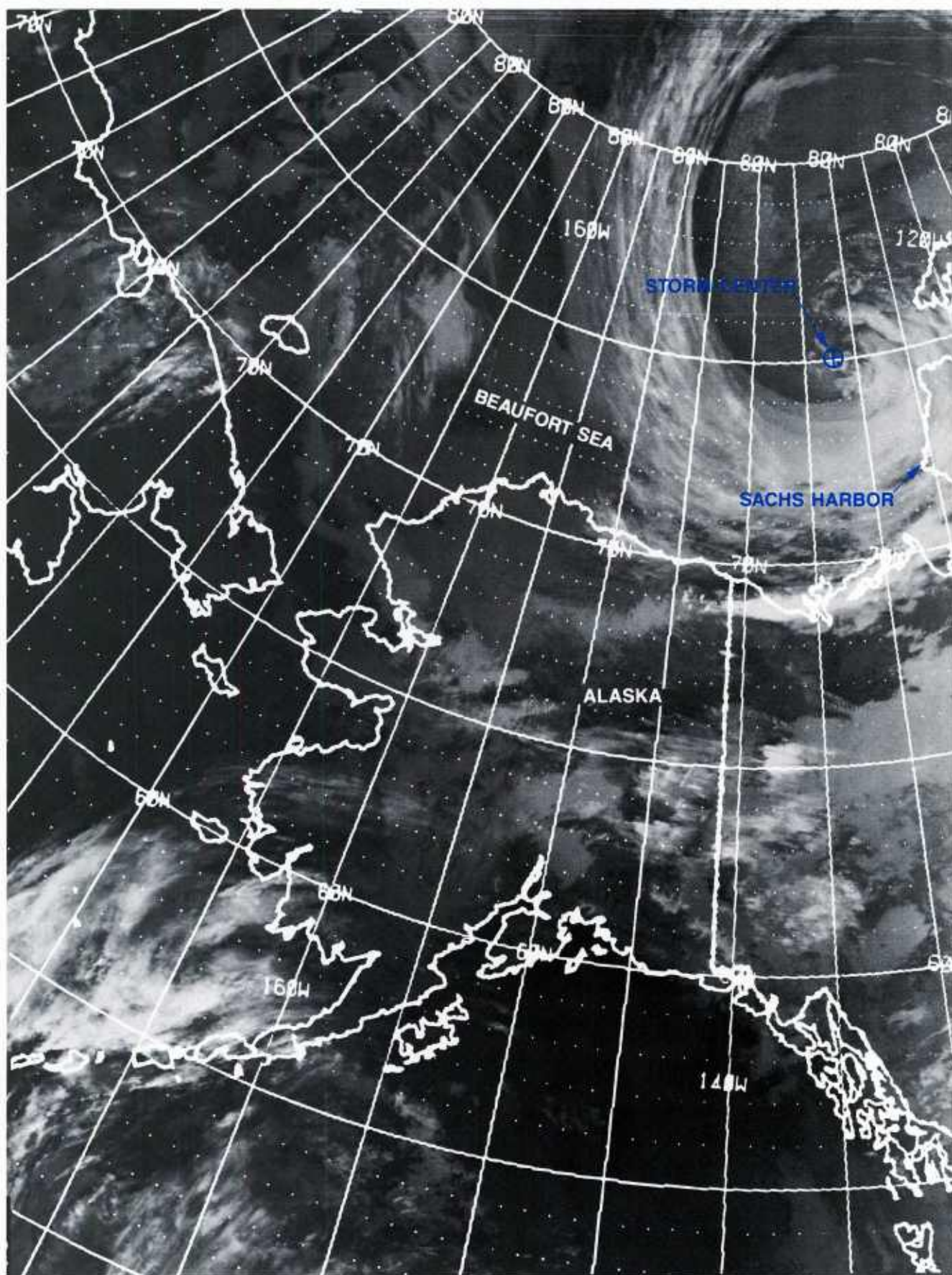


1A-29 DMSP infrared (TS) data. 17 September 1985, 1015 GMT.

Additional views of the system at 1015, 1523 and 1842 GMT on 17 September (Figs. 1A-29, 1A-30, and 1A-31, respectively) show the storm's further evolution to peak maturity. The approximate storm center is indicated by a  $\oplus$ .

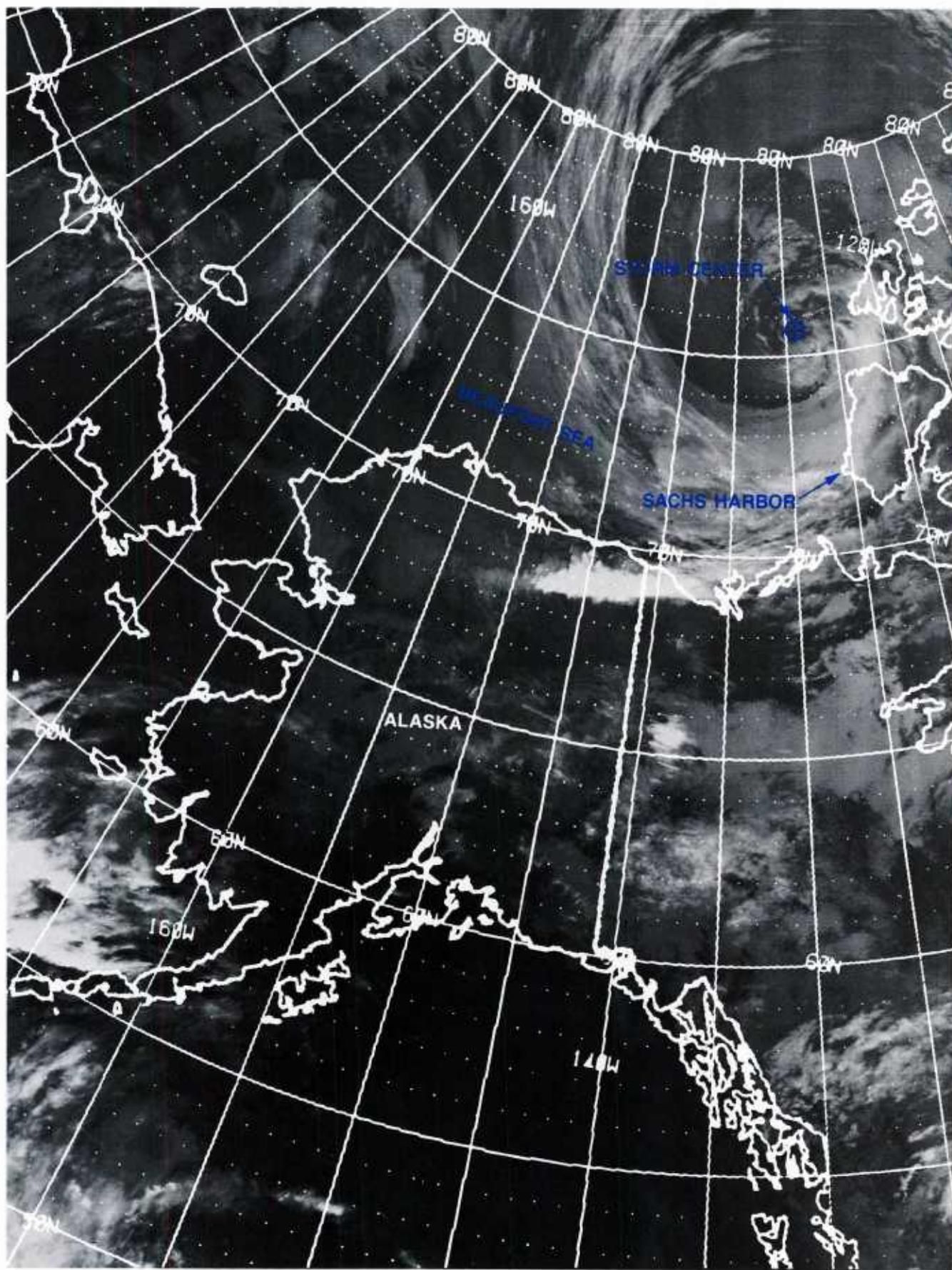
An Arctic frontal band developed in Figures 1A-30 and 1A-31. This front approached Sachs Harbor on 18 September. Evidence of increasing moisture associated with the band is shown on the Sachs Harbor time section (Fig. 1A-13a) on 18 September at 0000 GMT.





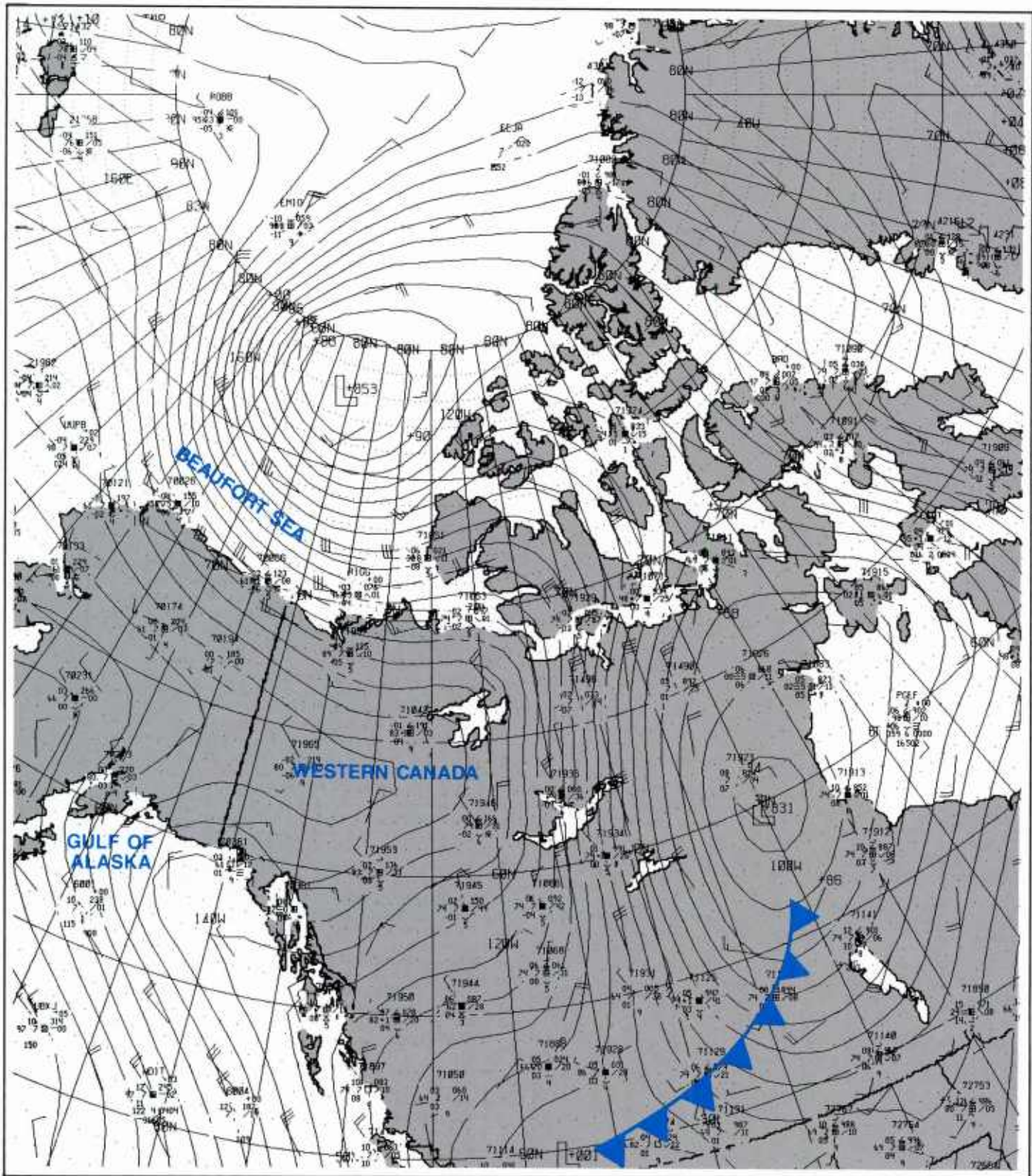
1A-30 DMSP infrared (TS) data. 17 September 1985, 1523 GMT.





1A-31 DMSP infrared (TS) data. 17 September 1985, 1842 GMT.





1A-32 FNOC surface analysis. 17 September 1985. 1200 GMT.

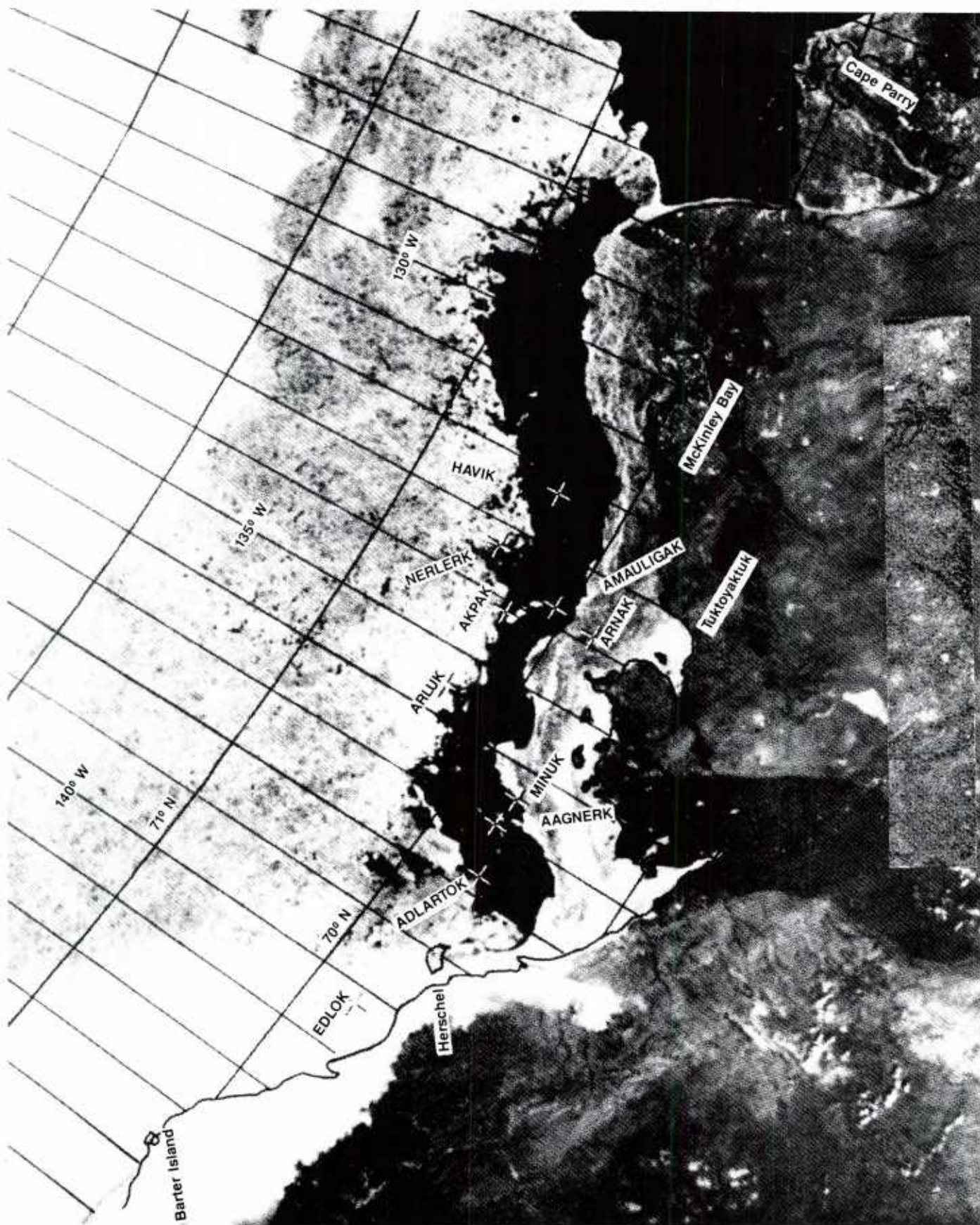
The FNOC surface analysis on 17 September at 1200 GMT (Fig. 1A-32) shows the strong sustained winds produced by this system along the North Slope.

Table 1, prepared by the Beaufort Weather Office, Edmonton, shows wind direction and wind speed in knots from 16-18 September 1985 at many of the North Slope stations. The long duration of strong winds over a three-day period is noteworthy.

Table 1 Wind log for the 16-18 September 1985 Beaufort storm period. (From Beaufort Weather Office 1985 Report).

Time GMT	Point Barrow BR11	XGB CIDS	Deadhorse SCC	Hammerhead McClure Exp 2	Barter Island BTJ	Edlok Exp 4	Komakuk YAJ	Tarsiut Molikpaq	Adlartok Exp 3	Minuk Kamotik	Havik Exp 1	Nerlerk Kulluk	Tuktuyaktuk YUB
16:00	2527G35		2422	2521	3017	2918	2915		3314	3320	3124		3313G20
01	2527G35	2622	2422G27	2624	2916	2918		3212			3023	3217	3212G21
02	2723G33		2522G29		2816	2918		3216	3318		3120	3320	3216
03	2924G33		2422G28		2822G28	2920	2518	3316	3110		3217	3220	3215
04	2823G33		2423G29		2725	2920	2520	3211	3015		3216	3214	3216
05	2823G33		2426G33	2426	2824	2618	2317	3310	3320		3317	3116	3416
06	2723G34		2426G33	2428	2828G35	2722	2715	3413			3117	2911	3412
07	2925G34		2429G34	2534	2729G35	2928	2416	2908	3015		2912	2612	3412
08	2925G36		2624G30		2733G39	3028	2415	3015	3015		2712		3509
09	3028G38		2723G31	2732	2834G40	2828	2415	3117	3020	3020	2614	2615	3506
10	2725G36		2522G28	2734	2830G35	2934	2418	3120	3030E		2714	2519	2907
11	2724G34		2523G28	2736	2930G35	2942	2418	3124	3030E		2516	2619	2710
12	2725G36		2626G35	2737	2830G35	2840	2713	3021	3030E	2825G33	2518	2619G26	2806
13	2626G38		2627G33	2736	2932G40	2932G40	2630	3125G33	3030E		2516	2519	2810
14	2723G37		2625G32	2735	2931G37	2932G38	2425	3023	3030E		2616	2821	2918
15	2723G36		2527G32	2839	2834G40		2420G25	3129	2835G40	2932			
16	2725G40	2640	2527G32	2739	2934G44	2940G50	2320G25	3130	2830G38			2924	2921G28
17	3023G37	2635	2527G32	2738	2836G44	2942G50	2118	2930G38	2835		2918	2920	2924G33
18	2716G33		2528G35	2740	2830G39	2934G46	2425G30	3030G42	2738G45	2838	2816	2720	2924G33
19	2819G33		2522G32		2939G46	2934G40		2930G42	2844G50		2720	2521	2922G32
20	2521G33	2535	2525G35	2736		2932G40	2418	2930G40	2840G48		2524	2825	2925G36
21	2820G35	2732G38	2522G32	2736	2934G42	2936G40	2628	2830G48	2832G40		2728	2830	2823G35
22	2725G34		2528G36	2734	2836G41	2928G34	2628	2930G40	2930G35		2730	2830G40	2924G35
23			2628G35	2731		2928G40	2530		2835		2734	2930	2925G35
17:00	3022G33		2628G35	2735	2937G45	2930	2726G34	2828	2832	2738	2817	2626	2823G32
01	2720G30		2726G32	2736	3032G39	2832	2420				2824		2823G38
02	2623G31	2735	2623G31		2936G46	2834	2416	2927G34	2925		2635	2633	2825G34
03	2820G30		2624G31	2735	2935G44	2838		2828	2935	2728G37	2534	2840	2820
04	2820G27		2623G30	2632	3037G42	2940	2520	2827	2840		2632	2833	2720G30
05			2725G34	2530	2934G39	2940	2317	2830	2935		2523	2632	2722
06	2921G30		2625G34	2630	2936G41	2942G48	2723G28			2728G38	2536		2825G29
07	2923G30		2726G34	2630		2934G40		2728	2840		2538	2640G45	2820G26
08	2719G31		2623G28		2935G43	2838G42	2427	2728G34	2735		2536	2627G30	2824G27
09	2817G28		2725G30	2624	2930G36	2940G44	2422	2725G31	2840G45	2930G42	2830	2730G34	2720G28
10	2920G32		2726G31		2931G36	2736G44	2324	2827	2838G45		2625	2735G40	2823G27
11	2818G28		2722G27		2934G41		2420	2824	2740		2827	2631G40	2824G29
12	2718G26		2623G29	2634	2934G40	2836G40	2823	2826G34	2735		2632	2730G38	2725G31
13	2718G30		2625G32	2638	2932G39	2932G38	2426	2725	2740		2628	2632	2726G30
14	2720G30		2624G33	2544	2934G41	2824G38		2833G45	2740	2736G46		2730	2724G30
15	2720G31		2627G35	2537	2835G43	2934G46	2320G30	2830G40	2740	2735G44		2729	2730G40
16	2820G29	2728G34	2626G36	2536	2932G41	2832G42	2325G30	2827	2740G50		2732	2833G45	2730G40
17	3023G32	2727	2626G35	2537	2839G44	2834G44	2424		2850			2744	2728G35
18	2620G33		2625G35	2537	2834G42	2834G40	2420	2827G38	2845G50	2734G46	2740	2734G45	2725G35
19	2917G32		2625G35	2536	2836G45	2942G50	2420	2827G38	2840G45		2540	2740G50	2728G40
20	2922G29	2635	2625G35		2937G45	2940G46	2420	2827G40			2730G38	2440	2729G40
21	2918G31	2632	2627G33	2536	2936G43	2940G46	2420	2827G40	2940		2332	2835G46	2730G40
22	2719G26	2634G37	2527G34	2538	2938G45	2938G50	2430	2930G40	2840G48		2433	2946	2725G38
23	2818G26		2526G32	2534	2837G44	2942G52	2624	2930G42	2940G45		2534	2742	2730G42
18:00	2717G26		2522G32	2530	2839G45	2942G52	2726	2925G40	2835G41	2734G42	2540	2744	2730G40
01	2518G23		2625G31	2430	2940G47	2946G54	2426	2830	2840		2638	2845G50	2830G40
02	2616G23	2732	2428G35	2430	2839G47	2842G55	2624	2930G38	2940G50		2540G46	2835G40	2825G40
03	2515G23		2523G33	2432	2937G46	2844G54	2530	2927G35	2840G50	2730G46	2727G34	2830G35	2829G38
04	2515G23		2526G32	2430	2934G41	2850G55	2430	2930G42	2840			2938G42	2725G35
05	2616G21		2526G30	2432	2830G41	2840G50	2325	2936G45	2840G50		2726G38	2943G48	2728G35
06	2611		2522G28	2530	2831G39	2942G48	2726	3040G45	3045	2930		2933	2721G26
07	2413			2523	2831G35	2840G46	2222	3138			2932	3045G50	2825G34
08	2410		2422	2524	2833G39	2832G38	2324		2840G45		2732	3030	2827G34
09	2412		2423	2222	2931G37	2832G38	2218	3035G40	2840	3125G38	2630	2933	2923G31
10	2208		2320	2126	2828G34	2828G34	2316	2933G40	3035		2830	2936G44	2820G26
11	2105		2316	2125	2927G34	2728G34	2318	3033G38	3030		2730	3030G34	2825G31
12	2212		2318		2925G28	2724G30	2618	2928G32	2830	2825G35	2927	2925G30	2820G25
13	1711			2320	2919	2716G20	2208	2928	2730		2817	2624	2820G26
14	1908			2318	2917	2715	2008	3028	2824		2718	2624	2820G27
15	1908	2108	2008	2211	3014	2310	1908	3024	2722	2726	2422	2622	2719G25
16	2309		2110	2311	2710			2715	2716		2628	2628	2718G28
17	2409	2004	2212	2210	2106		1006	2715	2515			2625	2520
18			2212	2311	1907	1505	0605	2514	2312	2720	2626	2623	2515

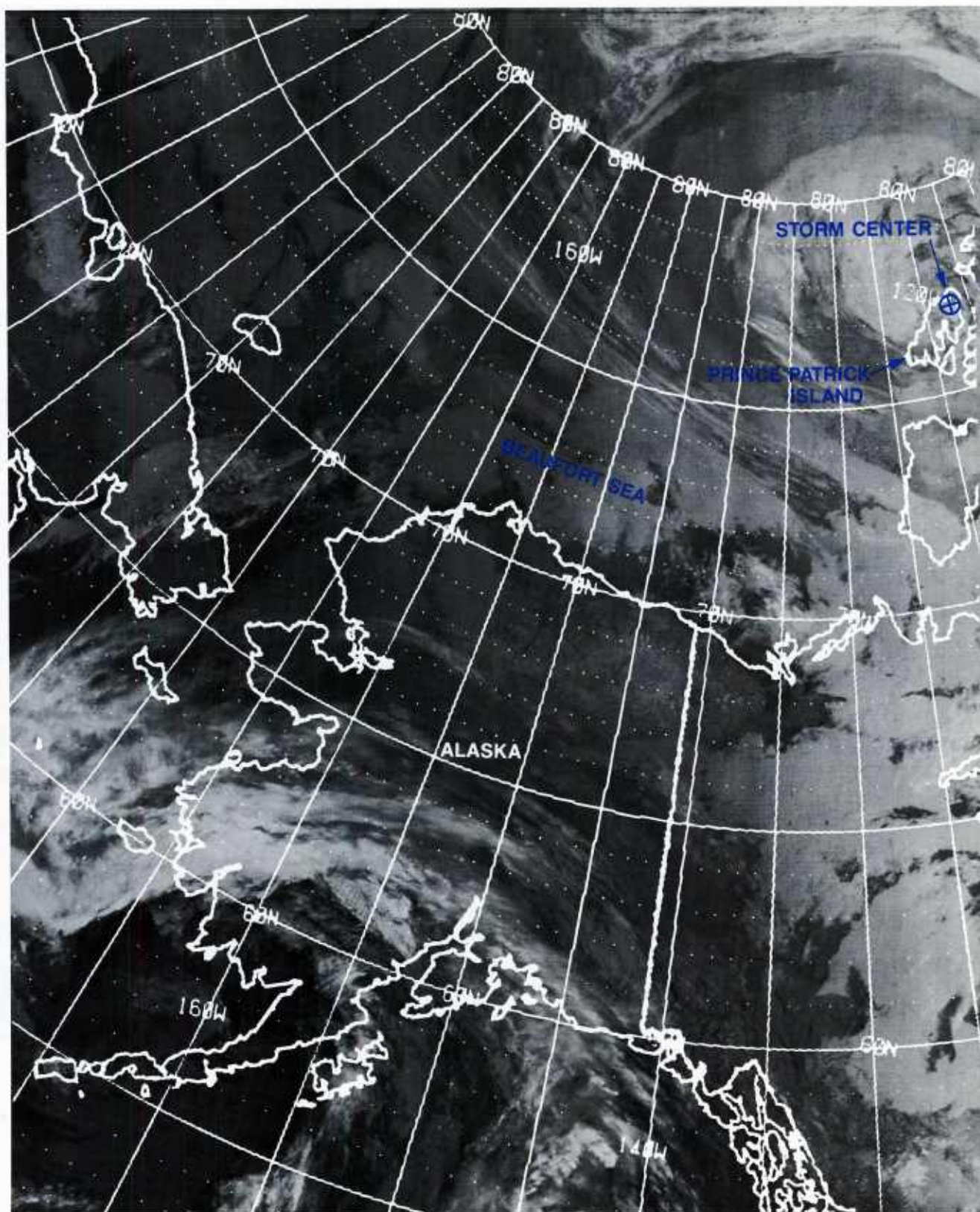




1A-34 NOAA-9 visual (CH 2) data. 5 June 1985 (From Beaufort Weather Office 1985 Report).

Figure 1A-34 is a NOAA visual image taken on a different date, 5 June 1985, which shows the location of many of these stations. Their vulnerability to prolonged strong westerly wind conditions under ice-free conditions is apparent.





1A-35 DMSP infrared (TS) data. 18 September 1985, 1501 GMT.

As indicated, a major factor in damage from this storm was the long duration of sustained strong winds. These began to subside on 18 September as the storm center moved NE. Figure 1A-35 is a final DMSP image of the storm system at 1501 GMT on 18 September with the center at 77N, 117W, near the northern shoreline of Prince Patrick Island.



The FNOC surface analysis on 18 September at 1200 GMT (Fig. 1A-36) concludes this study in revealing the abatement of winds along the North Slope and the approach of a protective ridge to again shield the area from the strong westerlies of large-scale cyclogenesis in the Beaufort Sea. Clear skies over the North Slope are apparent in the satellite data (Fig. 1A-35), and signal the end of this event.

### **Important Conclusions**

1. Large-scale cyclogenesis-producing strong winds along the North Slope of Alaska and off-shore waters does occur in the Beaufort Sea. Such storms are not frequent, but are more usual during the fall season, and are generally not shown in climatological storm tracks over the area. When open water exists along the coast, the fetch of westerly flow combined with a 2-3 day duration can build seas to in excess of 8 m.
2. Satellite data at frequent intervals (every 2-3 hours) are required to monitor movement and development of such systems.
3. Jet streaks around the periphery of slowly developing systems appear to play an important role leading to more rapid intensification. This is certainly not a new finding, but is important to emphasize. These jet streaks should be carefully monitored for position with respect to the storm system and for changes in satellite appearance.
4. Vertical time sections of key stations are useful in detecting lows, fronts, and jet cores and in understanding the 3-dimensional structure of weather events passing over a given location in the Arctic.
5. The 850 mb chart is especially useful in detecting frontogenesis and cyclogenesis in Arctic regions and in monitoring frontal movement.

### **References**

1. Parker, N., B. Thomson, J. Bullas, and W. Hume, 1985: "Beaufort Sea Storm," Scientific Services A.E.S., Western Region Report, 85-7, Twin Atria Bldg., 4999 98 Ave., Edmonton, Alberta, T6B 2X3, Canada, p. 26.
2. Bullas, J., 1985: Beaufort Weather Office 1985 Report, A.E.S., Twin Atria Bldg., 4999 98 Ave., Edmonton, Alberta, T6B 2X3, Canada, p. 191.





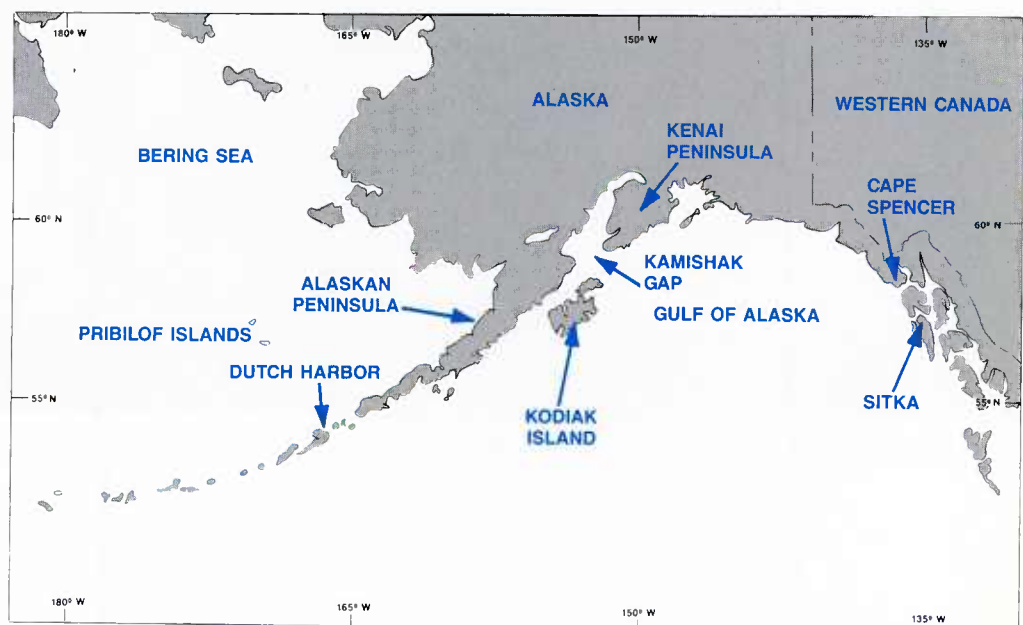
## Case 2 *Extreme Ship Icing Event—Western Gulf of Alaska*

The fishing vessel F/V Vestfjord, with a crew of five and one passenger, departed from the vicinity of Cape Spencer, Alaska (about 100 miles north of Sitka, Alaska) on 22 January 1989, en route to Dutch Harbor in the Aleutian Islands (Fig. 1A-37). The ship had missed the opening of the season for fishing king crab along the ice edge north of the Pribilof Islands and was hastening to make up for lost time.

At a speed of 9 kts, transit from Cape Spencer across the Gulf of Alaska to Kodiak normally takes about 3 days. However, Vestfjord almost immediately encountered high winds and high seas. Flow initially was from the west and southwest, which greatly reduced the ship's progress.

On the afternoon of 27 January, SE of the Kenai Peninsula, winds shifted to northerly as Vestfjord began to enter a very strong pressure gradient region that would yield very strong NW winds through the Kamishak Gap and south of the Alaskan Peninsula.

The vessel passed south of Kodiak on 28 January, in a region of severe cold air advection, with heavy super structure icing, due primarily to super-cooled sea spray. A weather report from the ship, approximately 60–70 miles SW of Kodiak Island on 29 January just prior to 1010 GMT, indicated northwest winds of 60 kts, in 27-foot seas. Air temperature was about  $-14^{\circ}\text{C}$ , and sea surface temperature about  $4^{\circ}\text{C}$ . Immediately after filing the report, the ship overturned and sank, with loss of all on board.



1A-37 Alaskan Regional Locator Map.

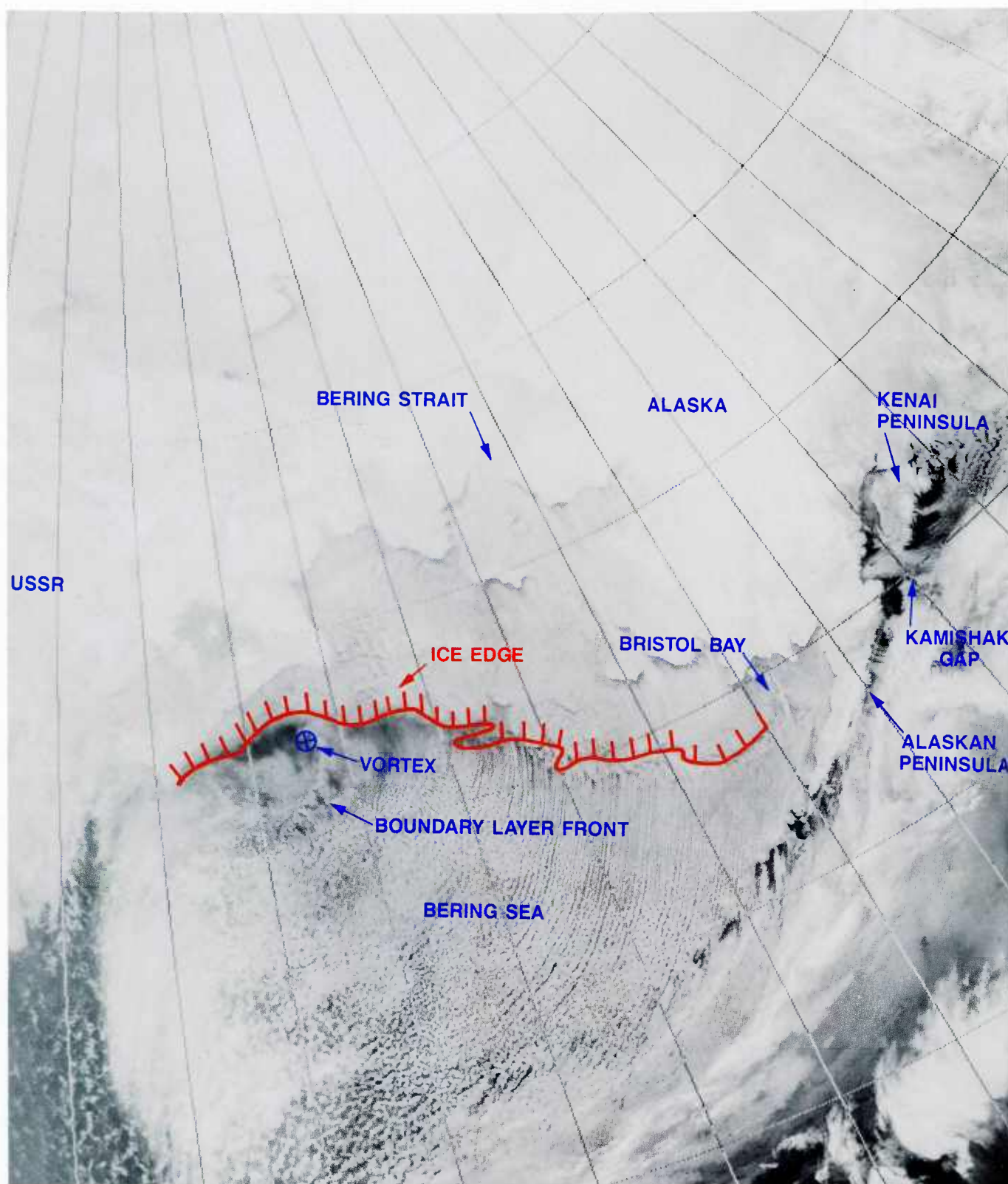
*27 January 1989*

DMSP infrared (TS) data received at 0617 GMT (Fig. 1A-38) show the effects of a cold surge into the Bering Sea. The ice edge is apparent, stretching from the coast of the USSR to Bristol Bay, just north of the Alaskan Peninsula. (Note that the image is poorly gridded and misaligned by over  $2^{\circ}$  latitude.) As shown in an enlargement (Fig. 1A-39), St Matthew Island is just north of the ice edge, but the Pribilof Islands, St Paul and St George, are in open water. Their outlines can be faintly seen through the cloud lines passing over the islands, apparently unaffected by the islands' topographic features which rise to 665 ft on St Paul and 1012 ft on St George.

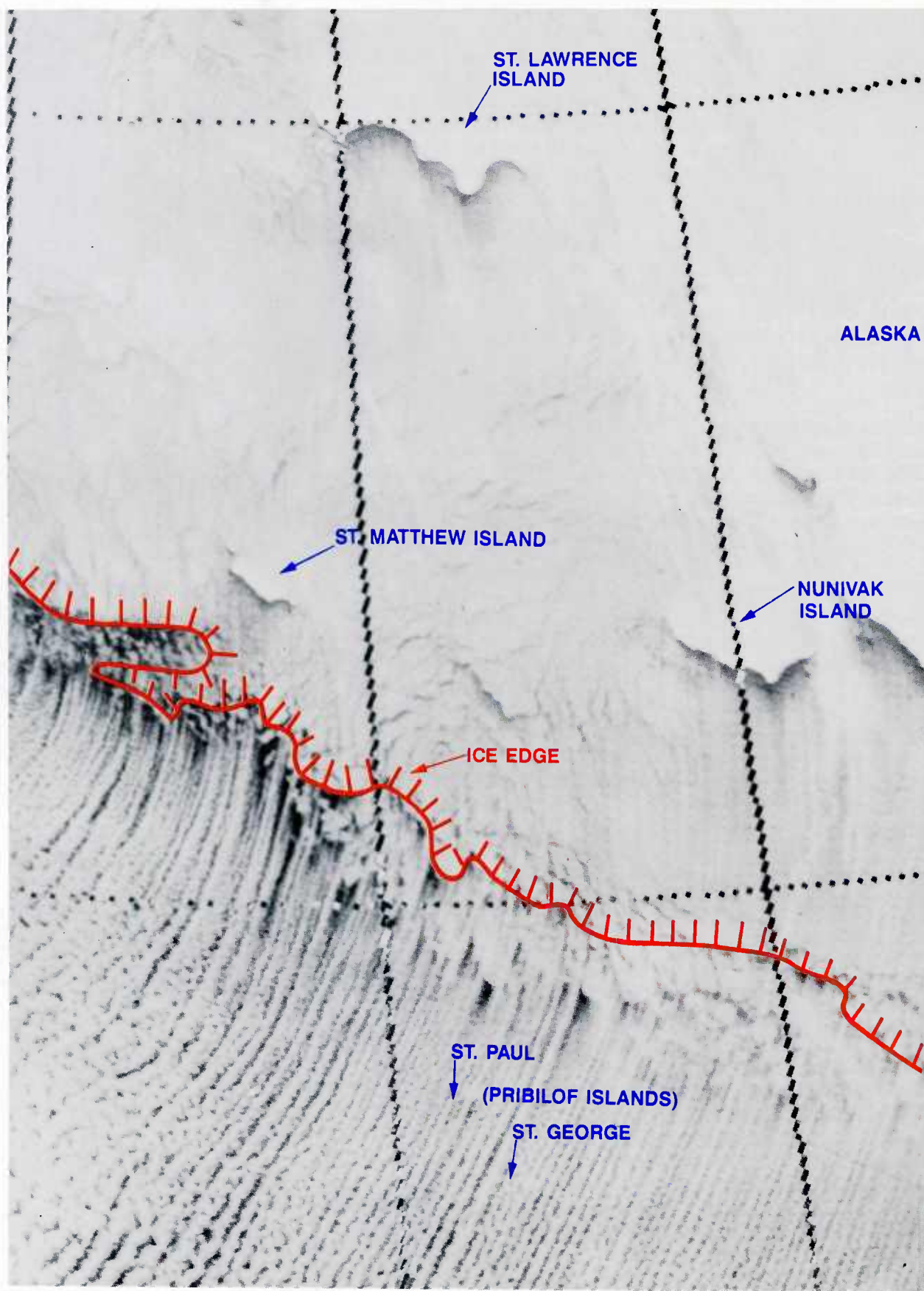
Near the western portion of the ice edge a mesoscale vortex is apparent, forming on the north end of a north-south-oriented boundary layer front (BLF). This implies the existence of an inverted trough in the area.

A northwesterly surge of air is apparent through the Kamishak Gap and other gaps along the Kenai and Alaskan Peninsulas.





1A-38 DMSP infrared (TS) data. 27 January 1989, 0617 GMT.



1A-39 DMSP infrared (TS) data enlargement. 27 January 1989, 0617 GMT.



The FNOC surface analysis for 0600 GMT (Fig. 1A-40) reveals the high pressure center (1033 mb) over western Siberia responsible for the cold outbreak. A long trough connects low pressure centers over the N. Pacific and passes through southeastern Alaska and the Yukon to a low centered just south of Great Slave Lake, in the District of Mackenzie, Canada. A strong pressure gradient is evident over the Aleutians, the Alaskan Peninsula, past Kodiak Island, the Kenai Peninsula, and into central Alaska. Note the satellite evidence that winds are blowing from the NW, perpendicular to the isobars, and along the pressure gradient in the Kamishak Gap and along the Kenai and Alaskan Peninsulas. This is the norm in that region under such an isobaric configuration and is an effect of the unique topography of the area.

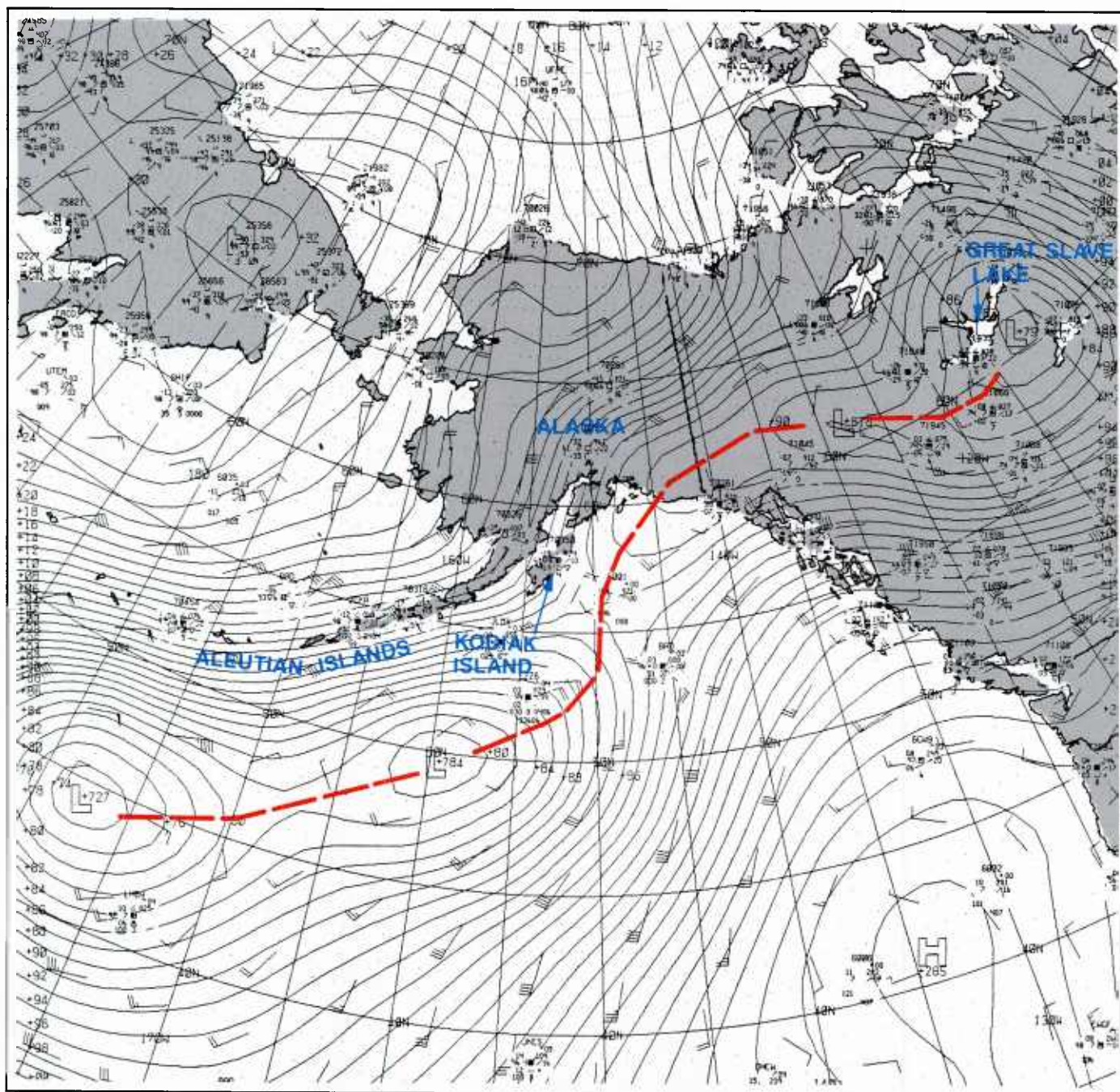
The surface analysis is not detailed enough to reveal the inverted trough associated with the boundary layer front near 175E. Twelve hours later, at 1840 GMT, another DMSP infrared (TS) image (Fig. 1A-41) shows that the surge is developing and moving eastward. Gap wind effects are evident all along the Alaskan Peninsula.

Northwest flow through the Kamishak Gap now extends further to the southeast and changes abruptly to northeasterly flow where the cloud lines disappear into an overcast veil of low clouds or fog. The north edge of this low overcast delineates the position of a mesoscale ridge. The trough line exists just south of this region, connecting the wave-like protuberances associated with low centers north of the overcast frontal band apparent in the southern portion of the image.

The mesoscale vortex in the boundary layer front, just south of the ice edge, has enlarged considerably in comparison to the previous view. However, it shows little vertical development or other signs of strength.

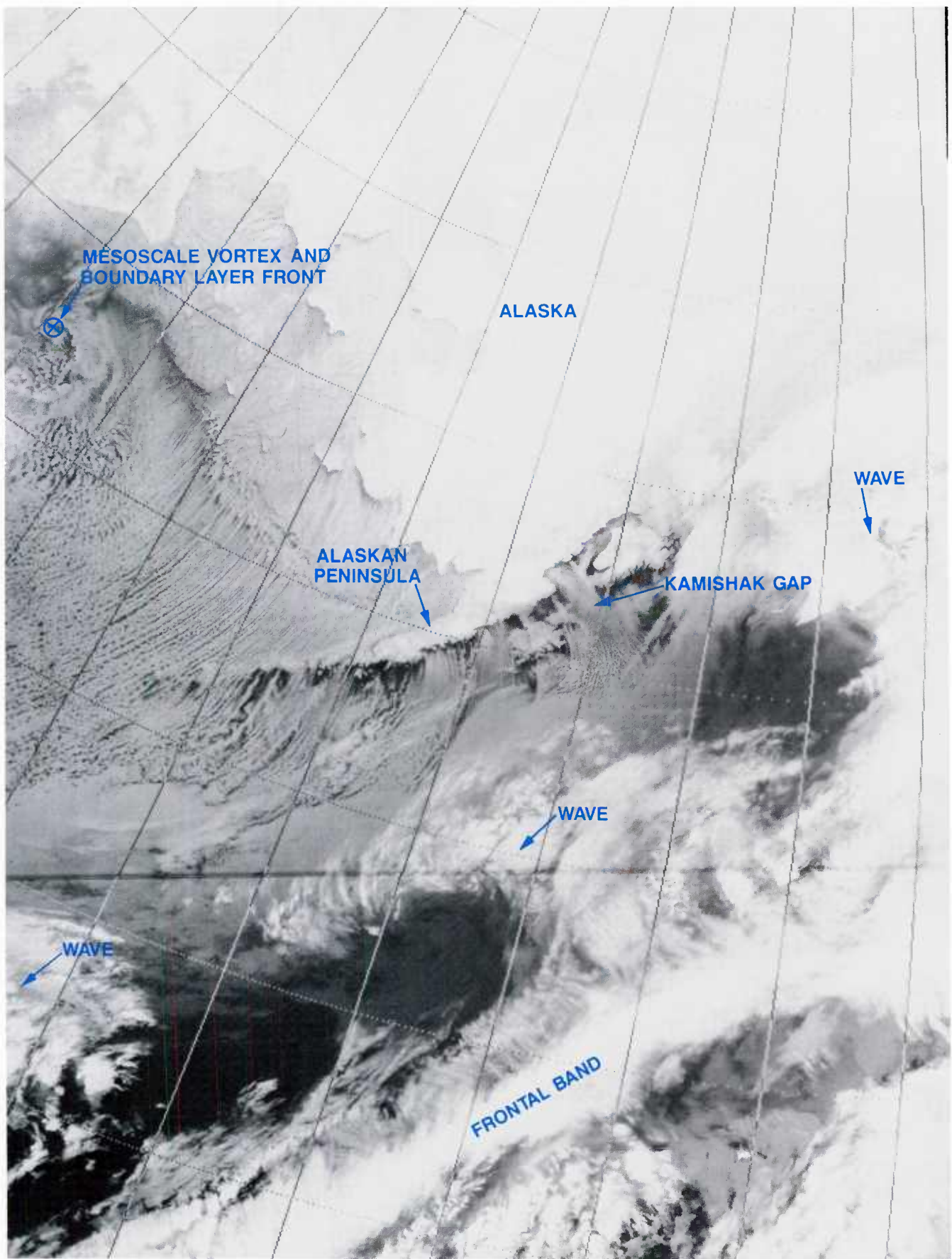
An enlargement of the Kamishak Gap region (Fig. 1A-42) reveals the significant changes of wind direction, on a mesoscale basis, within Cook Inlet. Winds are funneled from the NNE between the Chigmit Mountains, west and southwest of Anchorage, and the Kenai Mountains, south of Anchorage. Winds shift suddenly to NW in the lee of the Chinitna Peninsula, where an enhanced cloud line can be seen extending southeastward past the southern tip of the Kenai Peninsula. A short distance southeast of the Chinitna Peninsula, Augustine Island shows lee effects which indicate due-westerly flow. The separate flows converge into the enhanced cloud line extending leeward of the Chinitna Peninsula.

It is of interest that Augustine Island, with an elevation of 3927 ft, shows a clear wake effect, while the Barren Islands, between Kodiak and the Kenai Peninsula, show enhanced cloud trails. The Barren Islands have a maximum elevation of 1986 ft, considerably lower than Augustine. Kodiak's sounding for 28 January at 0000 GMT (Fig. 1A-43) reveals an inversion base near 870 mb, or about the 4200 foot level. The base was probably even lower near Augustine Island, since heat flux would tend to raise the base after the air passed over the water to Kodiak. This means that air flow passing Augustine Island would be largely forced around the island rather than over it, thereby creating a clear wake in the process. Air moving past the Barren Islands, on the other hand, could easily pass over the islands, inducing some upward vertical motion in the process, thereby giving rise to an enhanced cloud trail.

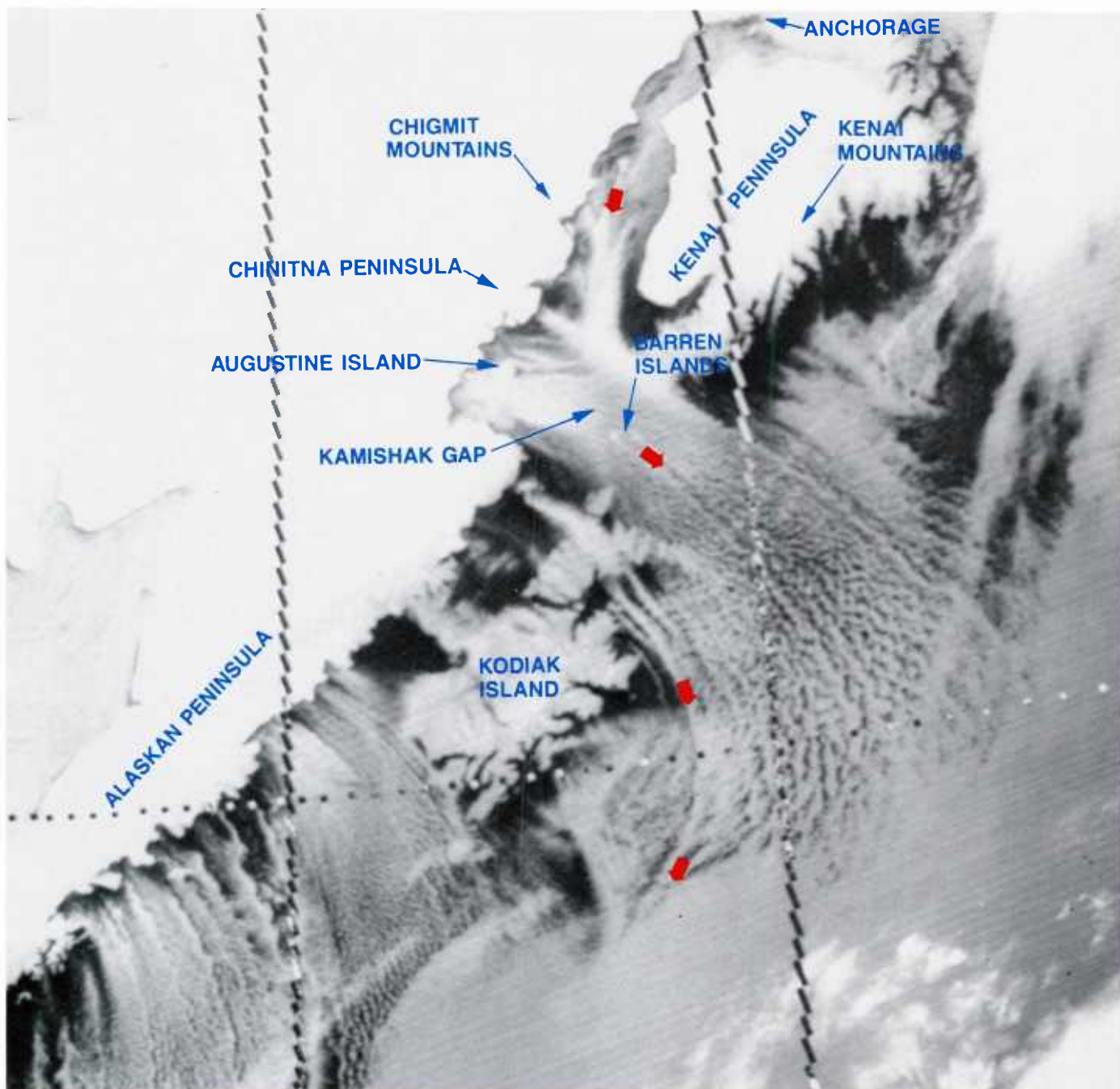


1A-40 FNOC surface analysis. 27 January 1989, 0600 GMT.





1A-41 DMSP infrared (TS) data. 27 January 1989, 1840 GMT.



1A-42 DMSP infrared (TS) data enlargement. 27 January 1989, 1840 GMT.

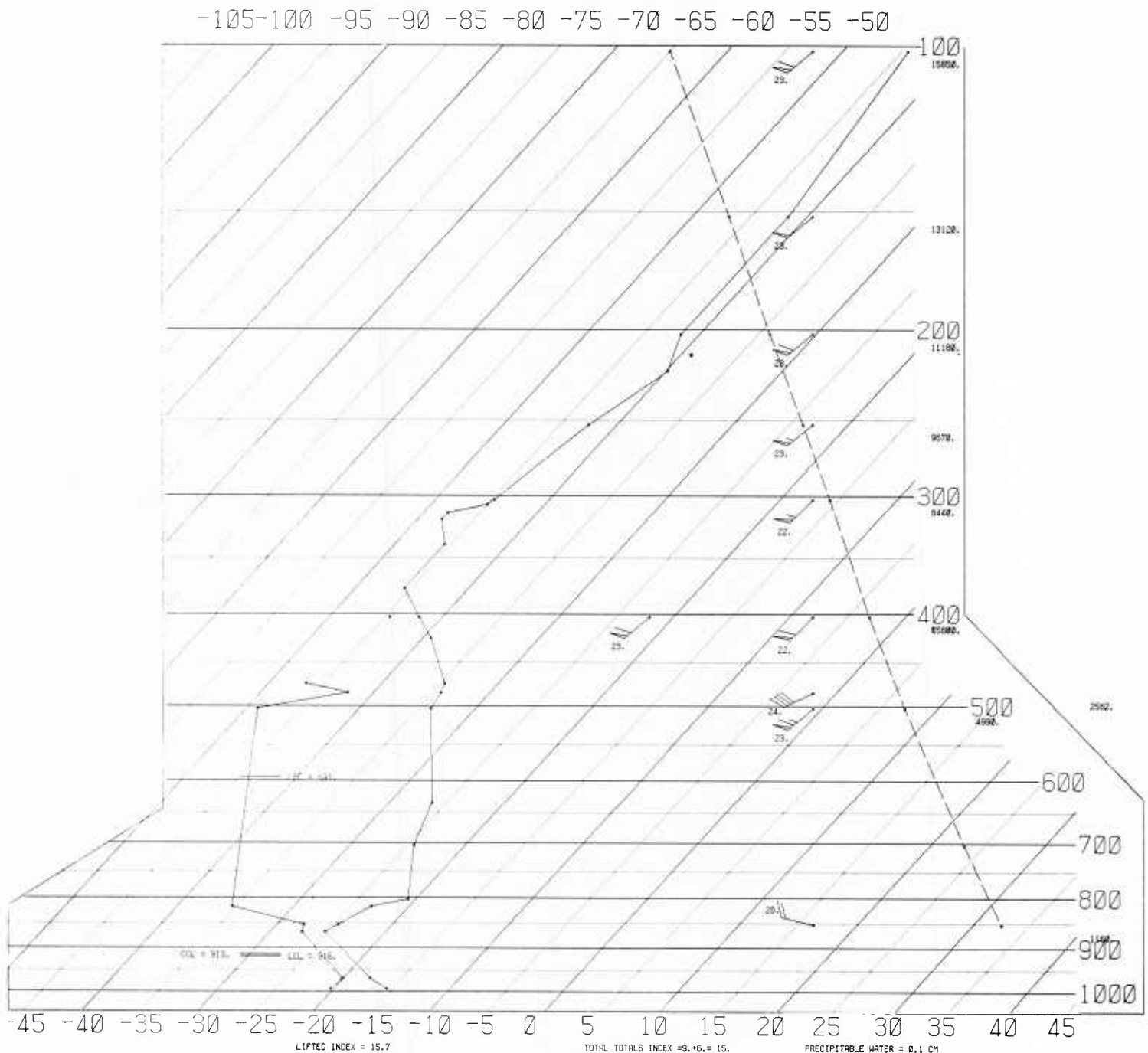


# SKEW T, LOG P DIAGRAM

890128

0000Z

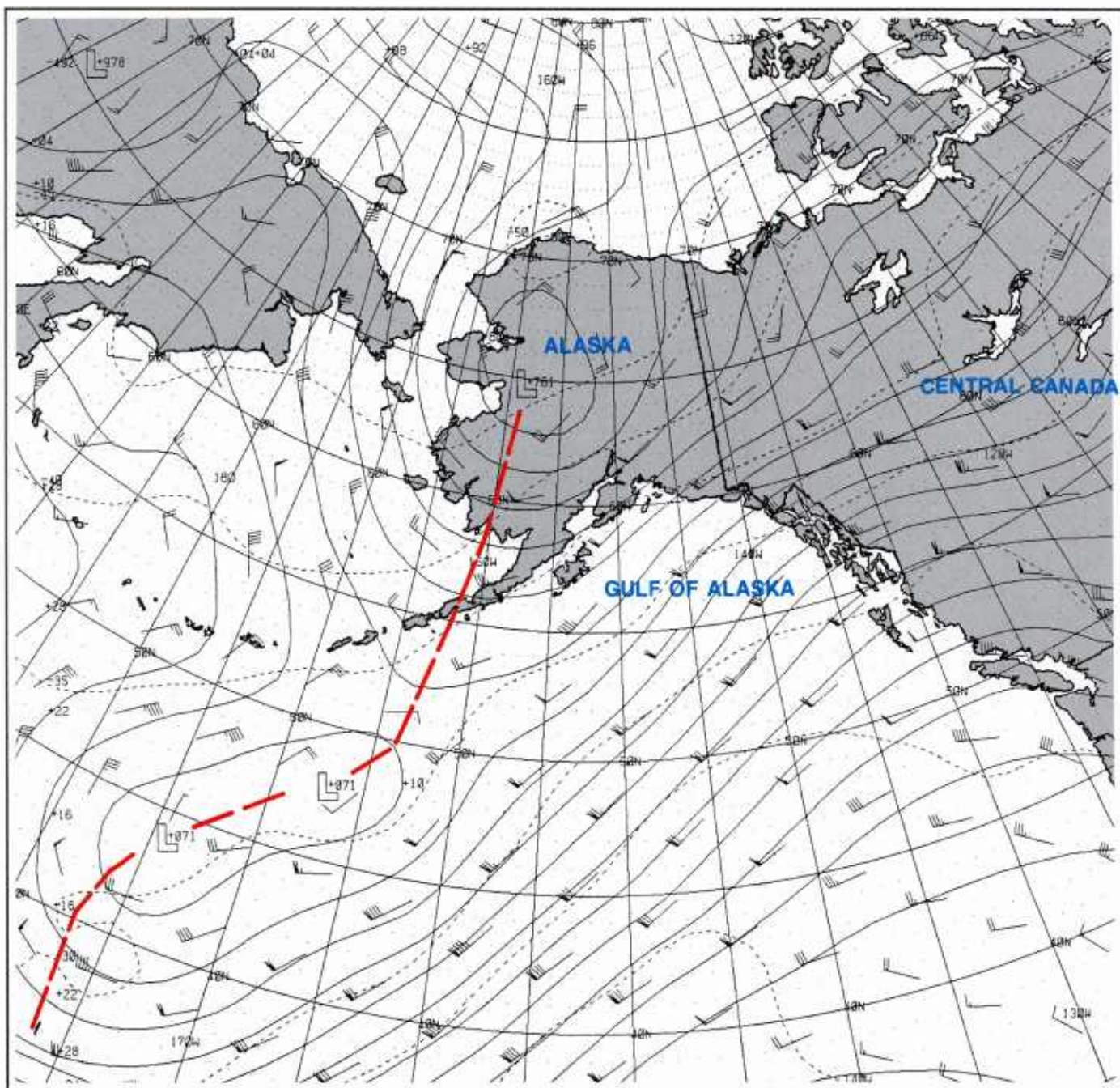
70350



1A-43 Radiosonde diagram for Kodiak Naval Station. 28 January, 0000 GMT.

Some useful mesoscale implications derive from the preceding analysis. Corner effects resulting in increased wind speed can be anticipated in wind flow around island barriers, as opposed to no wind speed increase when wind flows over the barrier. This increase can be considerable, causing much increased sea height and decreased surface visibility due to spray effects (Fett and Burk, 1981).

The clear wake may be a result of subsiding effects induced by entrainment of slow moving air in the immediate lee of the island into the faster moving current of air extending downstream on both sides from the island's edges.

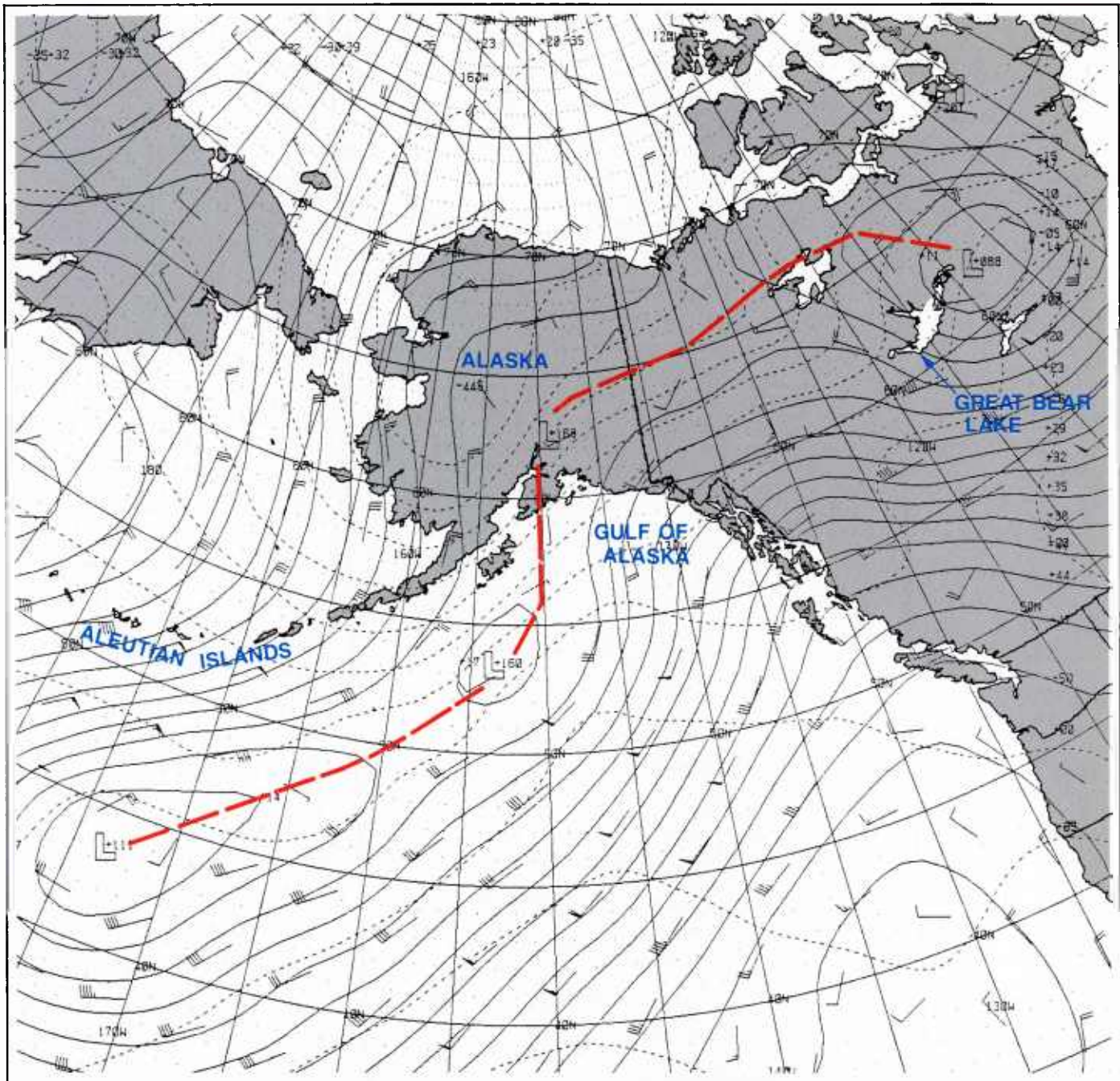


1A-44 FNOC 500 mb analysis. 27 January 1989, 1200 GMT.

The FNOC 500 mb analysis for 1200 GMT (Fig. 1A-44), shows the upper-level trough displaced northward from the surface position, as is commonly observed. Wind speeds increase from 25 kts at the base of the trough near the Alaskan Peninsula to 70 kts over SE Alaska. High-level speed divergence and positive vorticity advection favor cyclogenesis in the northern portion of the Gulf of Alaska.

Southeast of the trough, a jet stream maximum of 95 kts is found over the frontal band (Fig. 1A-41) which brings strong southwest flow into central Canada.

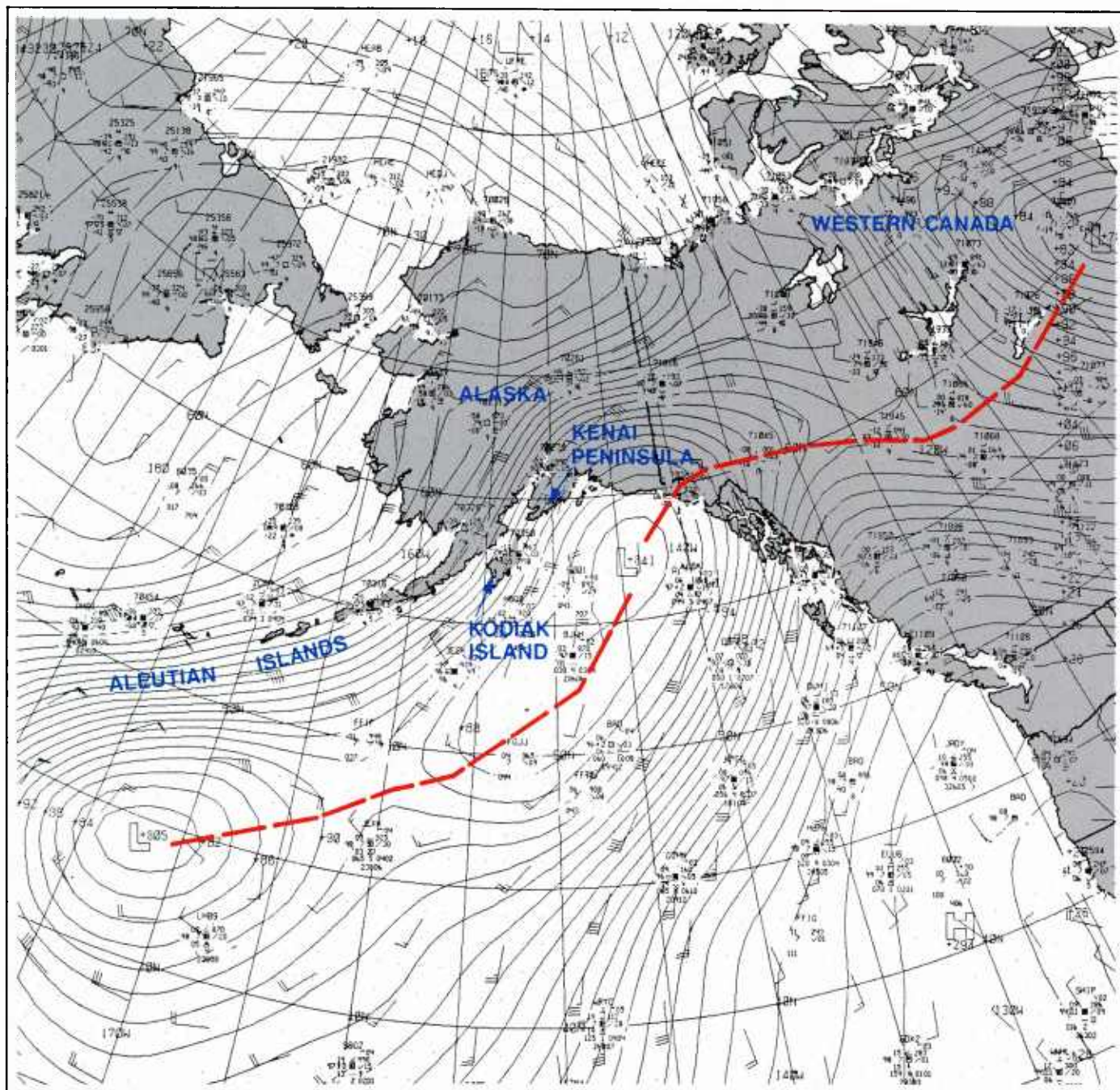




1A-45 FNOC 850 mb analysis. 27 January 1989, 1200 GMT.

The FNOC 850 mb analysis for 1200 GMT (Fig. 1A-45) shows the tremendously strong cold air advection extending down past the Aleutians. South of the trough, isotherm configuration corresponds to the frontal activity in that region.





1A-46 FNOc surface analysis. 27 January 1989, 1800 GMT.

The FNOc surface analysis for 1800 GMT is shown in Figure 1A-46. The analysis reveals the intensifying gradient through the Kodiak Island/Kenai Peninsula region that was to spell trouble for Vestfjord, just entering that area.

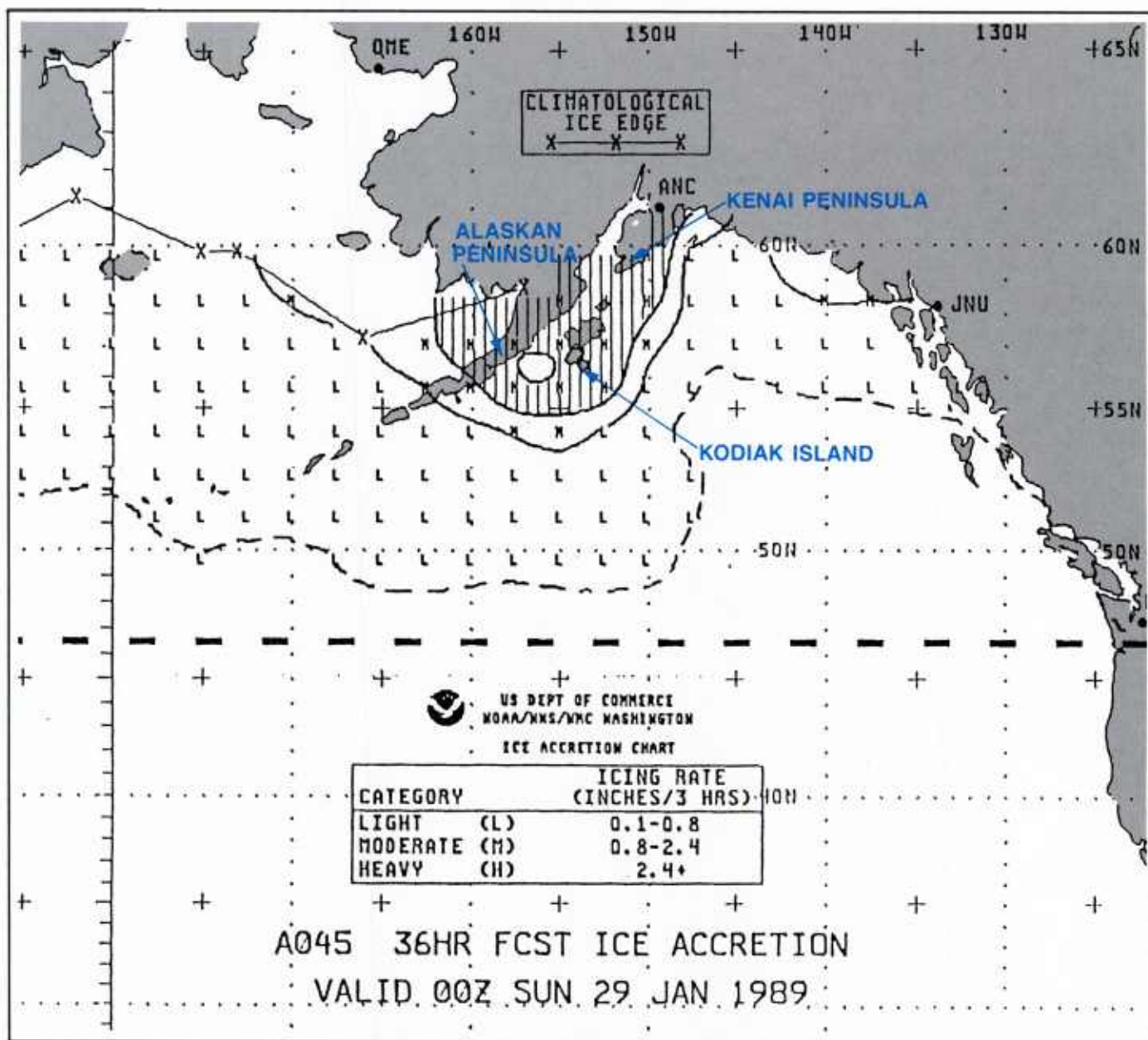
The Anchorage Marine Weather Forecast, issued on 27 January at 1146 GMT, valid from 3 AM Friday (Local Time) to 5 AM Saturday, with outlook to 5 AM Sunday (29 January 1989), read as follows:

*Area 3A. Barren Island and Kamishak Bay Waters.*

Storm Warning. NW winds to 50 kts increasing to 80 kts Friday night. Seas to 20 ft building to 35 ft Friday night. Heavy freezing spray. Lowest temperatures near 5 below.

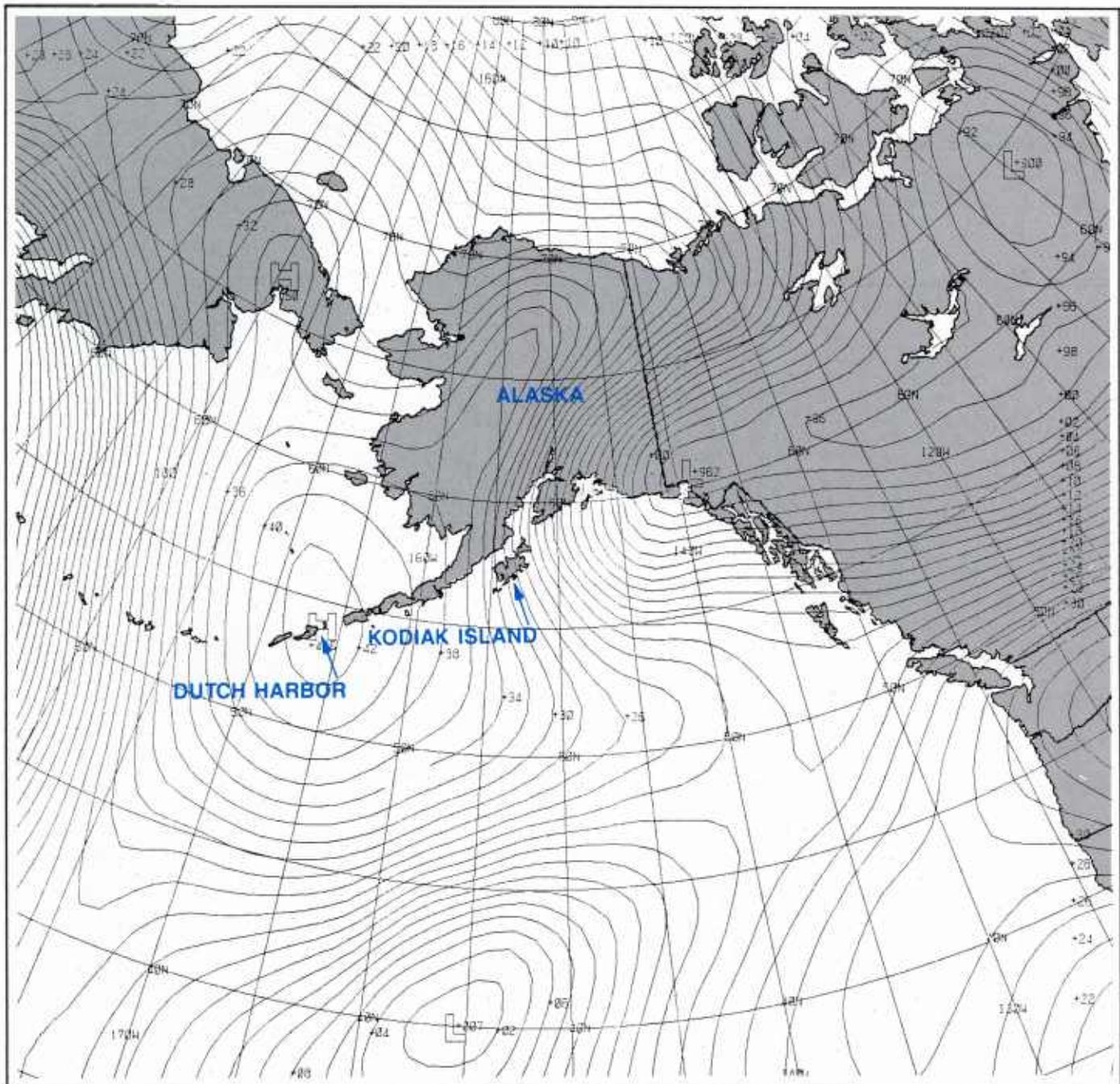
Outlook: NW winds to 80 kts.





1A-47 NOAA 36 hour forecast for ice accretion. Valid 29 January 1989 0000 GMT.

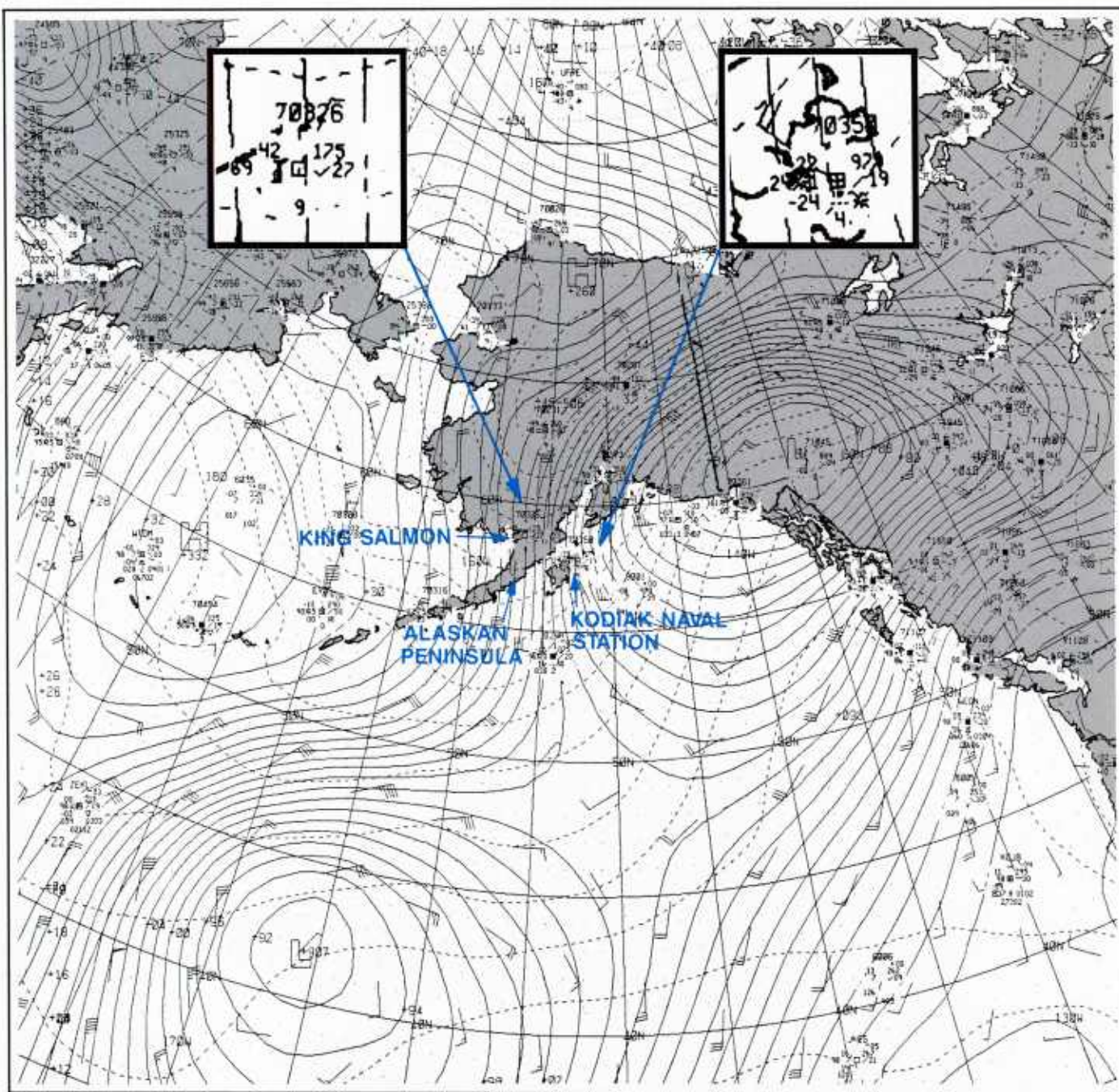
Figure 1A-47 is the NOAA 36-hour forecast for ice accretion, valid for 0000 GMT on 29 January 1989. The forecast indicates an area of heavy ice accretion surrounding the Kodiak and Kenai Peninsula region. Clearly, any fishing vessel having access to these warnings would head directly for the nearest port. For some reason, however, Vestfjord either did not receive or heed these warnings, or could not head for port, as it continued its route westward. The Captain possibly thought that he might outrun the system and, at any rate, be protected from high seas due to limited fetch in the lee of the Alaskan Peninsula.



1A-48 FNOC 48 hour surface prognosis. Valid 29 January 1989 1200 GMT.

The FNOC 48-hour surface prog (Fig. 1A-48), valid for 29 January 1989 at 1200 GMT (close to the time the ship sank), indicates that hopes for a more relaxed pressure field in the Kodiak Island area would not be achieved by that date. Calmer conditions could only be attained much further out on the Aleutian chain, with a high pressure center forecast directly over Dutch Harbor.





1A-49 FNOC surface analysis. 28 January 1989, 1200 GMT.

28 January 1989

The FNOC surface analysis for 1200 GMT (Fig. 1A-49) shows that the system was perhaps even more intense on this date. Isotherms on this analysis, drawn every 2°C, show one of the strongest cases of cold air advection in history. King Salmon, on the Alaskan Peninsula, reports a temperature of -42°C, while Kodiak Naval Station reports -22°C.

DMSP infrared (TS) data at 1434 GMT (Fig. 1A-50) show the cold surge in full force. Anticyclonic bending of the cloud streets south of the Aleutians coincides with a ridge line at that location. A small vortex seems to be forming near the Alaskan coast southwest of Prince William Sound, in the region where cyclogenesis might have been predicted based on the 500 mb analysis shown in (Fig. 1A-44).

A DMSP infrared (TS) view at 2002 GMT (Fig. 1A-51) shows the far western portion of the area. Remains of the decaying mesoscale vortex and BLF are apparent in a ring-like cloud pattern. The warm pattern in the ice on the southward lee of St. Lawrence Island is especially evident in this image and indicates a region of thinner refrozen ice, which radiates at a warmer temperature than the surrounding pack ice due to heat conduction from the underlying relatively warm sea. An enlargement of the ice edge is shown in Figure 1A-52. Comparison of this figure with Figure 1A-39, reveals that the ice is about 30 miles closer to St. Paul, in the Pribilofs, at this time, having been driven southward by the persistent, strong northerly winds over the pack ice.

#### *29 January 1989*

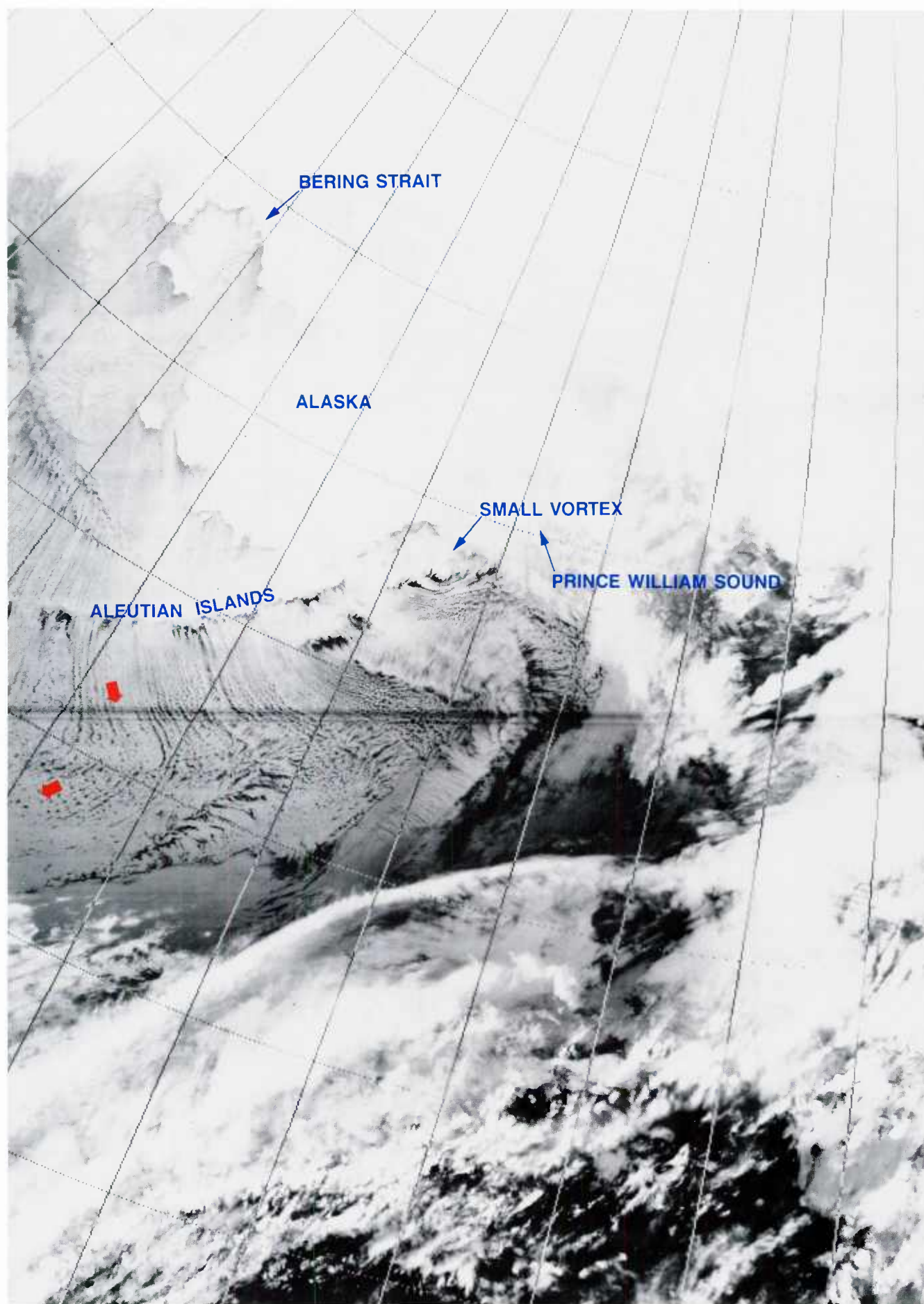
DMSP infrared (TS) data acquired at 0552 GMT (Fig. 1A-53) reveal a perfect fleur-de-lis cloud pattern (see Section 1B, Case 5), with northerly flow turning cyclonically to the east around a small vortex just south of the Kenai Peninsula, and the flow to the west turning anticyclonically about a high pressure center north of the Aleutians. Figure 1A-54 is the FNOC surface analysis for 0600 GMT, close to the time of the satellite data. The high pressure center is shown to the west, but the low just south of the Kenai Peninsula is not depicted on this analysis.

The 0000 GMT 500 mb analysis (Fig. 1A-55) shows an upper-level low displaced north of the suggested satellite-observed center with a position near Anchorage. The upper-level trough has moved slightly southeastward and is approaching Kodiak. Pronounced cold air advection on the west side of the trough is still apparent. At 850 mbs (Fig. 1A-56), pronounced cold air advection is evident from Kodiak Island southeastward.

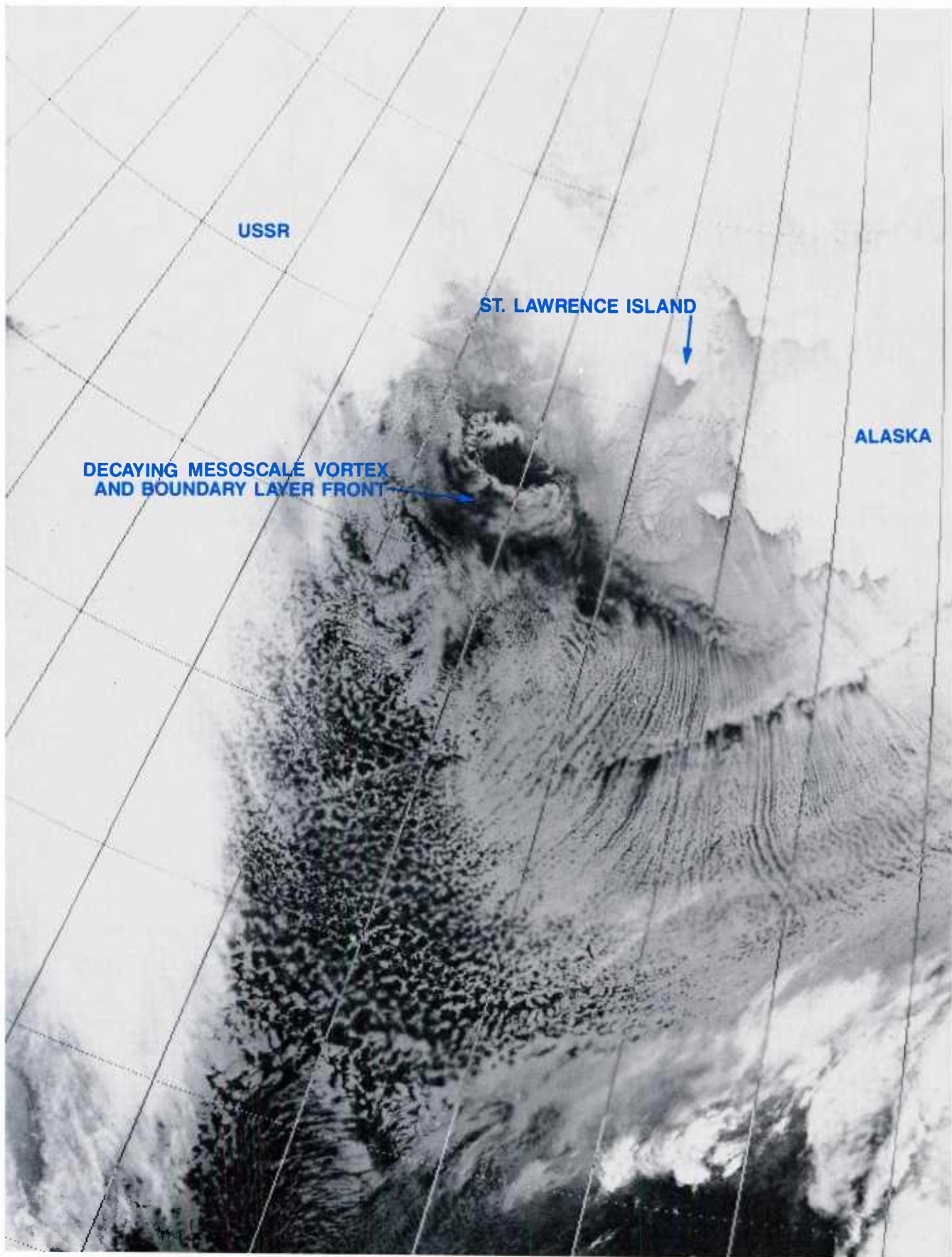
It is clear from the satellite data and the surface and upper-air analyses that conditions had not improved for the vessel Vestfjord, which was to sink shortly after the time of these data. (Its approximate position in Fig. 1A-53, at the time of the DMSP data, 0552 GMT, has been marked on the image with an "X". Vestfjord sank at 1010 GMT.)

It can be seen that the ship was located in an area of very moist, overcast conditions. Although the surface pressure gradient (Fig. 1A-54) suggests wind speeds of only 35-40 kts, the vessel itself, at the time, reported a sustained wind speed of 60 kts in 27-foot seas, and at least one other nearby ship (Fig. 1A-54) reported sustained winds of 50 kts. It is clear that, with an air temperature of  $-14^{\circ}\text{C}$ , supercooled sea spray could cause a rapid, and in this case disastrous, buildup of superstructure icing.



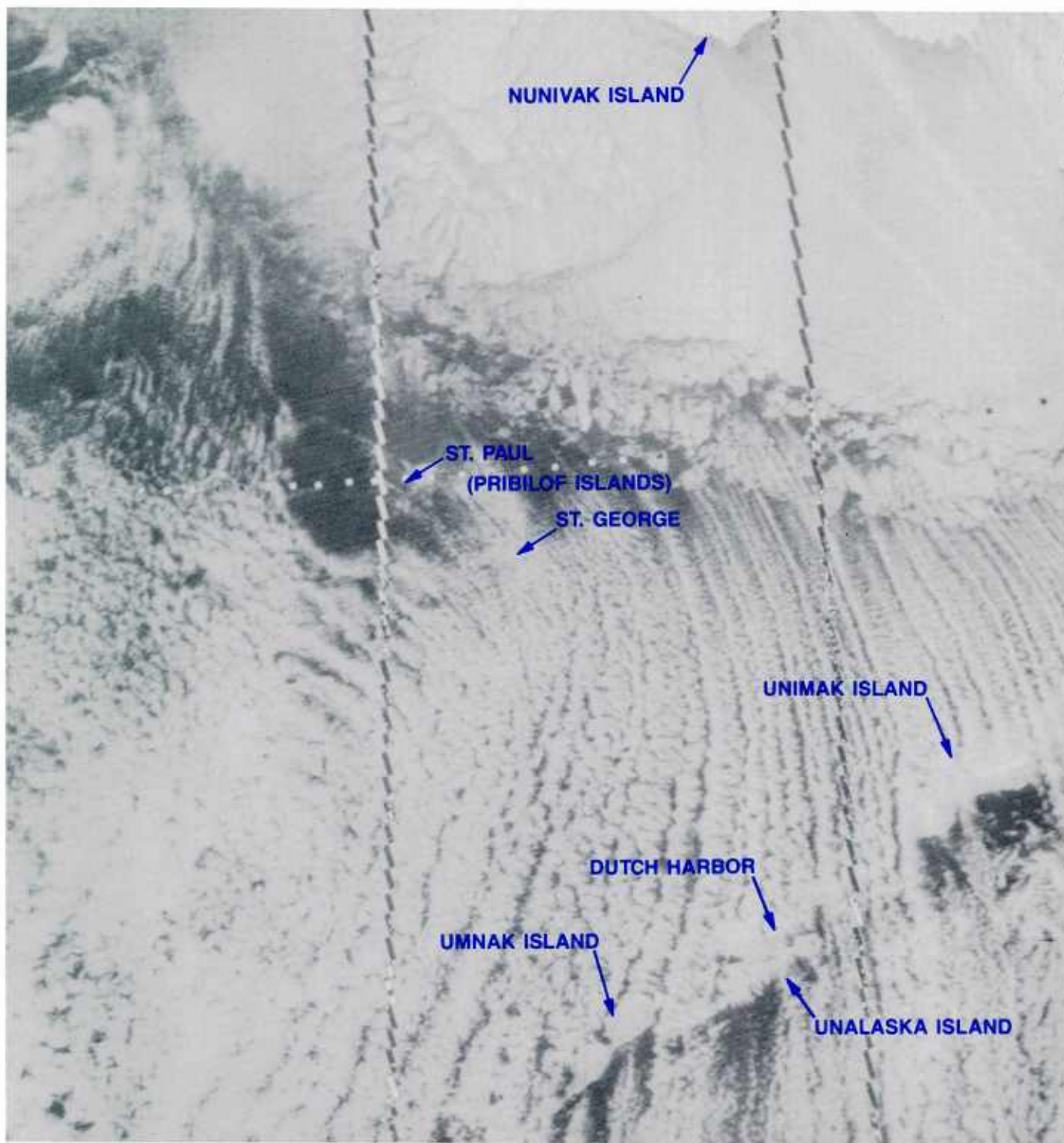


1A-50 DMSP infrared (TS) data. 28 January 1989, 1434 GMT.

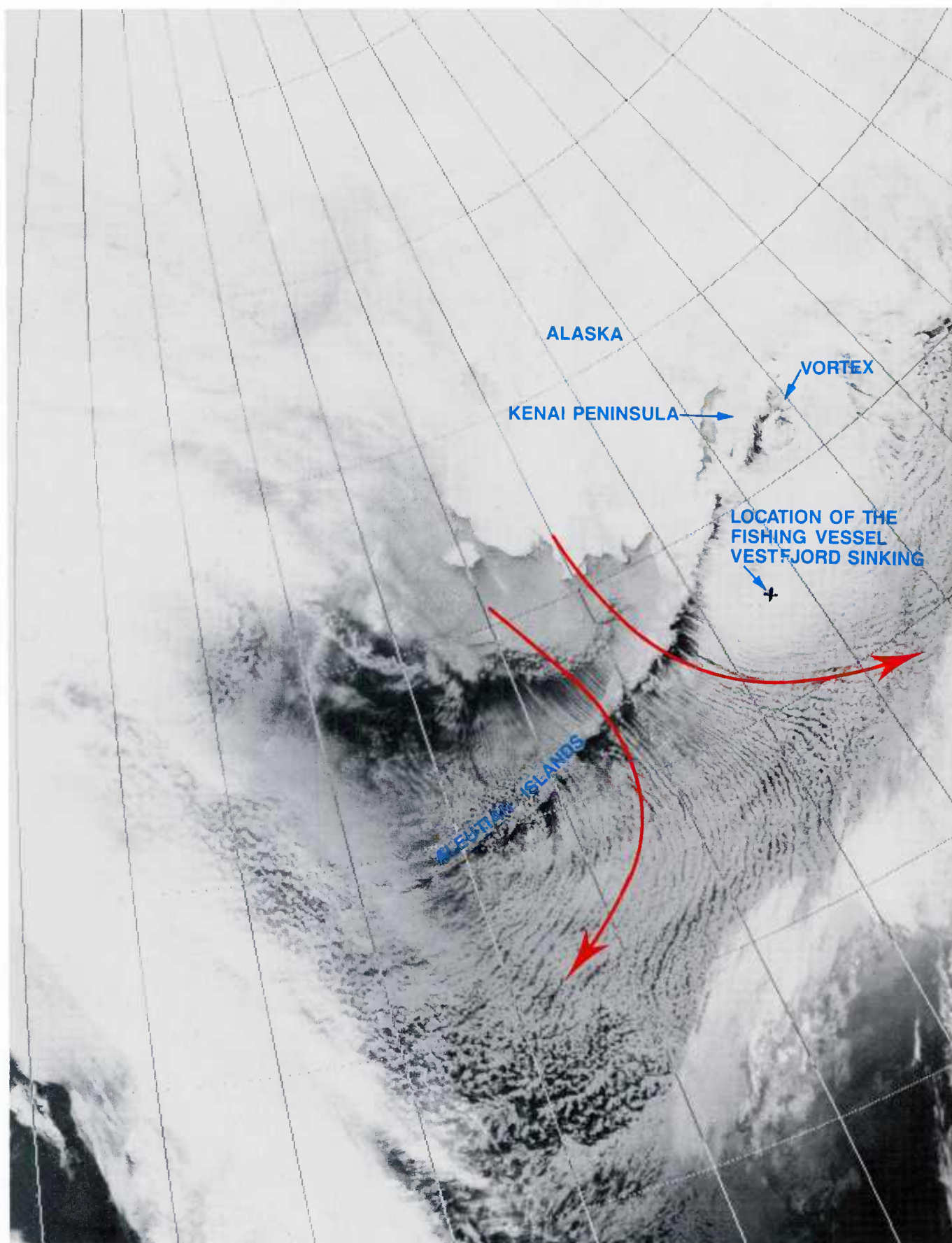


1A-51 DMSP infrared (TS) data. 28 January 1989, 2002 GMT.



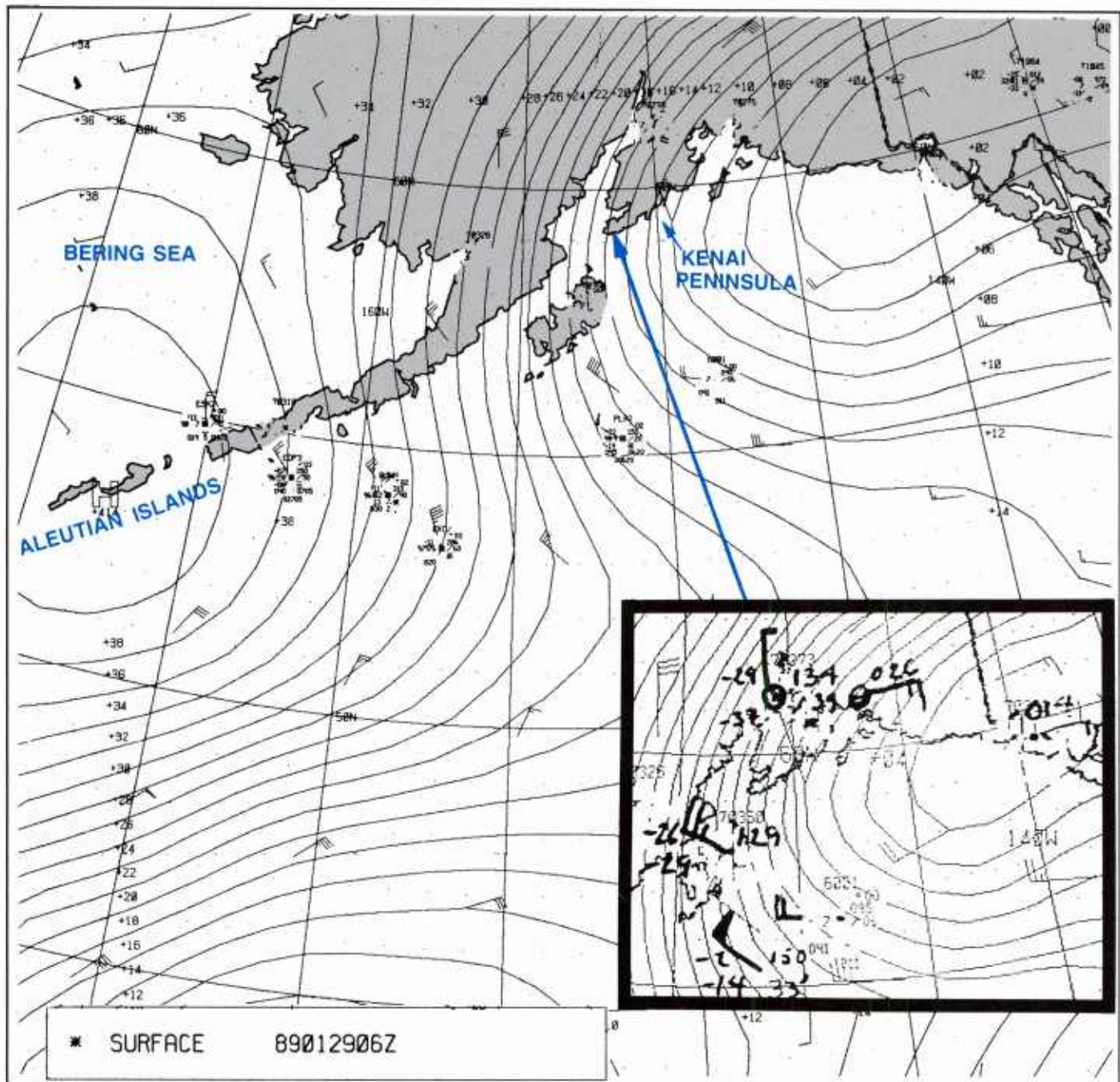


1A-52 DMSP infrared (TS) data enlargement. 28 January 1989. 2002 GMT.

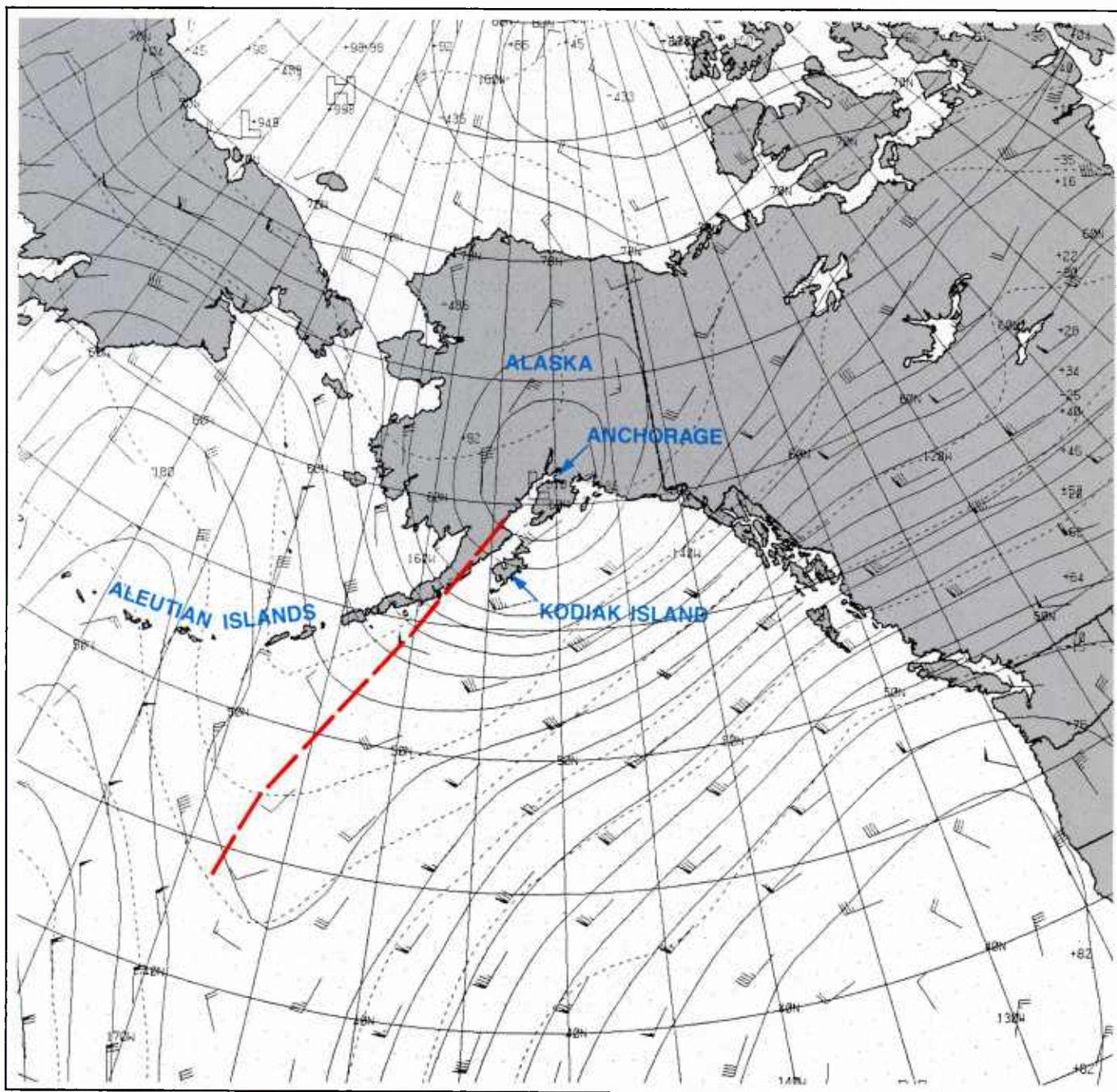


1A-53 DMSP infrared (TS) data. 29 January 1989, 0552 GMT.





1A-54 FNO surface analysis. 29 January 1989, 0600 GMT.



1A-55 FNOC 500 mb analysis. 29 January 1989, 0000 GMT.



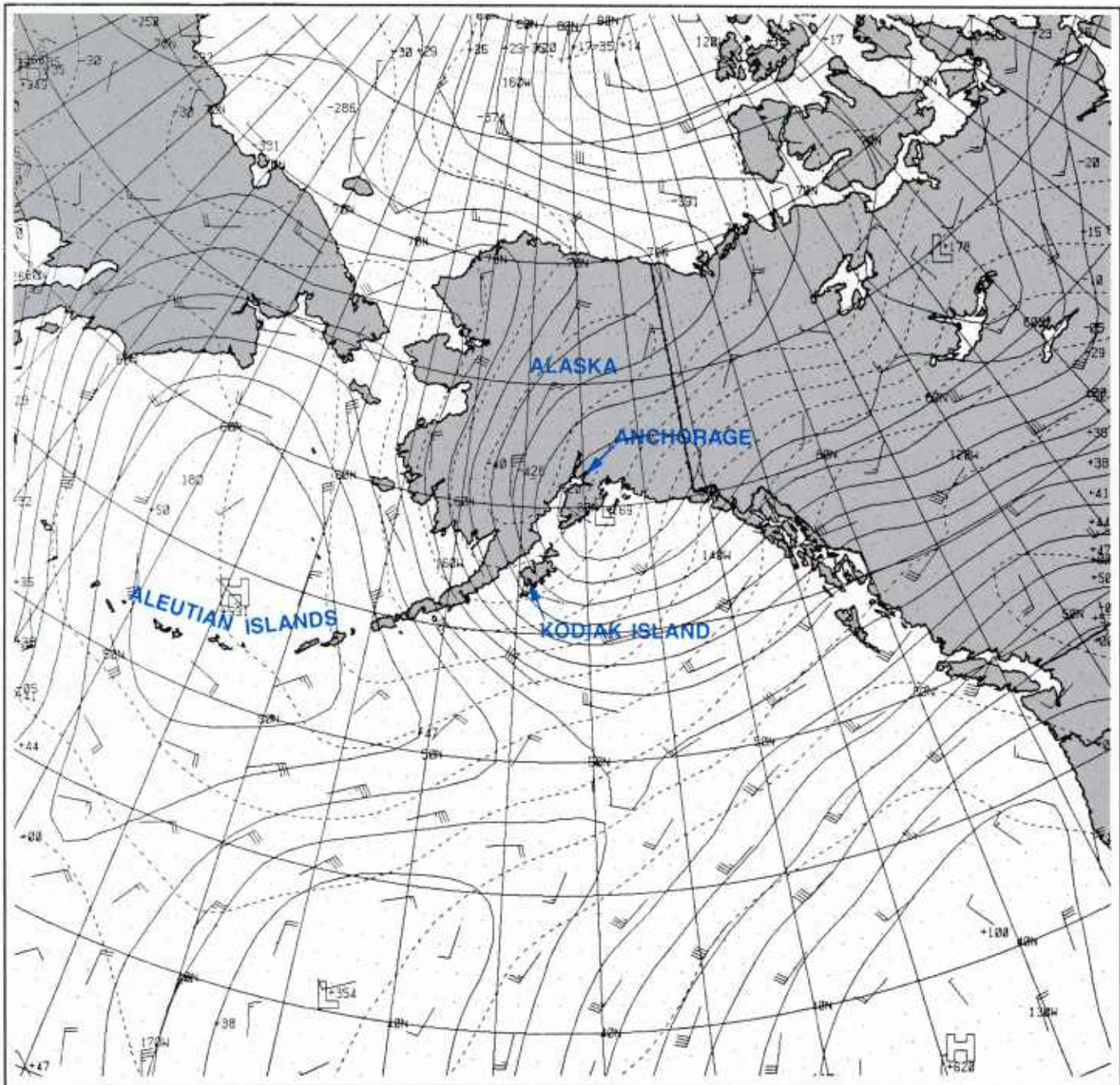


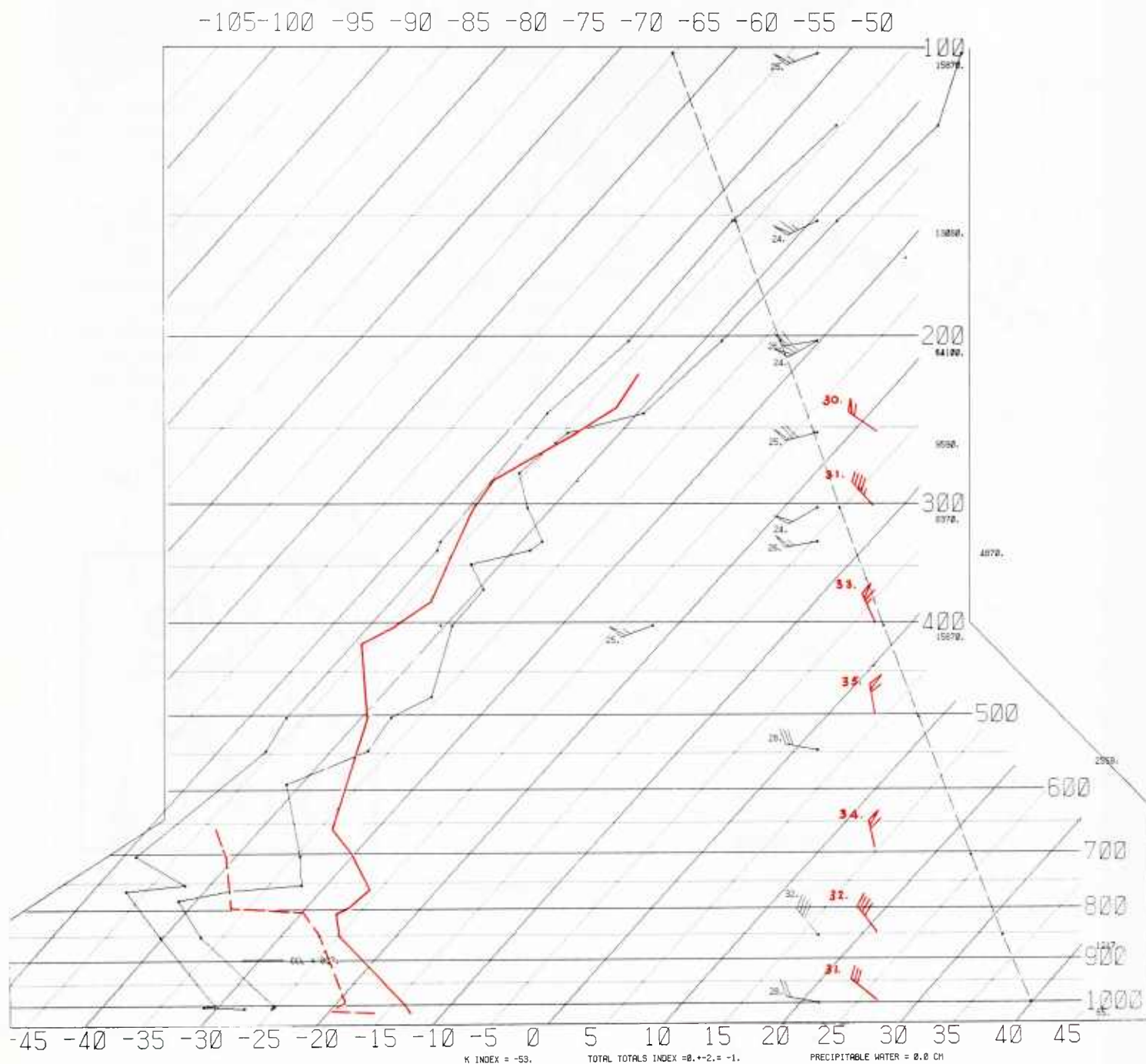
Fig. 1A-56 FNOC 850 mb analysis. 29 January 1989, 0000 GMT.

# SKEW T, LOG P DIAGRAM

890129

0000Z

70350



1A-58 Radiosonde diagram comparison for Kodiak Naval Station. 29 January 1989, 0000 GMT and 30 January 1989, 0000 GMT. Symbols and curves in red are for 30 January 1989, 0000 GMT.

The warming and drying effects are perhaps more clearly revealed in a comparison of radiosonde data showing conditions on Kodiak Island at 0000 GMT on 29 January versus 0000 GMT on 30 January (Fig. 1A-58). Temperature increases of as much as 12°C are apparent from the surface to 550 mb. Warm air advection is indicated on the 29 January data by the pronounced veering of winds from the 1000 to the 850 mb level. Additional warming appears subsidence-induced due to trough passage at upper-levels above 700 mbs.

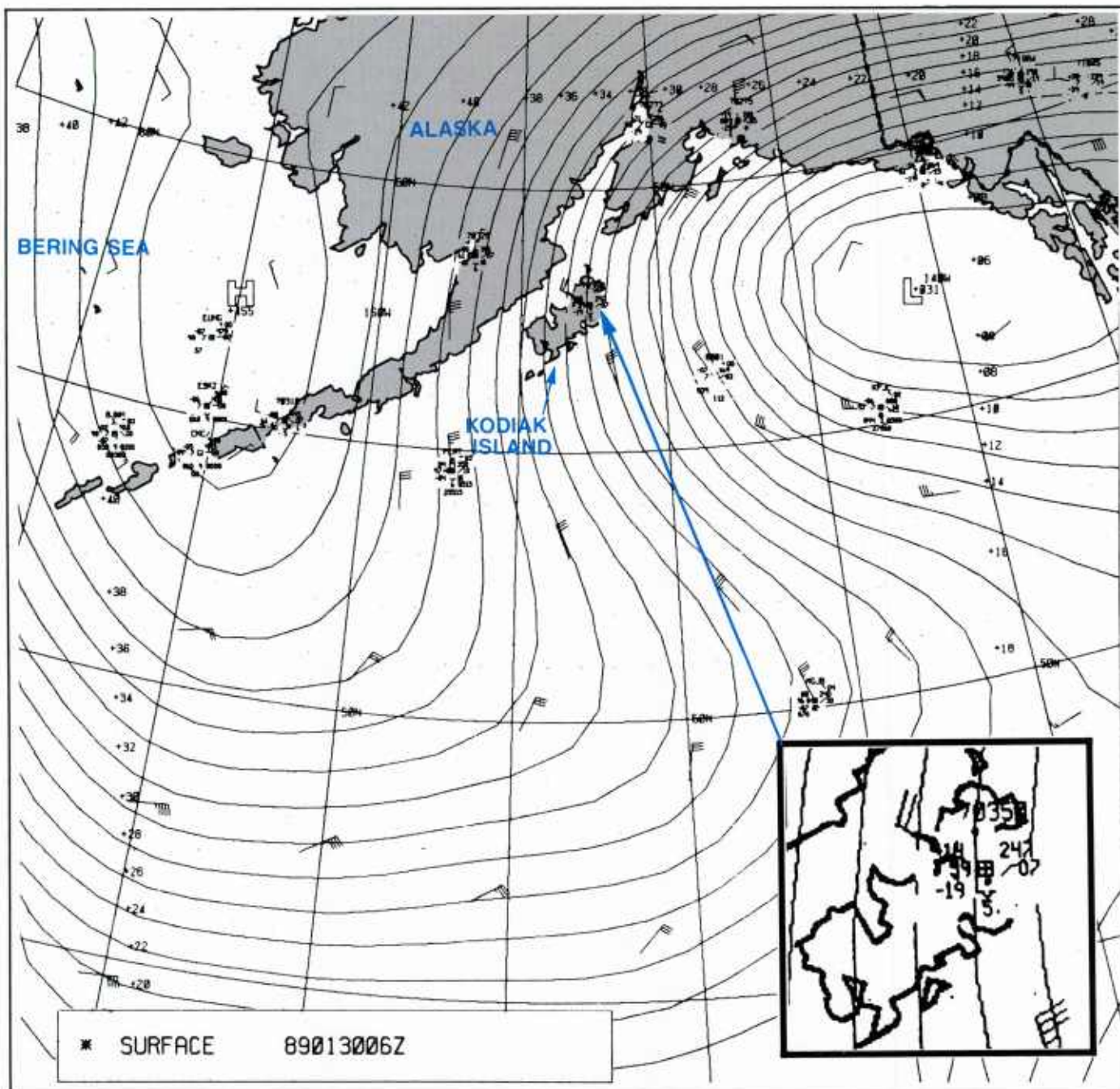


*30 January 1989*

The FNOC surface analysis for 0600 GMT (Fig. 1A-57), on first appearance, seems to indicate equally strong, unabated storm conditions. However, something significant happened in the weather experienced at Kodiak. Skies, which had been overcast, suddenly changed to only 2/8 coverage by 1800 GMT on 29 January. Temperatures, which had been reading around  $-25^{\circ}\text{C}$ , suddenly warmed to only  $-18^{\circ}\text{C}$ . Temperature-dew point spreads, similarly, which had been averaging  $2-3^{\circ}\text{C}$ , essentially doubled to 4 or  $5^{\circ}\text{C}$ .

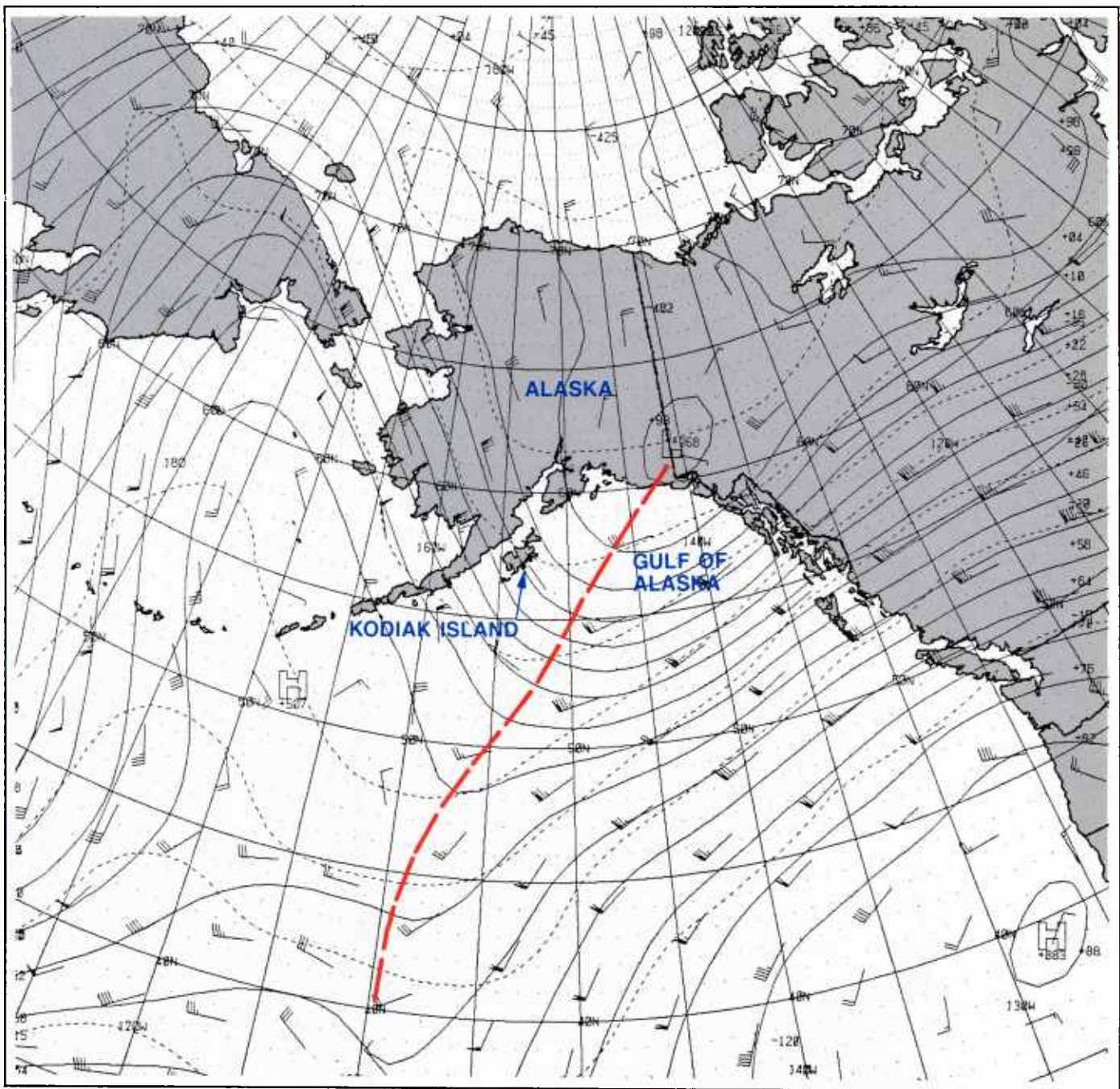
The dramatic warming and drying effects happened despite little evidence at the surface (Fig. 1A-54 and 1A-57) that any significant change in wind flow had occurred.

In a separate effort to document reasons for the warming that took place despite little change in appearance of the surface analyses (Figs. 1A-54 and 1A-57), 36-hour trajectories were run, utilizing the Navy Operational Regional Atmospheric Prediction System (NORAPS) model. Results indicated that low-level air over the Kodiak region on 29 January, at 0600 GMT, originated 36 hours earlier from central Alaska. On 30 January, however, 24 hours later, low-level air had its origin from over the northern Bering Sea—a much warmer region. Again, this surprising result would be difficult to envision, judging solely from the surface analyses (Figs. 1A-54 and 1A-57).



1A-57 FNOC surface analysis. 30 January 1989, 0600 GMT.





1A-59 FNOC 500 mb analysis. 30 January 1989, 0000 GMT.

Figure 1A-59 is the FNOC 500 mb analysis for 30 January at 0000 GMT. This analysis verifies that the trough had passed Kodiak by that time and now extended into the Gulf of Alaska.

The effect on the appearance of cloud forms over the area was equally dramatic. Figure 1A-60 is a DMSP infrared (TS) view of the region at 0913 GMT on 30 January. A comparison of this figure, unlike that acquired a little over 24 hours earlier (Fig. 1A-53), shows Kodiak under essentially clear, as opposed to overcast, sky conditions. The long, thin, tightly spaced cloud lines of Figure 1A-53 have been replaced by broader cloud lines and patches, still basically aligned from the northwest, but lacking the sharpness and clearly etched nature of the earlier view. The lack of vigor of cloud line development in Figure 1A-60 apparently reflects the reduced air-sea temperature difference brought about by effects associated with the passage of the upper-level trough and warm air advection at lower levels.

As earlier indicated, surface analyses for 29 and 30 January at 0600 GMT (Figs. 1A-54 and 1A-57), except for temperature differences, are quite similar, and strong winds and high seas surely existed on each of the two days. However, the icing problem was probably drastically reduced on 30 January because of the warmer surface air temperature.

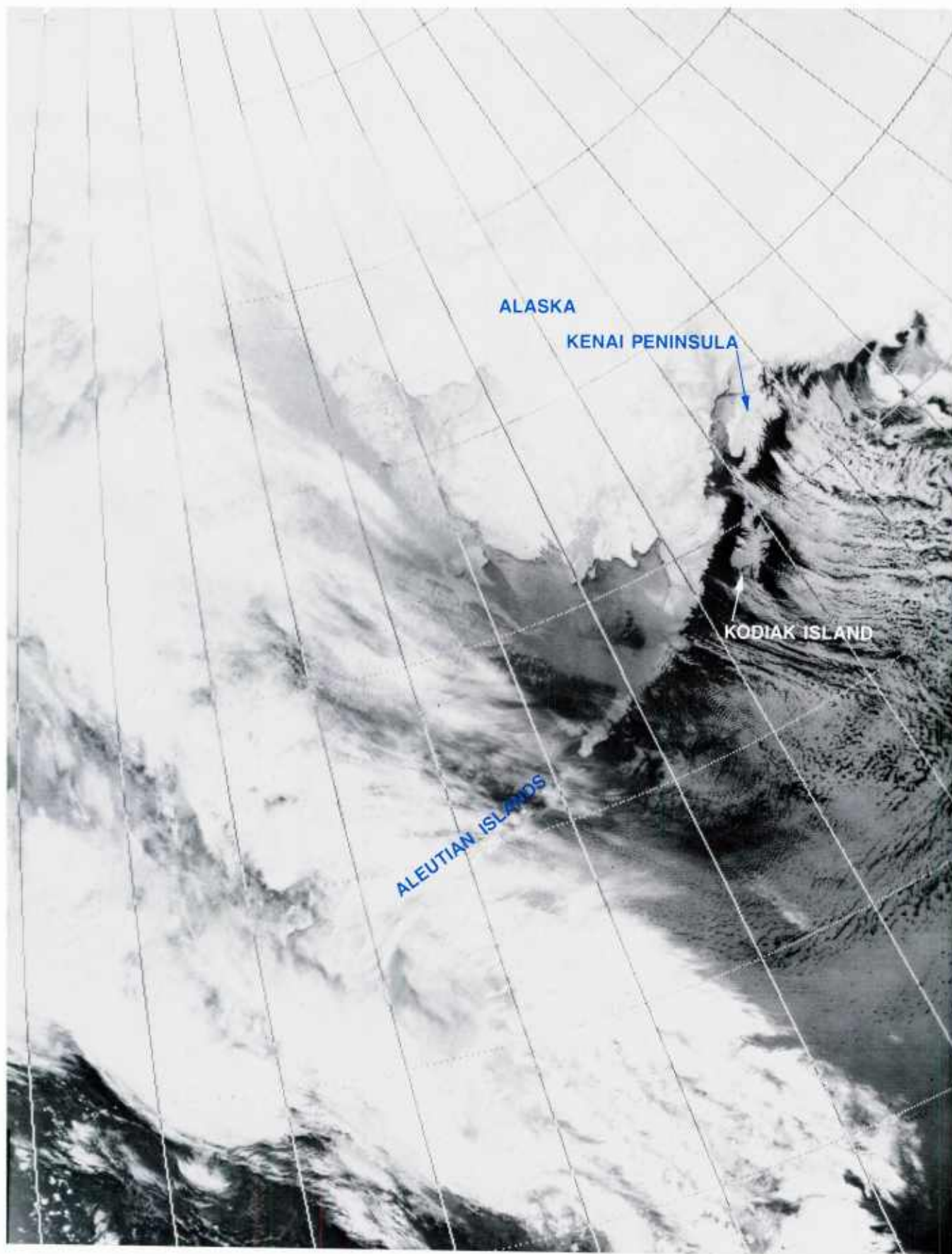
Figure 1A-61 is a chart showing icing nomograms for four values of sea temperature (Overland, Pease, and Preisendorfer, 1986). Assuming Vestfjord was in an area where sea surface temperature was  $3^{\circ}\text{C}$ , with an air temperature of  $-14^{\circ}\text{C}$ , heavy icing could be expected for winds of about 22 kts or greater. (Vestfjord reported 60 kts!) If the air temperature were  $-2^{\circ}\text{C}$ , as indicated by ship PLAT (55.3N, 151.5W) on 29 January at 0600 GMT (Fig. 1A-54), icing conditions would only be light, even if wind speeds exceeded 80 kts.

The lesson here is clear—extreme icing in the Gulf of Alaska is dependent upon extreme conditions of cold air advection. When air temperatures are lower than  $-14^{\circ}\text{C}$ , even a moderate wind of 20 kts can produce heavy icing. At 60 kts, under these conditions, a small ship is in immediate danger of becoming an ice cube—a situation experienced, unfortunately, by the crew and passenger aboard Vestfjord.

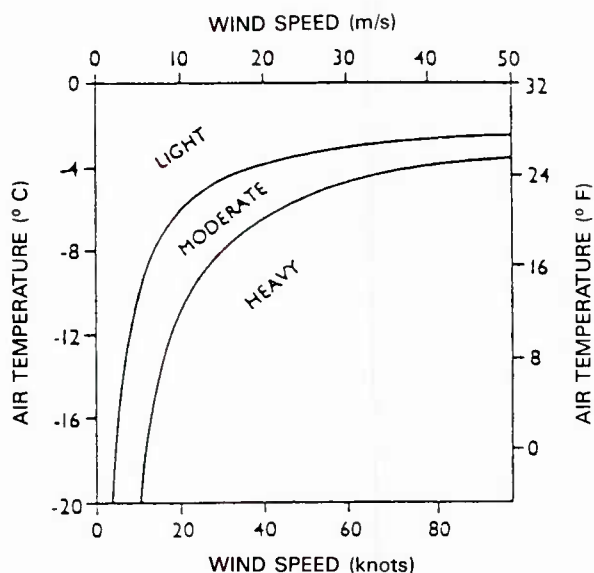
### **Important Conclusions**

1. Vessel icing in the Gulf of Alaska is dependent upon severe, but not uncommon, episodes of cold air advection.
2. Ship structural icing can be heavy if the air temperature is cold enough and wind speeds are high, even in water with temperature up to  $+7^{\circ}\text{C}$ .
3. Smaller vessels over cold water areas ( $< 7^{\circ}\text{C}$ ) should take immediate action to reach the nearest port whenever below-freezing temperatures, combined with a high wind warning, are forecast.
4. Icing conditions are especially likely in the region in advance of an approaching 500 mb trough.
5. Icing conditions may be expected to alleviate if lower-level warm air advection is indicated, accompanied by passage of an upper-level trough.
6. Warm air advection and 500 mb trough passage over the Gulf of Alaska during a winter-time cold surge can be detected in satellite data by noting changes in cloud line appearance and tendencies for a clearing of cloudiness, especially over and around island terrain.

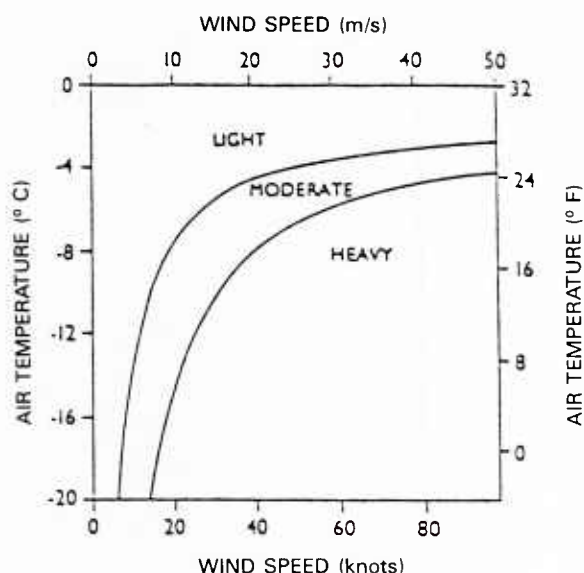




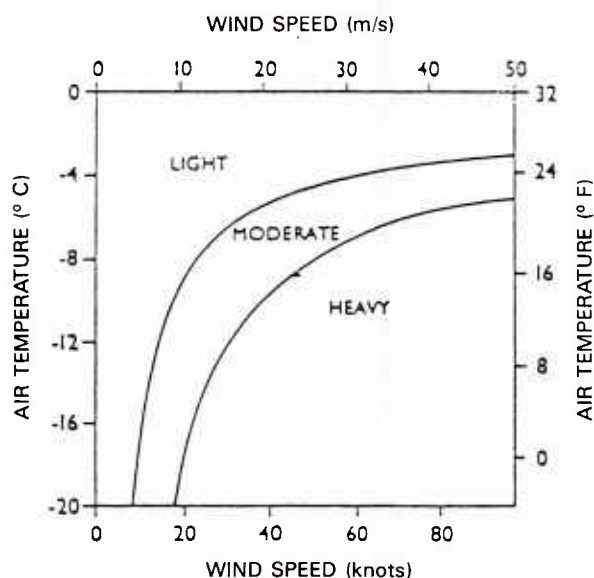
1A-60 DMSP infrared (TS) data. 30 January 1989, 0913 GMT.



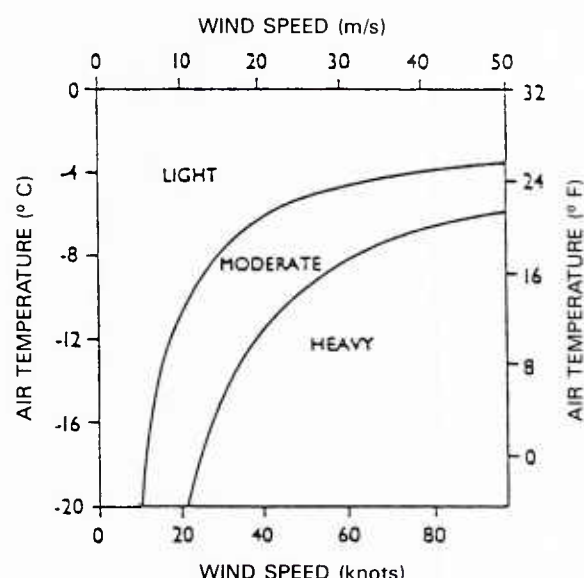
Icing conditions for vessels heading into or abeam of the wind for water temperature of  $+1^{\circ}\text{C}$  ( $34^{\circ}\text{F}$ )



Icing conditions for vessels heading into or abeam of the wind for water temperatures of  $+3^{\circ}\text{C}$  ( $37^{\circ}\text{F}$ )



Icing conditions for vessels heading into or abeam of the wind for water temperatures of  $+5^{\circ}\text{C}$  ( $41^{\circ}\text{F}$ )



Icing conditions for vessels heading into or abeam of the wind for water temperatures of  $+7^{\circ}\text{C}$  ( $45^{\circ}\text{F}$ )

Light Icing — Less than 0.7 cm/hr (0.3 in/hr)  
 Moderate Icing — 0.7 cm/hr (0.3 in/hr) to 2.0 cm/hr (0.8 in/hr)  
 Heavy Icing — Greater than 2.0 cm/hr (0.8 in/hr)

1A-61 Nomogram predicting rate of ice accumulation for vessels heading into or abeam of the wind.

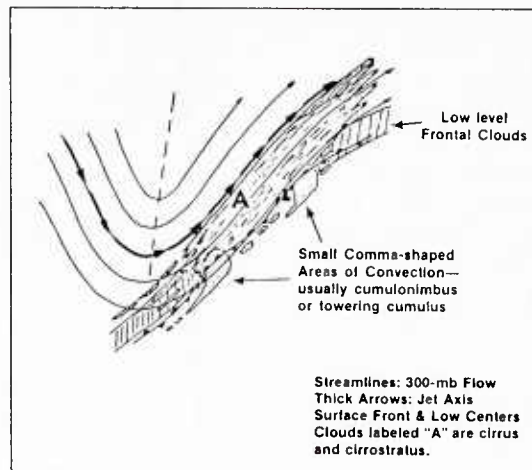
## References

1. Fett, R. W., and S. D. Burk, 1981: Island barrier effects as observed by satellite and instrumented aircraft, and simulated by a numerical model. *Mon. Wea. Rev.*, Vol 109, No. 7, 1527-1541.
2. Overland, J. E., C. H. Pease, and R. W. Preisendorfer, 1986: Prediction of vessel icing., *Jour. of Climate and Applied Meteor.*, No. 12, 1793-1806.

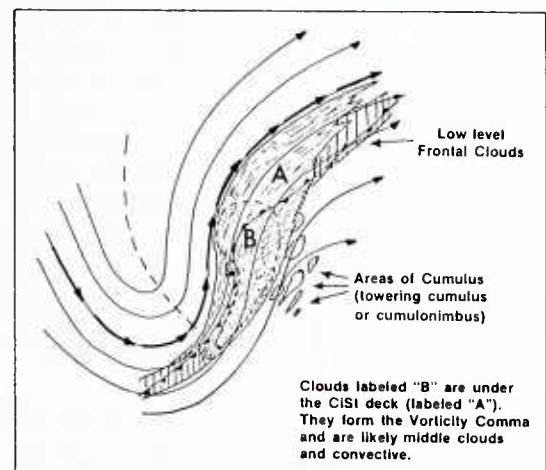


### Case 3 *Meridional Trough Cyclogenesis—A Severe Summer Storm Development in the Beaufort Sea (26–28 July 1982)*

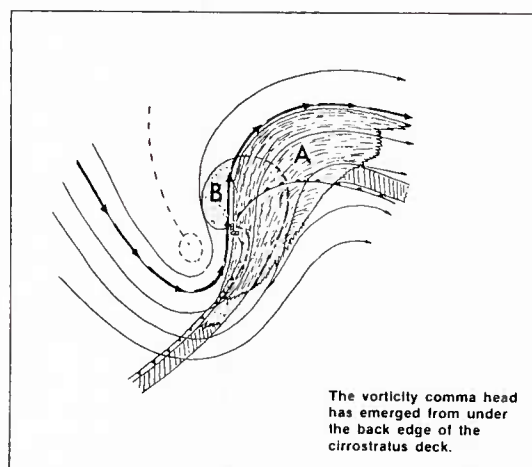
Meridional trough cyclogenesis has been estimated to occur in perhaps 25 percent of all storm developments (Weldon, 1975). A complete description of this form of cyclogenesis is included in NTAG Vol. 4, Part 1, Section 2A (Fett et al., 1984) and will not be repeated here. However, Fig. 1A-63a summarizes pertinent features, the most prominent of which is the clearly defined emergence of a vorticity comma head from under a multilayered band of frontal clouds in advance of an elongated, meridionally oriented trough axis. The comma head is composed of lower level overcast cloudiness. When the comma head emergence occurs adjacent to an especially enhanced “V-shaped” convective cloud formation, with cirrus evidence based on satellite observation of an upper level, short wave ridge intensifying immediately to the east of the frontal band, one can be sure that significant rapid cyclogenesis is in progress.



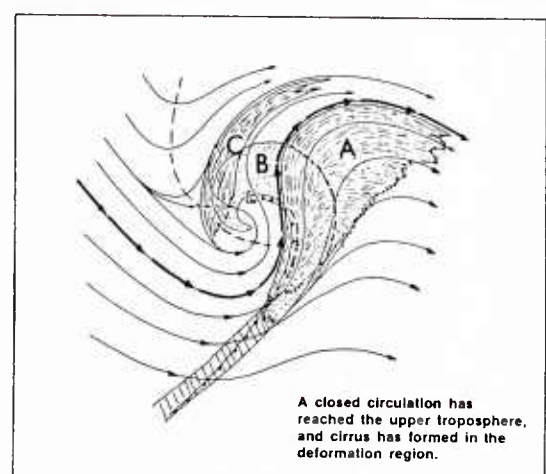
Meridional Trough Cyclogenesis, Phase 1.



Meridional Trough Cyclogenesis, Phase 2.



Meridional Trough Cyclogenesis, Phase 3.



Meridional Trough Cyclogenesis, Phase 4.

1A-63a Schematics showing the four stages of meridional trough cyclogenesis (from Weldon, 1975).

The storm development to be described was a summer (July) event. It produced near-hurricane force winds with waves up to 5 m over the Beaufort drill area and the Mackenzie River Delta region and forced the evacuation of personnel from Tarsiut Island. The storm developed rapidly and was not well analyzed or forecast (Black, 1982).

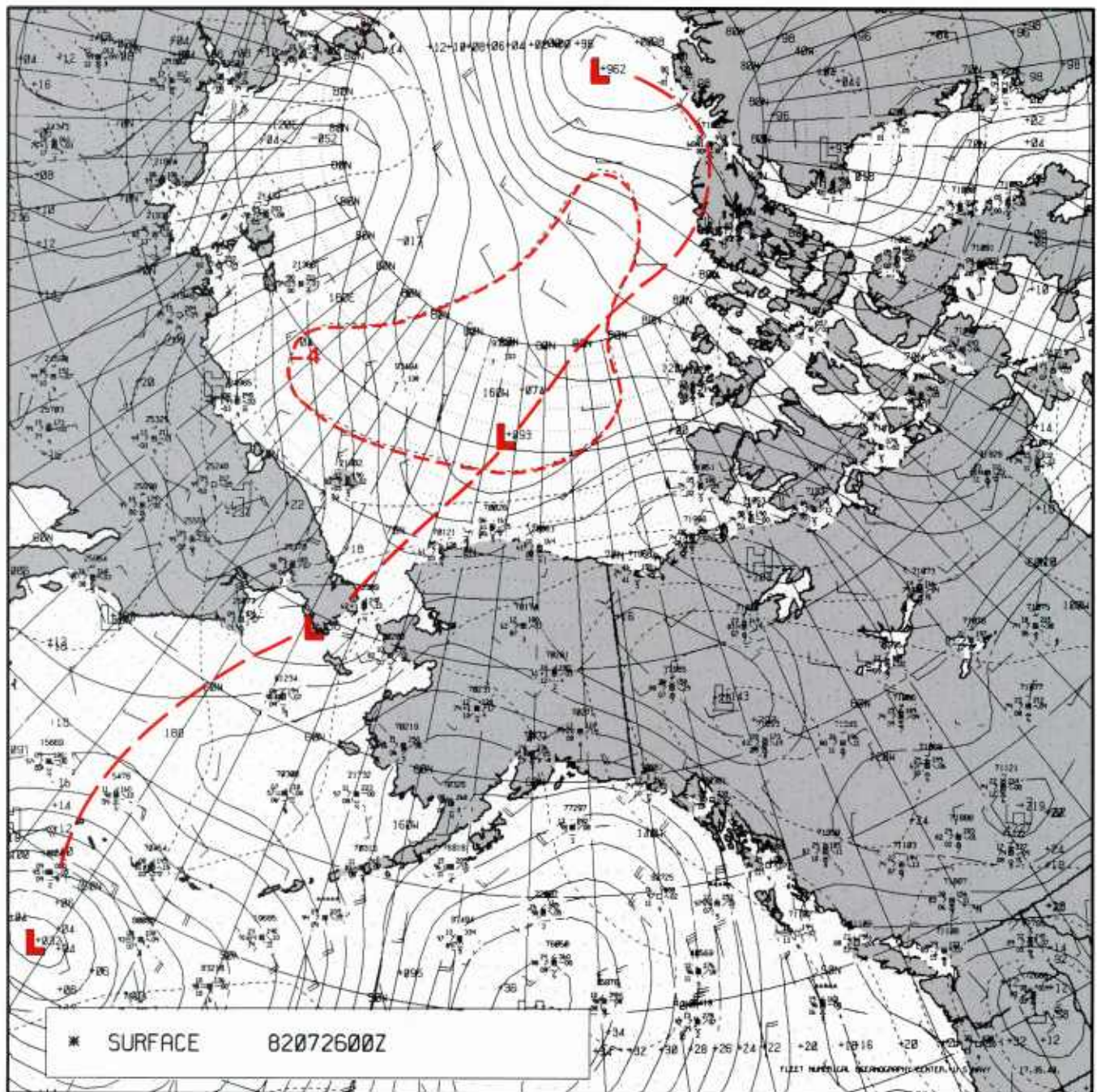
### *26 July 1982*

The FNOC surface analysis for 0000 GMT (Fig. 1A-64a) reveals a cold pocket of air encircling low pressure regions in the Arctic Ocean near 76°N 156°W. An elongated meridional trough extends southward from this region to a low near the Bering Strait and again southward through the Bering Sea. A northeastward extension to a low north of Greenland is also apparent. A similar pattern is shown in the FNOC 500-mb analysis (Fig. 1A-65a). In this analysis lows in the Arctic Ocean north of Alaska and near the Bering Strait are encircled by  $-25^{\circ}\text{C}$  isotherm emphasizing the cold nature of the trough. Black (1982) makes the very interesting observation “. . . that the trough over the Bering Strait provides an effective barrier between the Pacific stream over Alaska and the northerly flow over eastern Siberia.” This enhances baroclinicity in the region.

DMSP visible (LS) data acquired less than 2 hr prior to the 0000 GMT analyses (Fig. 1A-66a) reveal cloud vortices associated with each of the low center areas. A gridded version of these data is shown in Fig. 1A-67a. A cloud band extending between the lows suggests that they are joined by a front, as shown in Fig. 1A-67a. The frontal connection was adapted by NMC in a 0000 GMT surface analysis (not shown) and is further heightened by another DMSP visible (LS) image, acquired at 0001 GMT (Fig. 1A-68a), which shows rope clouds associated with the frontal zones extending from each of the lows. A gridded overlay to the depiction is shown in Fig. 1A-69a. Evidence of strong cold air advection sweeping behind the frontal zone and cloud vortex in the Bering Sea is shown by cloud streets in that region.

The low center over the Chukchi Sea is shown to be near vertically aligned, with low centers at the surface (Fig. 1A-64a), at the 500-mb level (Fig. 1A-65a), and in the satellite data (Figs. 1A-67a, 1A-68a, and 1A-69a), all appearing near the same location. The Barrow sounding for 0000 GMT (Fig. 1A-70a) verifies the expected southwesterly flow ahead of the front with a powerful 70-kt jet maximum apparent at the 400-mb level.



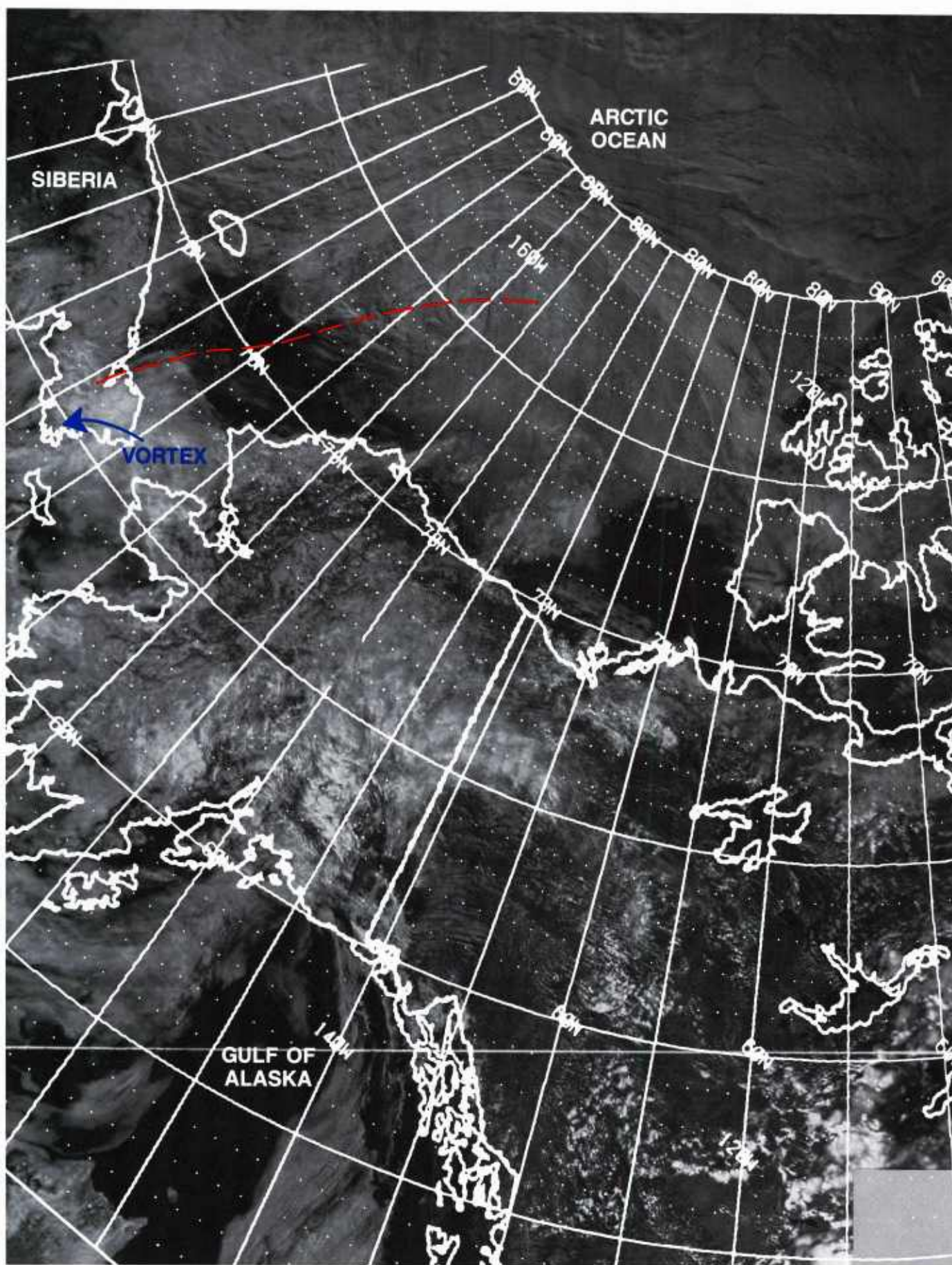


1A-64a FNOC surface analysis. 0000 GMT 26 July 1982.



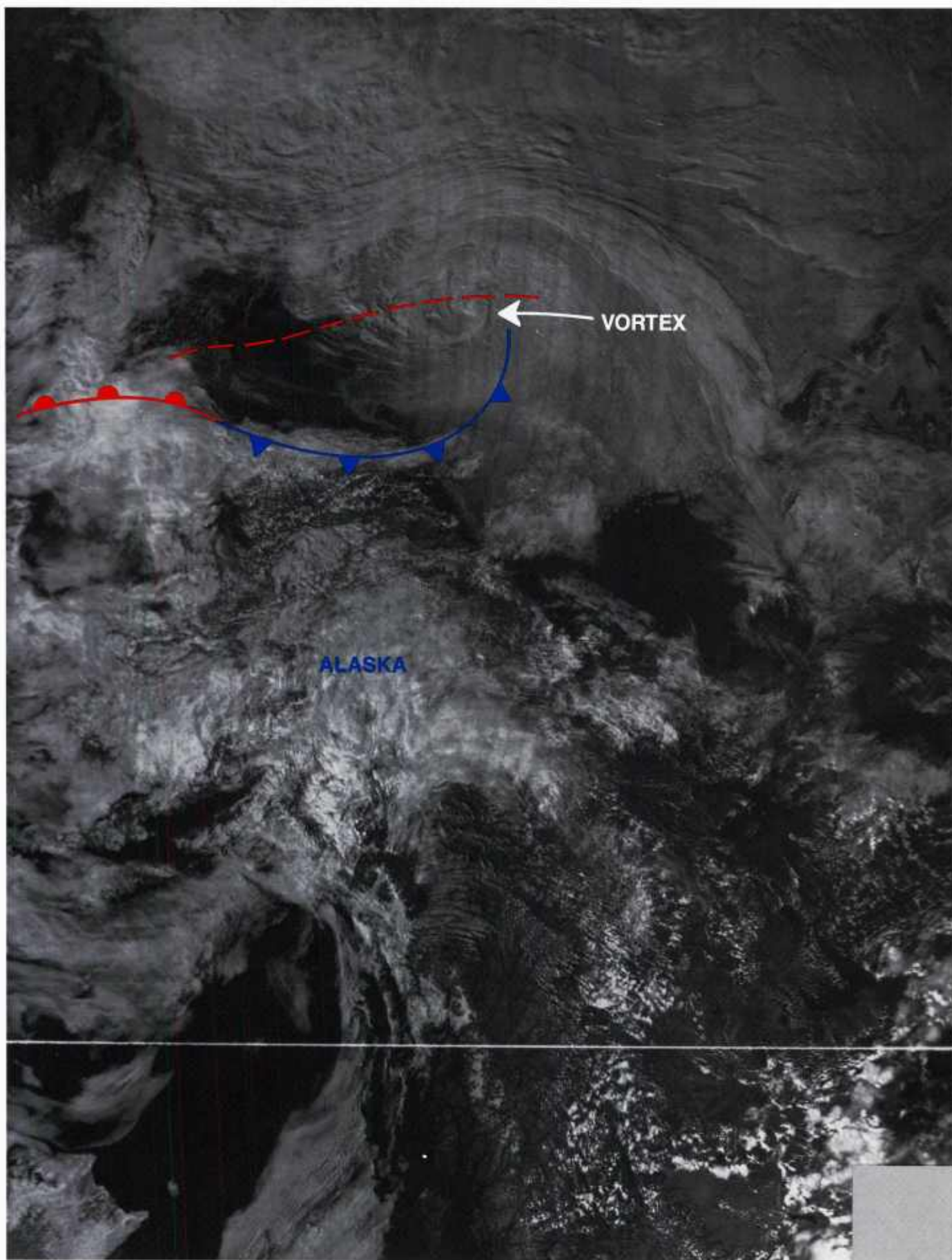






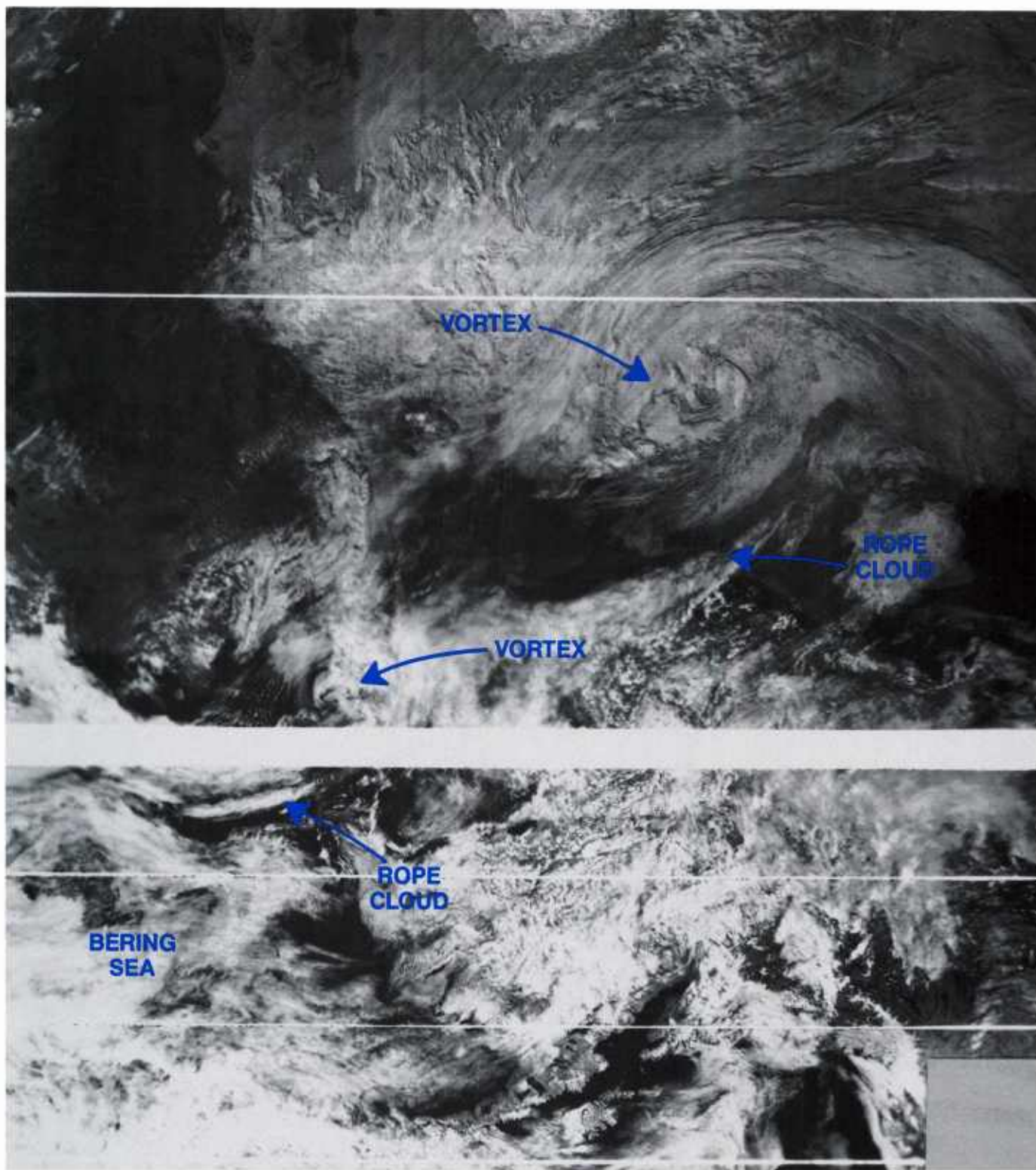
1A-66a DMSP visible (LS) data. 2219 GMT 25 July 1982.



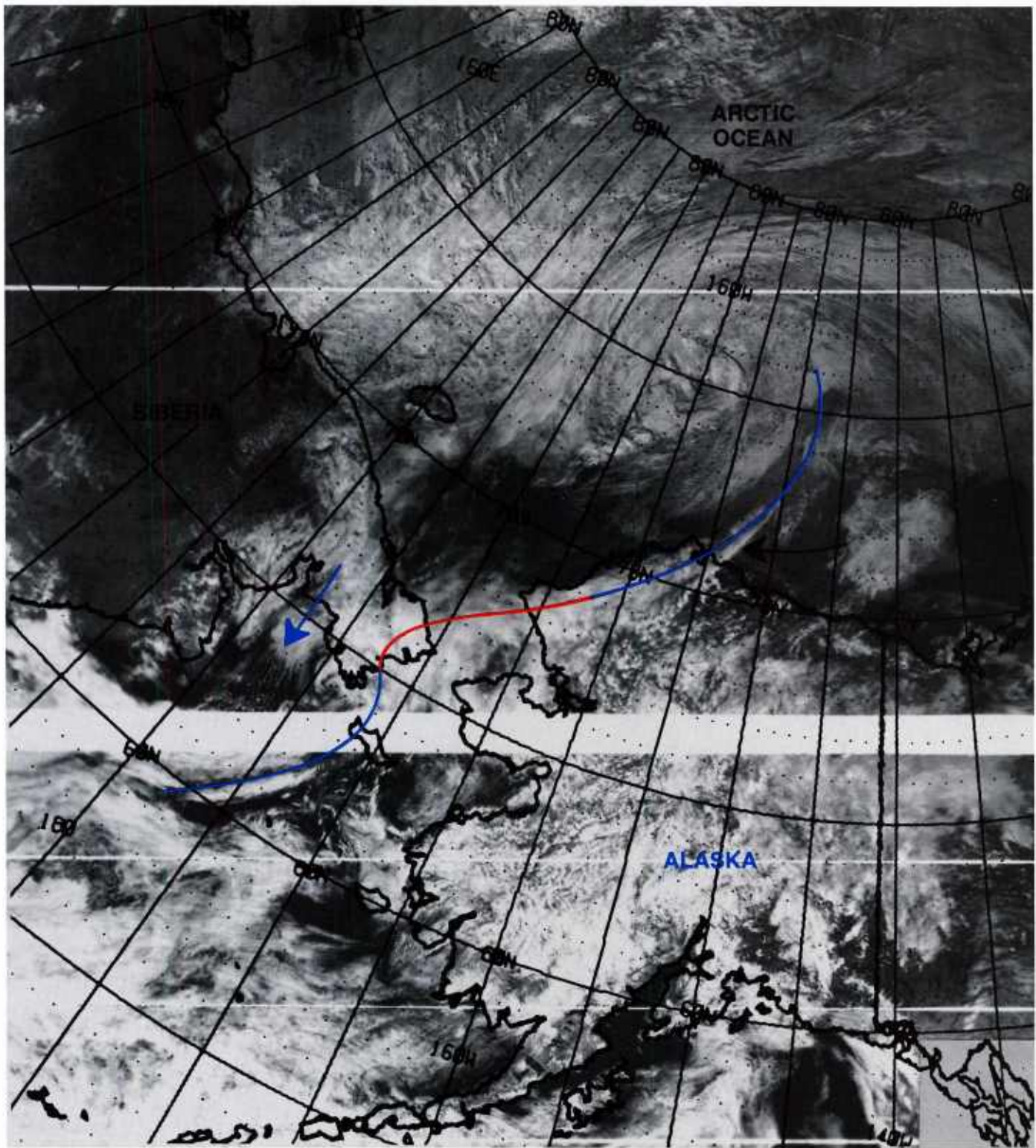


1A-67a DMSP visible (LS) data. 2219 GMT 25 July 1982, with overlay.





1A-68a DMSP visible (LS) data. 0001 GMT 26 July 1982.



1A-69a DMSP visible (LS) data. 0001 GMT 26 July 1982, with overlay.

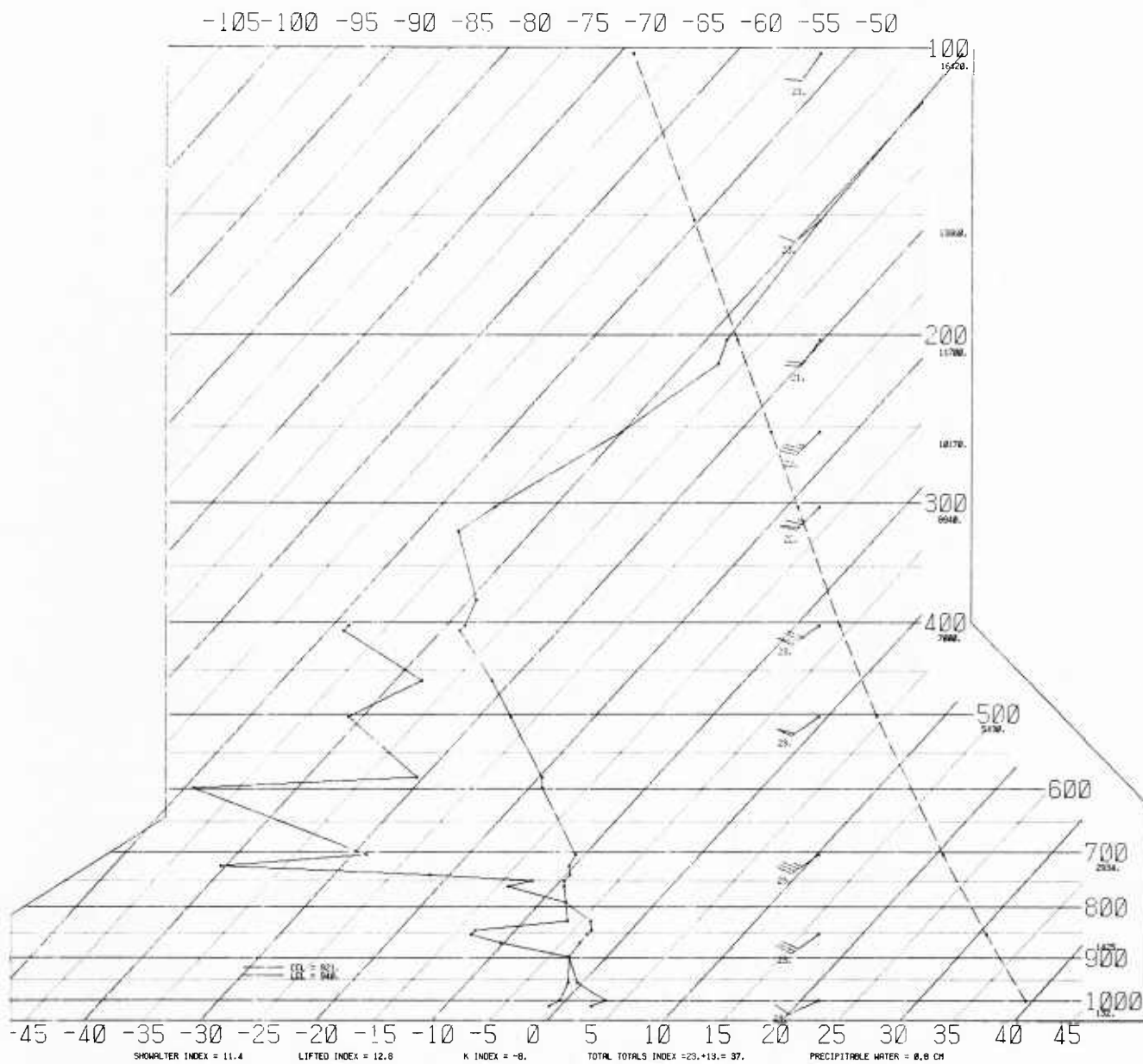


# SKEW T. LOG P DIAGRAM

820726

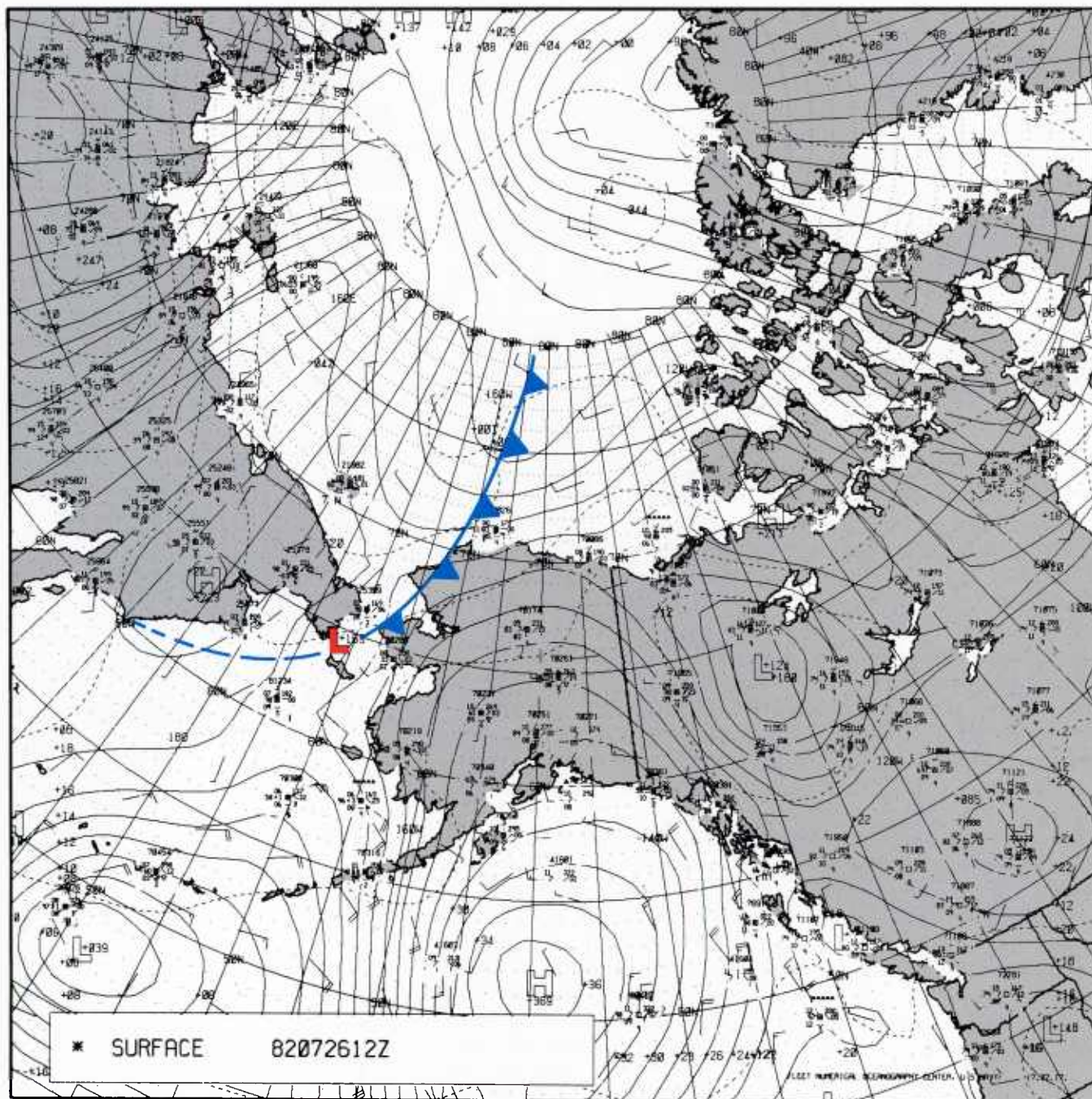
0000Z

70026



1A-70a Radiosonde data, Barrow, Alaska. 0000 GMT 26 July 1982.

The FNOC surface analysis for 1200 GMT (Fig. 1A-71a) shows low pressure dissipating over the Chukchi Sea with only a trough remaining, and the southernmost low near the Bering Strait filling from 1012.8 to 1016.5 mb. The deep meridional trough still connects the two areas and extends further southward into the Bering Sea. The NMC 1200 GMT frontal position in its northern portion has been superimposed on this analysis. The analysis indicates that the front has not yet passed Barrow, which shows a nonchanging 3 hourly pressure tendency.



1A-71a FNOC surface analysis. 1200 GMT 26 July 1982.



The FNOC 500-mb analysis for 1200 GMT (Fig. 1A-72a) also does not show much change in movement from the previous analysis (Fig. 1A-65a). A cold  $-25^{\circ}\text{C}$  isotherm continues to encircle low mesoscale centers still evident on the latter analysis. The Barrow sounding for 1200 GMT (Fig. 1A-73a) shows little change in wind direction or speed in comparison to the previous sounding (Fig. 1A-70a). The strong winds increasing in speed with height reach 50 kt and higher above 500 mb.

DMSP infrared (TS) data acquired at 1300 GMT (Fig. 1A-74a) suggest that neither of the low systems and associated cloud vortices have developed appreciably. In fact, they are difficult to locate precisely based on this particular image. The cold front drawn on this image does not extend as far north as the NMC analysis suggested, nor does it swing westward in its southern portion as indicated by NMC. Such positioning seems illogical based on satellite evidence of little cloud cover in those areas.

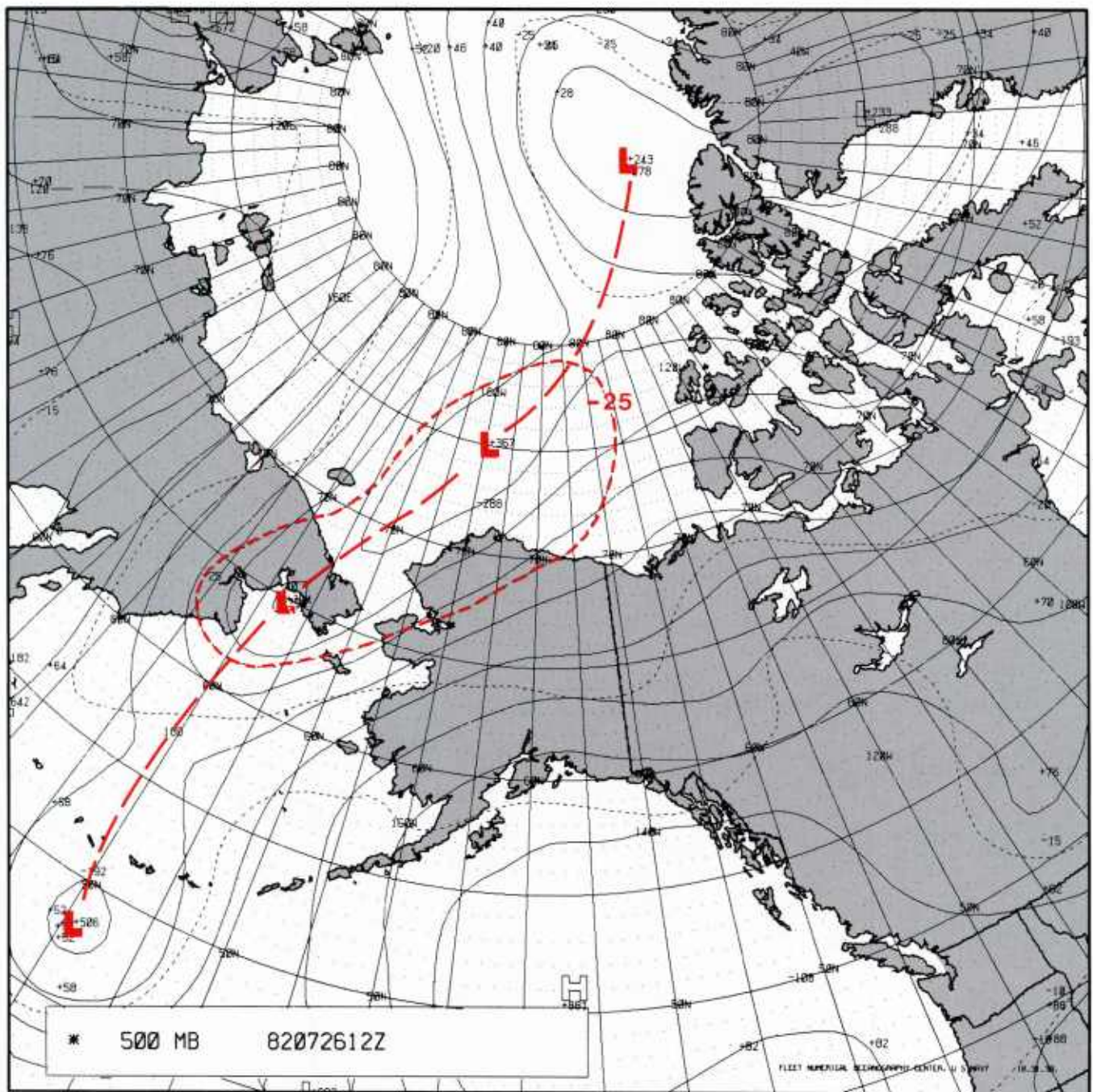
Evidence of gravity waves appears over the extreme northwest region of Alaska, near the frontal zone. This also relates well to the strong winds increasing with height in that region as suggested by the Barrow sounding (Fig. 1A-73a).

An enlarged DMSP visible channel (LF) view of the area in data acquired at 1449 GMT is shown in Fig. 1A-75a. The visible view shows detailed structure of the wave cloud and does suggest a low-level vortex near  $74^{\circ}\text{N}$   $168^{\circ}\text{W}$  to the northwest of the suggested jetstream axis.

Ridging over Alaska, evident at 1200 GMT (Fig. 1A-71a) continued as shown on the FNOC surface analysis for 1800 GMT (Fig. 1A-76a). The previously analyzed low near the Bering Strait moved sharply south-southeastward to a position just west of Bristol Bay. The storm appears to have deepened. Extremely strong winds are entering the storm's eastern quadrant. Not much evidence appears on this analysis of any development near the Bering Strait.

The DMSP infrared (TS) image for 2207 GMT (Fig. 1A-77a) shows evidence of ridging over Alaska using gravity wave indications and cloud streets as indicators of wind direction. The clear slot extending south from the Kenai Peninsula into the Gulf of Alaska is caused by and coincides with a sharp ridge over that region, also shown very distinctly in the FNOC surface analysis (Fig. 1A-76a).

More important for the purposes of this study is first evidence of impending rapid cyclogenesis shown in the region north of the Bering Strait, due west of Point Barrow. In this region small, comma-shaped cloud clusters appear, adjacent to a pronounced band of striated cirrus, associated with the jetstream in that region. This occurrence approximates Weldon's Phase I stage of meridional trough cyclogenesis, although the comma areas are not under the cirrus band as shown in Weldon's classic diagram (Fig. 1A-63a). Note that cloudiness north of the trough over the Arctic Ocean, leading to a multiple vortex region near the pole has begun slipping southward (compare Fig. 1A-77a with Fig. 1A-74a).



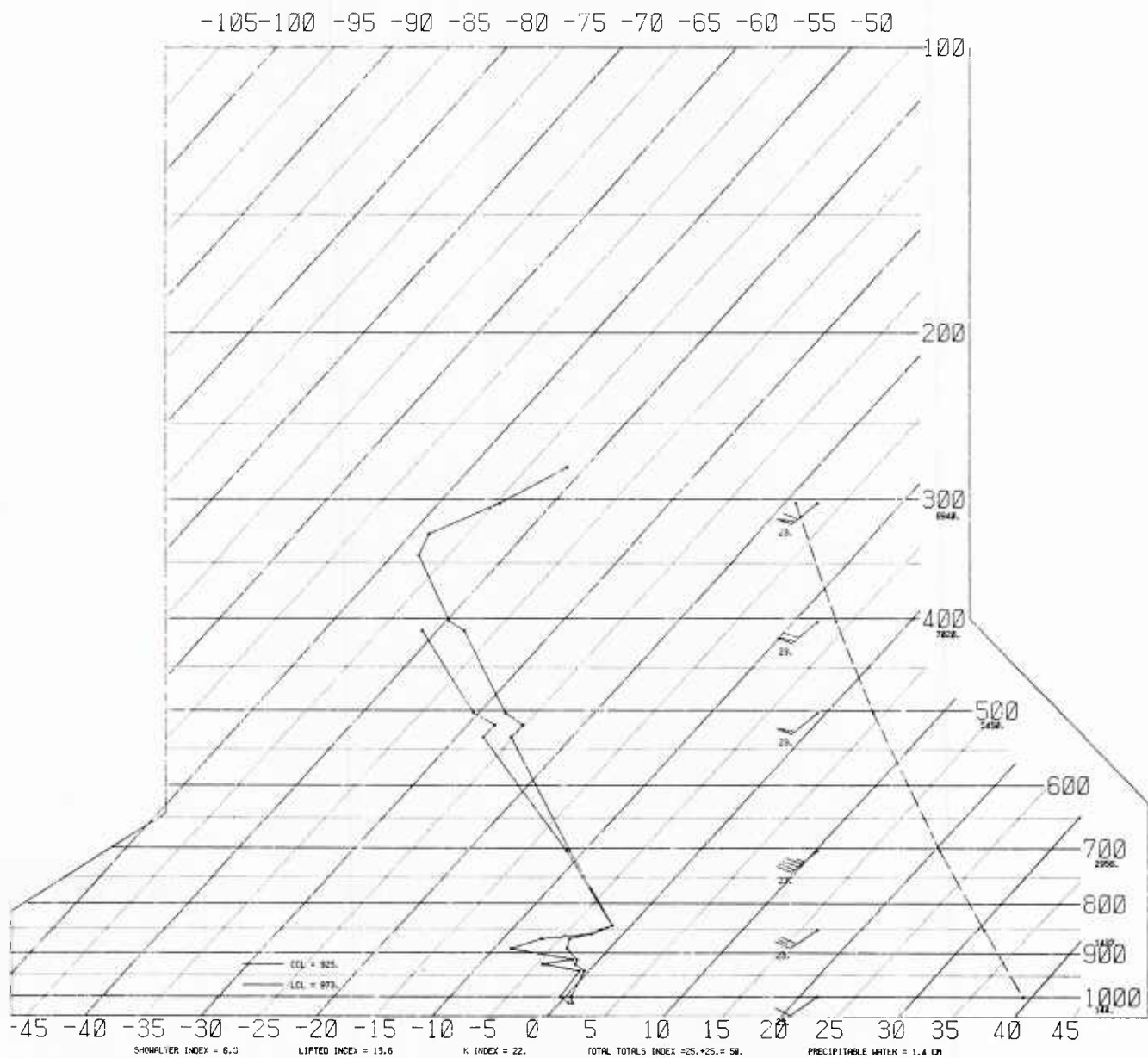


# SKEW T, LOG P DIAGRAM

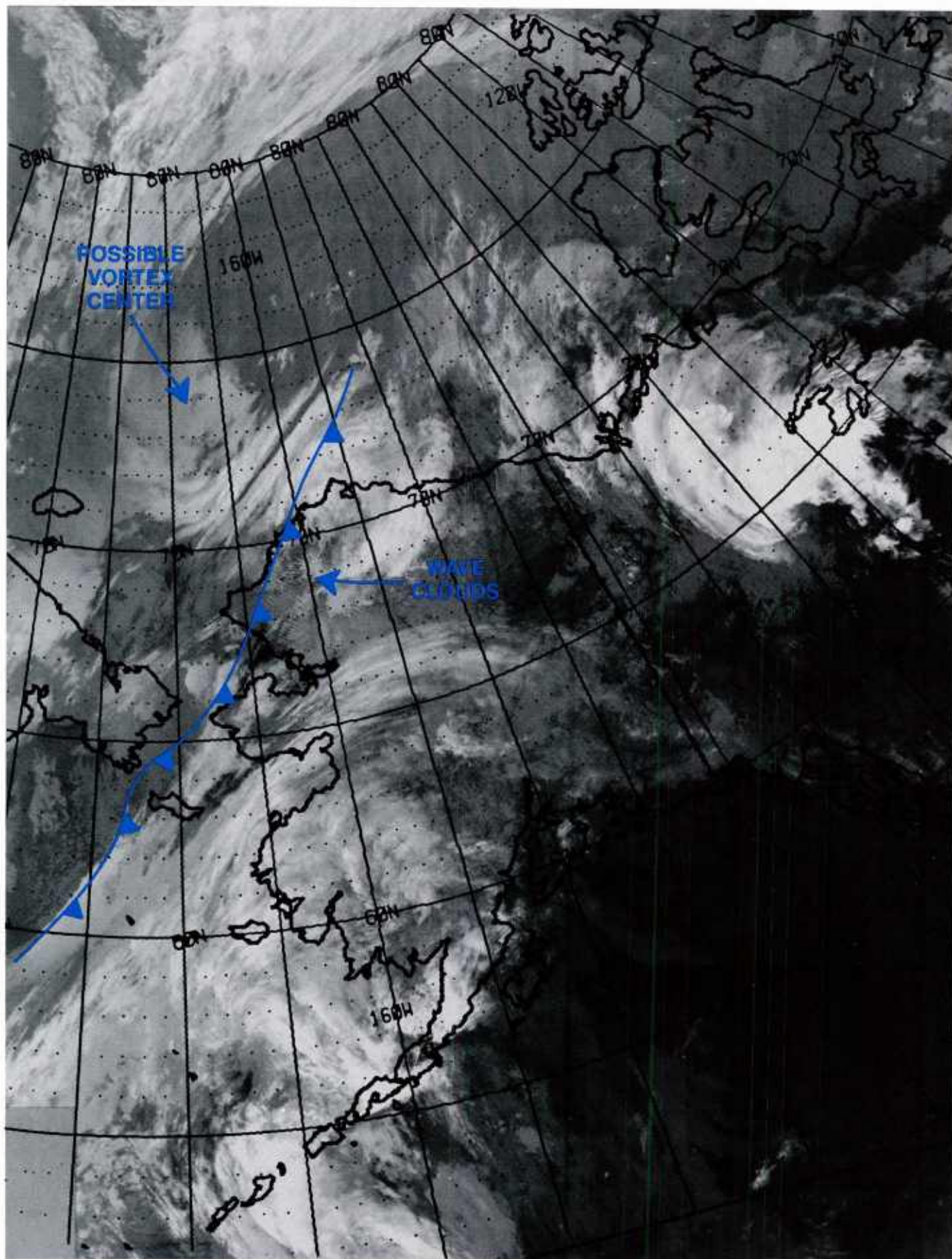
820726

1200Z

70026

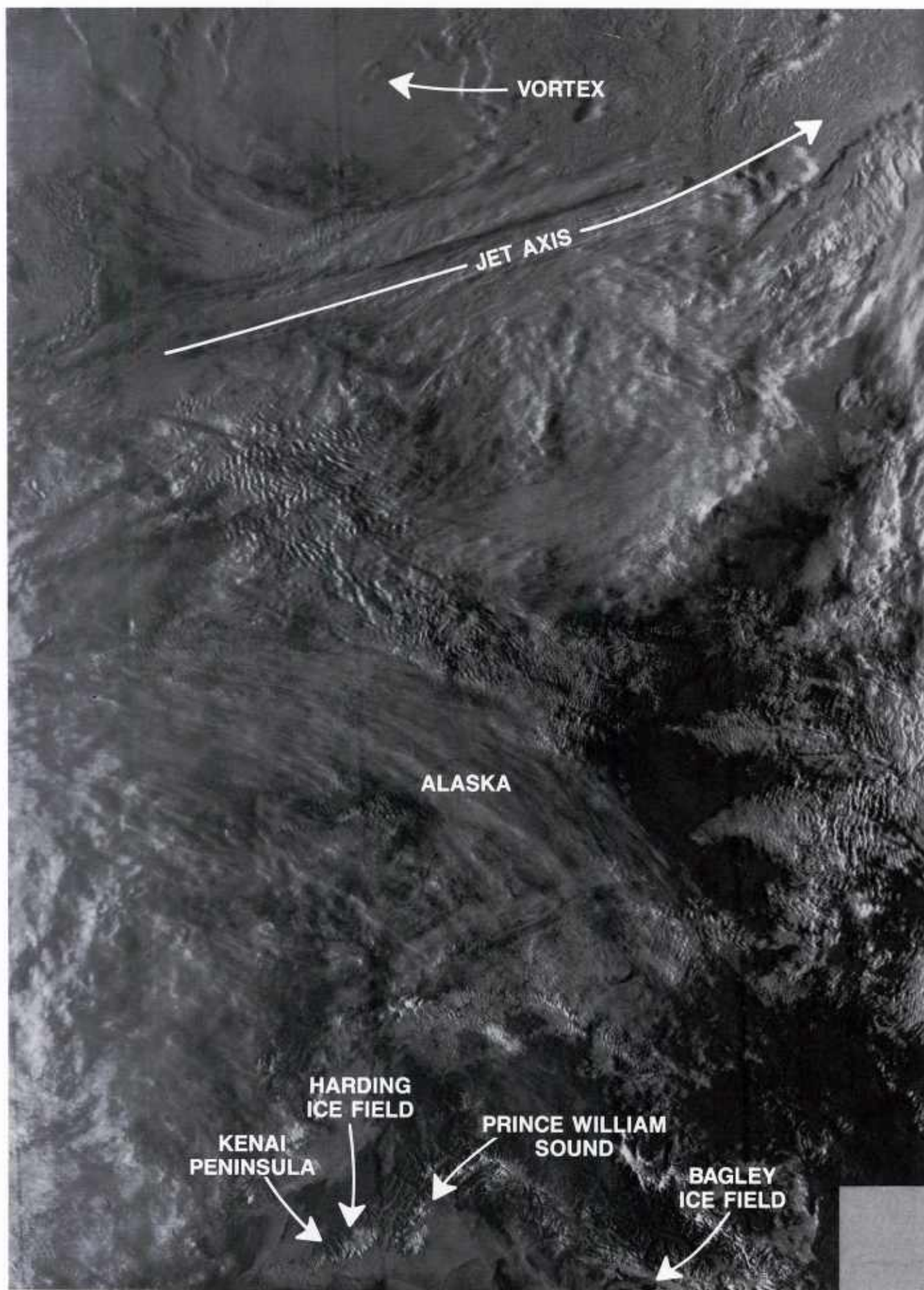


1A-73a Radiosonde data, Barrow, Alaska. 1200 GMT 26 July 1982.



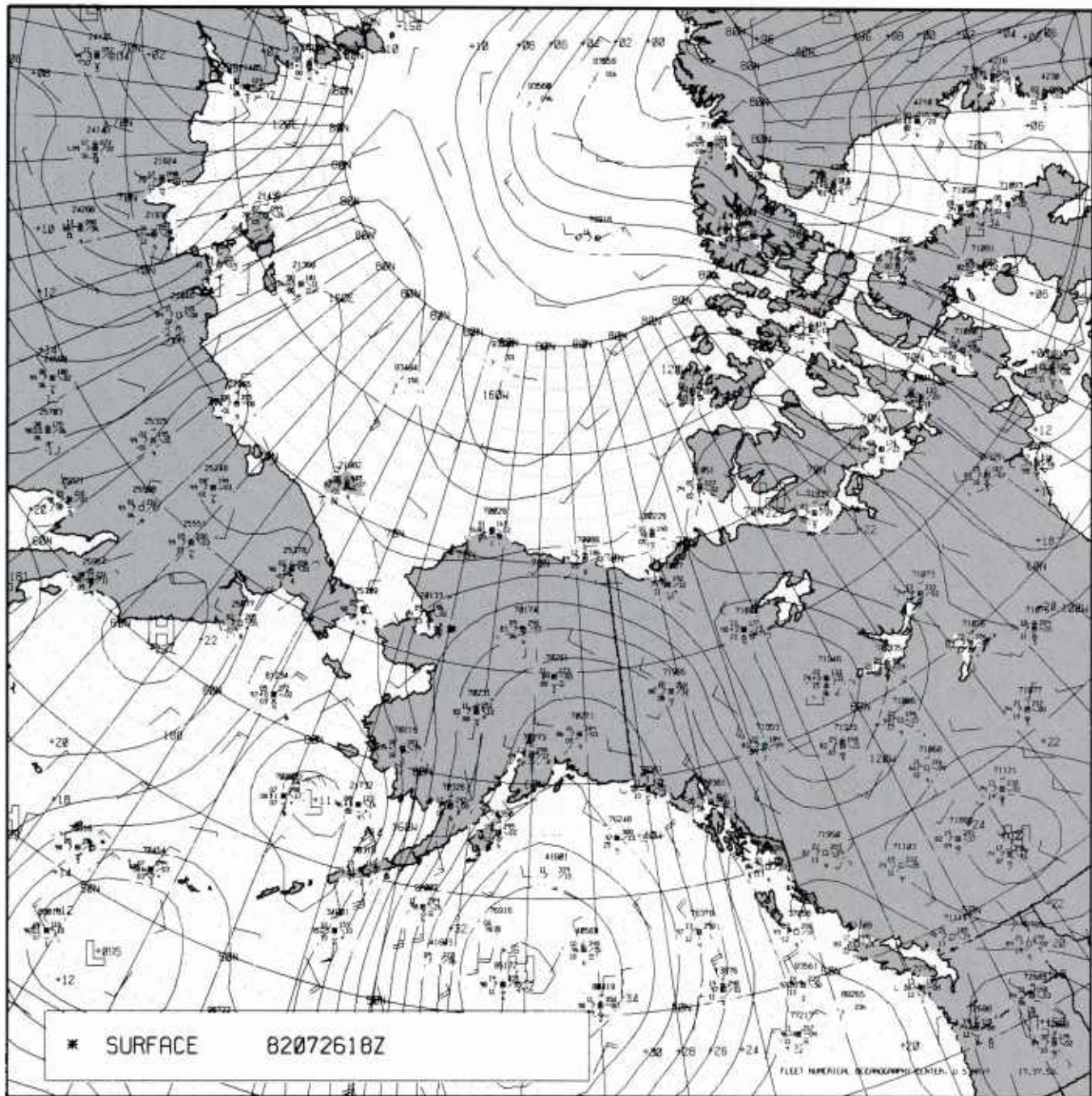
1A-74a DMSP infrared (TS) data. 1300 GMT 26 July 1982, with overlay.





1A-75a DMSP visible (LF) data (enlarged). 1449 GMT 26 July 1982, with overlay.

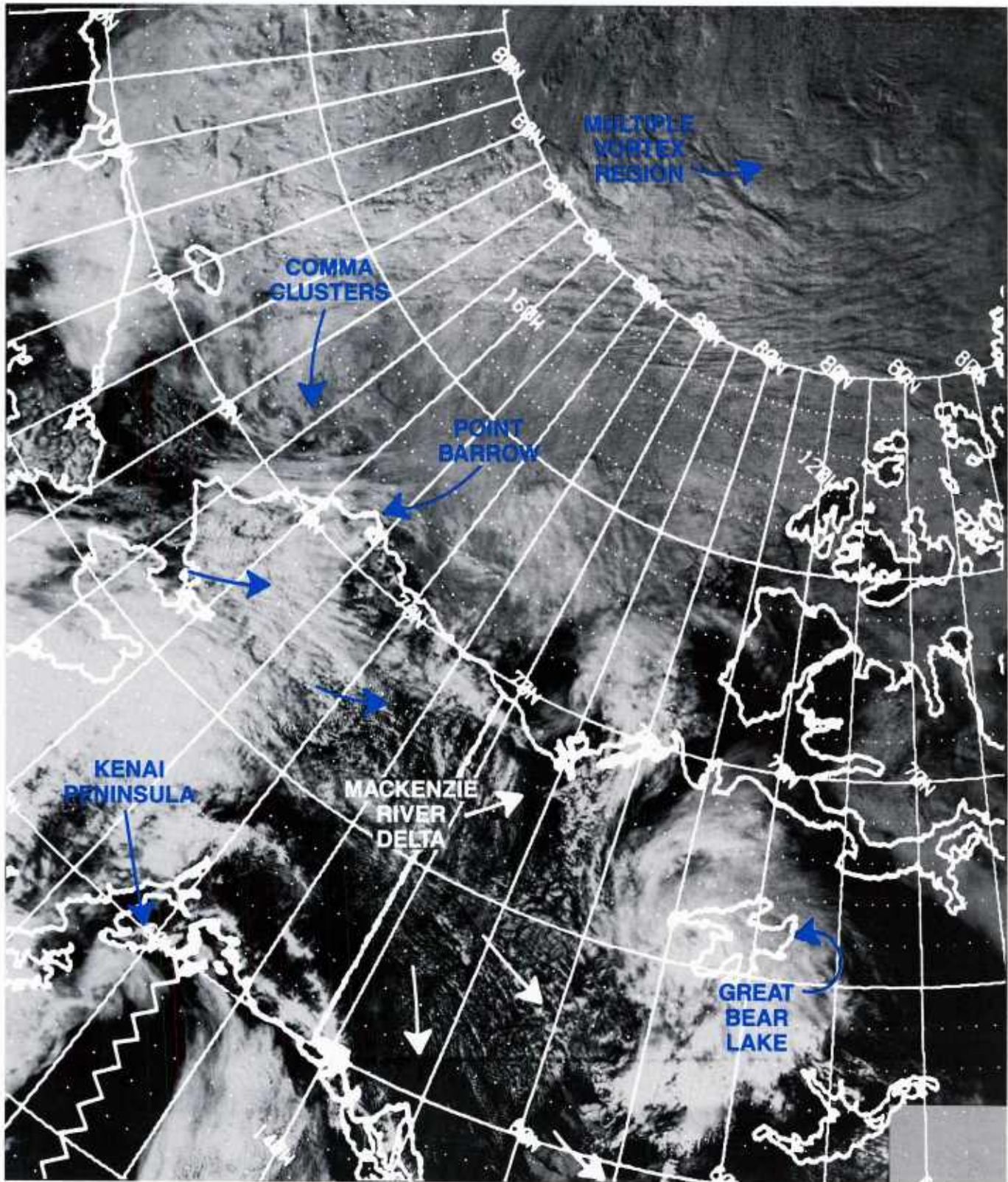




1A-76a FNOC surface analysis. 1800 GMT 26 July 1982.



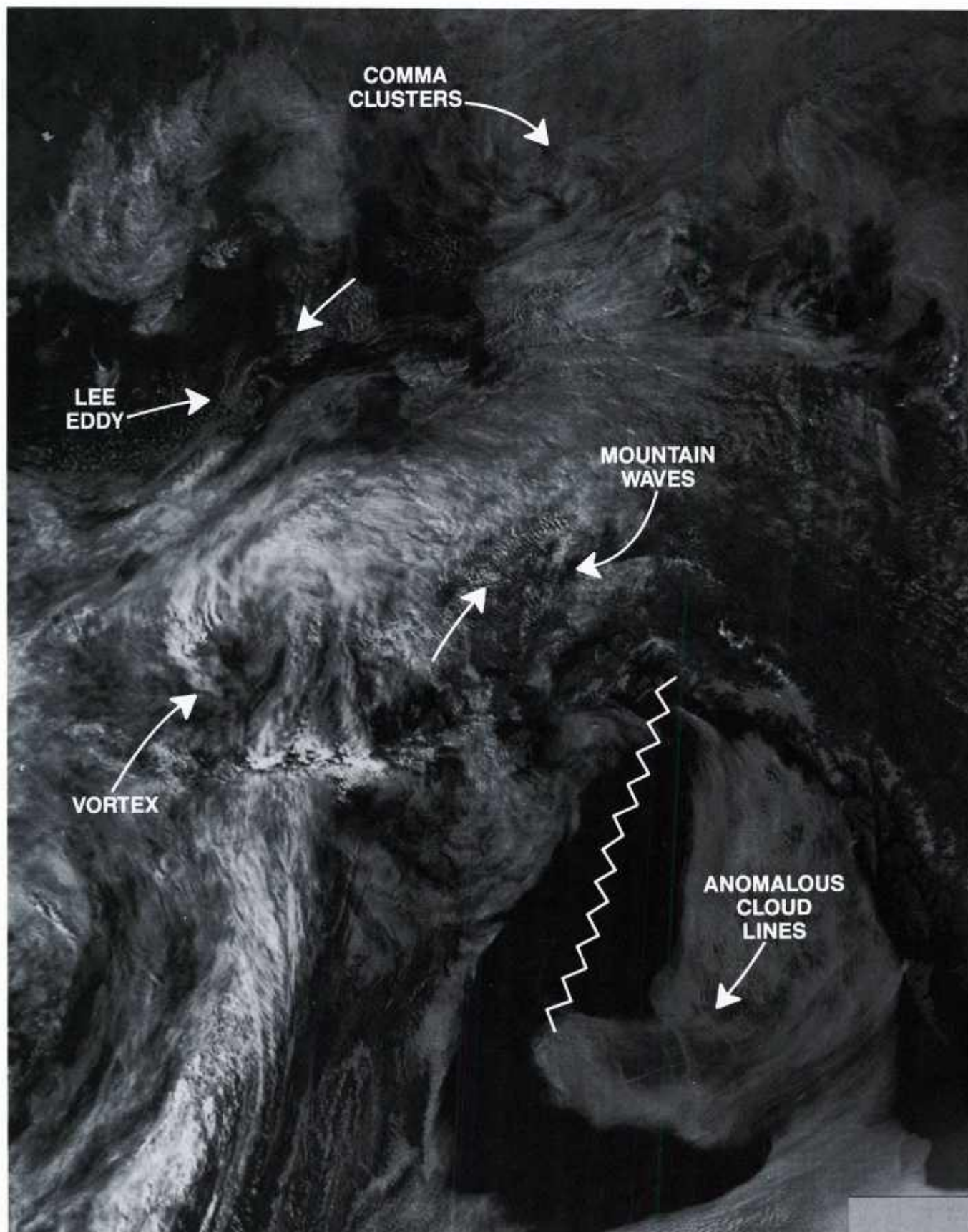
Also notable in Fig. 1A-77a is the strong cyclone development apparent over Great Bear Lake and a small additional development north of the Mackenzie River Delta. The delta region is characterized as a low, swampy, flooded region and this is apparent in the DMSP data, which show no cumulus development over that region, being deprived of the significant heating effect dry land would provide.



1A-77a DMSP visible (LS) data. 2207 GMT 26 July 1982, with overlay.



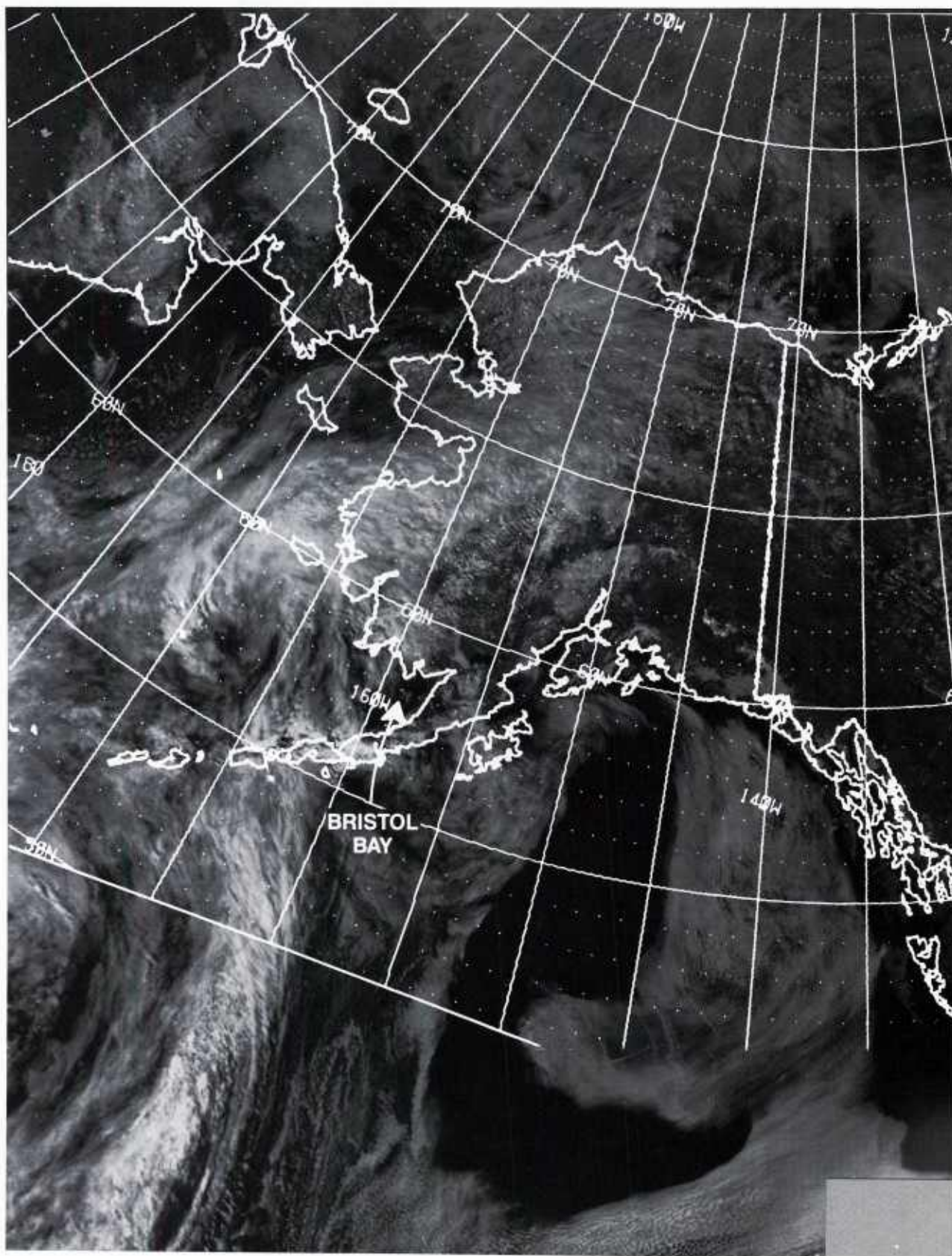
A DMSP visible channel (LS) view approximately 1½ hr later (Fig. 1A-78a) shows some slight intensification in convection within the comma cloud cluster group but no indication of deeper cyclogenesis. The vortex west of Bristol Bay appears quite intense with some embedded heavy deep convection.



1A-78a DMSP visible (LS) data. 2349 GMT 26 July 1982.



On a local scale the lee eddy south of the Chukchi Peninsula implies northerly flow in that region, while gravity waves over southeast Alaska imply southerly flow in that region, consistent with the cyclonic circulation between the two areas. The clear slot, implying a ridge line south of the Kenai Peninsula, persists on the image. Anomalous cloud lines near the high center imply fog and low ceilings in the vicinity. A gridded version of this image appears as Fig. 1A-79a.



1A-79a DMSP visible (LS) data. 2349 GMT 26 July 1982, with overlay.

27 July 1982

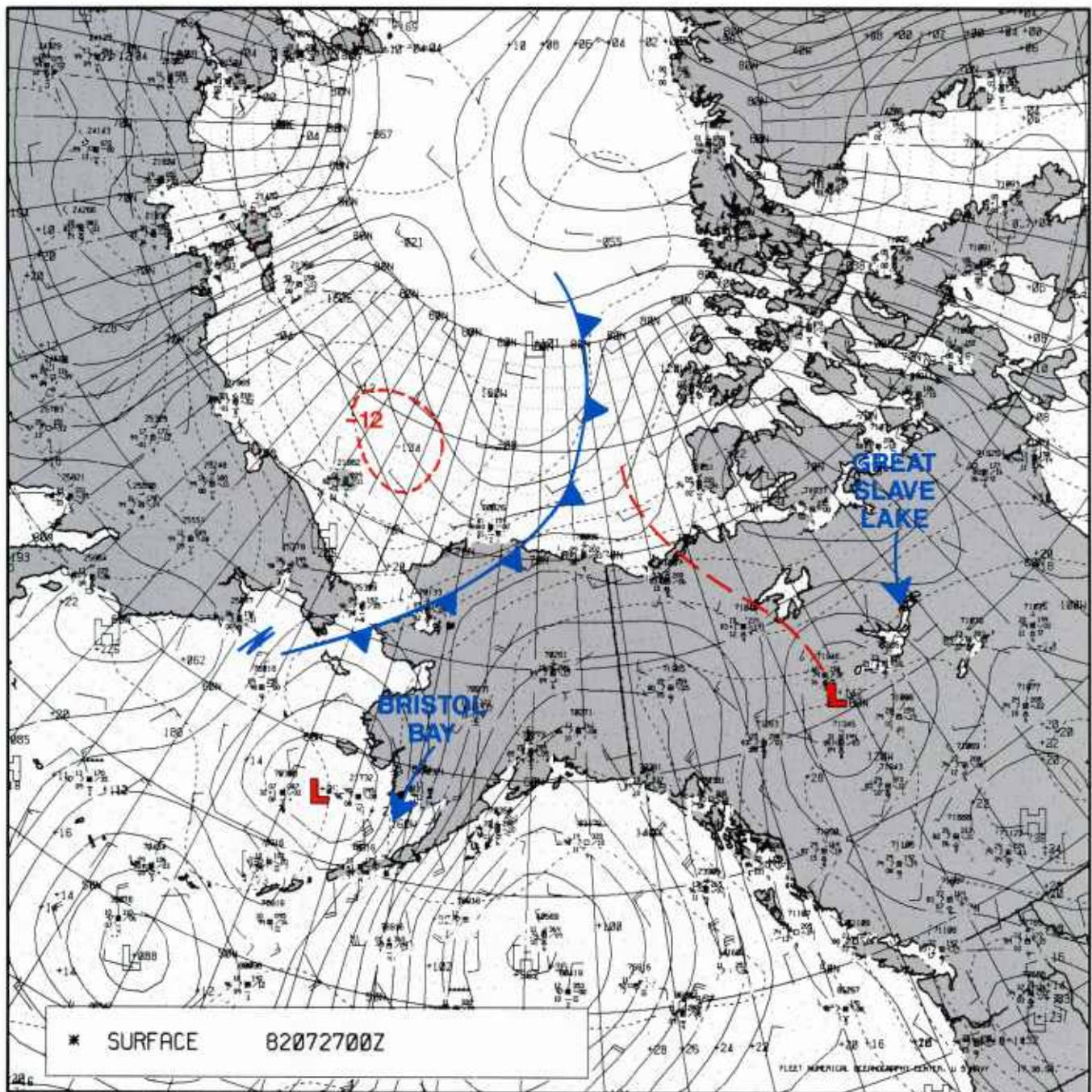
The FNOC 0000 GMT surface analysis (Fig. 1A-80a) with the NMC frontal position superimposed shows frontal movement past Point Barrow, but no serious signs of cyclogenesis along the North Slope at that time. The front is seen to be located in a region of packed isotherms with a cold ( $-12^{\circ}\text{C}$ ) pool of air behind the front over the Chukchi Sea. The low near Bristol Bay has deepened slightly with strong winds still entering its eastern quadrant. Ridging persists over Alaska, drifting slowly eastward, and a trough extends from Mackenzie Bay southeastward to a low near Great Slave Lake.

The FNOC 500-mb analysis (Fig. 1A-81a) shows the cold meridional trough now beginning to drift slowly eastward. Its position lags the surface position by several degrees. The 0000 GMT Barrow sounding (Fig. 1A-82a) shows that the trough, at levels 700 mb and above, had still not passed this location. Surface winds, however, were from the northwest, indicating frontal passage at this level, as shown in Fig. 1A-80a. By 1200 GMT (Fig. 1A-83a) winds had shifted at all levels reflecting the event.

The first DMSP image available on 27 July (Fig. 1A-84a) was an infrared (TS) view acquired at 1100 GMT. The image shows a classic view of the vorticity comma head emerging from the frontal band adjacent to a "V"-shaped convective cloud cluster formed by diverging upper level flow, with one branch turning strongly anticyclonically over Alaska, and the other branch turning cyclonically around the upper level low. Powerful vertical motion is induced within the cloud cluster by the upper level divergence. A lowering of pressure in the region is intimately associated with this pattern. It is important to note that the surface low is expected to be under the cirrus shield, near the inflection point, where flow changes from straight or cyclonic at upper levels to anticyclonic. This position has been marked by an *L* in Fig. 1A-84a. The position is several degrees east of the probable upper level position at this time. As Weldon (1975) indicated, "There is a tendency for the surface and upper level centers to rotate cyclonically with respect to each other, getting closer together until the systems are stacked vertically." Note that a secondary comma-shaped pattern of low cloudiness is apparent to the northeast of the major development. Convective comma cloud development to the southeast indicates additional vorticity associated with this system. The nearby presence of an upper cold low or trough is indicated by the cluster of cumulonimbus clouds to the southeast of the comma. Such juxtaposition is confirmed by the FNOC 500-mb analysis for 1200 GMT (Fig. 1A-85a). The position of an upper cold low immediately west of the thunderstorm area is shown in this analysis. The analysis obviously could have been adjusted slightly to show a cold trough over the thunderstorm area. The particular configuration shown in the satellite data would ordinarily imply strong potential for polar low development. However, a gridded version of the image (Fig. 1A-85b) shows that the systems will shortly be advected over land. Therefore, further strong intensification would seem improbable, since polar lows, like tropical cyclones, derive much of their energy from air-sea interaction.

Further to the south near Great Slave Lake, a cloud formation, sometimes called a "White Tornado," is evident (see NTAG Vol. 6, Section 1C: Fett et al., 1986). Such cloud formations are always associated with severe thunderstorms and, frequently, tornadic activity. From the foregoing discussion evidence of tremendous cloud development activity is shown, as documented by this one image.





1A-80a FNOC surface analysis. 0000 GMT 27 July 1982.





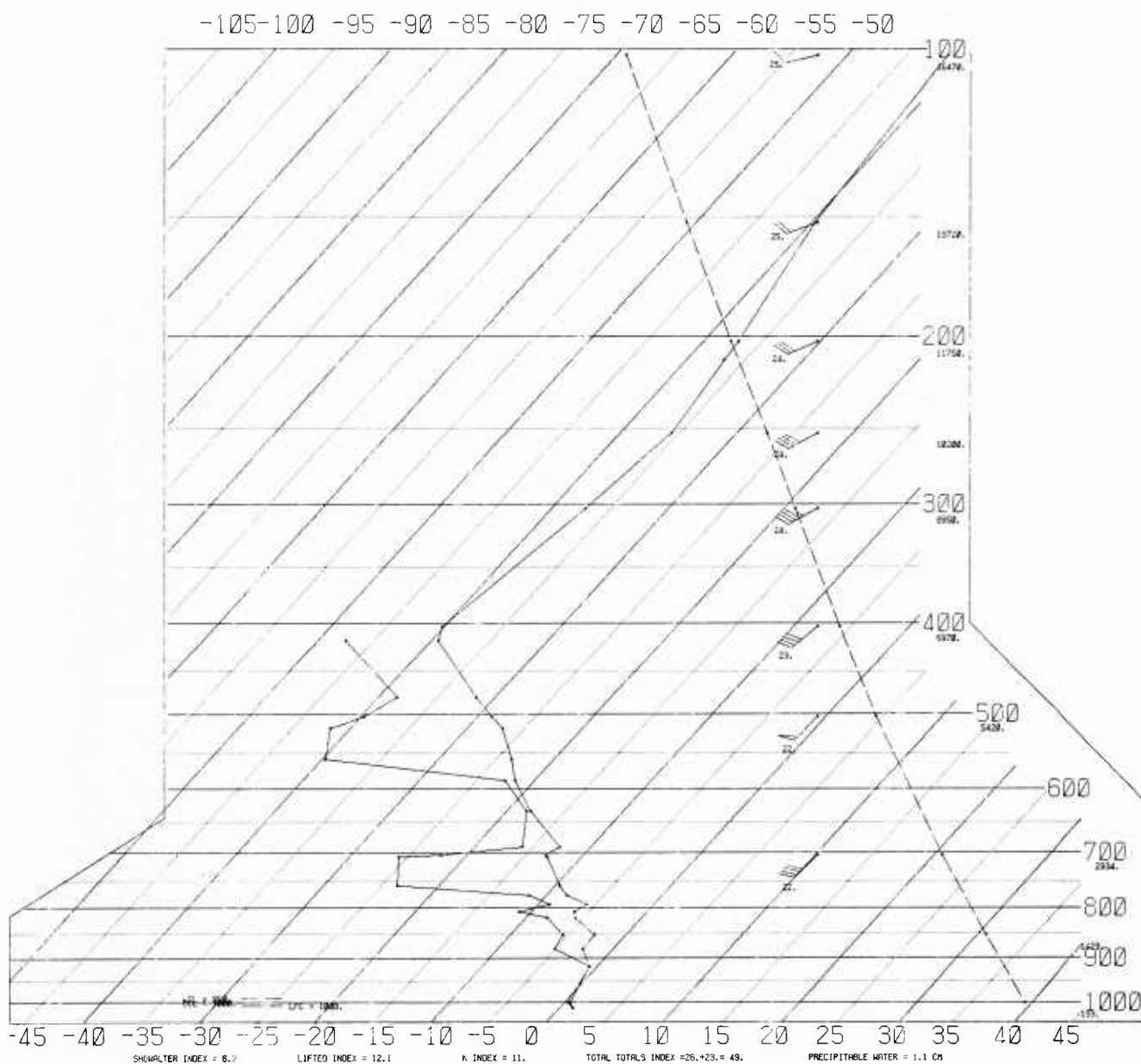


# SKEW T, LOG P DIAGRAM

820727

0000Z

70026



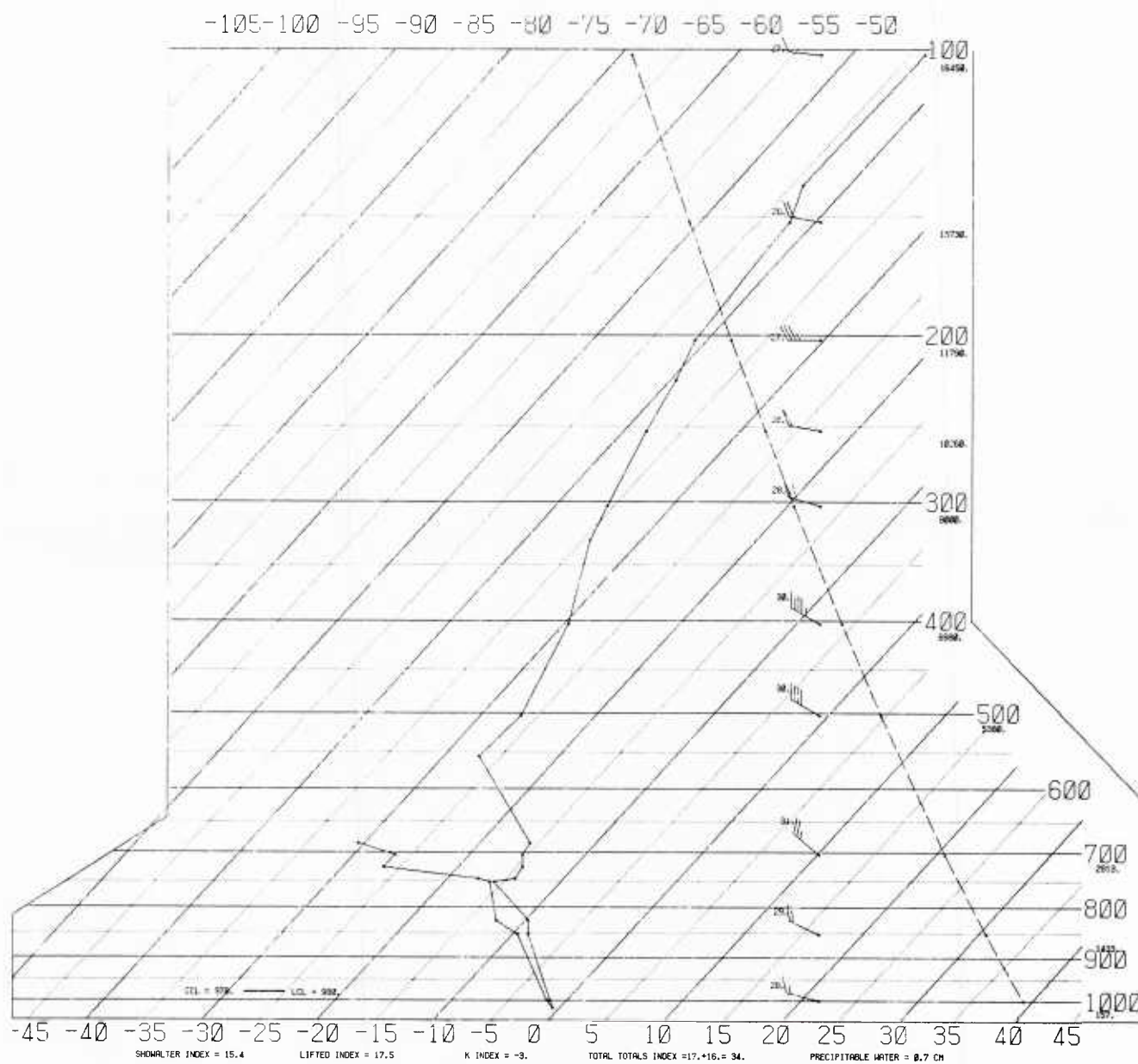
1A-82a Radiosonde data, Barrow, Alaska. 0000 GMT 27 July 1982.

# SKREW T, LOG P DIAGRAM

820727

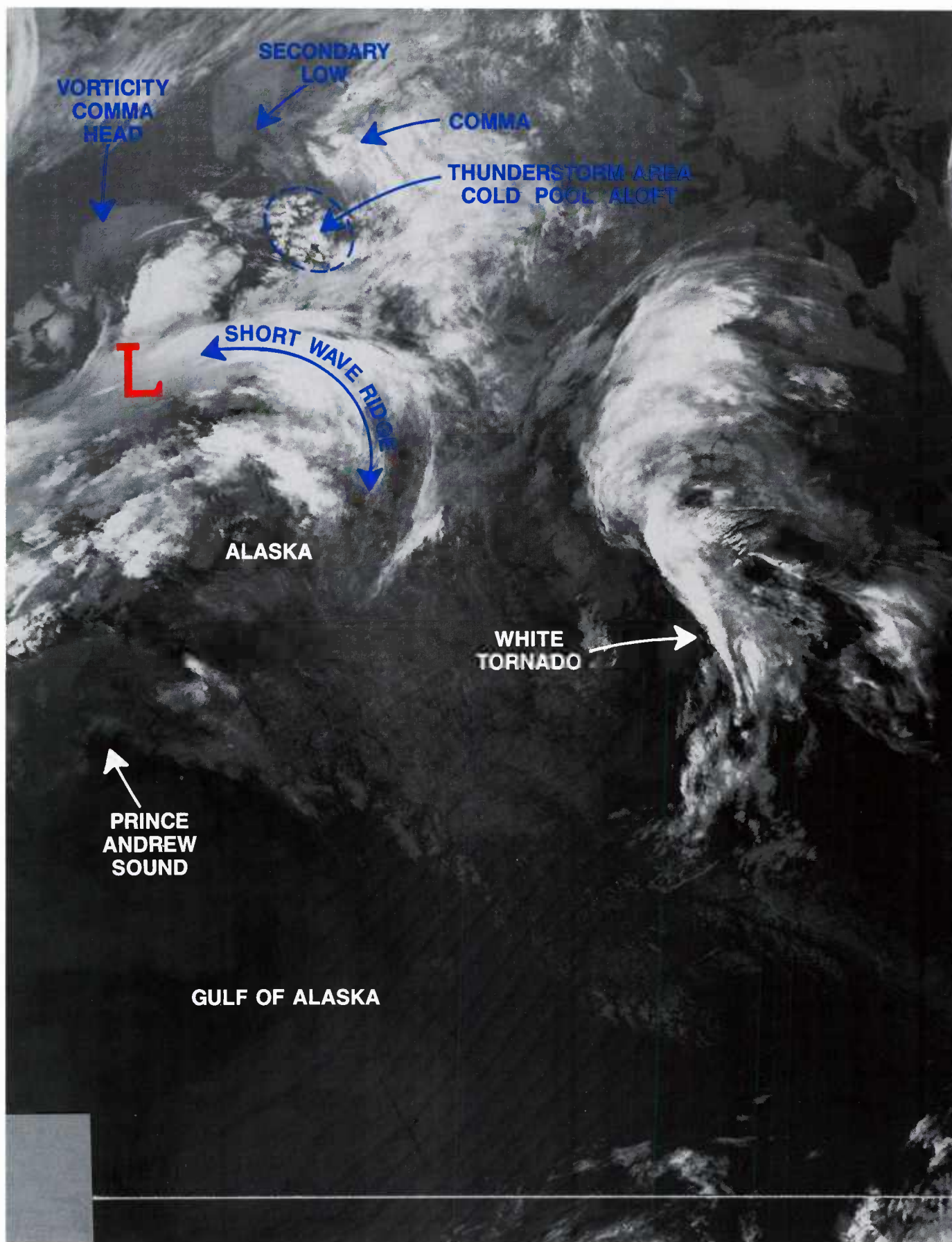
1200Z

70026

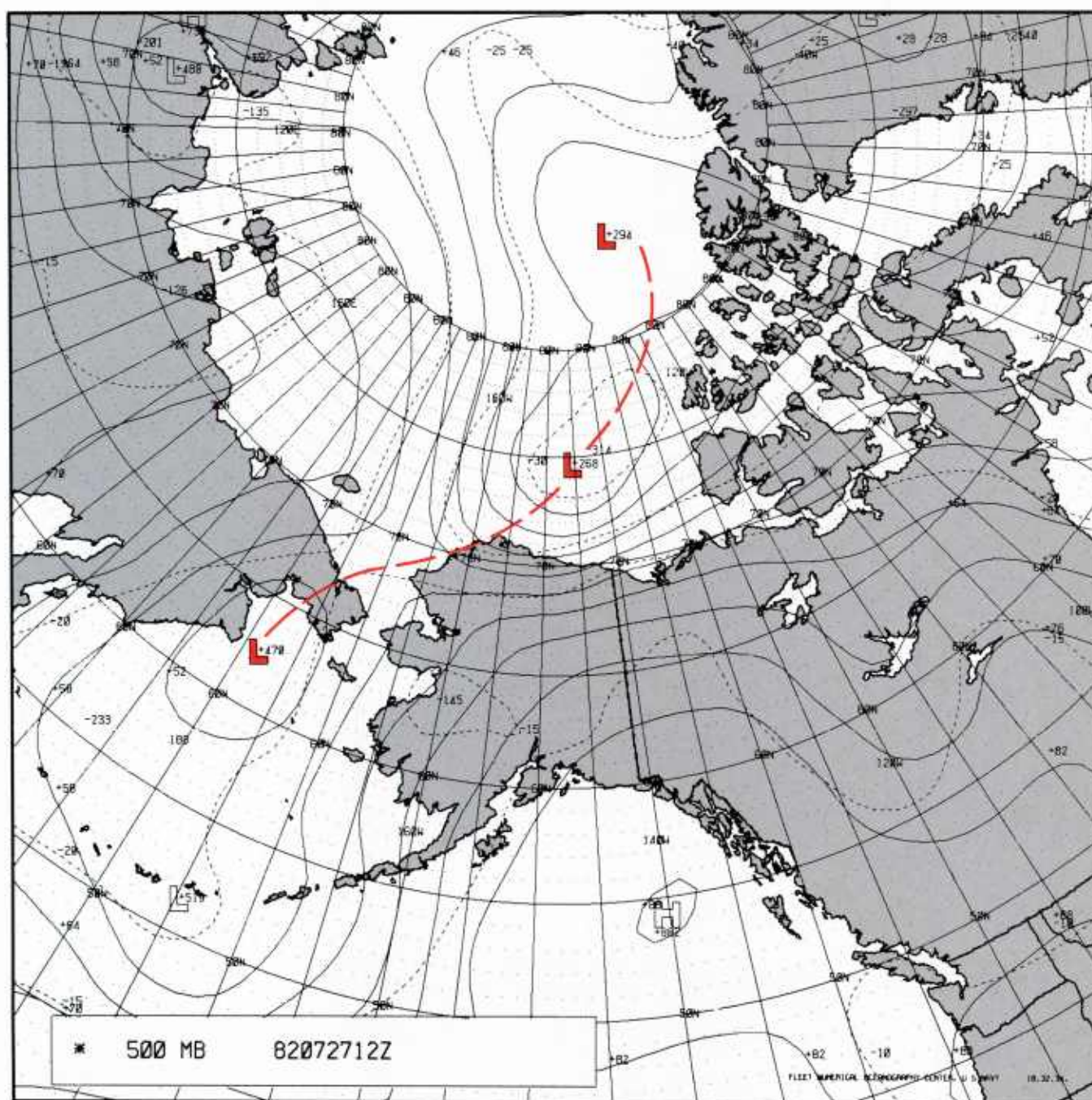


1A-83a Radiosonde data, Barrow, Alaska. 1200 GMT 27 July 1982.



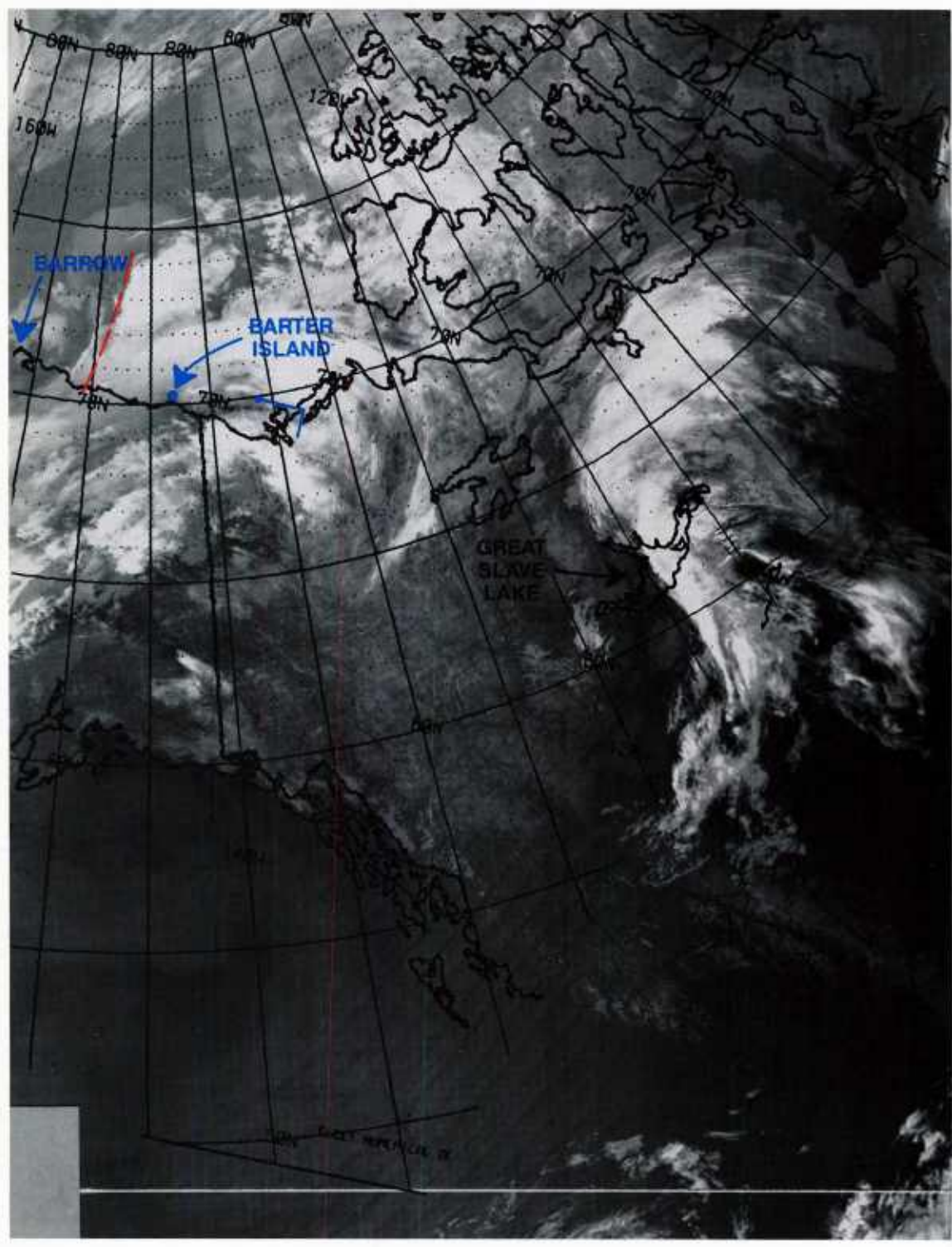


1A-84a DMSP infrared (TS) data. 1100 GMT 27 July 1982.



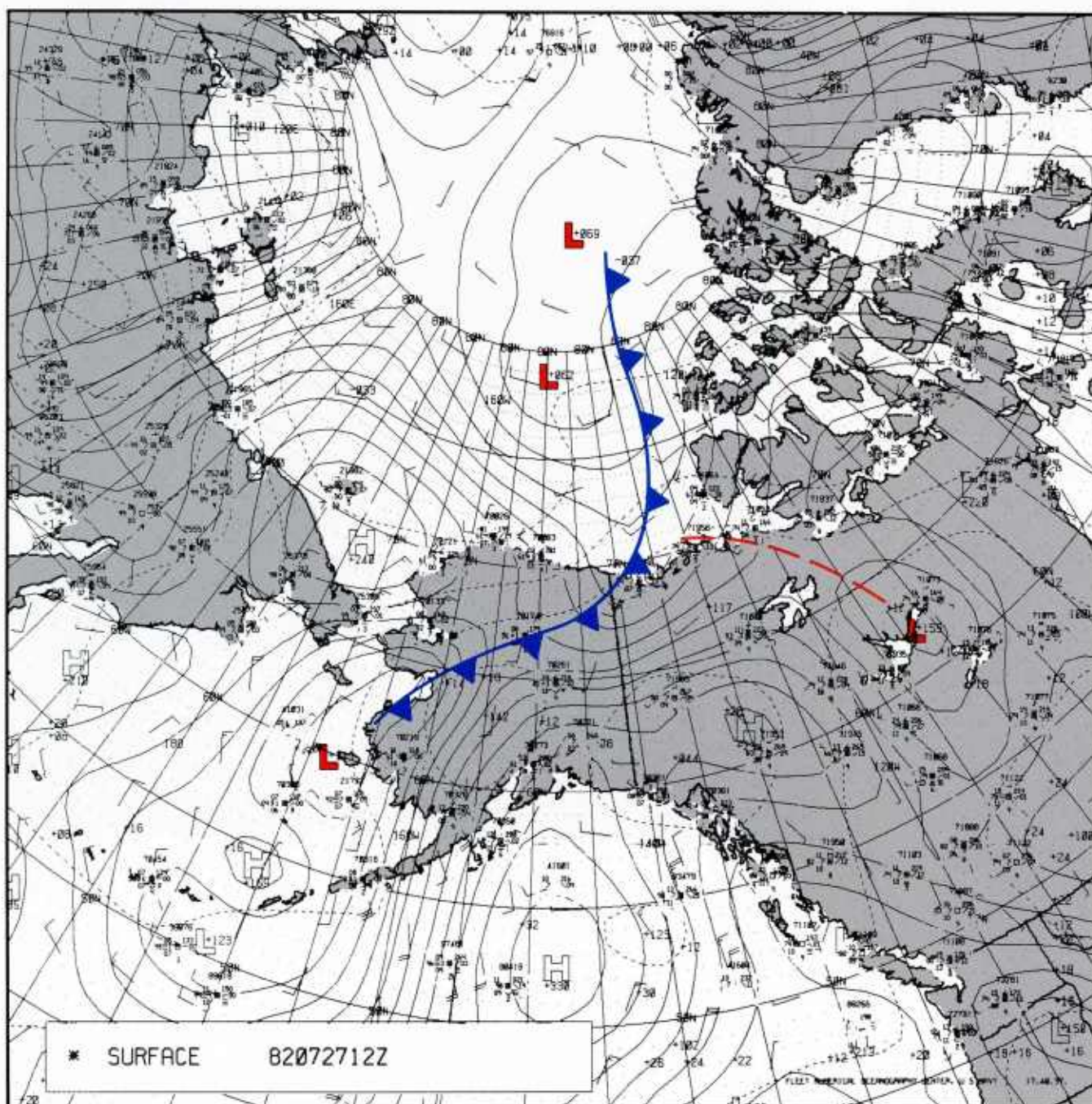
1A-85a FNOC 500-mb analysis. 1200 GMT 27 July 1982.





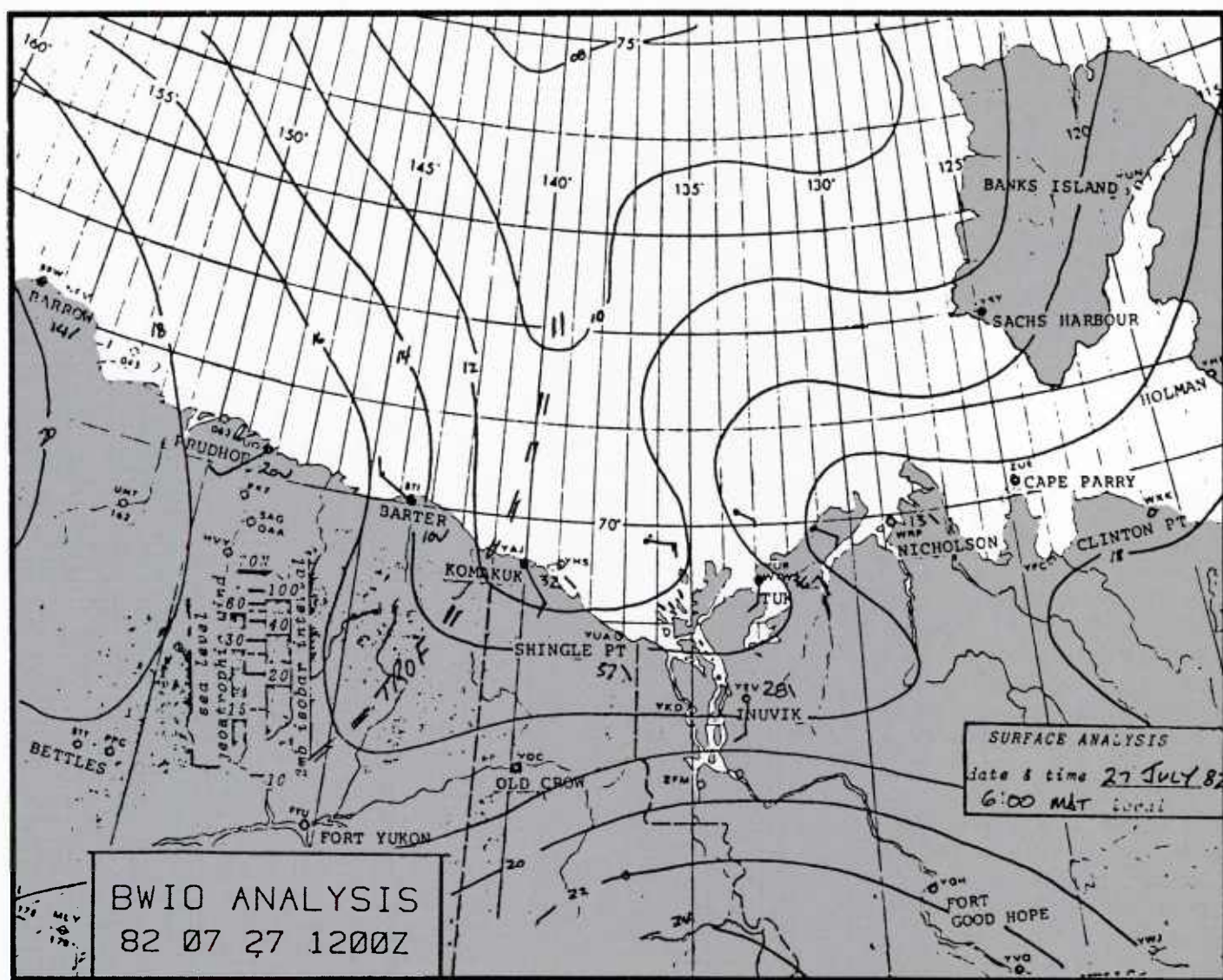
1A-85b DMSP infrared (TS) data. 1100 GMT 27 July 1982, with overlay.

The FNOC surface analysis for 1200 GMT (Fig. 1A-86a), with the NMC-derived frontal position superimposed, shows that the front had moved quite rapidly in the 12 hr since the preceding analysis (Fig. 1A-80a). A rate of 30 kt is implied. The Beaufort Weather Office surface analysis for the same time is shown for comparison (Fig. 1A-87a). The analysis reveals some of the 3-hourly pressure tendencies recorded as the system moved through the area. As indicated by Black (1982), "The pressure tendencies associated with the system became stronger as the low deepened. The 27/1200Z analysis shows a falling 37 tendency (falling 3.7 mb/3 hours) at Shingle Point, and a rising 20 at Deadhorse (Prudhoe Bay). At 27/1500Z, Inuvik showed falling 35, with Komakuk rising 48. By 27/1800Z the isallobaric gradient in Beaufort was at its strongest, with Nicholzen falling 49, Tarsiut rising 43, and Shingle Point rising 47."



1A-86a FNOC surface analysis. 1200 GMT 27 July 1982.





1A-87a Beaufort Weather Office surface analysis. 1200 GMT 27 July 1982.

An additional DMSP infrared (TS) view of the storm was acquired at 1300 GMT (Fig. 1A-88a). The storm systems have not changed dramatically in appearance from the preceding view (Fig. 1A-84a). However, the mesocyclone appearing on the north end of the convective complex is unique and especially well defined. An enlargement of the feature is shown in Fig. 1A-88b. Mesocyclones (having dimensions 4–40 km in meso beta scale) are associated with maximum downburst wind speeds of over 100 kt (Fujita, 1981). The suddenness of occurrence of such wind speeds can be devastating to ground structures, ships, oil rigs, etc., and upsetting to ground personnel in the region. Fortunately, this mesocyclone occurred well to the north, in the northern Beaufort Sea, some distance from human activities. Figure 1A-89a is a gridded version of the image to provide perspective.

The following comments by Black (1982) describe the severe weather effects that occurred on 27 July and are quoted essentially verbatim:

“By 1500Z, the low had definitely closed off, with a 1000 mb center at 70N 135W, just east of Tarsiut Island. Pressures were still falling 30–40 in advance. At 1600Z the M.V. Frank Broderick, 10 n mi west of Tarsiut, reported westerly winds gusting over 50 kt and 3 m waves.

“Tarsiut reported a wind shift from easterly to light westerly between 1300Z and 1500Z. Winds were 270/12 kt at 1600Z, increasing to 310/38G48 at 1700Z, and 310/50G65 at 1800Z. The last complete observation before evacuation of the island was taken at 1900Z. At that time, the winds were 310/48G63, and the significant wave height was 2½ metres. An unofficial report between 1900Z and 2000Z indicated the Tarsiut wind was a steady 60 kt from the northwest.

“The drillship Canmar Explorer 1, anchored 15 n mi east of Tarsiut at Kiggavik, reported a similar pattern. Gale force north westerlies developed by 1700Z, and persisted for 8 or 9 hours. At the Explorer 1, the maximum reported wind was 42 kt, and the maximum reported significant wave height was 4 metres. The weather record for Explorer 1 is incomplete, because the weather observer was too busy as a radio operator and air traffic controller to take observations. Tarsiut Island personnel were evacuated to Explorer 1, then transferred onshore.

“Three more drillships, the Canmar Explorers 2, 3, and 4, were anchored northeast of Tarsiut. They each reported 6 to 8 hours of gale force north-westerlies, with maximum winds of 40 kt, and significant wave heights reaching 4 to 5 metres.

“The pressure tendencies associated with the system became stronger as the low deepened. The 27/1200Z analysis shows a falling 37 tendency (falling 3.7 mb/3 hours) at Shingle Point, and a rising 20 at Deadhorse. At 27/1500Z, Inuvik showed falling 35, with Komakuk rising 48. By 27/1800Z the isallobaric gradient in the Beaufort was at its strongest, with Nicholzen falling 49, Tarsiut rising 43, and Shingle Point rising 47.

“The isallobaric gradient was strong enough to make an important contribution to the peak winds for the storm. Calculations show isallobaric wind components of the order of 30 knots at the peak of the storm.”

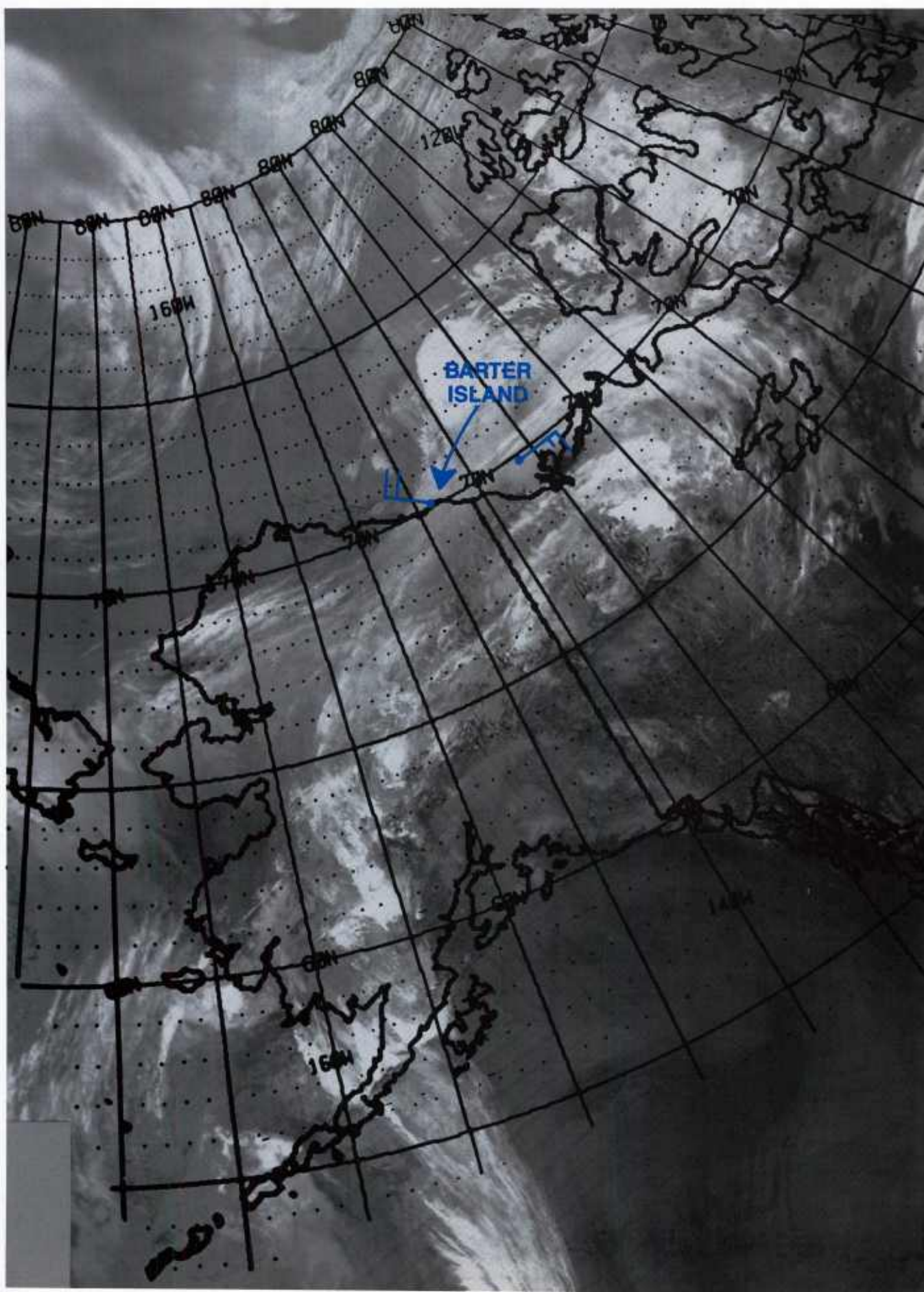




1A-88a DMSP infrared (TS) data 1300 GMT 27 July 1982.



1A-88b DMSP infrared (TS) data (enlarged). 1300 GMT 27 July 1982.



1A-89a DMSP infrared (TS) data. 1300 GMT 27 July 1982, with overlay.



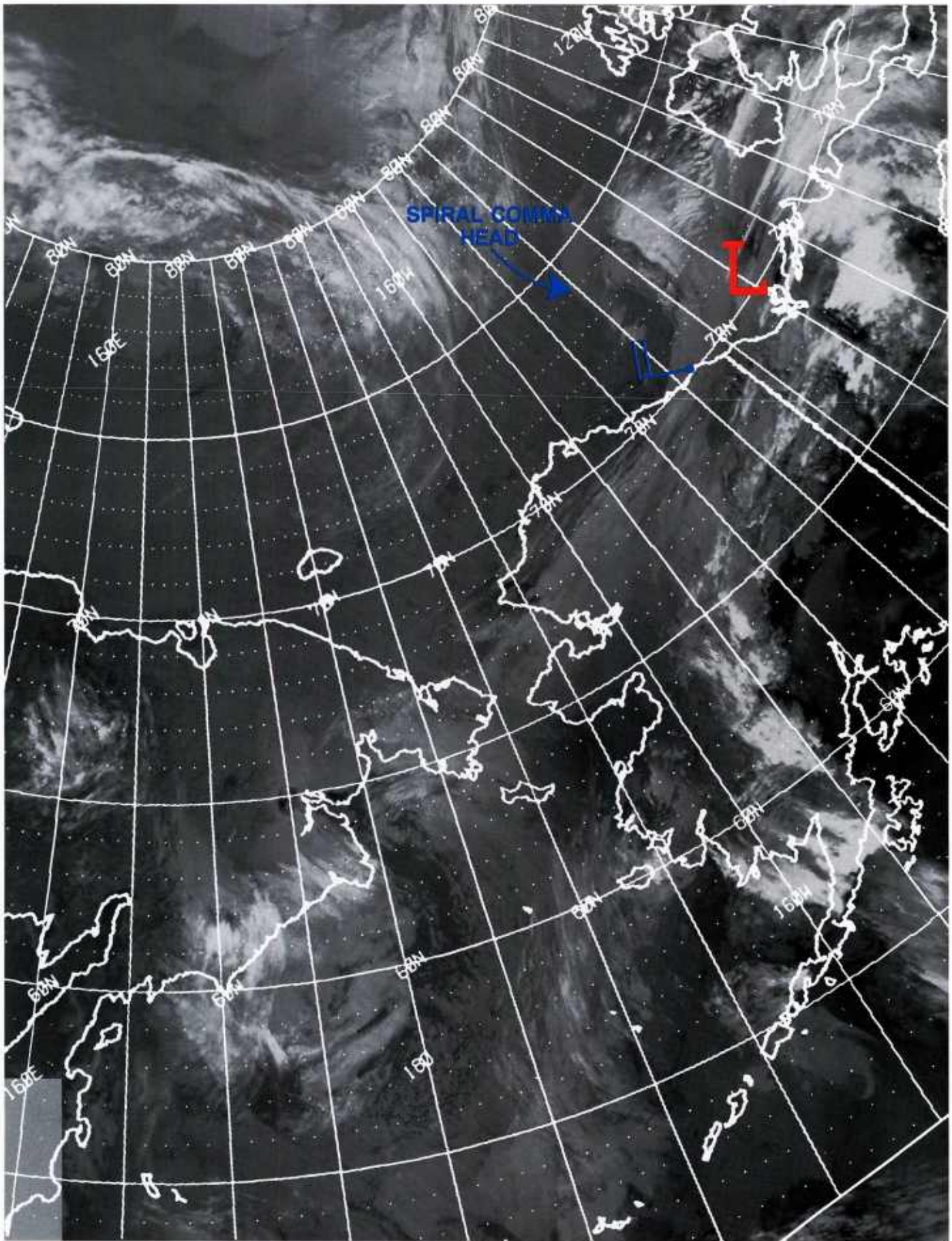
In the light of the preceding documentation by Black (1982) the DMSP infrared (TS) image acquired at 1500 GMT (Fig. 1A-90a) is of special interest. The image shows a weakening of the convective "V-shaped" cloud cluster, with no evidence of cloud lines to the west of that formation to define a closed circulation in that area. (Note, however, the northwest-southwest oriented cloud lines along  $150^{\circ}\text{W}$   $70.5\text{--}71.5^{\circ}\text{N}$ .) The low cloud, vorticity hook pattern is still evident, but apparently, according to the observation, a low center is closer to  $70^{\circ}\text{N}$   $135^{\circ}\text{W}$ , a somewhat surprising position, at least 180–200 n mi in advance of the upper level low. (An *L* is shown on Fig. 1A-90a to indicate the location of the surface low.) The low at this time has not been able to manifest itself through organization of the cloud lines around it.

By 2000 GMT low center position by satellite observation remains illusive. Figure 1A-91a shows DMSP visible (LF) data acquired at 2000 GMT. The storm is now clearly revealed in the extreme southeast portion of the Beaufort Sea, southwest of Banks Island. The shape of the storm appears to have changed, but this appearance is deceptive. The low vorticity comma head, clearly differentiated from the rest of the storm in the infrared data of Fig. 1A-90a, because of its warmer temperature, appears almost as bright as the rest of the storm in the visible channel data (Fig. 1A-91a). So the contrast is lost—but the shape has not changed. A careful scrutiny of the cloud lines around the vorticity comma head (Fig. 1A-91a) indicates straight northwesterly flow, so that low pressure should be somewhere to the northeast. However, with good supporting observations, the Beaufort Weather Office analysis for 1800 GMT (Fig. 1A-92a) shows a low centered near  $70.2^{\circ}\text{N}$   $133^{\circ}\text{W}$ . A gridded version of the DMSP visible data (Fig. 1A-93a) shows the low position relative to the cloud system. The storm was moving rapidly, and the satellite data are 2 hr older than the 1800 GMT surface analysis, so perhaps this position is not illogical.

FNOC's surface analysis for 1800 GMT (Fig. 1A-94a) shows only a trough in the region, but further advanced to the east, in a manner more consistent with the satellite evidence. (The analysis, incidentally, shows an excellent example of fog formation produced by advection of warm, moist air over cooler water into the low pressure region near Bristol Bay.) The storm was seen again in visible (LF) DMSP data at 2337 GMT (Fig. 1A-95a). Again, despite high winds recorded in the Mackenzie Bay area, more of a trough rather than a closed low is suggested.

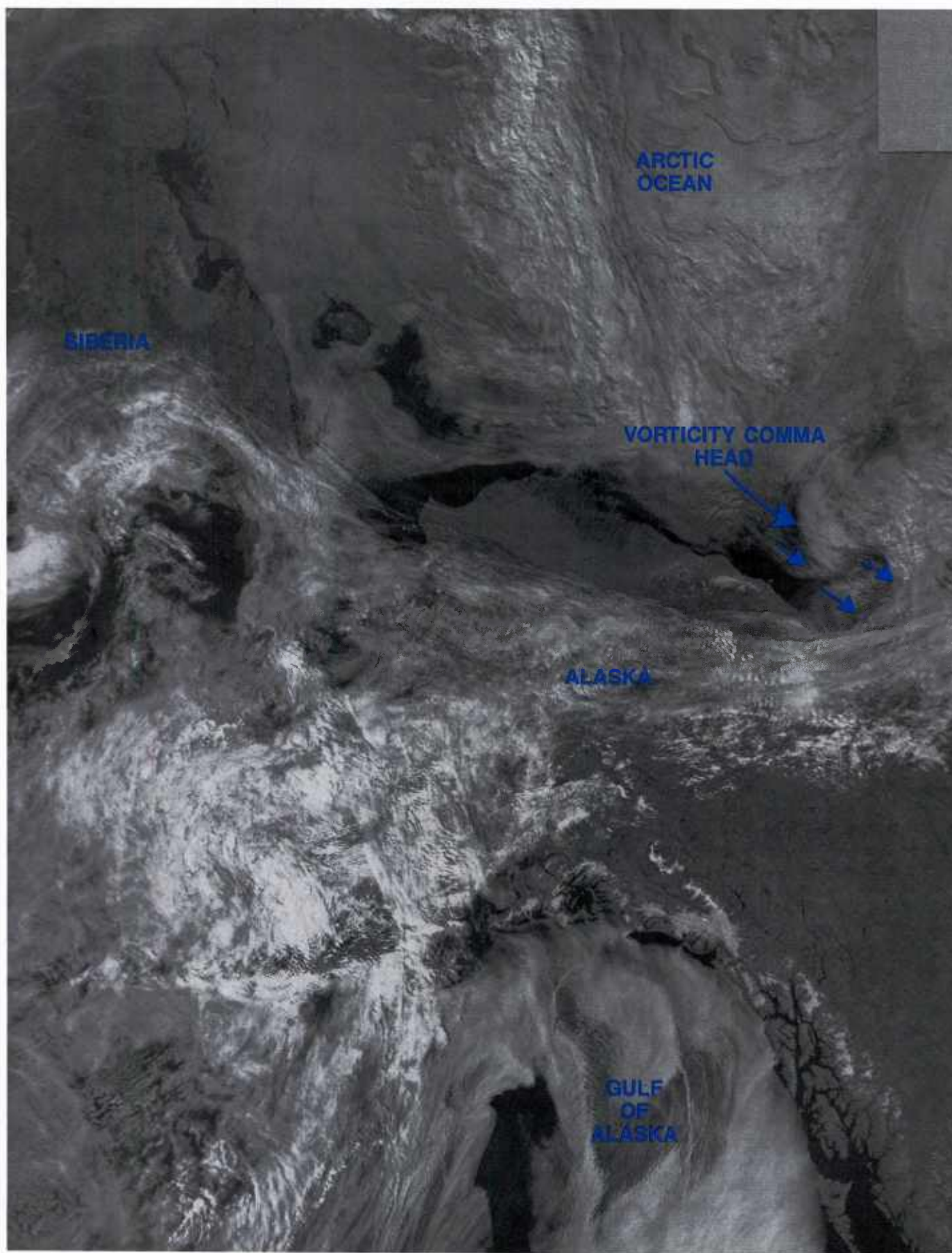
## *28 July 1982*

The FNOC surface analysis for 0000 GMT (Fig. 1A-96a) shows a sharp trough over Banks Island leading to a low well to the northwest. At 500 mb (Fig. 1A-97a) the FNOC analysis shows a cold low with a small  $-30^{\circ}\text{C}$  pool of air over Prince Patrick Island.

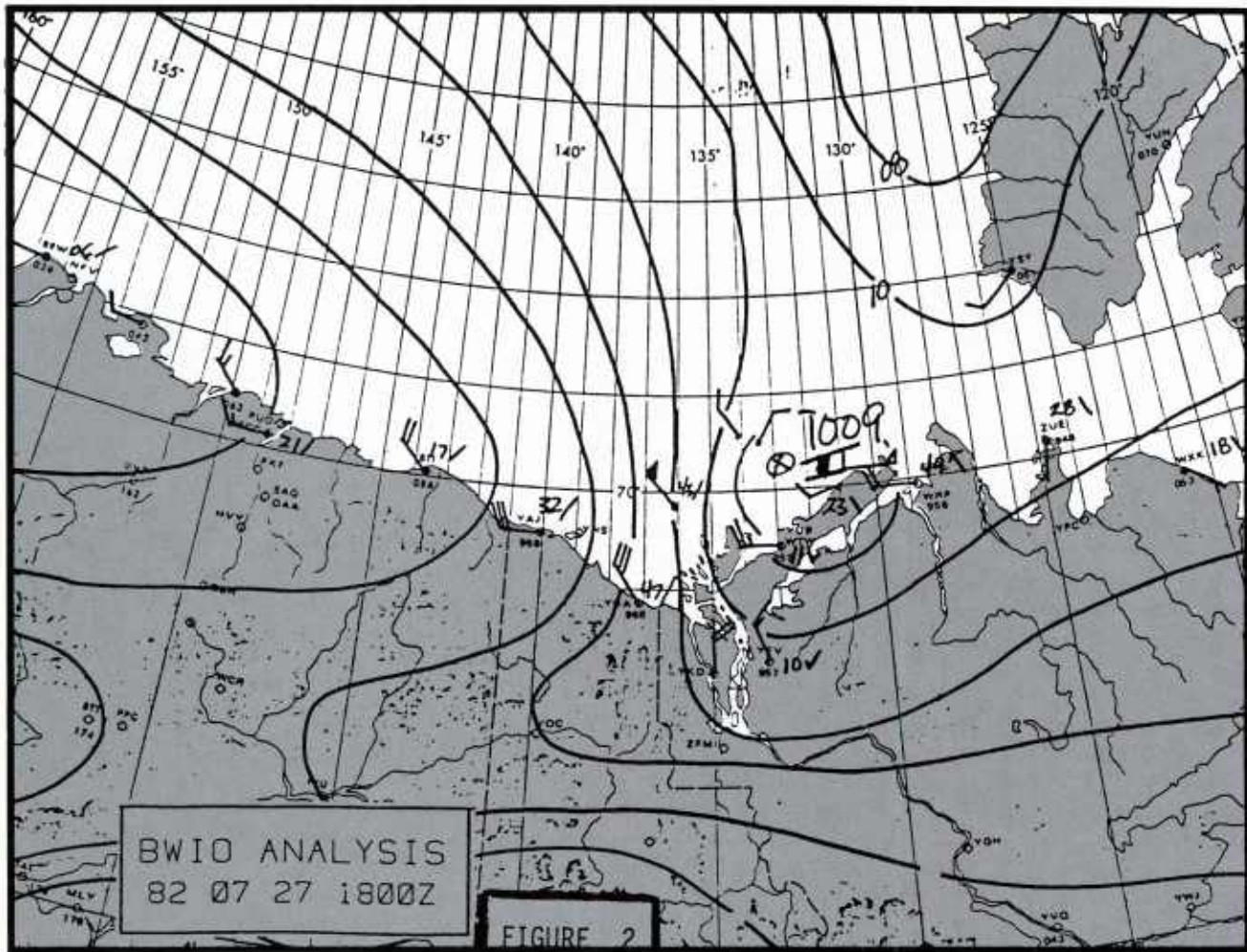


1A-90a DMSP infrared (TS) data. 1500 GMT 27 July 1982, with overlay.



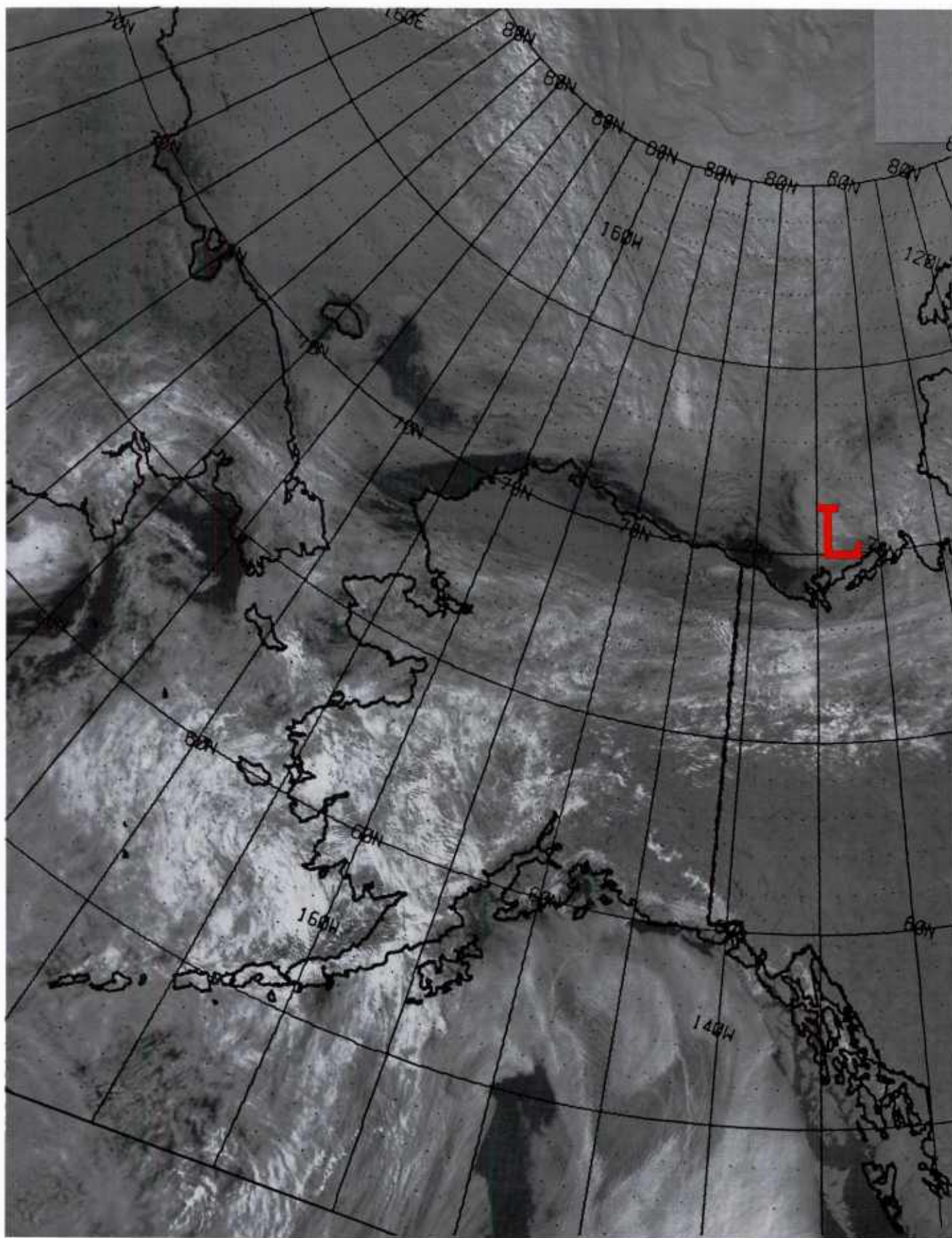


1A-91a DMSP visible (LF) data. 2000 GMT 27 July 1982.



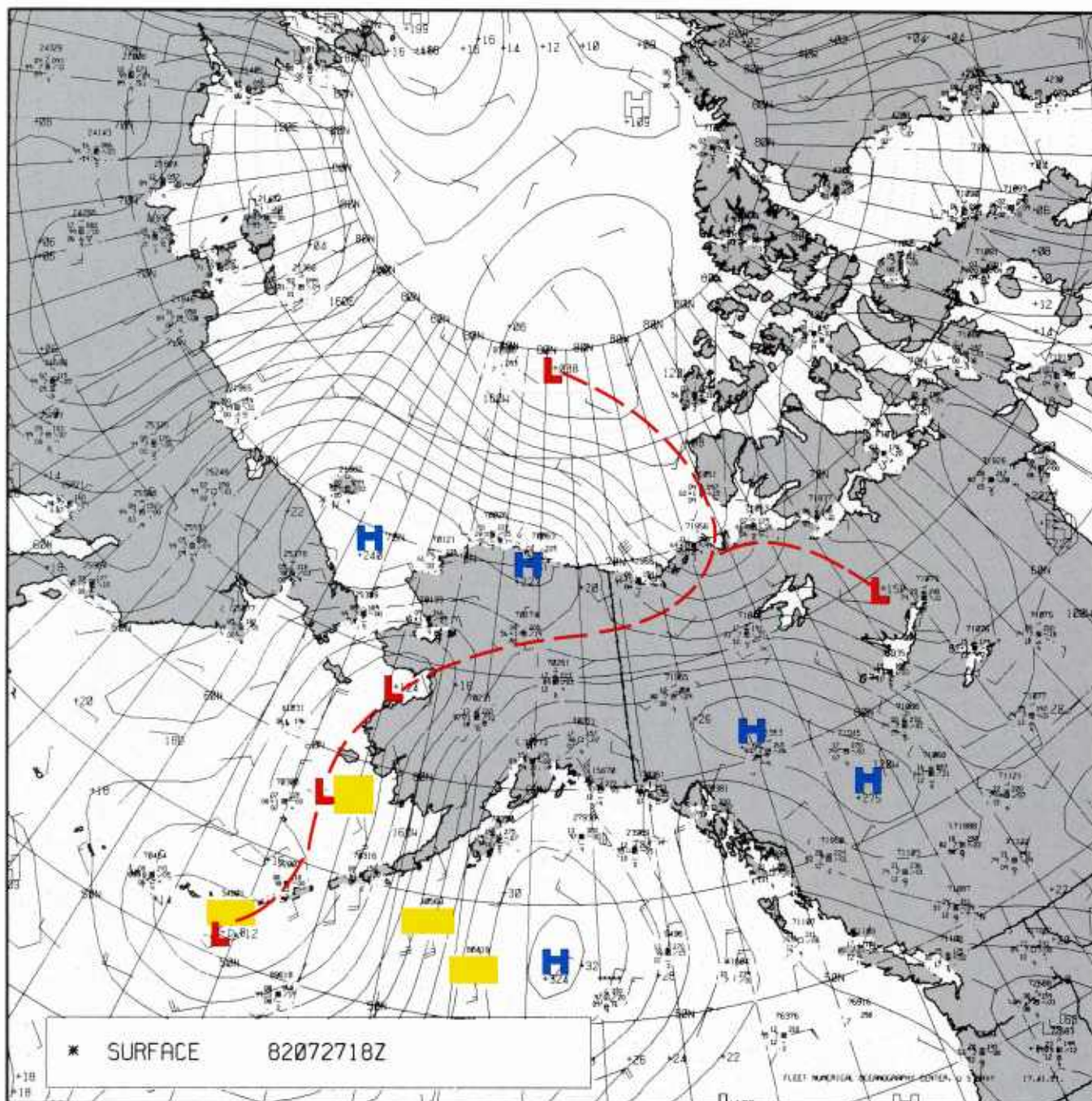
1A-92a Beaufort Weather Office surface analysis. 1800 GMT 27 July 1982.





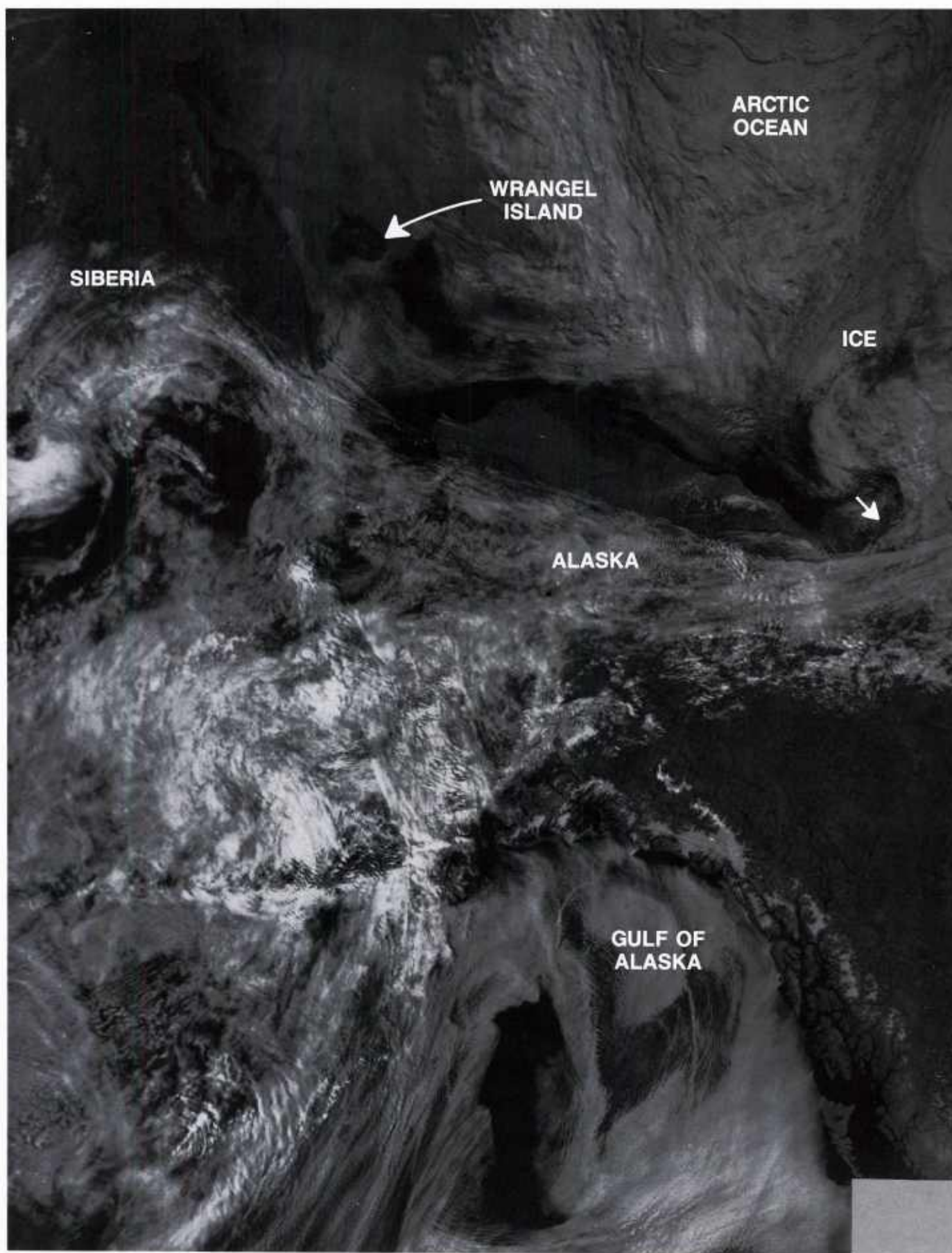
1A-93a DMSP visible (LF) data. 2000 GMT 27 July 1982, with overlay.





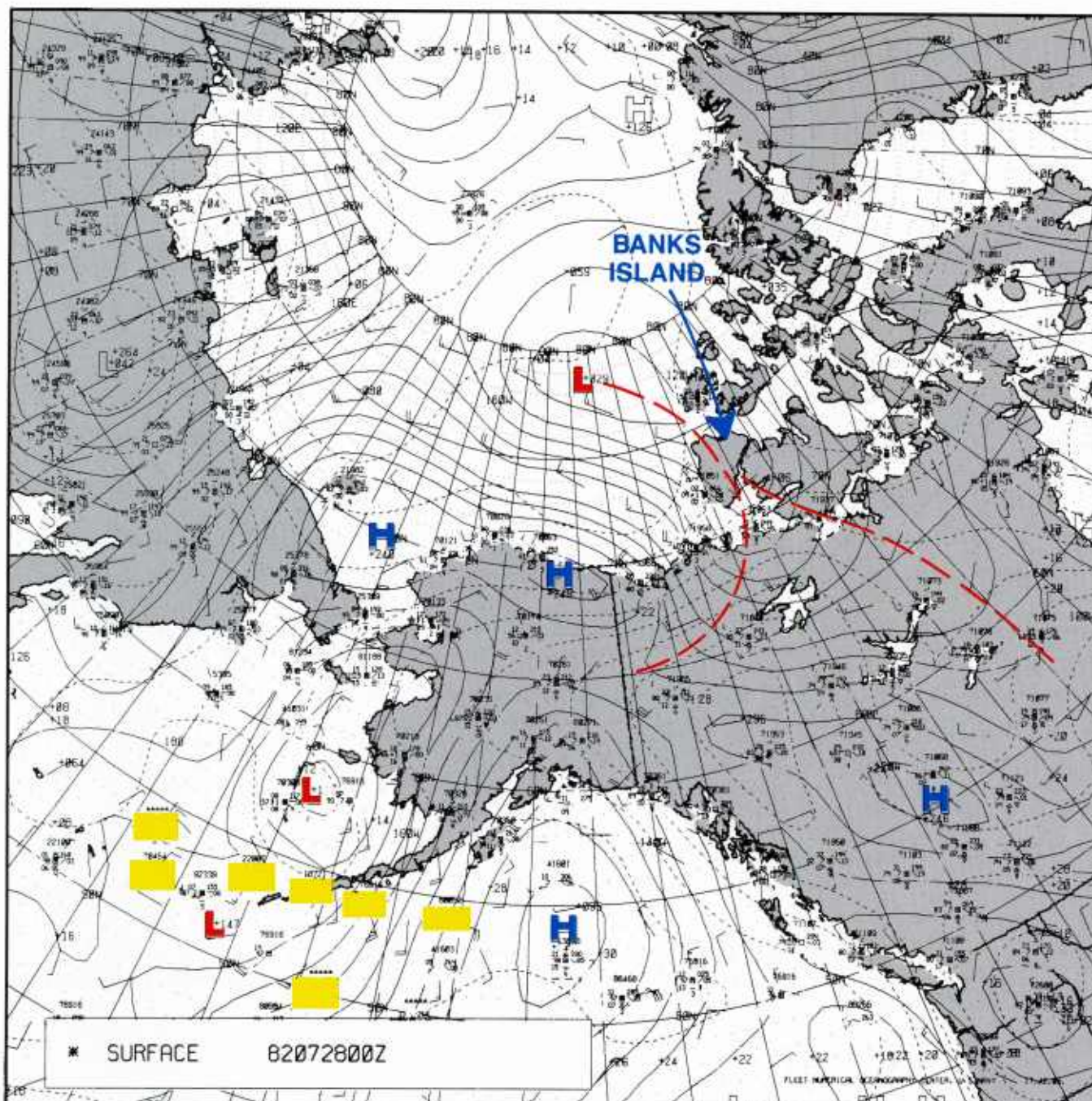
1A-94a FNOC surface analysis. 1800 GMT 27 July 1982.





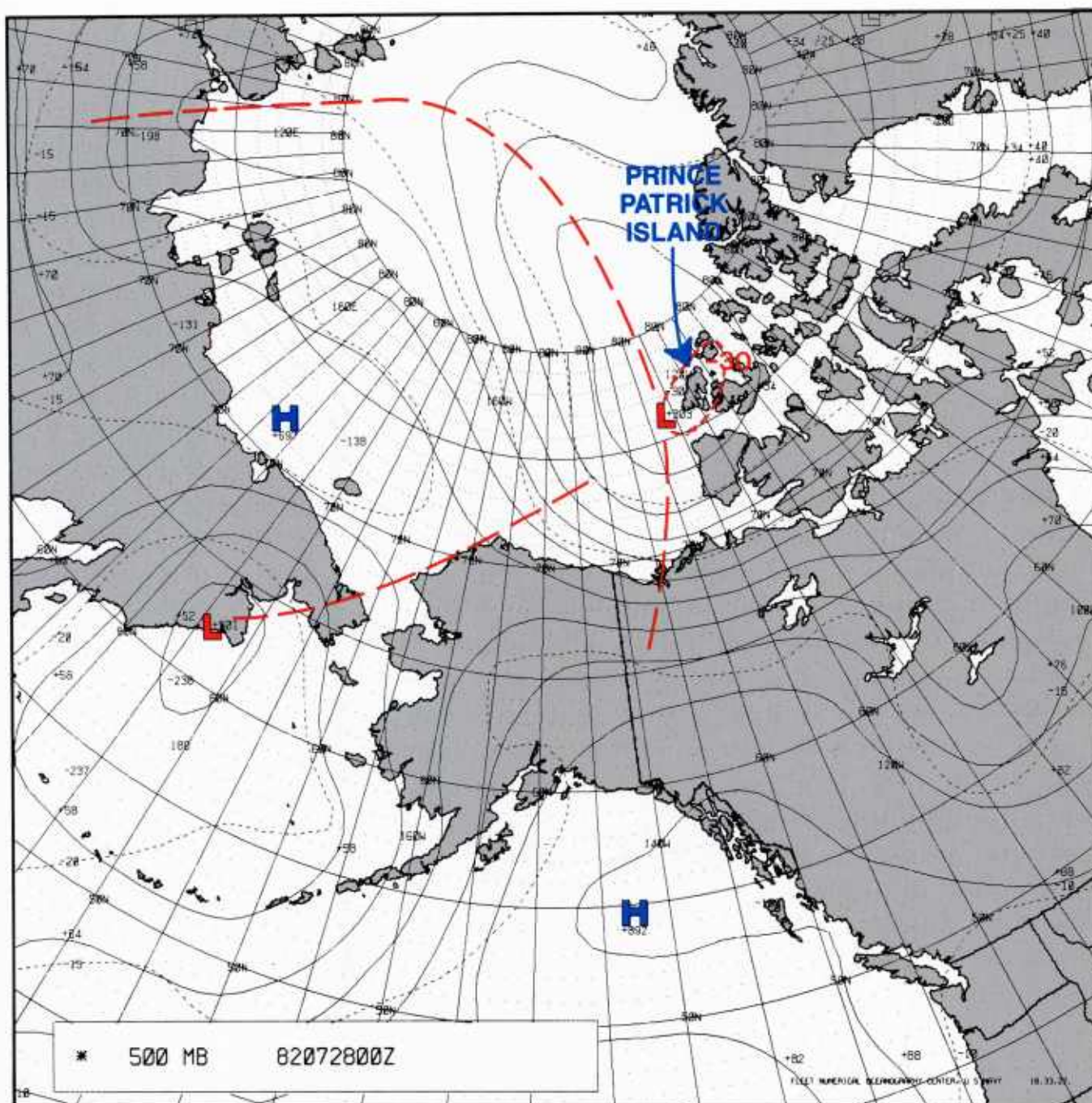
1A-95a DMSP visible (LF) data. 2337 GMT 27 July 1982.





1A-96a FNOC surface analysis. 0000 GMT 28 July 1982.





1A-97a FNOC 500-mb analysis. 0000 GMT 28 July 1982.

A final view of the storm as it moved over the Canadian Archipelago is shown in DMSP infrared (TS) data acquired at 1300 GMT (Fig. 1A-98a). The storm at this time has developed the characteristic hook that identifies it as a low that has deepened to 980–989 mb (see NTAG Vol. 3, Section 3A: Fett and Bohan, 1981). A series of small vortices extending northwest of the low center define a trough axis extending from this low.

The FNOC 1200 GMT surface analysis (Fig. 1A-99a) verifies a low center of 990 mb centered over the eastern coast of Victoria Island. As expected a trough axis extends from this low to the northwest.

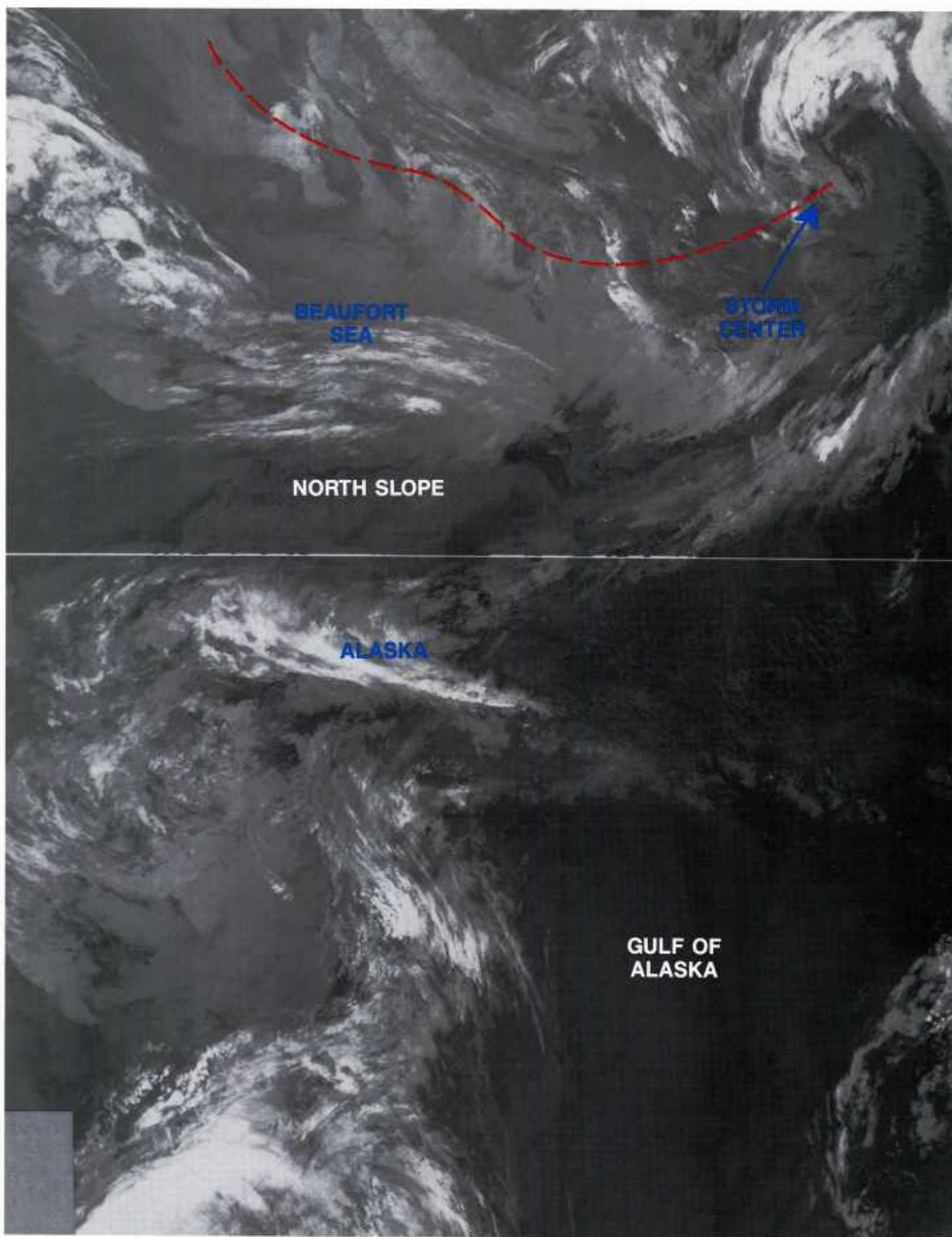
A gridded version of Fig. 1A-98a is shown as Fig. 1A-100a. The FNOC 500-mb analysis for 1200 GMT (Fig. 1A-101a) verifies that the low systems at this time are essentially vertically stacked. Subsequent analyses (not shown) indicated a stalling of the system with slowly rising central pressure characteristics.

### **Concluding Remarks**

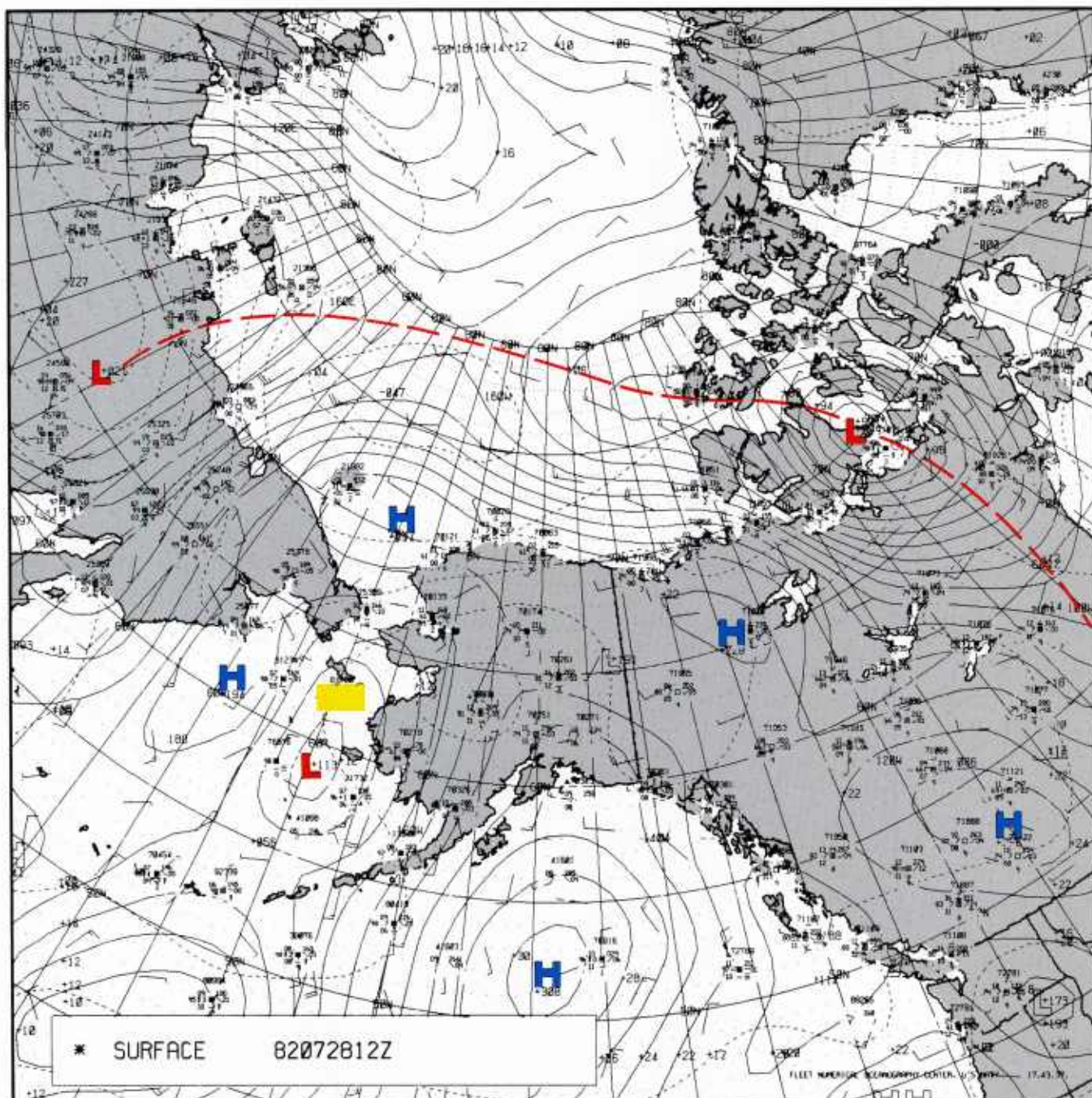
Black (1982) makes some interesting and valid observations concerning the development of this storm:

1. Mackenzie Bay is a favorable area for development. Lee troughing is induced over this region in a westerly to southwesterly flow.
2. A strong jet was noted over northern Alaska. Barter Island reported 121 kt at the 300-mb level on 27 July at 1200 GMT. On 28 July 0000 GMT, the surface low was positioned under the left exit of the jet.
3. Positive vorticity advection was noted over the region of development.
4. Cold air advection was evident aloft. The 500-mb, 700-mb, and 850-mb analyses all showed cold air advection during the development of the storm, thereby increasing potential energy available to the system.
5. A large area of open water existed around the Beaufort drill area, with a temperature of about 10 °C. This created a strong ocean-to-air flux of heat and moisture with attendant increased instability, and stronger surface winds.
6. The isallobaric wind was an important component of total wind speed.
7. Numerical forecast products, successful in showing a trough moving through the region, grossly underestimated intensity.



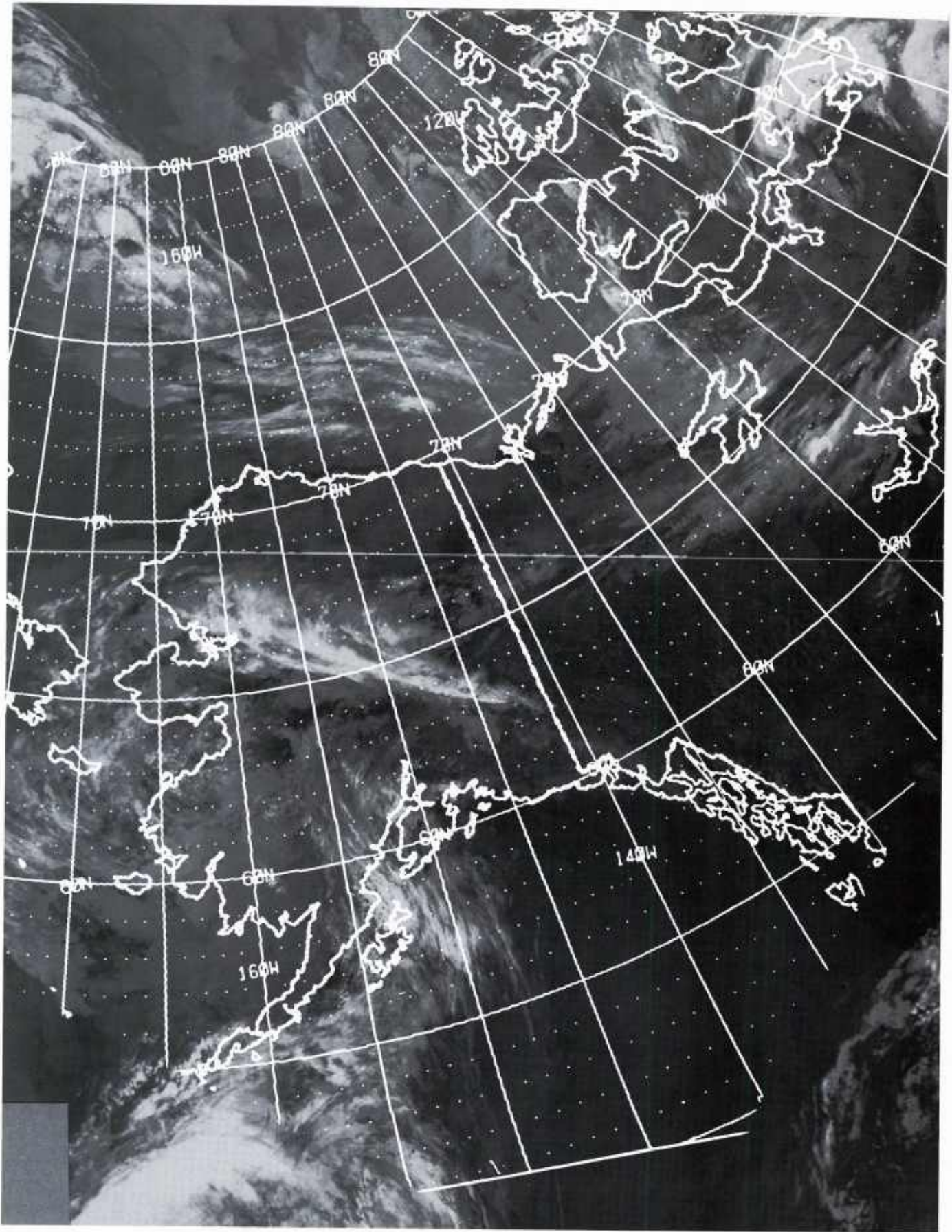


1A-98a DMSP infrared (TS) data. 1300 GMT 28 July 1982.



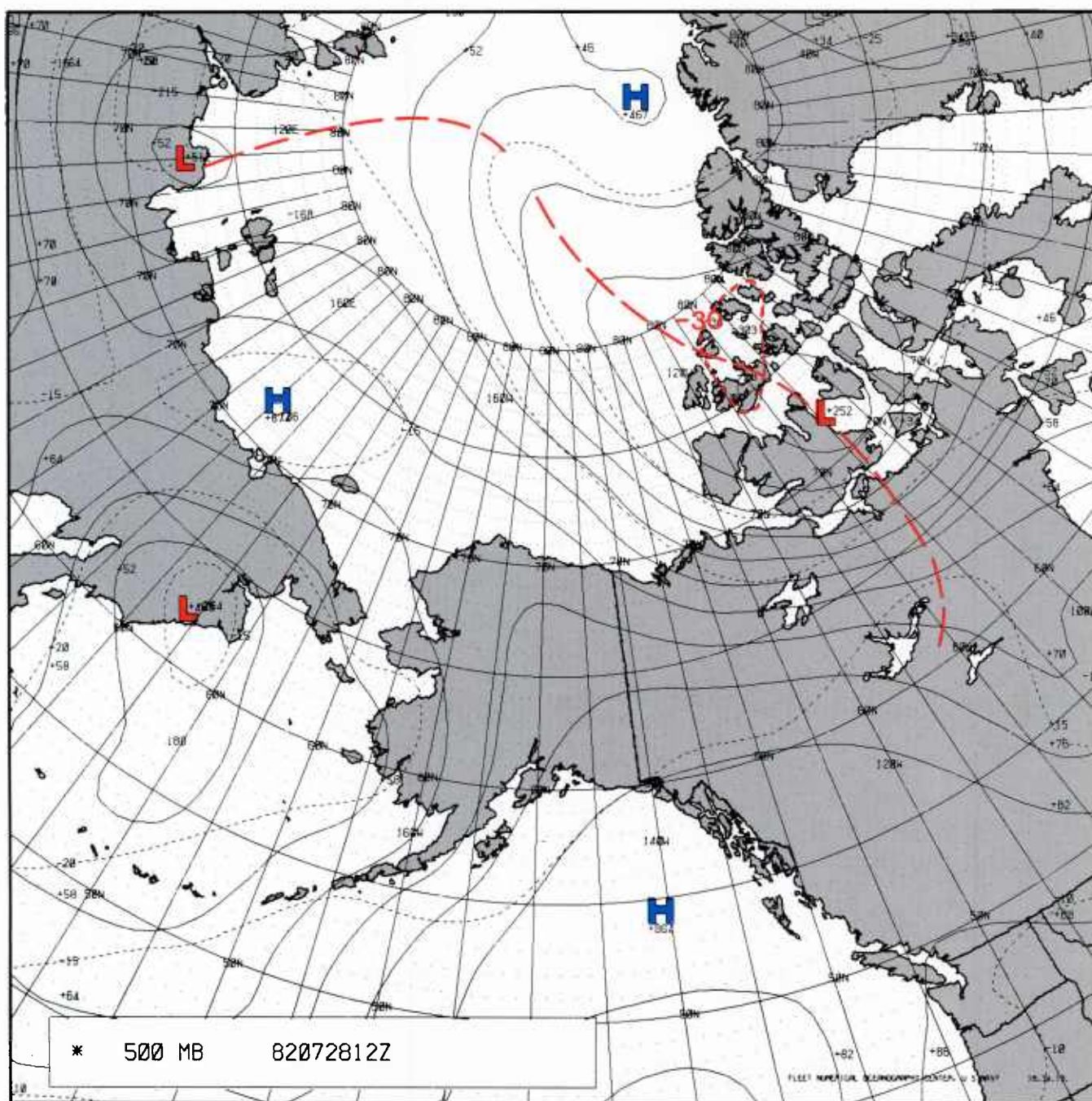
1A-99a FNOC surface analysis. 1200 GMT 28 July 1982.





1A-100a DMSP infrared (TS) data. 1300 GMT 28 July 1982, with overlay.





1A-101a FNOC 500-mb analysis. 1200 GMT 28 July 1982.



## Important Conclusions

1. Summer storms with winds approaching hurricane intensity can effect the North Slope and coastal region of northern Alaska.
2. Meridional-oriented troughs extending from the surface to upper tropospheric levels can promote rapid, intense, cyclogenesis.
3. Satellite data can provide the first significant clues of meridional trough cyclogenesis. Data should be monitored at frequent intervals (at least every 2–3 hr).
4. Numerical products may forecast meridional trough movement with reasonable accuracy. However, rapid cyclogenesis is unlikely to be revealed, on a reliable basis. The clue to a numerical forecast going awry may often be found through examination of satellite data over the region acquired on a timely basis.
5. The model of meridional trough cyclogenesis by Weldon (1975) appears realistic. However, careful monitoring of available surface observations is required to ascertain precise estimates of the surface low center movement and location.
6. Potential for mesocyclone development exists on the periphery of V-shaped convective cloud formations or white tornadoes.

## References

- Black, R.I., 1982: *Beaufort storm of July 27, 1982* (internal paper). Atmospheric Environmental Service, Edmonton, Alberta, Canada.
- Fett, R.W., and W.A. Bohan, 1981: Navy Tactical Applications Guide, Vol. 3, *North Atlantic and Mediterranean Weather Analysis and Forecast Applications*. NEPRF TR 80-07, Naval Environmental Prediction Research Facility, Monterey, CA 93943-5006, 200 pp.
- Fett, R.W., W.A. Bohan, and J. Rosenthal, 1984: Navy Tactical Applications Guide, Vol. 4, Part 1, *Eastern North Pacific Weather Analysis and Forecast Applications*. NEPRF TR 83-01, Naval Environmental Prediction Research Facility, Monterey, CA 93943-5006, 180 pp.
- Fett, R.W., W.A. Bohan, R.H. Whirtner, S.A. Hsu, S.W. Lyons, and J. Rosenthal, 1986: Navy Tactical Applications Guide, Vol. 6, *Tropics Weather Analysis and Forecast Applications*. NEPRF TR 86-02, Naval Environmental Prediction Research Facility, Monterey, CA 93943-5006, 182 pp.
- Fujita, T.T., 1981: Mesoscale aspects of convective storms. Preprint of Nowcasting Symposium 12-28 August 1981, Hamburg, Germany, SMPP Research Paper 191, University of Chicago, 8 pp.
- Weldon, Roger B., 1975: The structure and evolution of winter storms. Course Notes, National Weather Service Satellite Training (reprinted in Navy Tactical Applications Guide, Vol. 4, Part 1, *Eastern North Pacific Weather Analysis and Forecast Applications*, Sec. 2A, NEPRF TR 83-01, Naval Environmental Prediction Research Facility, Monterey, CA 93943-5006, 180 pp).

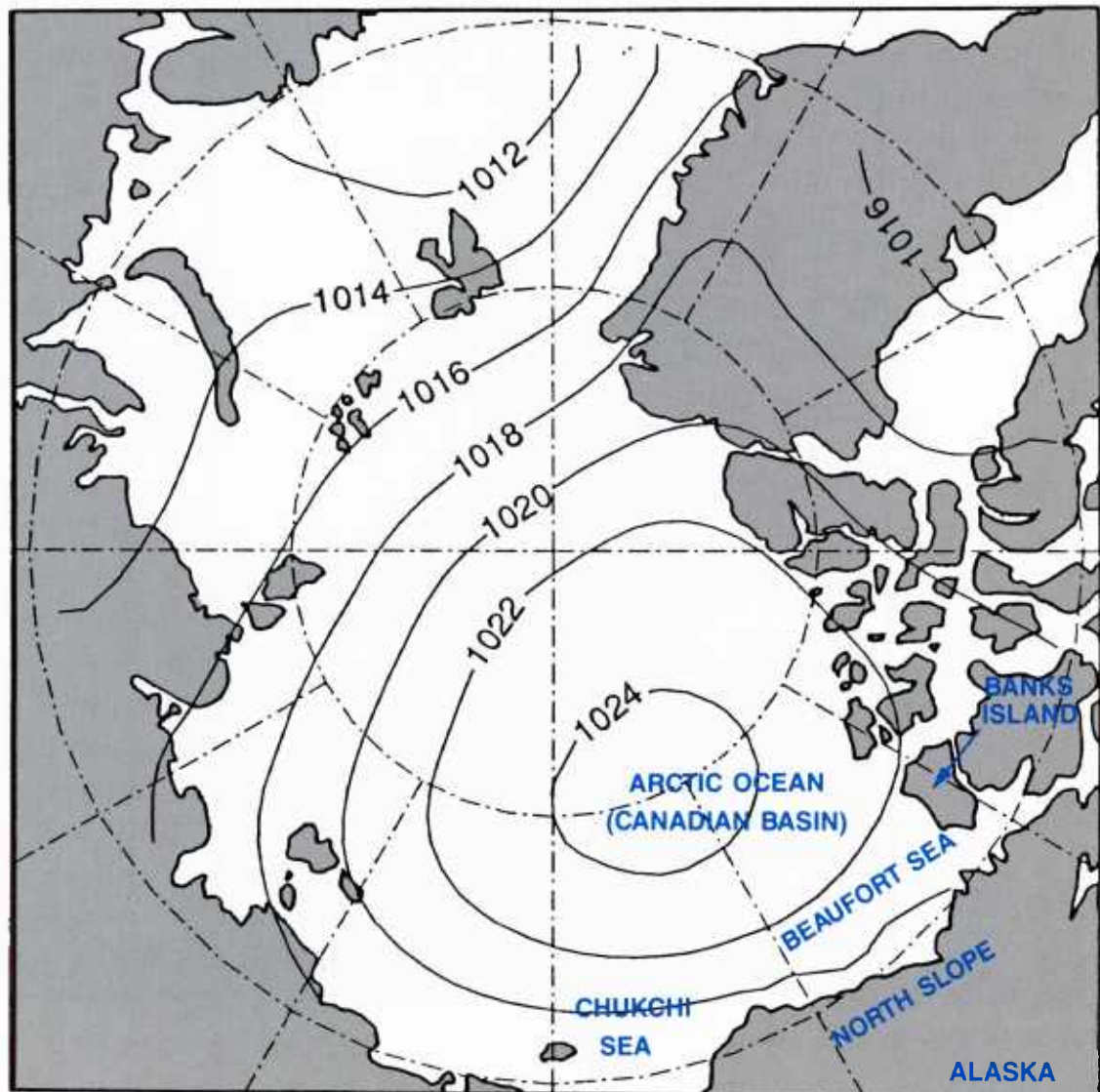




## *Case 1 Westward-Moving Low from the Chukchi to the East Siberian Sea*

During April, the monthly mean sea level pressure pattern (Figure 1B-1a) shows a large high-pressure cell centered over the Canada Basin of the Arctic Sea near 80N, 152W. The chart indicates that, under normal conditions, low-level systems over the Beaufort/Chukchi Seas should tend to track from east to west or northwest during this period.

It should also be noted that low clouds and/or aerosols are often produced as cold air from the ice pack flows over open leads and polynyi in the region. Favored locations for such effects are flaw leads along the west coast of Banks Island and the North Slope of Alaska and the Cape Bathurst polyna south of Banks Island. Such effects have been noted to extend long distances, sometimes covering much of the North Slope (see Section 3, Case 1).



1B-1a Mean monthly sea level pressure for April based on 8 years of buoy data over the Arctic.

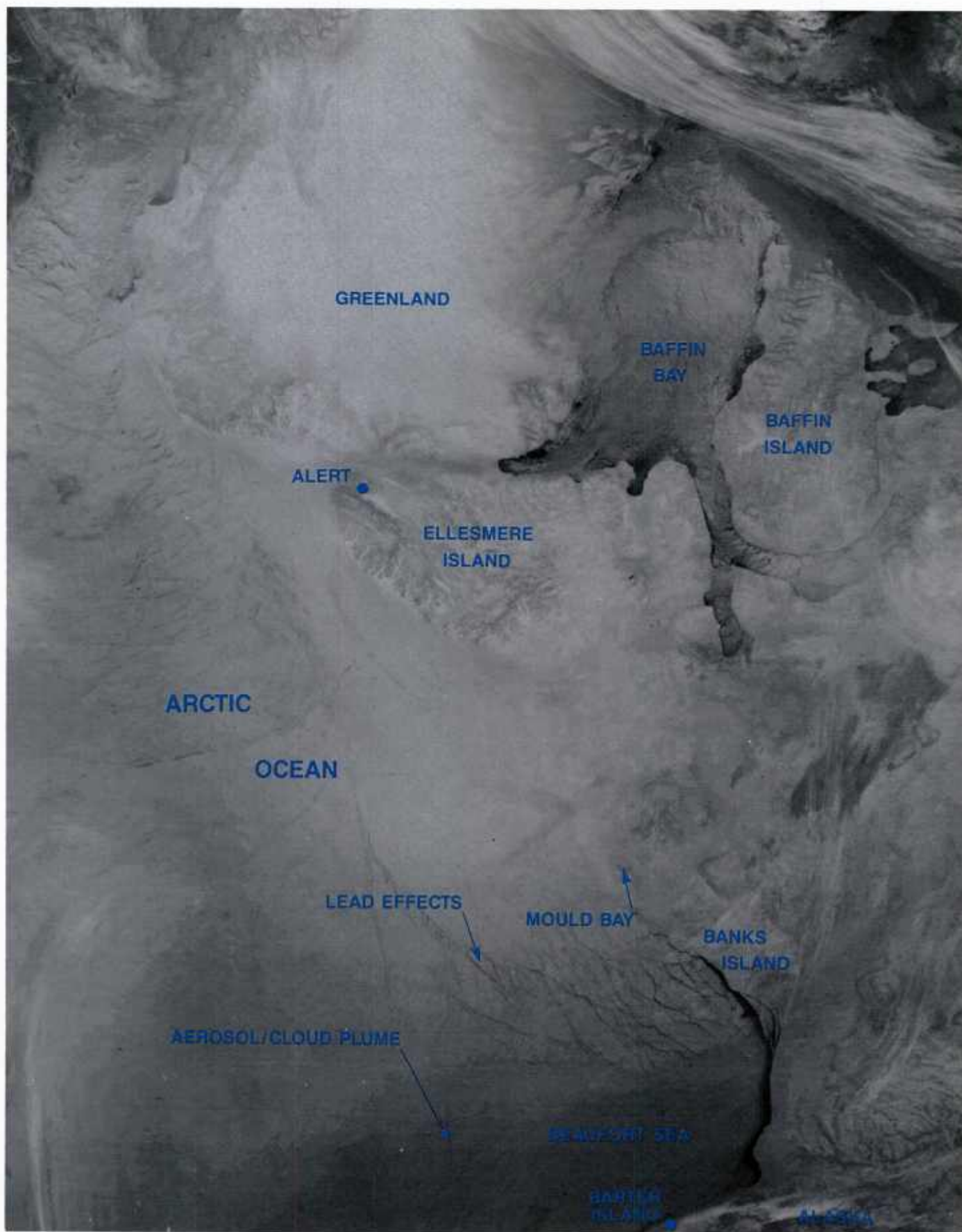
*15 April 1986*

DMSP infrared data acquired at 0700 GMT (Figure 1B-2a) show the region over the Arctic Ocean stretching from Greenland to the North Slope. Geographic boundaries are superimposed in Figure 1B-3a.

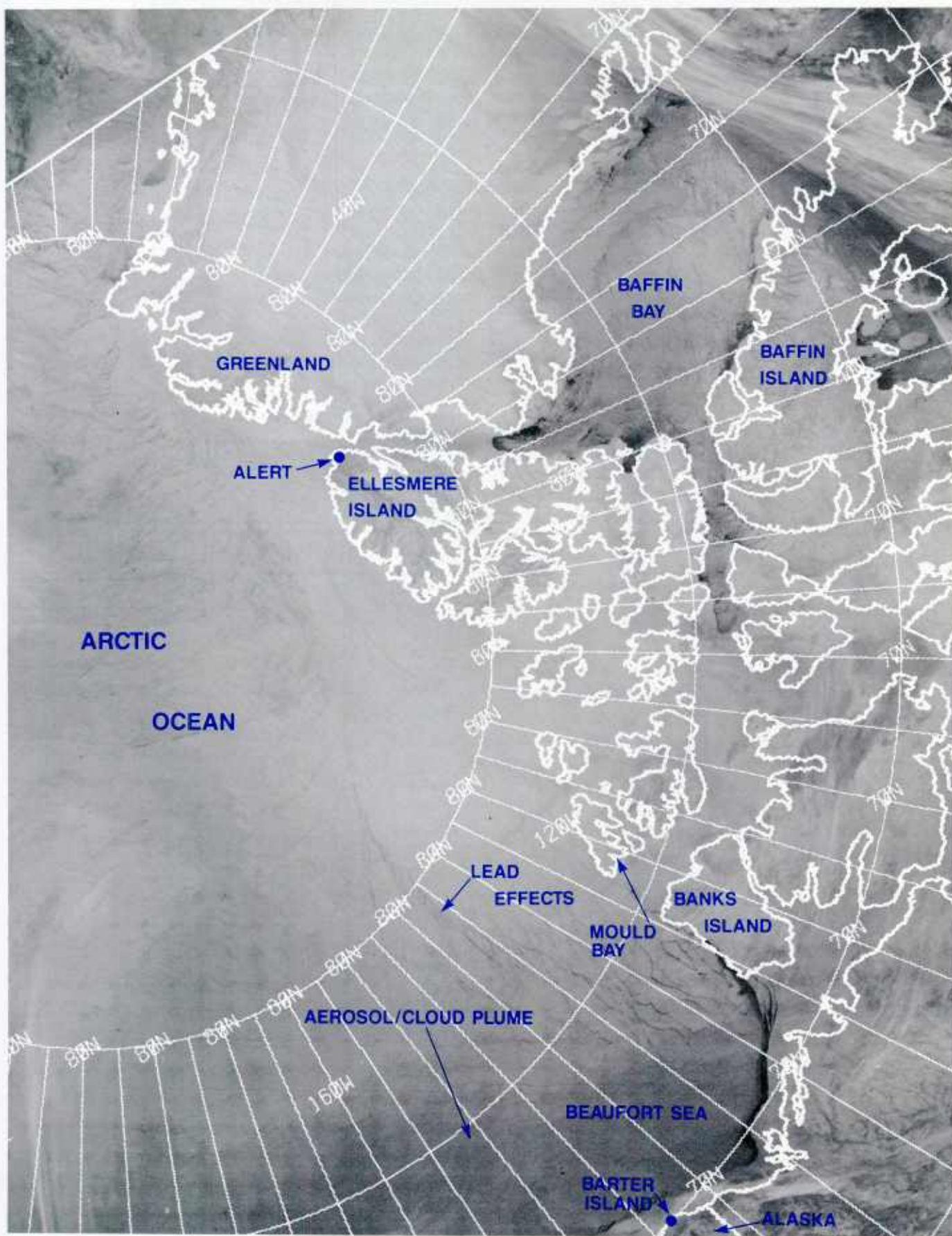
Little cloudiness is apparent in the DMSP imagery—especially over the Arctic Ocean ice pack, where detailed lead structure is apparent in most areas. Interpretation of clouds or aerosol effects in the Arctic, however, is dependent upon gray shade interpretation related to temperature changes. The numerous warm (darker gray) tones over the ice pack are normally associated with long-wave re-radiation by clouds or aerosols trapped under the strong low-level inversion existing over the pack ice. Wherever a lead or polynya is open, air/sea interaction effects cause a strong flux of moisture from the ocean to the air, resulting in aerosol and cloud generation.

On 15–16 April, during the time or near the time of these data, a NOAA WP-3D research aircraft flew from Alert, Canada, on Ellesmere Island (Figure 1B-2a), to Fairbanks, Alaska, in the center part of the state (Bridgman et al., 1988).





1B-2a DMSP infrared (TS) data. 15 April 1986, 0700 GMT.



1B-3a DMSP infrared (TS) data. 15 April 1986, 0700 GMT (with geographic boundaries).

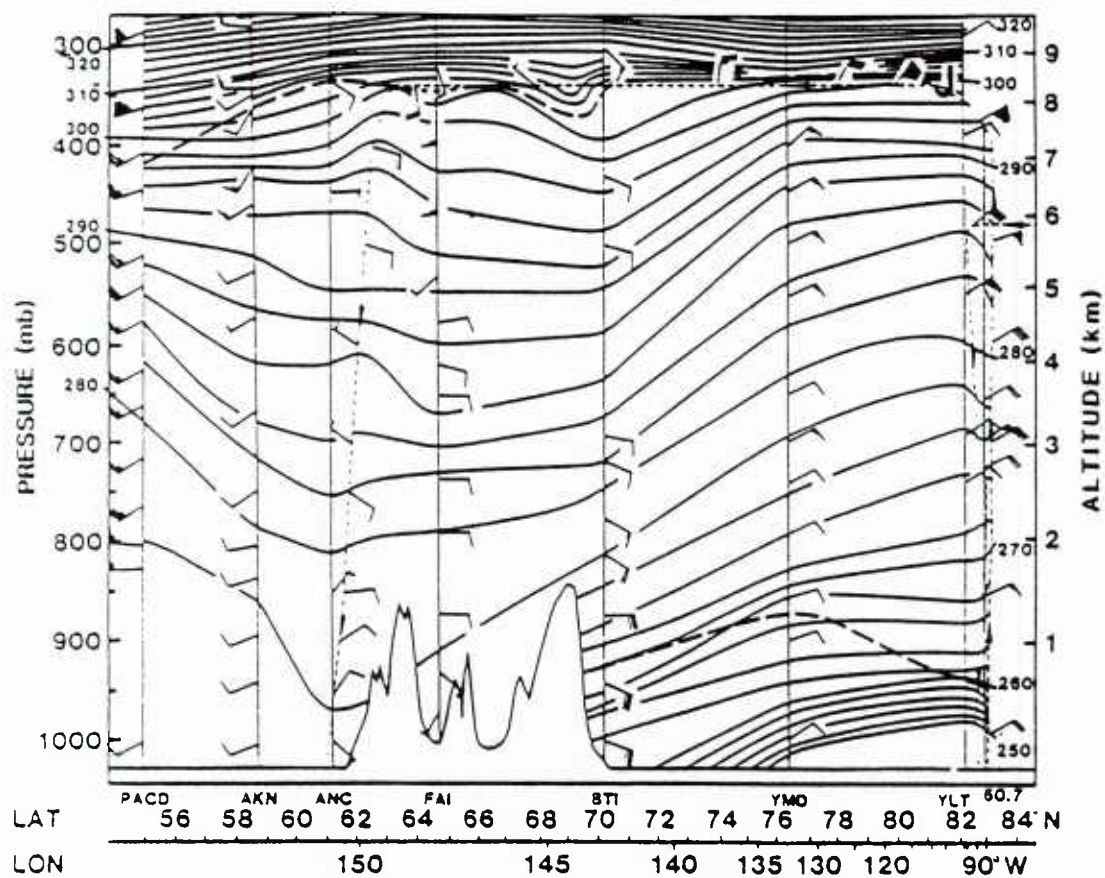


Figure 1B-4a is a latitude-altitude cross section showing conditions from Alert (YLT) past Fairbanks (FAI) to King Cove (PACD), Alaska. No major discontinuities appear except for the shallow cold frontal feature apparent between Mould Bay (YMD) and Barter Island (BTI). This feature is not particularly apparent in the satellite data (Figure 1B-2a) but may be associated with the presence of the cloud plume shown extending from the Banks Island area westward.

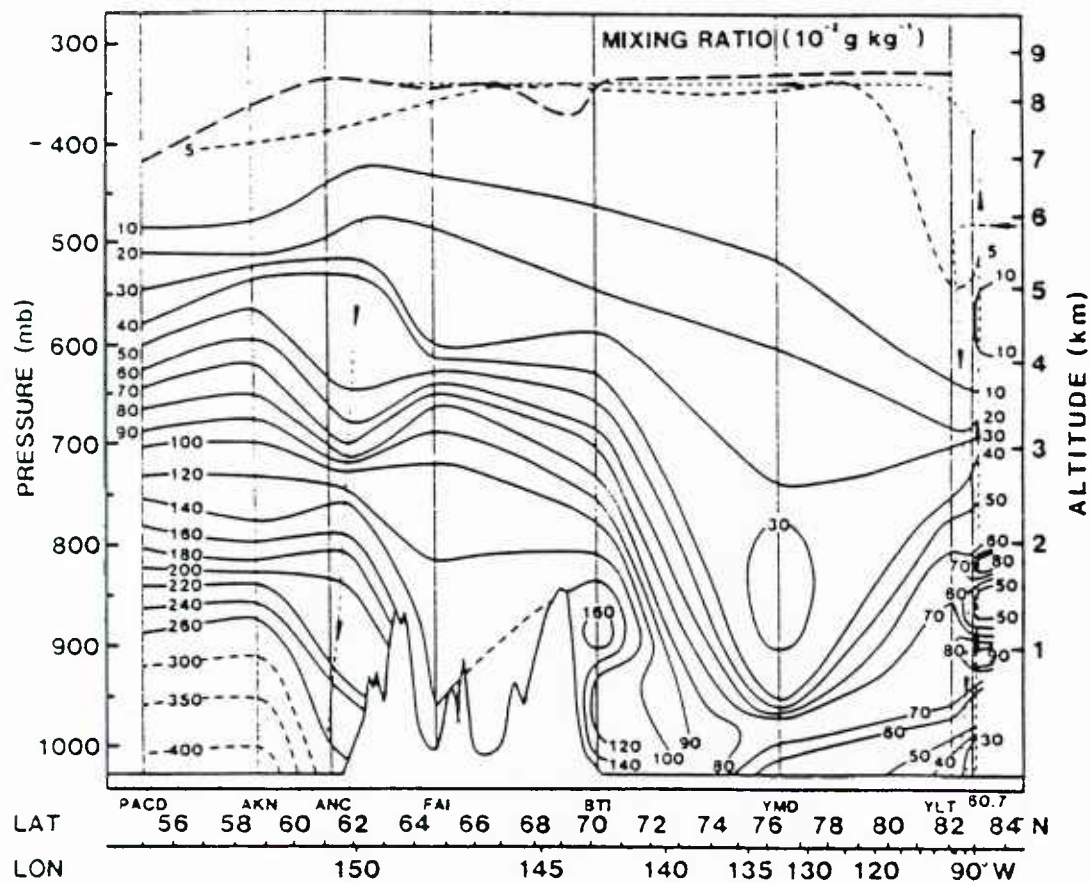
A corresponding latitude-altitude cross section of water vapor mixing ratio between Alert and Anchorage is perhaps more revealing (Figure 1B-4b). This cross section shows the strong moisture gradient existing between Mould Bay and Barter Island. This moisture gradient is almost surely associated with the aerosol/cloud plume revealed in the DMSP data (Figure 1B-2a). The moisture gradient and cloud plume also correspond well with the observation by Russ Schnell, aboard the WP-3D aircraft, that, as the aircraft approached the Alaskan coast, "conditions were obscured below and sun dogs could be seen in the obscuration," a fact indicating ice crystalline structure in this obscuration.

An additional DMSP visible view of the area on 15 April at 1556 GMT (Figure 1B-5a) reveals a cloud vortex due east of Wrangel Island. A cloud band from this system passes the Alaskan coastline near Barter Island. An overlay to this figure with geographic boundaries and coordinates (Figure 1B-6a) indicates that the vortex has a center position near 71N, 169W.

FNOC surface analyses for 15 April at 0000 GMT (Figure 1B-7a) and 1200 GMT (Figure 1B-8a) and for 16 April at 0000 GMT (Figure 1B-9a) do not succeed in resolving the cloud vortex system. In these analyses, however, note that Wrangel Island's observation (71.0N, 179.6W) shows a backing of the wind from easterly (Figure 1B-7a) to northerly (Figure 1B-8a) as the low center approached Wrangel Island and then a turn to southwesterly (Figure 1B-9a), indicating vortex passage. This also substantiates that the cloud vortex did have a closed circulation and that the surface charts (Figures 1B-7a, 1B-8a, and 1B-9a) are misanalyzed. At the same time, a low-pressure center south of the map area in Figure 1B-7a moved northward to 64N 145E (Figure 1B-8a) and then to 69.5N 157E (Figure 1B-9a). The movement of this system is emphasized to clarify that this is a different system than the cloud vortex we have been describing, yet is close to the same area. A careful assessment of this fact is necessary so that mistaken inferences do not occur.

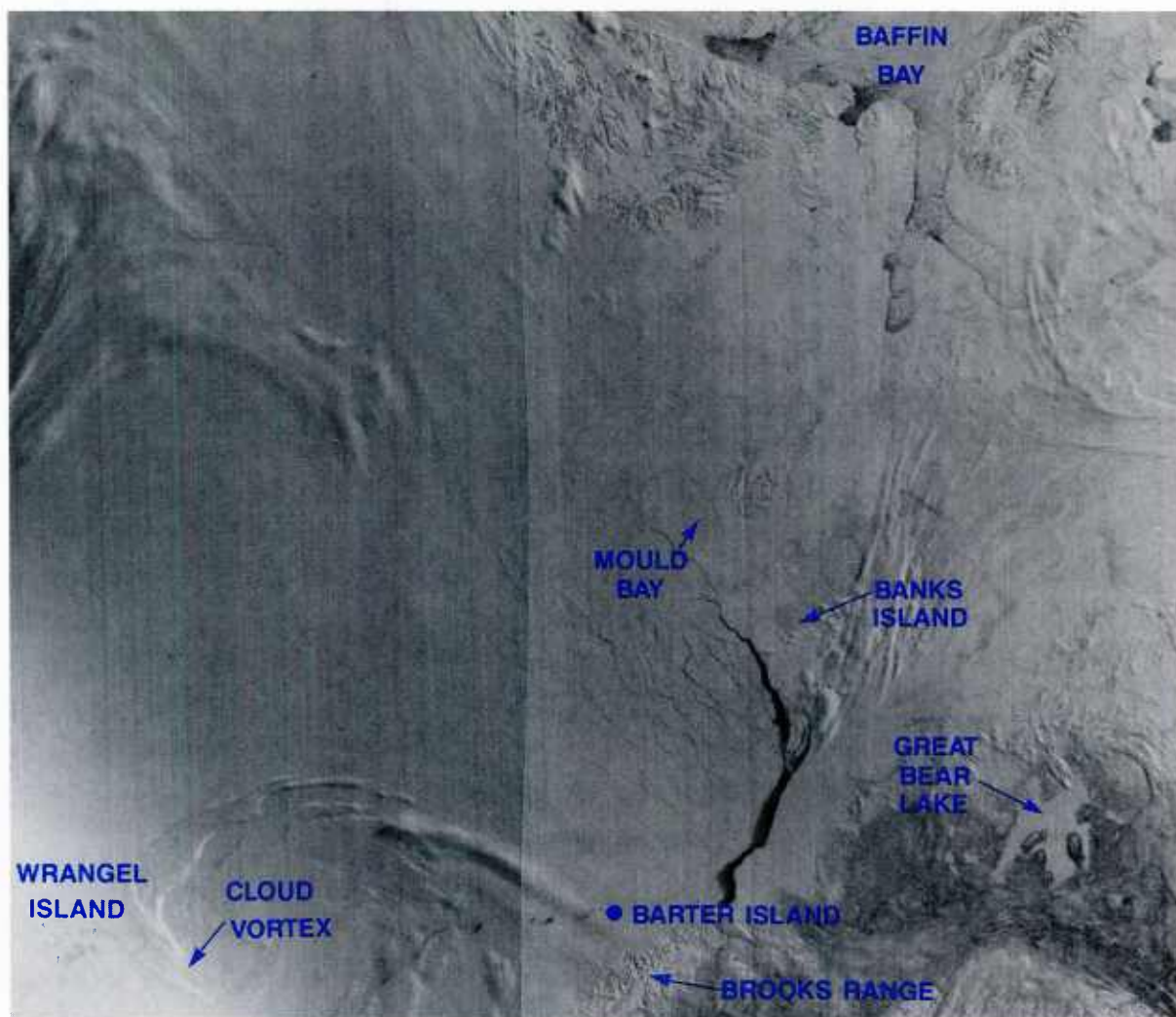


1B-4a A latitude-altitude cross-section from Alert (YLT), past Fairbanks (FAI), to King Cover (PACD), Alaska, 15-16 April 1986.

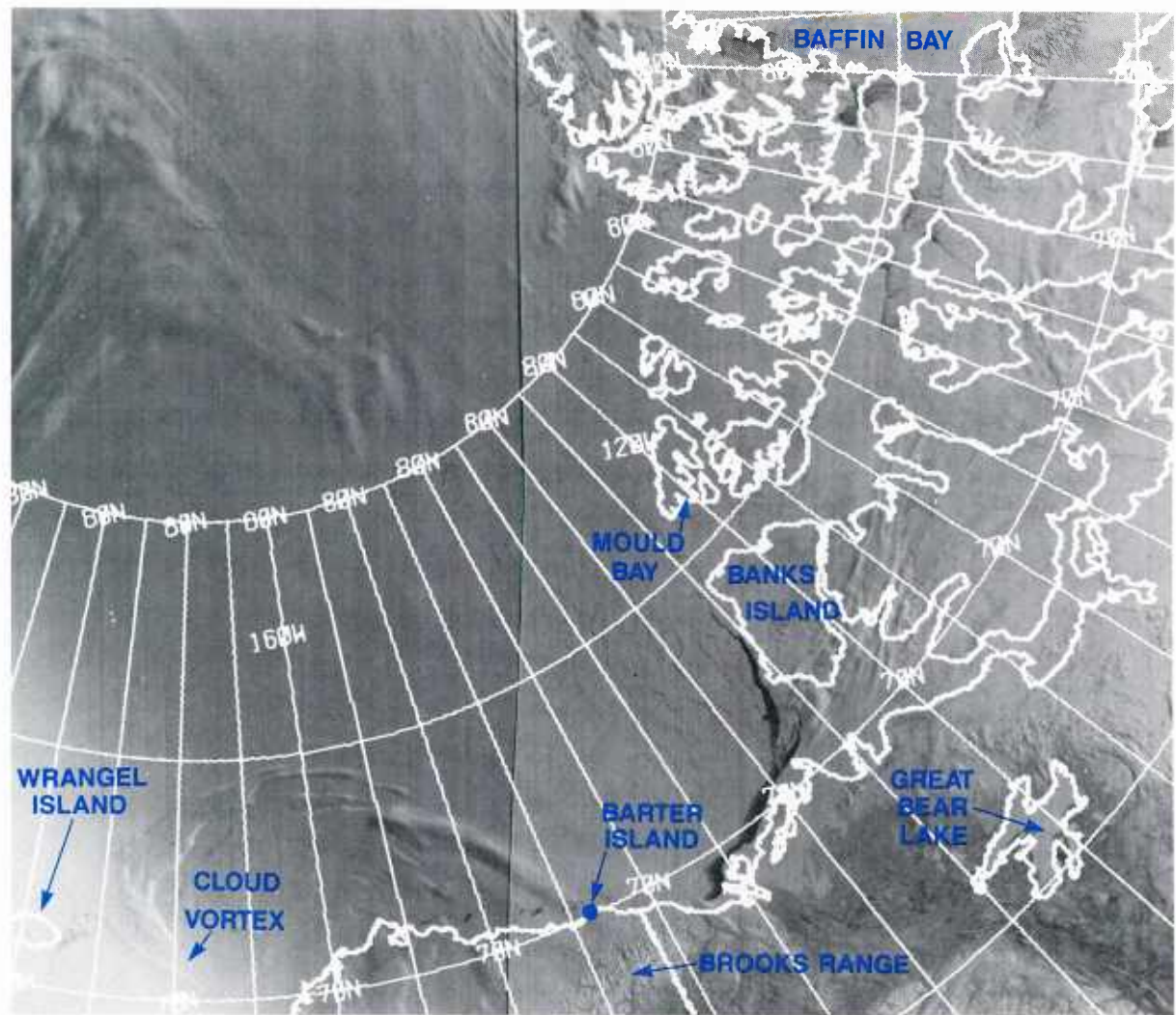


1B-4b A latitude-altitude cross-section of water vapor mixing ratio between Alert (YLT), past Fairbanks (FAI), to King Cover Alaska (PACD), 15-16 April 1986.





1B-5a DMSP visible (LF) data. 15 April 1986, 1556 GMT.

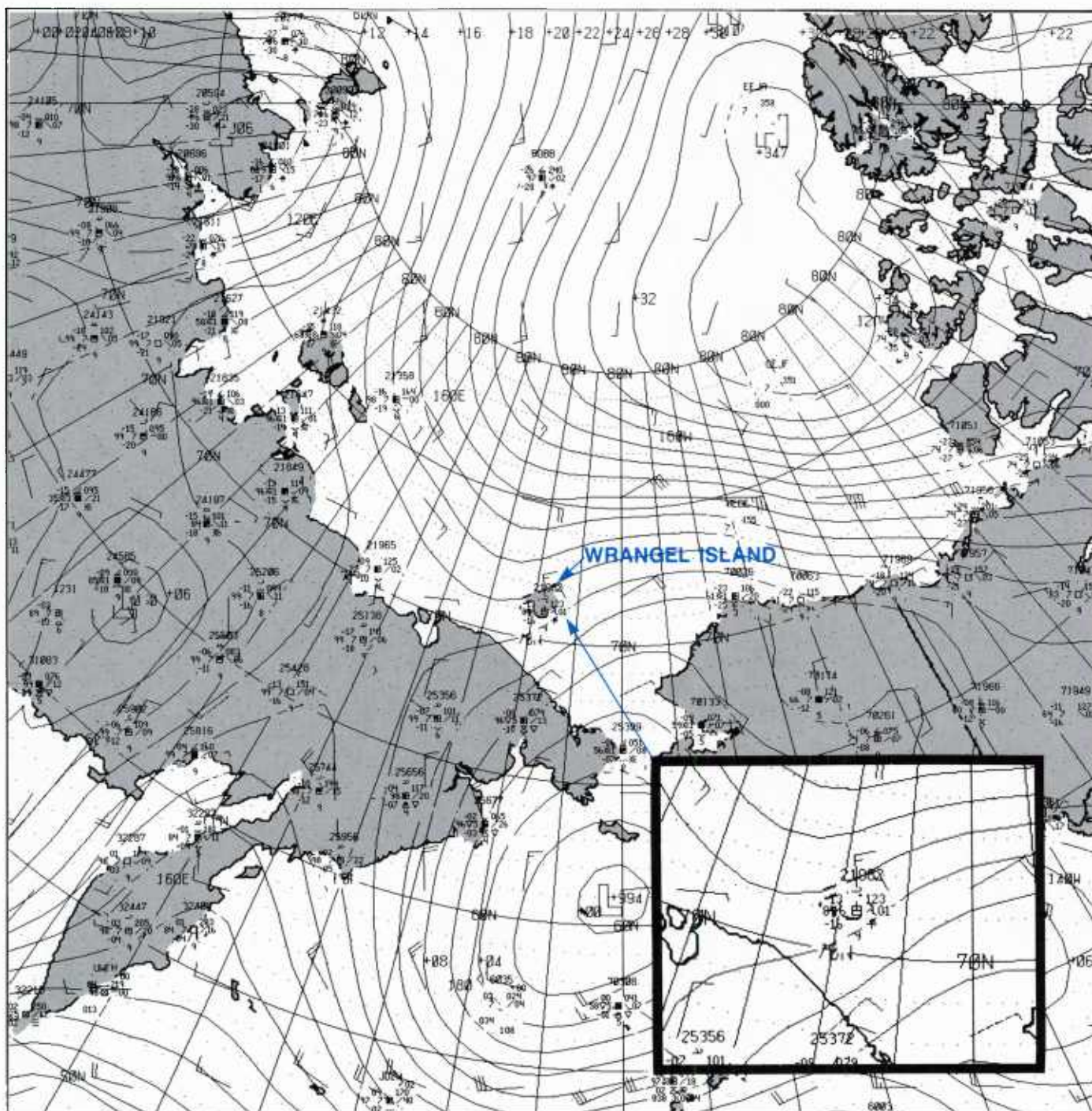


1B-6a DMSP visible (LF) data. 15 April 1986, 1556 GMT (with geographic boundaries).



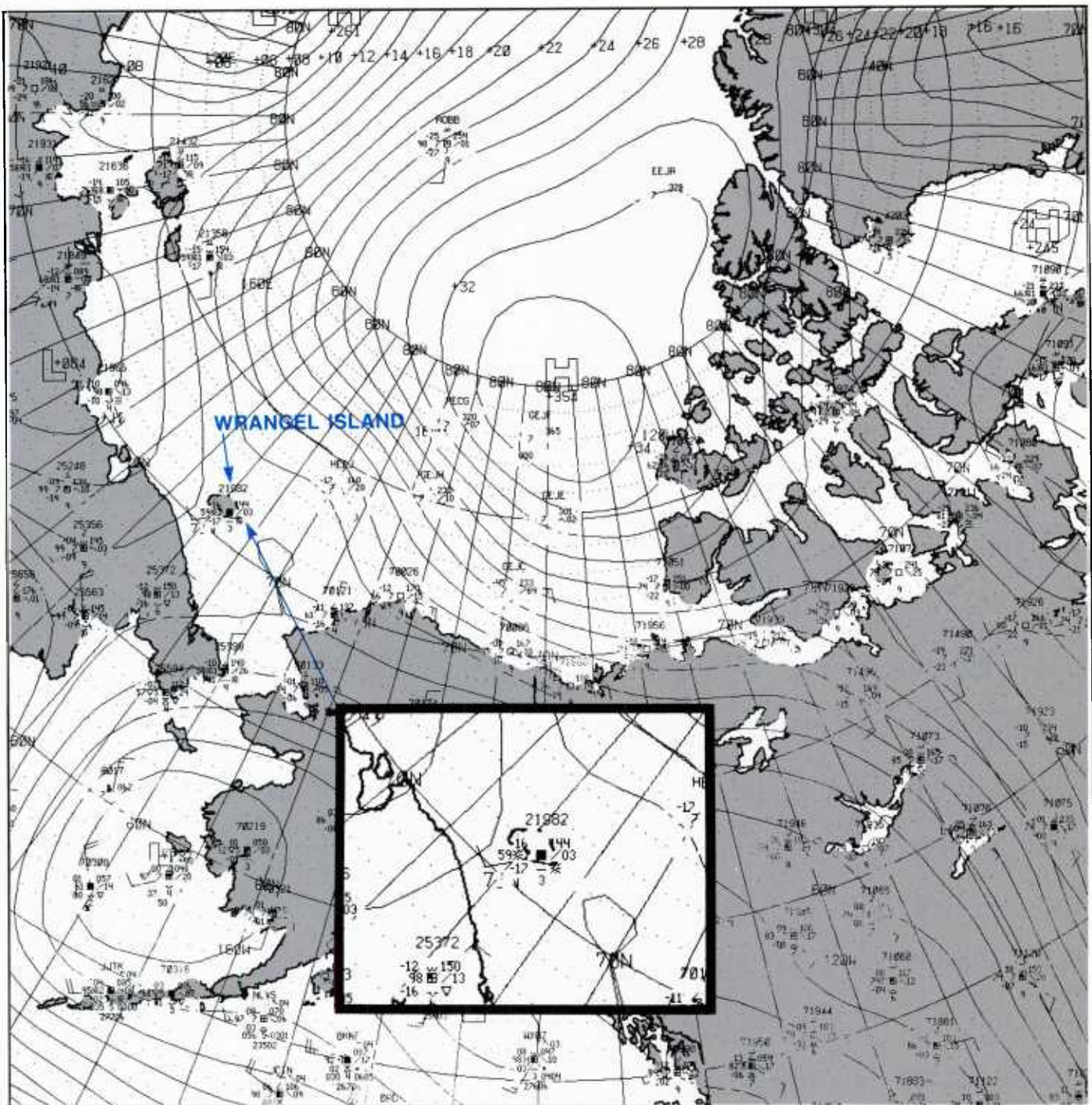






1B-8a FNOC surface analysis. 15 April 1986, 1200 GMT.





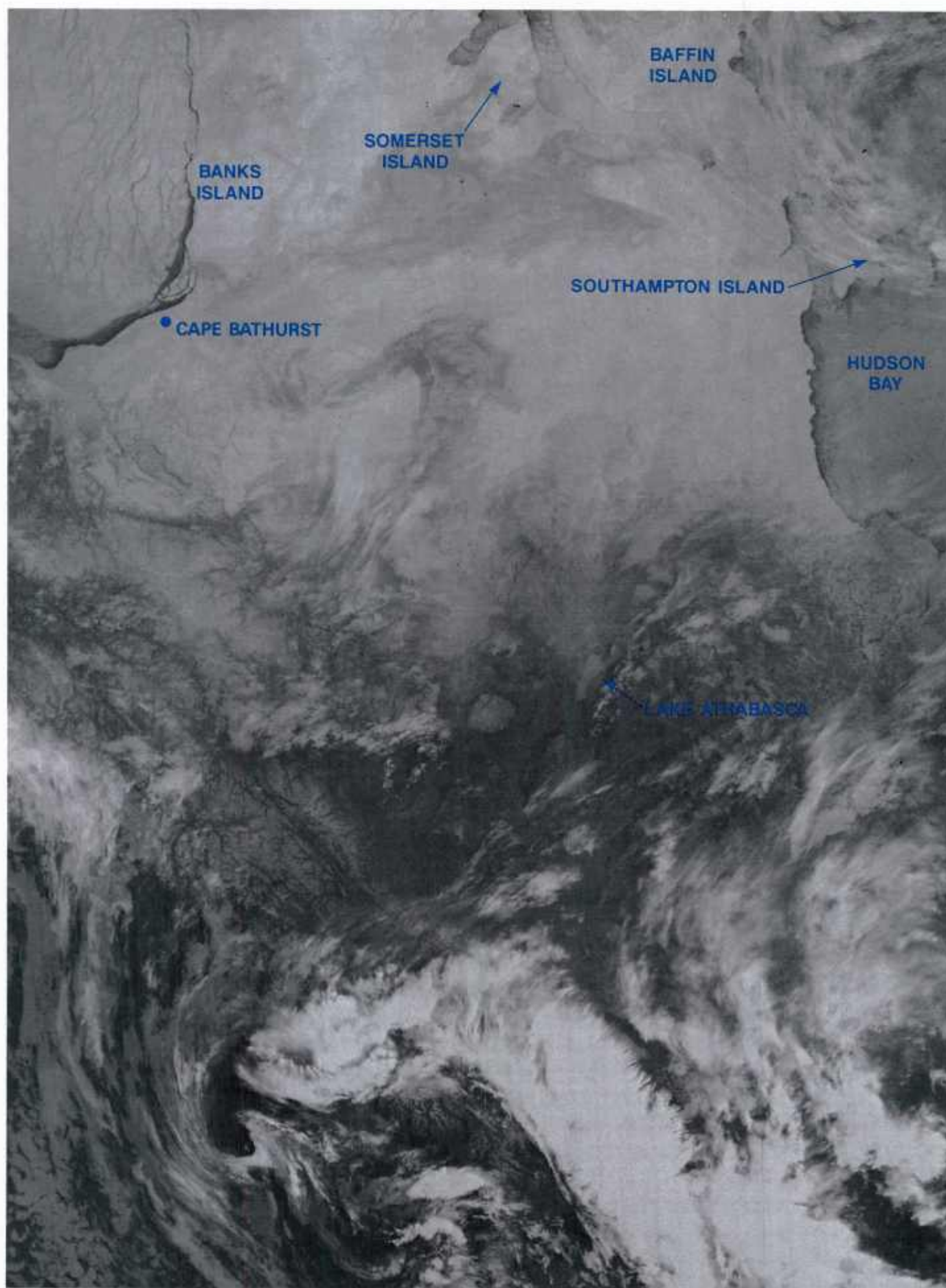
IB-9a FNOC surface analysis. 16 April 1986, 0000 GMT.

*16 April 1986*

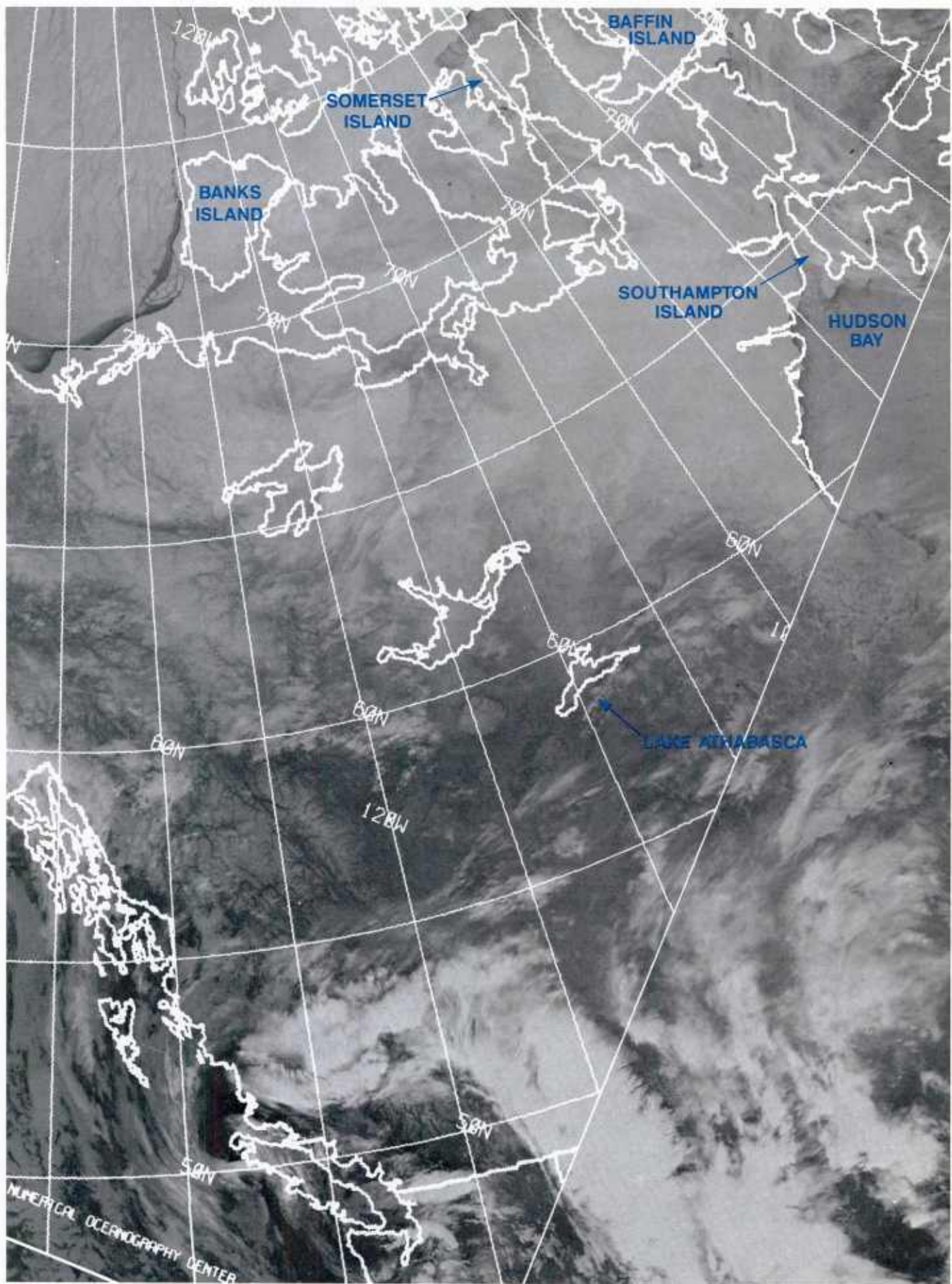
DMSP infrared data on this date at 0700 GMT (Figure 1B-10a) show continued evidence of aerosol/cloud generation from Banks Island leads and the Cape Bathurst polynya. An overlay to this figure (Figure 1B-11a) shows geographical boundaries.

At 1200 GMT DMSP infrared data (Figure 1B-12a) show a view of the vortex, now with a suggested center near 76N, 170E. An overlay to this figure (Figure 1B-13a) shows geographic boundaries. The gray tones of the major bands defining the vortex indicate that the bands are warmer than the ice pack to the north. This implies that the system is largely a low-level circulation with cloud tops radiating at a warm temperature near the top of the low-level inversion—probably near 900 mb. In this depiction the central portion of the vortex appears, at first glance, clear. Its internal temperature is apparently very close to that of the pack ice—obviously clear to the north. It will be shown in the discussion of the next image that this impression of a cloud-free interior is false; however, air/sea interaction effects in this image are noteworthy—in particular the plumes extending over the ice from a polynya on the south end of Banks Island and from near Cape Bathurst. Also, the North Slope region shows evidence of moisture plumes extending from a shore lead along the North Slope coast. The plumes extend southwestward suggesting that flow is from the northeast at low levels in this region.



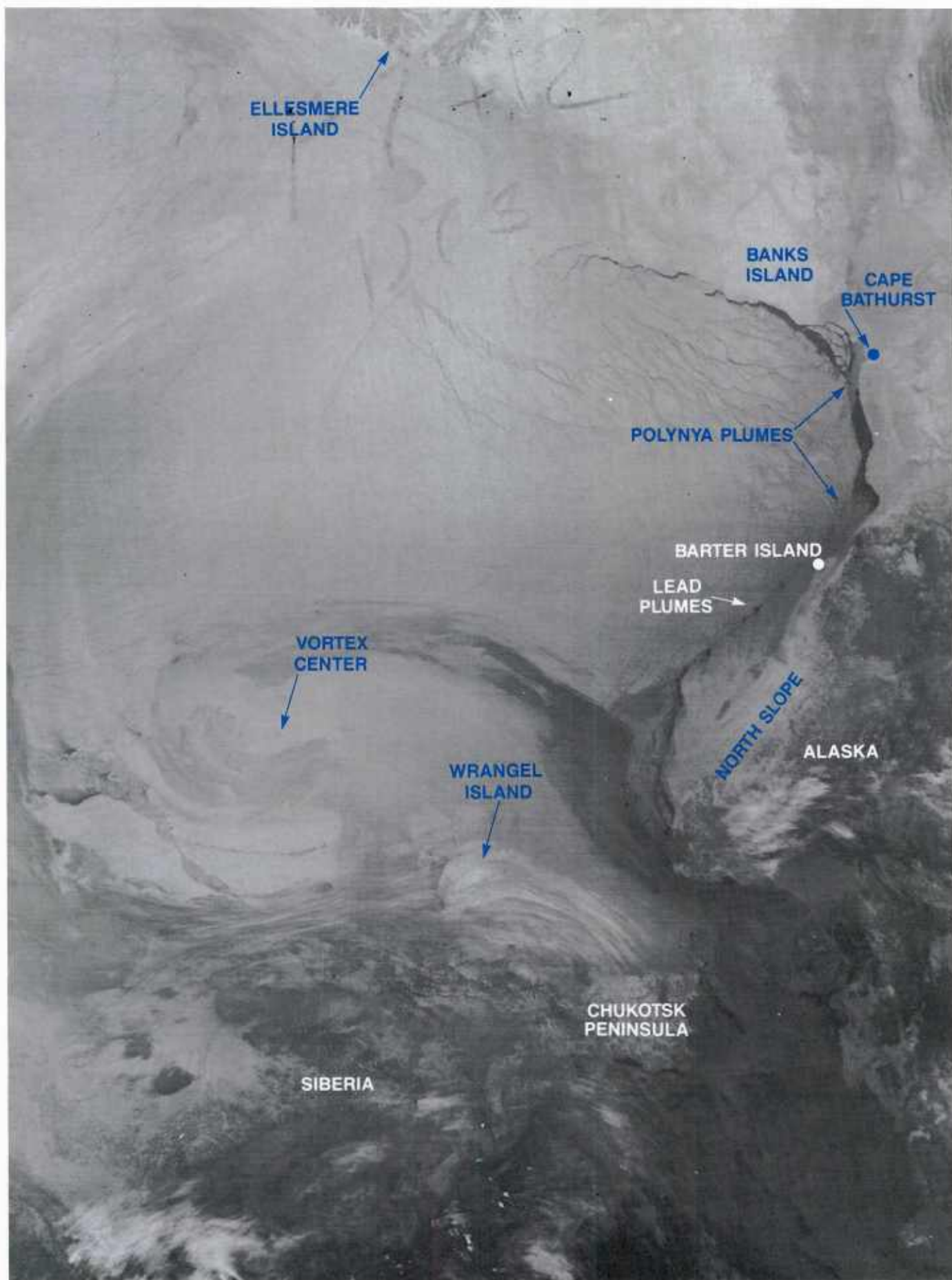


1B-10a DMSP infrared (TS) data. 16 April 1986, 0700 GMT.

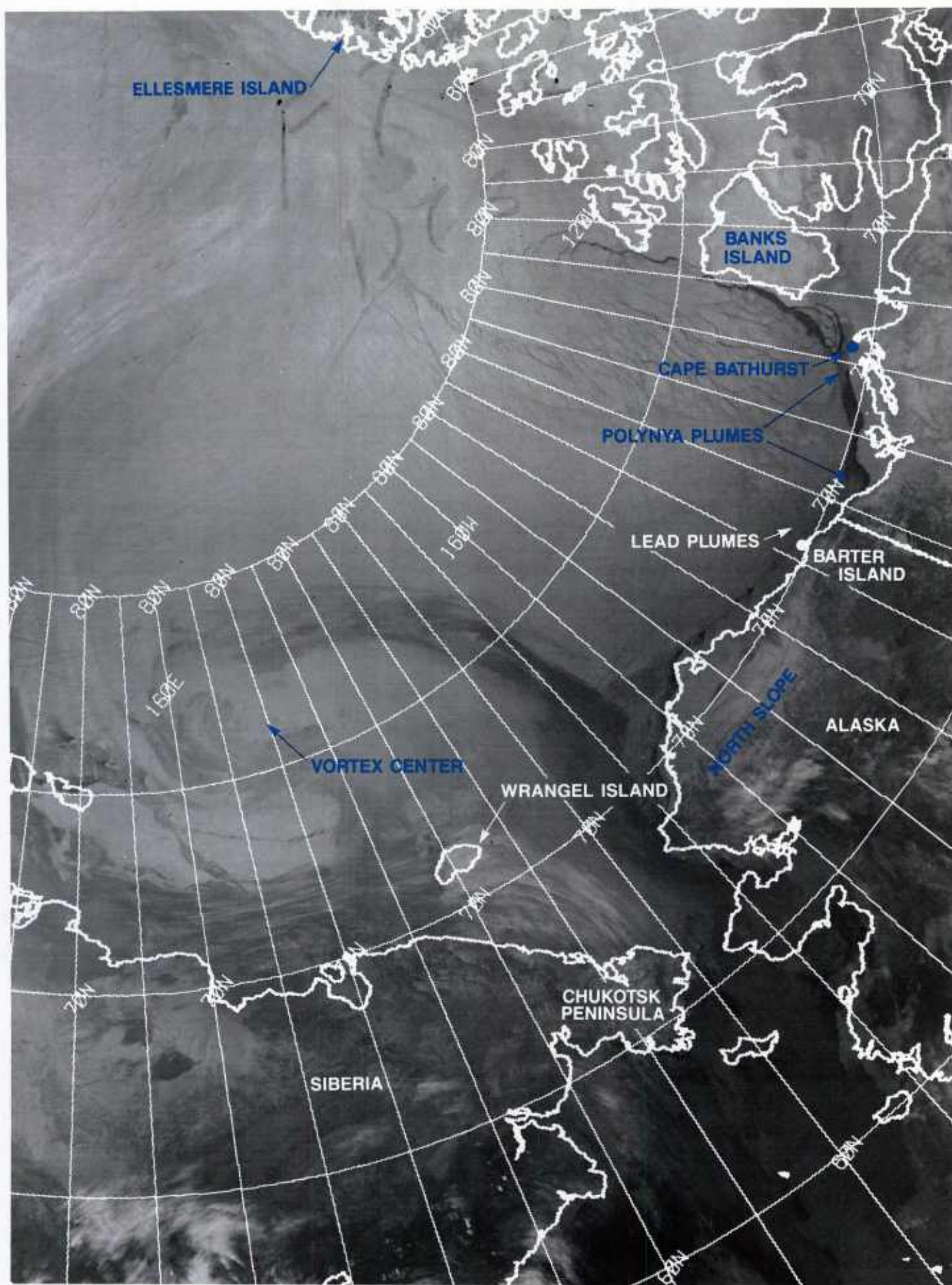


1B-11a DMSP infrared (TS) data (with geographic boundaries). 16 April 1986, 0700 GMT.





1B-12a DMSP infrared (TS) data. 16 April 1986, 1200 GMT.



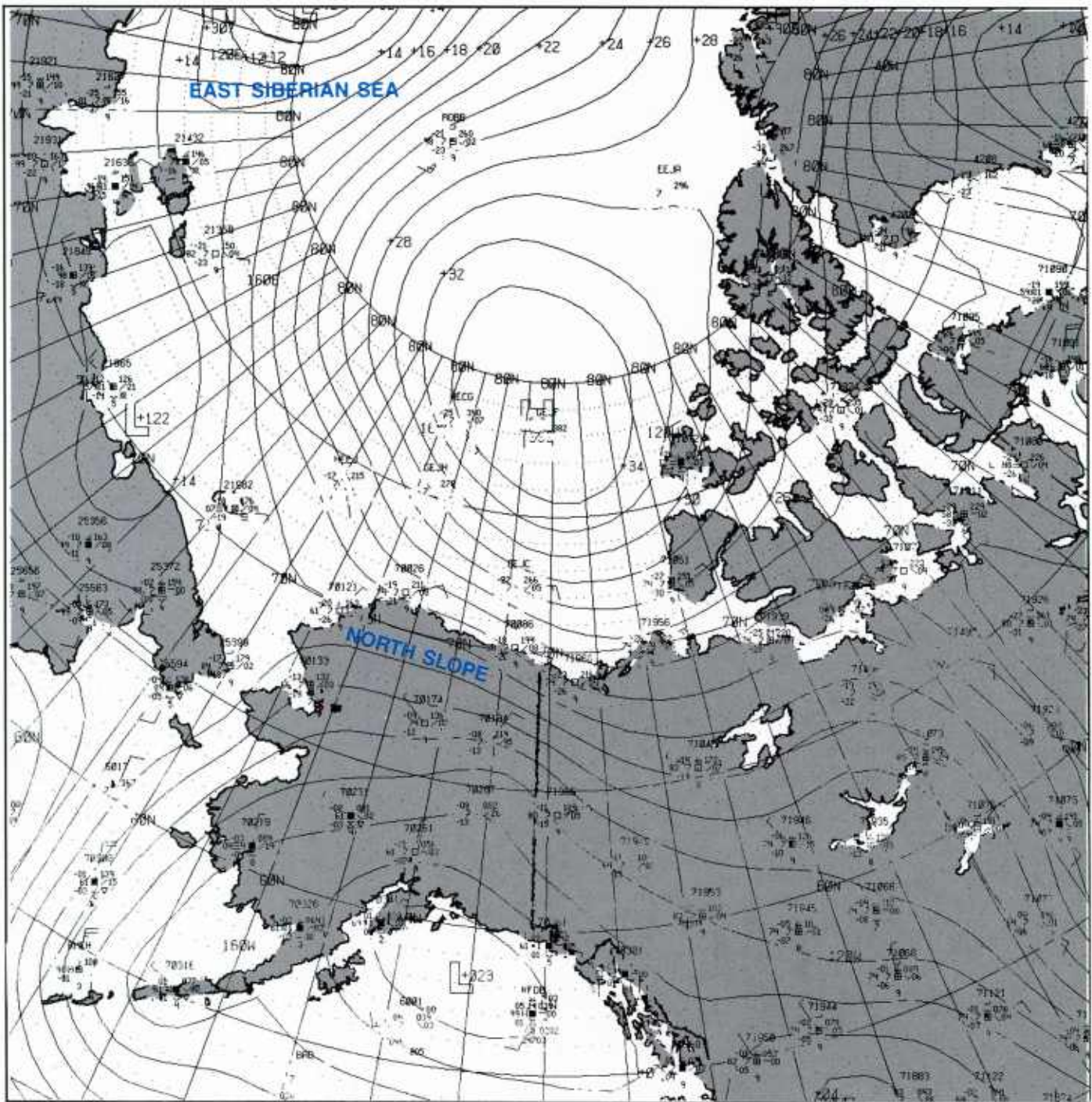
1B-13a DMSP infrared (TS) data (with geographic boundaries). 16 April 1986, 1200 GMT.



The surface analysis for 1200 GMT (Figure 1B-14a) verifies northeast flow over the North Slope but observations are too sparse to provide much substantiation of cloudiness or aerosol production from the lead effect. Note that the low center in the East Siberian Sea in the analysis is near 70.8N, 166.5E, some distance from the DMSP-suggested center near 76N, 170E. No evidence of a vortex at the map location appears in the DMSP data (Figure 1B-13a).

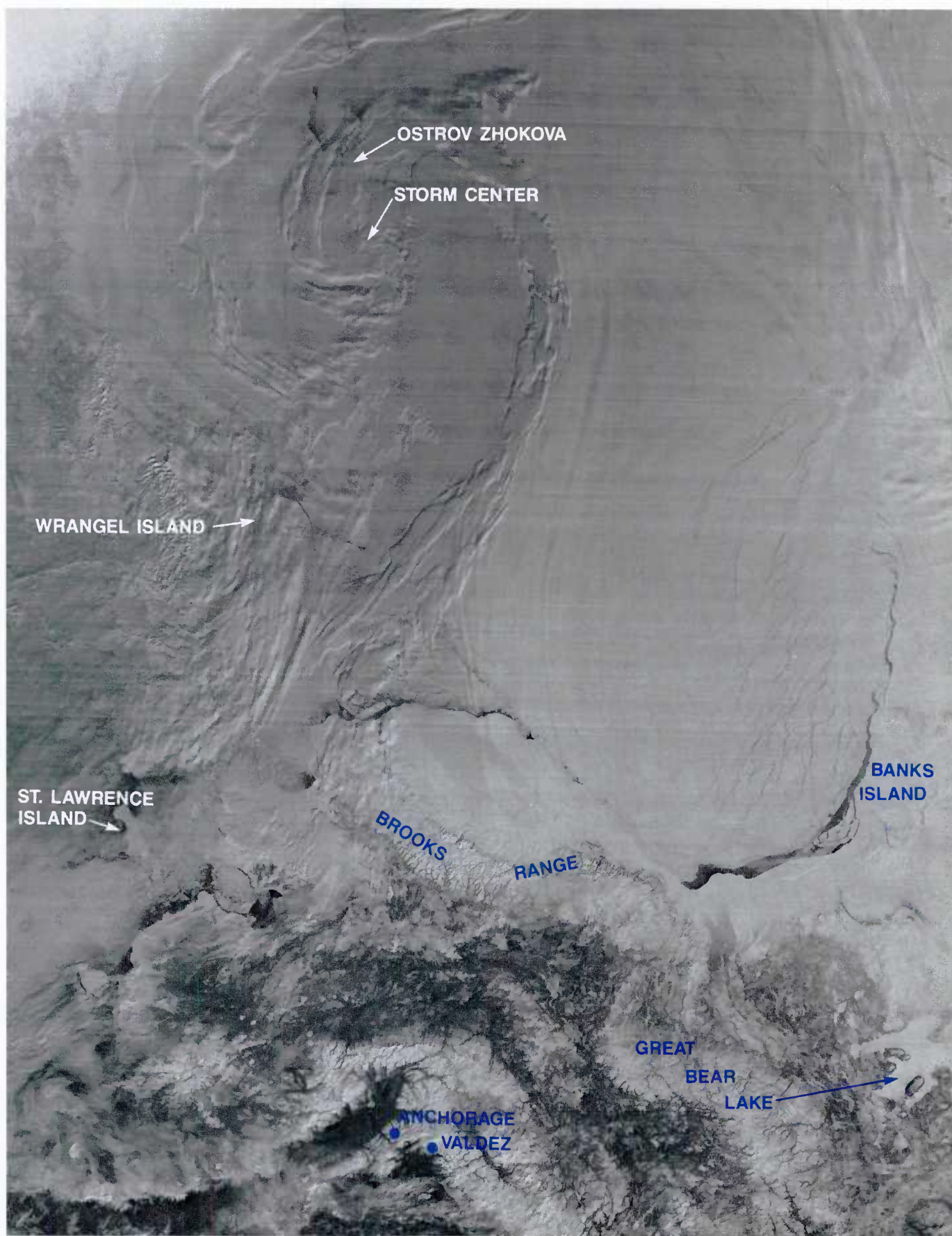
An excellent DMSP visible image shows the cloud vortex at 1900 GMT (Figure 1B-15a) with center near 76N 161E (Figure 1B-16a). The storm's interior is covered by a flat-appearing overcast, indicating that it has formed under a strong inversion. When this depiction is compared with the infrared view (Figure 1B-12a), it has to be concluded that the interior cloudiness is very low and therefore its cloud-top temperature is close to the temperature of the ice-pack. Fortunately, a station in the region, Ostrov Zhokhova (76.1N 152.8E, Station No. 21358), has sounding data. A RAOB from this station, at 1200 GMT on 16 April (Figure 1B-17a), reveals the extremely strong low-level inversion with a moist layer near the surface with dry air at all elevations above. The interior cloudiness has a top at a lower level than the enhanced cloud band encircling the periphery. This conclusion is also shown in Figure 1B-15a by the shadow of the encircling band which falls on the lower level cloudiness. A RAOB from the same station at 0000 GMT on 17 April (Figure 1B-18a) shows a more elevated inversion. This may reflect changed conditions in the warm cloud band encircling the storm.

The FNOC surface analysis for 16 April at 1800 GMT (Figure 1B-19a) shows a low center in the East Siberian Sea near 73.4N, 161.8W. The location of this FNOC surface analysis low center is getting closer to but is still south of the DMSP-viewed center at 76N, 161E (Figure 1B-16a).



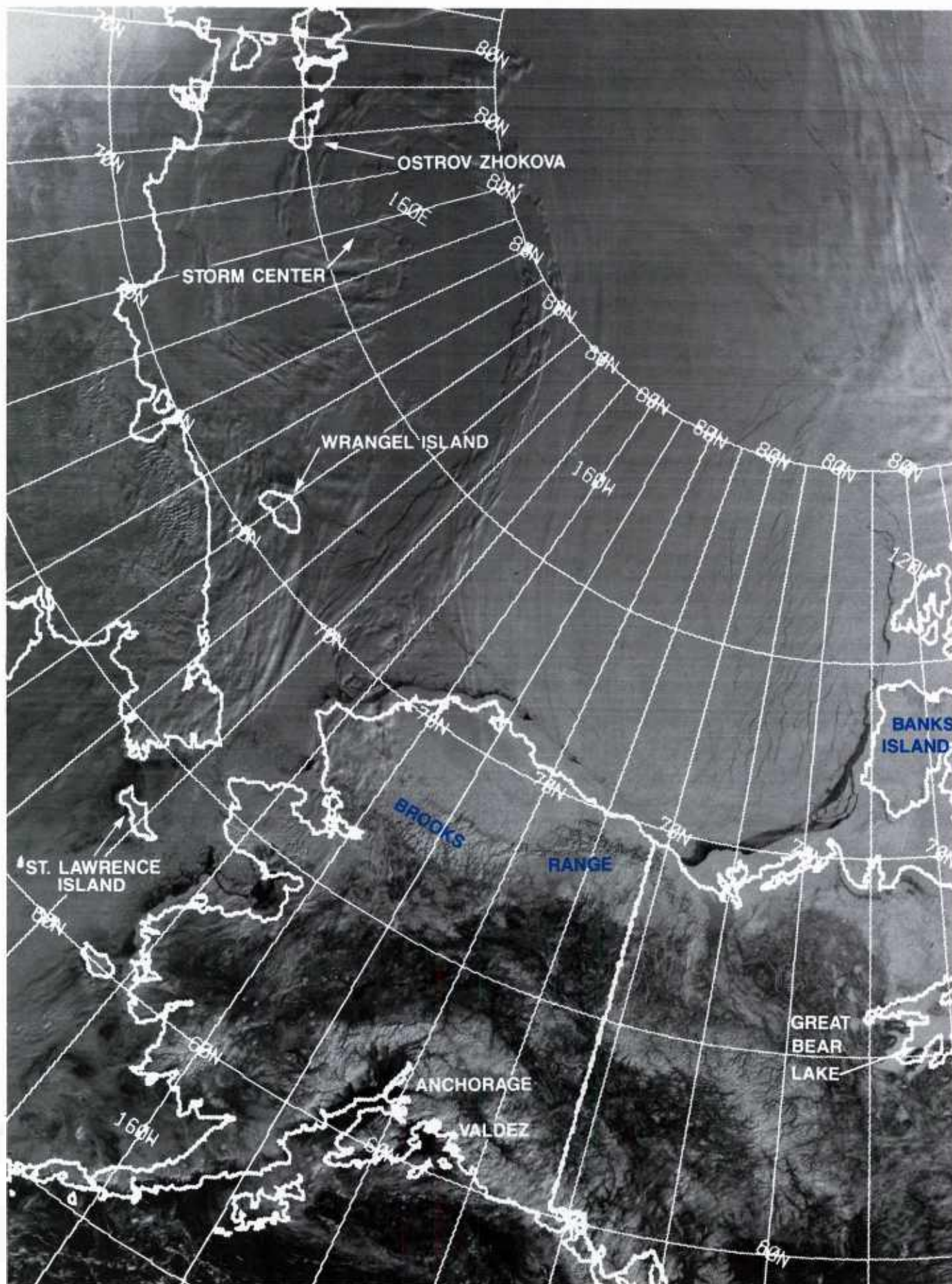
IB-I4a FNOC surface analysis. 16 April 1986, 1200 GMT.





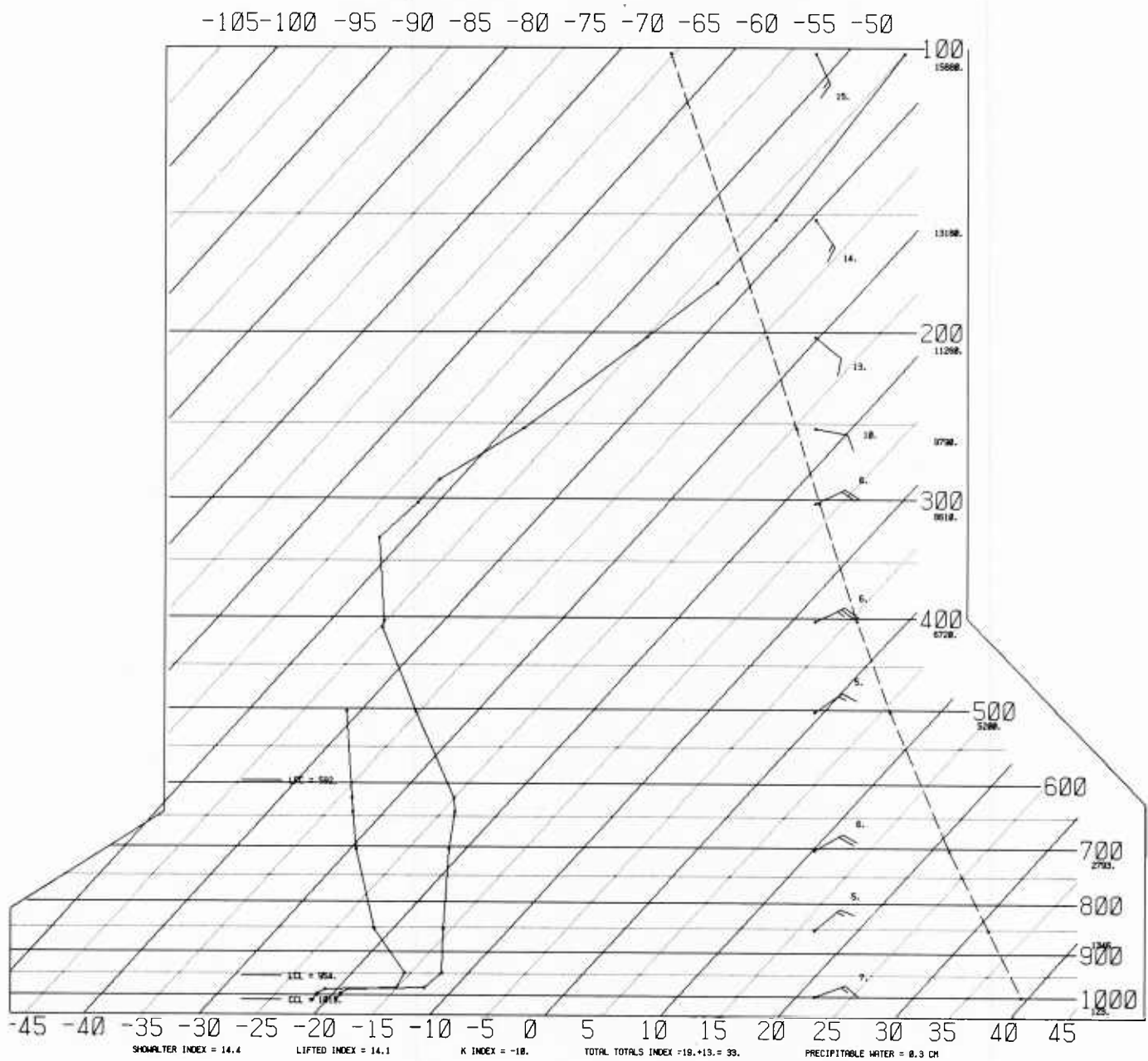
1B-15a DMSP visible (LF) data. 16 April 1986, 1900 GMT.



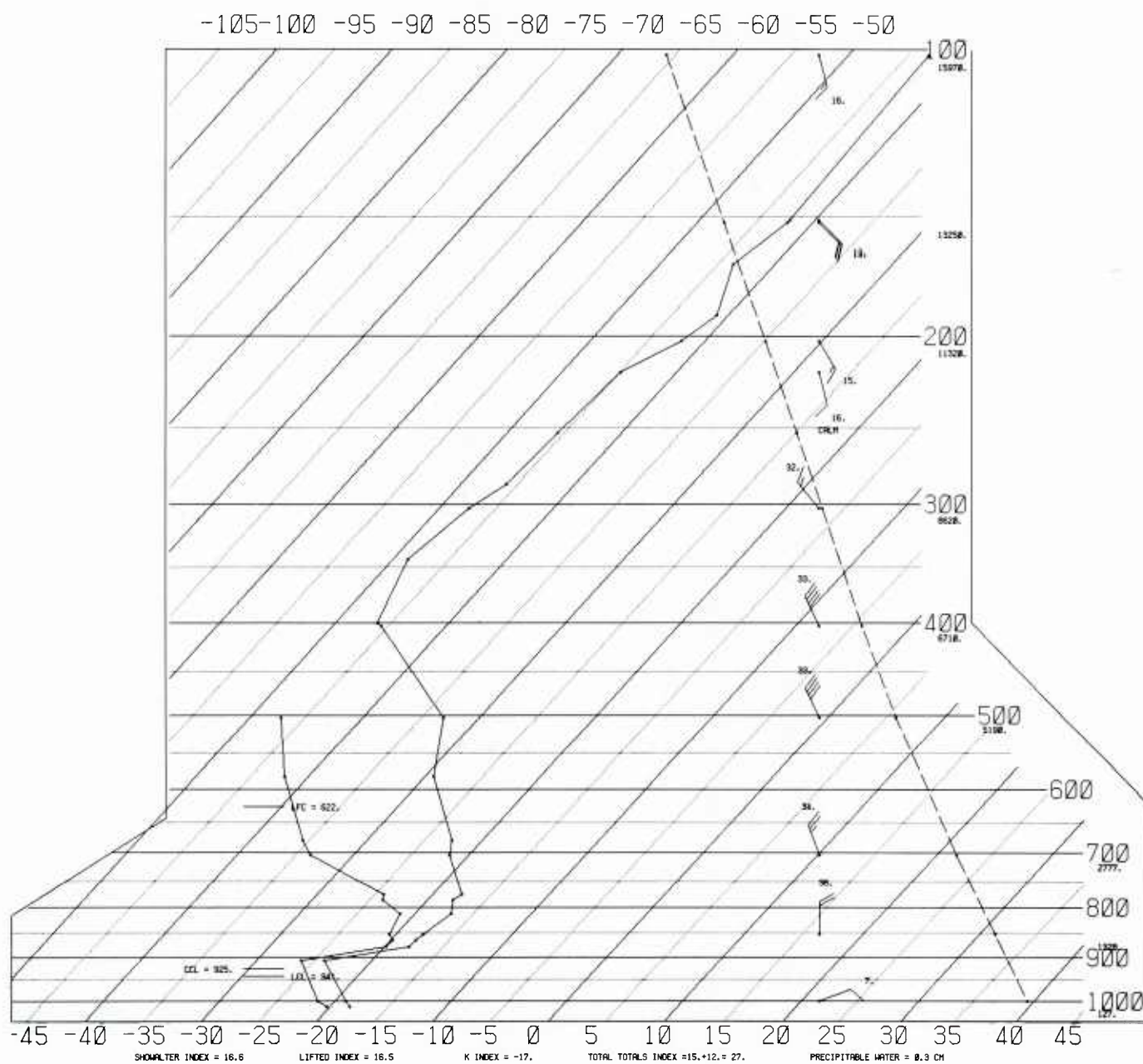


1B-16a DMSP visible (LF) data (with geographic boundaries). 16 April 1986, 1900 GMT.



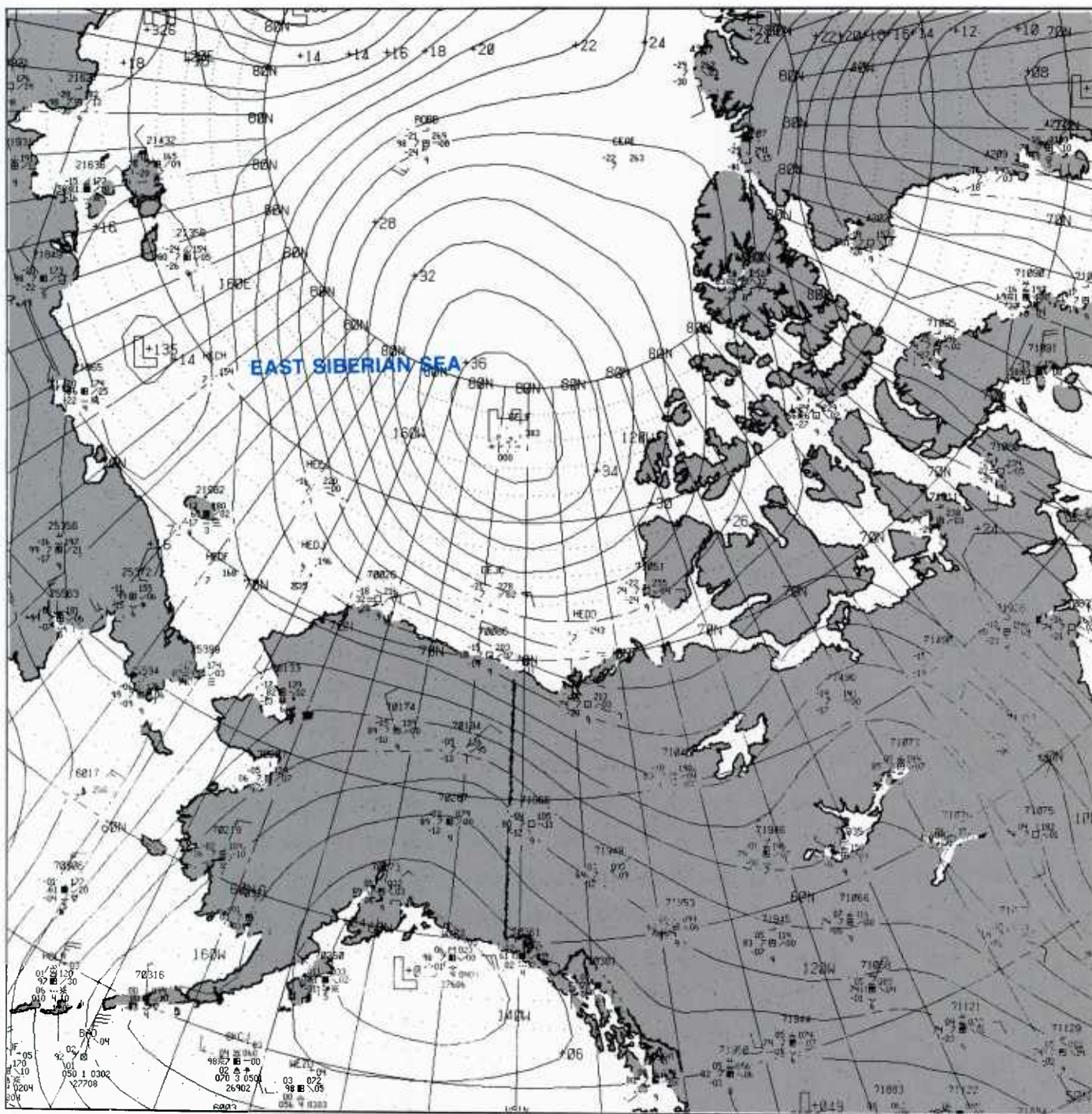


1B-17a Ostrov Zhokhova (76.1°N, 152.8°E) radiosonde data. 16 April 1986, 1200 GMT.



1B-18a Ostrov Zhokhova (76.1°N, 152.8°E) radiosonde data. 17 April 1986, 0000 GMT.





An infrared DMSP depiction, just an hour earlier than the visible data, is shown in Figure 1B-20a. A gridded view of the infrared depiction is shown in Figure 1B-21a. Figures 1B-20a and 1B-21a are especially interesting because very subtle gray shade variations show many regions where open leads and polynyas are venting moisture into the atmosphere over large areas. The shore lead along the North Slope is especially active. Barter Island appears to be under the influence of the plume emanating from an apparent polynya just northwest of Mackenzie Bay. A RAOB for this station, at 1200 GMT (Figure 1B-22a), shows strong ESE winds of 30 knots blowing past the station at low levels and the sounding reveals saturated conditions apparently resulting from plume formation in a shallow layer near 980 mb. A pronounced surface-based inversion provides a cap preventing dispersion of the plume to higher elevations. Note that an outer moist region seems to sweep from the Cape Bathurst area northwestward around the periphery of the cloud vortex system.

#### *17 April 1986*

A final DMSP infrared view of the region on this date at 1200 GMT is shown in Figure 1B-23a. A gridded version of this image is shown in Figure 1B-24a. The vortex center at this time is somewhat ill-defined but suggested near 75.5N, 160E. The FNOC surface analysis for this time (Figure 1B-25a) shows only a trough in that region; but, as we have seen using DMSP data, it has been possible to track a fairly well-defined low regularly from an initial position east of Wrangel Island 48 hours earlier. FNOC surface analyses never did resolve this feature.

The gridded DMSP image (Figure 1B-24a) is additionally interesting because it documents the existence of a very pronounced plume extending from the Amundsen Gulf or Cape Bathurst region. This plume sweeps over the North Slope and exits into the Chukchi Sea north of Cape Lisburne.

Surface winds, as shown on the surface analysis (Figure 1B-25a), are very strong from the northeast and are responsible for the notable westward extension of the plume.

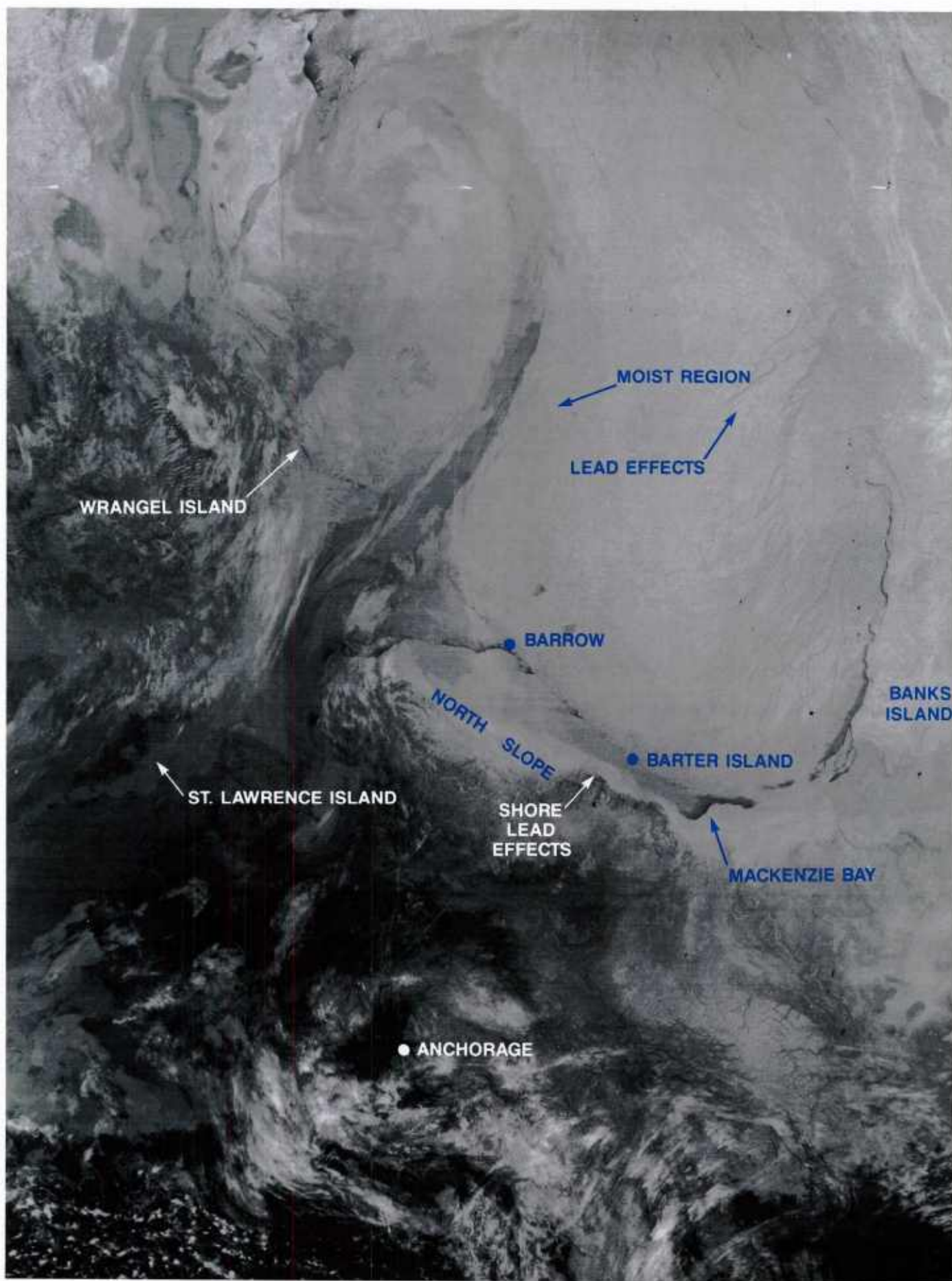
#### **Important Conclusions**

1. Low centers in the Arctic are more reliably detected and monitored by satellite than in conventional surface analysis.
2. During the month of April, shallow low-level, low-pressure systems in the Beaufort/Chukchi Sea have tendencies to track eastward toward the East Siberian Sea.
3. Much of the haze, aerosols, and low-level cloudiness in the Arctic are formed as a result of air-sea interaction effects in which a strong moisture flux from the sea to the air occurs over open water regions in leads and polynyas.
4. The infrared sensor is useful in delineating low-level moisture, haze, aerosols, and clouds. These will normally appear as a warmer (darker) shade of gray against the cold surface of the ice pack.

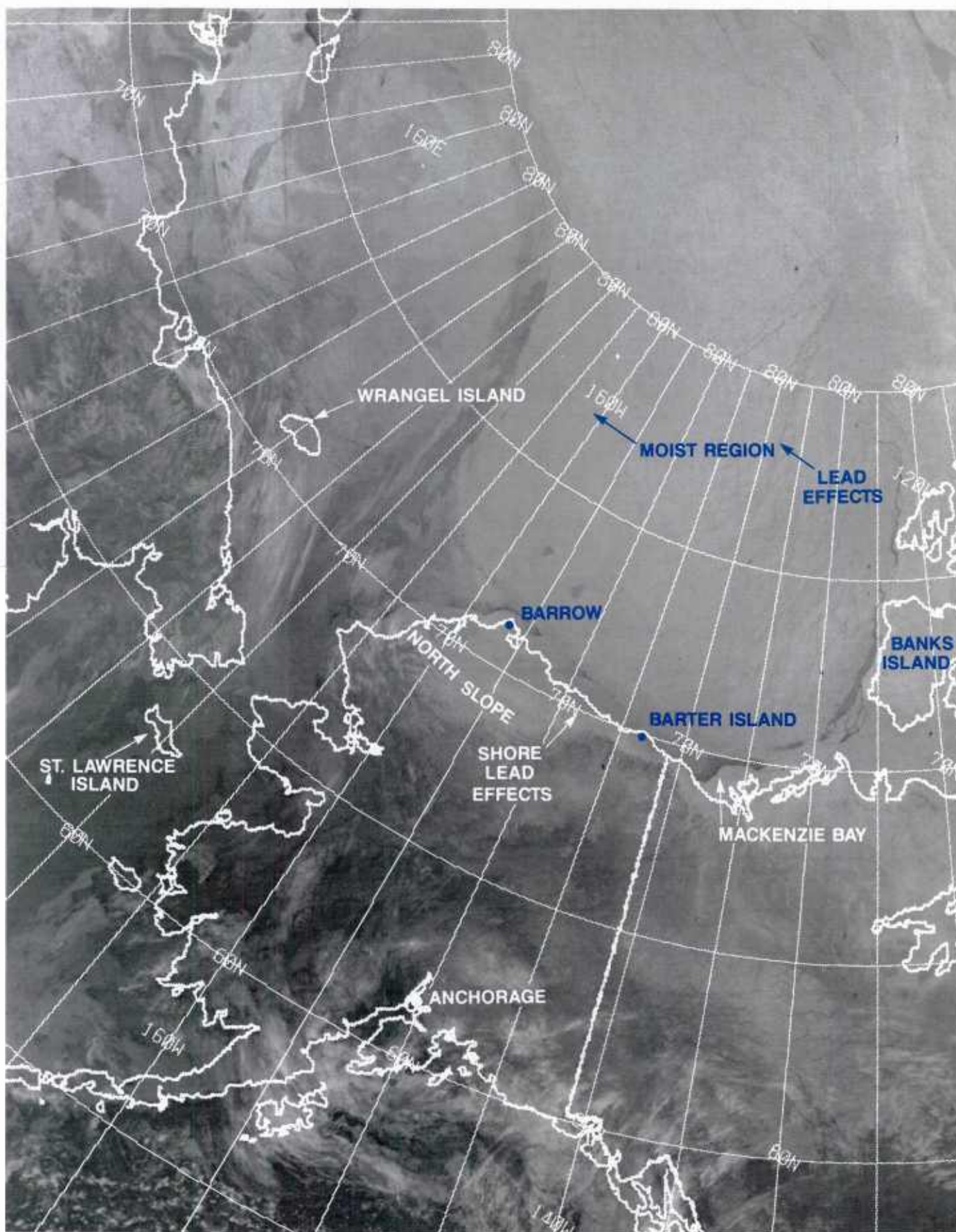
#### **Reference**

Bridgman, H.A., R.C. Schnell, G.A. Herbert, B.A. Bodhaine, and S.J. Oltmans, 1988: Meteorology and haze structure during AGASP II, Part 2: Canadian Arctic Flights, 13-16 April 1986, *J. Atmos. Chem.*



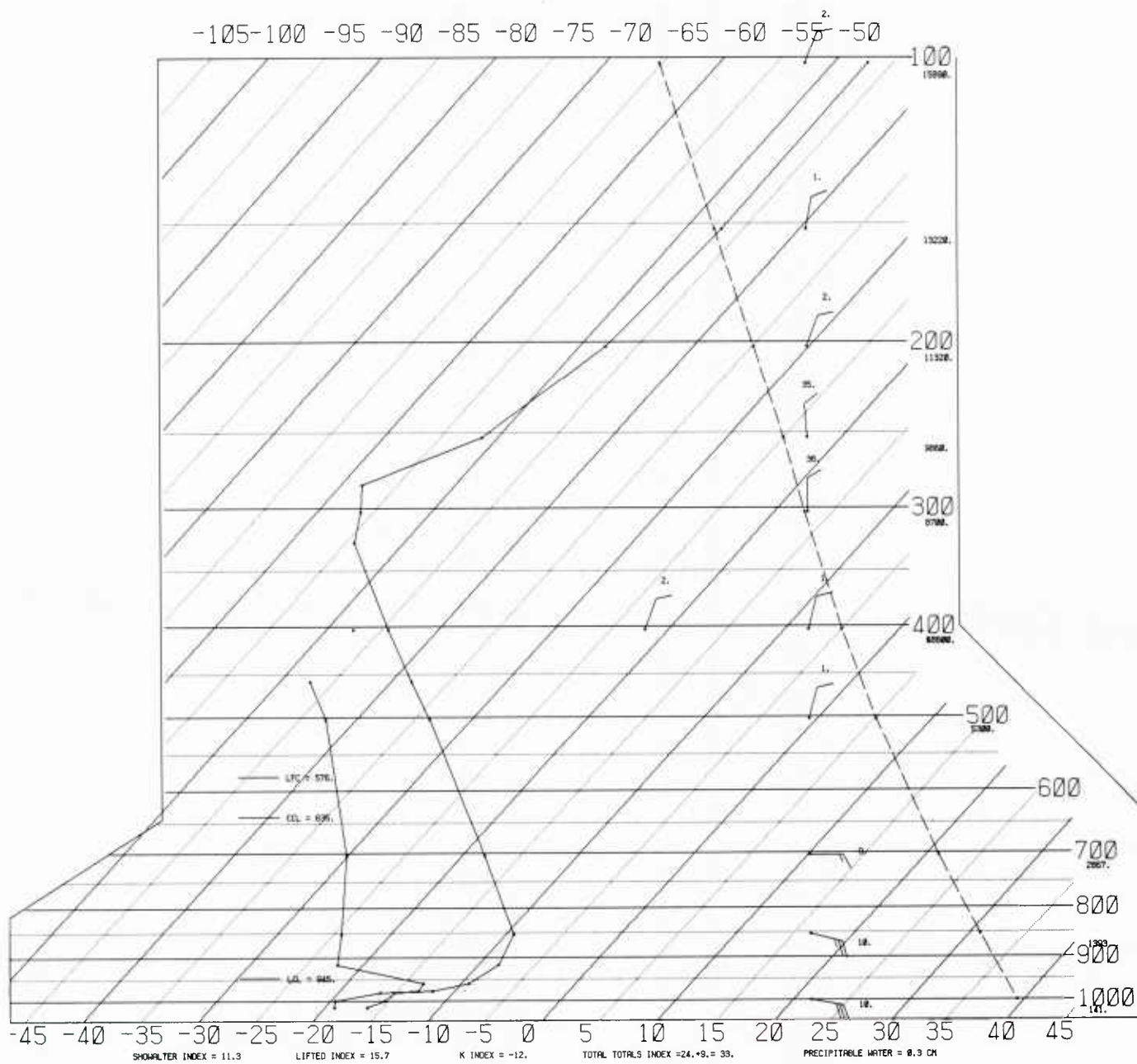


1B-20a DMSP infrared (TS) data, 16 April 1986, 1700 GMT.

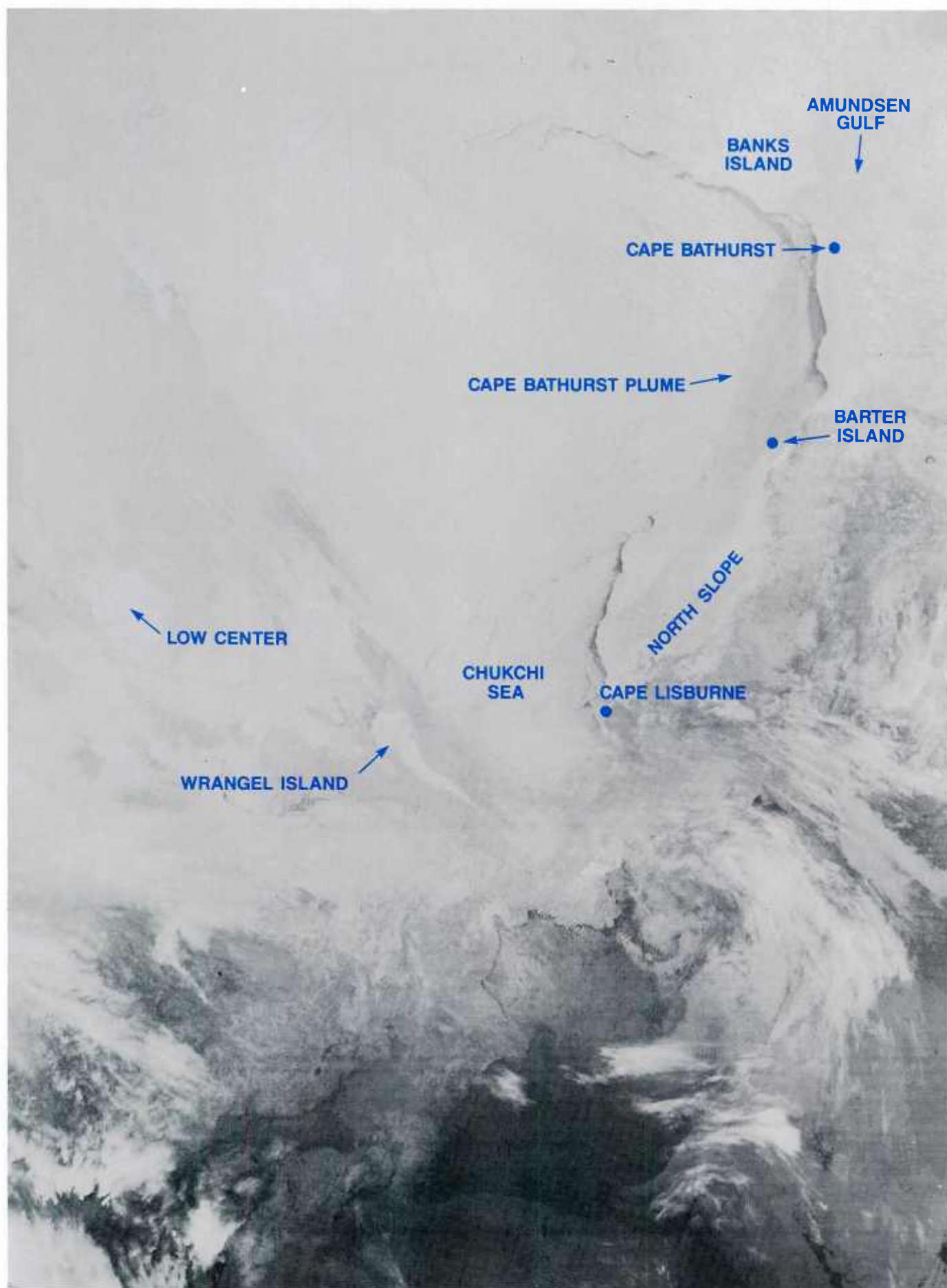


1B-21a DMSP infrared (TS) data (with geographic boundaries). 16 April 1986, 1700 GMT.



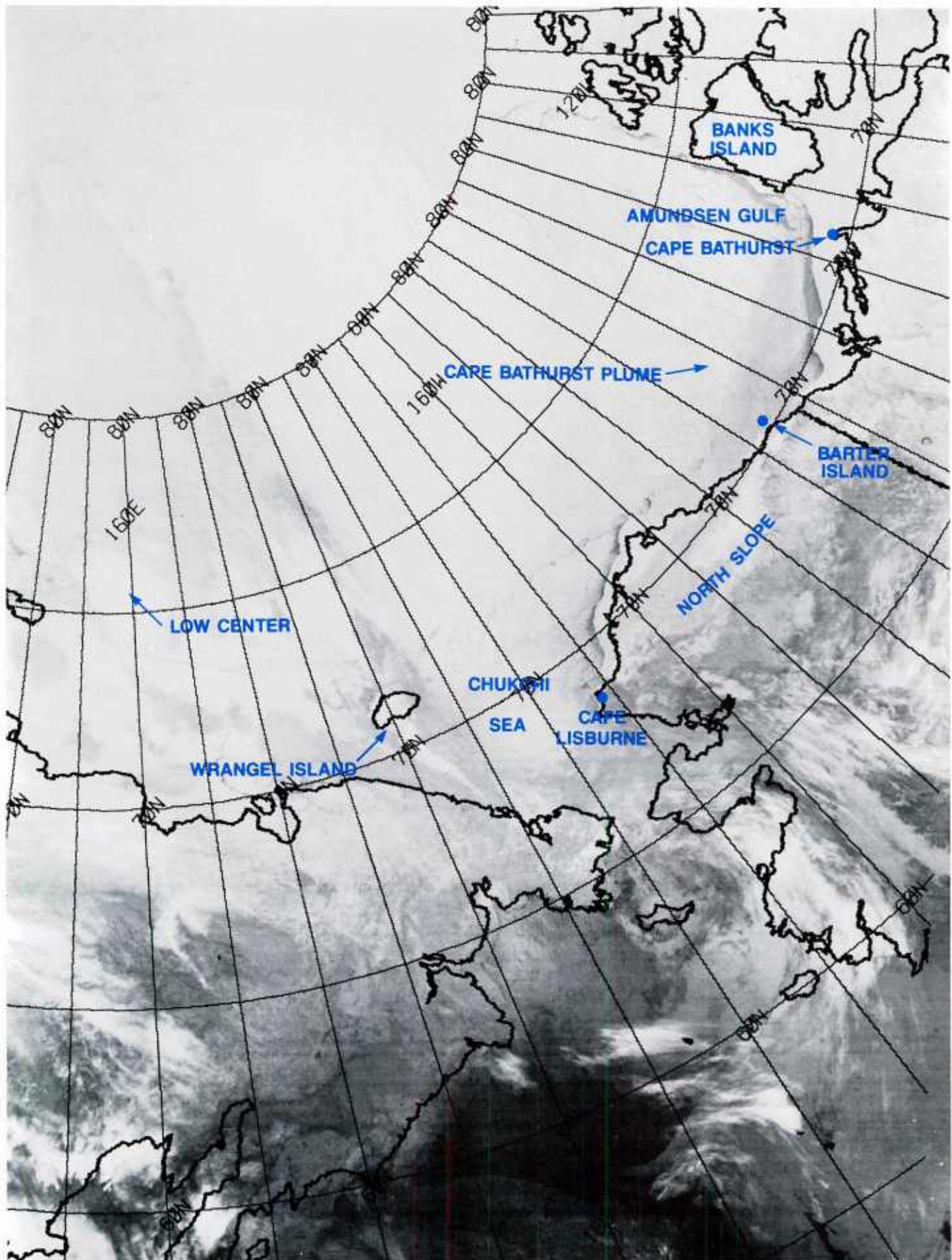


1B-22a Barter Island (70.1°N, 143.6°W) radiosonde data, 16 April 1986, 1200 GMT.



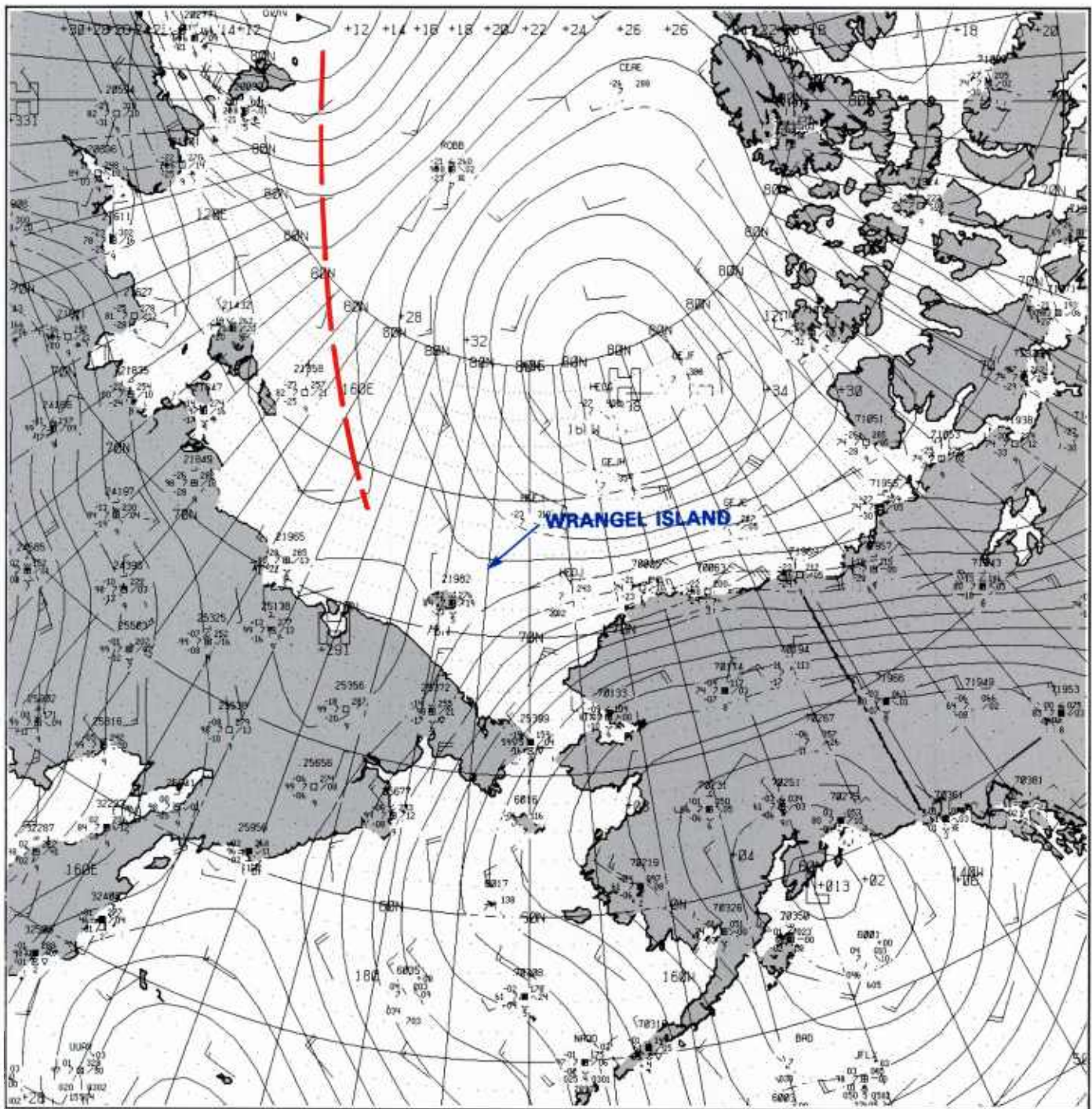
1B-23a DMSP infrared (TS) data. 17 April 1986, 1200 GMT.





1B-24a DMSP infrared (TS) data (with geographic boundaries). 17 April 1986, 1200 GMT.





1B-25a FNOc surface analysis. 17 April 1986, 1200 GMT.



## *Case 2 The “Col Cloud” Frontal Interconnections*

A distinctive-appearing cloud form present in many satellite images in the Arctic, as well as midlatitudes, is termed the “col cloud”: an elongated, lens shaped, low cloud mass, with a width on the order of 100–150 n mi and a length of 300–900 n mi. The cloud radiates at a warm temperature and appears as a dark gray shade in satellite infrared imagery. It often seems isolated from other cloud forms but in reality is a southward extension of frontal cloudiness stretching into a region of higher pressure, where the flow is no longer turning cyclonically in the trough containing the frontal band. At times the cloud seems definitely associated with a col, having higher pressure east and west of the cloud and lower pressure north and south. The major importance of being able to recognize this cloud pattern is the additional insight it provides in terms of frontal analysis, and the fact that the col cloud is always associated with a region covered by fog or low stratus. Its progress, along with that of the main front, can be monitored, sometimes for 2–3 days or longer and therefore is very useful in forecasts to pinpoint major regions of poor weather with known characteristics.

### *Col Cloud Over China—28 February 1987*

Figure 1B-28a is a DMSP infrared (TS) imagery over China, acquired at 2300 GMT on 28 February 1987. The frontal position from NMC's surface analysis on or at 0000 GMT 1 March 1987 has been superimposed on the image. Note that orographic wave clouds show good connection with the frontal position (see additional examples in NTAG Vol. 8, Part 1: Fett, 1990).

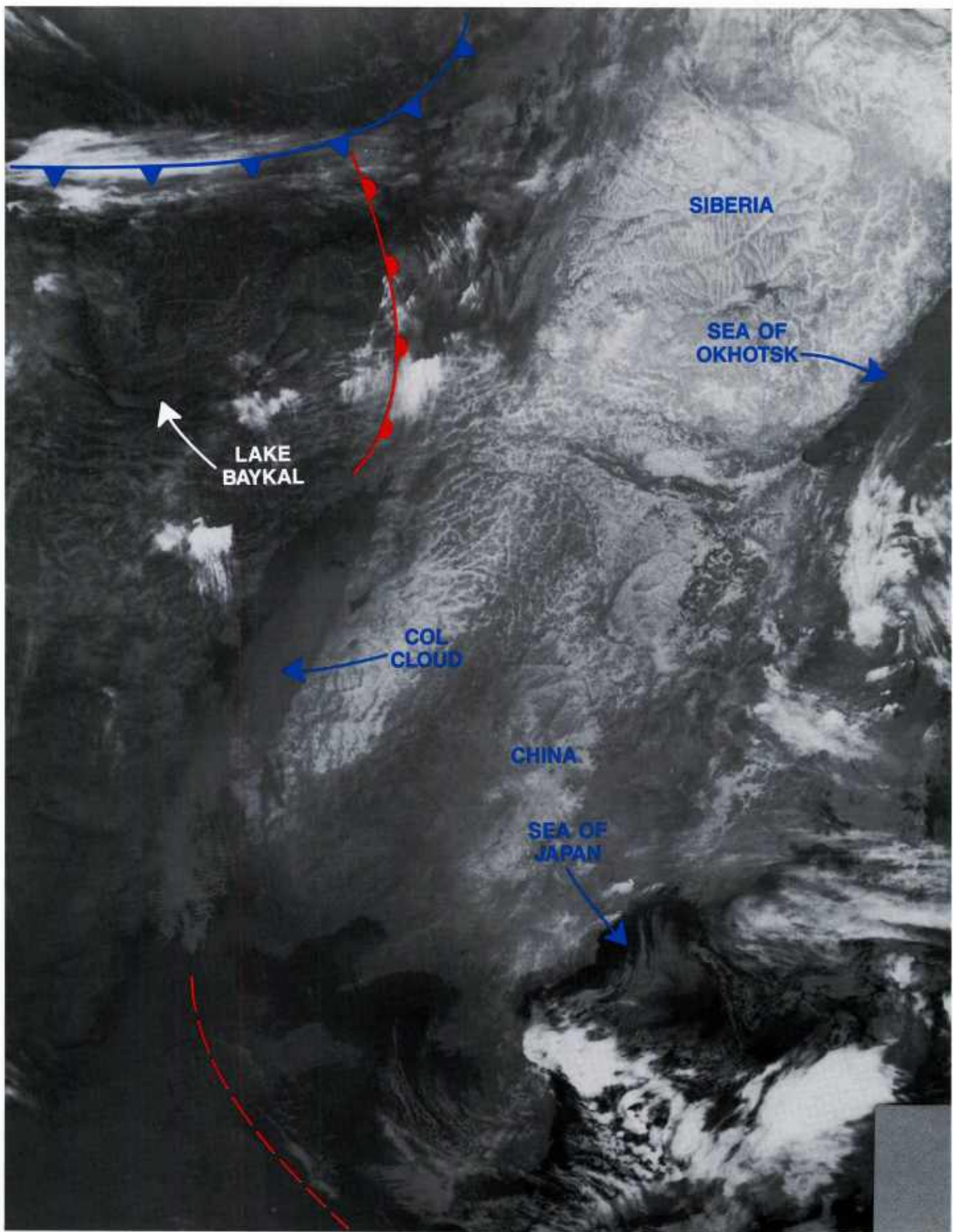
The terminus of the warm front on its southern extremity coincides with the beginning of a col cloud that extends southward over 750 n mi across the mainland of China. Gravity waves on its southern extremity suggest a northerly jetstream influence over that region, also implied by the nature of cloud striations from wave clouds further to the north.

The NMC surface analysis at 0000 GMT on 1 March 1987 is shown in Fig. 1B-29a with the dashed outline of the col cloud superimposed. It can be seen that the col cloud is a logical extension of the analyzed warm front southward, through a region of high pressure. It might even be argued that the position of a previous cold front extends further southward along the dashed line shown in the analysis to link with the frontal location shown over the Pacific from 130°–170°E.

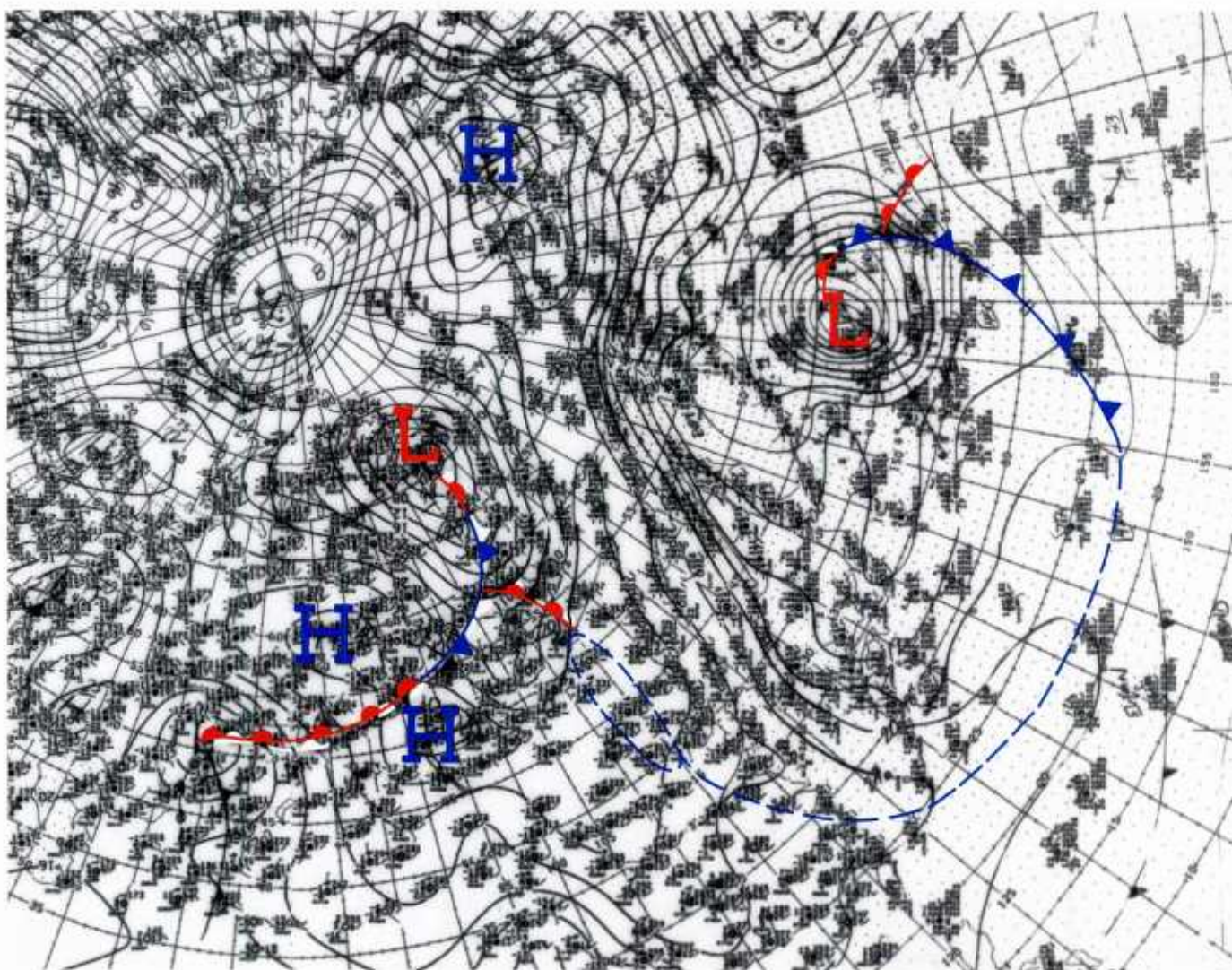
#### **Reference**

Fett, R.W., 1990: Navy Tactical Applications Guide, Vol. 8, Part 1, *Arctic: Greenland/Norwegian/Barents Seas Weather Analysis and Forecast Applications*. NEPRF TR 89-07, Naval Environmental Prediction Research Facility, Monterey, CA 93943-5006, 200 pp.





1B-28a DMSP infrared (TS) data. 2300 GMT 28 February 1987.



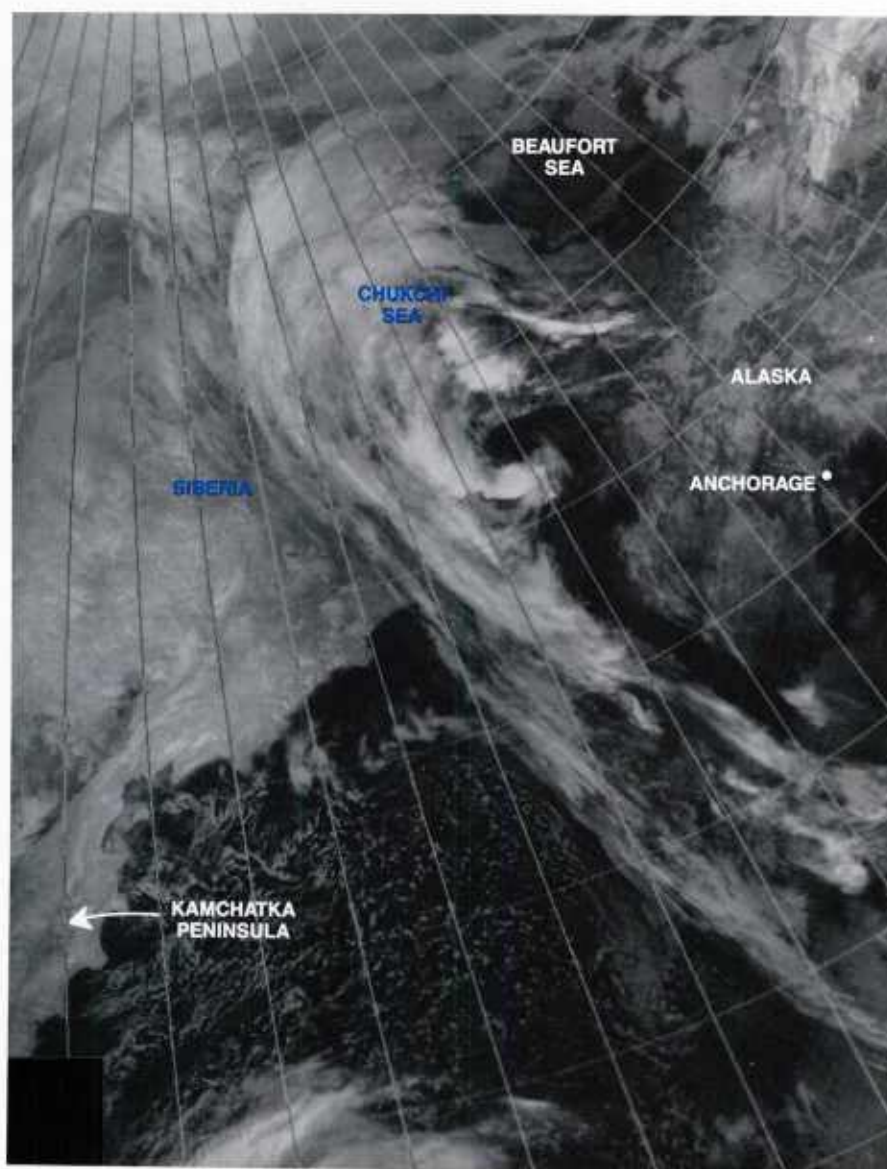
1B-29a NMC surface analysis. 0000 GMT 1 March 1987.



*Case 3 Frontal Movement/Col Cloud Formation Over Alaska  
(19–21 February 1989)*

*19 February 1989*

The DMSP infrared (TS) data acquired at 0632 GMT (Fig. 1B-31a) reveal a meridionally oriented band of multilayered clouds extending north-northwestward across the Bering Sea into Siberia. The cloud striations bend anticyclonically suggesting a ridge influence extending into the upper elevations over the Chukchi and Beaufort Seas.



1B-31a DMSP infrared (TS) data, 0632 GMT 19 February 1989.

The NMC 850-mb analysis (Fig. 1B-32a) at 1200 GMT shows that this high was a warm core high with a pocket of warm air centered over southeast Alaska. Warm core highs increase in intensity aloft; hence the vigorous circulation implied by the anticyclonically-turning cirrus striations in the satellite data. A packing of isotherms across Siberia and into the Chukchi and Beaufort Seas indicates a frontal zone in that region.

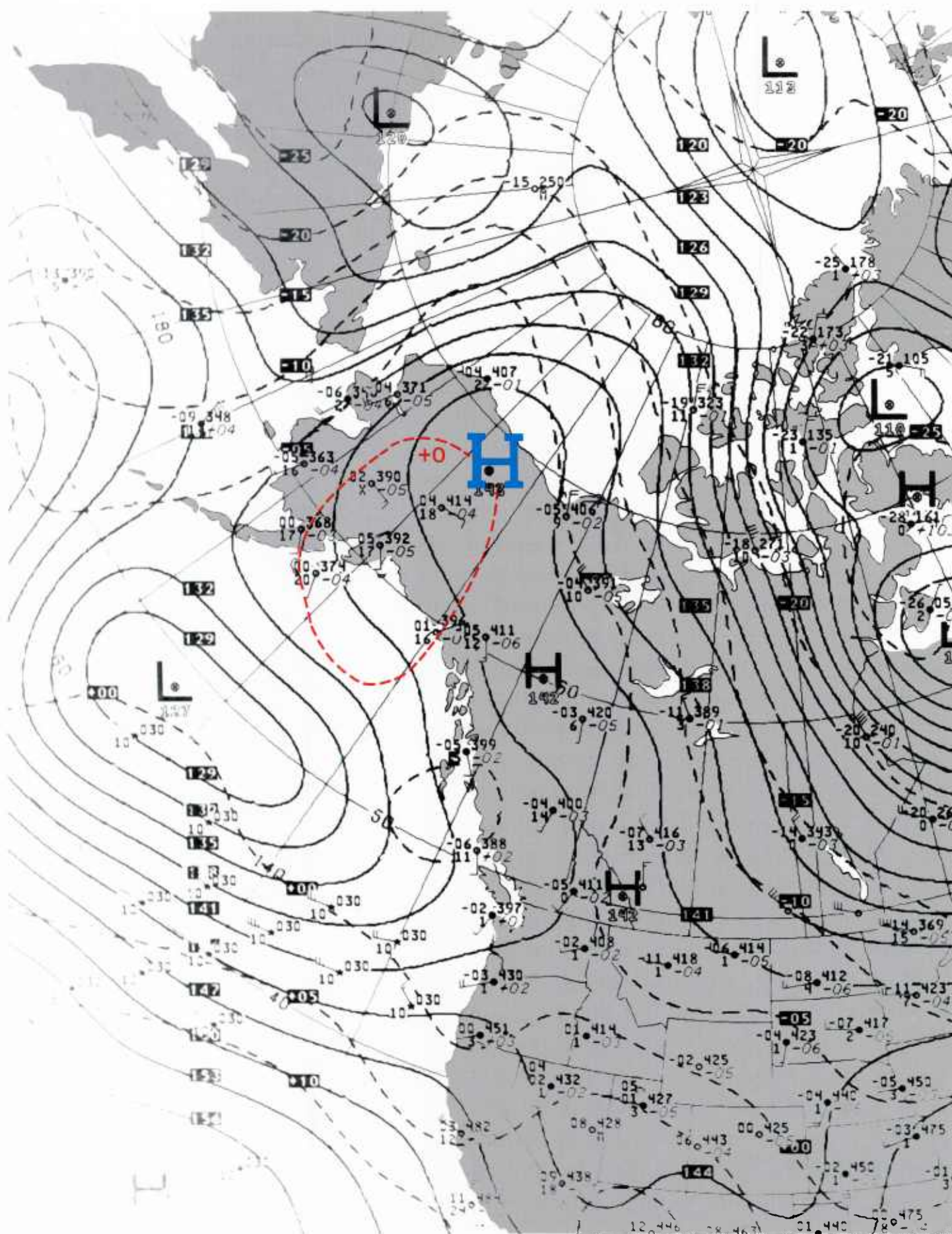
Figure 1B-33a is the NMC surface analysis for 0600 GMT. The analysis reveals low pressure over the northeastern tip of Siberia and a stationary front in the region of the packed isotherms noted on the 850-mb analysis (Fig. 1B-32a). Cumulonimbus cloudiness with snow showers is reported at 66°N 170°W in the region of heavy convective activity apparent near that location in the DMSP data (Fig. 1B-31a). A long narrow trough is analyzed extending southward over the Bering Sea. By 1745 GMT the cloudy band had moved considerably northward and eastward as shown in the DMSP infrared data (TS) (Fig. 1B-34a). Strong jetstream winds at this time have produced orographic wave cloud effects apparent at several locations over western Alaska, notably the Askinauk Mountains; the Kigluaik, Kougarok, and Bendelben Mountains on the Seward Peninsula; and the De Long Mountains and Lookout Ridge in the Brooks Range. Low pressure is suggested near 75°N 155°W.

The NMC surface analysis for 1800 GMT (Fig. 1B-35a) shows a low center near 75°N 172°W at the same latitude but well to the west of the suggested center based on satellite data. The analysis continues to show the long north-south oriented trough line extending from the low center through the Bering Strait and a stationary frontal zone over the Beaufort Sea.

### *20 February 1989*

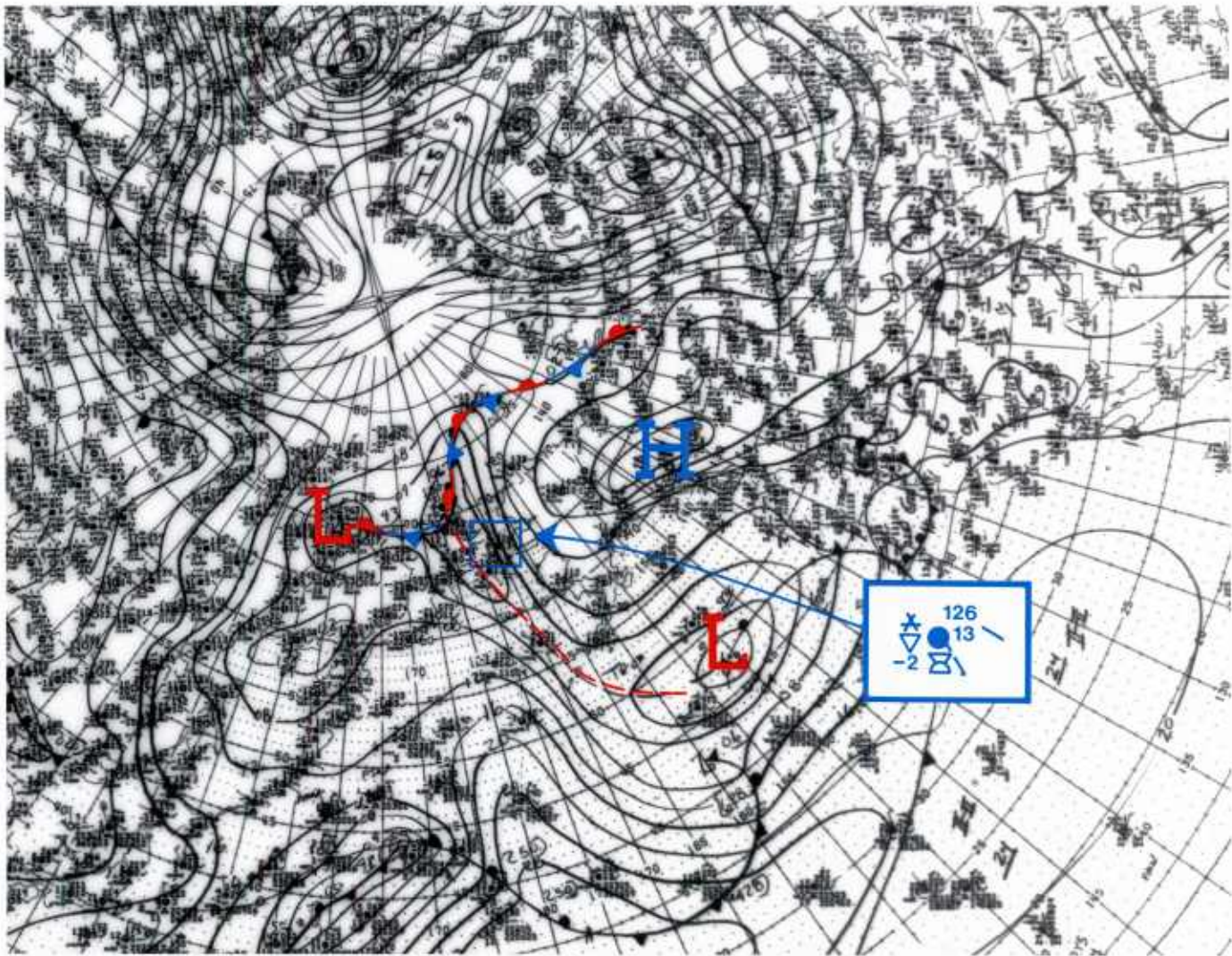
The DMSP infrared (TS) data received at 0438 GMT on this date (Fig. 1B-36a) are of special interest. The data continue to reveal a long north-south oriented, striated band of cloudiness passing over the western portion of Alaska. The cloudy band, however, terminates and merges into a warm gray shade area from 61°N down to the Aleutians, which largely block the protrusion of the gray shade to more southerly latitudes. The implication is that flow is northerly in that area. Suppression of higher level cloudiness, along with the warm gray shade effect, suggests that anticyclonic conditions exist over the region and that the gray shade is caused by radiation from the tops of virtually overcast but unresolved elements of low stratus or stratocumulus cloudiness, capped by a strong inversion. Strong winds aloft are still apparent in the DMSP data, especially over northern Alaska, where a lee wave cloud is apparent on the northern slope of the Endicott Mountains.





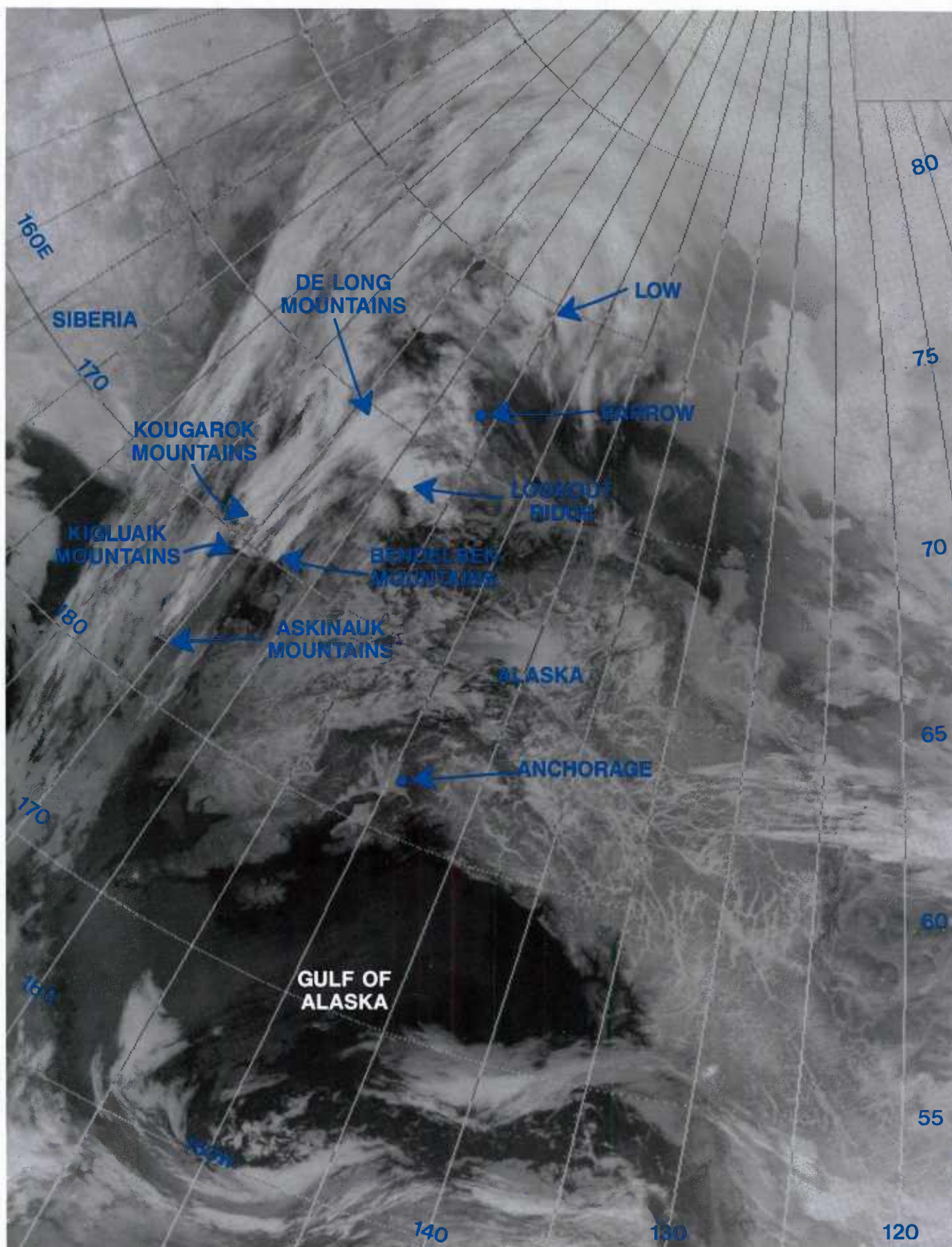
1B-32a NMC 850-mb analysis, 1200 GMT 19 February 1989.





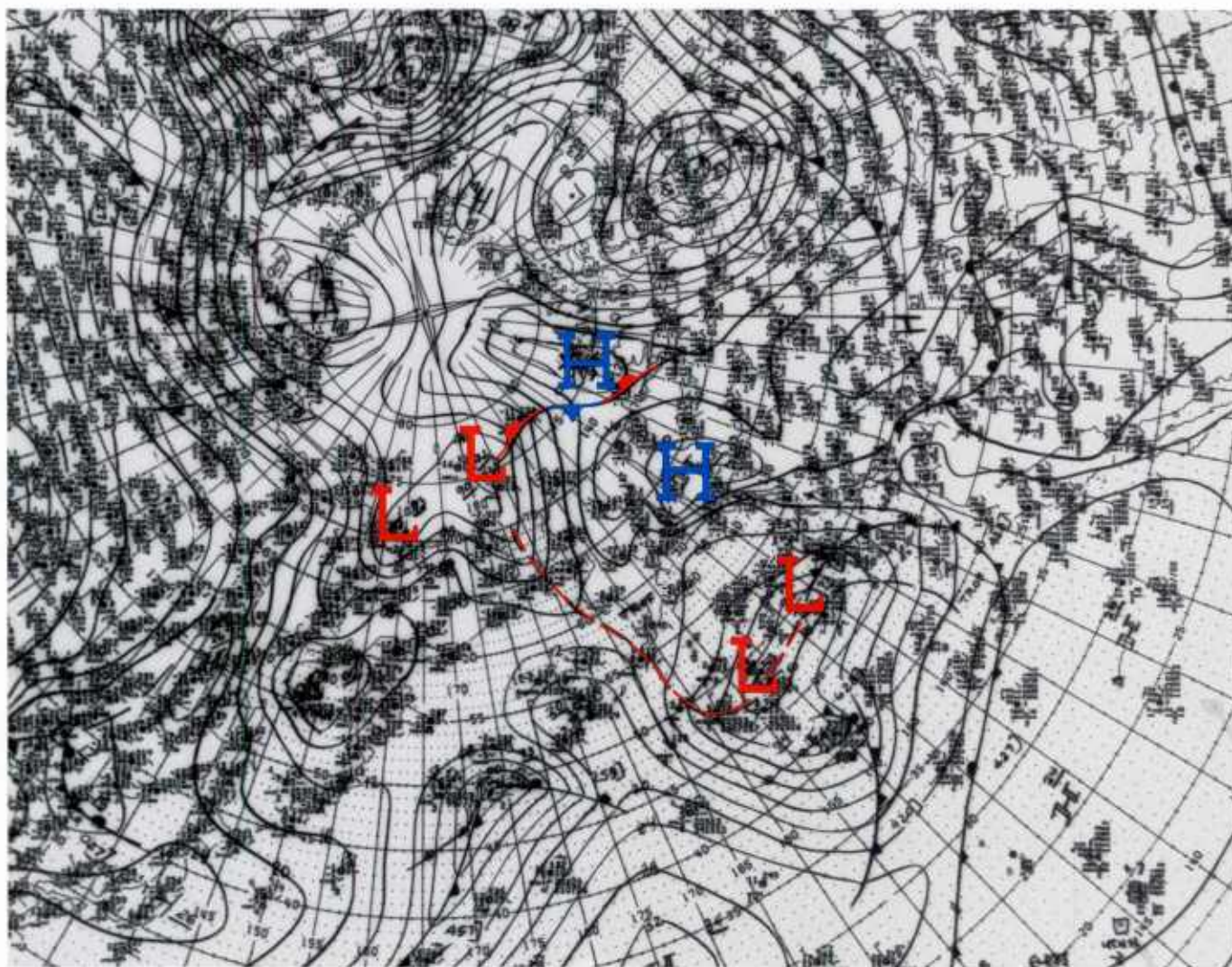
1B-33a NMC surface analysis. 0600 GMT 19 February 1989.





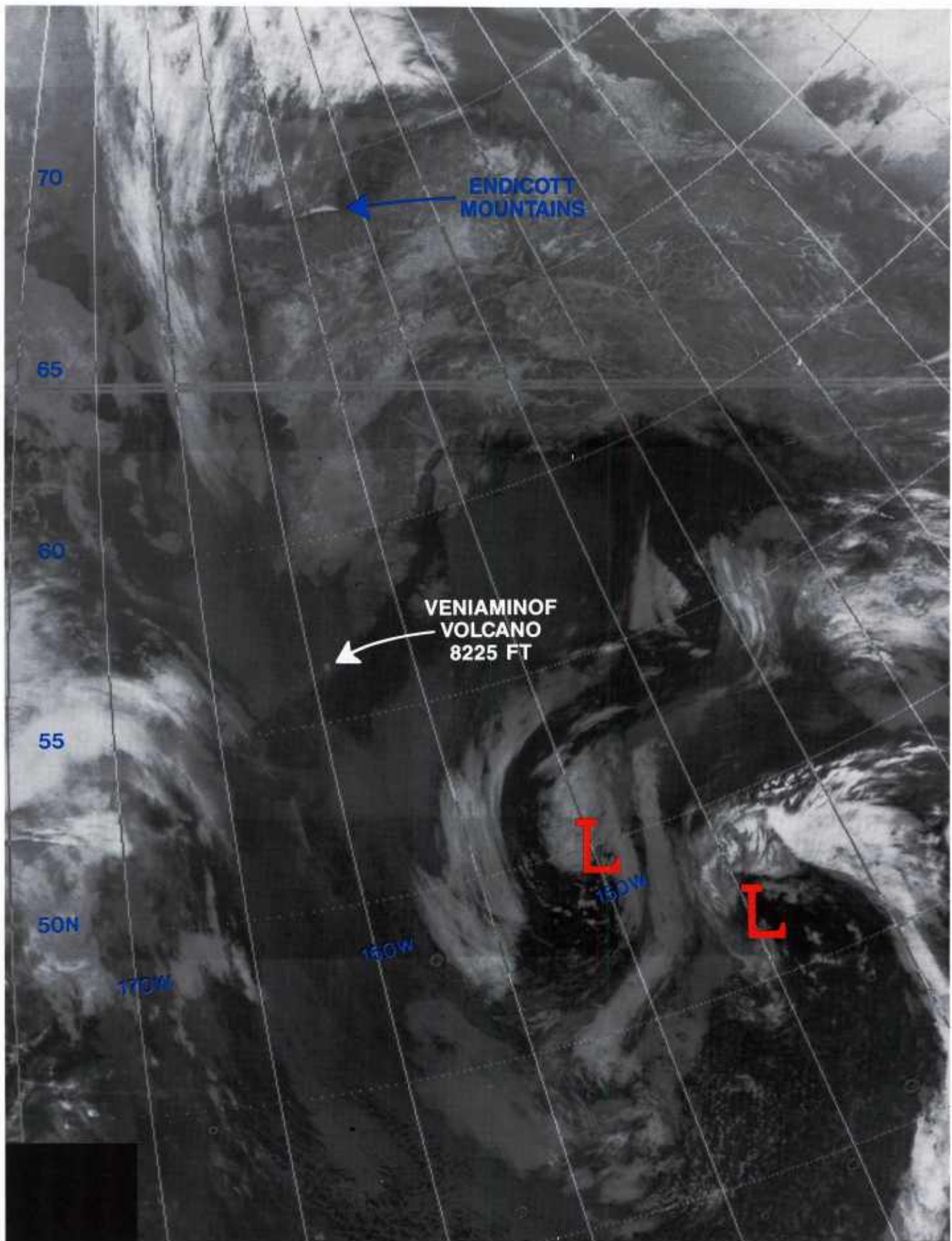
1B-34a DMSP infrared (TS) data. 1745 GMT 19 February 1989.





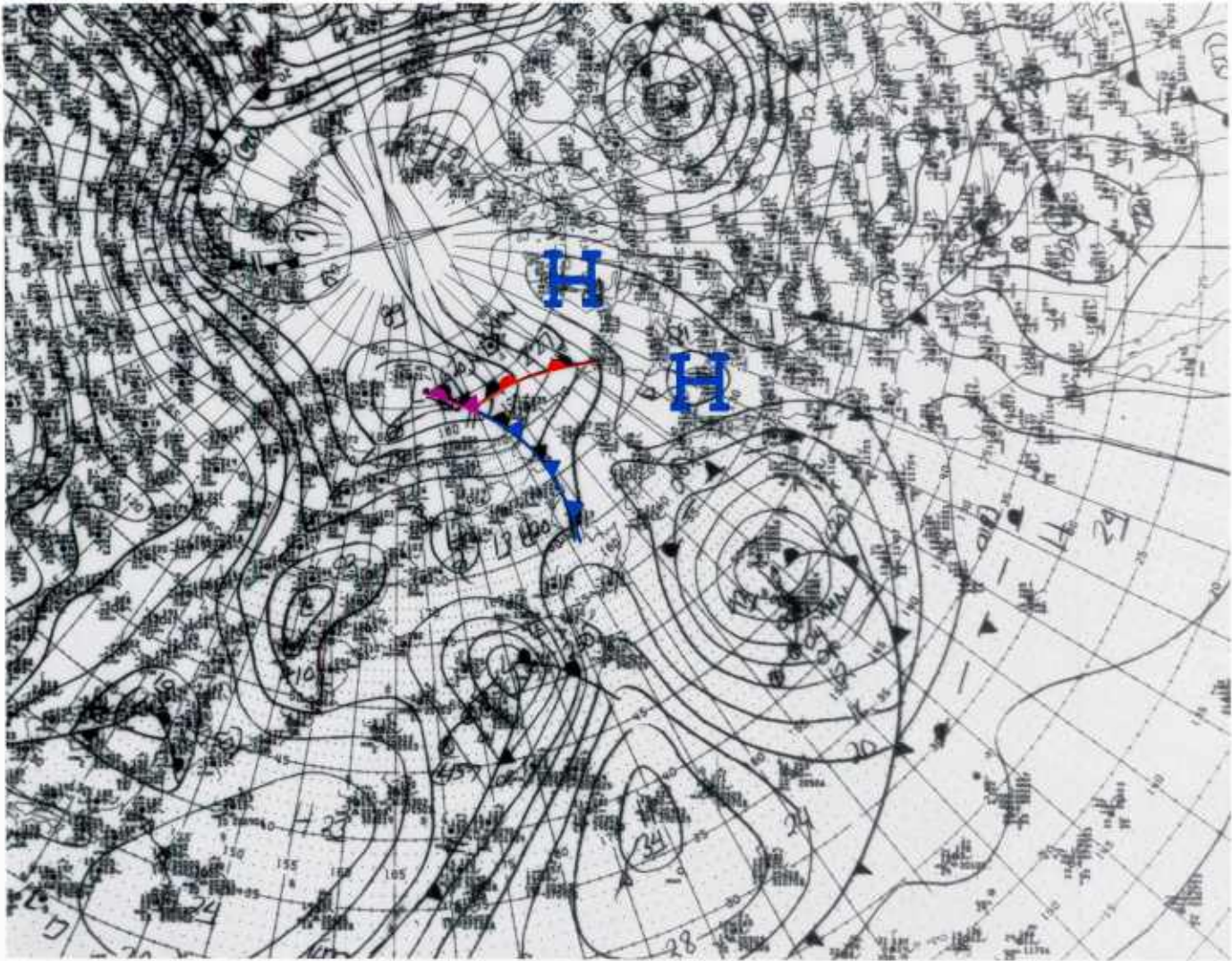
1B-35a NMC surface analysis. 1800 GMT 19 February 1989.





1B-36a DMSP infrared (TS) data. 0438 GMT 20 February 1989.

The NMC surface analysis for 0600 GMT (Fig. 1B-37a) verifies the protrusion of a ridge line over the gray shade area, while individual surface reports in the region confirm overcast conditions with stratocumulus cloudiness.



1B-37a NMC surface analysis. 0600 GMT 20 February 1989.



The NMC analysis at this time indicates a cold front coinciding with the band of striated cloudiness previously identified as a trough. Note the logical extension of the newly analyzed cold front southward through the gray shade region, past the Aleutians, to a vortex located near 50°N 150°W. Previous NMC analyses (Figs. 1B-33a and 1B-35a) explicitly showed this connection as a trough line. The NMC analysis does not show the low at 50°N 150°W. This low has probably formed as a result of vorticity in the trough connecting the northern low with the major low analyzed and shown in the satellite data near 47°N 145°W. Higher pressure in a col-like region, now north of the Aleutians, separates the two systems.

By 1400 GMT a very interesting cloud form appears evident, as shown in DMSP infrared (TS) data acquired at 1449 GMT (Fig. 1B-38a). Note the abrupt transition of cloud top temperatures from cold, north of the Brooks ridge line, to warm, in the elongated cloud mass to the south. This is the col cloud, a region of overcast low stratus or fog representing the frontal band in a region where flow is no longer strongly cyclonic.

Figure 1B-39a, the NMC surface analysis for 1200 GMT, shows that a ridge line extends over the col cloud region. Figure 1B-40a, the corresponding NMC 850-mb analysis, shows a col in the area of the cloud formation.

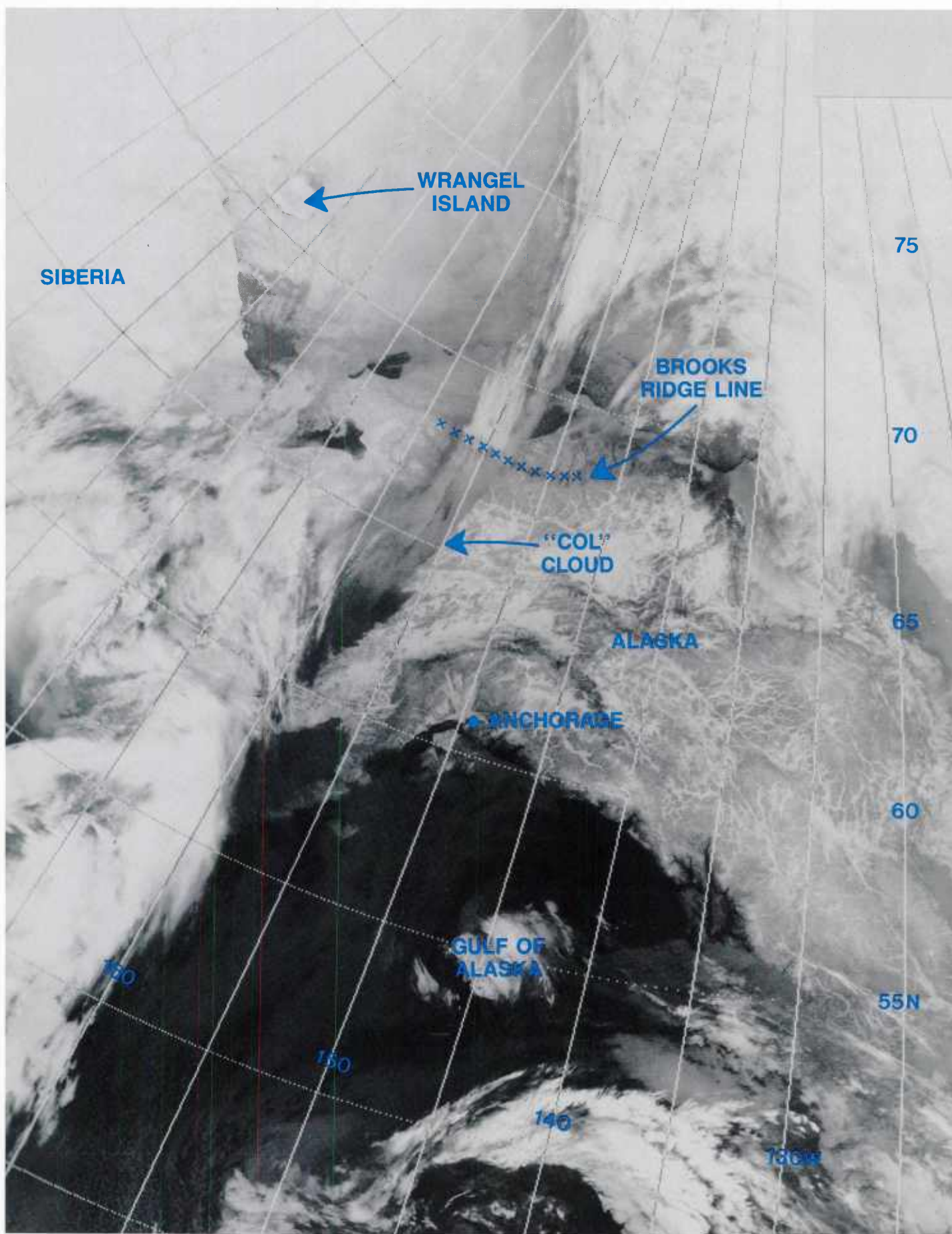
By 1725 GMT, as the front moved past Barrow, DMSP infrared (TS) data (Fig. 1B-41a) revealed that the col cloud now extended over the Brooks Range and was influencing weather on the North Slope of Alaska. Strong anticyclonic turning of upper level cloudiness east of the frontal zone corresponds with the position of a warm ridge evident on the NMC 1800 GMT surface analysis (Fig. 1B-42a). The analysis also shows that a ridge exists over the frontal position in central Alaska corresponding to the position of the col cloud.

## *21 February 1989*

The front continued its eastward movement fairly rapidly and by 0607 GMT (Fig. 1B-43a) was approaching the extreme eastern portion of the Beaufort Sea near Banks Island. The DMSP infrared (TS) data in the above figures reveal very warm cloud top temperatures south of Banks and extending over the Mackenzie River Delta. Inuvik, near 68.3°N 133.5°W was under the warm cloud region, and its sounding for 1200 GMT is shown in Fig. 1B-44a. The sounding reveals saturated conditions from the surface to about 900 mb (~3,300 ft). Winds were calm at the surface and 10 kt or less through the 800-mb level. The NMC surface analysis for 0600 GMT (Fig. 1B-44b) shows the cold front extending through a ridge near Inuvik and along the North Slope of Alaska. Inuvik's observation indicated overcast skies with stratus-type cloudiness. Although the original shape of the col cloud can no longer be discerned, conditions associated with it are thus seen to persist.

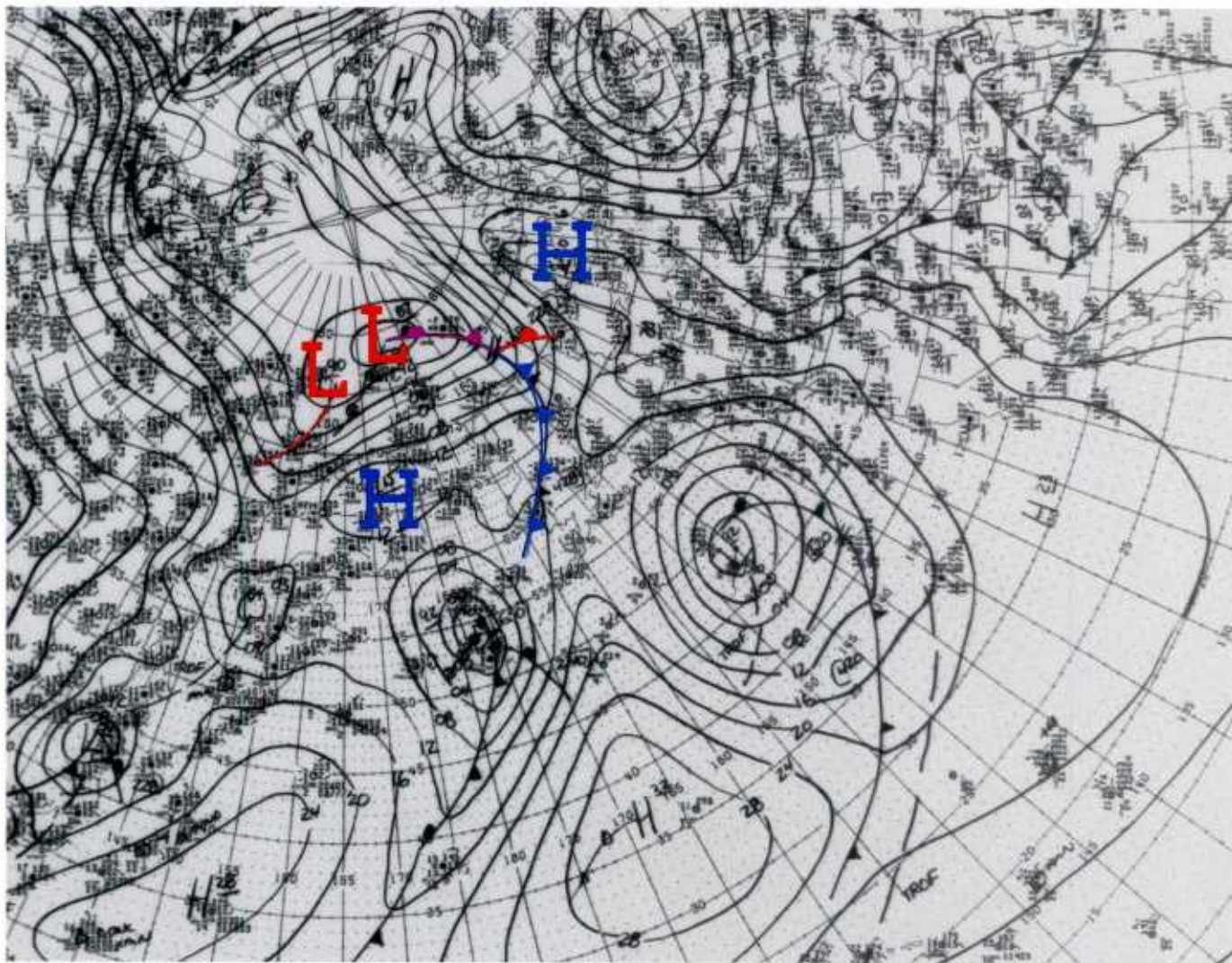
### **Important Conclusions**

1. An important feature associated with many cold frontal systems in the Arctic is the col cloud: a cloud that appears in infrared data, is often lens-shaped, and has dimensions of 100–150 n mi in width and 300–900 n mi in length.
2. The col cloud and associated weather can persist for 24–48 hours or longer, tracking in tandem with the associated cold frontal movement.
3. Ceilings are typically low, and visibilities are poor under the col cloud region.



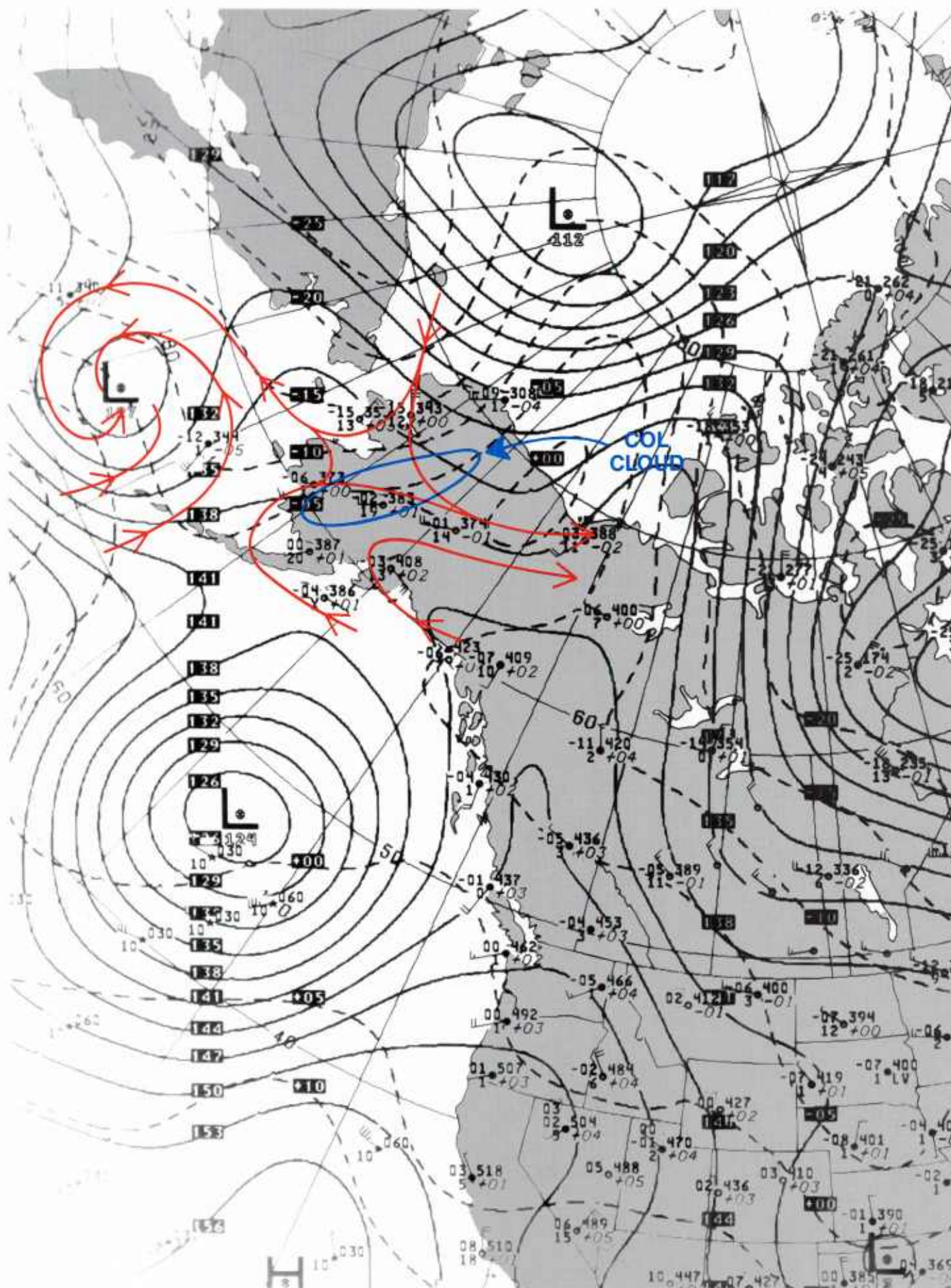
1B-38a DMSP infrared (TS) data. 1449 GMT 20 February 1989.





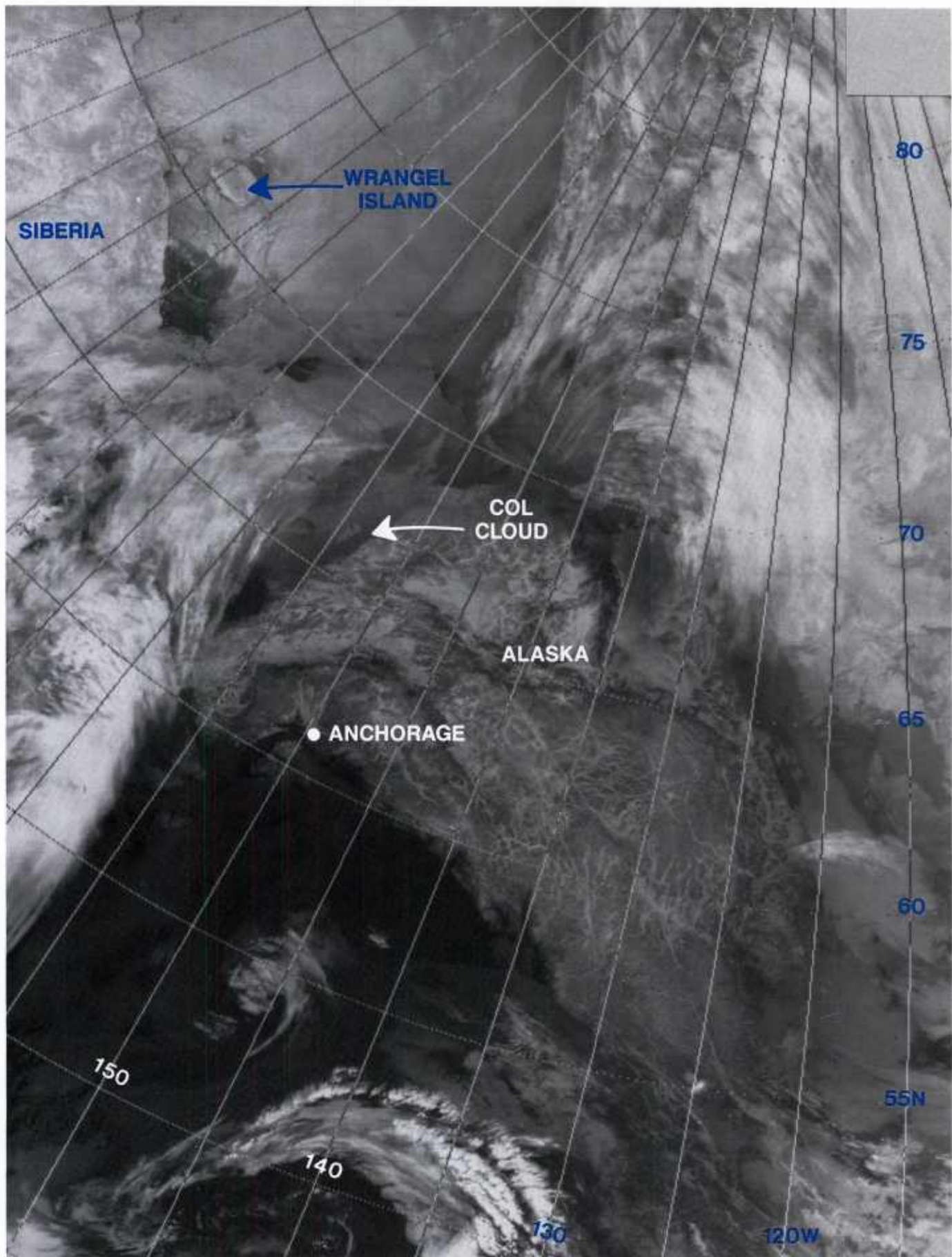
1B-39a NMC surface analysis. 1200 GMT 20 February 1989.





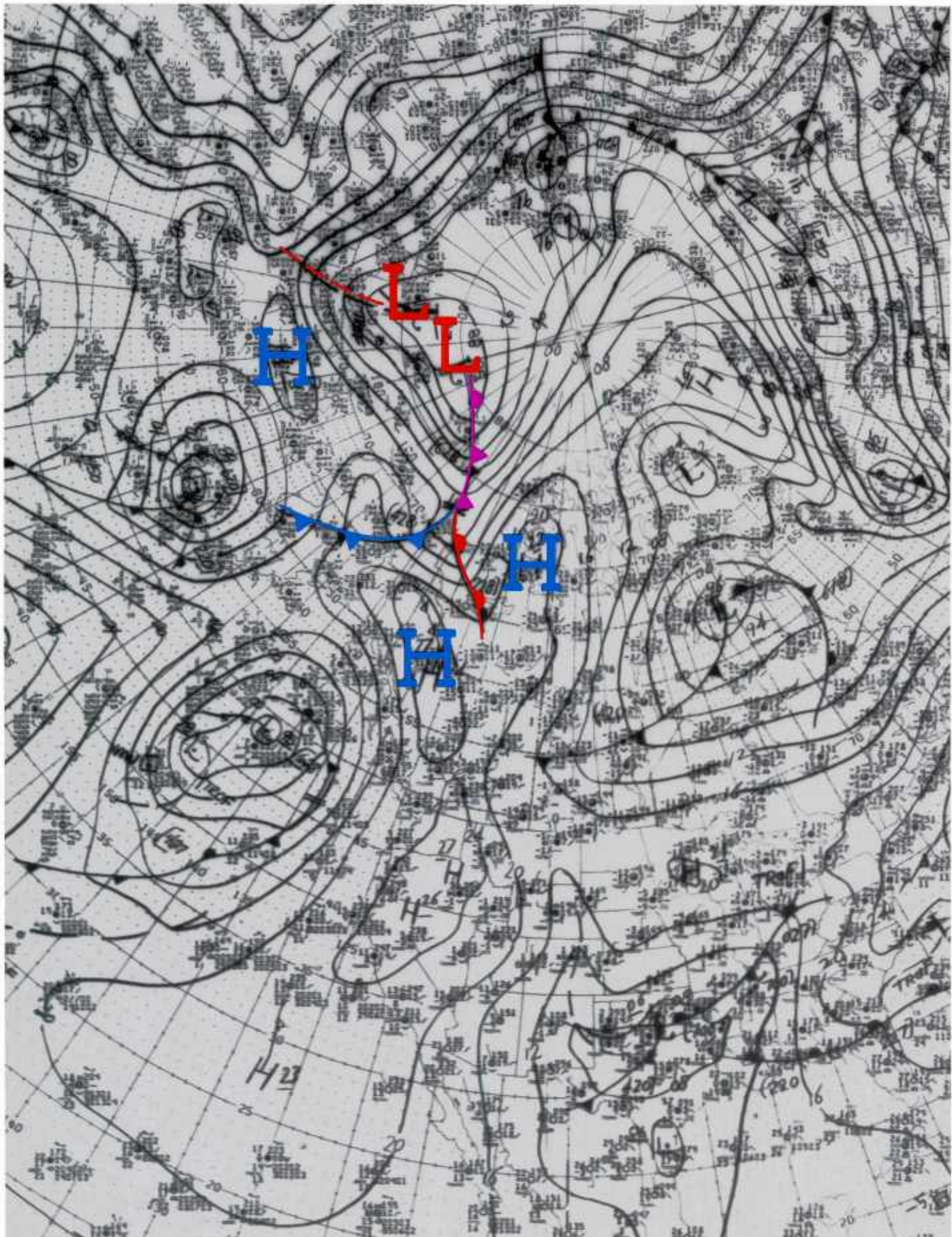
1B-40a NMC 850-mb analysis. 1200 GMT 20 February 1989.





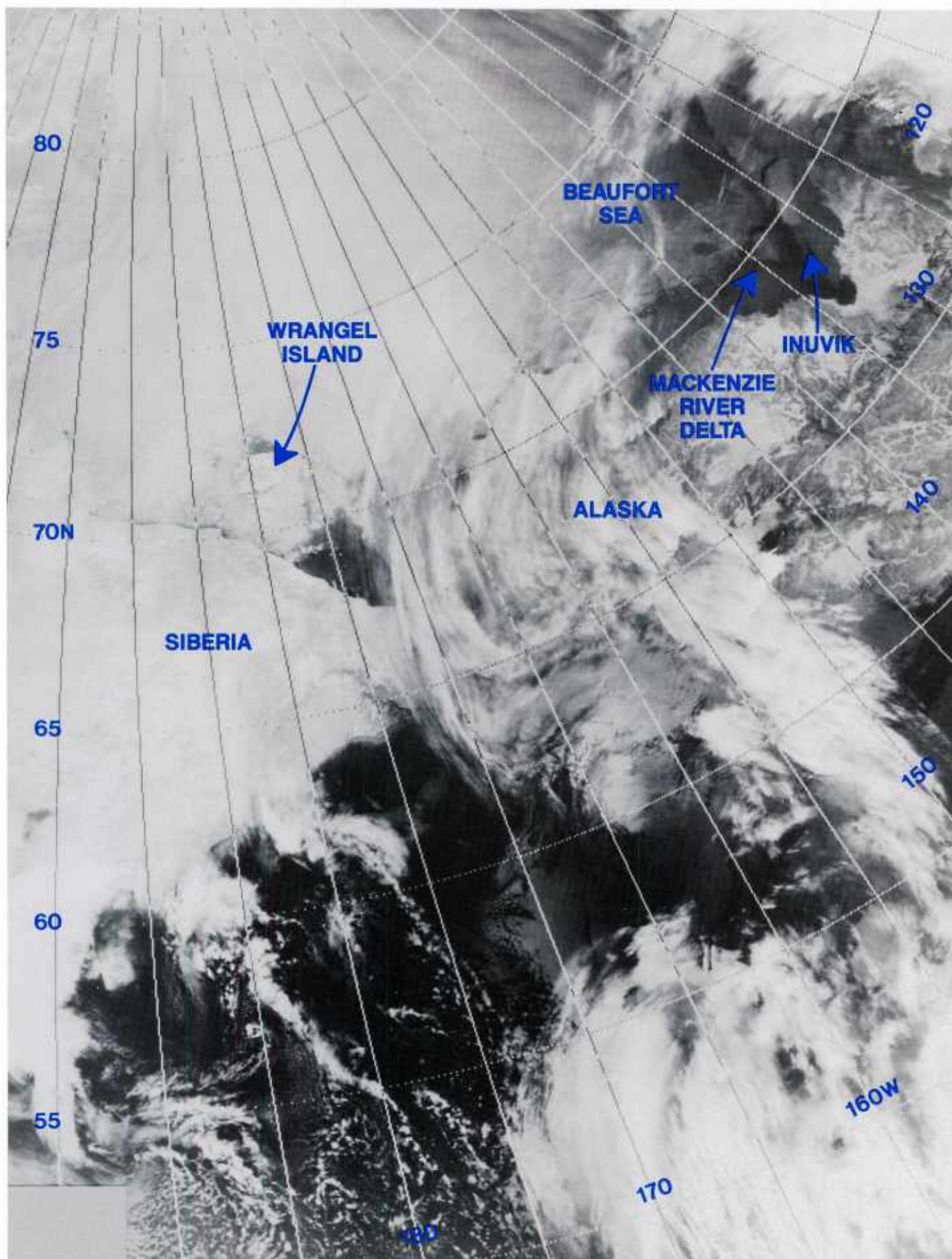
1B-41a DMSP infrared (TS) data. 1725 GMT 20 February 1989.





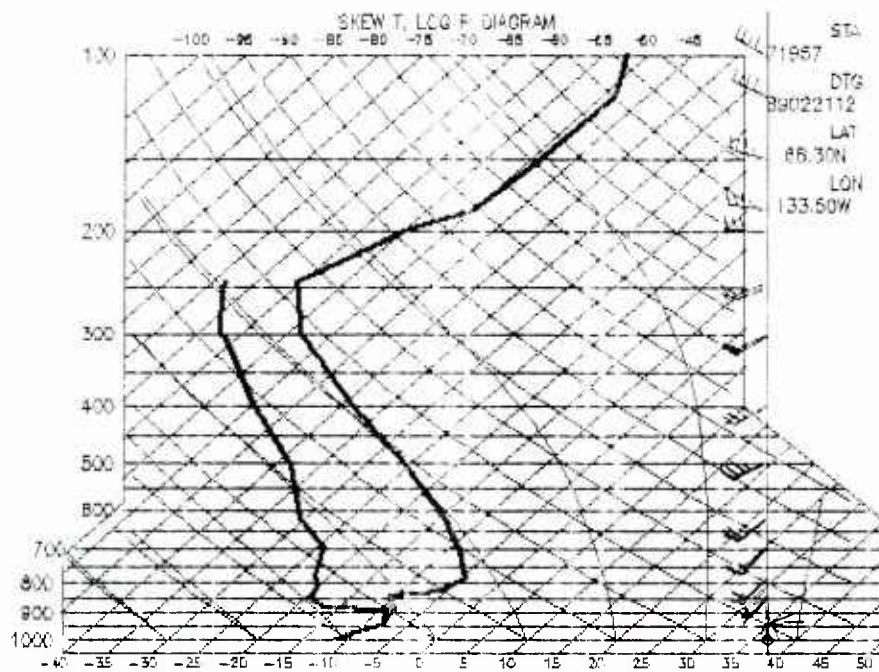
1B-42a NMC surface analysis. 1800 GMT 20 February 1989.



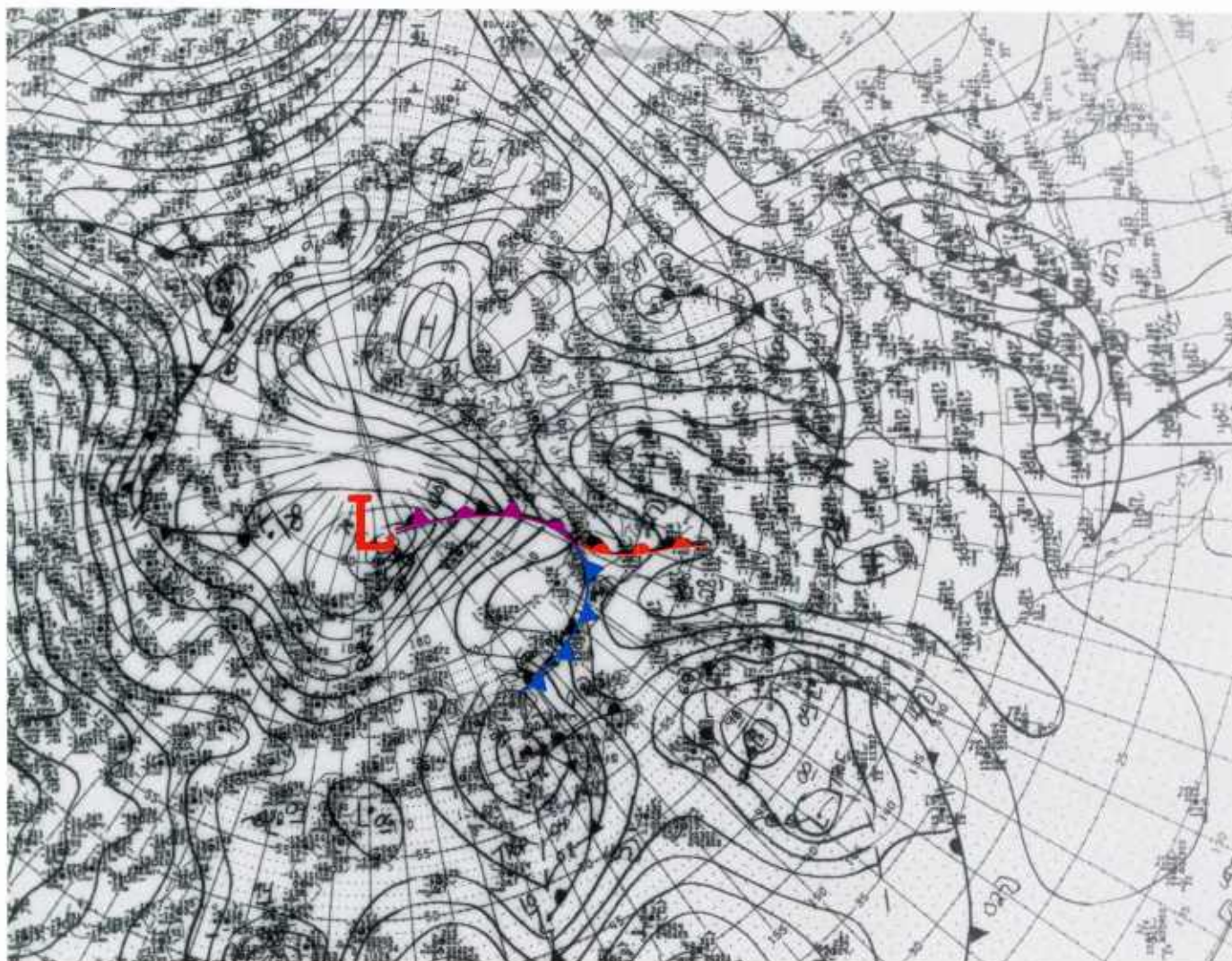


1B-43a DMSP infrared (TS) data. 0607 GMT 21 February 1989.





1B-44a Radiosonde data for Inuvik, NWT, Canada. 1200 GMT 21 February 1989.



1B-44b NMC surface analysis. 0600 GMT 21 February 1989.



*Case 4 Col Cloud Effects—East Siberian Sea*

*14 February 1983*

Figure 1B-45a is a DMSP infrared (TS) view of the Arctic Ocean north of Siberia and Alaska, acquired at 2321 GMT. The warm overcast region extending out of Siberia into the East Siberian Sea near  $155^{\circ}$ – $160^{\circ}$ E is conspicuous as a prominent feature. The warm temperatures defining its shape imply that the cloudiness forming the feature is trapped beneath a strong low-level inversion. Cloudiness is banked up against mountainous terrain on the east side of this feature; lowlands extend considerably further beyond its western boundary.



1B-45a DMSP infrared (TS) data. 2321 GMT 14 February 1983.

The strong inversion over the region is shown by the radiosonde data for Cherskiy (68.8°N 161.3°E) at 0000 GMT on 15 February 1983 (Fig. 1B-46a). The temperature increased from  $-37.5^{\circ}\text{C}$  at the surface to  $-16^{\circ}\text{C}$  near the 900-mb level. Any cloudiness trapped under such an inversion would appear much warmer than the surrounding noncloudy environment in satellite infrared data.

Curiously, the warm cloudiness extends eastward over the East Siberian Sea toward Wrangel Island and then loops northward into an apparent Arctic frontal zone. A low-level vortex is implied by curvature effects perceptible in the region just west of Wrangel Island. A possible analysis of the situation is shown in Fig. 1B-47a, a gridded overlay to Fig. 1B-45a. According to this interpretation, as the front moved eastward across the ice pack, frictional effects and slower winds impeded the progress of its southern boundary, causing fragmentation across the East Siberian Sea.

The appearance of the cloudy region just west of Cherskiy and its position relative to the northward portion of the frontal zone suggest that it might have developed as a col cloud. In other words it could represent the fractured remains of a frontal zone whose northern portion had moved on to the east. The surface analysis at 0000 GMT on 15 February, with suggested frontal position superimposed (Fig. 1B-48a), verifies that this cloudiness is occurring in a col region, as is other especially enhanced cloudiness northeast of Wrangel Island. The high pressure center shown near Wrangel Island is probably erroneously analyzed. The existence of the vortex immediately to the west of Wrangel (not analyzed on the original FNOC analysis) suggests that the trough to the north extended deeper into that region. The position of this trough has been drawn on Figs. 1B-47a and 1B-48a, leading southward from the apparent cloud vortex center of the Arctic front over the Arctic Ocean to a secondary vortex on the front (Fig. 1B-47a). The vortex has broken up the smooth structure of strongly suppressed adjacent cloudiness.

### **Important Conclusions**

1. Much of the cloudiness of Arctic fronts is very low level, capped by a strong inversion.
2. Many coastal cloudiness effects may be remnant effects of Arctic fronts that have fragmented, moving faster over the ice pack, with southern extensions impeded in speed by frictional effects of terrain.
3. This example demonstrated that Arctic frontal width can extend to 300 n mi or more. Therefore, cloudiness associated with Arctic fronts may be slow in passing a given location.

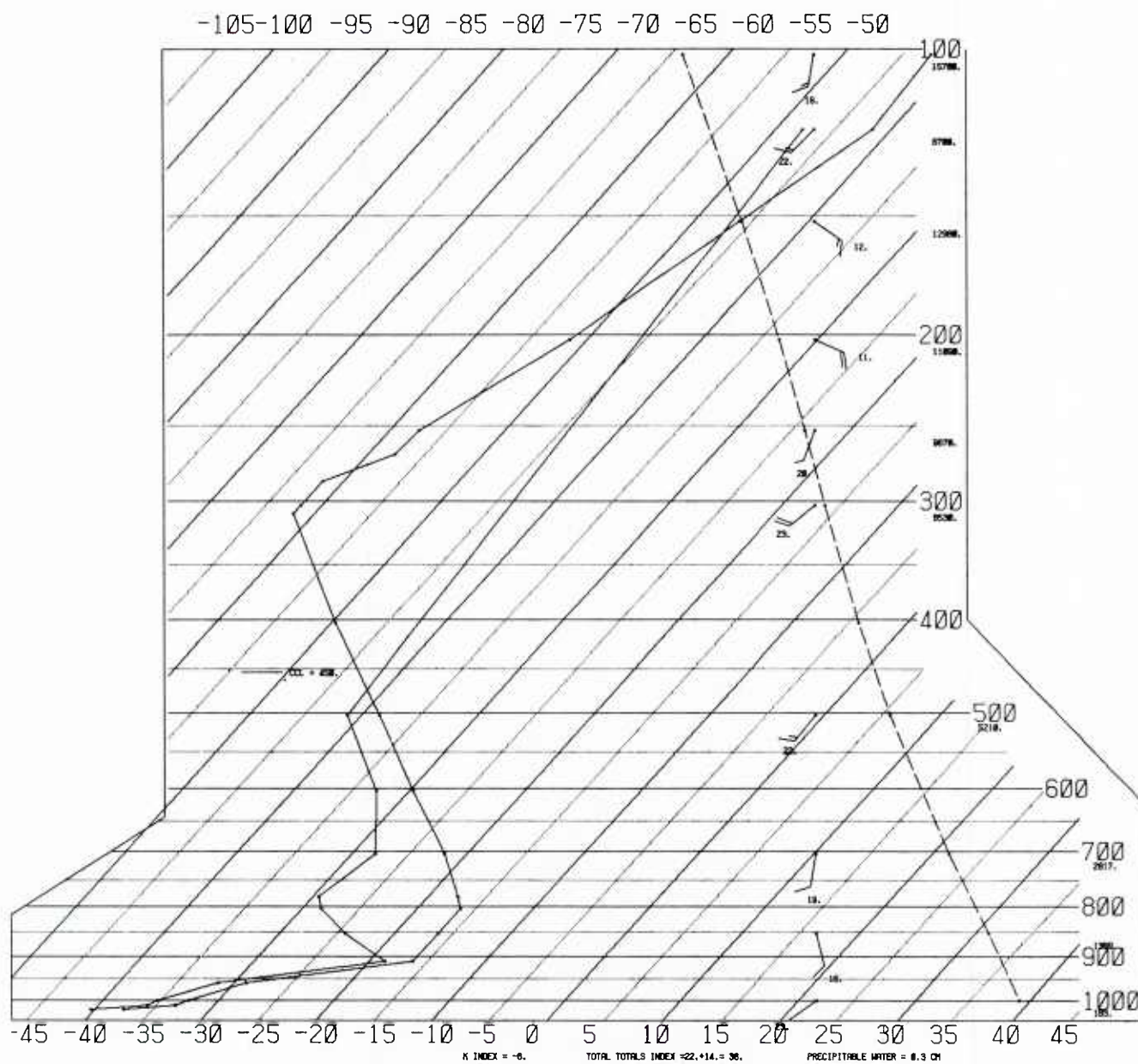


# SKEW T, LOG P DIAGRAM

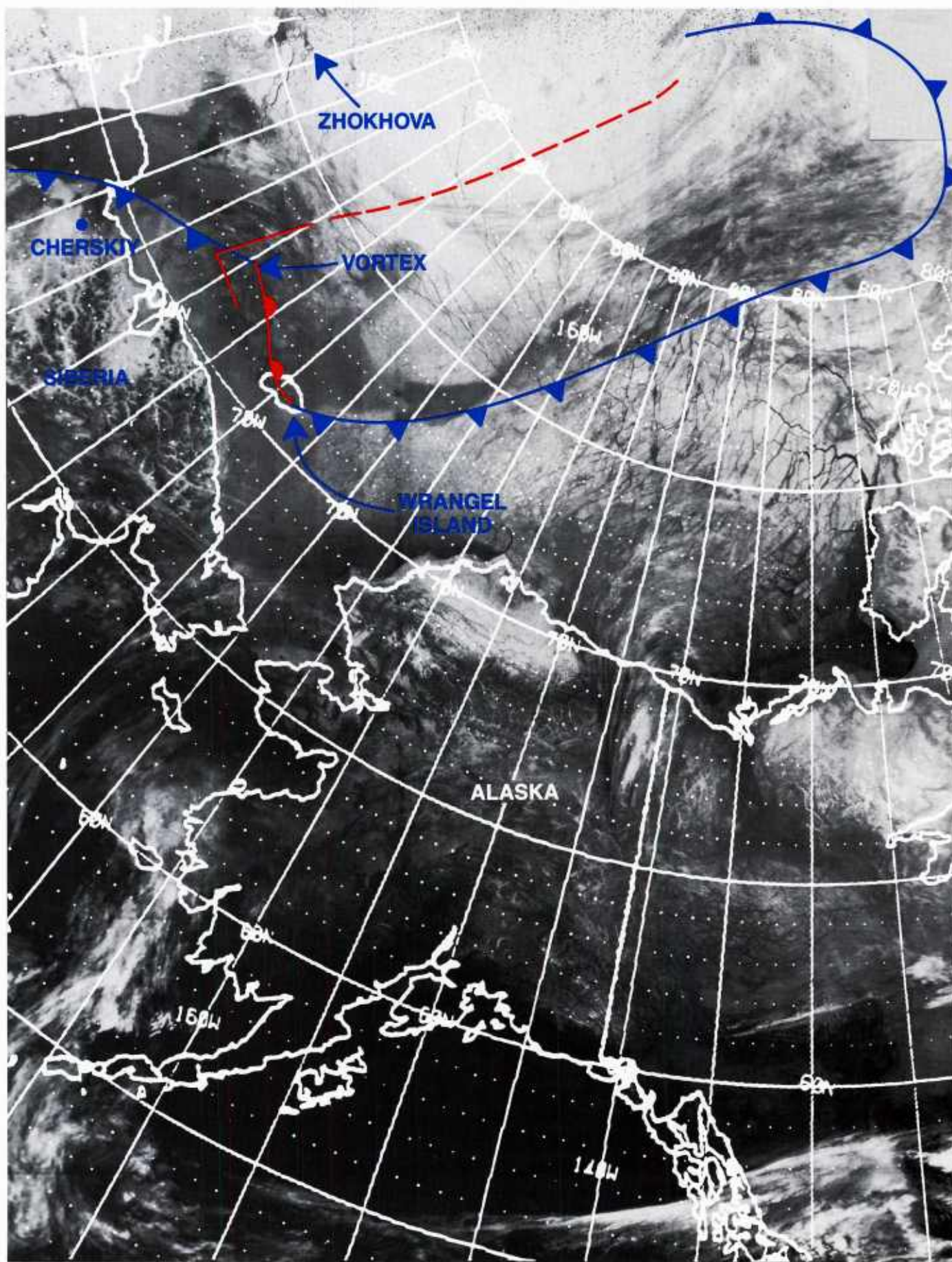
830215

0000Z

25123

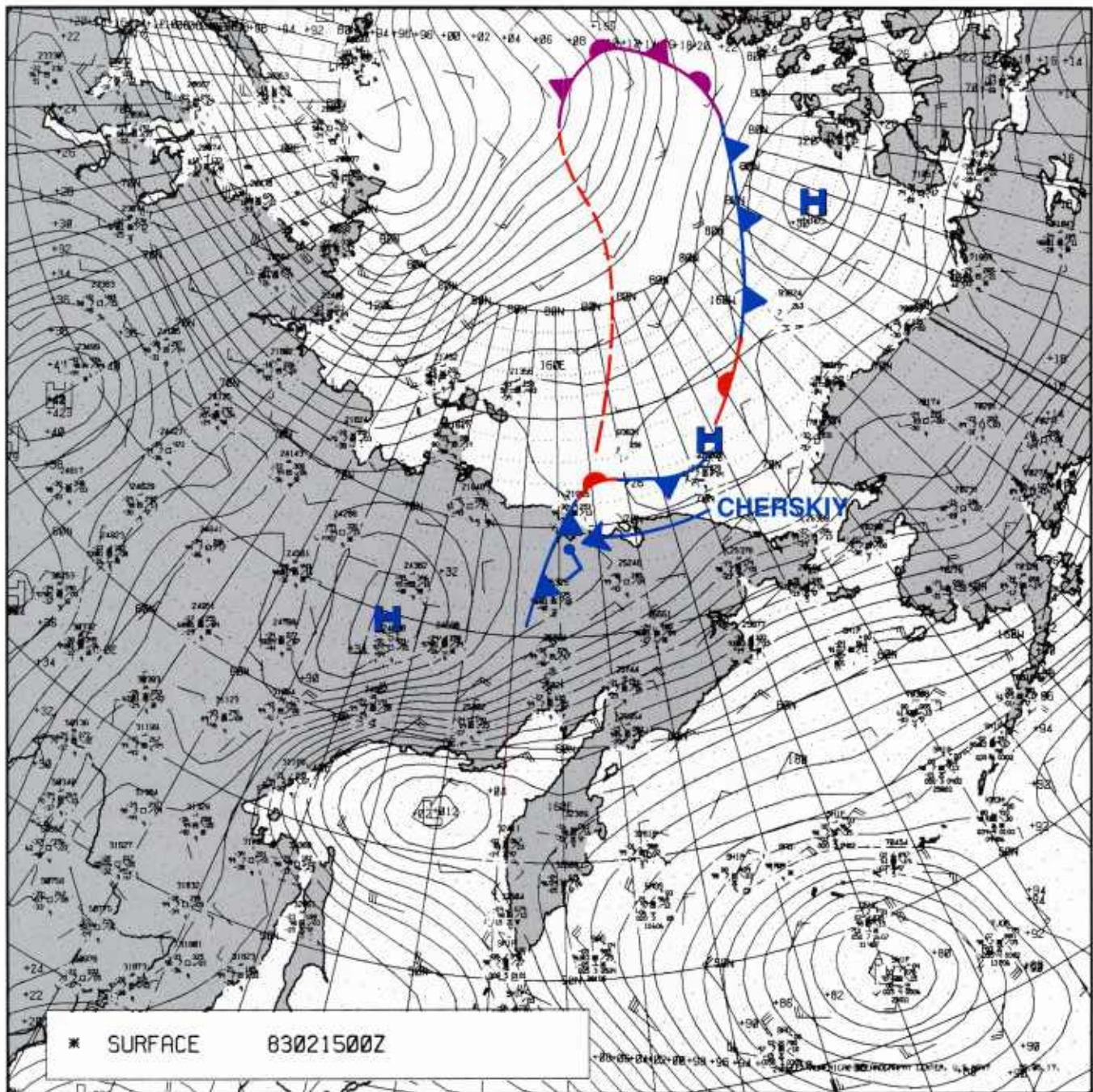


1B-46a Radiosonde data for Cherskiy, USSR. 0000 GMT 15 February 1983.



1B-47a DMSP infrared (TS) data. 2321 GMT 14 February 1983, with overlay.





1B-48a FNOC surface analysis. 0000 GMT 15 February 1983.

*Case 5 Arctic Fronts and the "Fleur-de-lis" Cloud Pattern  
(16-19 April 1989)*

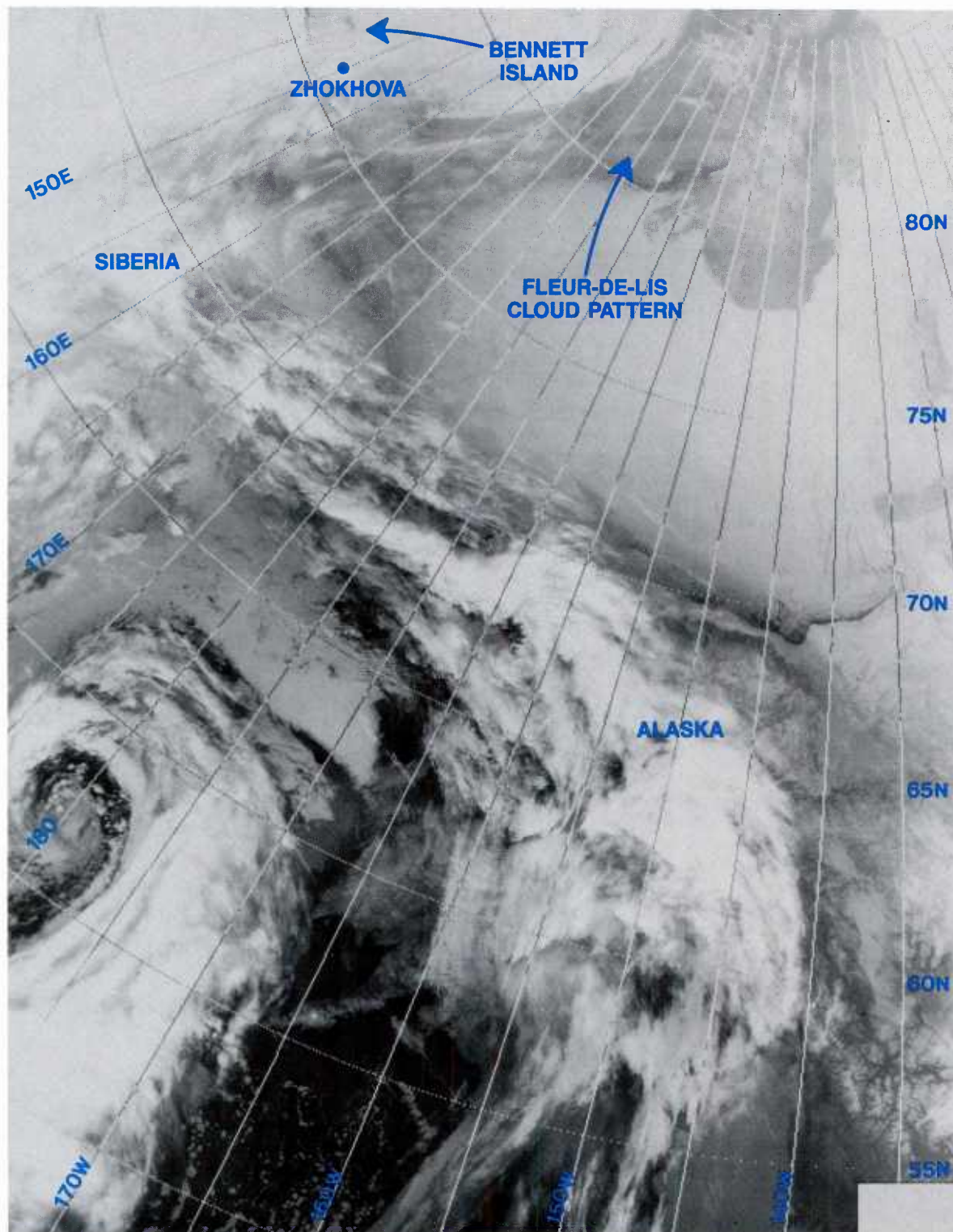
The fleur-de-lis cloud pattern has been previously described in NTAG Vol. 8, Part 1, Section 1E (Fett, 1990). The pattern is associated with a core of high speed winds that flow parallel to a broad, frontlike band of clouds that splits at the downstream end into an anticyclonic gyre on the right-hand side, coinciding with a ridge or anticyclonic vorticity maximum, and a cyclonic gyre on the left-hand side, coinciding with a trough or cyclonic vorticity maximum. The top of the formation has flow coming from the opposite direction, opposing the major band or stem, creating a deformation zone or col.

The pattern is often seen over the Arctic Ocean as a warm cloud feature indicating its low-level nature and the presence of a low-level inversion. The feature in fact is a shallow Arctic front characterized by low ceilings and foggy low-level conditions.



16 April 1989

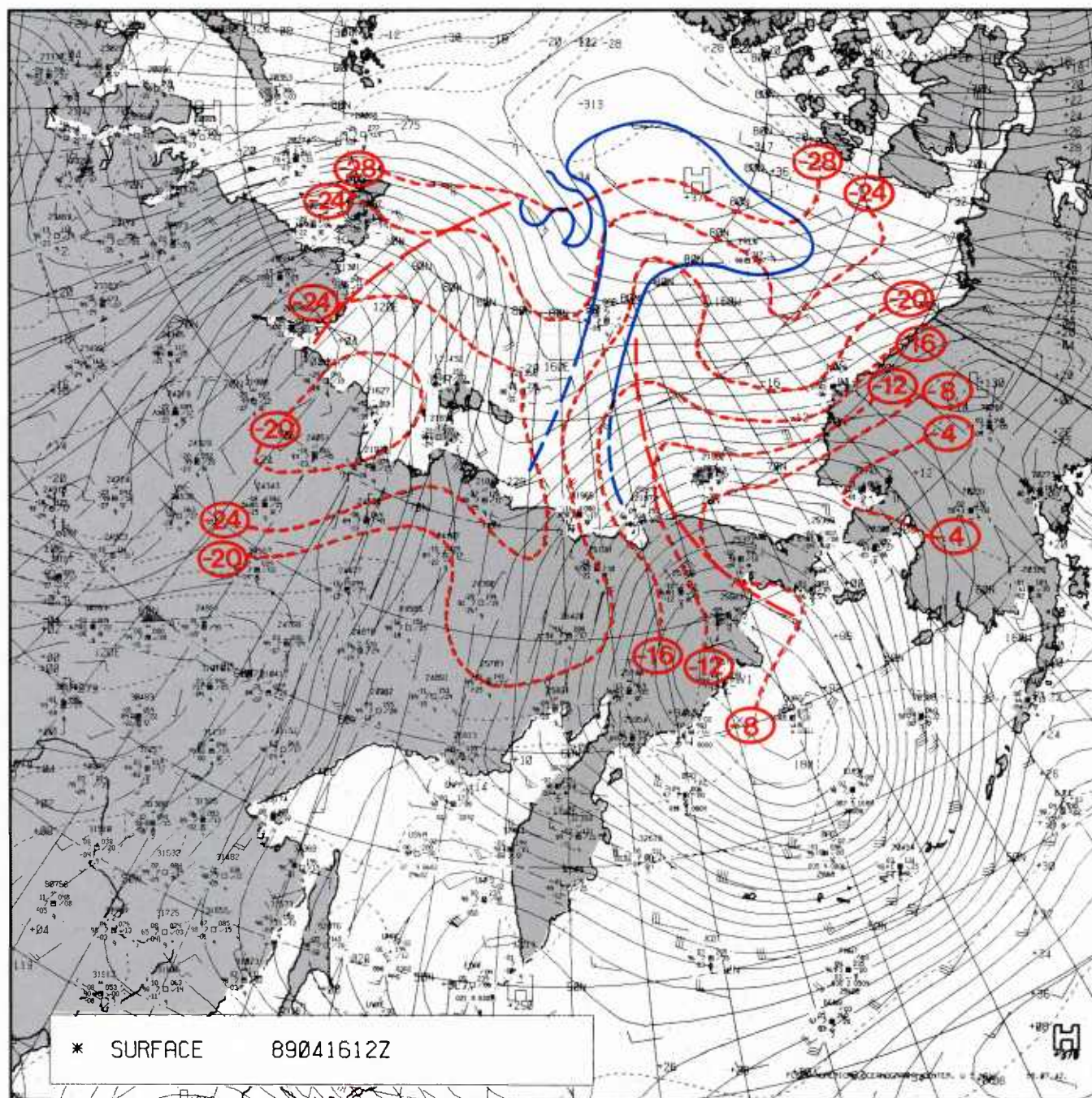
The DMSP infrared (TS) data acquired at 1503 GMT (Fig. 1B-50a) reveal the fleur-de-lis cloud pattern stretching northeastward over the Arctic Ocean from Siberia, just east of the New Siberian Islands (70°N 150°E). Bennett Island (76.7°N 149.7°E), in the New Siberian Group, can be seen in the clear, west of the frontal band in the DMSP data. The position of the island of Zhokhova, partially obscured by cloudiness, is shown in Fig. 1B-50a. The low-level nature of the cloud pattern can be inferred from the warm temperatures that define its shape.



1B-50a DMSP infrared (TS) data. 1503 GMT 16 April 1989.



The FNOC surface analysis for 1200 GMT, about 3 hr prior to the DMSP data, is shown in Fig. 1B-51a. The approximate outline of the fleur-de-lis cloud pattern and an isotherm analysis has been superimposed on the figure. It can be seen that an inverted short wave trough and warm tongue of air exist on the east side of the cloud pattern along the stem. A major lobe at the top part of the pattern overlaps high pressure on the east side, and the pattern extends into another trough on the west side. A small cloud vortex is suggested by the satellite data in the trough region on the west side. A station under the cloud band near 79.2°N 171°E, reporting at various times as ship UYAJ, indicates an overcast sky condition with a base of lowest clouds (strati) as code 4 (1,000–1,999 ft).



1B-51a FNOC surface analysis. 1200 GMT 16 April 1989.



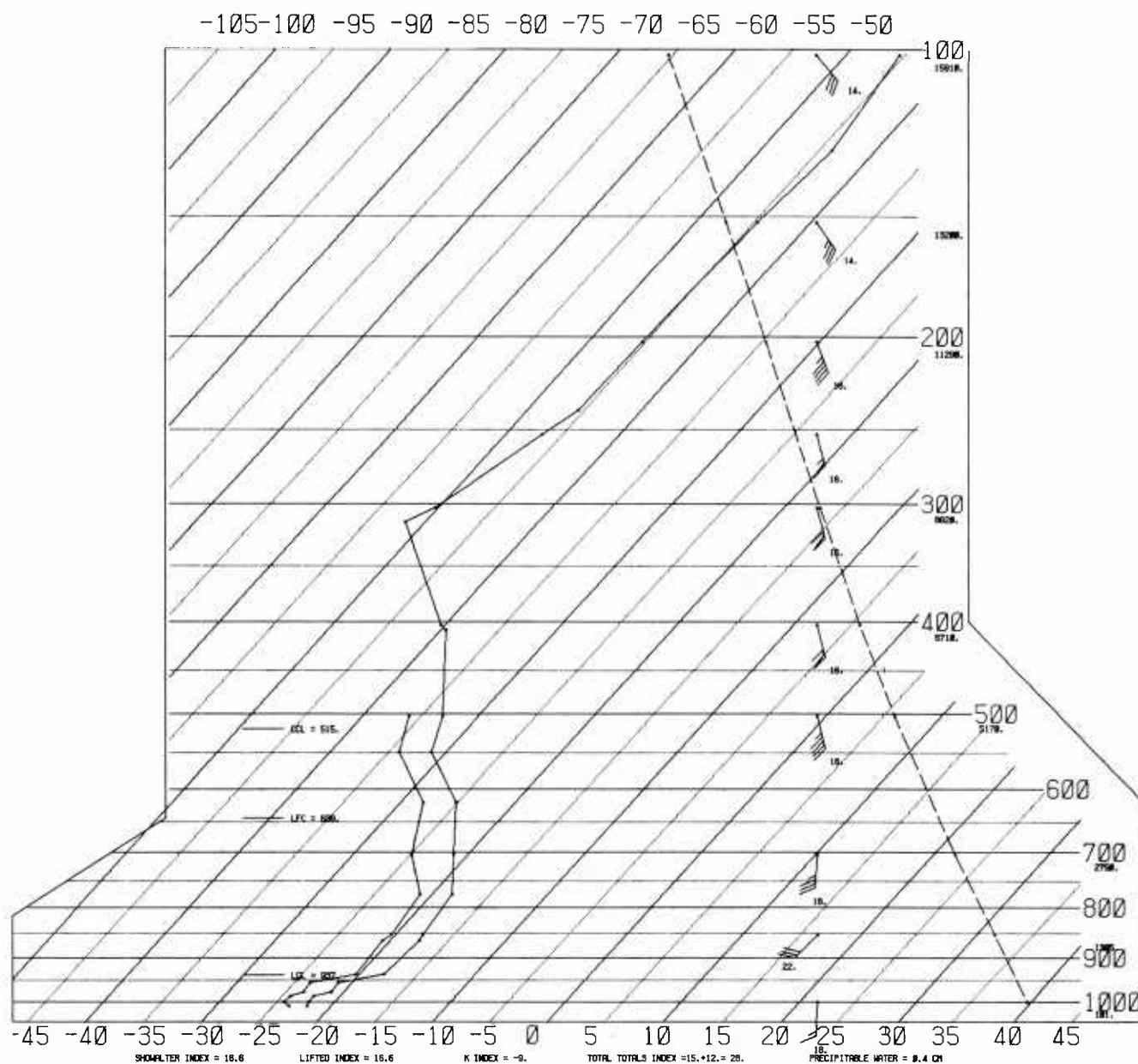
The island of Zhokhova (76.1°N 152.8°E) showed upper level conditions in its RAOB at 0000 GMT for 16 April (Fig. 1B-52a), different from what one might have anticipated based on the surface analysis. At 850 mb, winds are indicated as southwesterly at 30 kt. This direction is in perfect alignment with the stem of the fleur-de-lis cloud pattern.

# SKEW T, LOG P DIAGRAM

890416

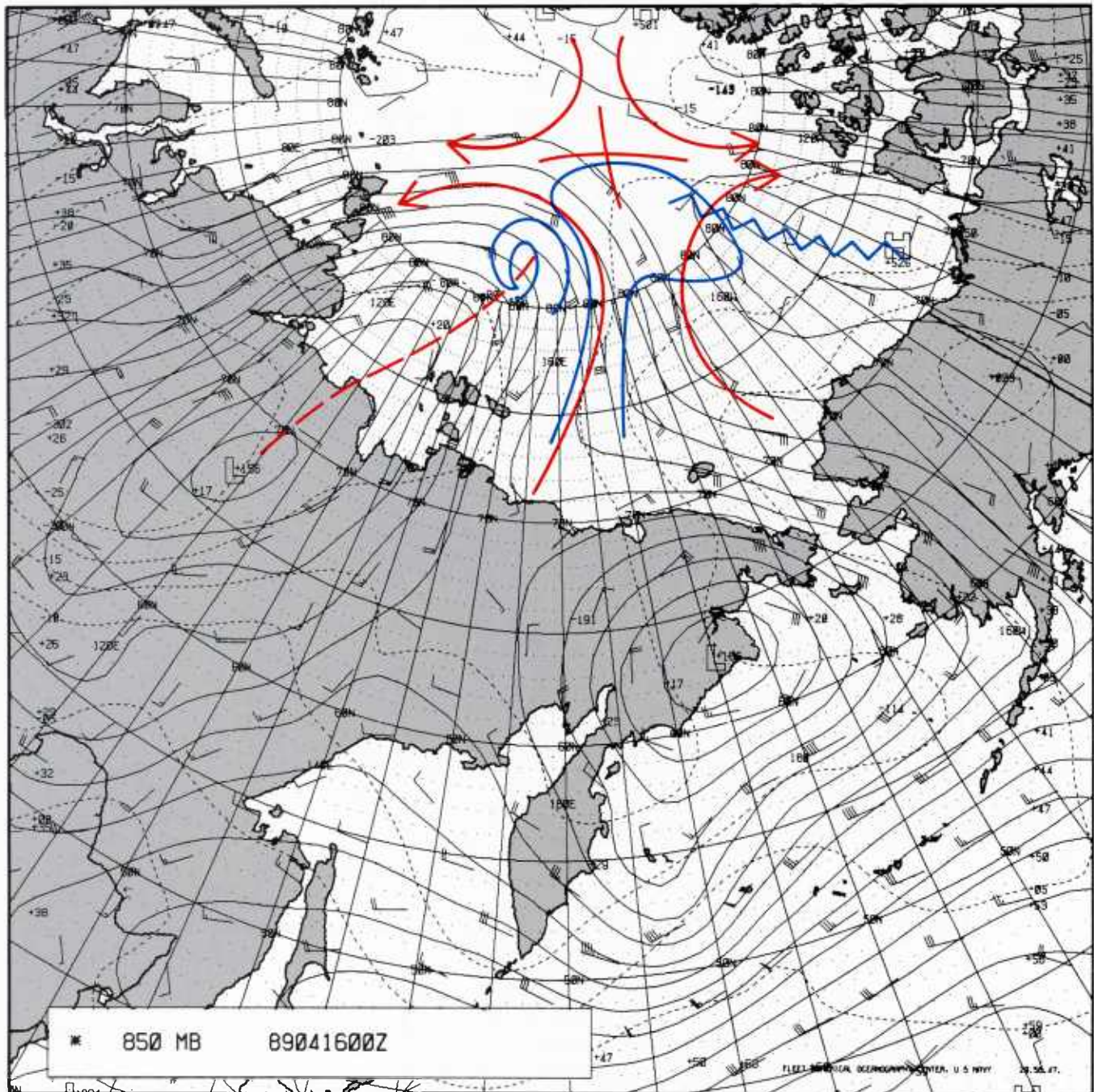
0000Z

21358



1B-52a Radiosonde data for Zhokhova, U.S.S.R. 0000 GMT 16 April 1989.

The FNOC 850-mb analysis at 0000 GMT on 16 April (Fig. 1B-53a), with a streamline analysis superimposed, reveals confluent flow leading into the stem of the fleur-de-lis cloud pattern. Cyclonic and anticyclonic lobes on the northern end form the col associated with that region of the fleur-de-lis.



1B-53a FNOC 850-mb analysis (streamlines and cloud pattern superimposed). 0000 GMT 16 April 1989.



The FNOC 500-mb analyses for 0000 GMT (Fig. 1B-54a) and 1200 GMT (Fig. 1B-55a) substantiate southerly to southwesterly flow. These analyses also confirm the existence of a jet core aloft parallel to the western edge of the fleur-de-lis cloud pattern.

### *17 April 1989*

The DMSP infrared (TS) data acquired at 0621 GMT (Fig. 1B-56a) show that the pattern has moved northwestward. This suggests that the steering influence on the system was the large high pressure area centered over the Arctic Ocean north of Alaska, evident on the surface analysis (Fig. 1B-51a) as well as upper level analyses (Figs. 1B-53a, 1B-54a, and 1B-55a). A secondary vortex, apparently lower level, is evident on the north side of the stem of the fleur-de-lis pattern. The area of warm cloudiness near the southern portion of Banks Island and the plume extending from its western shore are likely air-sea interaction effects producing fog and/or low stratus from open leads and polynyi in that region.

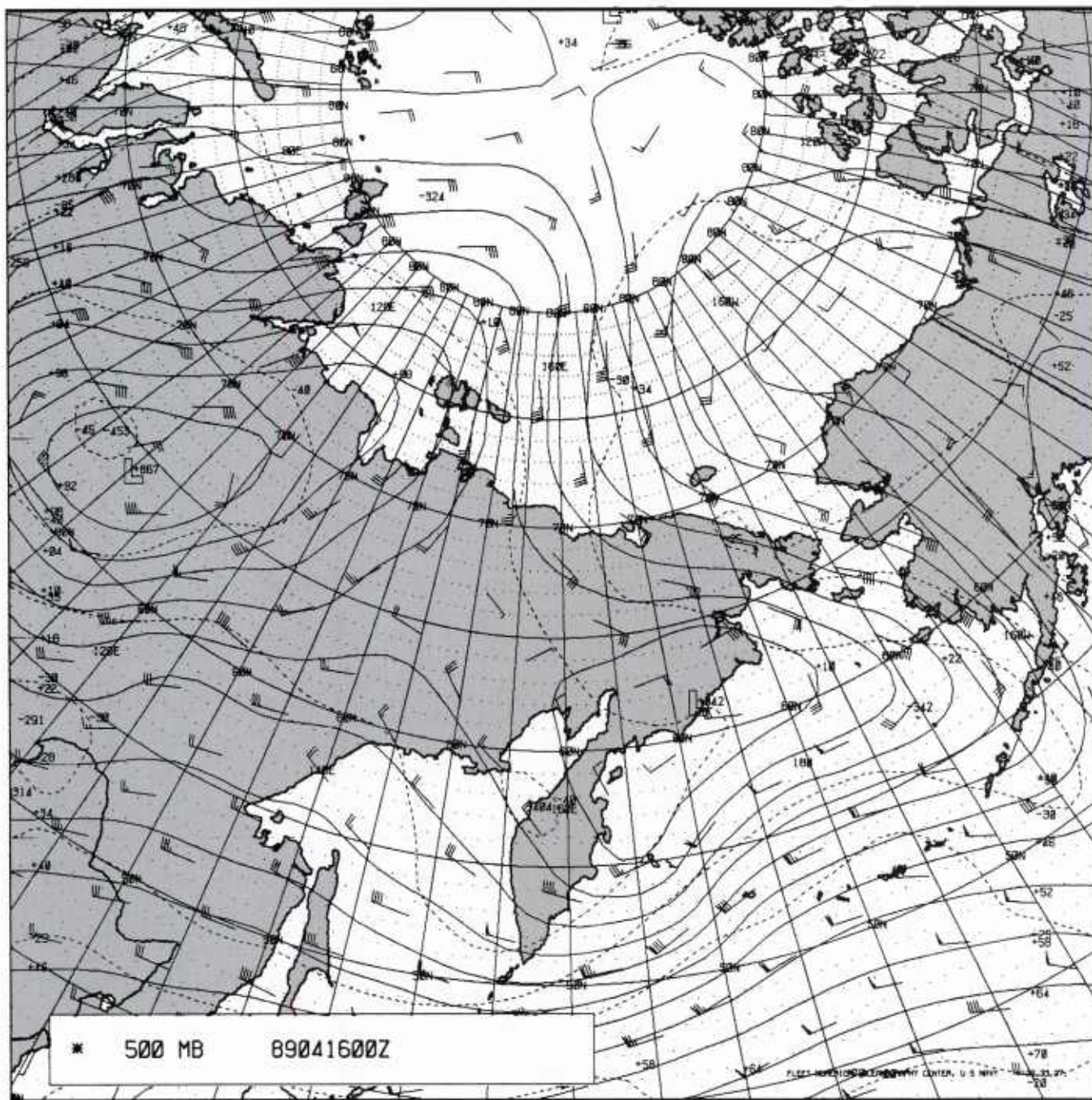
The FNOC 1200 GMT surface analysis, with cloud pattern and isotherms superimposed (Fig. 1B-57a), reveals a warm pocket of air and high pressure that continues to characterize the area on the east side of the band. Cold air is present on the west side of the band.

The FNOC 850-mb analysis for 1200 GMT, with cloud pattern and streamlines superimposed (Fig. 1B-58a), shows anticyclonic flow encircling the fleur-de-lis pattern. Warm temperatures and a high pressure center are evident on the southern side.

The FNOC 500-mb analysis for 1200 GMT (Fig. 1B-59a) continues to reveal a jetstream running parallel to the stem of the fleur-de-lis pattern and turning anticyclonically about the high pressure system to the south. Infrared data (TS) received at 1715 GMT on 17 April (Fig. 1B-60a) and visible DMSP data (LF) (Fig. 1B-61a) received over the same area about 1½ hr later are especially interesting. The infrared data (Fig. 1B-60a) show that the fleur-de-lis has rotated in a clockwise pattern during the past 24 hr, probably in response to the dominant anticyclonic flow over the region. The northeast side of the pattern is now lengthened into a frontlike pattern that appears to turn cyclonically into a vortex near 87°N 135°N.

The DMSP visible data (Fig. 1B-61a) reveal the flattened appearance of much of the cloudiness associated with the fleur-de-lis pattern. Shadows on the northern and western boundaries of some of this cloudiness indicate the Sun's position to the southeast and also the fact that some of the clouds in the pattern are casting their shadows on lower level underlying cloudiness. The outline of cloud patterns from the infrared data (Fig. 1B-60a) has been superimposed in Fig. 1B-62a to aid in interpretation. The flat top to much of the cloudiness is an additional indication that the area is capped by a strong low-level inversion.

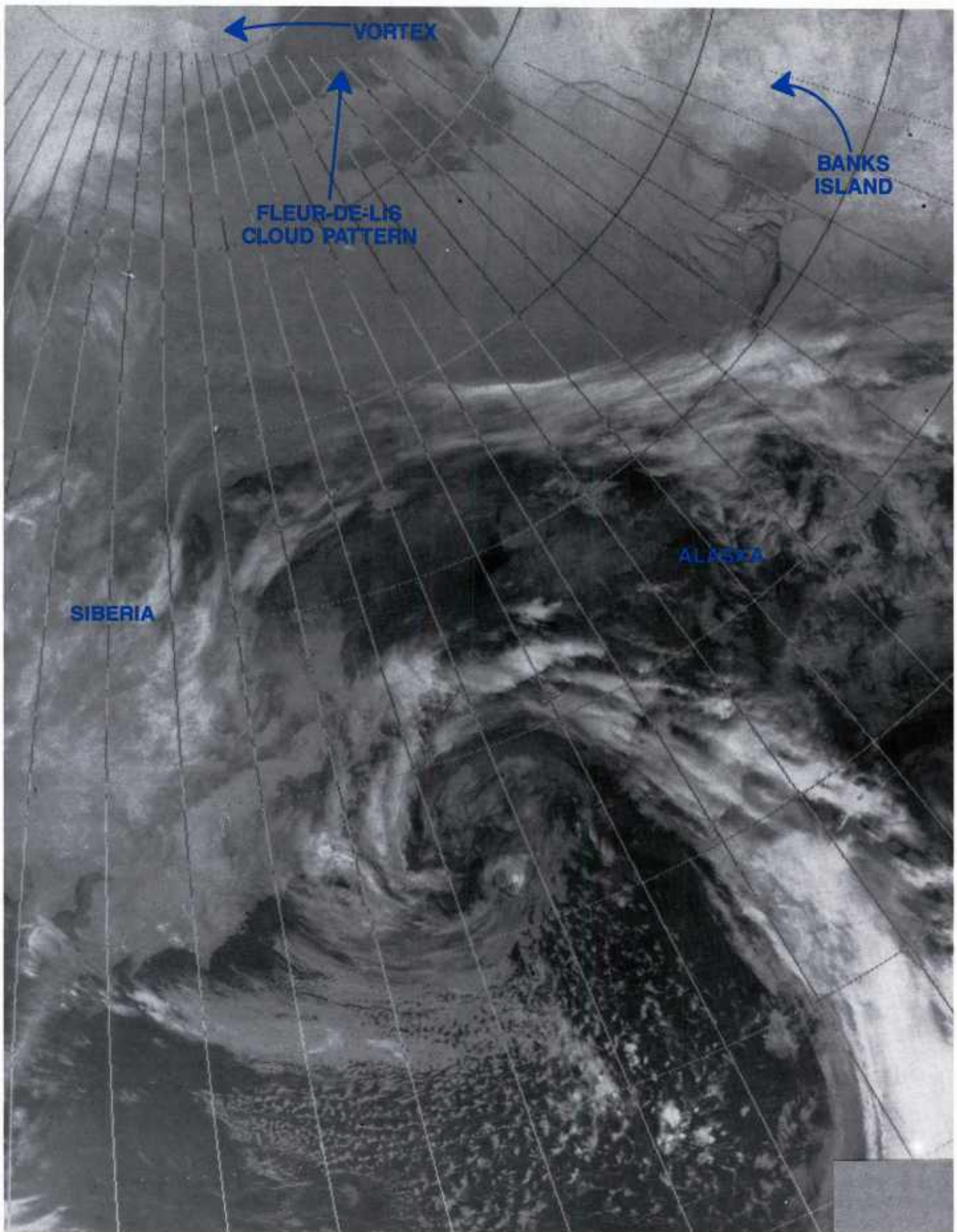
A new massive protuberance of cloudiness entering the Arctic Ocean region is evident to the southwest, bearing resemblance to another fleur-de-lis pattern. Note in particular the warm and flattened nature of this cloud region.



1B-54a FNOC 500-mb analysis. 0000 GMT 16 April 1989.

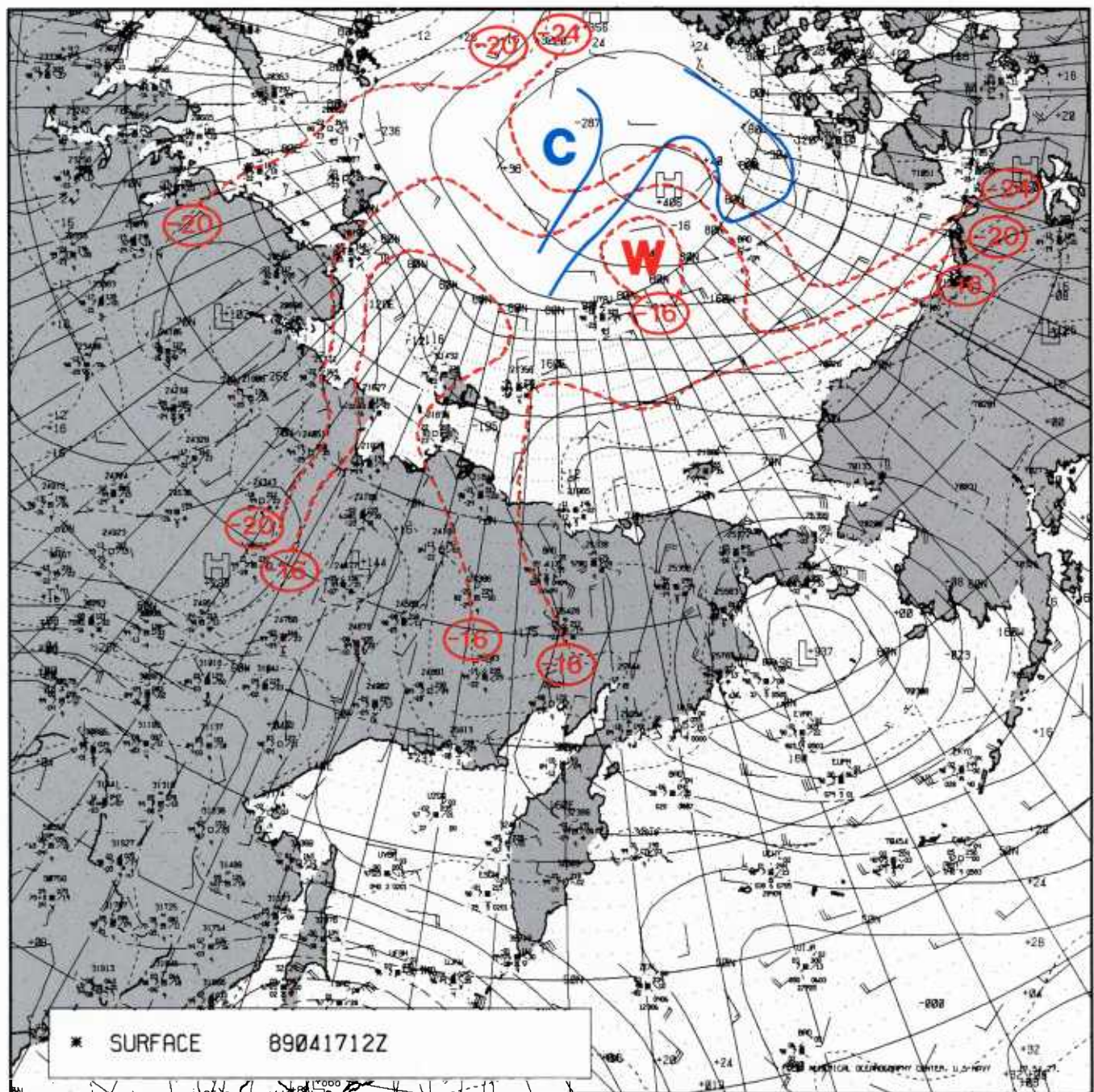






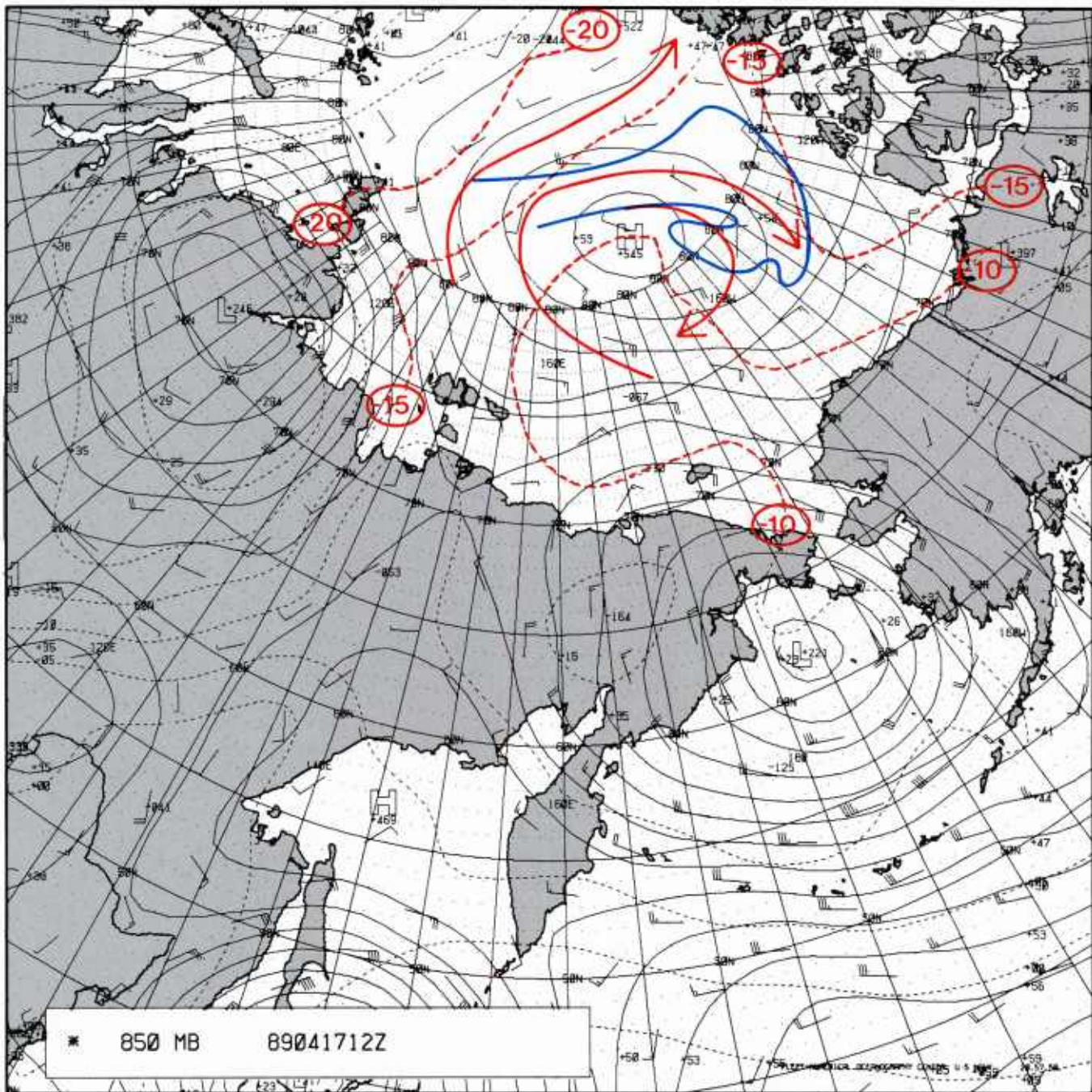
1B-56a DMSP infrared (TS) data. 0621 GMT 17 April 1989.





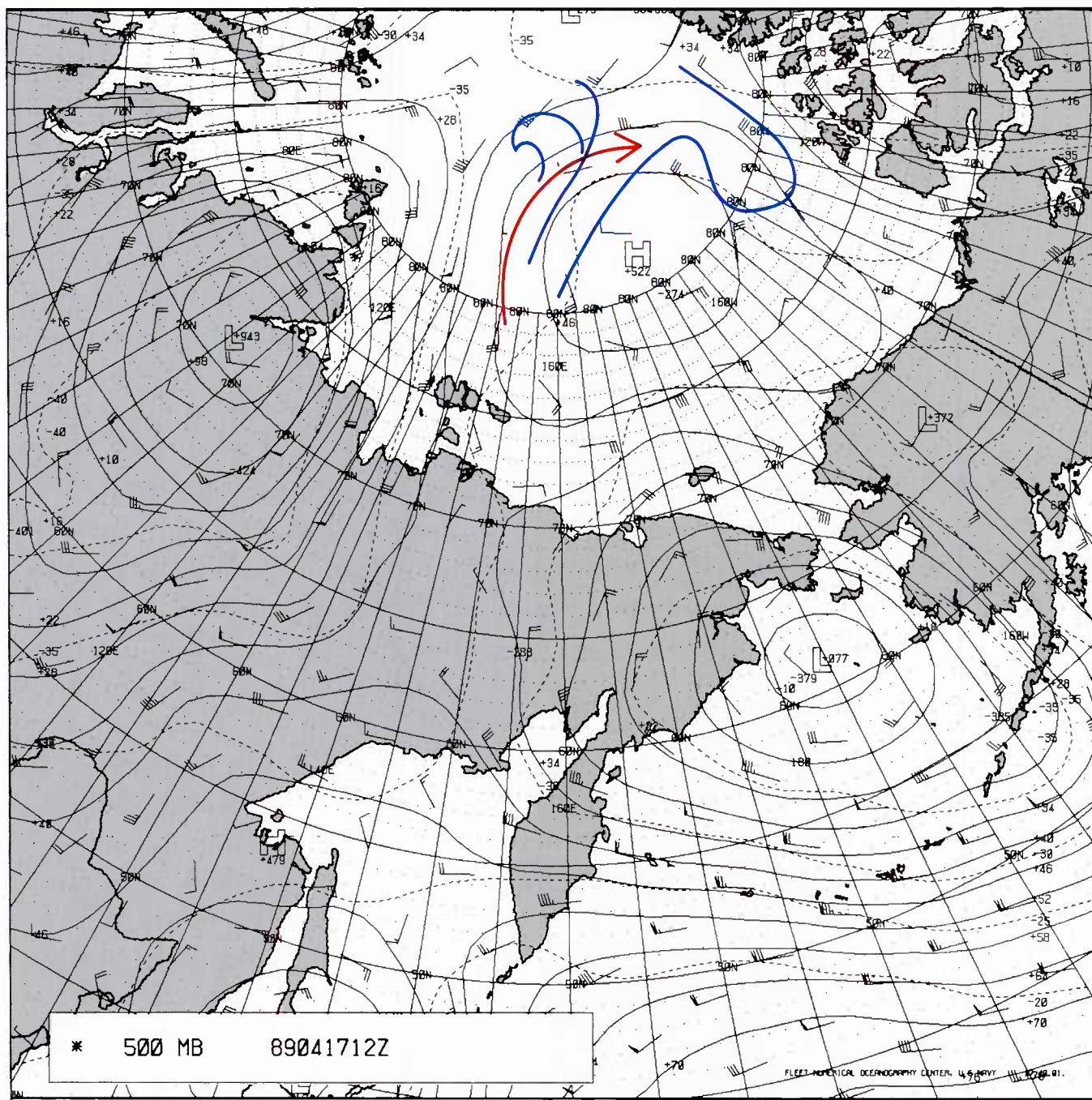
1B-57a FNOC surface analysis (cloud pattern and isotherm analysis superimposed). 1200 GMT 17 April 1989.



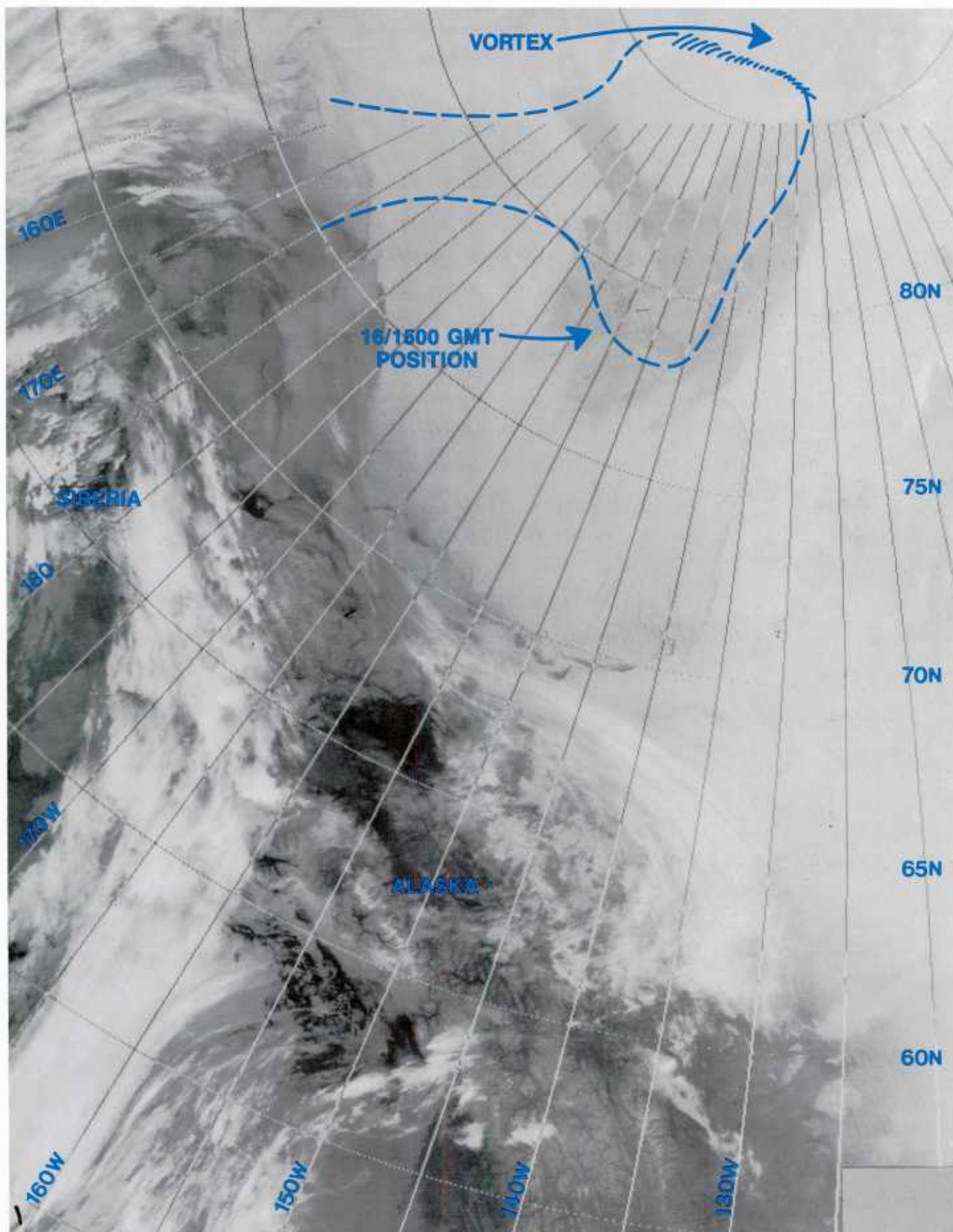


1B-58a FNOC 850-mb analysis (cloud pattern, streamline analysis, and isotherm analysis superimposed).  
1200 GMT 17 April 1989.



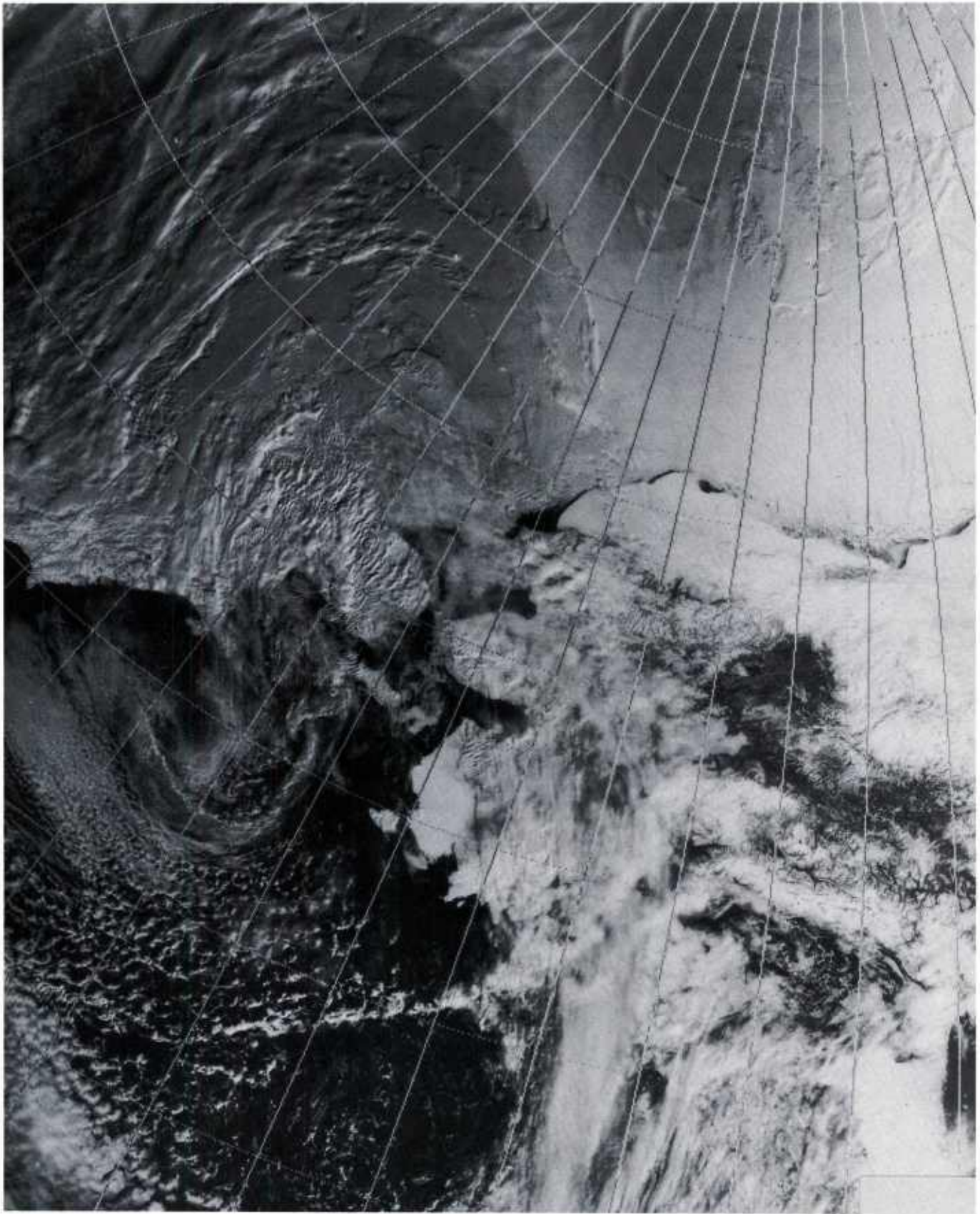


1B-59a FNOC 500-mb analysis (cloud pattern and streamline analysis superimposed). 1200 GMT 17 April 1989.



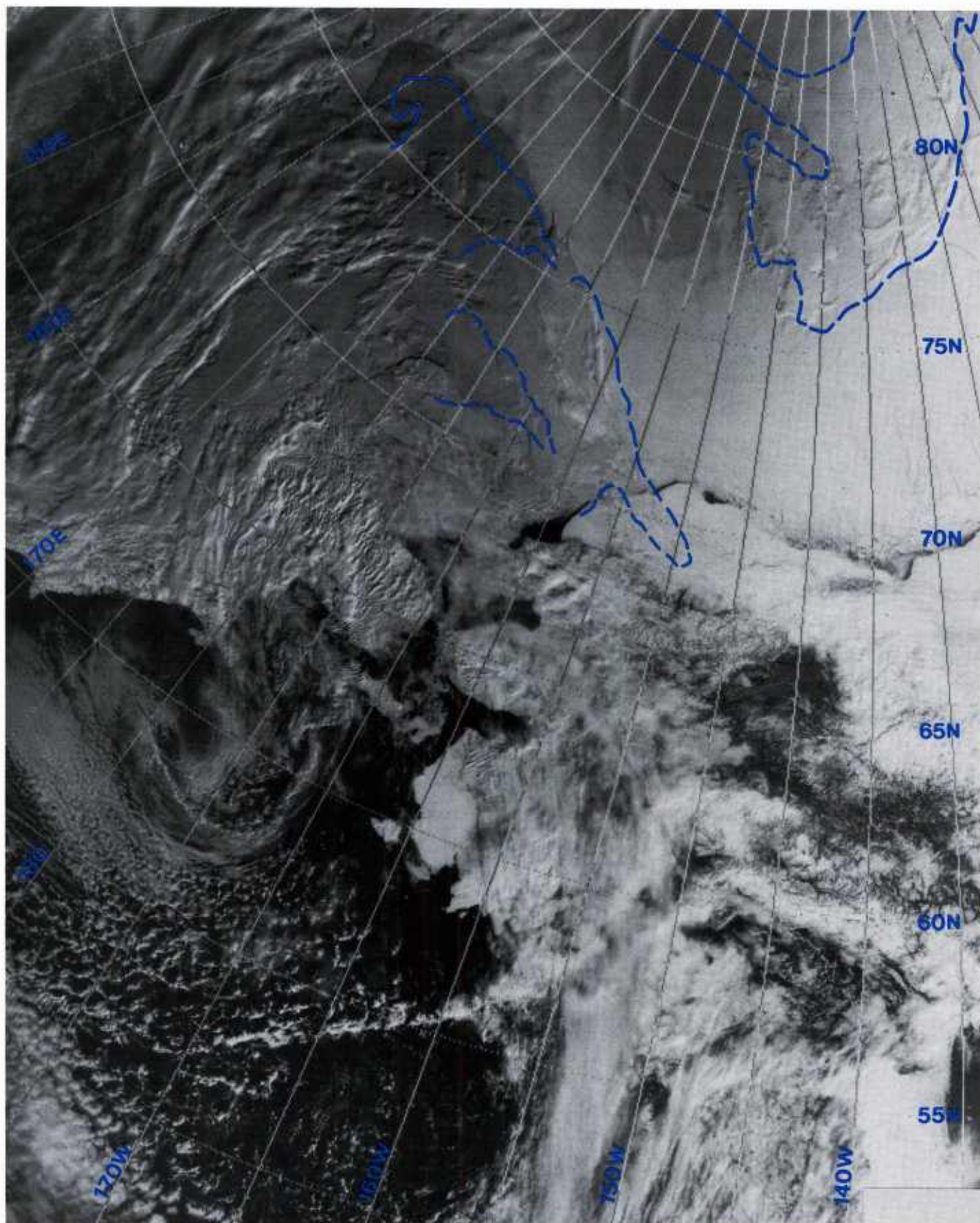
1B-60a DMSP infrared (TS) data. 1715 GMT 17 April 1989.





1B-61a DMSP visible (LF) data. 1857 GMT 17 April 1989.



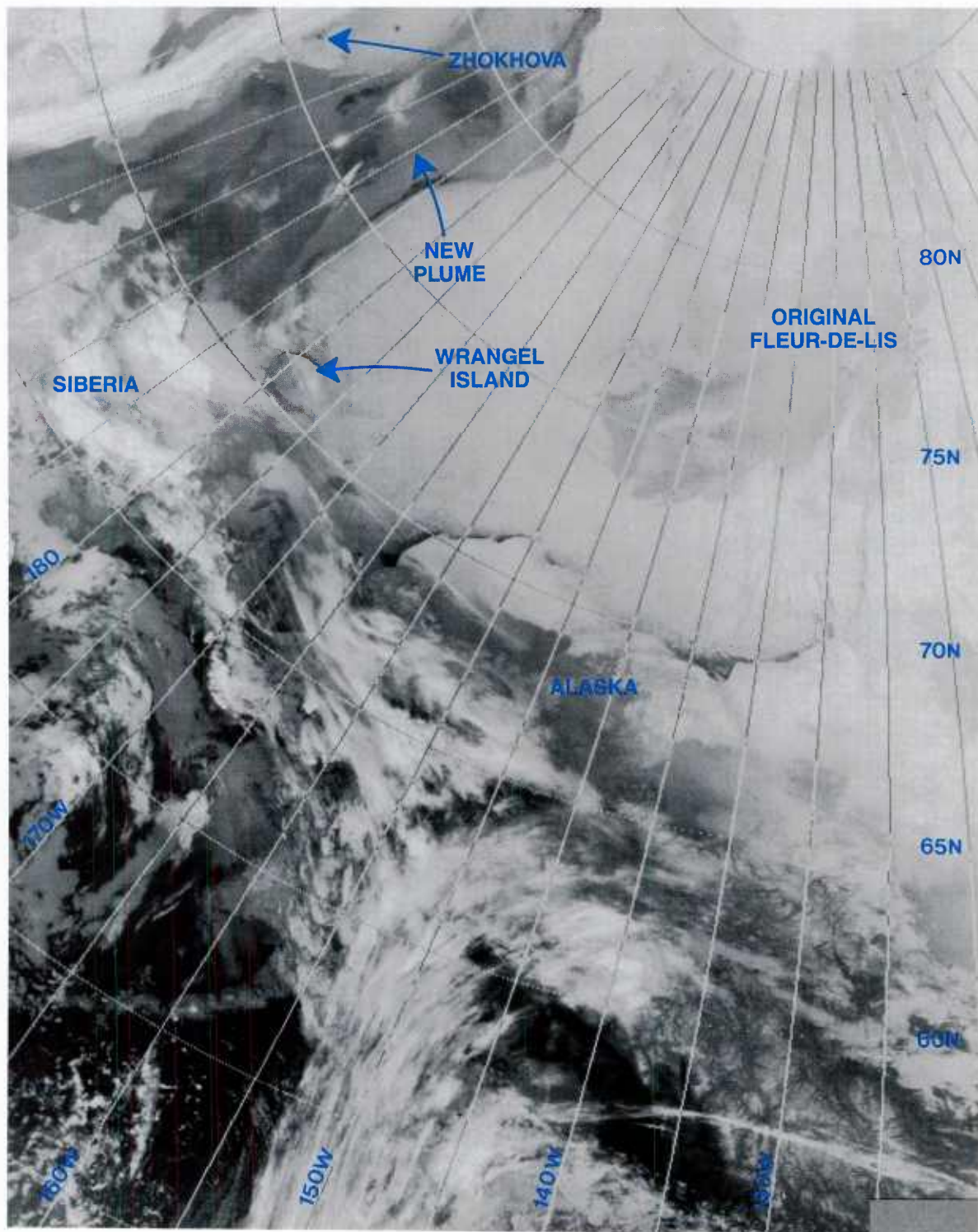


1B-62a DMSP visible (LF) data. 1857 GMT 17 April 1989, cloud pattern from Fig. 1B-60a superimposed.



18 April 1989

The DMSP infrared (TS) data acquired at 1437 GMT (Fig. 1B-63a) indicate that the old fleur-de-lis pattern seems to be breaking up over the eastern Arctic Ocean region leaving still recognizable debris of cloudiness drifting over the area under the persistent low-level inversion. Cloud top temperatures in the region of the original fleur-de-lis are somewhat cooler suggesting a lower height under the inversion. The new plume to the west appears dominant and energetic at this time with an overlying streak of cirrus cloudiness that would normally suggest the presence of a jetstream or strong winds aloft over that area. (This hypothesis will later be shown to be in error.)



1B-63a DMSP infrared (TS) data. 1437 GMT 18 April 1989.

The DMSP visible (LF) data 4 hr later at 1837 GMT (Fig. 1B-64a) provide excellent details showing the multilayer structure of the new plume and the flattened appearance of much of the cloudiness. These details continue to indicate the presence of a strong low-level inversion.

The multiple layer and inversion structure at low levels is well illustrated by RAOB data from Cherskiy, U.S.S.R. ( $68.8^{\circ}\text{N}$   $161.3^{\circ}\text{E}$ ) (Fig. 1B-65a) which reveals three inversions or stable layers below 840 mb. Note that 850-mb winds at Cherskiy are from the northeast at 15 kt. This feature relates well to the direction of alignment of topographic wave clouds evident southwest of Wrangel Island (Figs. 1B-63a and 1B-64a).

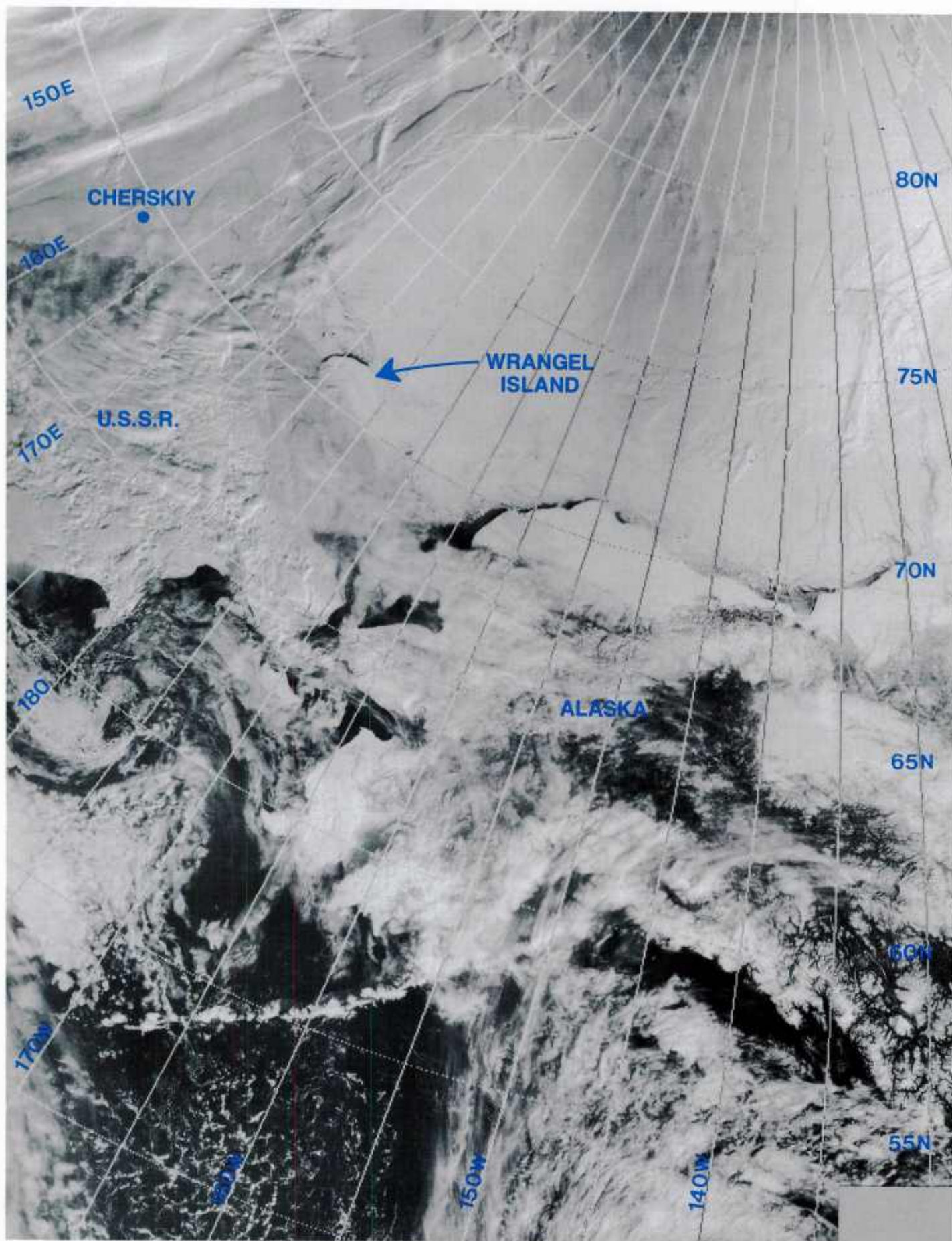
The FNOC 850-mb analysis for 1200 GMT (Fig. 1B-66a) shows that a ridge line exists between Cherskiy and the plumes of north-south oriented cloudiness to the west, where winds become southerly in alignment with the plumes. The ridge line over the region is consistent with subsidence and the noted low-level inversions.

The 500-mb analysis for 1200 GMT (Fig. 1B-67a) is of interest because it does not verify a jet association with the cirrus band extending in a north-south direction between latitudes  $65^{\circ}$ – $80^{\circ}\text{N}$  along  $155^{\circ}\text{E}$ . Rather it shows a confluent streamline of moderate speed in the northern portion, where southerly winds are evident, and a similarly confluent streamline in the southern portion, where northerly flow is evident. A col separates the two flow regimes between  $71^{\circ}$ – $88^{\circ}\text{N}$ .

If this analysis is realistic one might conclude that many cirrus bands in the Arctic are the result of such confluence and that the  $180^{\circ}$  ambiguity, in terms of flow direction, is not always obvious. Another conclusion is that not all similarly appearing cirrus streaks are jetstream associated.

Fortunately, this hypothesis can be tested with DMSP visible (LF) data acquired at 2348 GMT on this date (Fig. 1B-68a) when the cirrus plume can be seen again still oriented north-south between latitudes  $67^{\circ}$ – $73^{\circ}\text{N}$  along approximately  $152^{\circ}$ – $153^{\circ}\text{E}$ . The FNOC 500-mb analysis for 19 April 0000 GMT, valid a few minutes after the time of the DMSP data (Fig. 1B-69a), reveals that the streak is located along the convergence asymptote of a col over that exact location.





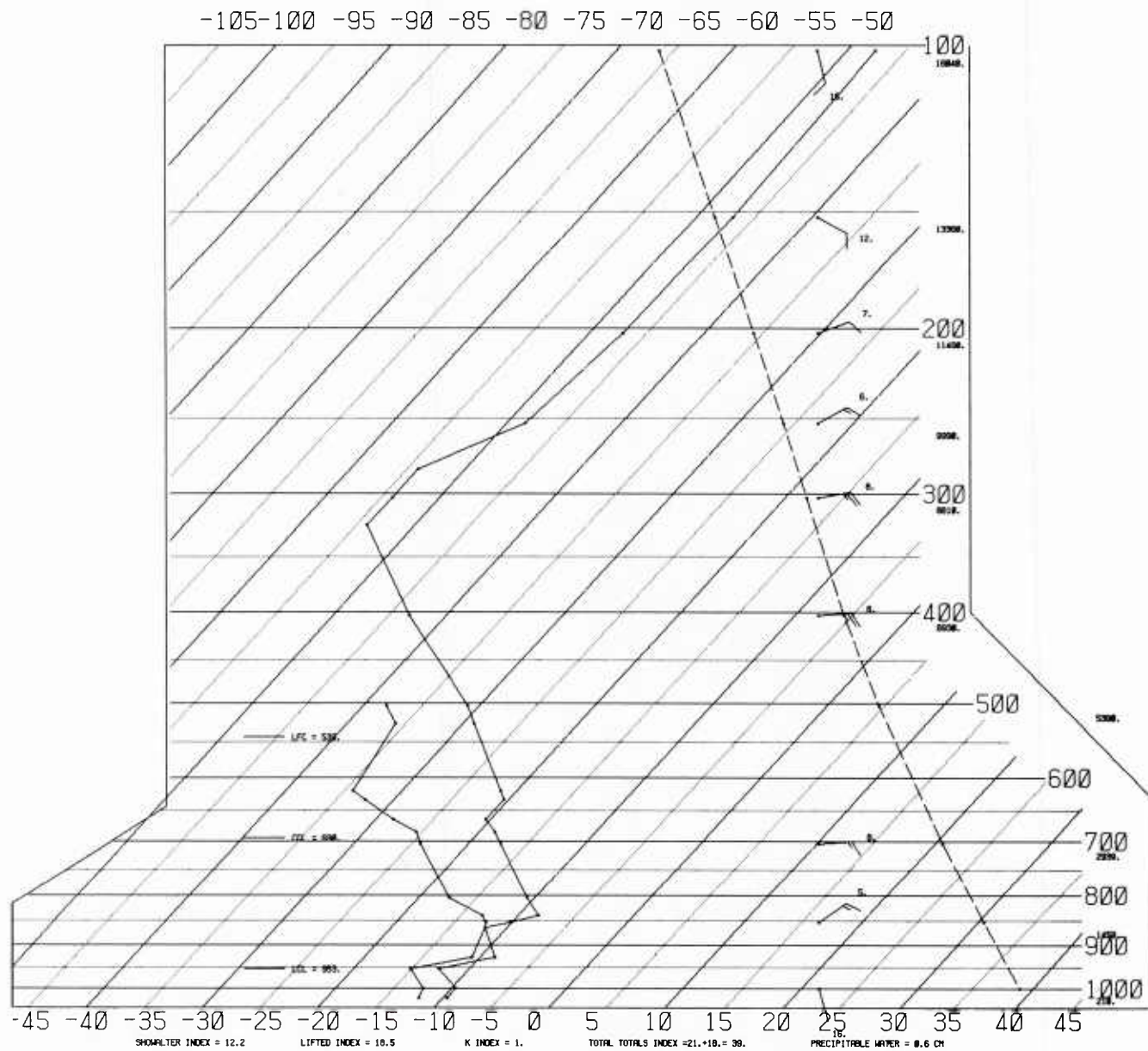
1B-64a DMSP visible (LF) data. 1837 GMT 18 April 1989.

# SKEW T, LOG P DIAGRAM

890418

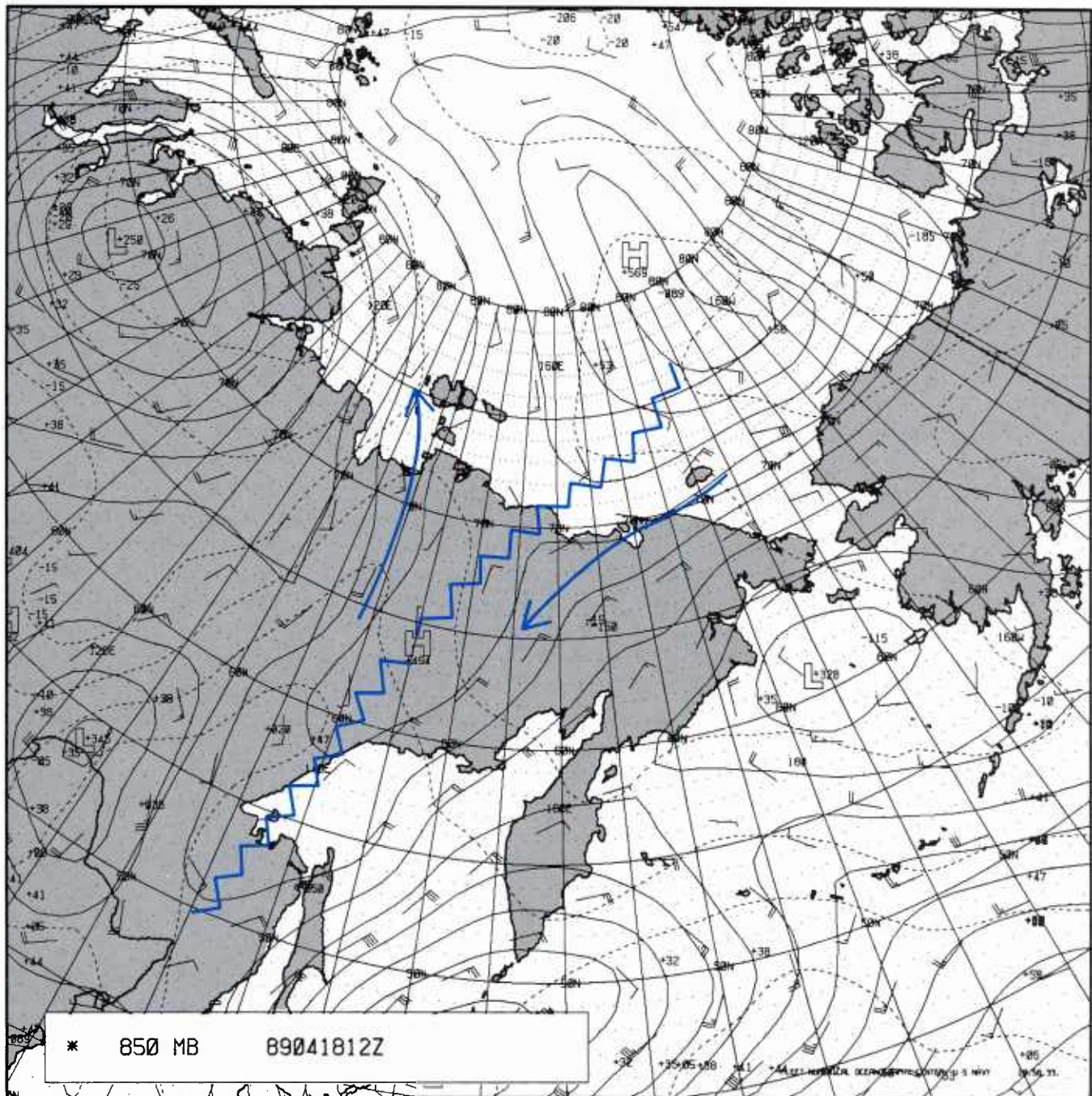
1200Z

25123



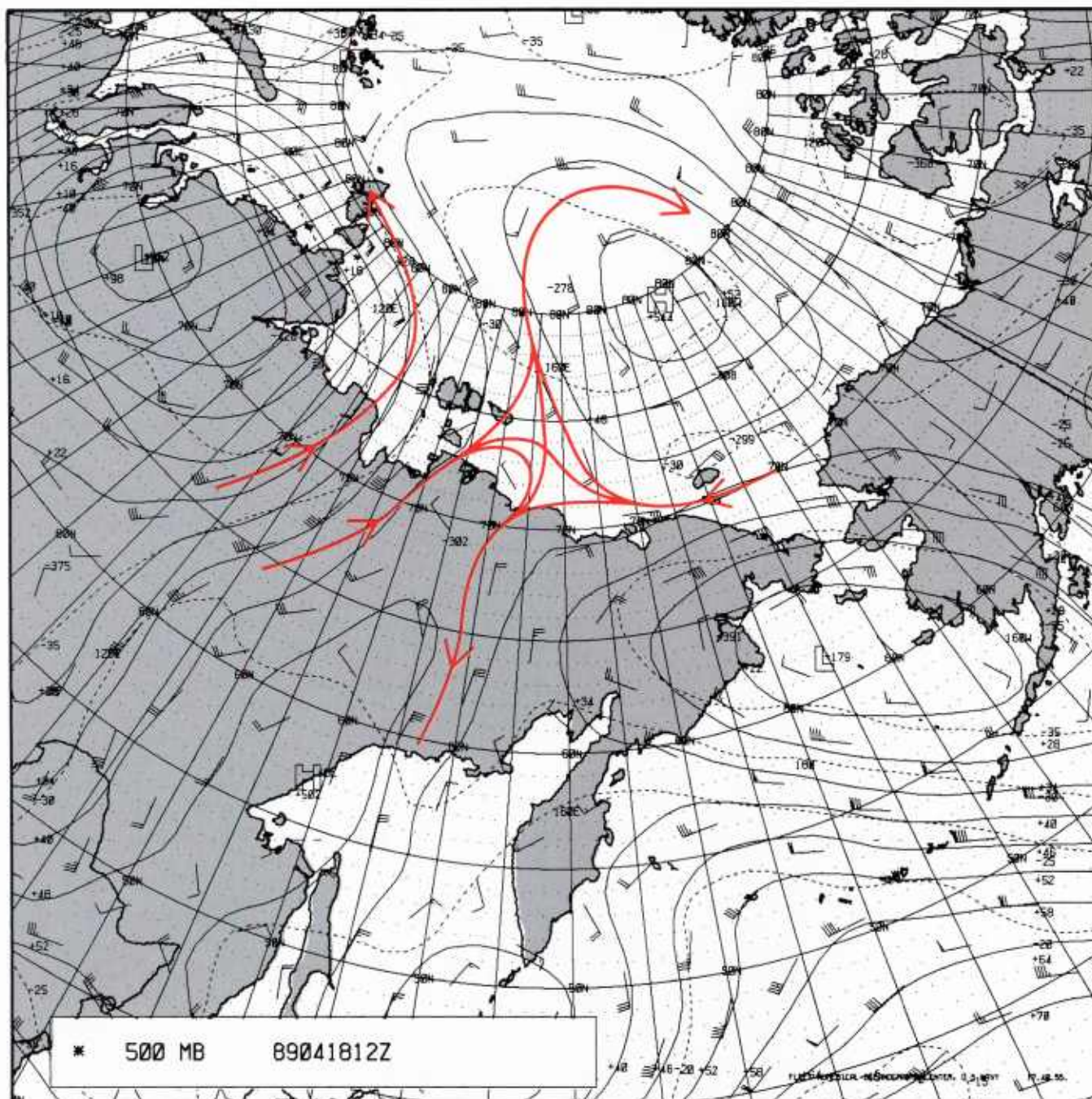
1B-65a Radiosonde data for Cherskiy, U.S.S.R. 1200 GMT 18 April 1989.





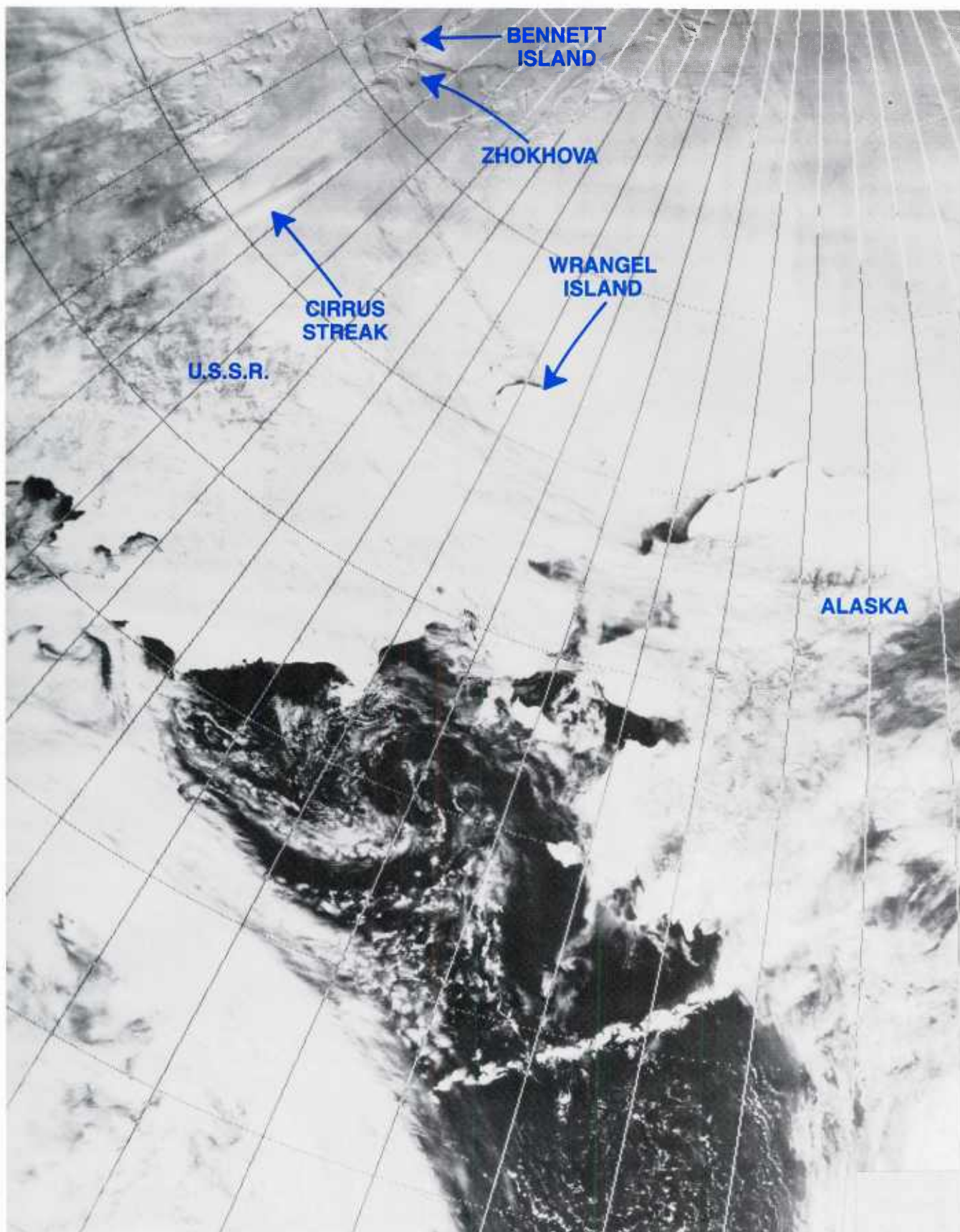
1B-66a FNOc 850-mb analysis. 1200 GMT 18 April 1989.



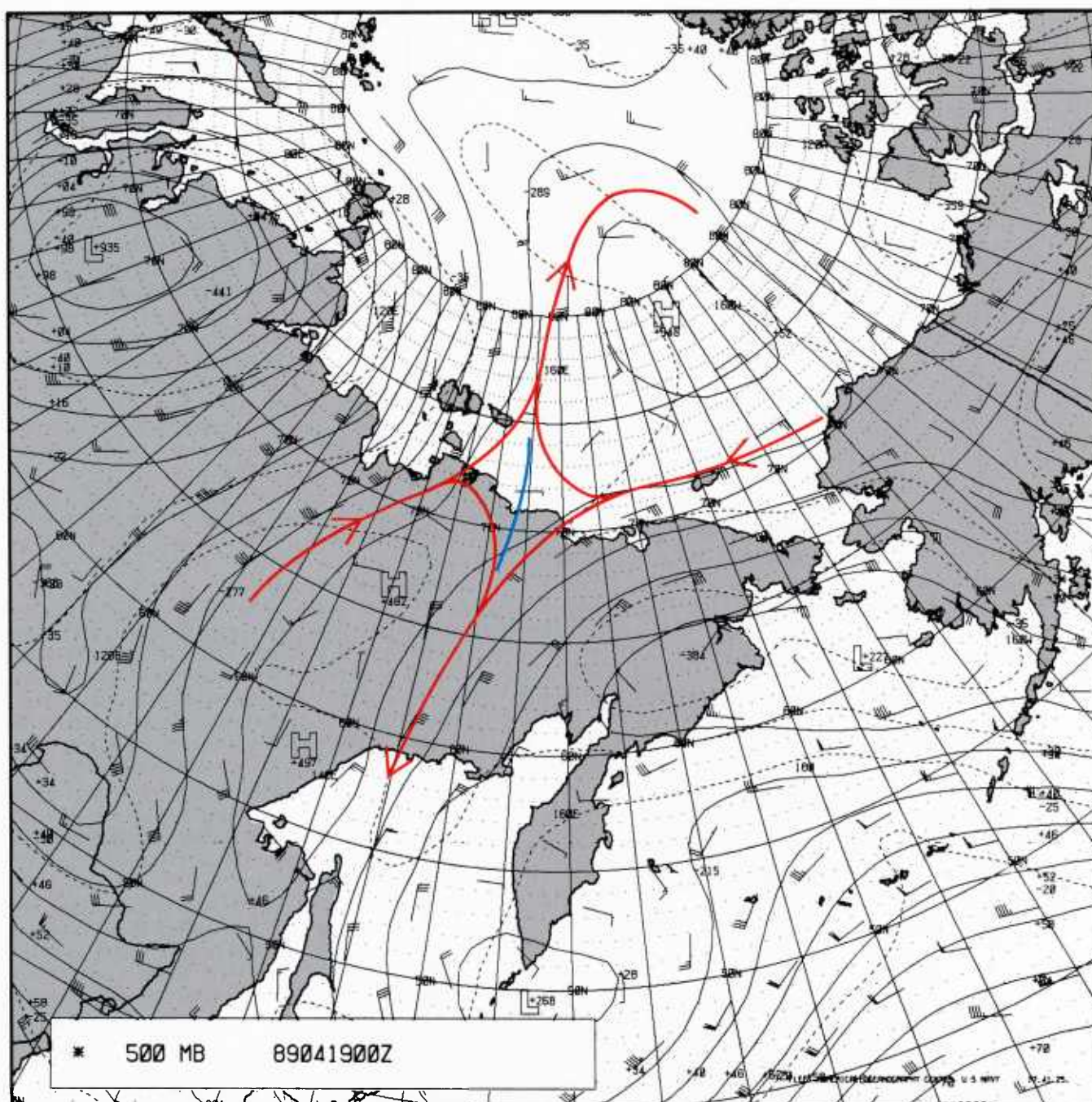


1B-67a FNOC 500-mb analysis (streamline analysis superimposed). 1200 GMT 18 April 1989.





1B-68a DMSP visible (LF) data, 2348 GMT 18 April 1989.



1B-69a FNOc 500-mb analysis (streamline analysis superimposed). 0000 GMT 19 April 1989.



*19 April 1989*

Some spectacular views of the central Arctic Basin were obtained on this data by the DMSP spacecraft. Figure 1B-70a is an infrared (TS) view at 0949 GMT. The new plume has surged into the central basin to merge with cloudiness from the first fleur-de-lis cloud pattern system and has produced low overcast conditions, filling most of the Canada Basin with some of the cloudiness of the system apparently flowing over the North Slope of Alaska.

The stem of the new fleur-de-lis pattern extends north-northeastward from the coast of the Soviet Union in the region of  $150^{\circ}$ – $160^{\circ}$ E. The separation of the pattern to the left and right in the area  $80^{\circ}$ – $85^{\circ}$ N implies high pressure to the right and low pressure to the left.

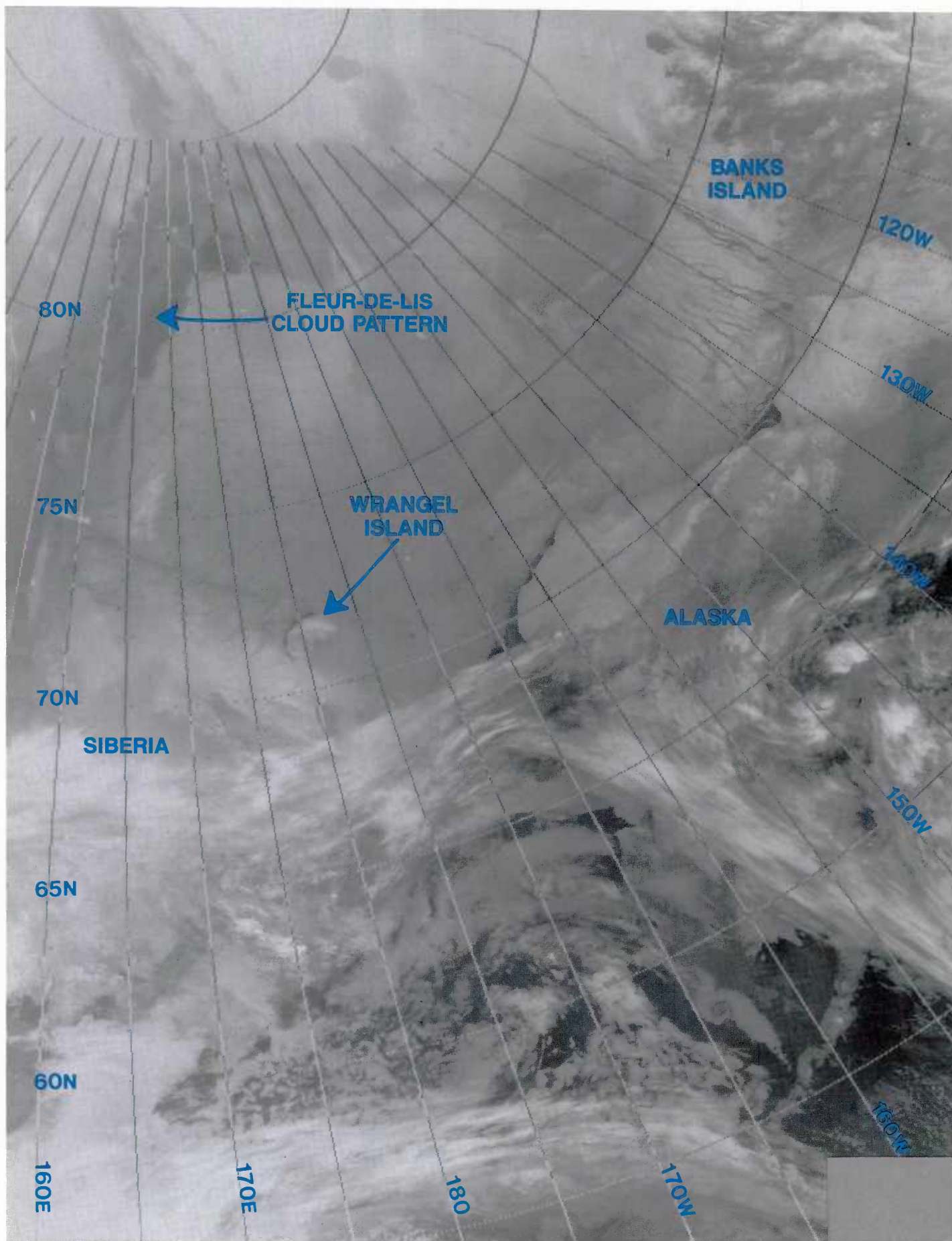
The FNOC surface analysis for 0000 GMT (Fig. 1B-71a), as well as the 500-mb analysis for the same time (Fig. 1B-69a), reveals that the flow is contained and apparently induced by flow between high pressure over the Arctic Ocean and low pressure over central Russia. The high pressure center over the central Arctic Ocean, near  $78^{\circ}$ N  $175^{\circ}$ W, could be very misleading in terms of expected cloud cover. The average meteorologist not familiar with the region would find, instead of expected clear skies with high pressure, actual weather consisting of an enormous area of dense, low overcast.

Continued evolution of the system in DMSP infrared (TS) data obtained at 1607 GMT is shown in Fig. 1B-72a. The warmer temperature of the stem of the fleur-de-lis pattern implies low cloudiness at a higher level than other cloudiness over the high pressure region north of Alaska. Cooler temperatures in this latter area imply lower cloud tops, but still capped by a low-level inversion. This region east of Wrangel Island, extending over the Beaufort Sea, has temperatures almost as cold as the surrounding pack ice. This feature implies very low cloudiness, and perhaps even a foggy condition, with a base of clouds at sea-surface level. A bright orographic cloud plume from mountainous terrain on Wrangel Island indicates easterly flow consistent with indications on the 500-mb analysis (Fig. 1B-69a) showing 30 kt easterly winds over the region.

A final DMSP view in visible (LF) data acquired at 1958 GMT is shown in Fig. 1B-73a. Islands of grounded sea ice (labeled 1, 2, and 3) are especially evident in this image (see Section 3C). Close examination of the region north of Alaska shows overcast, very flat appearing, low-level cloudiness covering much of the area. This is the remnant of the fleur-de-lis plume shown 3 days earlier in Fig. 1B-50a.

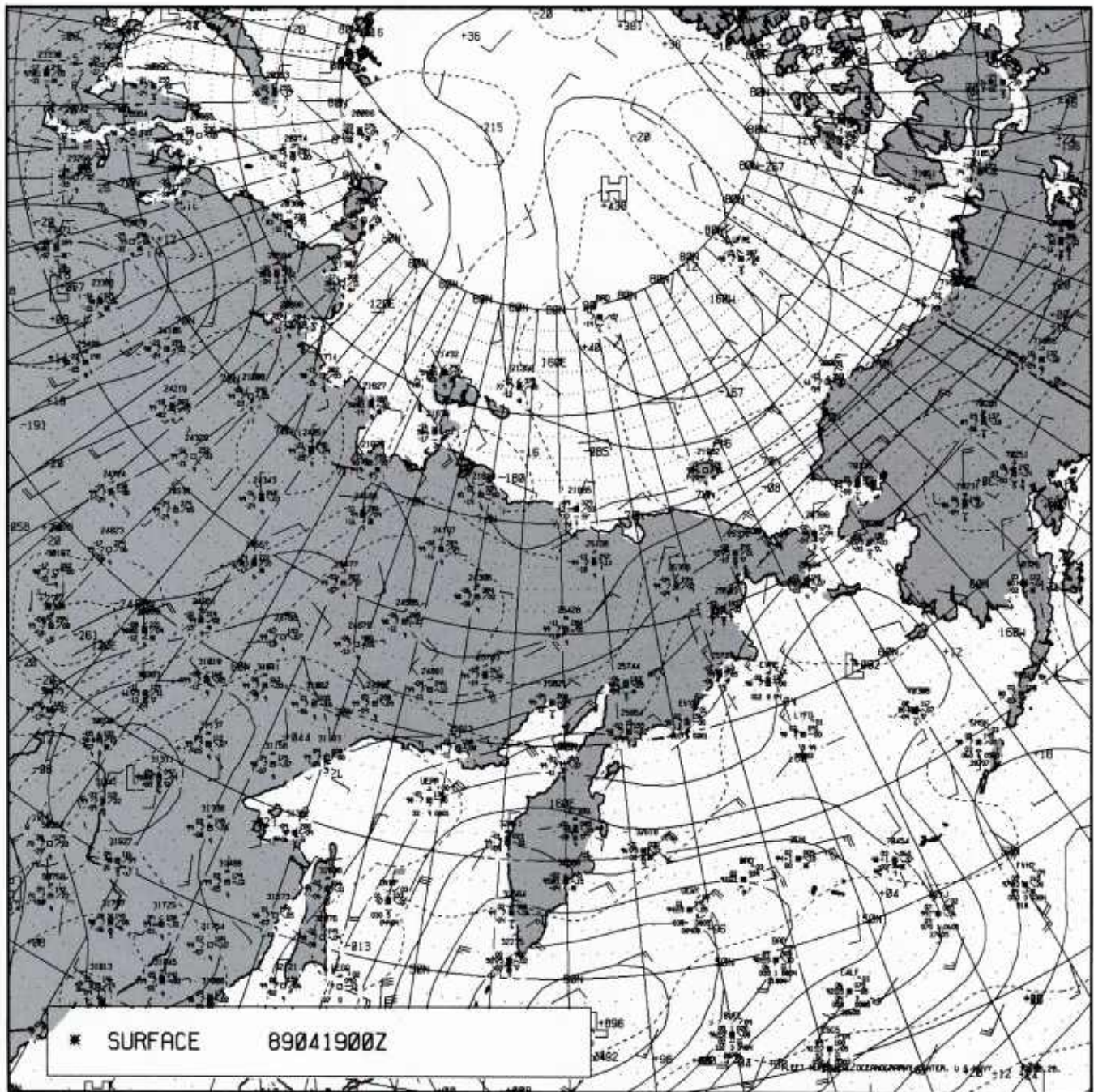
Much cirrus cloudiness is evident in this visible image, not particularly noticeable in some areas in the infrared data (Fig. 1B-72a). As noted in NTAG Vol. 1, cirrus cloudiness is mainly detectable in DMSP visible data, through forward scattering of light, when the OLS scanner is pointed in the direction of the Sun (which is to the southeast at the time of data observation). Thin cirrus clouds are often invisible when the scanner points in a direction away from the Sun. It is therefore of special interest to see an apparent cirrus streak over the fleur-de-lis pattern in the northwest portion of the image that is not apparent in the infrared data (Fig. 1B-72a). A possible explanation for this aberrant behavior is that the cirrus clouds are rendered visible primarily as a result of the shadow the band produces on the underlying surface. The band itself may be too thin to cause a noticeable change in radiative effect in the infrared channel. The major cirrus streak may appear somewhat brighter due to sufficient backscattering. However, note that a parallel streak to the north is apparent only as a shadow, indicating a more diffuse nature.

The final FNOC surface and 500-mb analyses to relate to the above data are shown in Figs. 1B-74a and 1B-75a, respectively. The flow pattern favors periodic projection of fleur-de-lis type cloudiness into that region of the Arctic.

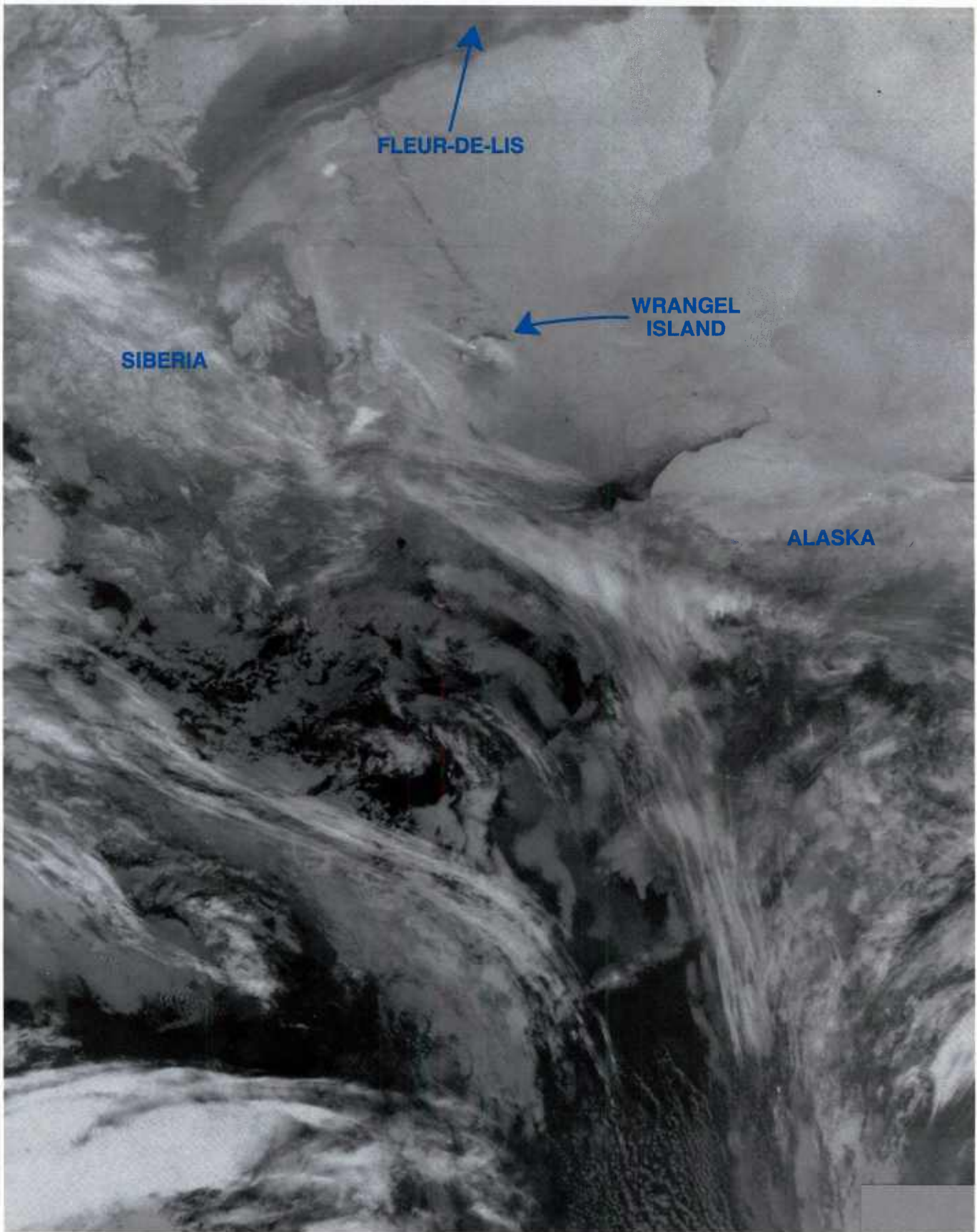


1B-70a DMSP infrared (TS) data. 0949 GMT 19 April 1989.



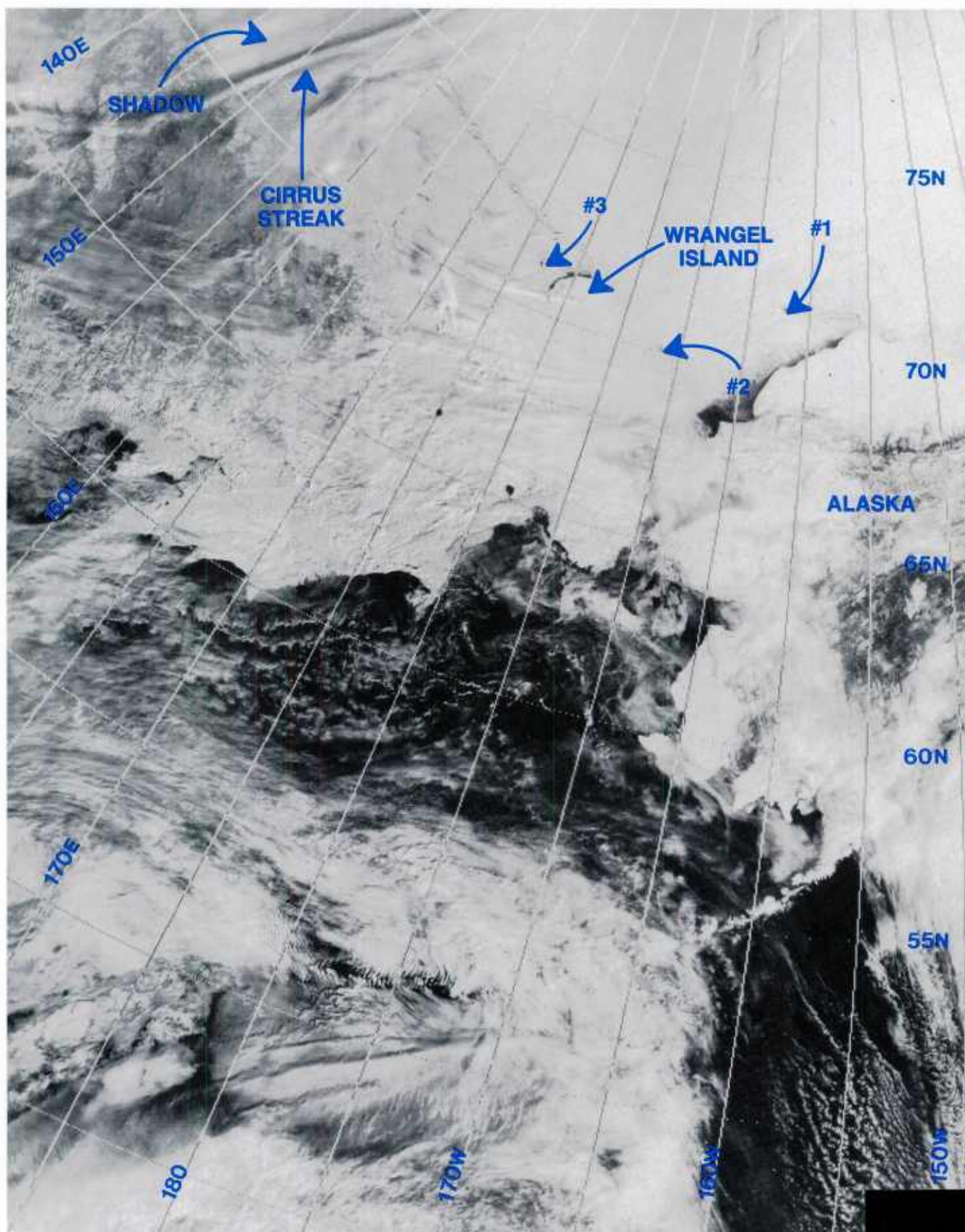


1B-71a FNOC surface analysis. 0000 GMT 19 April 1989.



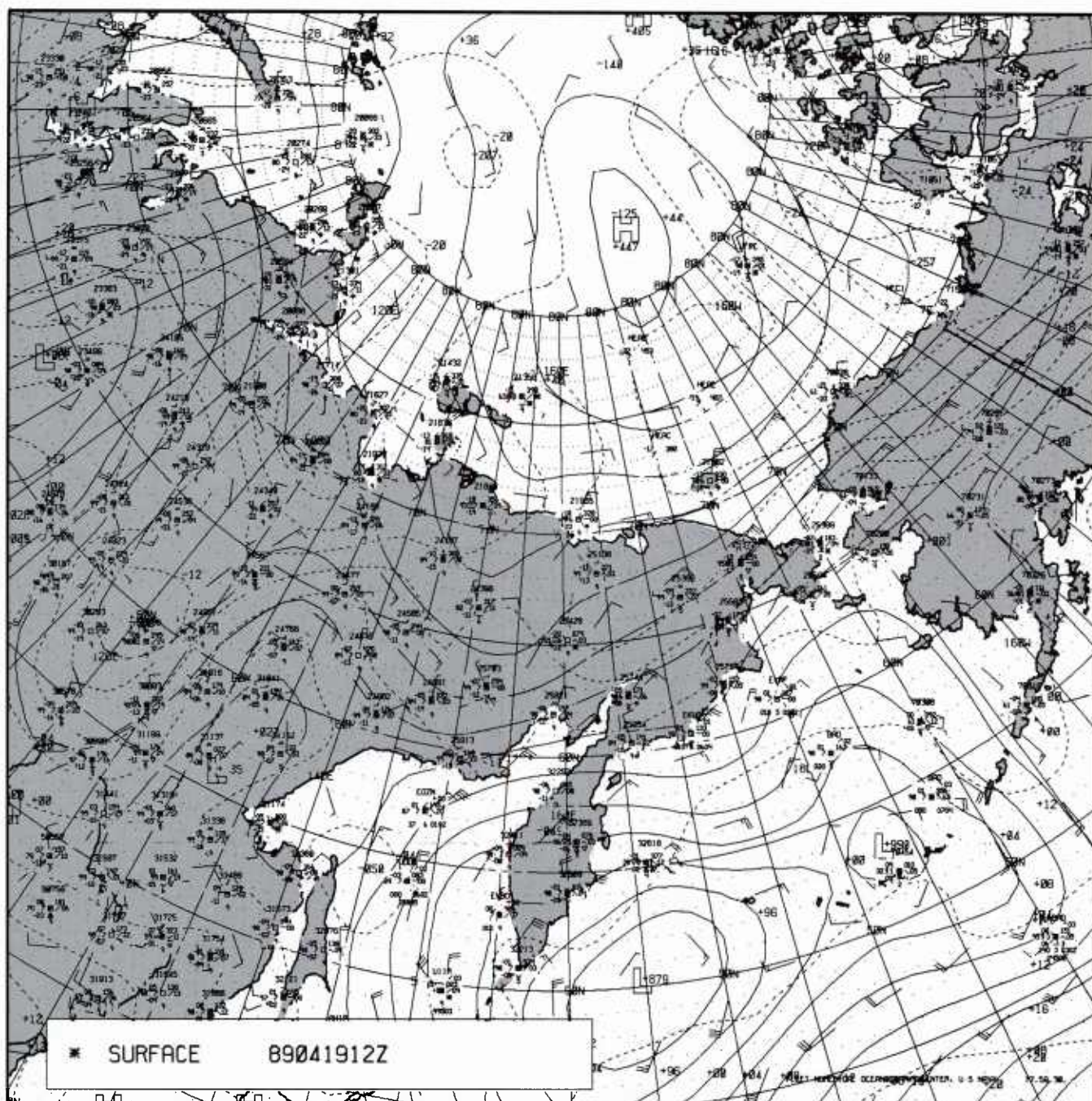
1B-72a DMSP infrared (TS) data. 1607 GMT 19 April 1989.





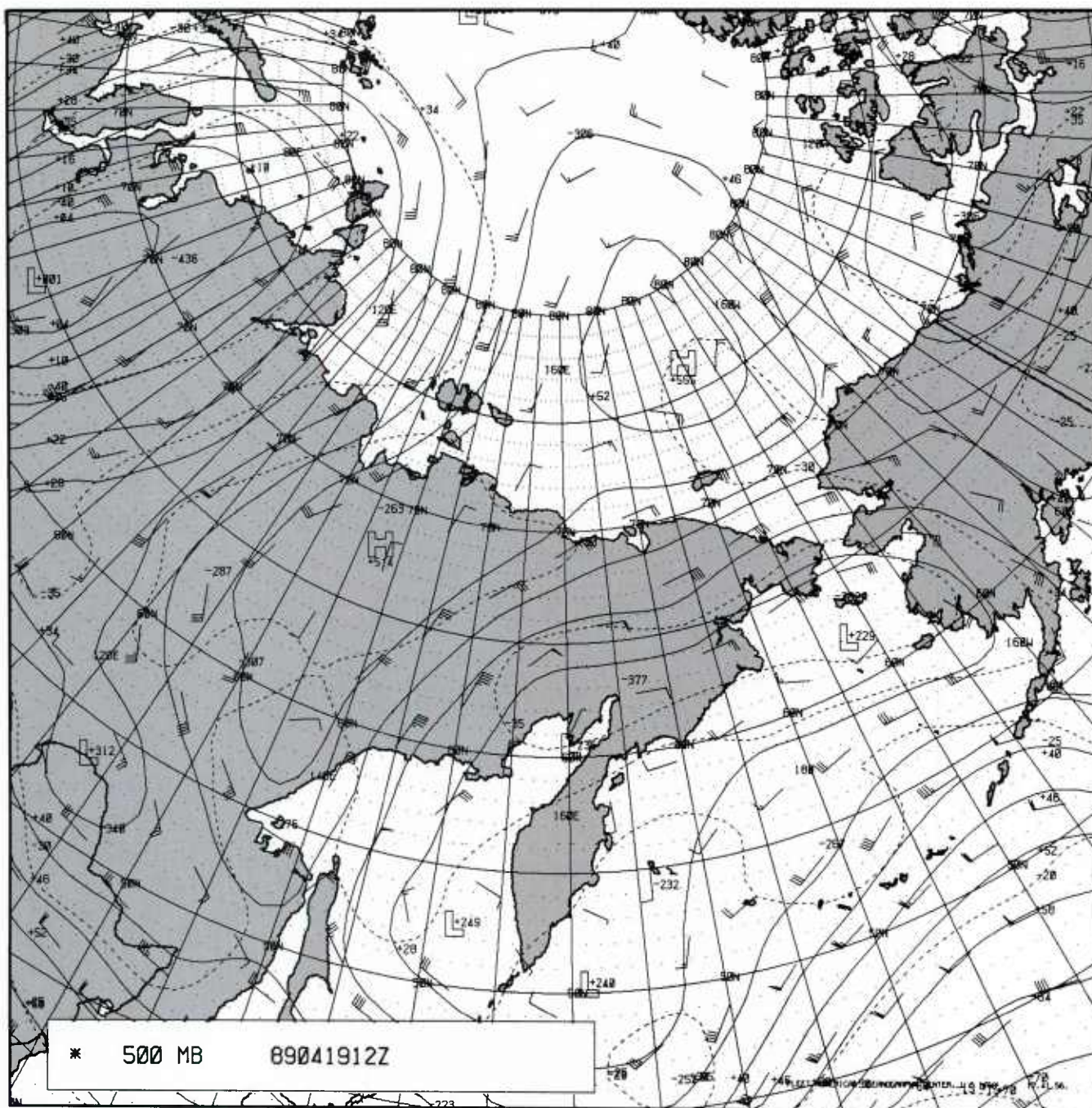
1B-73a DMSP visible (LF) data. 1958 GMT 19 April 1989.





1B-74a FNOC surface analysis. 1200 GMT 19 April 1989.





1B-75a FNOC 500-mb analysis. 1200 GMT 19 April 1989.

### **Important Conclusions**

1. The fleur-de-lis pattern is associated with enormous areas of dense, low overcast stratus and fog, capped by one or more low-level inversions.
2. A high pressure pattern favors fleur-de-lis cloud pattern production over the central Arctic Ocean, with low pressure over central Russia and a moderate gradient producing southerly flow into the Arctic Ocean from the Siberian region.
3. A southerly jetstream between the high and low pressure systems seems to be associated with the development of the pattern.
4. Meteorologists expecting clear sky conditions associated with a massive high pressure region centered over the Arctic Ocean are apt to be surprised by satellite evidence of a dense, low overcast.
5. Thin cirrus bands or streaks over the Arctic region, and perhaps other areas of the world, may be related to upper level convergence with the band of cirrus forming along the asymptote of convergence in the center of a col.

### **Reference**

Fett, R.W., 1990: Navy Tactical Applications Guide, Vol. 8, Part 1, *Arctic: Greenland/Norwegian/Barents Seas Weather Analysis and Forecast Applications*. NEPRF TR 89-07, Naval Environmental Prediction Research Facility, Monterey, CA 93943-5006, 200 pp.





# Section 2

## *Polar Lows*

2A	<i>Introduction to Polar Lows</i> .....	2A-1
----	---	------

2B	<i>Case Studies</i>	
----	---------------------	--

	Polar Low Development .....	2B-1
--	-----------------------------	------

### *Case Studies*

1	<i>Polar Low Development in the East Siberian/ Chukchi/Beaufort Sea Region</i> .....	2B-2
---	--	------





## 2A *Introduction to Polar Lows*

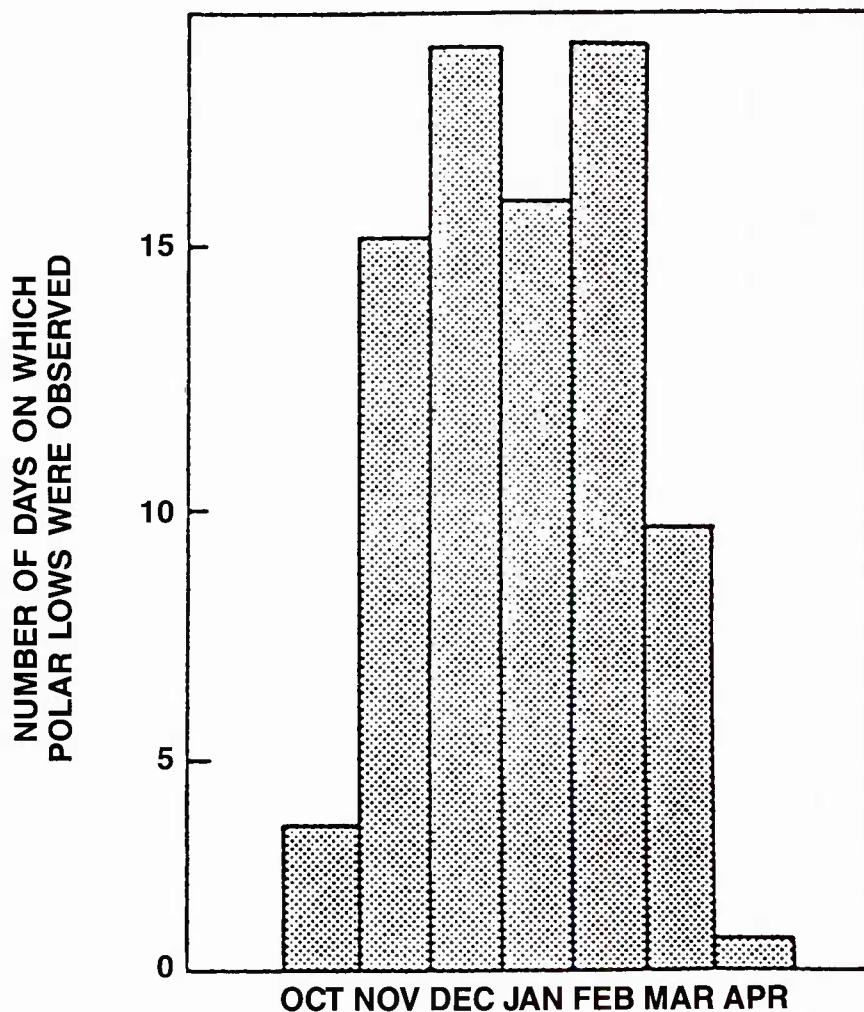
The term "polar lows" has been applied to various subsynoptic Arctic disturbances. Both the theory of these systems and an unambiguous definition of a polar low are evolving. Small cloud vortices have a tendency to develop in regions where cyclonic vorticity is maximized. These cloud vortices may occur along trough lines extending from closed lows or in regions of cyclonic horizontal shear in wind speed. In such regions, despite the cloud vortex, a closed wind circulation implying a pressure minimum does not exist; hence, the term polar low seems inappropriate for the description of such features. At the same time, it is agreed that these types of cloud features may evolve into polar lows. The distinction is similar to that made in tropical meteorology, of an easterly wave which has not yet evolved into a tropical depression (a closed tropical circulation having a wind speed of less than 34 kt). For the purposes of this publication, using similar logic, a cloud vortex in the cold air behind a frontal system in the Arctic will be referred to as only a polar vortex or cloud vortex until it can be ascertained that (1) a closed circulation and pressure minimum exists, and (2) minimum wind speeds of 35 kt or more have been attained. At that point, the polar vortex or cloud vortex will be referred to as a polar low. This reference seems especially fitting since the term polar low has, in recent years, come to connote an intense Arctic storm of at least tropical storm and often hurricane intensity. Excluded from the above definition are those comma-shaped cloud systems that occur in close proximity to major frontal boundaries (Businger, 1987).



Businger (1987), using NOAA satellite data, conducted a detailed study concerning the number of days per month in which “. . . vigorous polar lows (exhibiting a well developed spiral cloud structure and high cloud tops indicated by cold radiative cloud-top temperatures) were present. . .” over the Gulf of Alaska or the Bering Sea during the period 1975–1983 (Fig. 2A-2a). The figure indicates maximum frequency in late fall through early spring, with the peak development period being November through February.

Several synoptic and subsynoptic features have been shown to be associated with polar low development in the Bering Sea and Gulf of Alaska region. Businger (1987) showed that environmental factors conducive to the development of strong polar lows include (1) a deep outflow of Arctic air over open water, (2) a cold synoptic scale closed low aloft, (3) differential positive vorticity advection associated with a small synoptic-scale trough or vortex at 500 mb, and (4) significant negative height and temperature anomalies throughout the troposphere.

Brown (1986) pointed out that development of high latitude polar lows is inevitably associated with cloud street structures. The role of Arctic boundary layer fronts—the boundary between air that has been warmed on a long path over the sea and air that has just left snow-covered land or the ice pack—as a source of baroclinic instability that can lead to polar low development has been addressed by Shapiro and Fedor (1989).



2A-2a Histogram of the number of days per month on which polar lows were observed in polar-orbiting satellite imagery over the Gulf of Alaska or the Bering Sea during the period 1975–1983 (Businger, 1987).

The conditions favorable for polar low development, as noted above, are of synoptic scale. A typical scenario includes (1) the stalling and gradual dissipation of a mature synoptic-scale cyclone leaving behind a large cold vortex aloft; (2) establishment within the synoptic regime of a subsynoptic scale baroclinic zone, such as a boundary layer front through convergence of low-level flow regimes, a boundary between warm air wrapping around the mature cyclone due to the frontal occluding process and ambient cold air, or any other mechanism resulting in a baroclinic zone development; and (3) for development of the more intense polar lows (dubbed "Arctic hurricanes") the passage of a jet maximum (jet streak), typically associated with a secondary trough spokewheeling around the upper low and passing over the lower level baroclinic development (Emanuel and Rotunno, 1989).

Polar low development tends to be episodic because the basic forcing patterns are of synoptic "spatial" scale, while the temporal scale is extended due to dissipating mature cyclones becoming nearly stationary over the Bering Sea region. It is not unusual for several polar lows to be occurring within the region at one time with the formation and dissipation processes going on for several days.

The favorable location for polar lows is generally in the western and southern sectors of dissipating synoptic lows. Because the polar lows develop some distance away from the center of the synoptic low, they are likely to have moderate to strong steering flow over them. As a result they will move at a velocity representative of the steering flow and not with the movement of the dissipating synoptic low. The more intense the polar low and related vertical development, the higher in the atmosphere will be the representative steering level. Steering is actually an integrated result of the flow throughout the layer of the atmosphere interacting with the low; but generally speaking, the flow near the midpoint of the vertical development of the low will be representative of the integrated or mean steering flow. Because of the suppressed atmosphere of the high latitudes, even strong polar lows will likely have a representative steering level closer to 850 mb instead of the 500 mb that is generally used as a rule of thumb for synoptic scale midlatitude features. A speed of advance of 30 kt is not unusual for well developed polar lows. Because of the relatively small horizontal extent of the Bering Sea and Gulf of Alaska and the tendency to dissipate rapidly once over land, a polar low exists, on the average, only a day or two. Only under optimum forcing and migration path can a given polar low persist for several days. Because forcing is localized and polar lows are small in size, they can develop rapidly, frequently reaching maximum development within 12 to 24 hr from initial development, and also dissipate rapidly.

Analysis of aircraft and radiosonde data collected during field experiments has shown that some polar lows have warm cores. Satellite imagery frequently shows an "eye" similar to that seen in tropical cyclones and surrounding strong convection. The warm core configuration is likely associated with the strong convective activity. This thermodynamic structure has led to the coining of the term "Arctic hurricane."

Because of their small scale and localized forcing, polar lows are usually below the resolution of existing operational numerical models. However, the models can depict the favorable synoptic scale patterns. Forecasters should closely monitor the numerical analyses and prognoses for existing or developing favorable synoptic conditions. Equally important is the utilization of satellite imagery and conventional observations.



### **Forecast Aid for Initial Development**

1. Cold air outbreak and formation of low-level cloud street patterns.
2. Large negative anomalies in upper level temperature and heights.
3. Development of a low level baroclinic zone such as an Arctic front due to convergence of air streams with different over-water flow length or "wrap-around" warm air slots to the west and south of occluding frontal systems.
4. Upper level short wave trough and/or jet maximum moving over low-level features.

After initial development occurs as a result of low level baroclinic conditions, the polar low clouds, which are generally of convective form, begin to organize into the classic comma shape. If favorable upper air conditions exist, further intensification will occur that can result in winds reaching hurricane force. During the development process of polar lows certain sequences of cloud signatures can be seen in satellite imagery. Initial development typically occurs along Arctic fronts or other convergence or baroclinic zones that exhibit recognizable enhanced cloud development and organization.

Intensifying polar lows tend to have highly symmetric, spiral-shaped cloud signatures with vigorous cumulonimbus surrounding a clear area or eye. Polar lows at this stage of development will have central pressures 4 to 8 mb below ambient sea level pressure with winds in the 30- to 40-kt range and their cloud pattern will be 100 to 200 n mi in diameter. To reach "Arctic hurricane" status requires increased low level convergence or upper level divergence resulting in the cloud pattern becoming asymmetrical with an anticyclonically curved cirrus shield reflecting the outflow region. The cirrus shield may cover the cumulonimbus surrounded eye. At this stage the cloud pattern will have a diameter of 300 to 400 n mi, the central surface pressure will be near 970 mb; and the winds will be in the 40- to 60-kt range.

During passage of an Arctic hurricane in March of 1977, St. Paul Island recorded a pressure drop from 985 mb to 972 mb in 3 hr and then back up to 985 mb 3 hr after passage. Concurrently the air temperature rose from  $-7^{\circ}$  to  $-3^{\circ}\text{C}$ , reflecting the warm core nature of these most intense polar lows, and then back down. A Soviet icebreaker caught in this same Arctic hurricane encountered winds over 60 kt, 30-ft waves, lightning, snow, and sea spray, resulting in heavy super structure icing, rapidly changing pressure and temperature, and passage through an "eye-like" calm, clear, warm area.

### **Forecast Aids for Intensification**

1. Development or movement of an upper air negative height anomaly of about 200 m over an oceanic region. Over the Bering Sea and Gulf of Alaska this in general means 500-mb heights below 5,000 m.
2. Negative 500-mb temperature anomalies of  $-6^{\circ}\text{C}$  equates to a 500-mb temperature of generally  $< -36^{\circ}\text{C}$  for this area.
3. Approach of an upper level jet streak or area of positive vorticity advection.

Other environmental features that have been recognized in studies of polar low episodes include

1. Existence of a synoptic scale low-pressure trough such as the remnants of a dissipating occluded low.
2. An area of enhanced SST gradient in the vicinity of the area of potential.
3. Isobar packing to the west of an area conducive to, or of already developed, polar lows.
4. A steep surface temperature gradient of about 10°C over 120 n mi to the west of the area of potential.
5. A very low tropopause height on the order of 6,000 m.

#### References

- Brown, R.A., 1986. The planetary boundary layer precursor to the polar low. Proceedings of the International Conference on Polar Lows, Oslo 1986, The Norwegian Meteorological Institute.
- Businger, S., 1987. The synoptic climatology of polar-low outbreaks over the Gulf of Alaska and the Bering Sea. *Tellus*, 39A, 307-325.
- Emanuel, K.A., and R. Rotunno, 1989. Polar lows as arctic hurricanes. *Tellus*, 41A, 1-17.
- Shapiro, M.A., and L.S. Fedor, 1989. A case study of an ice-edge boundary layer front and polar low development over the Norwegian and Barents Seas. *Polar and Arctic Lows*, P.F. Twitchell, E.A. Rasmusson, and K.L. Davidson (Eds.), Deepak Publishing, Hampton, VA, 257-278.





## **2B**   *Case Studies*

### *Polar Low Development*

This section presents examples of Polar Low development in the East Siberian/Chukchi/Beaufort Sea region. DMSP visible and infrared imagery as well as surface and 500 mb analyses are used to illustrate this development.

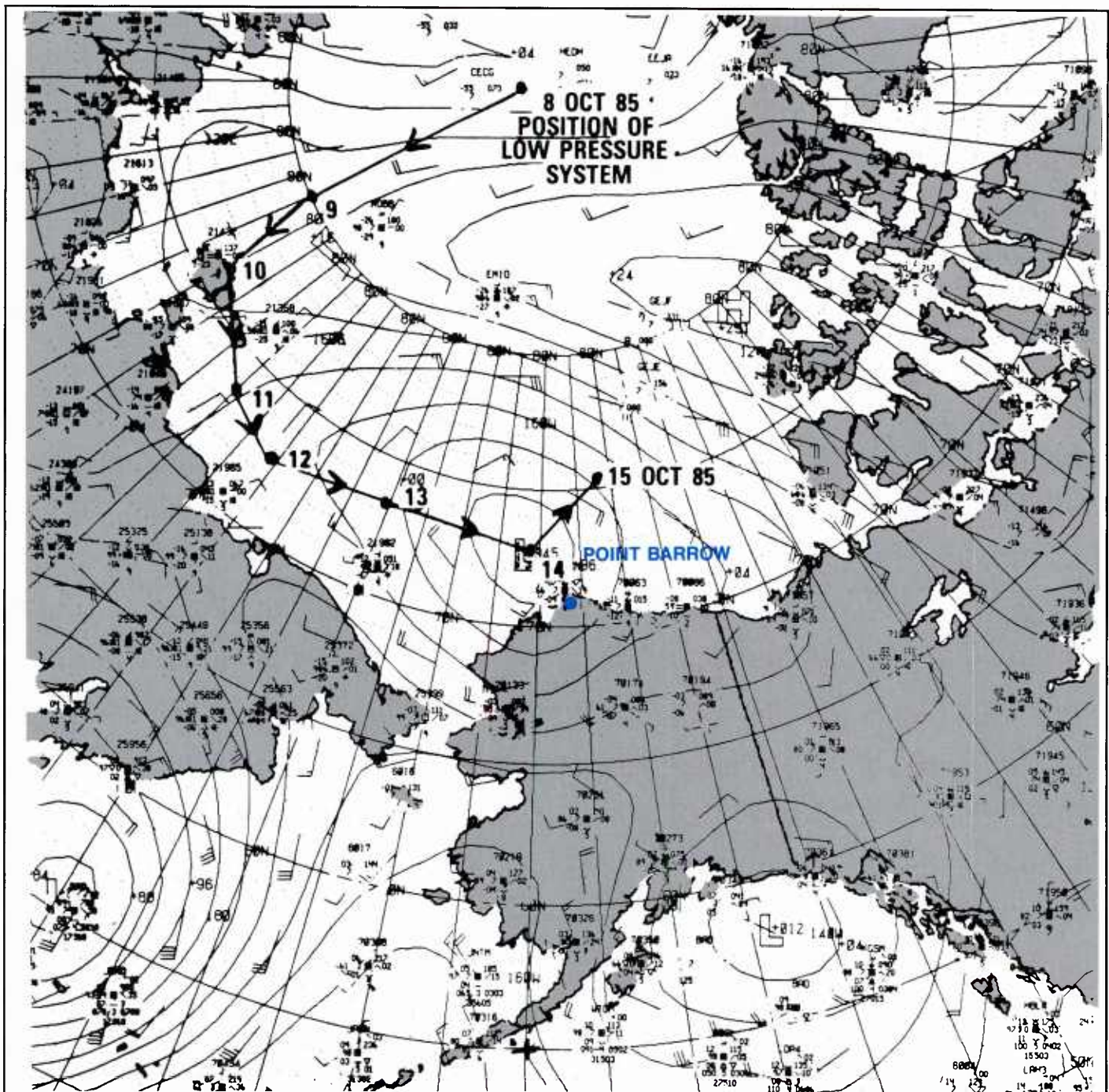


*Case 1 Polar Low Development in the East Siberian/Chukchi/Beaufort Sea Region*

*October 1985*

A low pressure system centered near the North Pole on 8 October was observed to track regularly in a southward, then in an eastward direction, reaching the northwest coast of Alaska by 14 October (Figure 2B-2a).

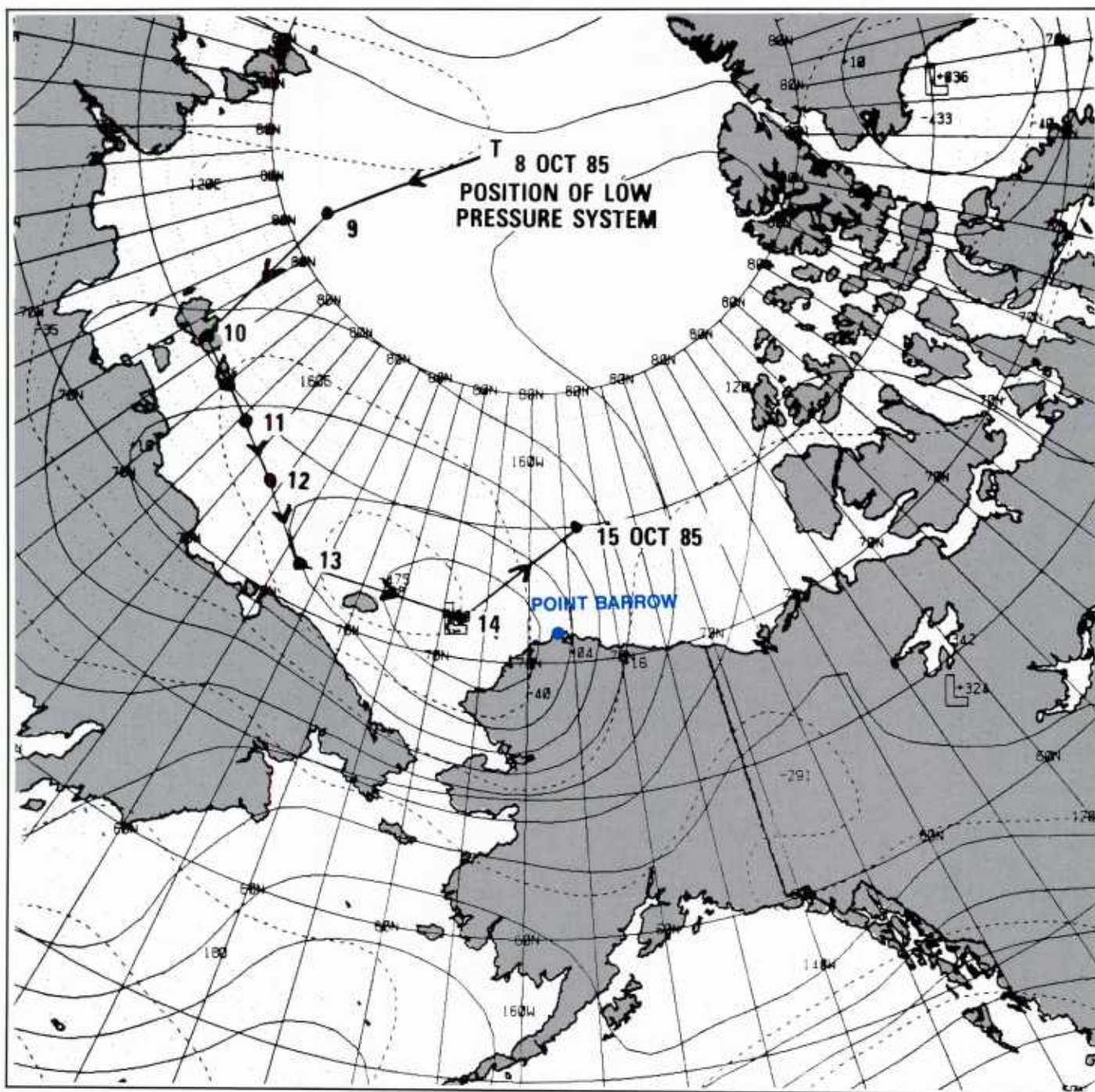
A 500 mb low and cold pool of air, apparently associated with this system, also was observed moving generally in tandem with the surface feature (Figure 2B-3a). Twelve- and twenty-four-hour Fleet Numerical Oceanography



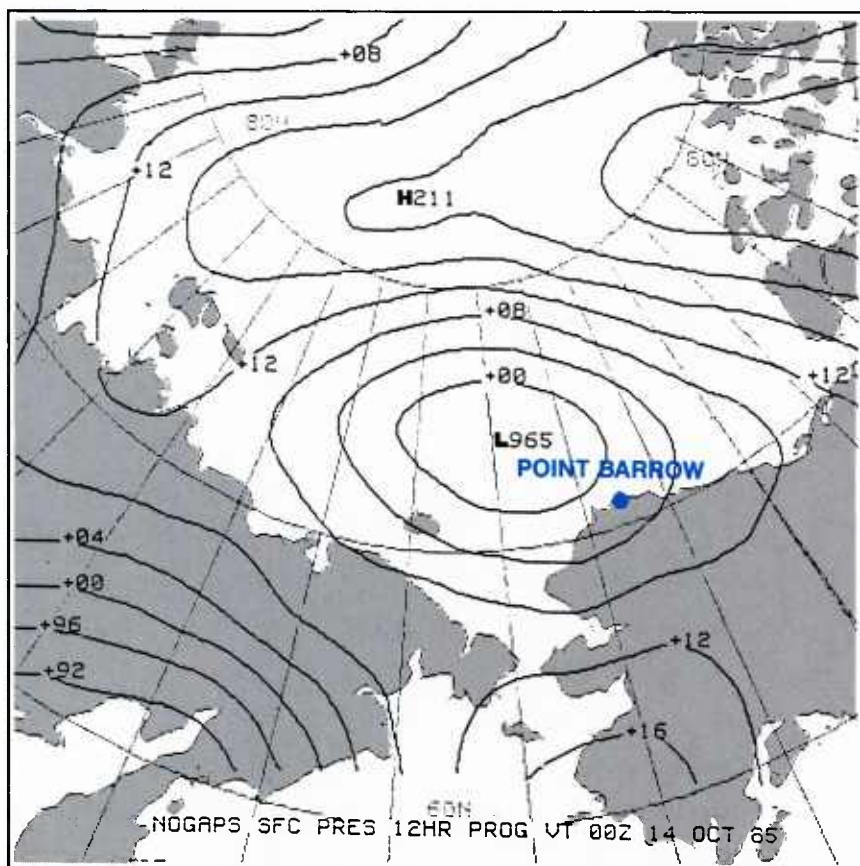
2B-2a FNOC surface analysis with low center track data, 8-14 October 1985.



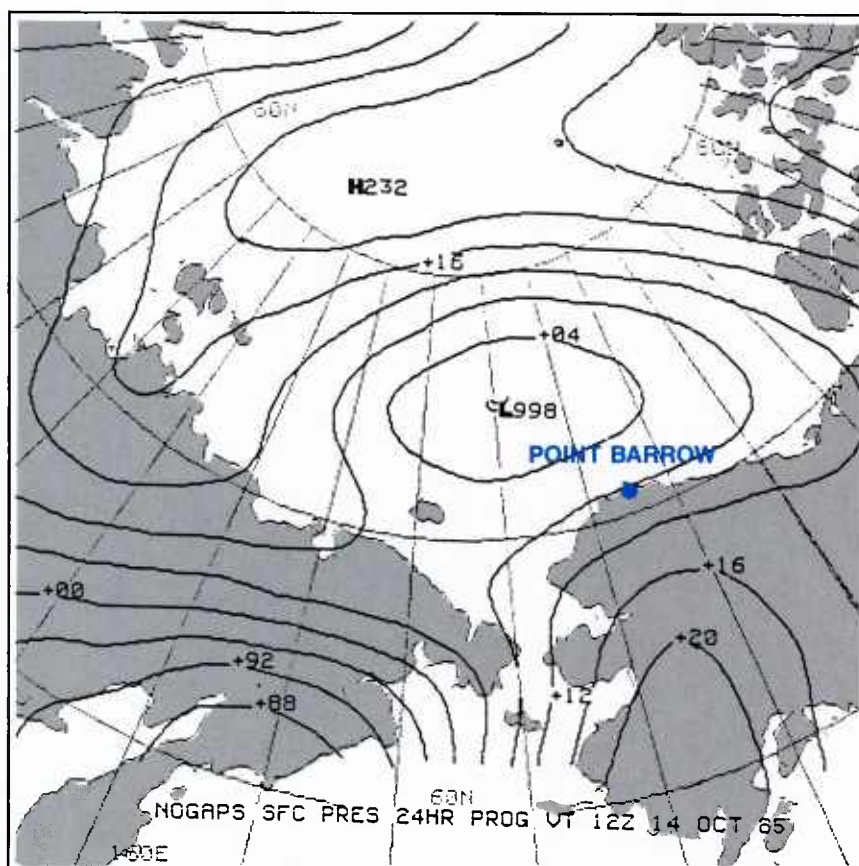
Center (FNOC) surface forecast charts valid for 0000 GMT (Figure 2B-3b) and 1200 GMT (Figure 2B-3c), respectively, on 14 October predicted a 996.5 (0000 GMT) and a 999.8 mb (1200 GMT) low to be located near 72.5N, 170W at the end of the forecast periods. Since the low was not particularly intense and, in fact, was predicted to fill slightly with time, there appeared to be no cause for concern on the part of ships or coastal installations in that region. The U.S. Coast Guard Icebreaker *Polar Sea* was operating in the vicinity of Point Barrow at the time (70.9N, 160.7W) approximately 210 nm southeast of the low's projected position. At about 0130 GMT on the 14th, the *Polar Sea* was suddenly and unexpectedly struck with winds in excess of 60 kt that shifted from southeast to southwest as the barometer bottomed out at 29.2 in. Hg (989 mb).







2B-3b FNOC 12-hour surface prognosis. Valid: 14 October 1985, 0000 GMT.



2B-3c FNOC 24-hour surface prognosis. Valid: 14 October 1985, 1200 GMT.

SUBJ: AWS-85 DAILY SITREP: 13 OCT 85

1. 140200Z OCT 85 POSIT: 70:53N 160:42W

2. WX: TEMP 26F SST: 32F

BARO: 29.24 SIG: OVC/SNOW

WINDS: 240/67KTS VIS: .3NM

SEAS: 240/7FT, CONFUSED, INCREASING

3. SUMMARY OF ACTIVITIES:

D. 131700H: WINDS SUDDENLY AND UNEXPECTEDLY INCREASED TO 60KTS AND CONTINUED TO INCREASE TO 70KTS WITH GUSTS TO 75KTS; WINDS OF THIS MAGNITUDE NOT FORECASTED OMEGA ANTENNA BLOWN DOWN. BOTH ANTENNAS HAVE BEEN RECOVERED. ADVISE BARROW RADIO VIA H.F. OF PRESENT WINDS/WX BARO. BOTTOMED OUT QUICKLY TO 29.20 AND NOW SLOWLY RISING.

4. INTENTIONS:

A. PROCEED TO KODIAK. SOA MAY HAVE TO BE REDUCED IF CONDITIONS CONTINUE TO DETERIORATE.

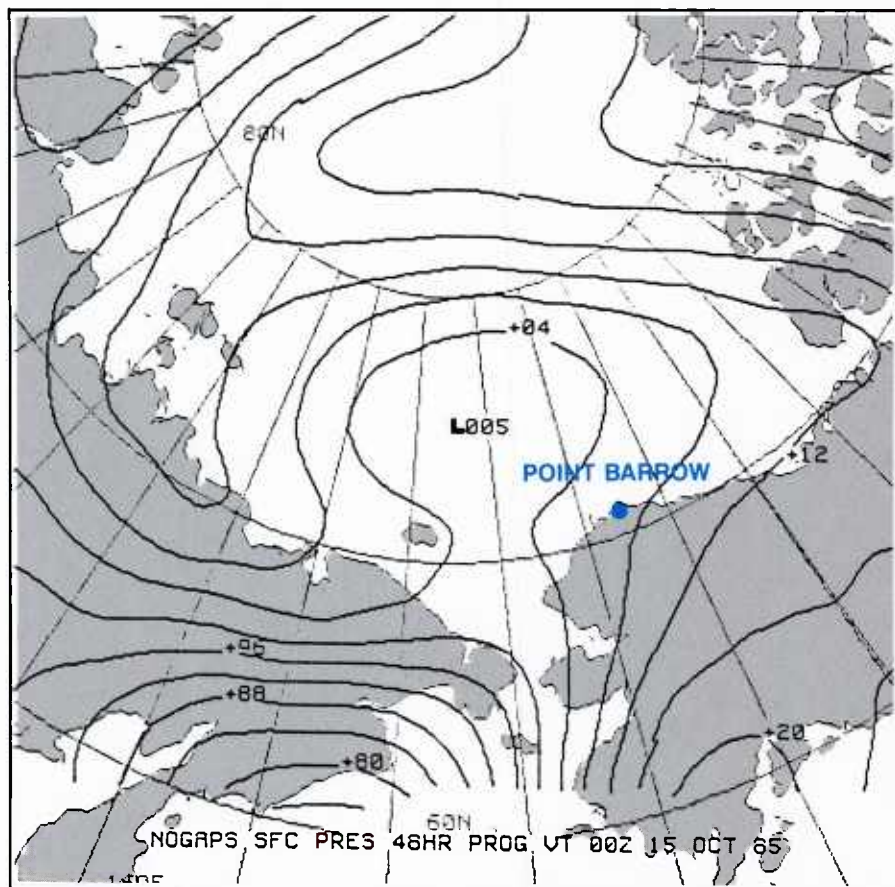
2B-4a Situation Report from *Polar Sea* to NPOC. 14 October 1985, 0200 GMT.

Figure 2B-4a is a copy of the situation report transmitted by *Polar Sea* to Navy authorities describing the occurrence. As noted in the message, winds continued to increase to 70 kt with gusts to 75 kt as equipment was blown down and overboard. At about this time (14/0600 GMT), a forecast specifically prepared for the *Polar Sea* by the Naval Polar Oceanography Center (NPOC), Suitland, Maryland, was received indicating that they could expect generally undisturbed weather with southerly winds of 15-20 kt for the next 24 hours. This forecast was consistent with the Navy Operational Global Prediction System (NOGAPS) numerical model's 48-hour forecast, valid for 15 October at 0000 GMT (Figure 2B-5a), showing further filling of the low over the Chukchi Sea and a weak pressure gradient that would produce southerly flow over the north coastal region of Alaska. The NPOC forecast was also made without benefit of the *Polar Sea*'s 14/0000 GMT observation.

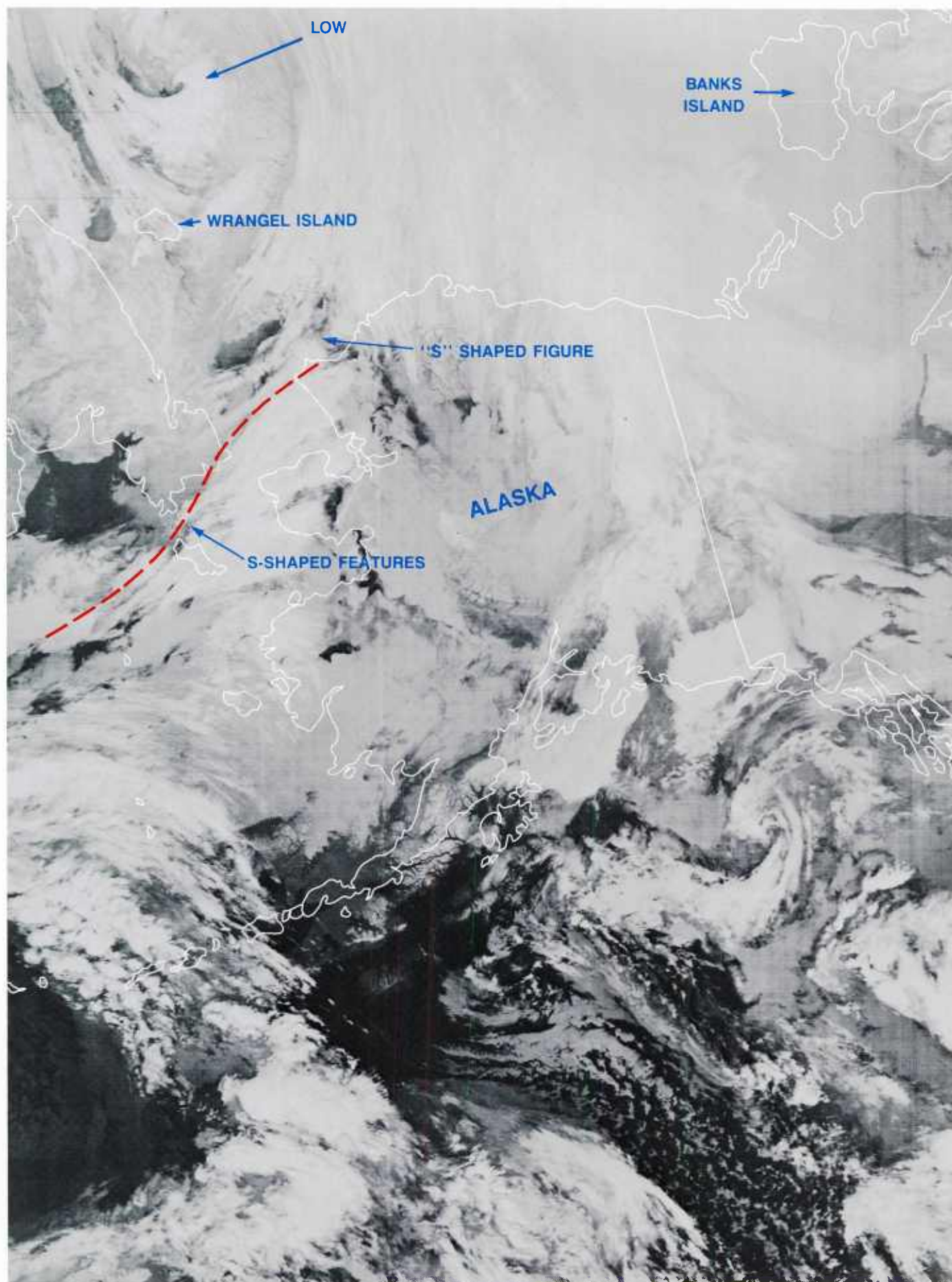


Obviously, this is an excellent example of faulty analysis and forecast guidance; however, the forecast was not illogical based on the long history of the storm as it traveled over the Arctic Ocean for about a week and failed to demonstrate the explosive cyclogenesis which occurred late on 13 October.

What were the special features that favored intense polar low development at that specific time? To attempt to find an answer to this question, the full set of DMSP data, available NOAA data, surface and upper-air charts, and RAOB data were assembled.

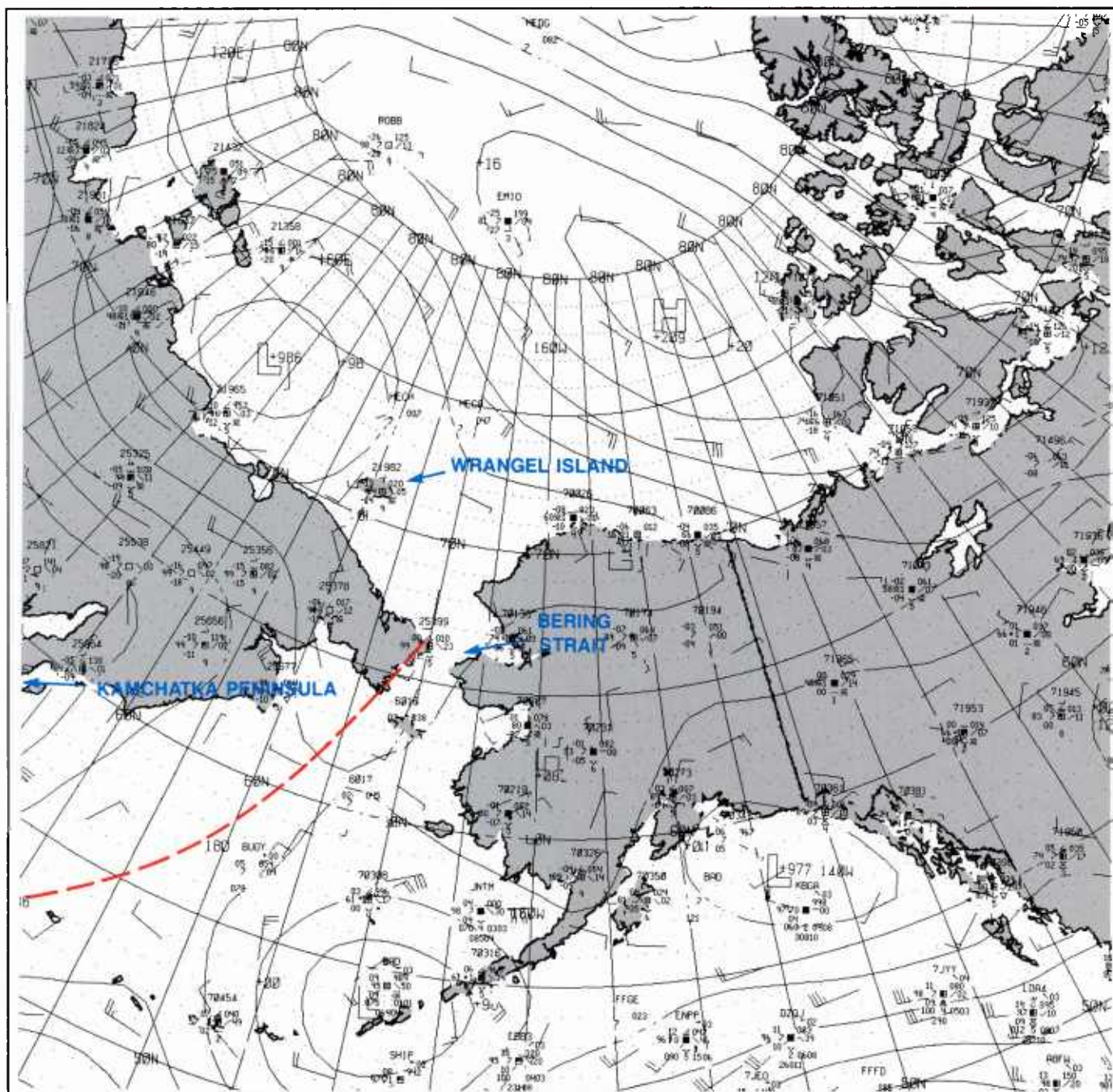


2B-5a FNOC 48-hour NOGAPS prognosis. Valid: 15 October 1985, 0000 GMT.



2B-6a DMSP infrared (TS) data. 11 October 1985, 1901 GMT.



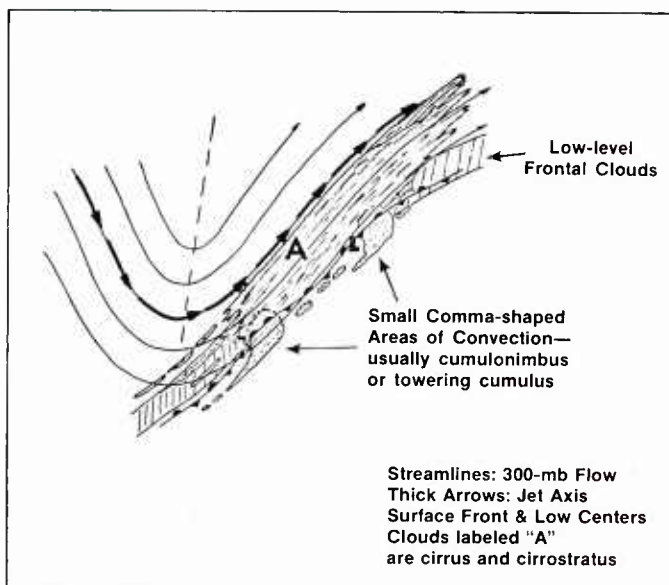


2B-7a FNOC surface analysis, 11 October 1985, 1800 GMT.

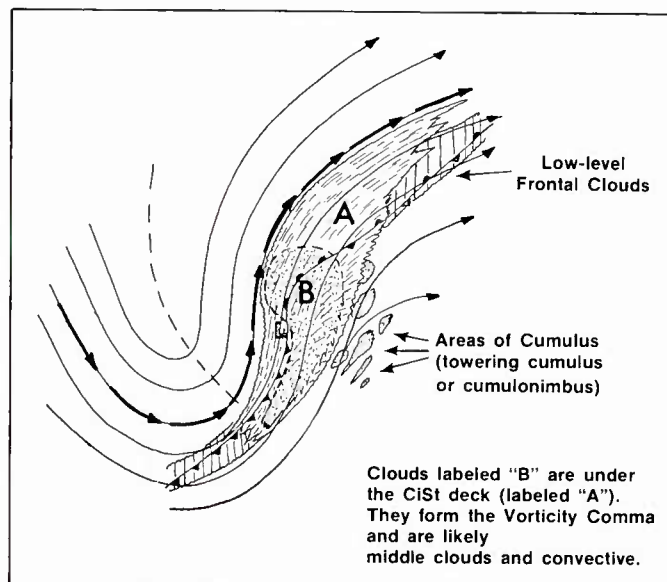
### 11 October 1985

The study begins on 11 October, about 3½ days prior to the polar low event. At 1901 GMT on this date, DMSP IR data (Figure 2B-6a) revealed an intense-appearing comma-shaped low about 670 km east of Wrangel Island. The surface analysis for 1800 GMT (Figure 2B-7a) clearly documented the existence of low pressure in that region. Wind observations, however, are inadequate to determine maximum intensity of the system, which surely exceeded the 20 kt indication of the nearest reporting station well to the south of the center (70.5N, 160.5E).

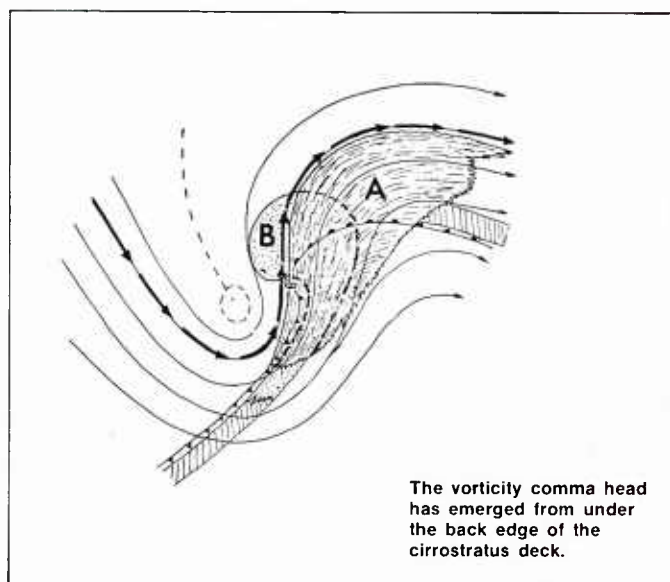
The DMSP data (Figure 2B-6a) revealed another significant feature extending over the Bering Strait. This feature was a lazy S-shaped convective cloud band with the western edge convex to the north and concave to the south. The position of the cloud band coincides with a trough, shown in the surface analysis as extending from the Bering Strait well to the south past the Kamchatka Peninsula.



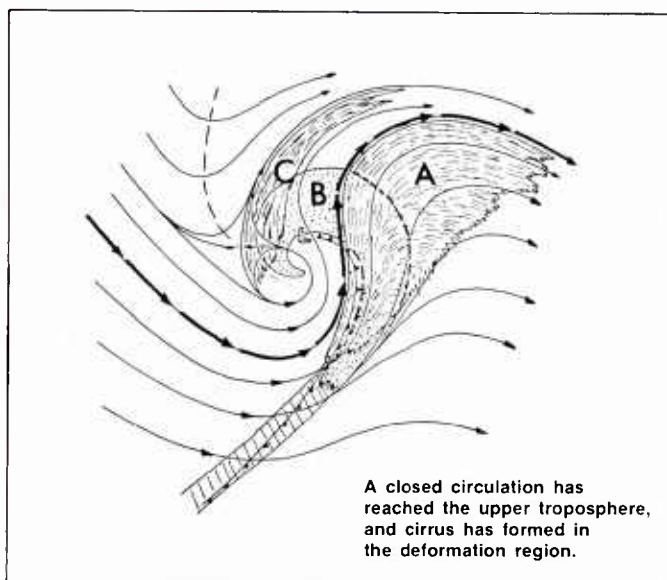
Meridional Trough Cyclogenesis, Phase 1.



Meridional Trough Cyclogenesis, Phase 2.



Meridional Trough Cyclogenesis, Phase 3.

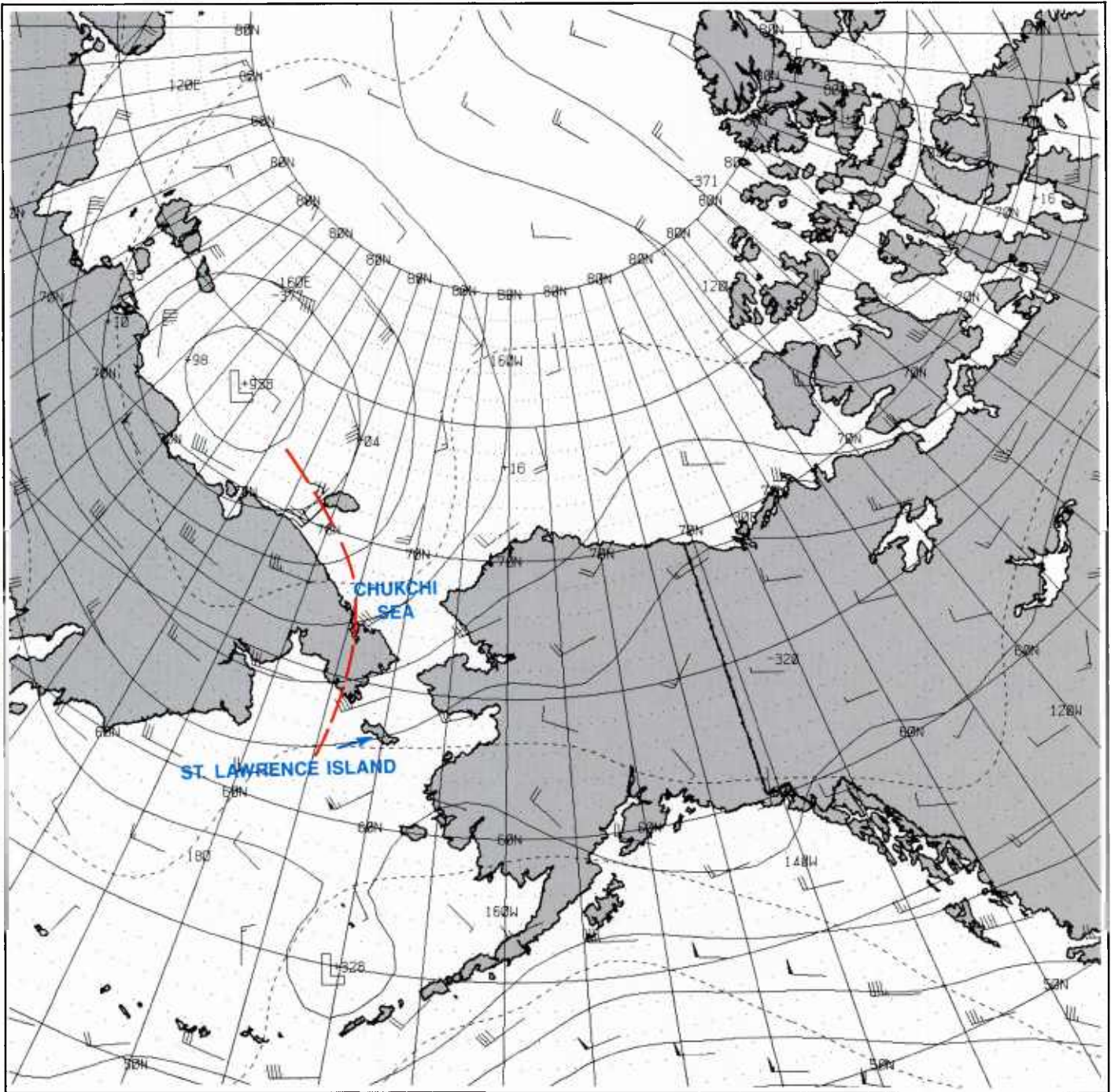


Meridional Trough Cyclogenesis, Phase 4.

2B-8a Meridional Trough (Type 1) Cyclogenesis (From NTAG Vol. 4, Section 2A, pp. 2A-6 and 2A-7).

This type of cloud feature in such a trough position has been identified by Weldon (Figure 2B-8a) as a pattern appearing in "Meridional Trough (Type 1) Cyclogenesis" (see NTAG Vol. 4, Sec. 2A, pp. 2A-6 and 2A-7). At this stage of development, Weldon's model indicates that a jet axis parallels the western edge of the cloud band. In addition, a short wave trough extends from the northwest into the concave section. A short wave ridge is predicted to be located downstream from the trough over the convex section. Rapid development often occurs following this condition at the same time as a comma-shaped cloud vortex emerges from under the convex region.



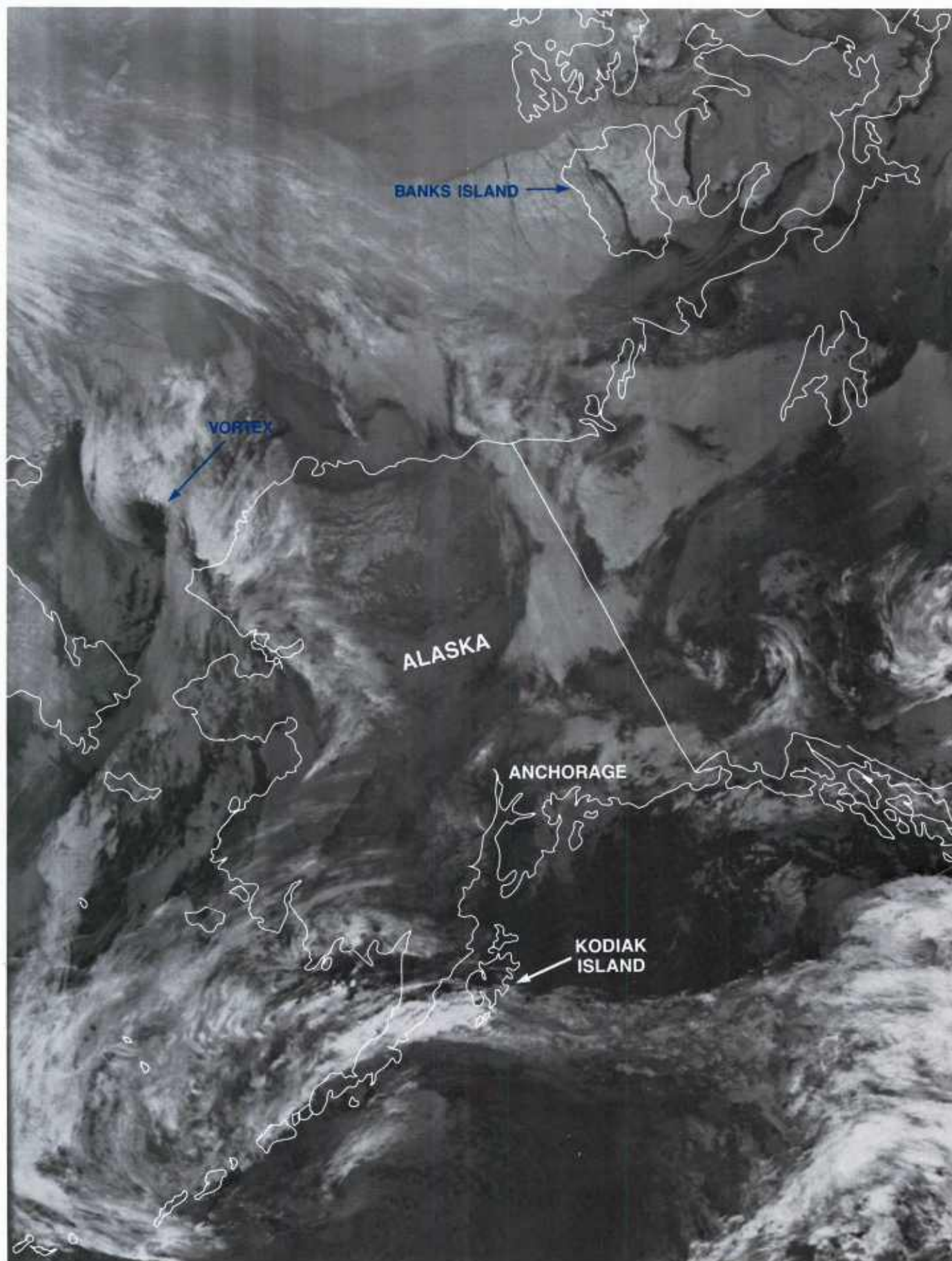


2B-9a FNOC 500 mb analysis. 12 October 1985, 0000 GMT.

### 12 October 1985

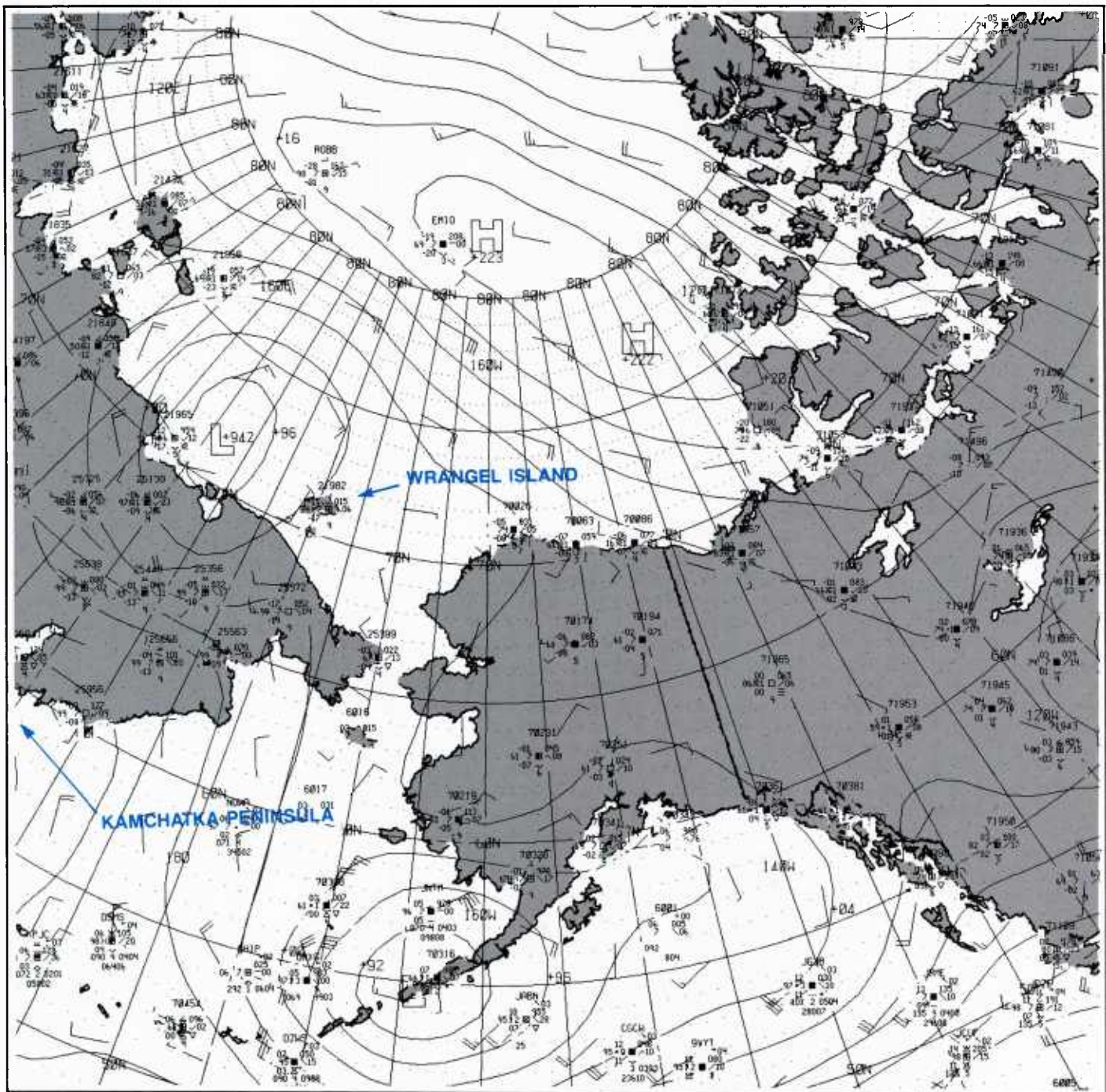
The 500 mb analysis for 0000 GMT (Figure 2B-9a) shows an upper cold low very near the position of the surface low shown in Figure 2B-7a. A short wave trough is suggested, as implied by the satellite data, over the Chukchi Peninsula. Upper air wind vectors are not adequate to verify the jet presumed to be paralleling the western edge of the cloud in Figure 2B-6a, although a 65 kt wind is indicated very near that area just south of St. Lawrence Island.





2B-10a DMSP infrared (TS) data. 12 October 1985, 0504 GMT.





2B-11a FNOc surface analysis. 12 October 1985, 0000 GMT.

### 12 October 1985 (cont)

Early on this date (0504 GMT), DMSP data (Figure 2B-10a) reveal that a cloud vortex has formed in the Bering Strait as implied by the previously described data (Figure 2B-6a). The cloud-free center creates an eye-like appearance, apparently induced by strong subsiding motion into this region, which normally occurs during the intensification process.

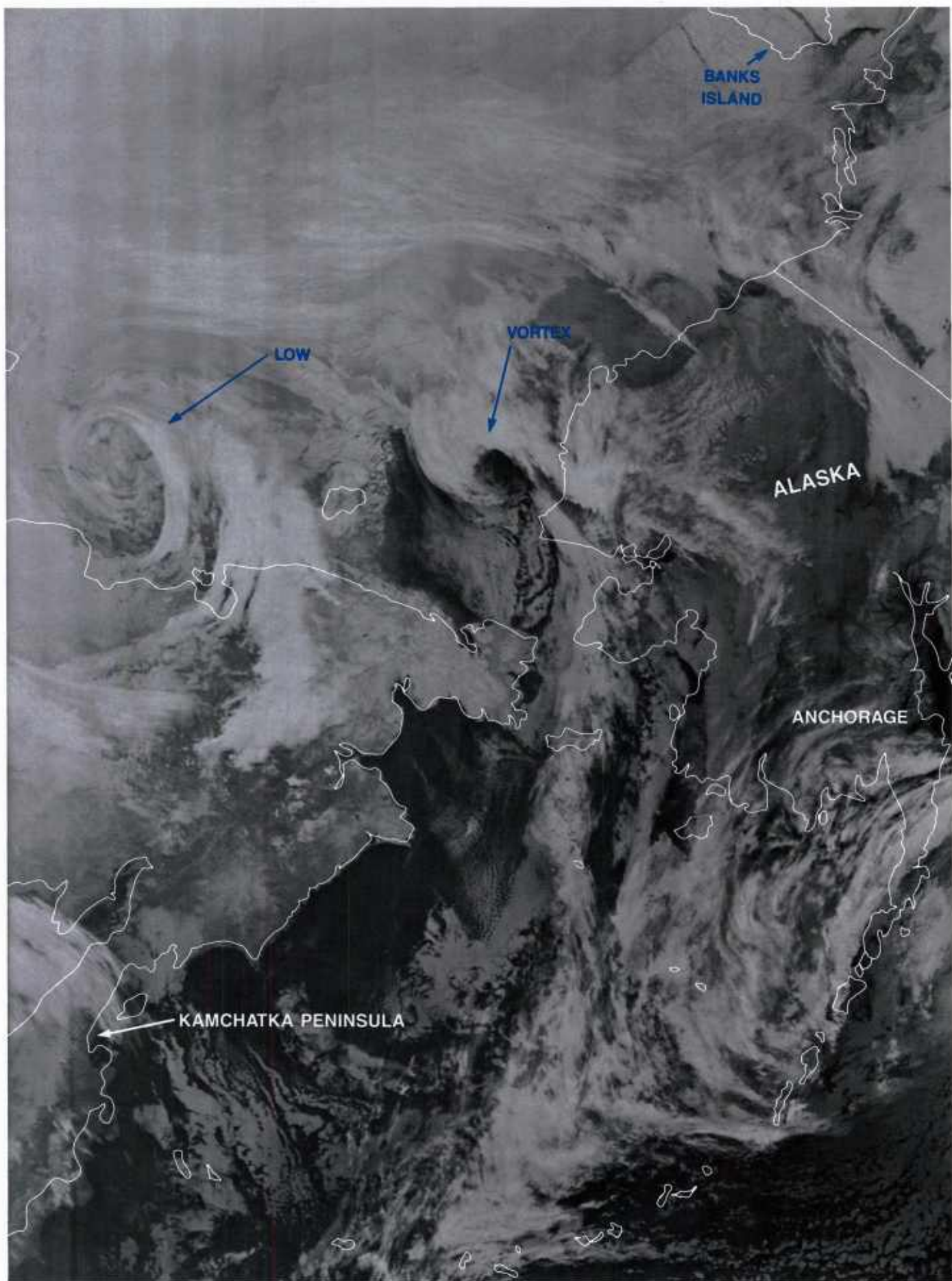
The FNOc surface analysis (Figure 2B-11a) shows cyclonic-turning winds in that region, but no low center or strong winds are indicated. This analysis also shows the further movement of the low in the East Siberian Sea toward Wrangel Island.

Another DMSP view of both systems was obtained 1½ hours later at 0634 GMT (Figure 2B-12a). The meridional nature of the trough extending south from the vortex is well revealed by a generally north/south oriented cloud band leading up to the vortex north of the Bering Strait. Cloud lines all down the coastline of Asia toward the northern Kamchatka Peninsula indicate offshore northwesterly flow out to the convergent band close to the trough-line. This is also verified in the surface analysis (Figure 2B-11a).

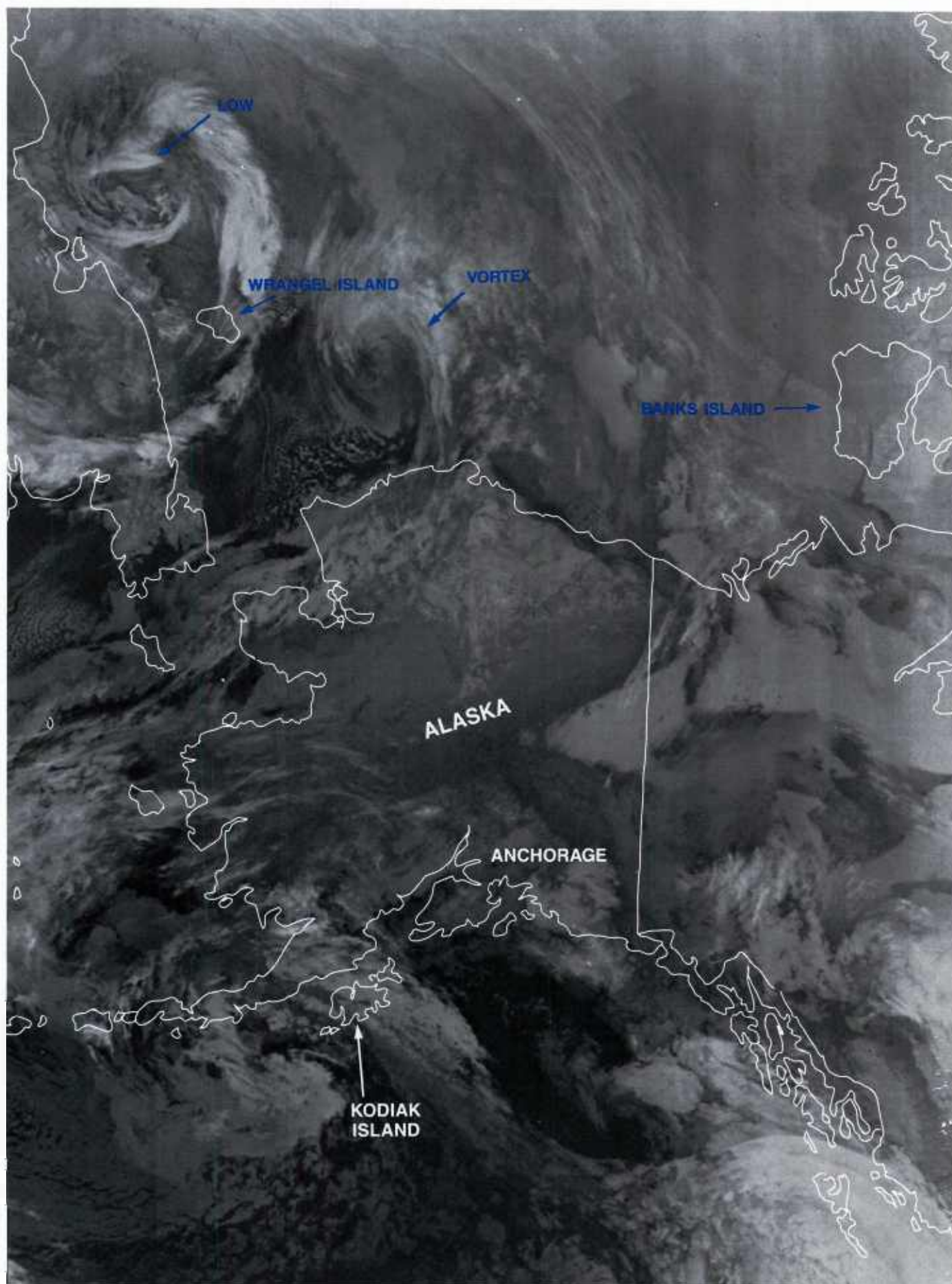
The low in the East Siberian Sea appears to have weakened near its center portion, but a squall line has formed in its eastern quadrants; surface pressures are falling rapidly in that region (Figure 2B-11a).

The next good view of the storm systems was obtained at 1437 GMT (Figure 2B-13a). This view shows that the vortex north of the Bering Strait has moved northward, approaching the ice edge east of Wrangel Island. The East Siberian Low has moved southeastward. The lows appear to be under the influence of the Fujiwhara effect, showing a tendency to rotate cyclonically about one another.



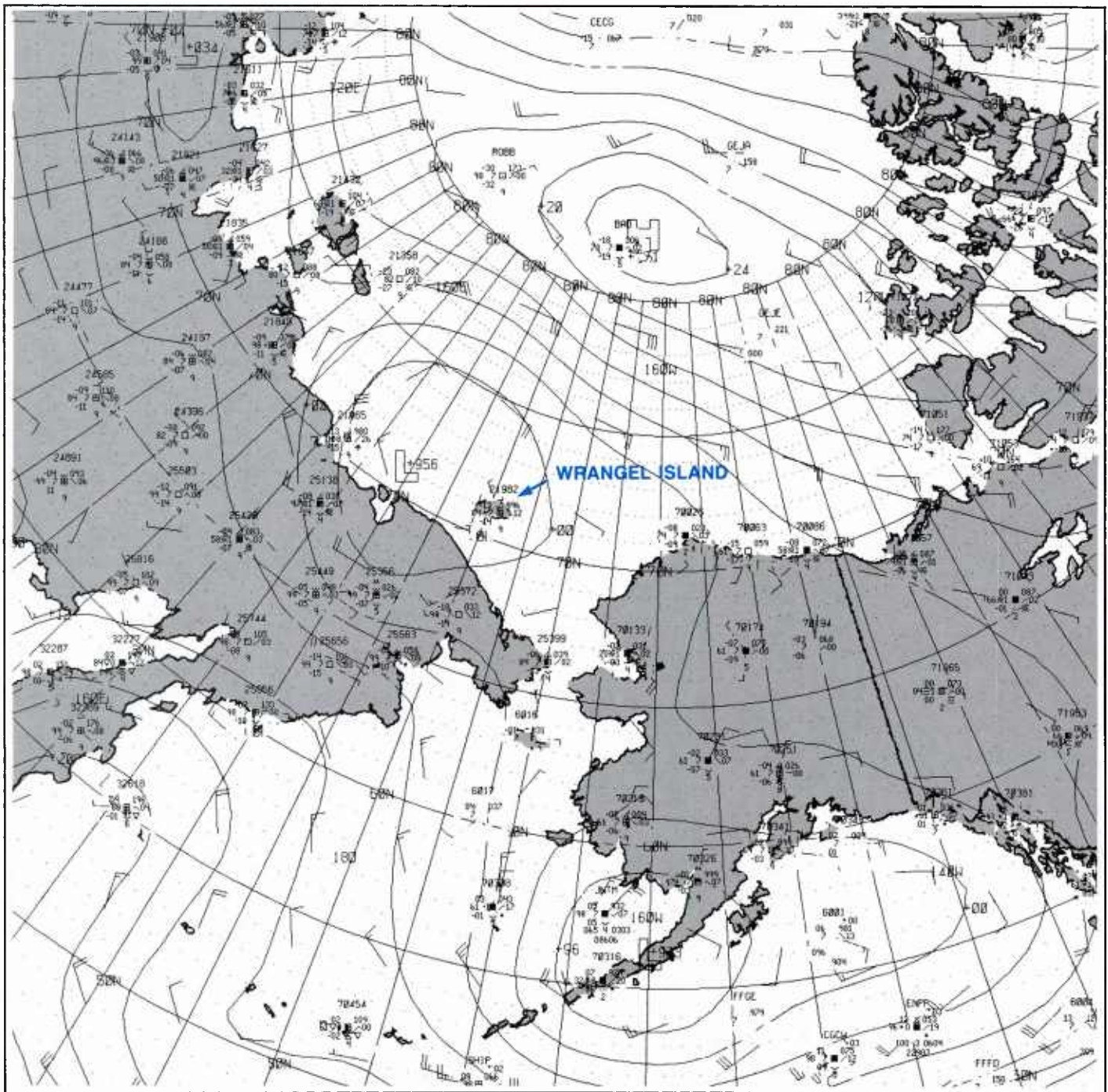


2B-12a DMSP infrared (TS) data. 12 October 1985, 0634 GMT.



2B-13a DMSP infrared (TS) data. 12 October 1985, 1437 GMT.

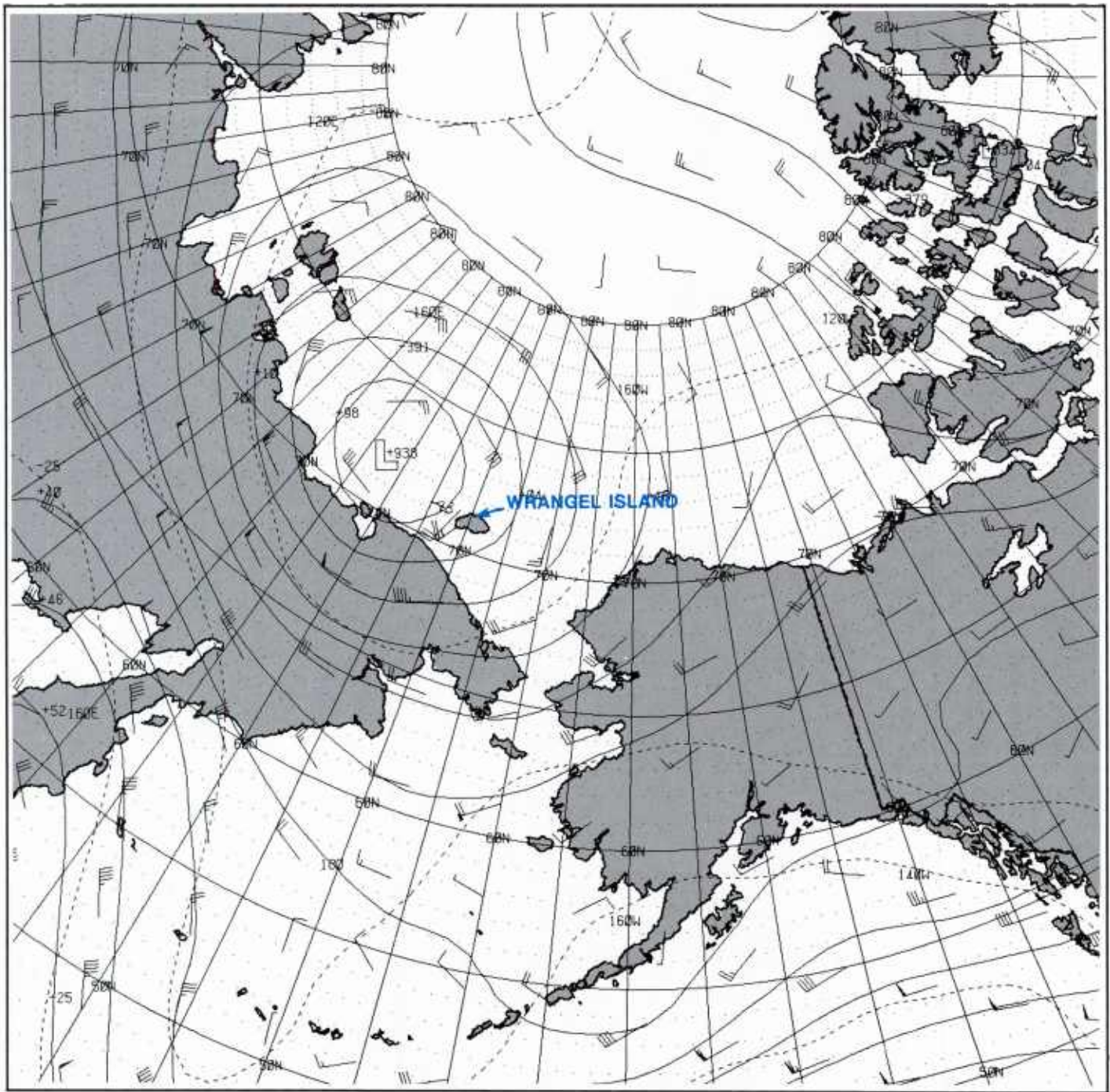




2B-14a FNOC surface analysis. 12 October 1985, 1200 GMT.

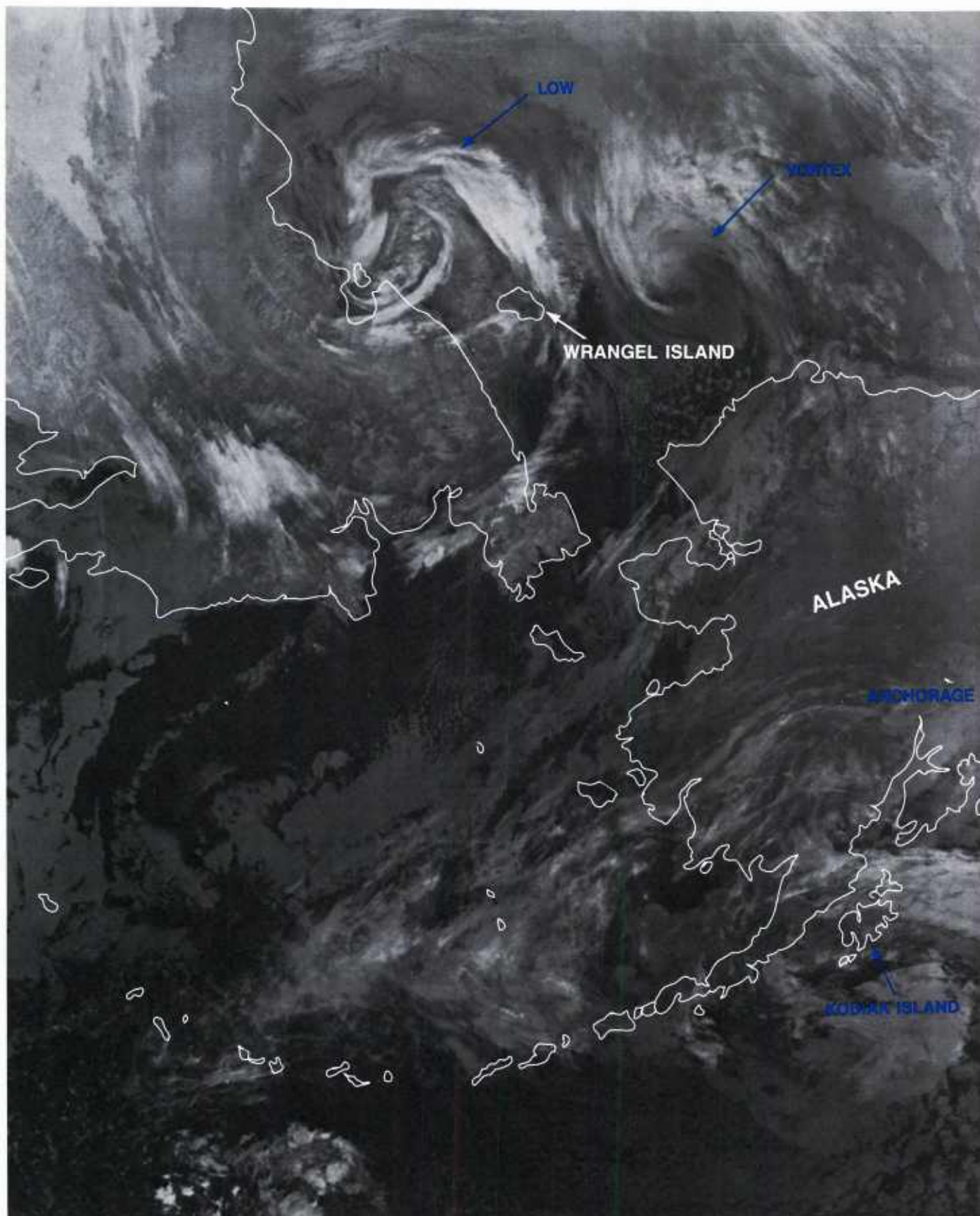
The surface analysis for 1200 GMT (Figure 2A-14a) still does not explicitly show the easternmost low, i.e., the vortex, but does show pressures falling rapidly from Wrangel Island southward. The 500 mb analysis for the same time (Figure 2A-15a) shows further movement of the upper cold low toward Wrangel Island. Cold temperatures of less than  $-35^{\circ}\text{C}$  are being advected to a position over the open water north of the Bering Strait.





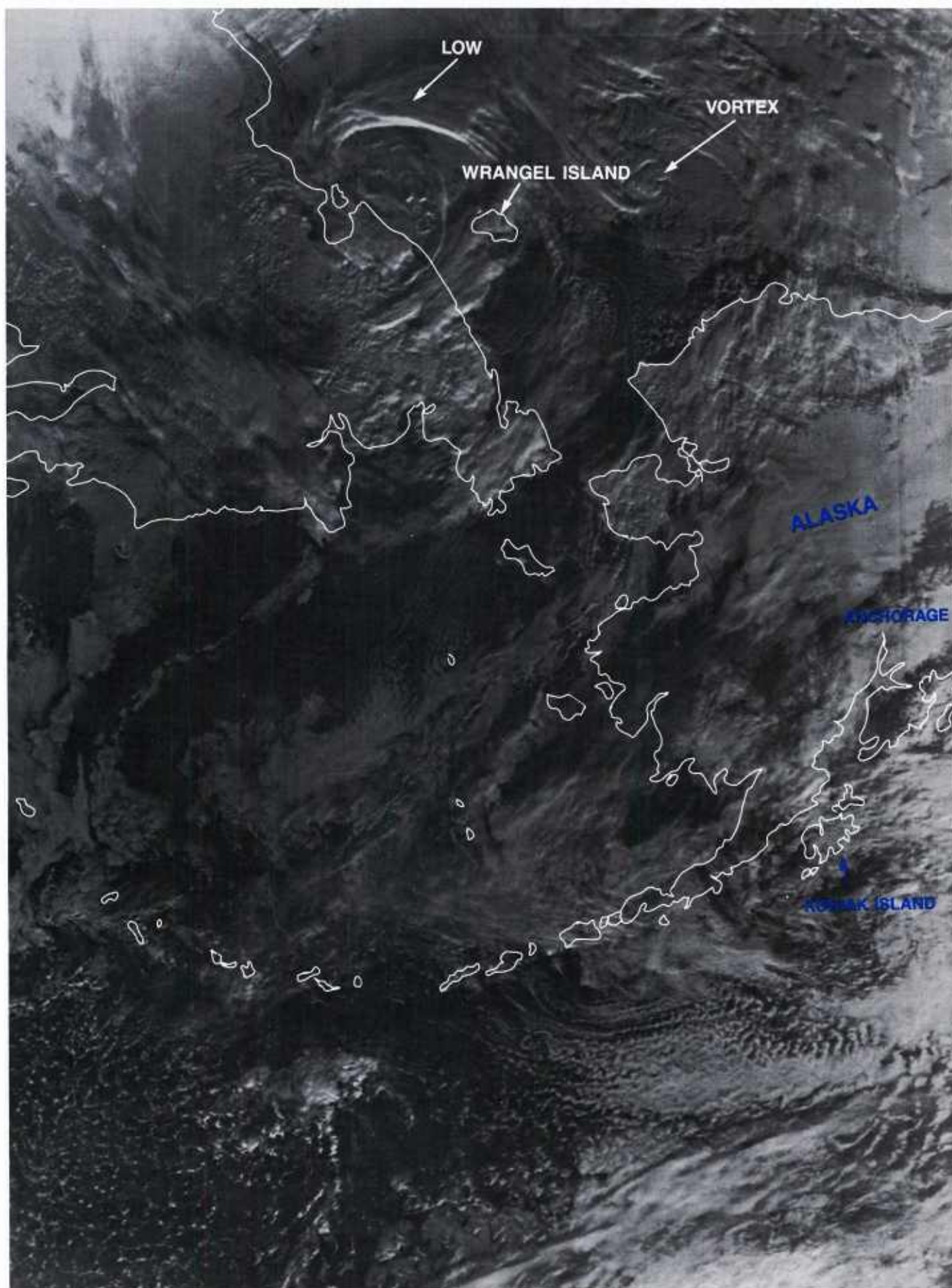
2B-15a FNOC 500 mb analysis. 12 October 1985, 1200 GMT.





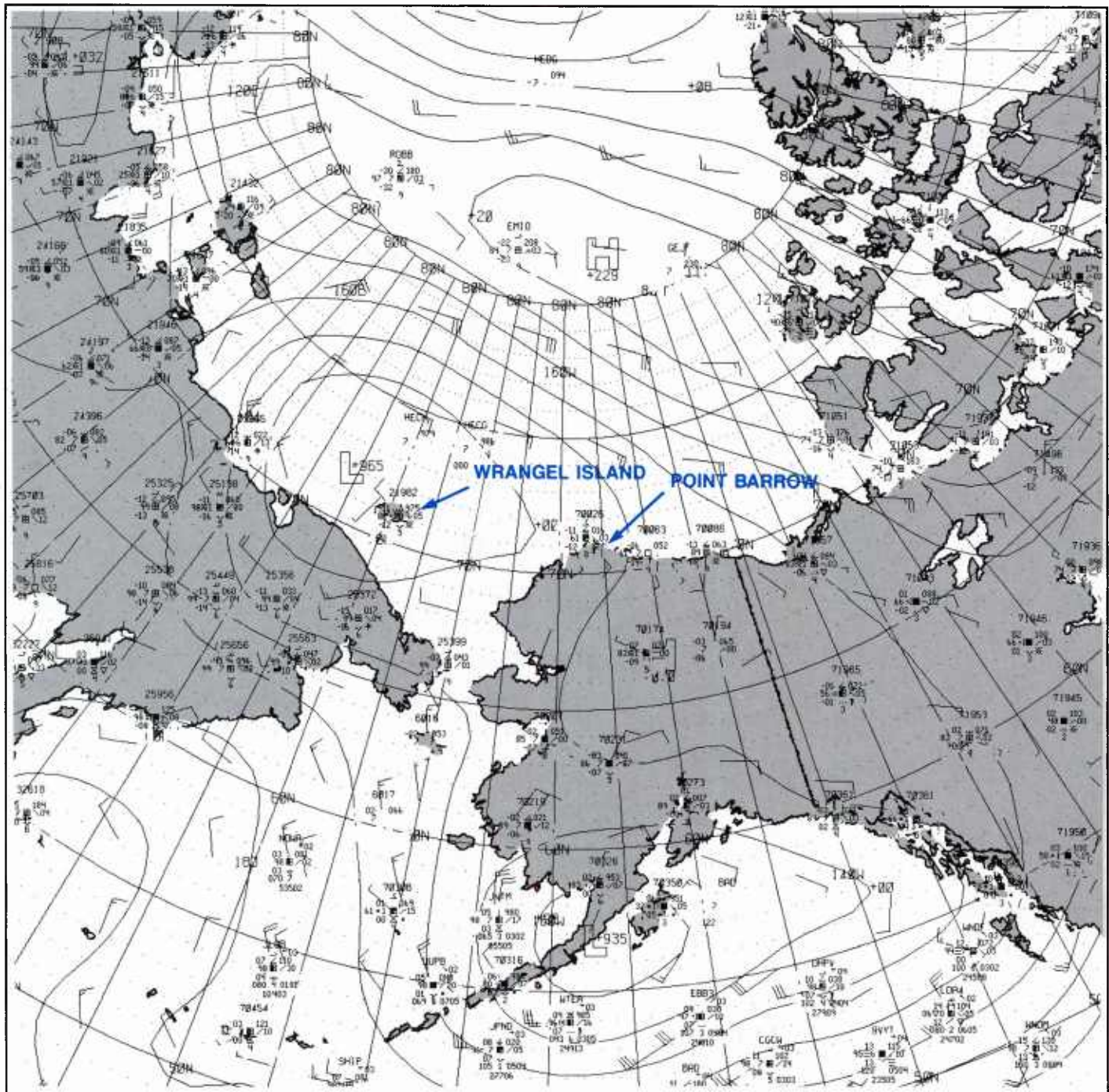
2B-16a DMSP infrared (TS) data. 12 October 1985, 1635 GMT.

Additional DMSP views of the two storms on 12 October were obtained at 1635 GMT (Figure 2B-16a) and at 2022 GMT (Figure 2B-17a). These views substantiate a continued Fujiwhara effect as the easternmost storm is advected northward over the ice pack and the other storm approaches Wrangel Island.



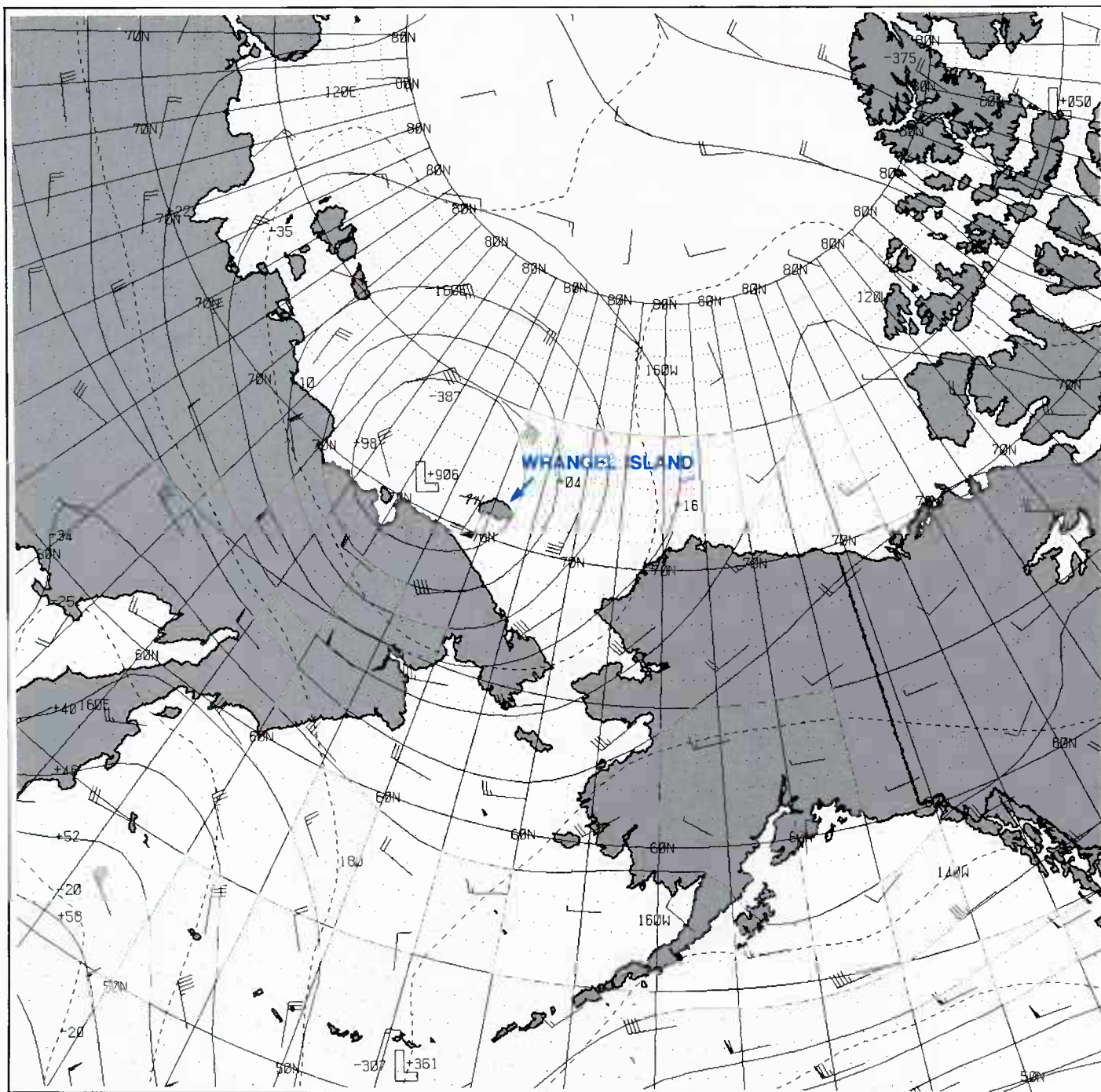
2B-17a DMSP infrared (TS) data. 12 October 1985, 2022 GMT.





2B-18a FNOC surface analysis. 12 October 1985, 1800 GMT.

The 1800 GMT FNOC surface analysis is shown in Figure 2A-18a. The analysis still does not incorporate the low center associated with the easternmost storm. However, Wrangel Island's northwest wind and Pt. Barrow's southeast wind at 15 kt, together with the other computer-produced indications, clearly suggest a closed circulation center somewhere east of Wrangel Island.



2B-19a FNOC 500 mb analysis. 13 October 1985, 0000 GMT.

### 13 October 1985

The FNOC 500 mb analysis for 0000 GMT (Figure 2B-19a) shows continued movement of the synoptic-scale upper cold low toward Wrangel Island. Temperature aloft over Wrangel Island, at the 500 mb level, dropped from  $-30^{\circ}\text{C}$  as the cold low approached, on 10 October at 0000 GMT, to  $-44^{\circ}\text{C}$  on 13 October at 0000 GMT.



A DMSP view of the storm area at 0609 GMT on 13 October is shown in Figure 2B-20a. This view is about 10 hours after that of Figure 2B-17a. The East Siberian low is still very apparent with center of circulation near Wrangel Island. The easternmost low, i.e., the vortex, that had been moving north of the Bering Strait, however, is ill-defined and apparently dissipating over the ice cap well to the north.

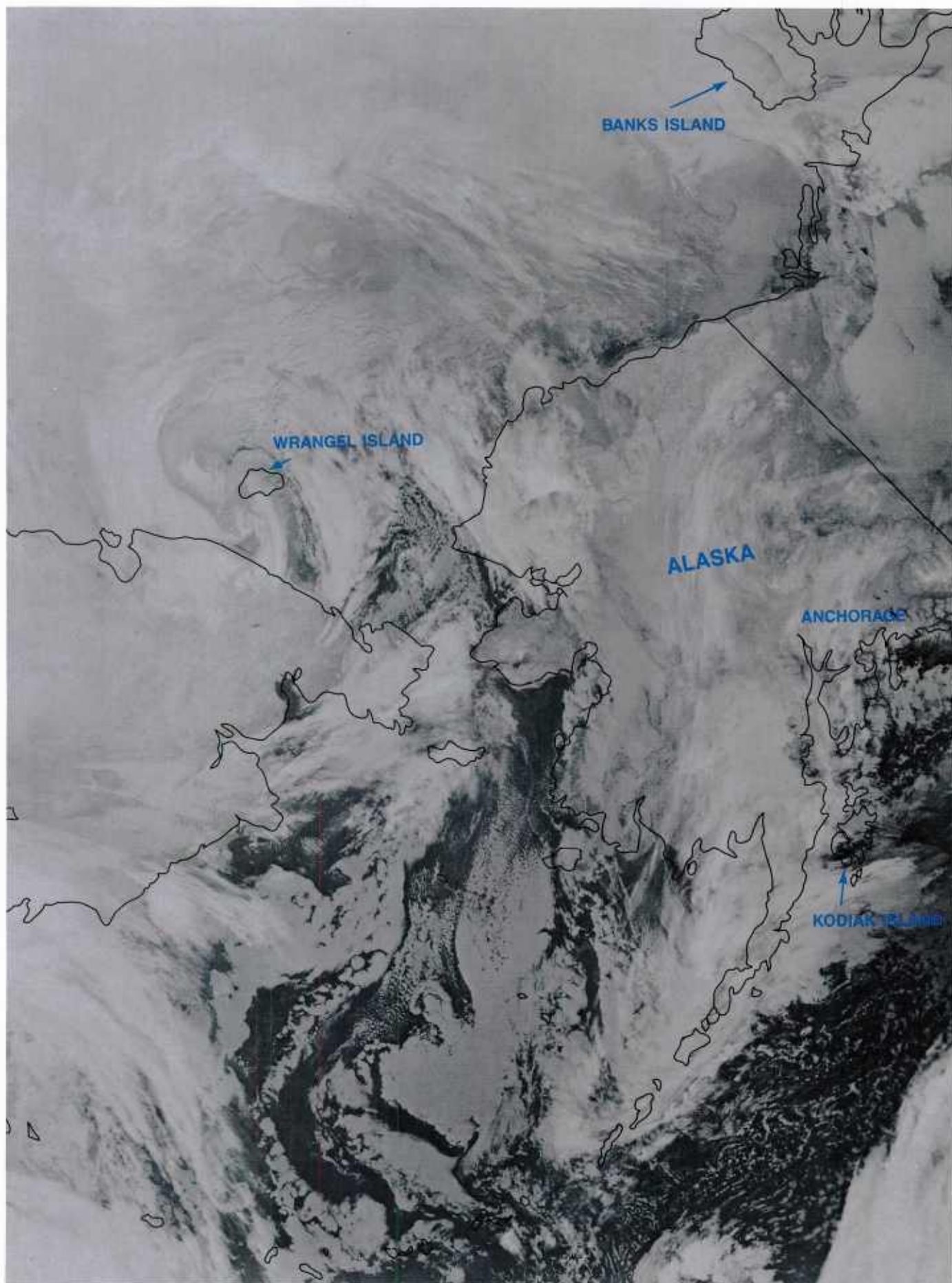
DMSP data for 1436 GMT (Figure 2B-21a) reveal that an intense squall line has developed, associated with the circulation of the low near Wrangel Island. The squall line is seen as a convective band of clouds sweeping northward from the Bering Sea, over the Seward Peninsula, and into the Chukchi Sea, where a series of cumulonimbus clusters seems to form a hook- or comma-shaped cloud configuration. Cloud lines in the Bering Strait indicate westerly flow in that region, while a vortex cloud center is apparent just south of Wrangel Island.

The center position of the low indicated in the DMSP data (which is south of Wrangel Island) disagrees with low center placement on the FNOC surface analysis for 1200 GMT (Figure 2B-22a). It is possible that the analysis, for the first time, is indicating the position of the dissipating low, i.e., the vortex, that had moved northward over the ice pack, while it is failing to resolve satellite evidence of the low passing south of Wrangel Island.

Additional DMSP views of the low near Wrangel Island at 1617 GMT (Figure 2B-23a), at 1821 GMT (Figure 2B-24a, infrared, and Figure 2B-25a, visible), and at 2002 GMT (Figure 2B-27a) show the vortex moving off the ice and over the open water of the Chukchi Sea. The visible view (Figure 2B-25a) is especially interesting in that the edge of the pack ice is fairly clearly delineated, stretching from the north slope of Alaska, passing just north of Point Barrow, and westward to a position just east of Wrangel Island.

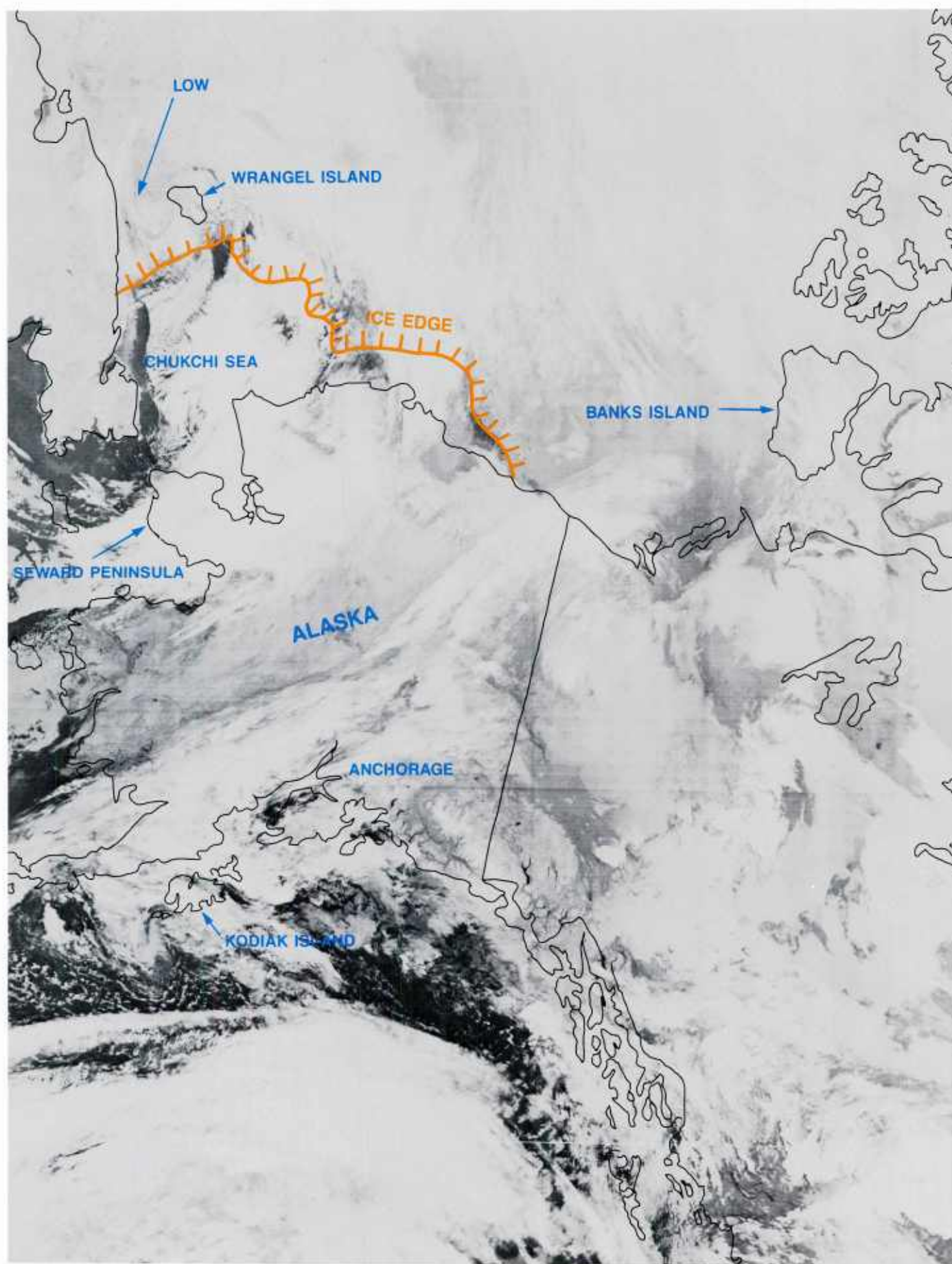
The vortex does not appear very intense in these views. It is the hook-shape of the squall line with a possible low center forming just north of the Seward Peninsula that attracts attention. The potential for the small vortex moving off the ice toward the apex of the hook-shaped convective cloud band and inducing rapid cyclogenesis is significant (see the discussion of Weldon's (Figure 2B-26a), "Cold Air Vortex Cyclogenesis" in NTAG Vol. 4, Part 1, Sec. 2A, p. 2A-10). Another aspect of this particular cloud system configuration, however, also seems significant. The enhanced convection over the open water north of the Bering Strait is indicative of unstable conditions due to a cold pool of air aloft (associated with a cold low). That this condition exists is shown by the FNOC 500 mb analysis for 1200 GMT (Figure 2B-28a).

The outline of the cloud configuration at 1436 GMT (Figure 2B-21a) has been superimposed on this analysis. It can be seen that temperatures lower than  $-35^{\circ}\text{C}$  extend over the open water in the Chukchi Sea. The hook-shaped convective cloud band also lies to the east of a short wave trough in a region of positive vorticity advection. The appearance of convective open-celled regions of cumulonimbus over open water south of a convective cloud band has been noted in other regions just prior to polar low development. Compare, for example, Figure 2B-24a with a DMSP view over the Iceland region on 13 February 1984 (Figure 2B-29a). Both are examples of precursor cloud configuration prior to polar low evolution. The distinctive pattern of open-celled cumulonimbus south (or in this example—west) of a major convergent band of intensified convection is easy to assess. A cloud vortex or vorticity maximum within the field of enhanced open-celled convection is apparent in both examples.

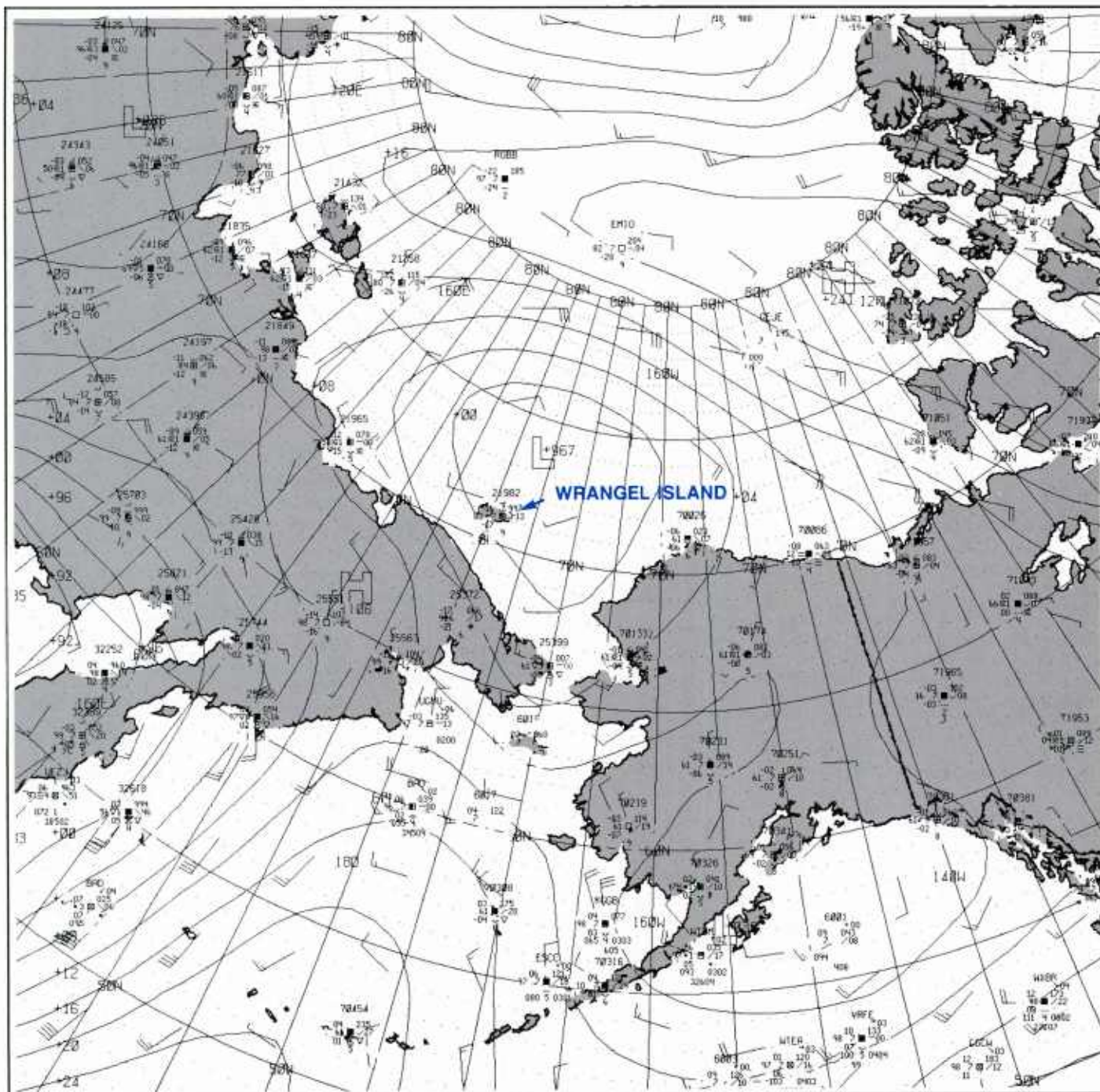


2B-20a DMSP infrared (TS) data. 13 October 1985, 0609 GMT.



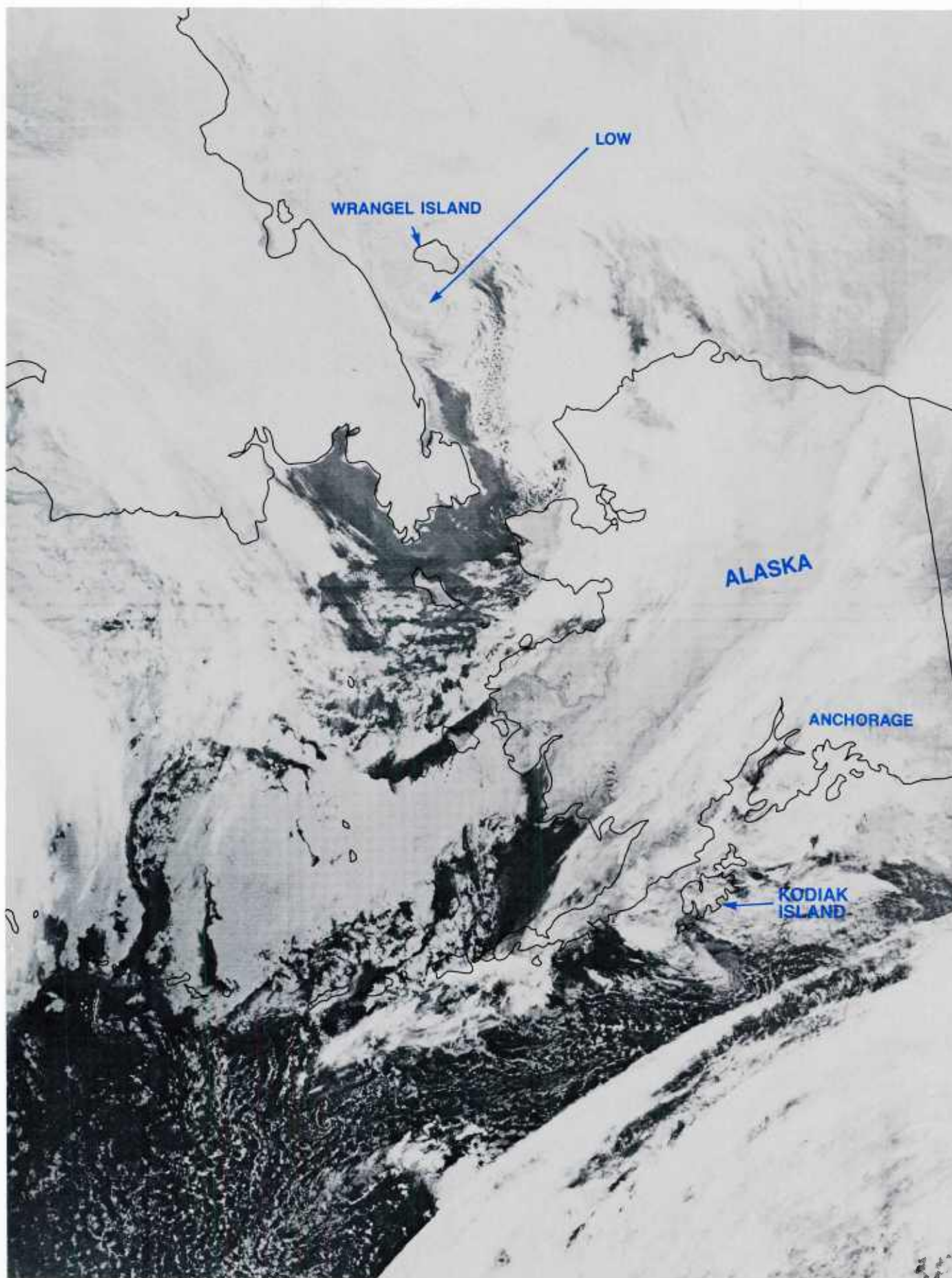


2B-21a DMSP infrared (TS) data. 13 October 1985, 1436 GMT.

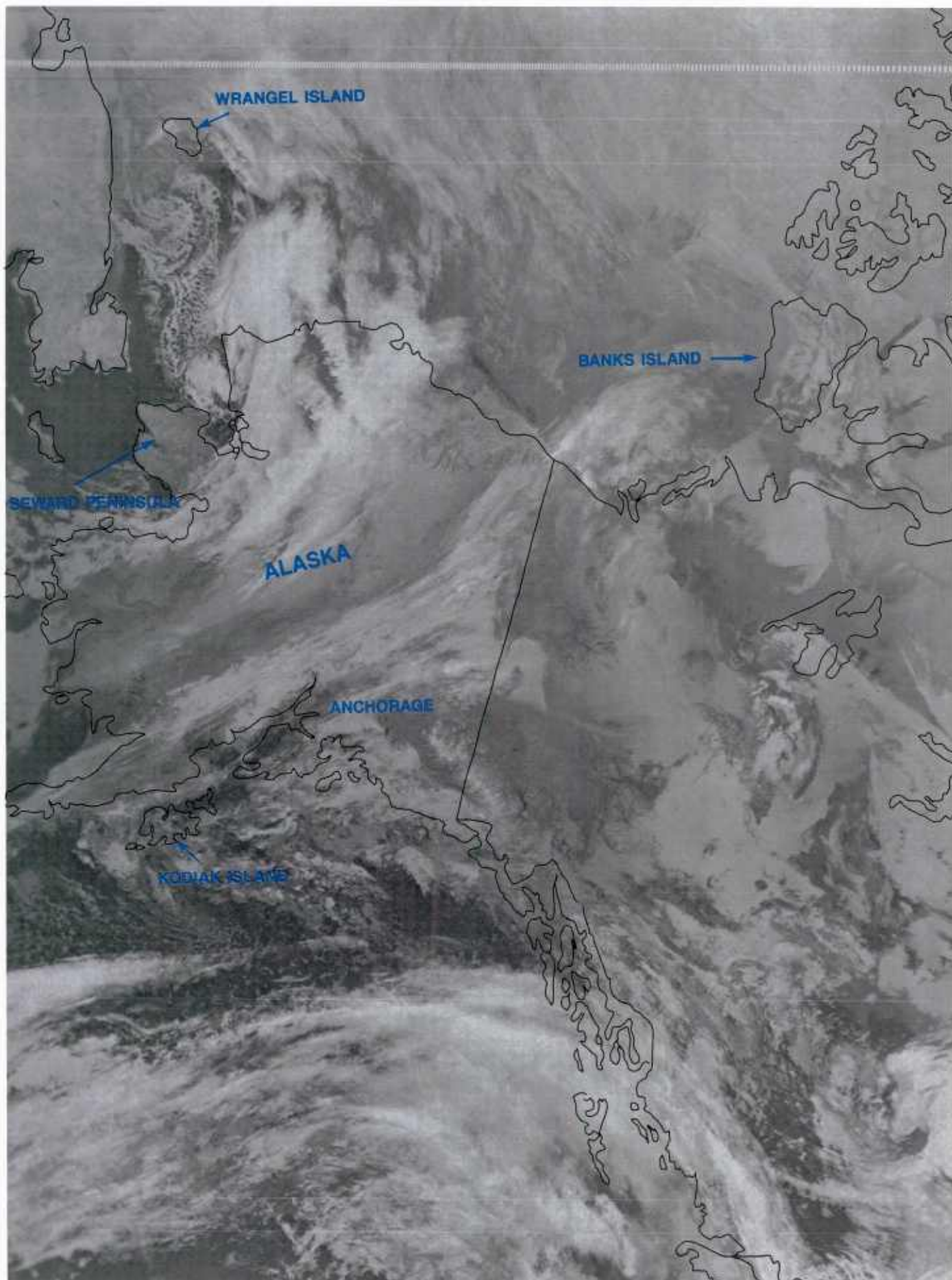


2B-22a FNOG Surface analysis. 13 October 1985, 1200 GMT.



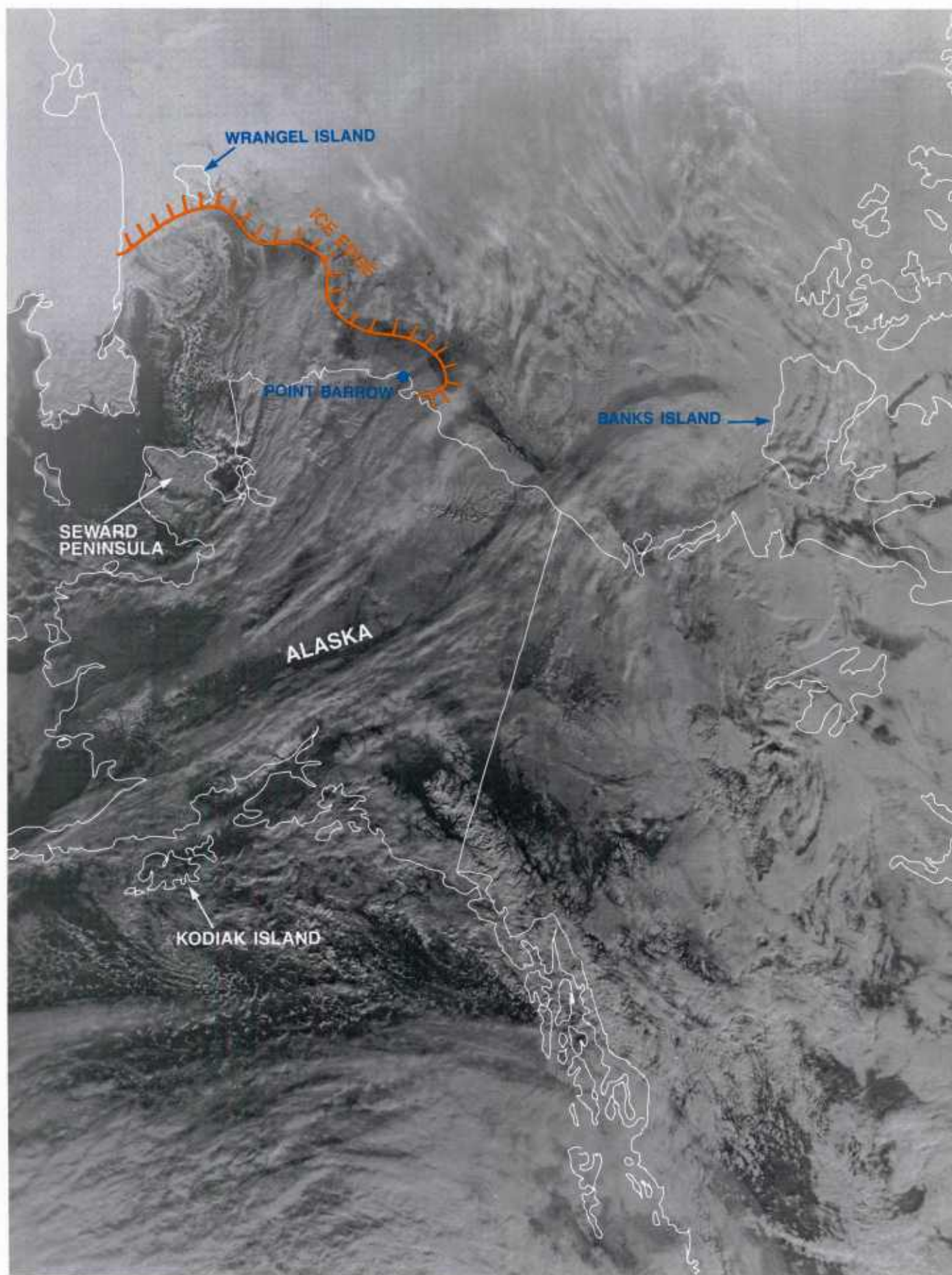


2B-23a DMSP infrared (TS) data. 13 October 1985, 1617 GMT.

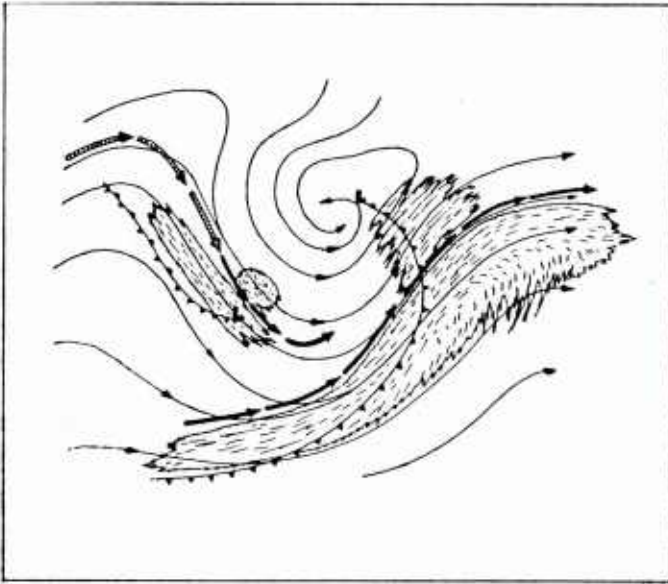


2B-24a DMSP infrared (TS) data. 13 October 1985, 1821 GMT.

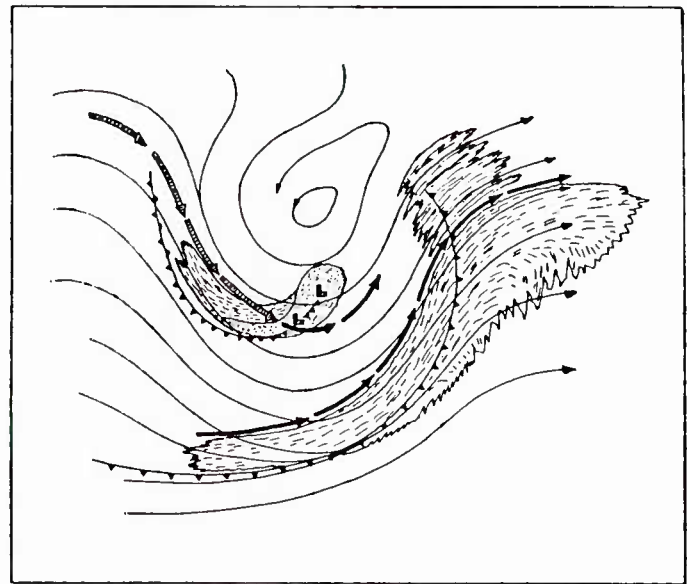




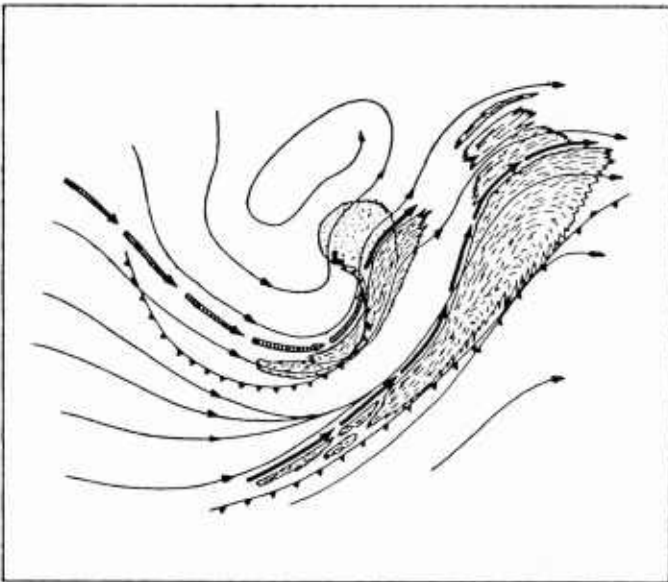
2B-25a DMSP visible (LF) data. 13 October 1985, 1821 GMT.



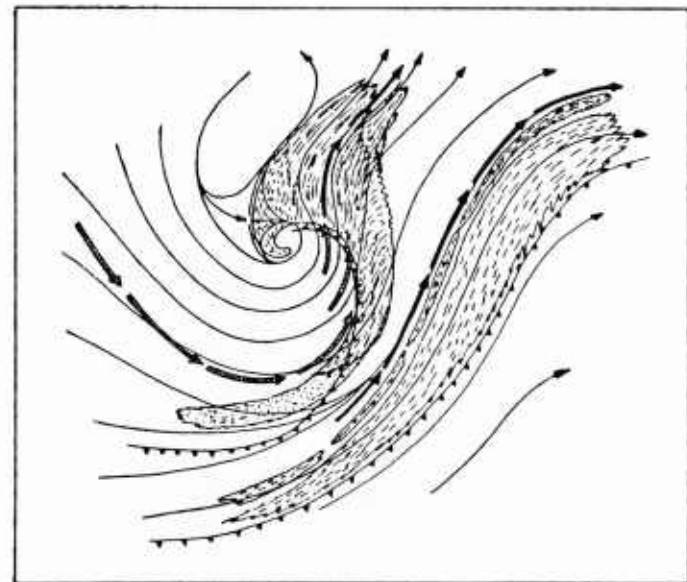
Cold Air Vortex Cyclogenesis, Phase 1.



Cold Air Vortex Cyclogenesis, Phase 2.



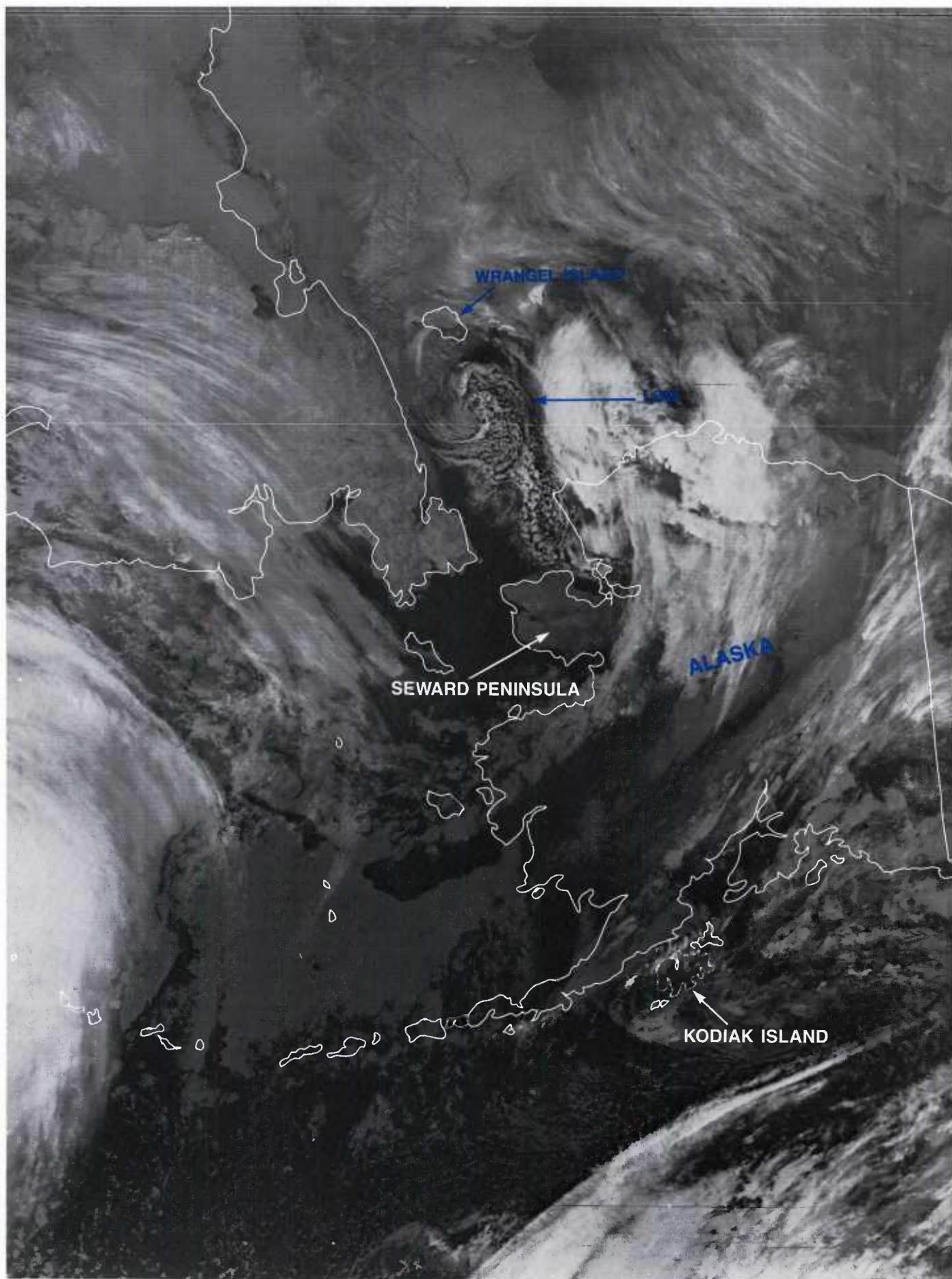
Cold Air Vortex Cyclogenesis, Phase 3.



Cold Air Vortex Cyclogenesis, Phase 4.

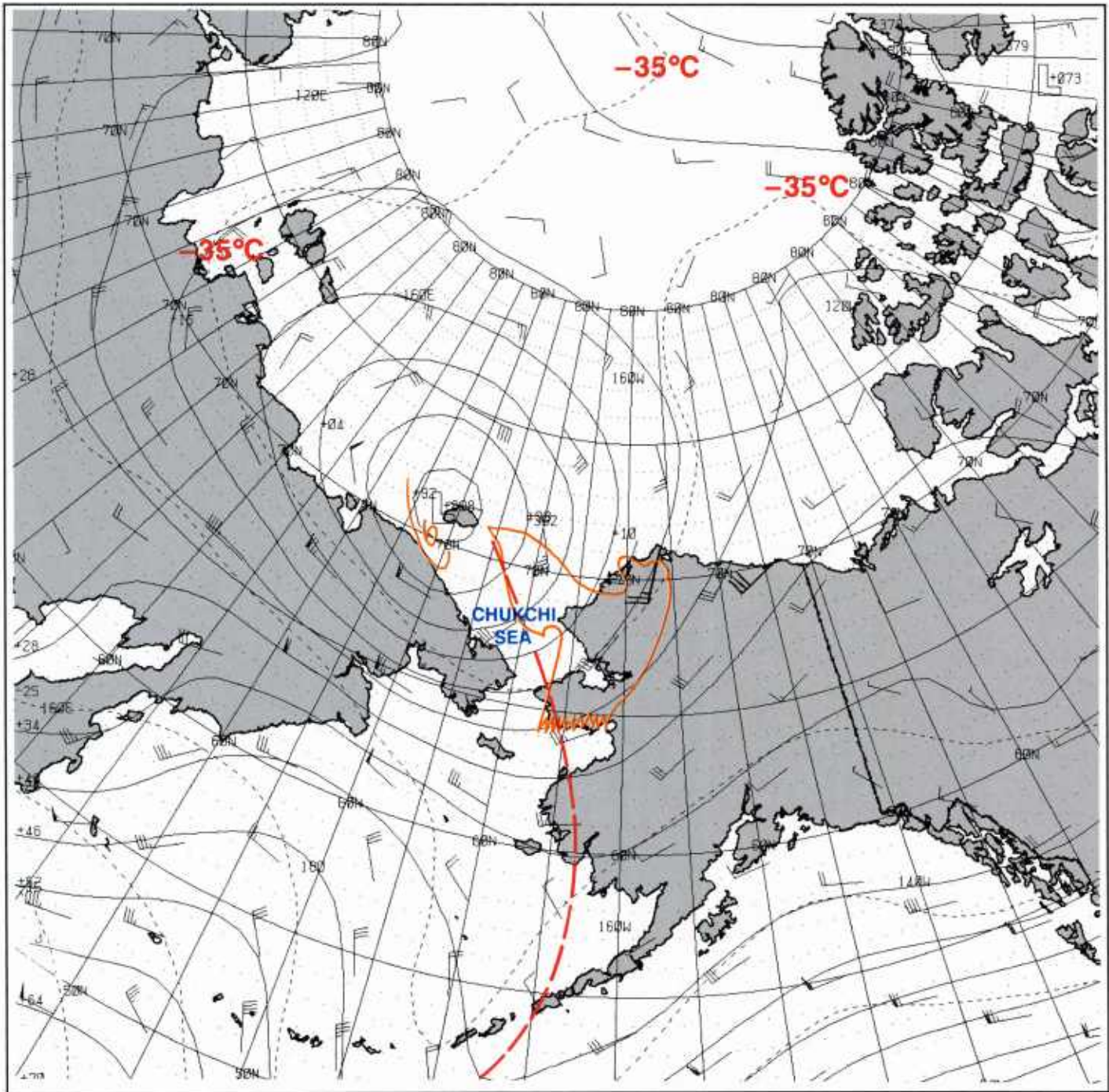
2B-26a Cold Air Vortex Cyclogenesis (From NTAG Vol. 4, Part 1, Section 2A, p. 2A-10).





2B-27a DMSP infrared (TS) data. 13 October 1985, 2002 GMT.

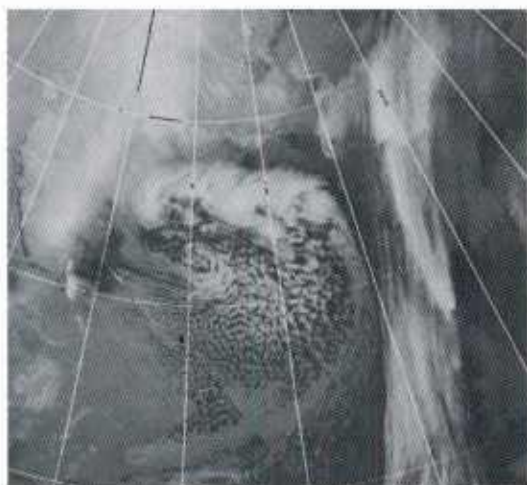




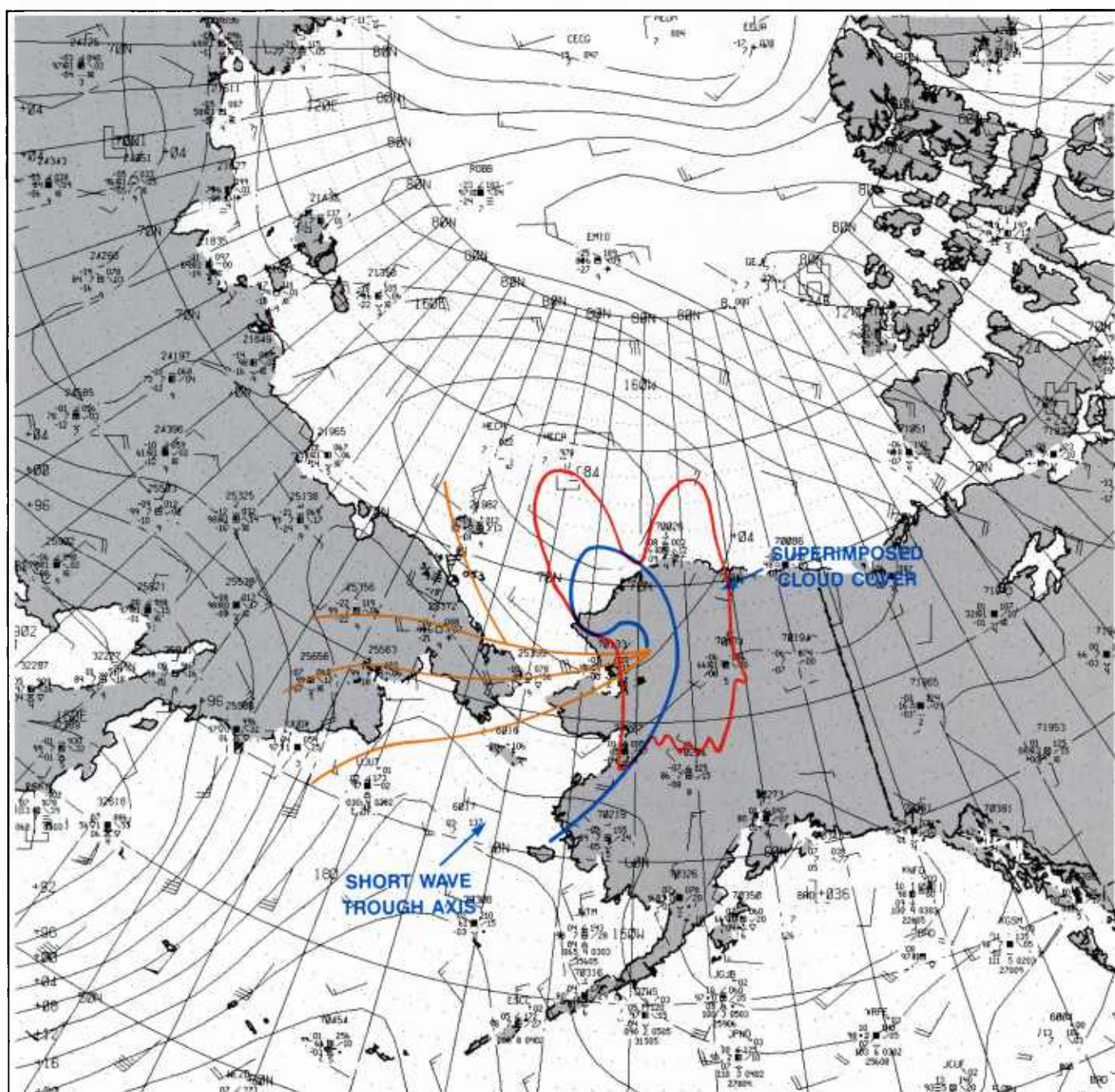
2B-28a FNOC 500 mb analysis. 13 October 1985, 1200 GMT (with superimposed cloud outline from Fig. 2B-21a).

The surface analysis for 1800 GMT (Figure 2B-29b) shows that winds with speeds of 20-30 kt encircle a portion of the storm region although the low center indicated is analyzed well north of where major action appears to be occurring based on the satellite information. The short wave trough axis is oriented in a north/south direction through the Bering Strait just west of the convective band axis that has moved inland over Alaska by the time of Figures 2B-24a and 2B-25a, revealing a cloud-free view of the Seward Peninsula.



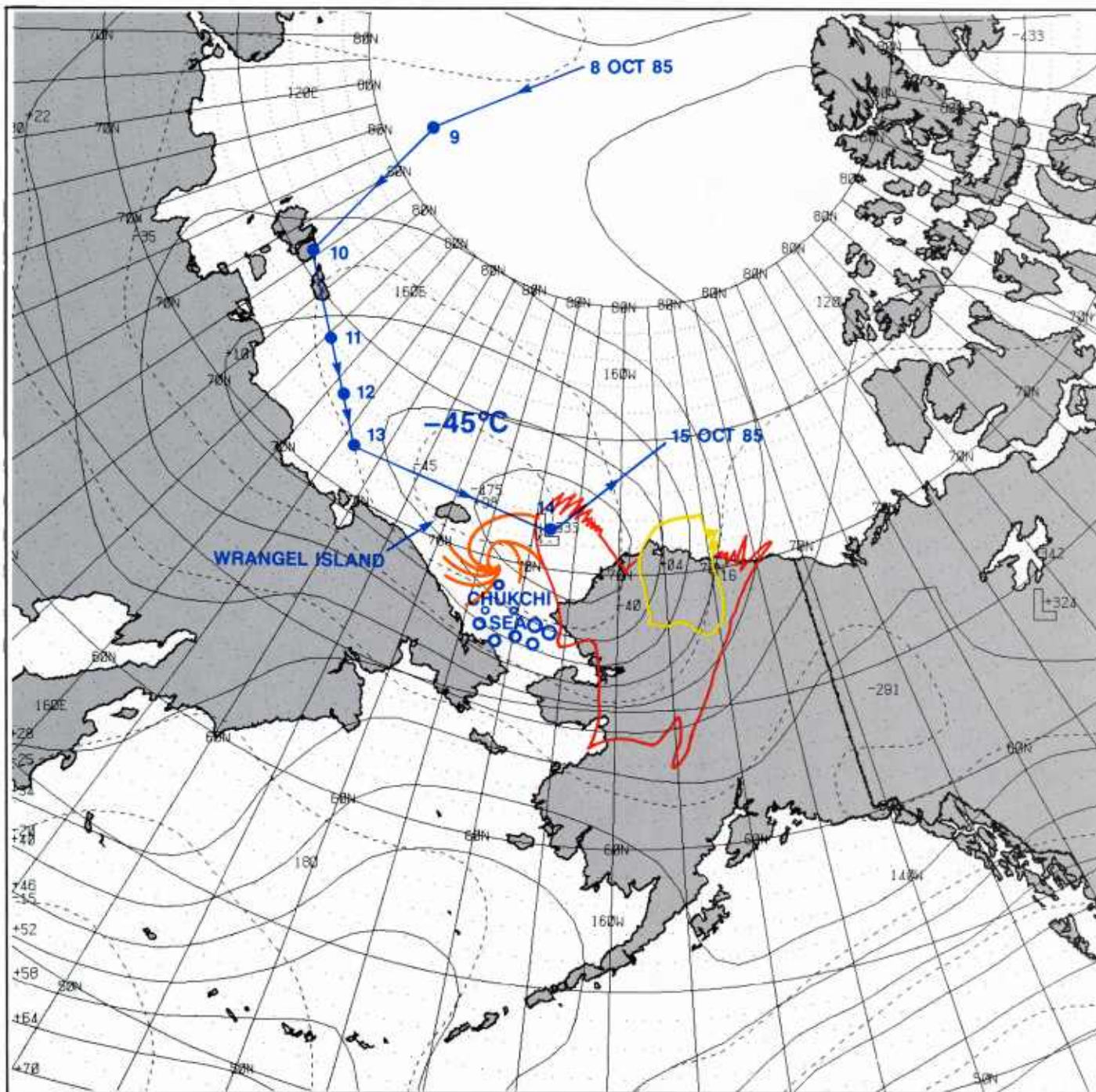


2B-29a DMSP infrared data  
near Iceland. 13 February 1984.



2B-29b FNOG surface analysis. 13 October 1985, 1800 GMT.



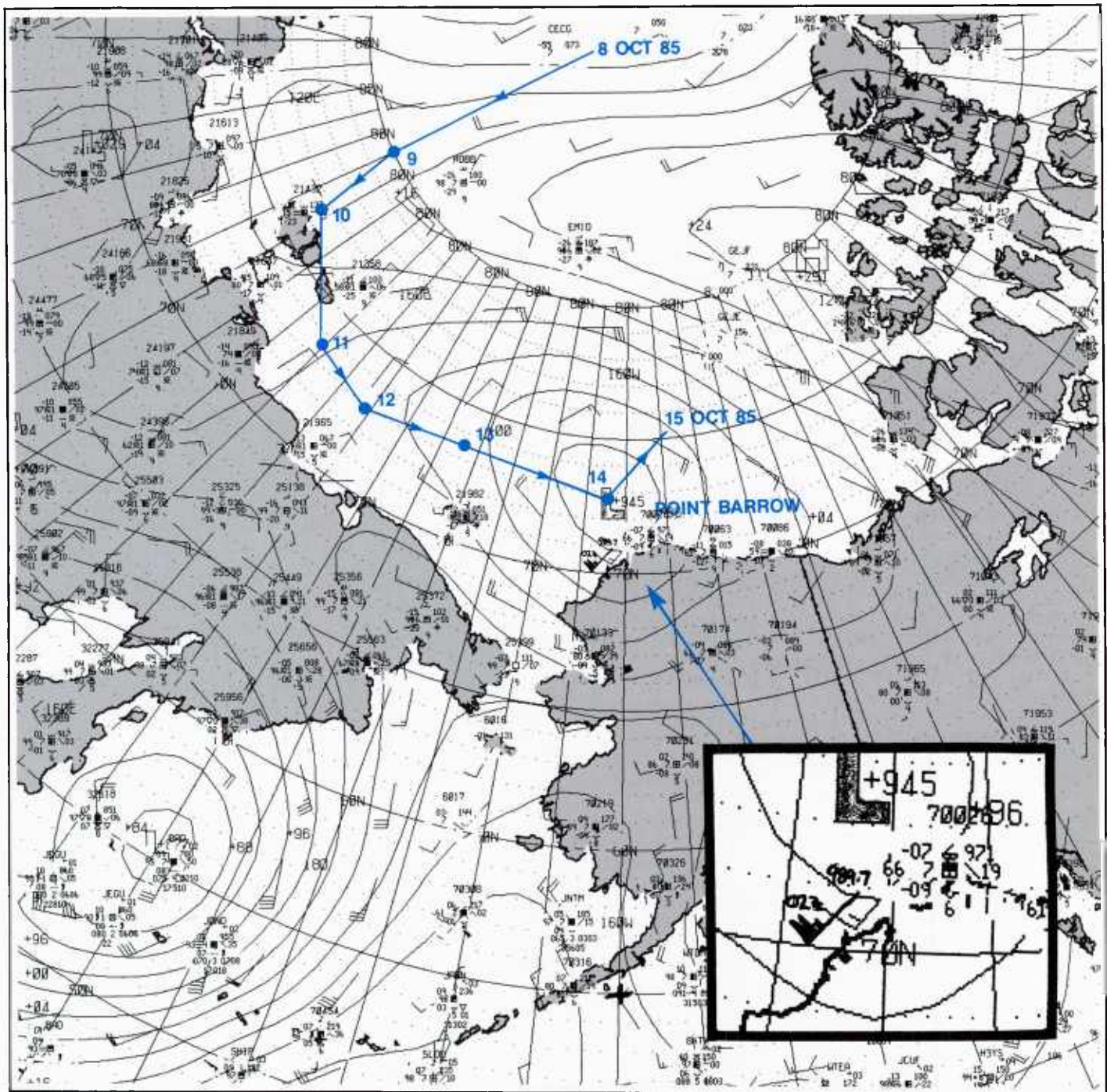


2B-30a FNOC 500 mb analysis. 14 October 1985, 0000 GMT (with superimposed cloud outlines from Fig. 2B-27a).

### 14 October 1985

The FNOC 500 mb analysis for 0000 GMT (Figure 2B-30a), with cloud outlines of the DMSP data as shown in Figure 2B-27a superimposed, is interesting in that the cold dome of air with temperatures lower than  $-45^{\circ}\text{C}$  is shown passing over Wrangel Island into the Chukchi Sea. The corresponding surface analysis (Figure 2B-31a) shows a 994.5 mb low just northwest of Point Barrow. Judging from this analysis, one would not suspect that in two hours winds of more than 60 kt could be experienced while operating in the Beaufort Sea near Pt. Barrow. (The wind report from *Polar Sea* has been plotted in this analysis near 70.8N, 161.5W.)





2B-31a FNOC surface analysis. 14 October 1985, 0000 GMT.

Two hours after the *Polar Sea* report, at 0406 GMT, DMSP data (Figure 2B-32a) revealed cloud forms around the developing center. Note the large convective clusters of cumulonimbus just off the northwest coast of Alaska southwest of the center. Subsiding motion is beginning to clear out the region of eye formation.

A superb view of the developing storm less than two hours later at 0548 GMT (Figure 2B-33a) reveals convection associated with the vorticity center, formerly over the Chukchi Sea, moving onto the northwest coast of Alaska, southwest of Pt. Barrow. Frigid Arctic air from off the ice pack is seen through cloud strait indications flowing toward that center. A huge squall line formation lies just north of the developing center.

An eye begins closing off in a view two hours later at 0752 GMT (Figure 2B-34a). Figures 2B-35a (1000 GMT), 2B-36a (1200 GMT), and 2B-37a (1300 GMT) show the conclusion of this process as the storm moved on-shore just southwest of Pt. Barrow.

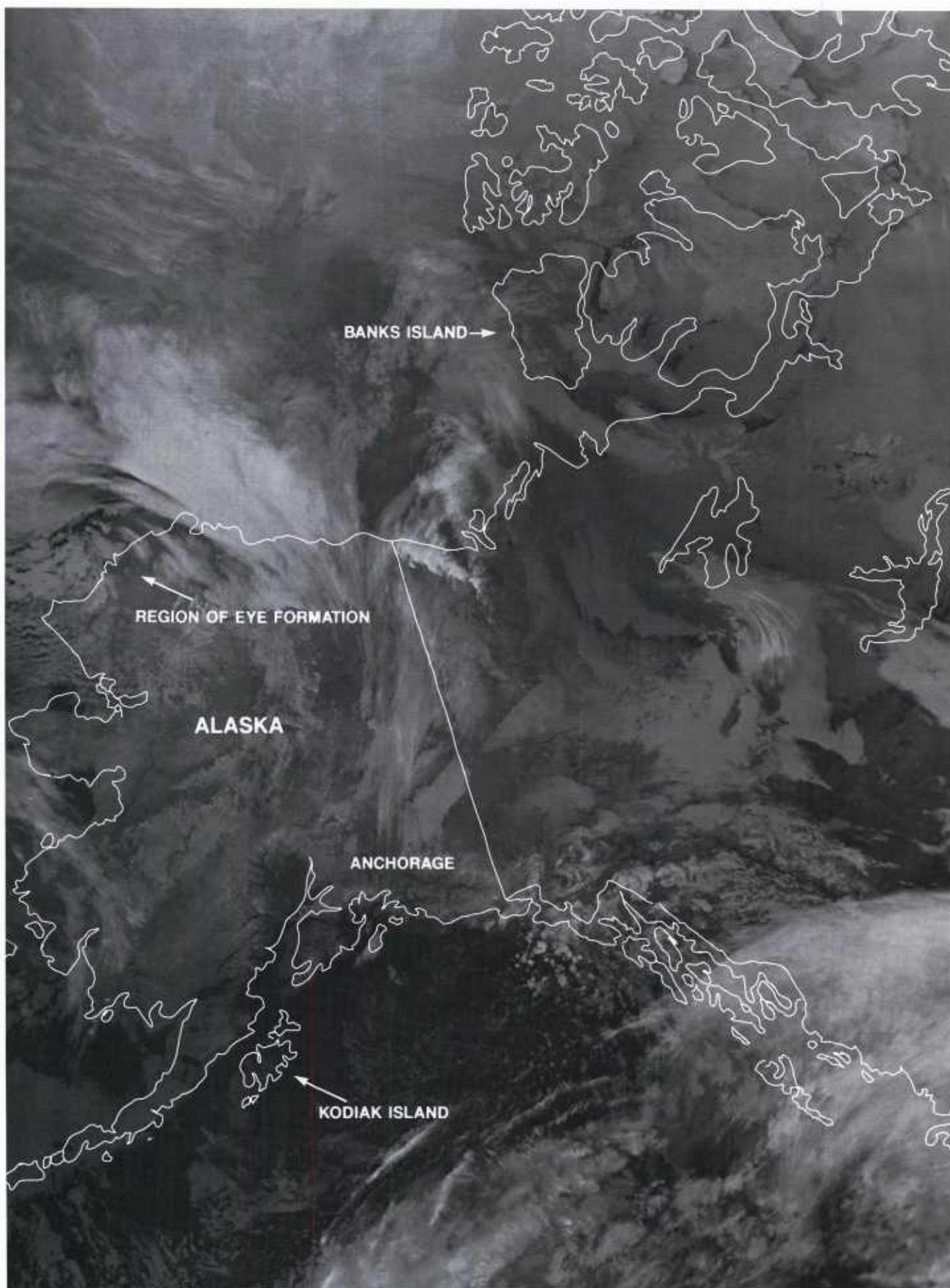
Figures 2B-32a through 2B-35a document, in satellite views, the birth of a polar low off the northwest coast of Alaska during a period of less than six hours, starting with no recognizable cloud vortex and developing to a distinct hurricane-like eye appearance. It is noteworthy that *Polar Sea* encountered hurricane-force winds prior to recognizable cloud vortex formation. This was the period of explosive deepening.

### *Epilogue*

In fairness to the forecasters at NPOC, Canadian forecasters at the Beaufort Weather Office and Arctic Weather Centre, Edmonton, Alberta, also failed to analyze and forecast the development of this storm. They noted that “progs fail to properly analyze 500 mb cold low and missed the surface low entirely. . . .” Their comment was that the storm was “not forecast type and totally ignored by progs.”

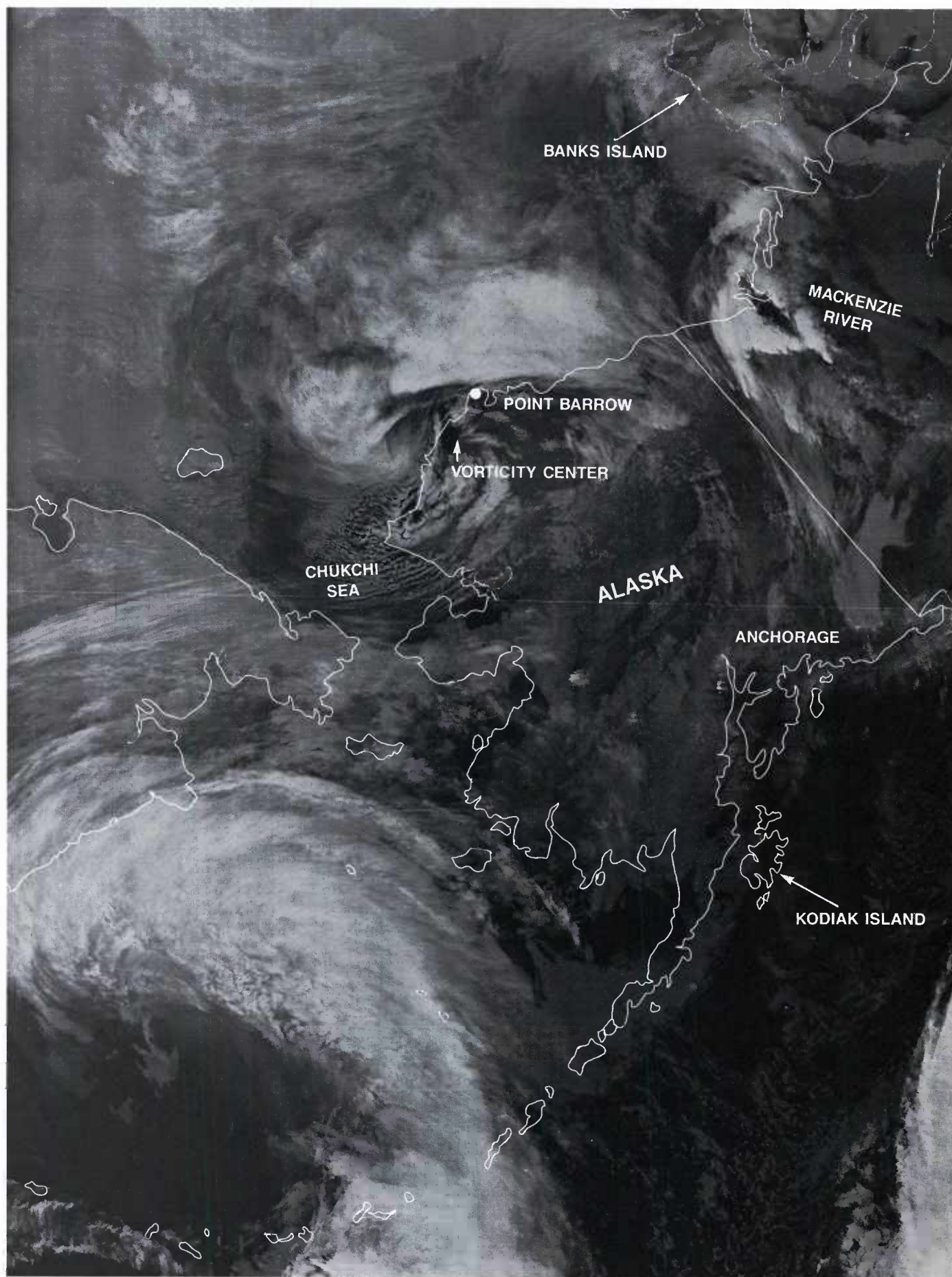
Ed Hudson of the Beaufort Weather Office prepared summary surface analyses that depicted the storm as it approached the Alaskan coast on 14 October at 1200 GMT (Figure 2B-38a), moved inland passing just south of Pt. Barrow by 1800 GMT (Figure 2B-38b), and then moved out into the Beaufort Sea on 15 October at 0000 GMT and 0600 GMT (Figures 2B-39a and 2B-39b) (Beaufort Weather Office 1985 Report). He noted strong winds associated with the storm, with Prudhoe Bay and nearby Deadhorse reporting gusts to 52 and 54 kt, respectively, at 14/2000 GMT, and peak winds of 75 kt recorded at Prudhoe Bay at 14/2035 GMT. Lack of confidence in prog products caused major forecast uncertainty as the storm entered the Beaufort Sea.





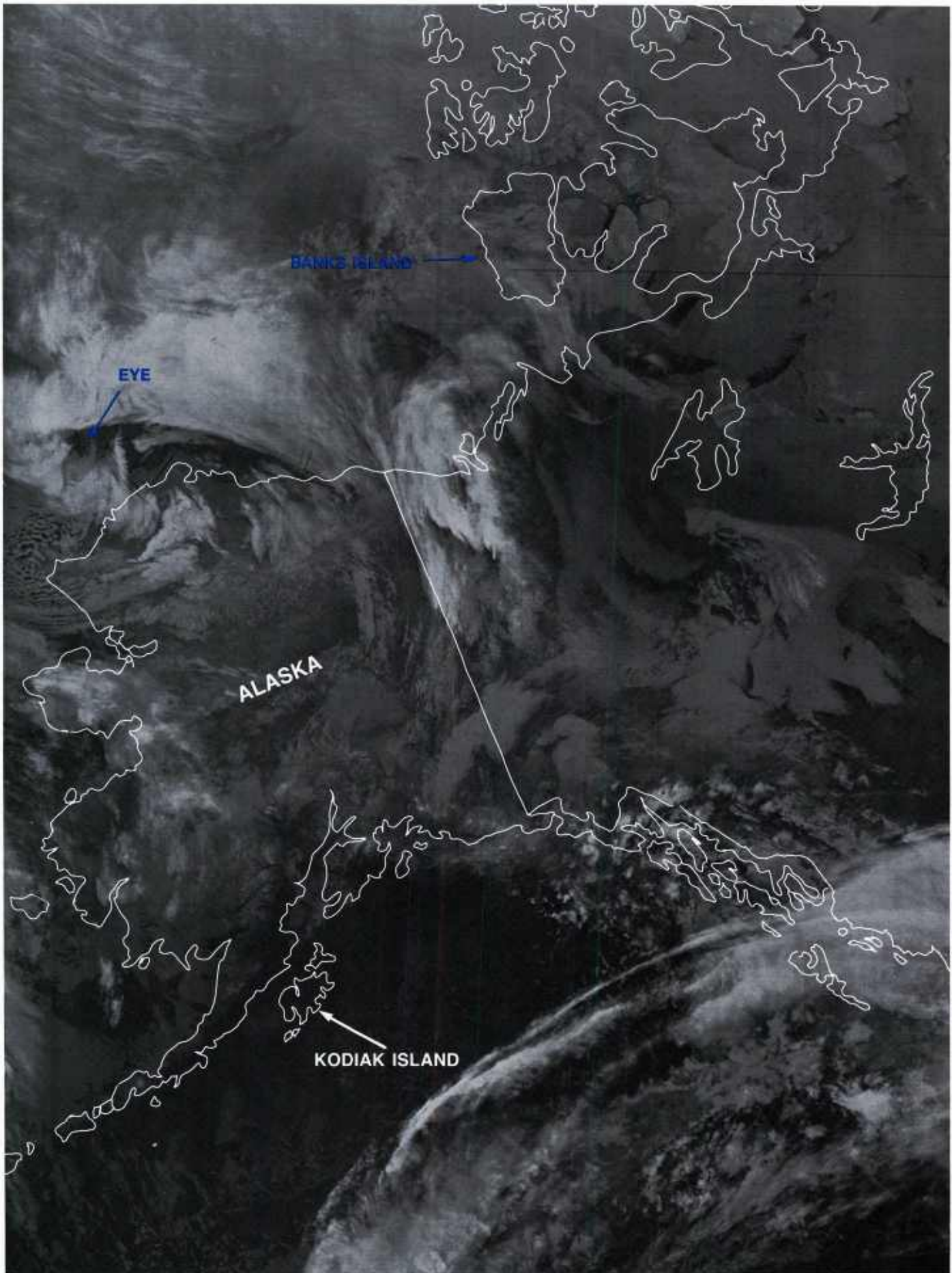
2B-32a DMSP infrared (TS) data. 14 October 1985, 0406 GMT.



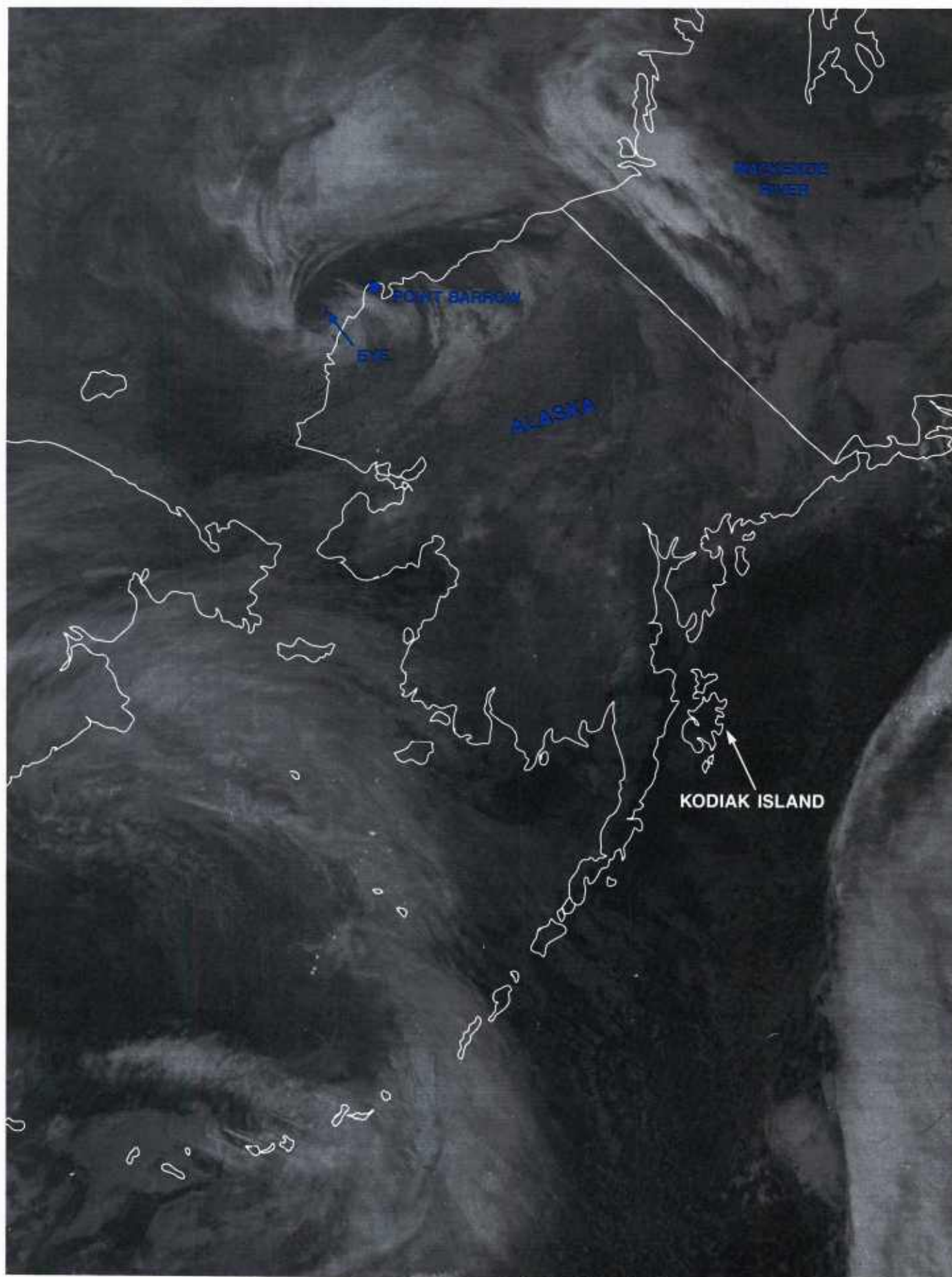


2B-33a DMSP infrared (TS) data. 14 October 1985, 0548 GMT.



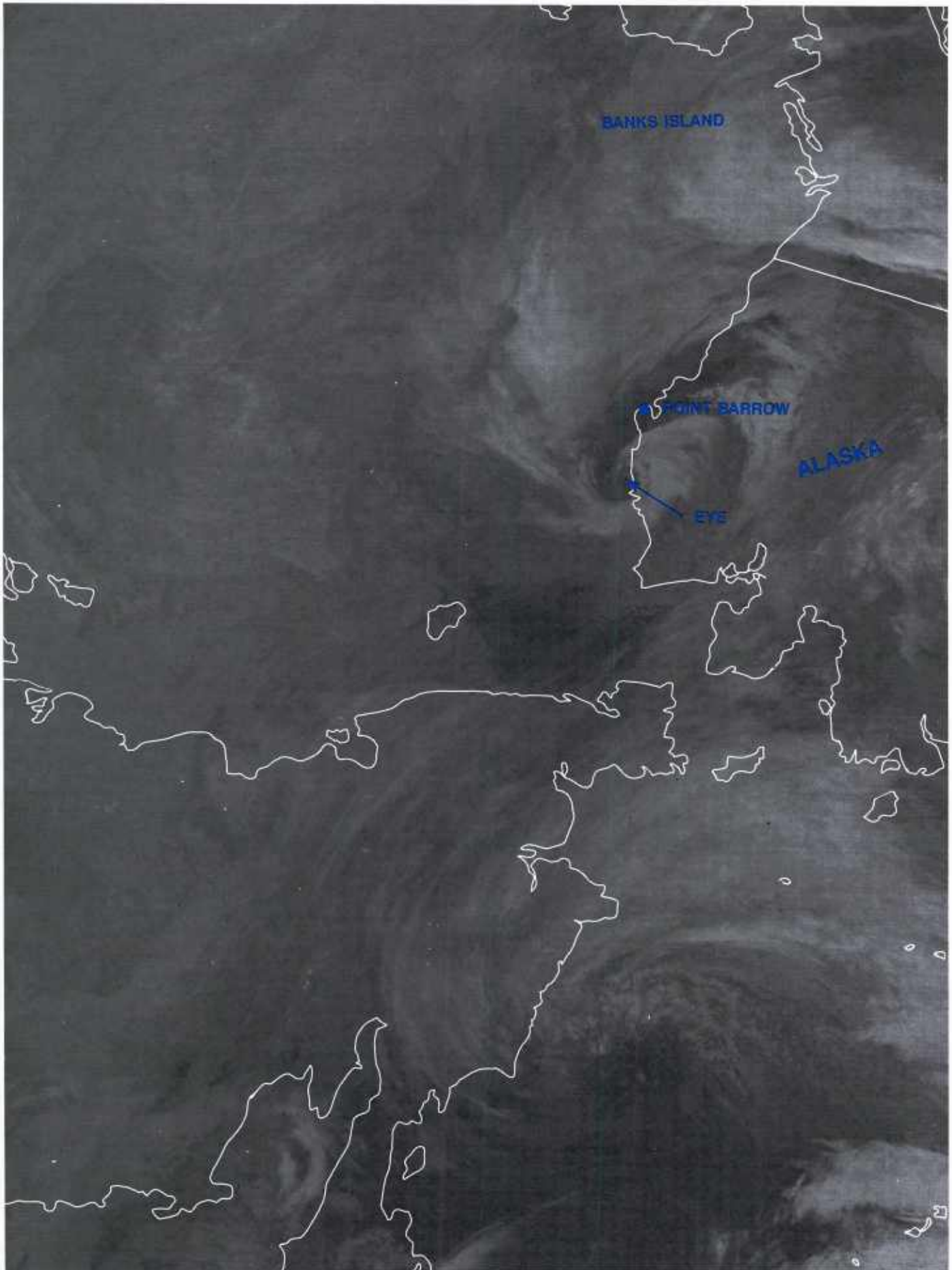


2B-34a DMSP infrared (TS) data. 14 October 1985, 0752 GMT.

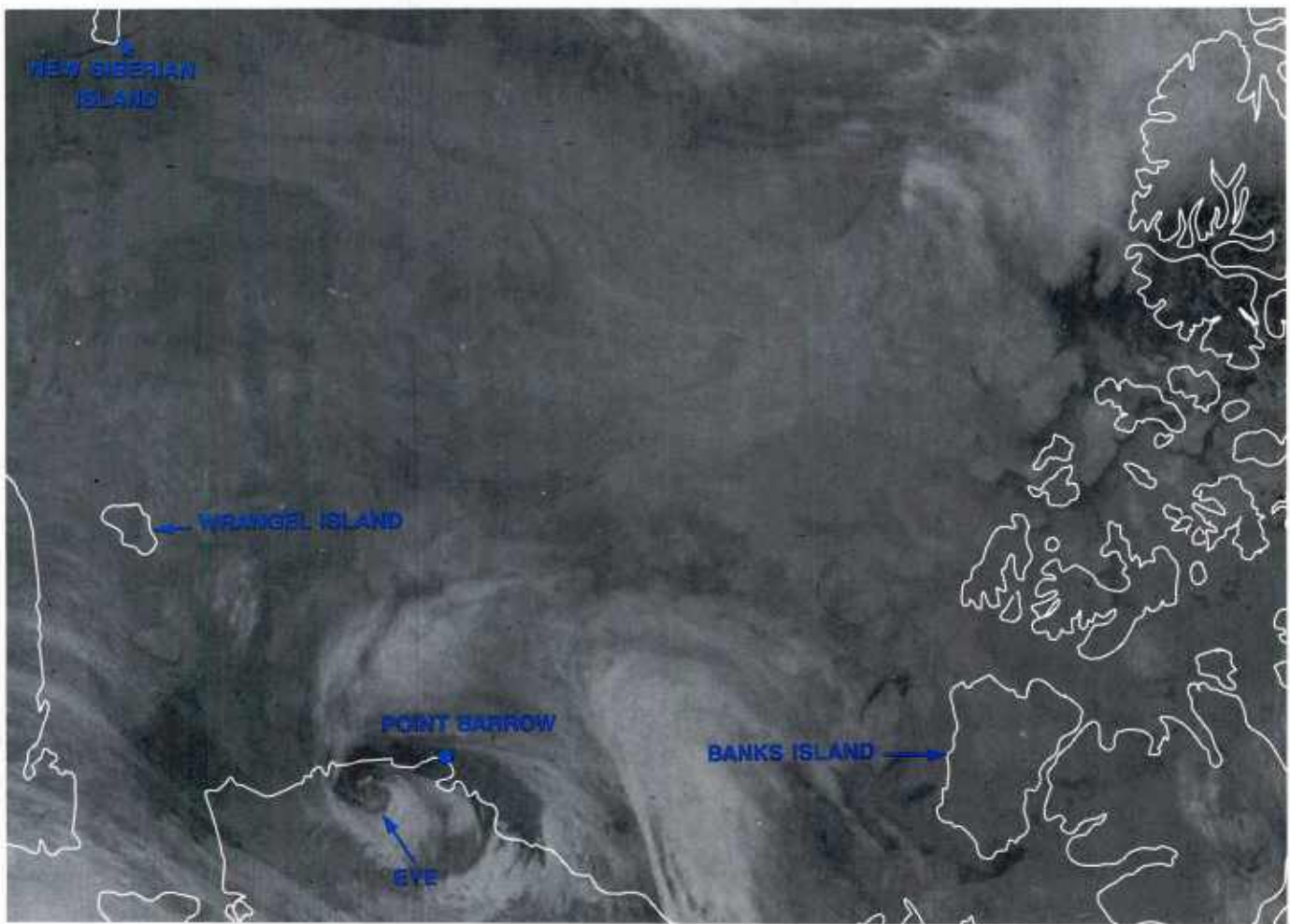


2B-35a DMSP infrared (TS) data. 14 October 1985, 1000 GMT.



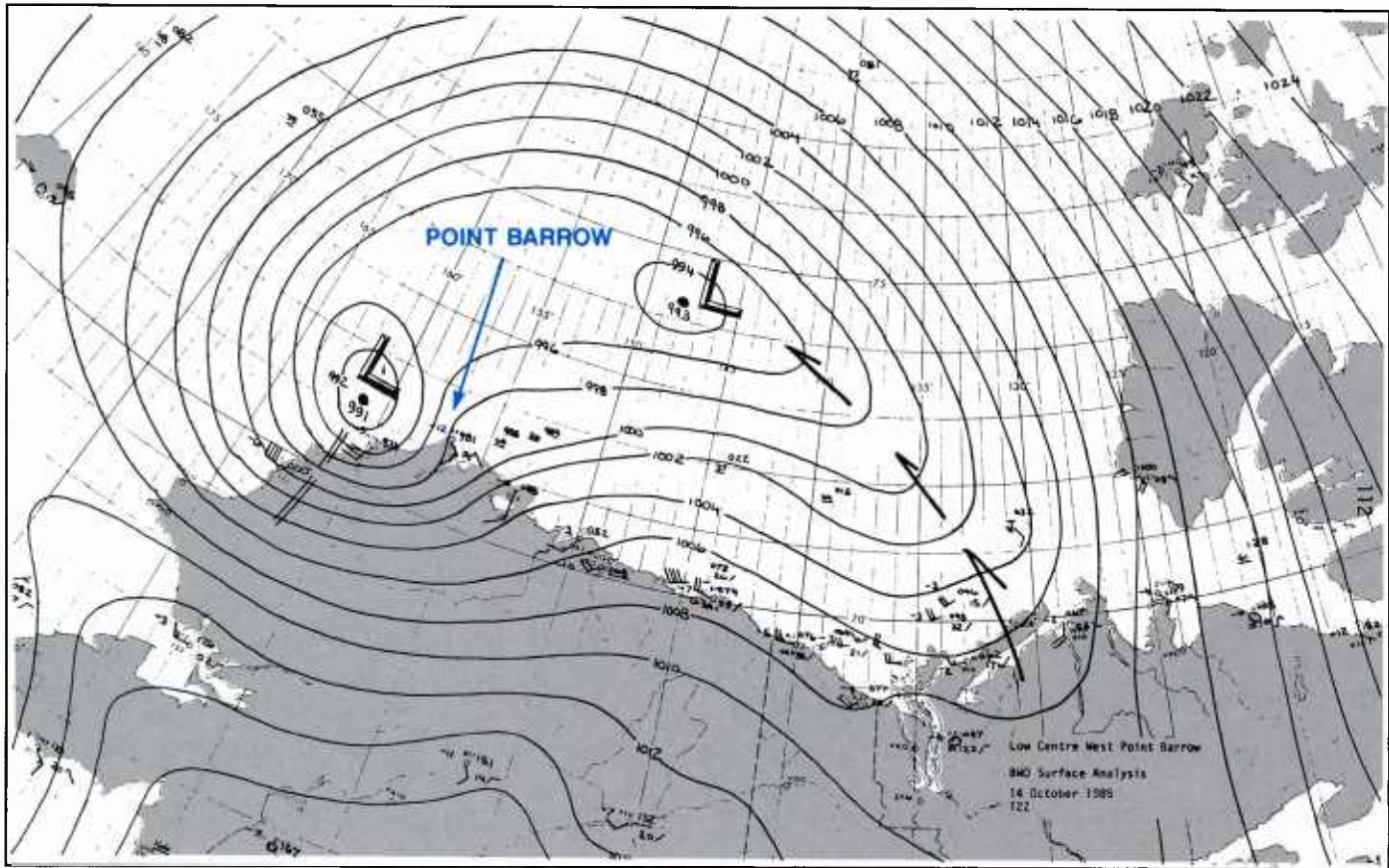


2B-36a DMSP infrared (TS) data, 14 October 1985, 1200 GMT.

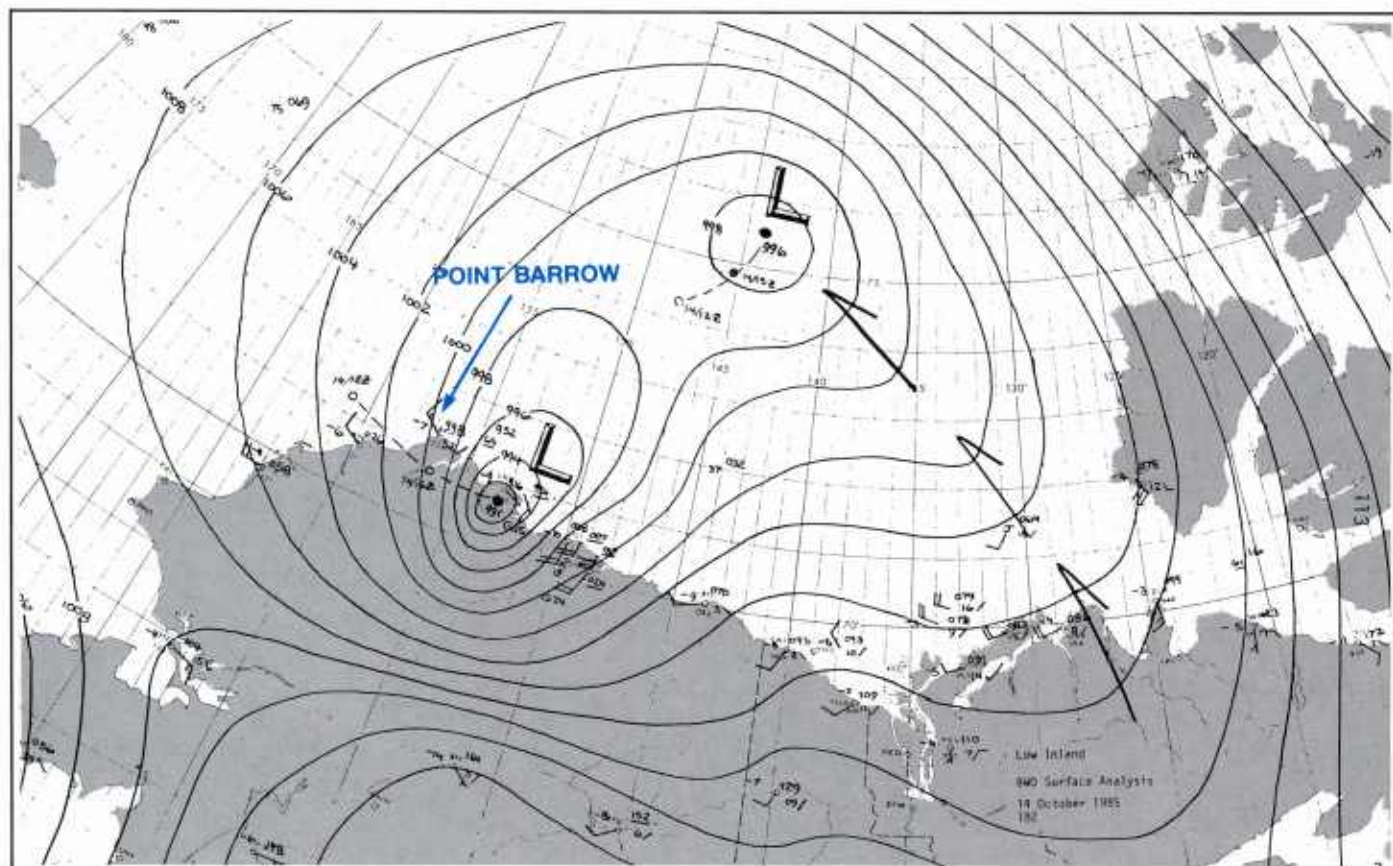


2B-37a DMSP infrared (TS) data. 14 October 1985, 1300 GMT.



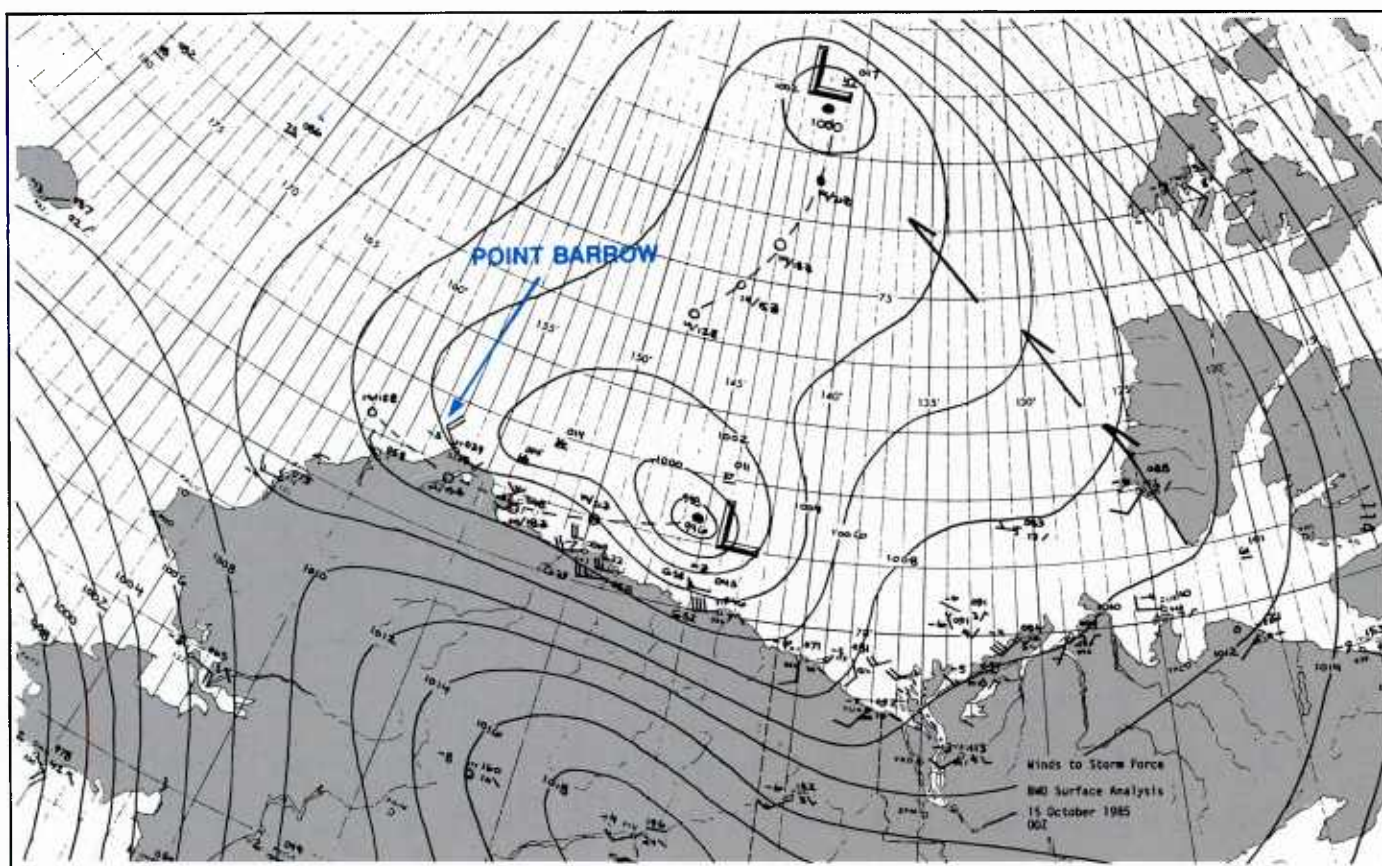


2B-38a Beaufort Weather Office surface analysis. 14 October 1985, 1200 GMT.

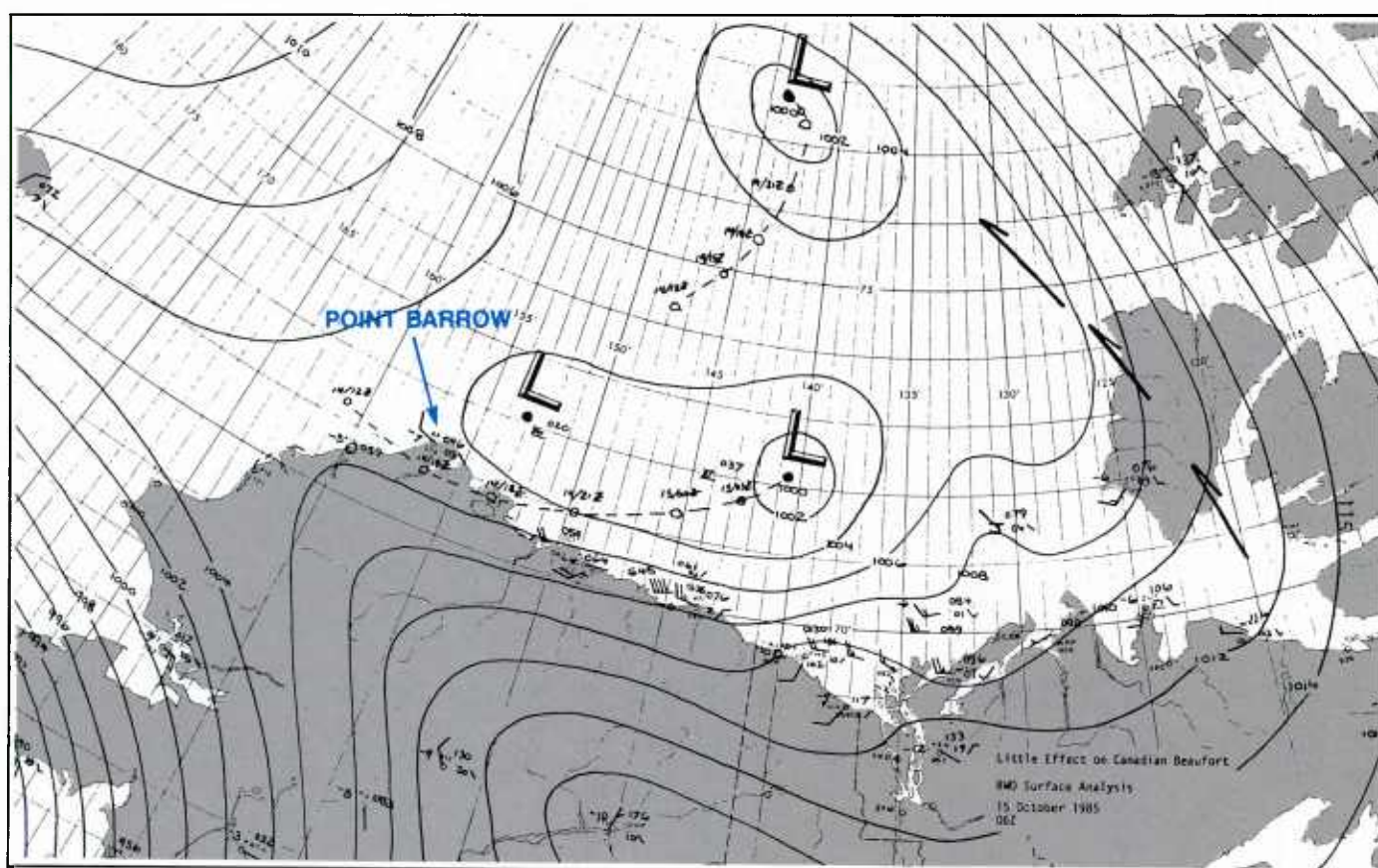


2B-38b Beaufort Weather Office surface analysis. 14 October 1985, 1800 GMT.





2B-39a Beaufort Weather Office surface analysis. 15 October 1985, 0000 GMT.



2B-39b Beaufort Weather Office surface analysis. 15 October 1985, 0600 GMT.



### **Important Conclusions**

1. Intense polar lows of the type experienced in the Greenland/Norwegian/Barents Sea also develop in the region of the East Siberian/Chukchi/Beaufort Sea.
2. Satellite data at frequent intervals (every 2–3 hours) are required to monitor the development of polar lows. Coverage should start in the vicinity of Wrangel Island and extend eastward continuously over the Beaufort Sea.
3. Surface analyses should incorporate satellite evidence of vortex development at the earliest opportunity. Hurricane-force winds in polar lows, however, can occur prior to recognizable cloud vortex formation. Precursor signs discussed in this paper can give warning prior to development.
4. A cold 500 mb low appears to be an essential ingredient in severe polar low development. Cold temperatures aloft act to destabilize the atmosphere and give rise to open-cellular cumulonimbus production over water south or west of the convective cloud band in which development will occur. Such development serves as a useful precursor indication of potential for polar low development.
5. Whenever surface lows and upper cold lows track together in eastward movement over the ice pack toward Alaska, they should be continuously monitored for signs of potential polar low development.

### **Acknowledgement**

The assistance of Ed Hudson, Beaufort Weather Office, in assembling material for this study, and briefings by personnel of the Arctic Weather Centre, Edmonton, related to Arctic research, are gratefully acknowledged.

### **Reference**

Beaufort Weather Office 1985 Report. Available from Atmospheric Environment Service, Twin Atria Bldg., 4999 98th Ave., Edmonton, Alberta, Canada T6B 2X3.





# Section 3

## *Local-Scale Atmospheric Phenomena and Effects*

### *3A Leads and Polynyi: Air/Sea Interaction Effects*

Introduction .....	3A-1
--------------------	------

#### *Case Studies*

1 Fog and Stratus Formation—Cape Bathurst Polynya, 11–12 October 1985.....	3A-2
2 Low-Level Wind Direction Determination From Lead Effects.....	3A-8
3 Low-Level Inversion Effects in the Arctic.....	3A-13

### *3B Mountain-Gap Winds*

Features Associated with the Development of Mountain-Gap Winds.....	3B-1
--	------

#### *Case Studies*

1 The Kamishak Gap Wind .....	3B-2
2 A Synoptic Intensification of the Kamishak Gap Wind .....	3B-6

### *3C Islands of Grounded Sea Ice: Their Use in Detecting Changes in Direction of Ice Motion and Their Role in Lead Formation .....*

3C-1

#### *Case Studies*

1 Ice Drift Reversal and Lead Formation in the Chukchi and East Siberian Seas .....	3C-2
--	------

<b>3D</b>	<b><i>Characteristic Structure and Seasonal Changes in Arctic Sea Ice .....</i></b>	<b>3D-1</b>
	<i>Case Studies</i>	
	1 <i>Satellite Detection of Flooded Sea Ice .....</i>	3D-3
<b>3E</b>	<b><i>Land and Sea Breezes .....</i></b>	<b>3E-1</b>
	<i>Case Studies</i>	
	1 <i>Sea Breezes Along the Alaskan Beaufort Seacoast ..</i>	3E-3
	2 <i>Land Breezes Along the Alaskan Beaufort Seacoast .....</i>	3E-13
<b>3F</b>	<b><i>Orographic Cloud Formations and Other Unique Cloud Effects .....</i></b>	<b>3F-1</b>
	<i>Case Studies</i>	
	1 <i>Use of Orographic Cloud Plumes in Defining Arctic Frontal Location .....</i>	3F-3





### *3A Leads and Polynyi: Air/Sea Interaction Effects*

#### *Introduction*

Leads and polynyi in the Arctic undergo continuous change with respect to size, configuration, and air/sea interaction activity, due to effects of ocean current, wind flow, and air/sea temperature differences. The energy exchange due to heat and moisture flux from the open water in leads and polynyi is tremendous. Although small in area compared to the total ice cover, the net energy loss from a narrow open lead has been estimated to be over 800 times that from similar area ice floes over 3 meters thick (Badgley, 1966). Thus, relatively small open areas can contribute 20–30% of the total surface heat budget (Maykut, 1978).

It has even been shown that the moisture flux from a single large polynya, the North Water polynya of Baffin Bay, has contributed measurably to the growth of the Greenland ice cap (Müller et al., 1973; Müller, 1979).

It is intuitively obvious that heat and moisture flux can be maximized under a unique set of meteorological conditions and similarly minimized under still another set of quite different conditions. Ideal conditions for heat and moisture loss from the ocean include strong surface winds, cold air temperatures, dry air, and a pattern of cold air advection coming over the area. Such conditions are frequently found on the east side of high latitude high pressure centers and on the west side of high latitude low pressure centers. Winds over the lead or polynya location, under such conditions, back with height, reflecting the on-going process of cold air advection.



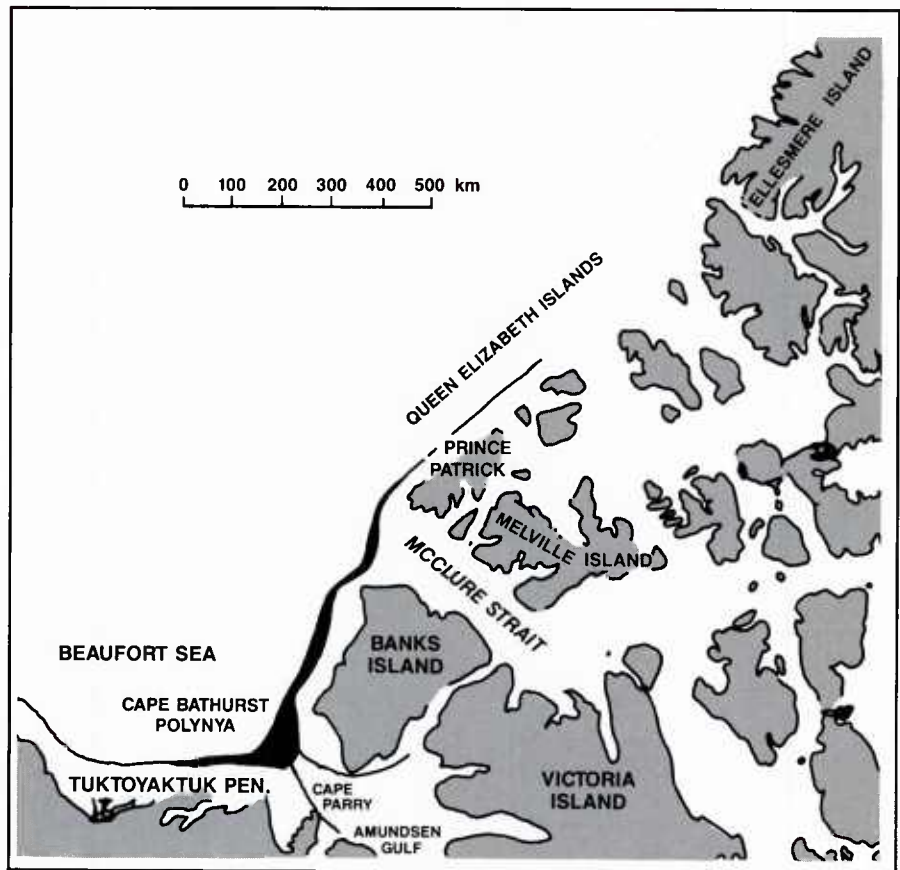
*Case 1 Fog and Stratus Formation—Cape Bathurst Polynya,  
11–12 October 1985*

*11 October 1985*

Figure 3A-2a shows the position of a shore lead in the Beaufort Sea passing west of Prince Patrick and Banks Islands. The lead widens to polynya proportions near Cape Bathurst at the entrance to the Amundsen Gulf and seems to recur in that location annually most years.

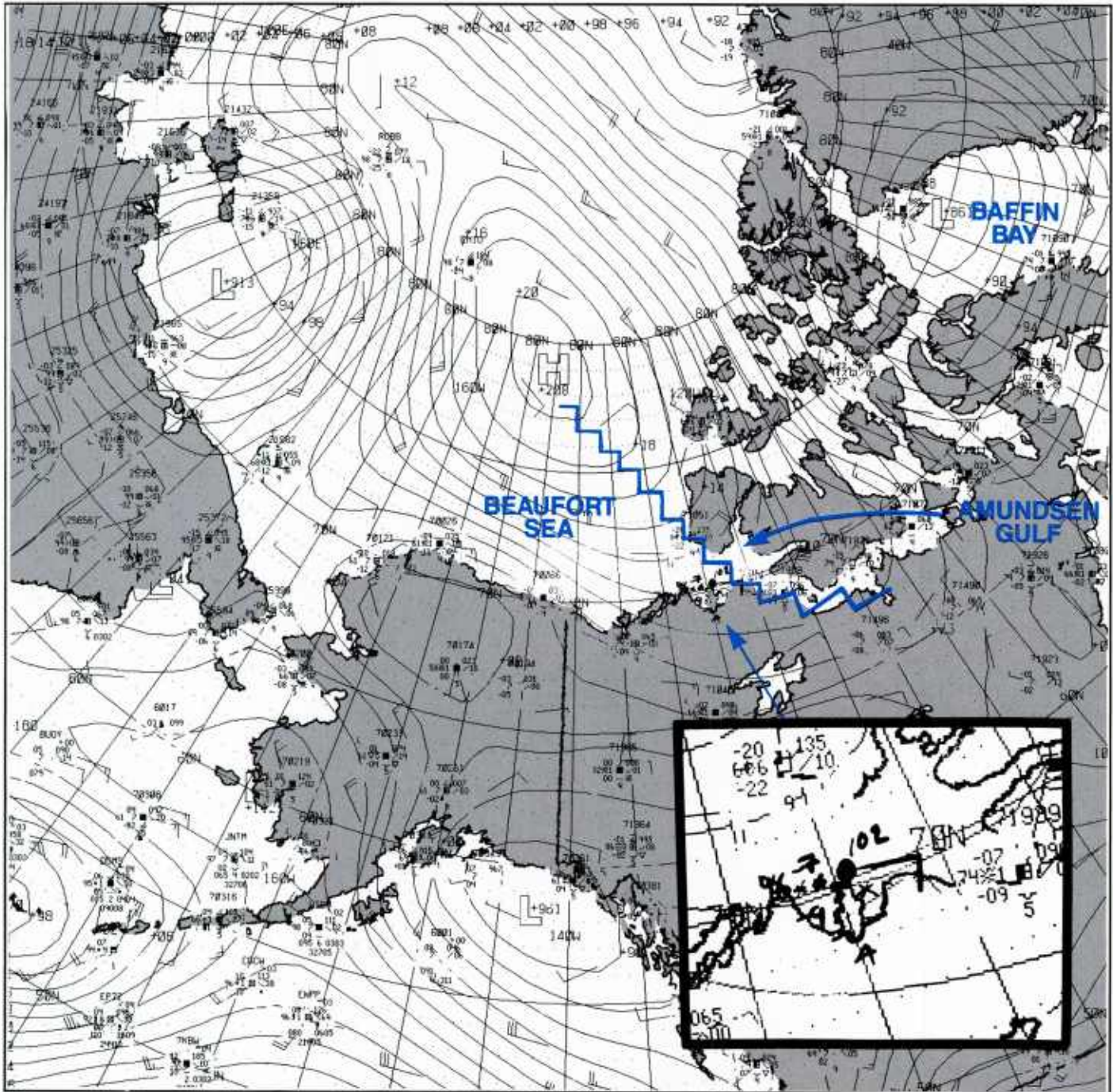
The surface analysis for 11 October at 0600 GMT is shown in Figure 3A-2b. The analysis shows that a surface ridgeline extended from a high pressure center in the Beaufort Sea near 78N, 148W, past Banks Island and southeastward past Victoria Island over the Amundsen Gulf. The pressure gradient is reasonably strong with reports of 20–30 kt winds in the Gulf region. Low pressure over Baffin Bay combines with the high pressure over the Beaufort Sea to produce a strong pressure gradient over the entire Canadian Archipelago under equally strong conditions of cold air advection.

DMSP infrared data on 11 October at 0853 GMT (Fig. 3A-3a) show a large, warm, cloud plume, which extends westward along the north coast of the Northwest Territories, over the Mackenzie River delta, between Cape Parry and Barter Island, toward Point Barrow. (The outline of Alaska, operationally-produced, is slightly askew on this image.) The source of the plume is the open water region around the southern portion of Banks and Victoria Islands. The southeastern tip of Banks Island is obscured by one plume which emanates from a small open water area in the Prince of Wales Sound, which separates Banks from Victoria Island.



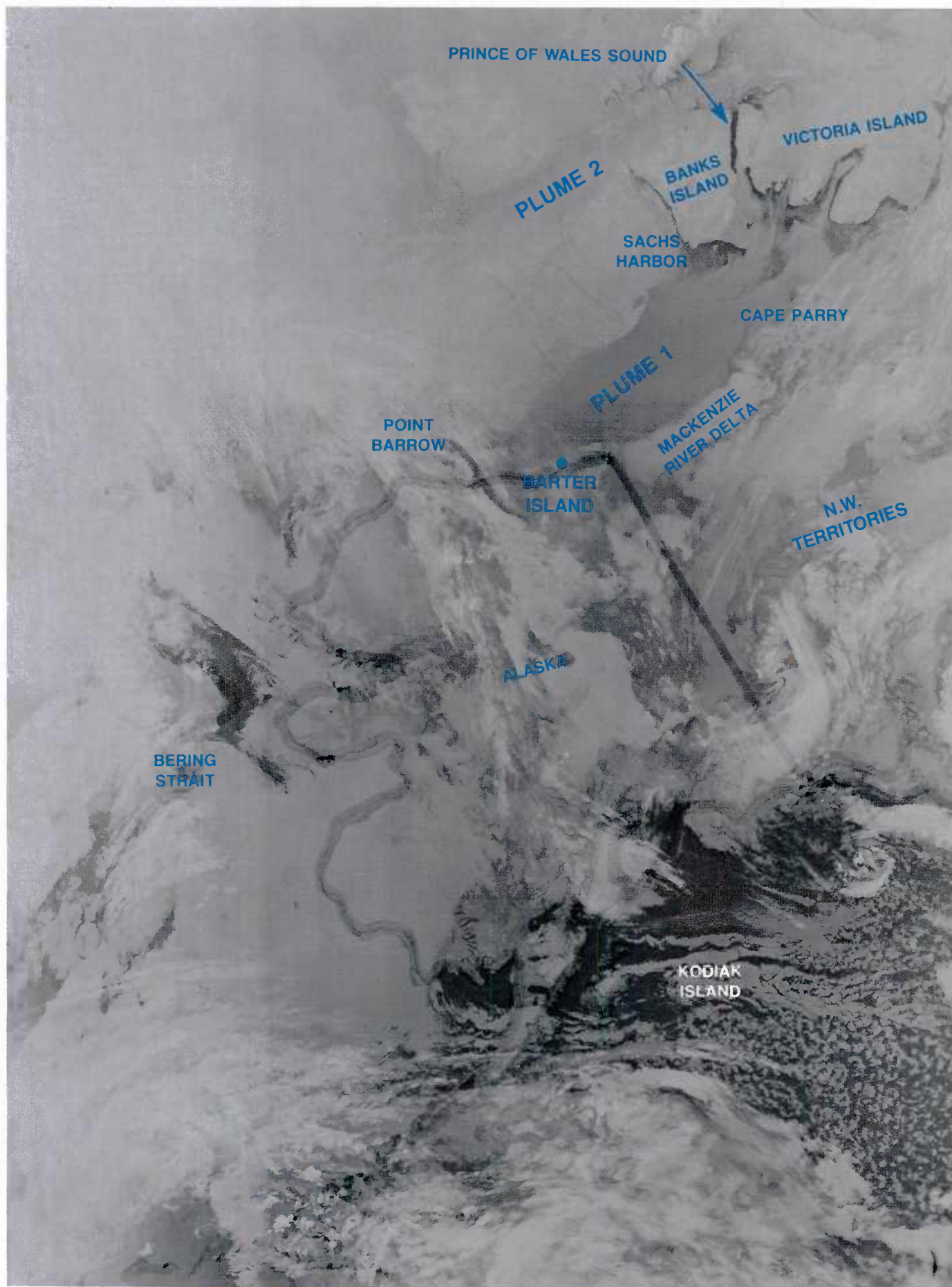
3A-2a Locator chart showing shore lead and polynya location near Banks Island [after Smith and Rigby, 1981].

Cape Parry (70.2N, 124.7W) is a reporting station located under the plume about 120 nm south of Sachs Harbor. Air passing over Cape Parry with wind flow from the east had the opportunity to be warmed by the open water in the Amundsen Gulf. On the 0600 GMT surface analysis (Fig. 3A-2b), Cape Parry reported a temperature of  $-7^{\circ}\text{C}$  as opposed to  $-20^{\circ}\text{C}$  reported at the same time by Sachs Harbor. Continuous light snow was falling over Cape Parry from a stratocumulus cloud base indicated between 300 and 600 m. Sachs Harbor was located north of the plume (Fig. 3A-2b) under clear skies and was experiencing the effects of less modified Arctic air. Subsiding air associated with the ridge line produced a sharp inversion within and near the polynya area.



3A-2b FNOC surface analysis. 11 October 1985, 0600 GMT.

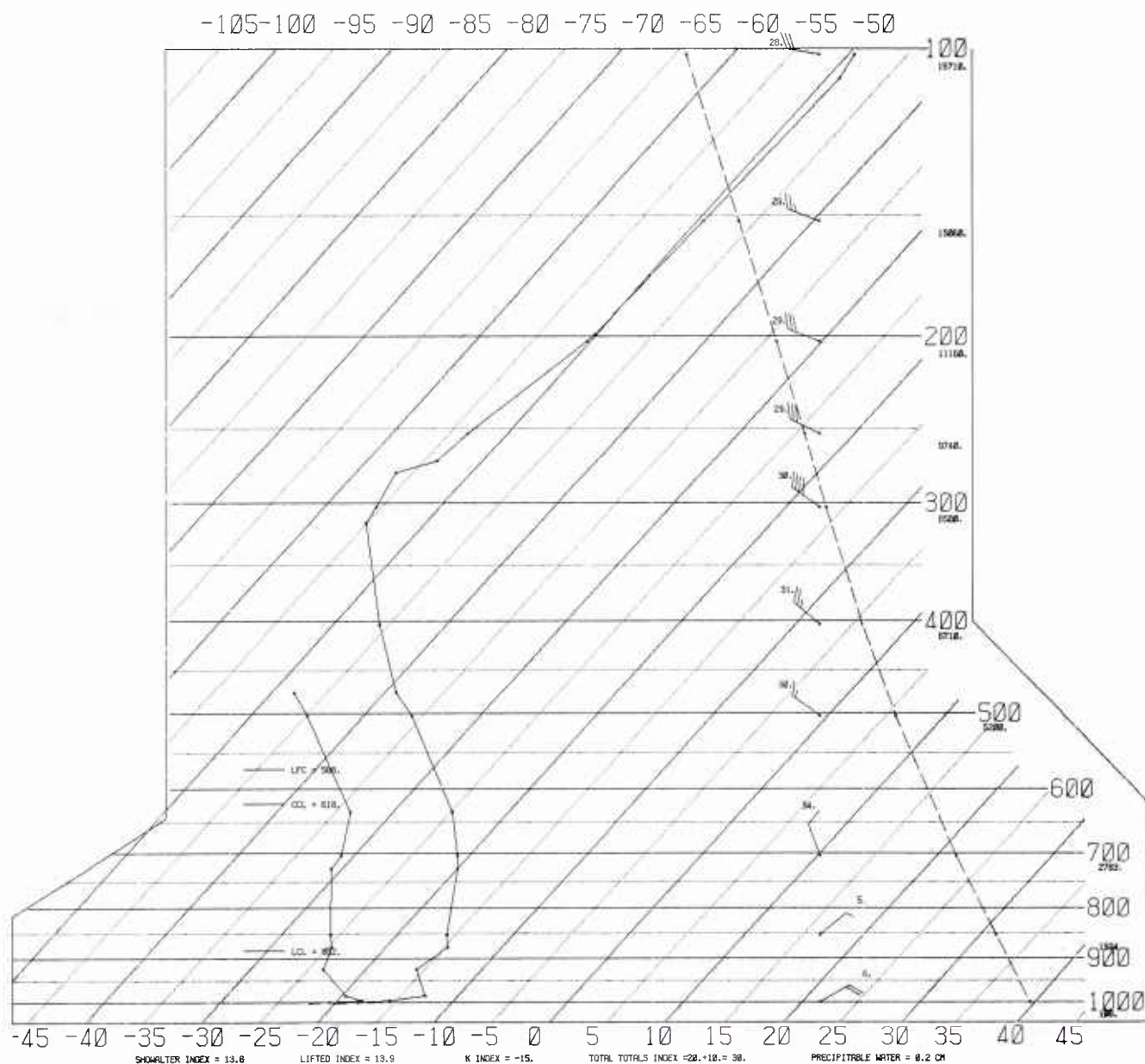




3A-3a DMSP infrared (TS) data. 11 October 1985, 0853 GMT.

The 11 October 1200 GMT sounding for Sachs Harbor (Fig. 3A-4a) shows a pronounced inversion with a very shallow moist layer near the surface and quite dry conditions in the clear air above. Note the pronounced backing of winds with height indicative of cold air advection.

Barter Island was under the extreme western fringe of the plume, reporting light continuous snow with about 3 miles visibility. Base of the overcast stratocumulus deck reported over the station was estimated at 200–300 m (Fig. 3A-2a). The 1200 GMT sounding for Barter Island (Fig. 3A-5a) reflects

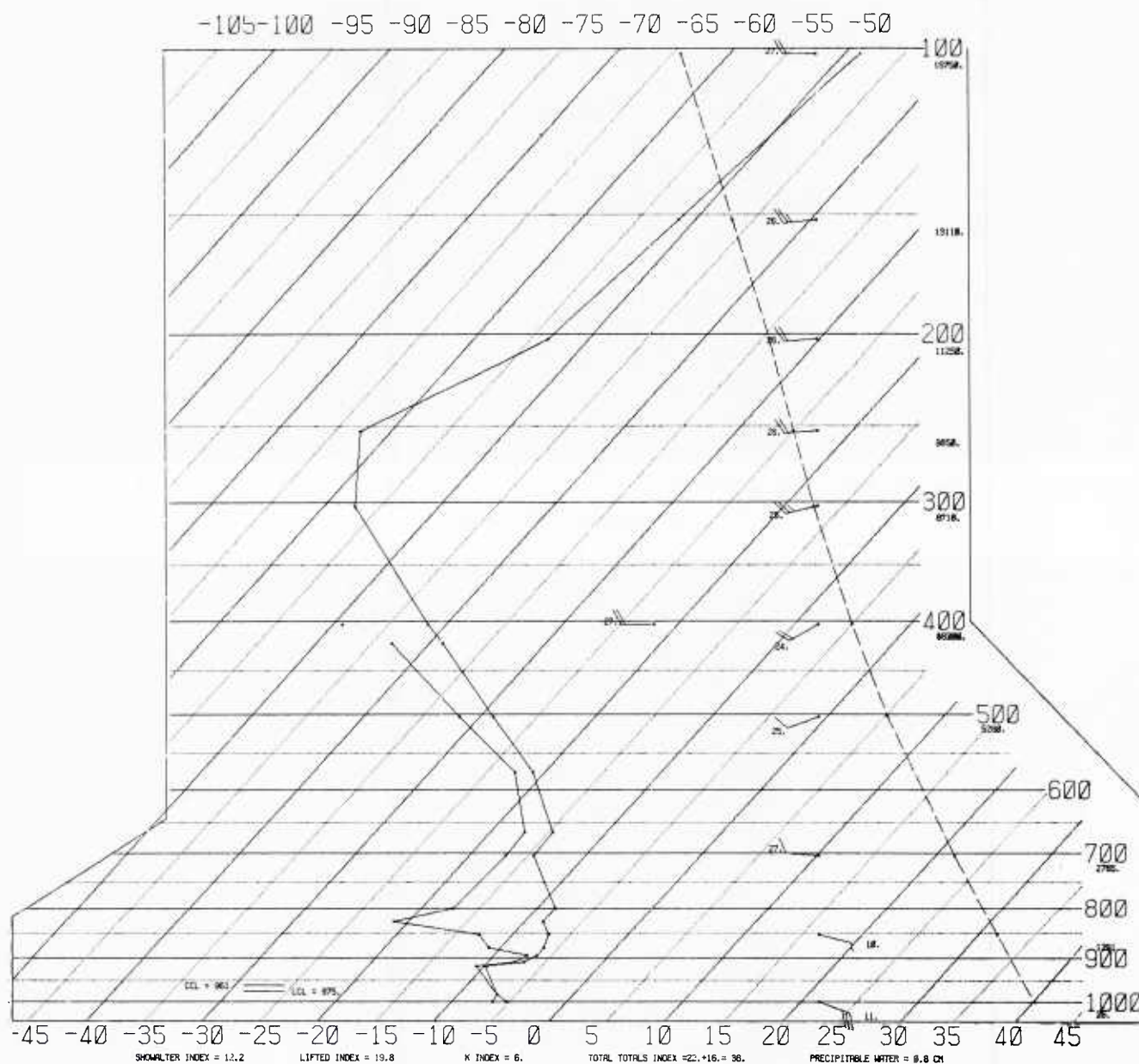


3A-4a Sachs Harbor (72°N, 125.3°W) radiosonde data. 11 October 1985, 1200 GMT.



these moist low level conditions, capped by an inversion with base near 920 mb and top near 850 mb. This would suggest that the plume thickness was about 2,000–2,500 ft and confined to the low levels. (The moist layer starting at 700 mb is apparently caused by mid-level cloudiness suggested in the data from the satellite passing over the western tip of the plume.)

Although not as obvious as the plume south of Banks Island a second plume is suggested on the north end of the island (Fig. 3A-3a). This plume also stretches to the west.



3A-5a Barter Island (70.1°N, 143.6°W) radiosonde data. 11 October 1985, 1200 GMT.

*12 October 1985*

Plume development persisted into the next day and at 1400 GMT a DMSP infrared view (Fig. 3A-6a) reveals the second plume extending from the north end of Banks Island almost 1,800 miles across the Arctic ice cap.

The plume was also evident at 1802 GMT (Fig. 3A-6b), four hours later, as revealed in a NOAA-8 infrared image acquired by the Canadian Arctic Weather Center at Edmonton, Alberta, Canada. Both the NOAA and DMSP images show part of this plume originating from the Thomsen River in the north-central portion of Banks Island. The rest of the plume apparently is formed from the shore lead shown in Figure 3A-1a and from smaller leads in the McClure Strait, between Banks and Prince Patrick Islands.

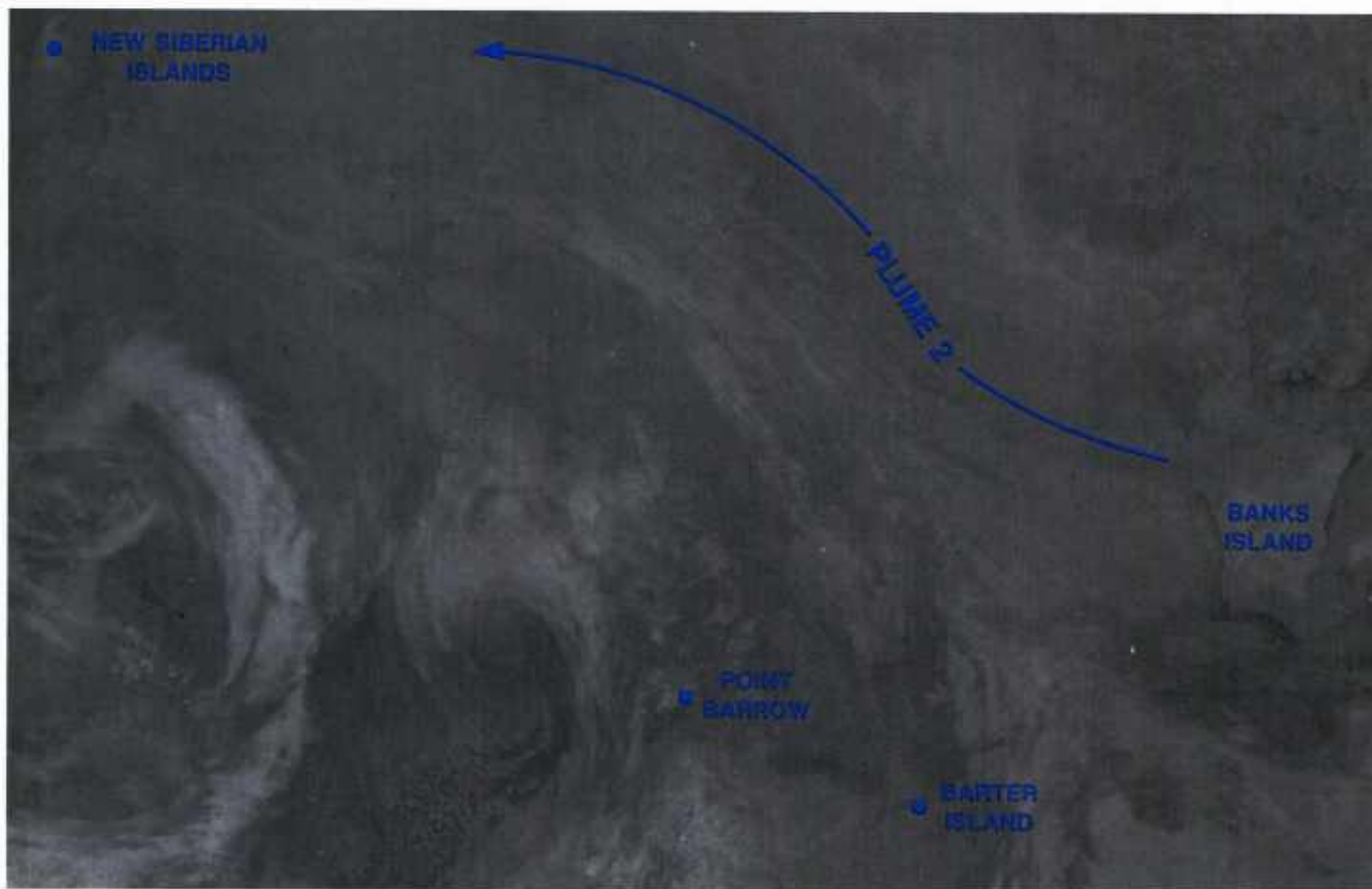
Persistence of this plume over a 2-day period and the continuous 1,800 mile length of the plume implies very stable flow such as might be anticipated under an extremely strong low level inversion near a ridgeline associated with a high pressure center. Additionally, the long fetch of the plume implies good advective influence and an elongation of the ridge northeast of the plume axis.

The surface analysis for 12 October at 1200 GMT (Fig. 3A-7a) verifies the existence of an elongated WNW-SSE ridgeline extending northwestward from Banks Island. The plume apparently was advected west-northwestward by the moderate 20–30 kt southeasterly flow that existed south of the ridgeline. The example demonstrates the fantastic potential in the Arctic for spreading clouds and pollution intact over vast areas of the Arctic without appreciable dispersion. It also demonstrates the type of meteorological conditions likely to produce such effects.

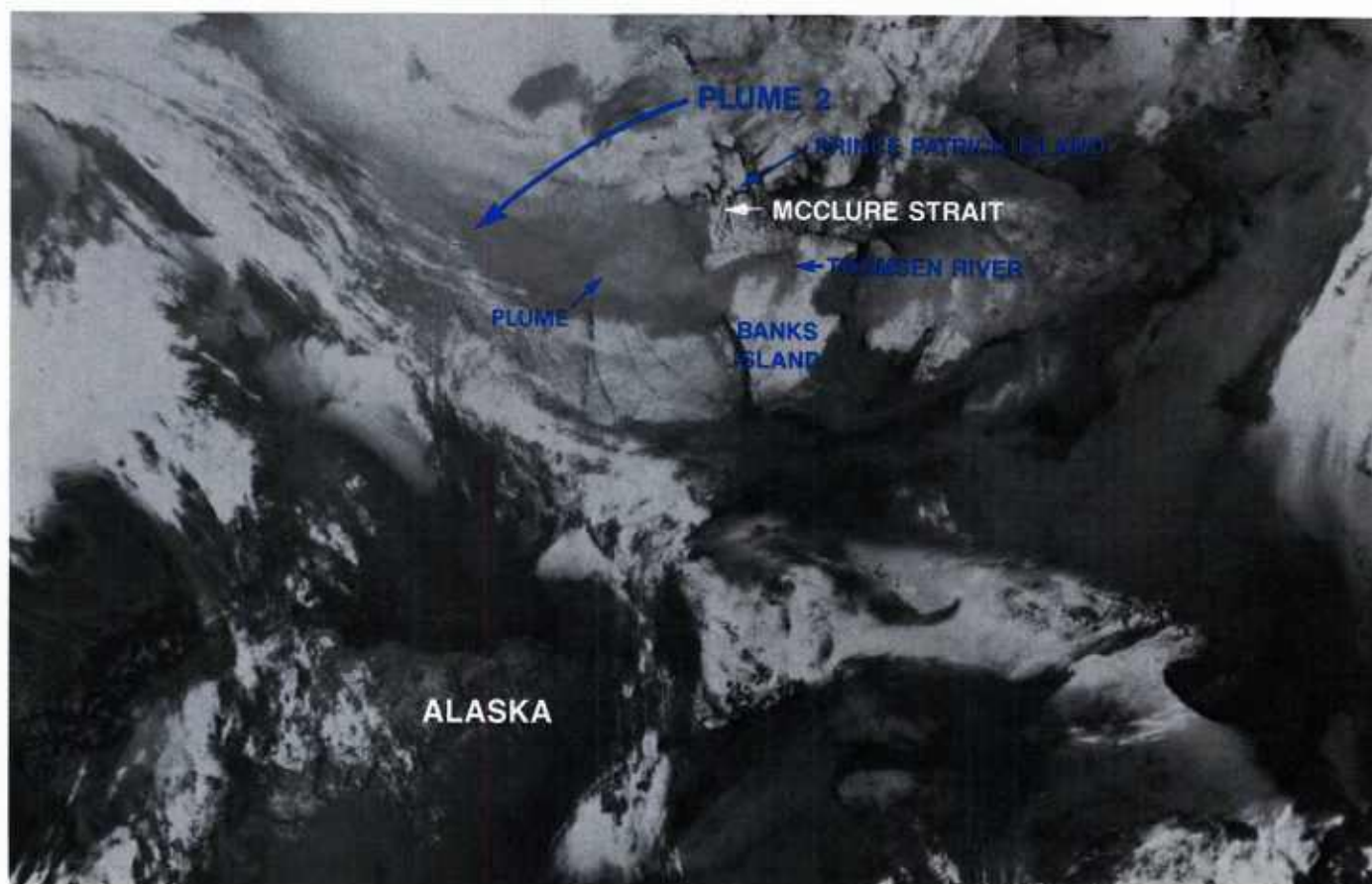
### **Important Conclusions**

1. The shoreline lead in the Beaufort Sea near Prince Patrick and Banks Islands, and the Cape Bathurst Polynya south of Banks Island, is an important source of aerosols, low cloudiness, fog, and snowfall along the north coast of Alaska and over the Beaufort Sea.
2. Aerosols, fog, and low cloudiness effects produced in the open water areas near Banks and Prince Patrick Islands can spread for several thousand miles over the ice cap, given favorable advective conditions and a stable boundary layer.
3. Optimum conditions for such effects include a high center over the central Arctic with ridgeline extending southeastward toward the Canadian Archipelago and passing near the northern portion of Banks Island, with low pressure over Baffin Bay. Under such circumstances a strong pressure gradient over the region gives moderate northerly flow and cold, dry air advection into the region of numerous leads and polynyi of the central Canadian Archipelago.
4. Although not discussed, it can be seen in Fig. 3A-7a that continuous snowfall is reported over much of the central Canadian Archipelago. Almost universally the snow is from an overcast deck of stratocumulus with bases in the 300–600 m range, similar to that produced from the Cape Bathurst Polynya. The suggestion is that much of the snowfall in this entire region can be attributed to the air/sea interaction effects over leads and polynyi.

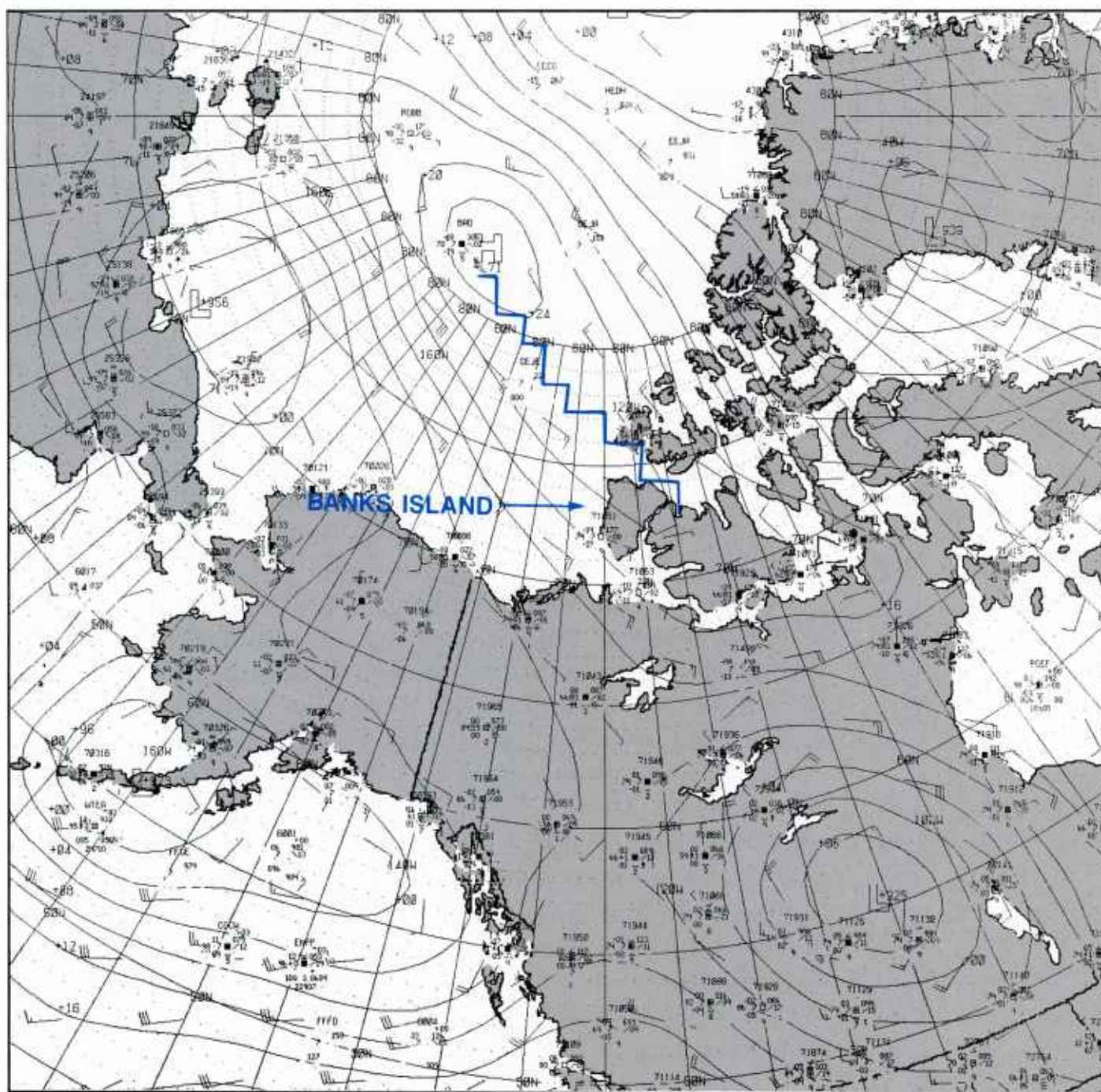




3A-6a DMSP infrared (TS) data. 12 October 1985, 1400 GMT.



3A-6b NOAA-8 infrared (Ch 4) data. 12 October 1985, 1802 GMT.



3A-7a FNO surface analysis. 12 October 1985, 1200 GMT.

#### References

- Badgley, F.I., 1966: Heat budget at the surface of the Arctic Ocean, in *Proceedings of the Symposium on the Arctic Heat Budget and Atmosphere Circulation*, edited by J.O. Fletcher, pp. 267-277, Rm 5233, NSF, Rand Corp., Santa Monica.
- Maykut, G.A., 1978: Energy exchange over young sea ice in the central Arctic, *J. Geophys. Res.*, **83**, No. C7, 3646-3658.
- Müller, F., A. Okamura, and R. Braithwaite, 1973: *Geograph Helvet.*, **2**, 111-117.
- , North Water Project, 1979: Prog. Rep. VI, Swiss Fed. Inst. of Tech., Zurich.
- Topman, D.R., R.G. Perkins, S.D. Smith, R.J. Anderson, and G. Denhartog, 1983: Polynyas in the Canadian Archipelago, 1, Introduction and Oceanography, *J. of Geophys. Res.*, **88**, No. C5, 2888-2899.
- Smith, M., and B. Rigby, 1981: Distribution of polynyas in the Canadian Arctic, Oceans. paper 45, Can. Wildlife Serv., Environment Canada.

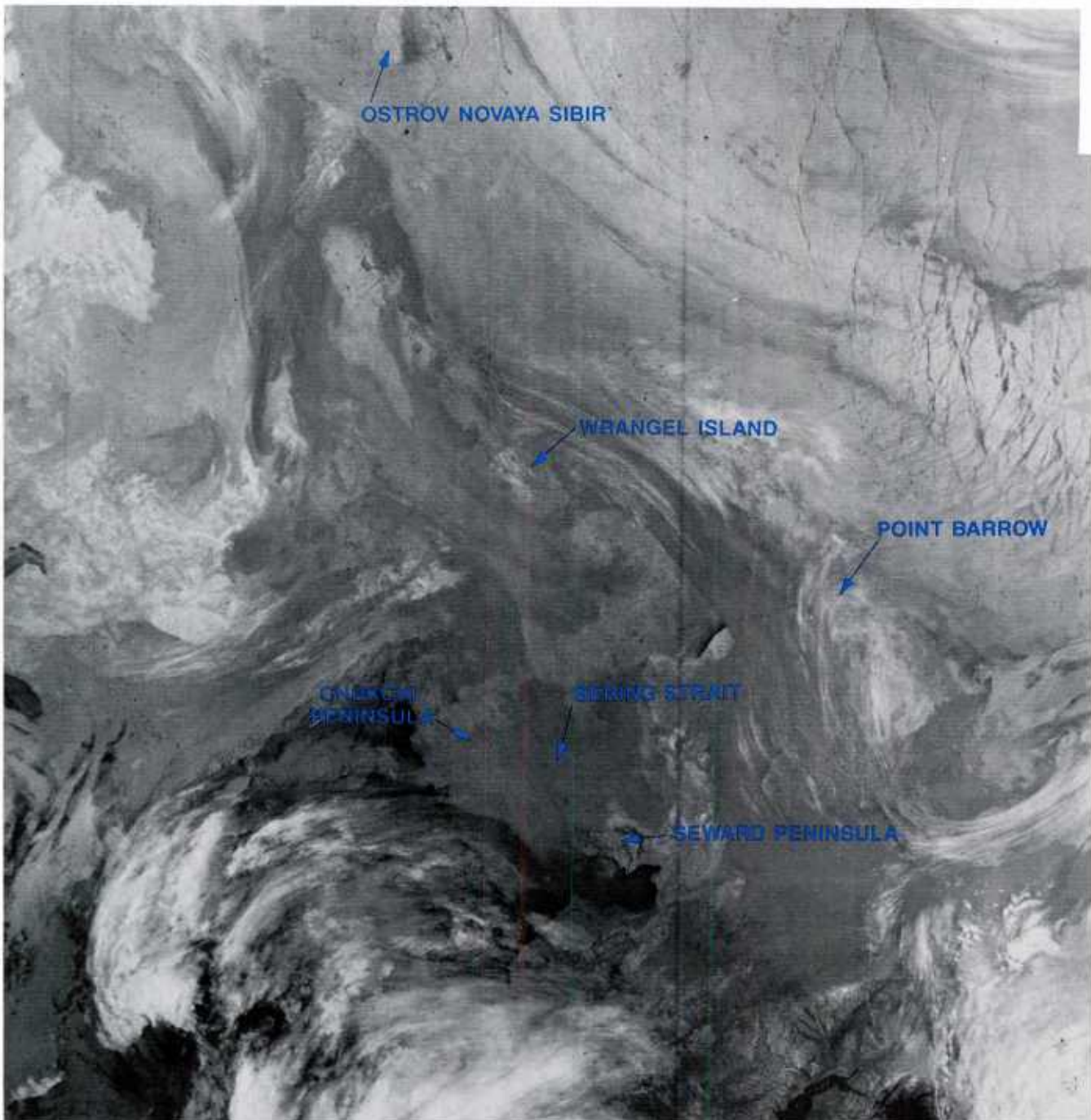


## Case 2 Low-Level Wind Direction Determination From Lead Effects

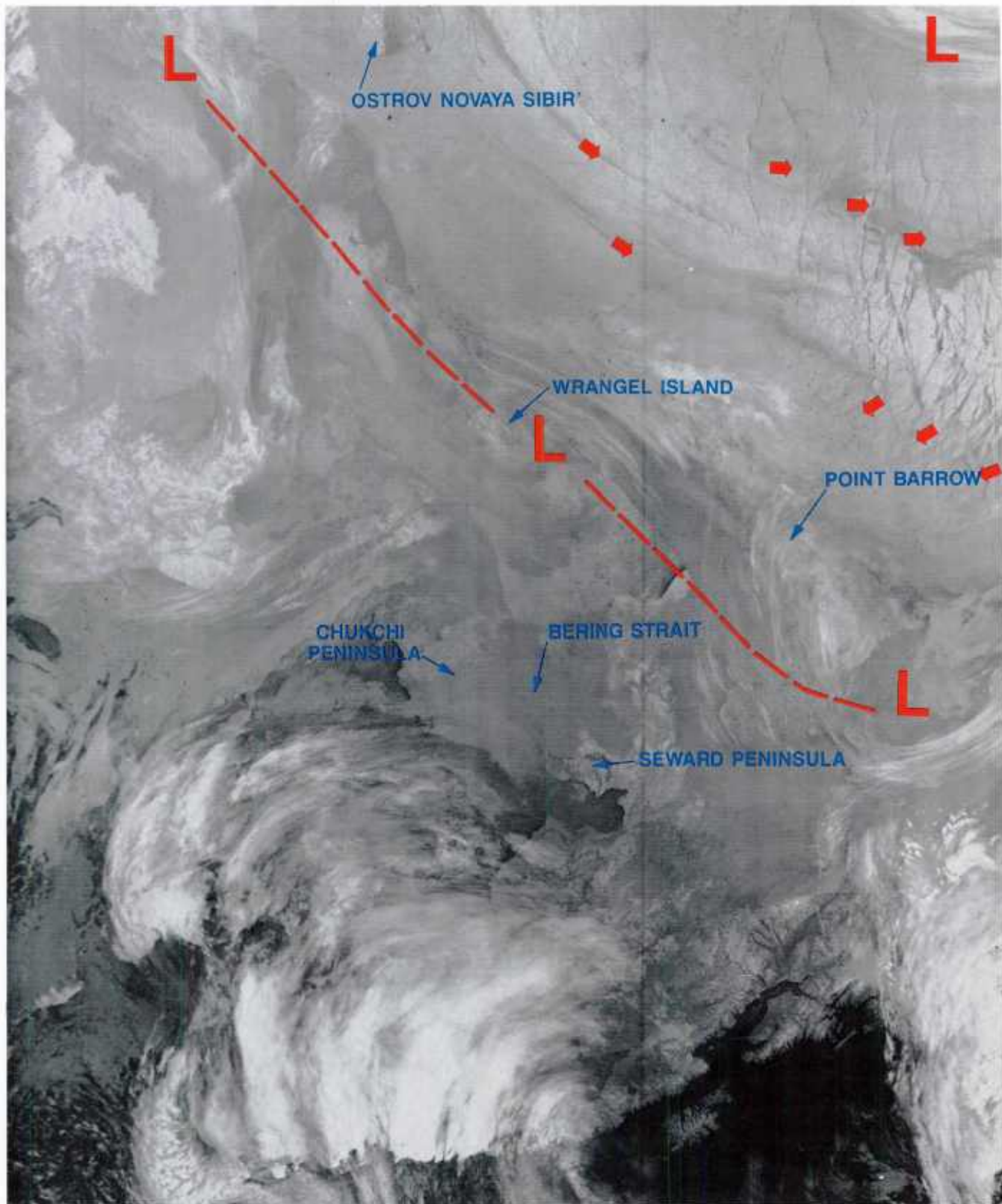
10 February 1983

DMSP infrared data acquired at 0022 GMT (Fig. 3A-8) show cloud features over the East Siberian/Chukchi/Beaufort Sea regions.

A low pressure system is implied to the north and a number of cyclone vortices are suggested, stretching E-W from right center to the upper left corner of the image. A number of low-level cloud plumes are apparent emanating from open leads in the ice cap. The cloud plumes appear warm because they are low-level and capped by the strong inversion normally existing over the ice pack.



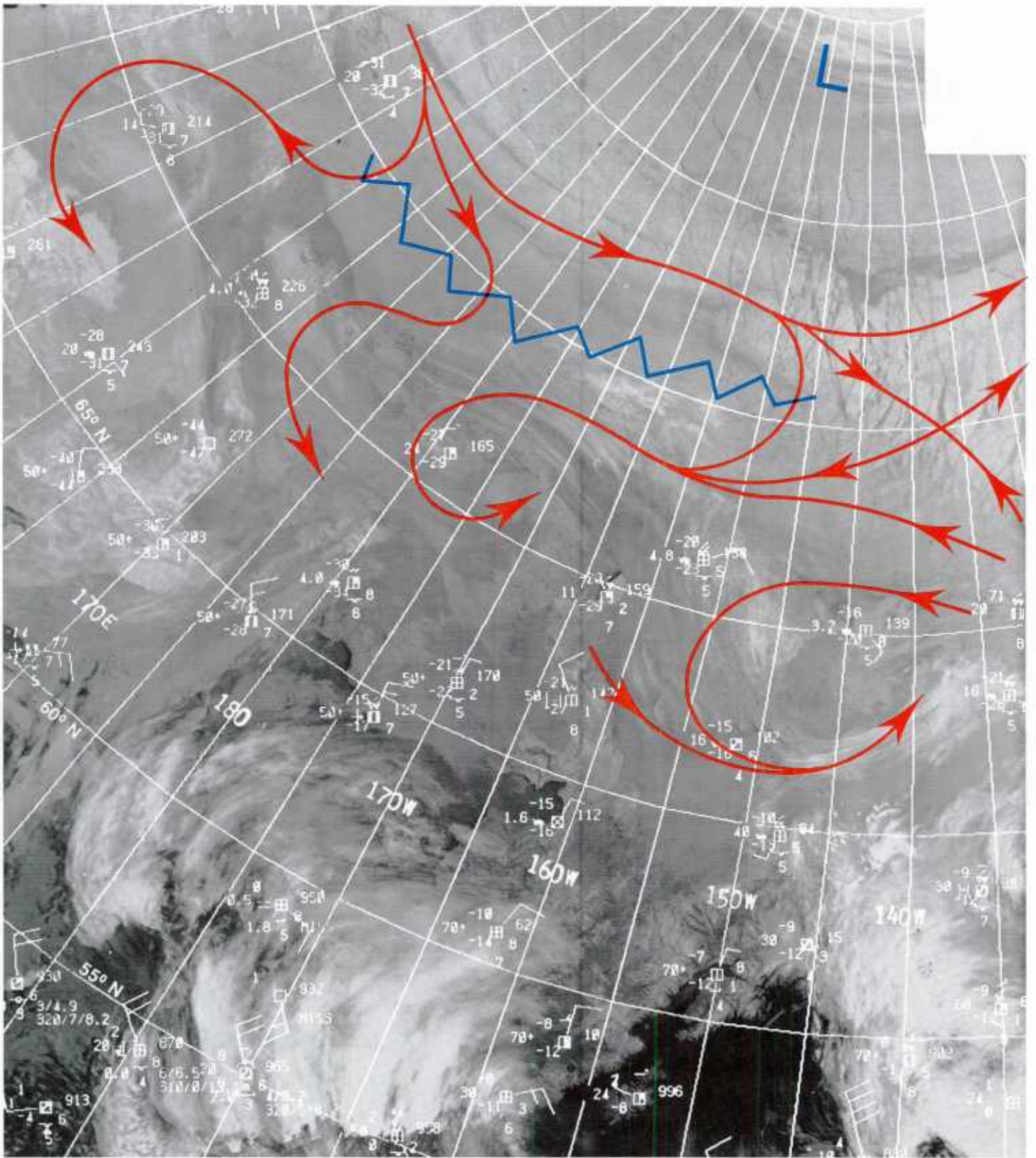
3A-8 DMSP infrared (TS) data. 10 February 1983, 0022 GMT.



3A-9 Annotations including arrows suggesting direction of low level flow and trough line (dashed line) position for Fig. 3A-8.

Figure 3A-9 is an overlay to the image pointing out some of these features and other geographical features of the area. Direction of low-level wind flow is inferred from the cloud plumes having leads as their source of moisture. A trough would be anticipated connecting low centers, which would imply that a narrow ridge existed on the north side of the trough line.

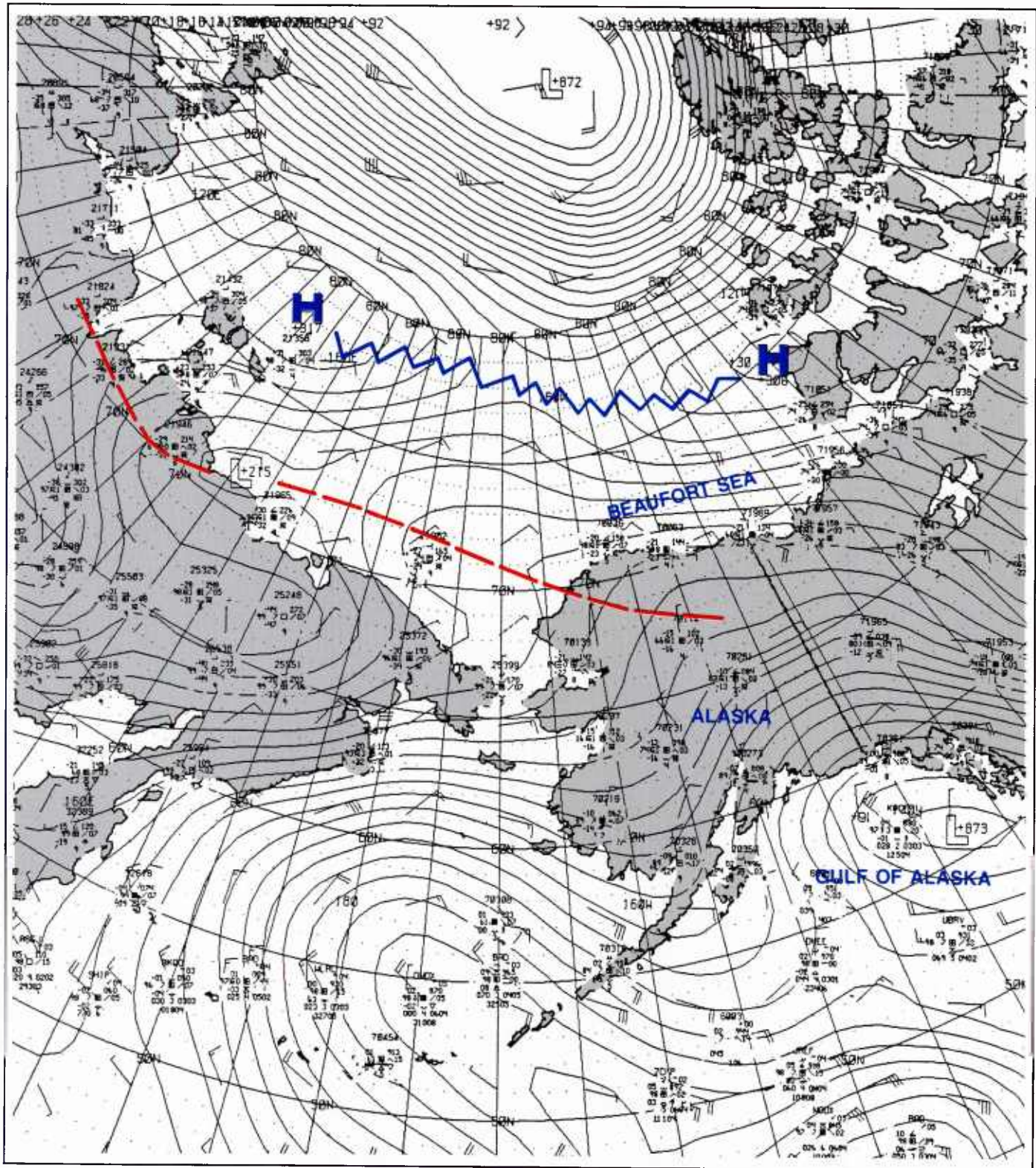




3A-10 Additional overlay for Fig. 3A-8 showing surface observations and hand-drawn streamline analysis.

Figure 3A-10 is an overlay with superimposed grid, surface reports, and streamlines, to add additional detail, which is scant over the ice cap.





3A-11 FNOC surface analysis. 10 February 1983, 0000 GMT.

The results of this hand-analysis compare quite well with the FNOC surface analysis on 10 February at 0000 GMT (Fig. 3A-11). The main discrepancy seems to be in the position of the ridge line, which is analyzed further north on the FNOC analysis. Since there are no observations to confirm this position it seems quite likely to assume that the hand-analysis is more accurate. More important, however, the exercise shows that quite a good analysis could have been derived by using the satellite data alone.



### *Case 3 Low-Level Inversion Effects in the Arctic*

The strong low level Arctic inversion of winter, often ground based, performs a number of useful functions that aid in the analysis of satellite infrared data. Low clouds trapped below the inversion radiate long-wave radiation reflecting the higher temperature of the cloud's top, trapped within the inversion layer. When such cloudiness is formed as a result of cold air advection over warmer water and resulting condensation, the cloud acts as a tracer of low-level wind direction. Mountainous or hilly terrain that rises through the inversion will have its slopes warmed by higher temperatures aloft while valley areas remain cold. The infrared sensor is therefore able to discriminate between valley areas and higher terrain. High ridge lines and mountain peaks that extend well above the top of the inversion again turn cold and radiate in infrared data as cold spots or lines surrounded by areas of warmer temperatures of the lower slopes. Detection of the existence or nonexistence of such effects leads to immediate useful information concerning the low-level structure of the atmosphere.

*24 January 1983*

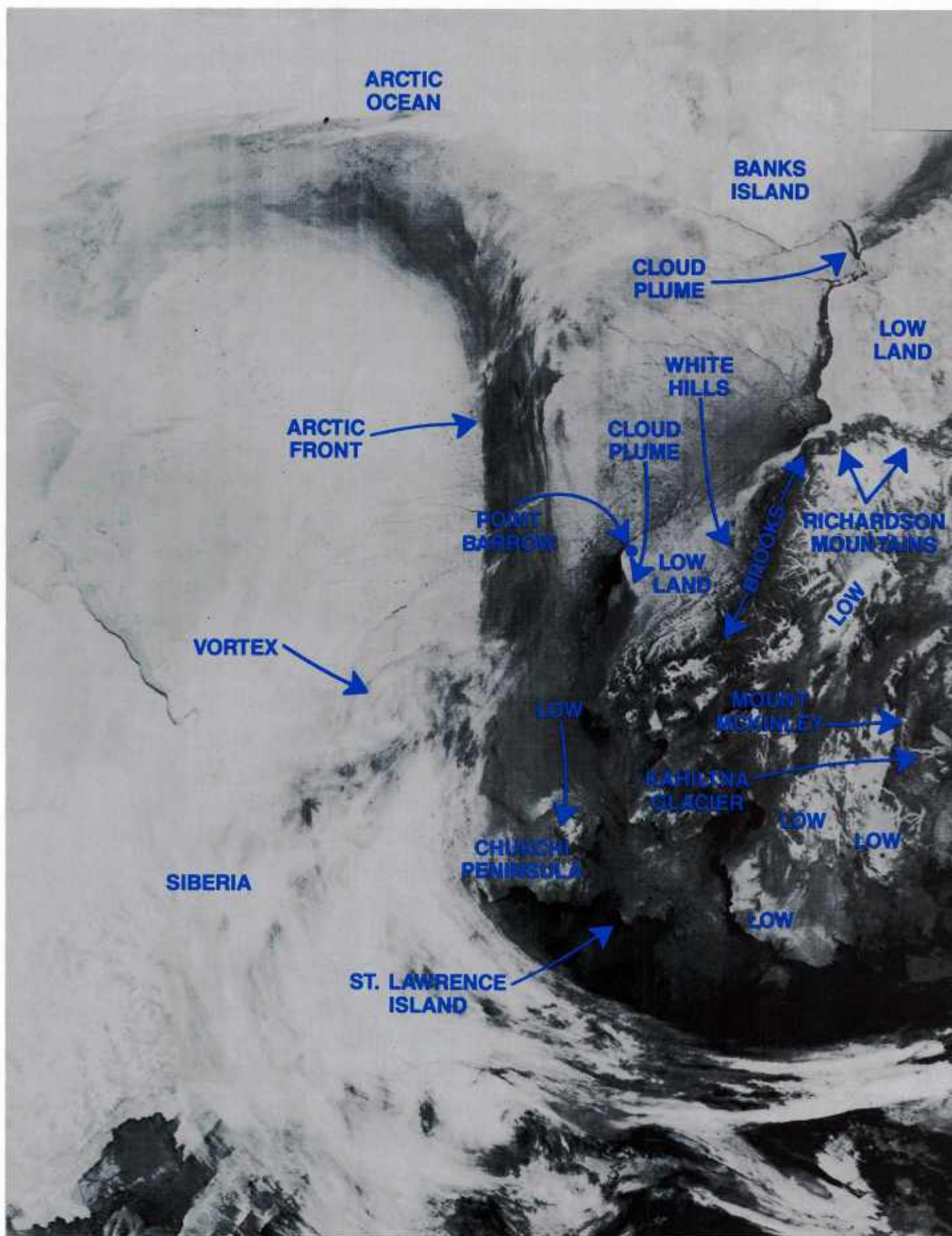
The DMSP infrared (TS) data acquired at 1545 GMT (Fig. 3A-14a) show cloud and terrain details over the Alaska - Arctic Ocean area. A gridded version of Fig. 3A-14a is shown as Fig. 3A-15a. Especially evident in the figures is the low level Arctic front which extends northeastward to an apparent low center in the Arctic Ocean, with its southern extremity near the Chukchi Peninsula of Siberia. A midlevel vortex is also seen in that region overlying Wrangel Island.

The frontal cloudiness is apparently trapped under an extremely strong low-level inversion over that region. Figure 3A-16a is the 1200 GMT sounding from Barrow, Alaska. It reveals a surface-based inversion with surface temperature of  $-26.7^{\circ}\text{C}$ . The top of the inversion is at 900 mb (near 1,000 m, or 3,200 ft) with a temperature of about  $3^{\circ}\text{C}$ , almost  $30^{\circ}$  warmer than at the surface.

The FNOC surface analysis for 1200 GMT (Fig. 3A-17a) with frontal cloud pattern superimposed suggests that the front has occurred as the result of a surge of moist air between low pressure over the New Siberian Islands and high pressure west of Wrangel Island, in the manner of a fleur-de-lis cloud formation (see Section 1B, Case 5). The front contains no severe weather but only low overcast cloudiness in a weak wind field.

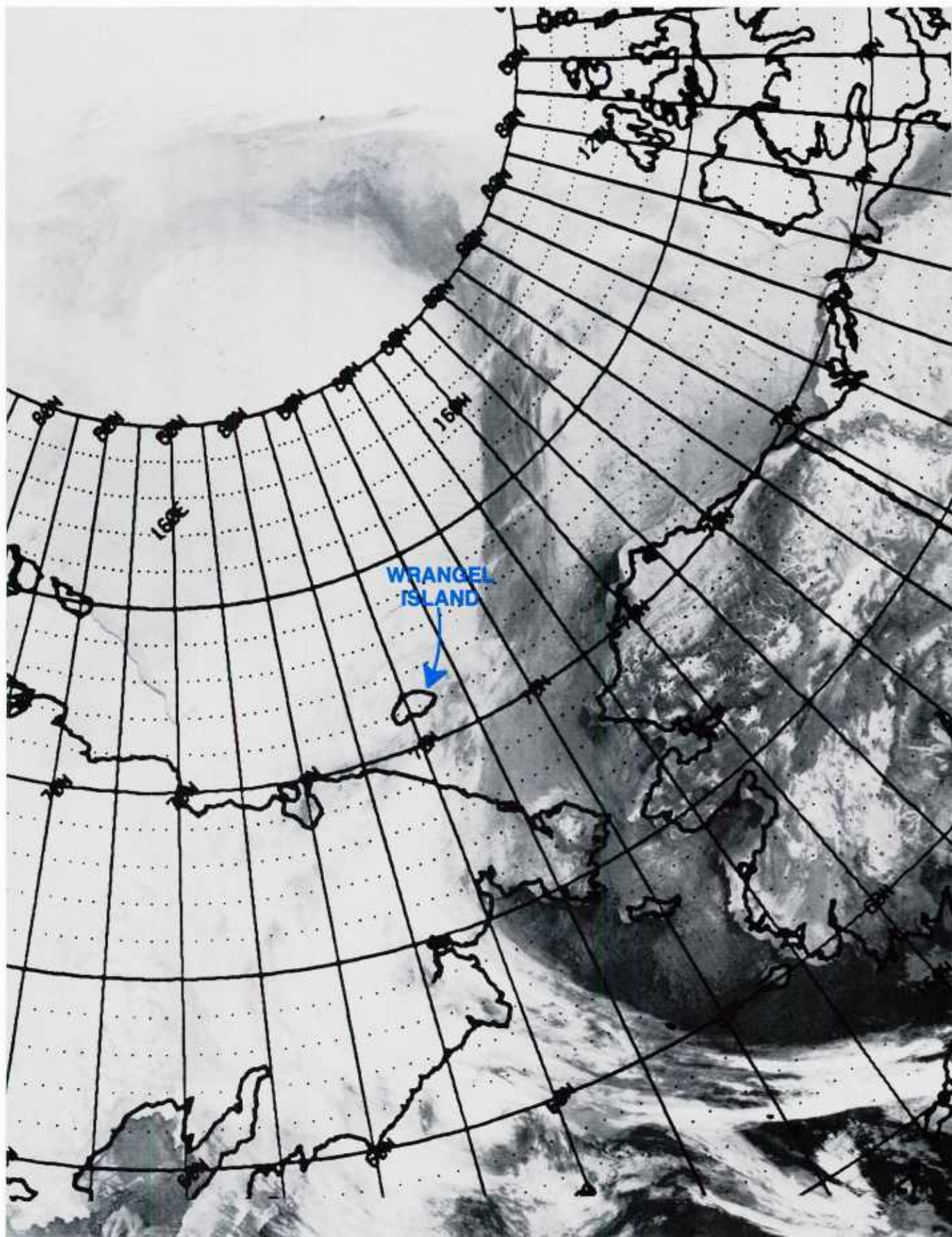
Warm cloud plumes emanating from open water regions, one south of Banks Island and the other west-southwest of Point Barrow, delineate low-level wind direction in those regions. The Banks Island (Amundson Gulf) plume indicates northwesterly flow, while the plume near Point Barrow suggests northeasterly flow. Flow from these respective directions is verified in the FNOC surface analysis (Fig. 3A-17a).





3A-14a DMSP infrared (TS) data. 1545 GMT 24 January 1983.





3A-15a DMSP infrared (TS) data. 1545 GMT 24 January 1983, with overlay.

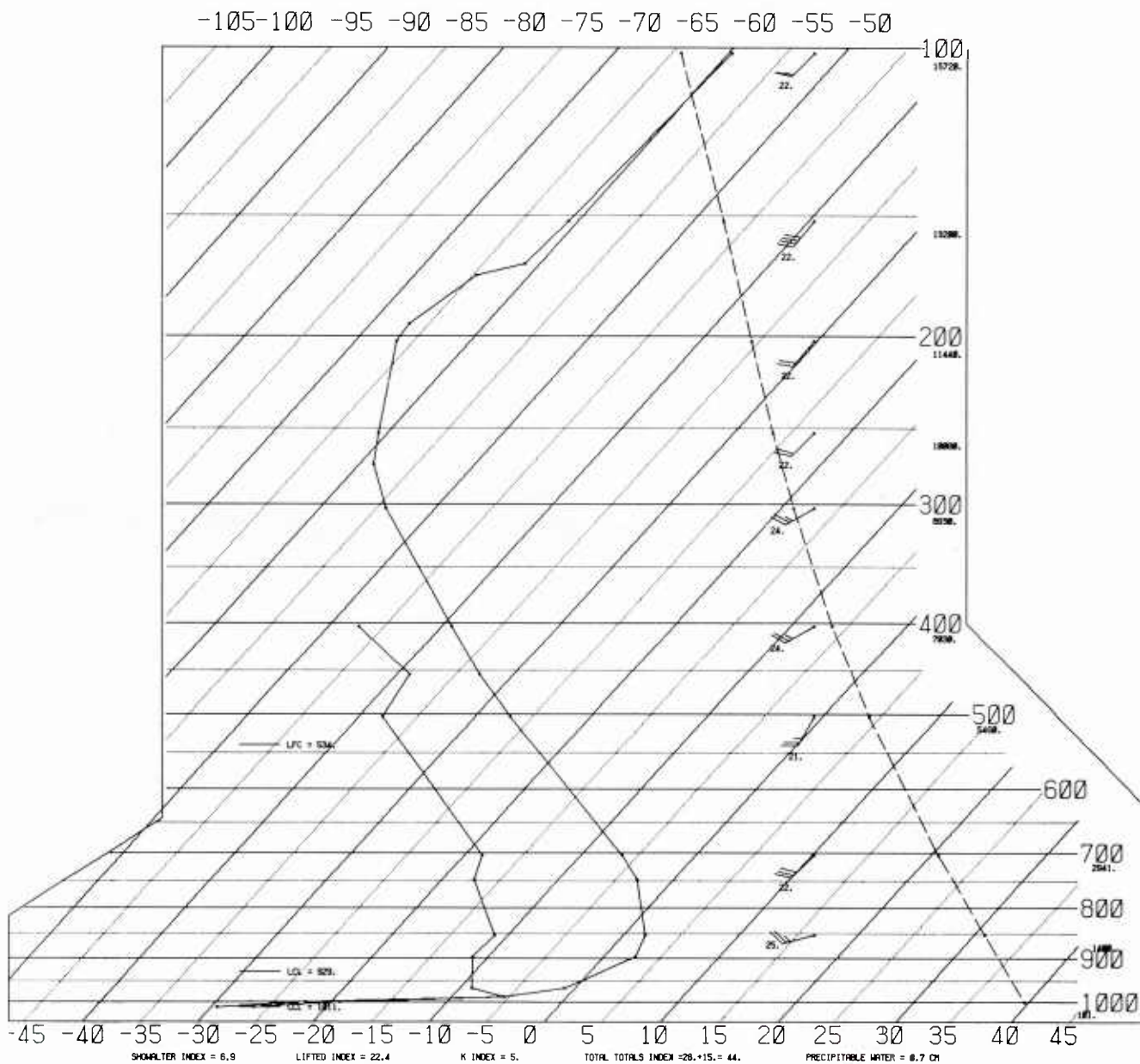


# SKEW T, LOG P DIAGRAM

830124

1200Z

70026



3A-16a Radiosonde data for Barrow, Alaska. 1200 GMT 24 January 1983.

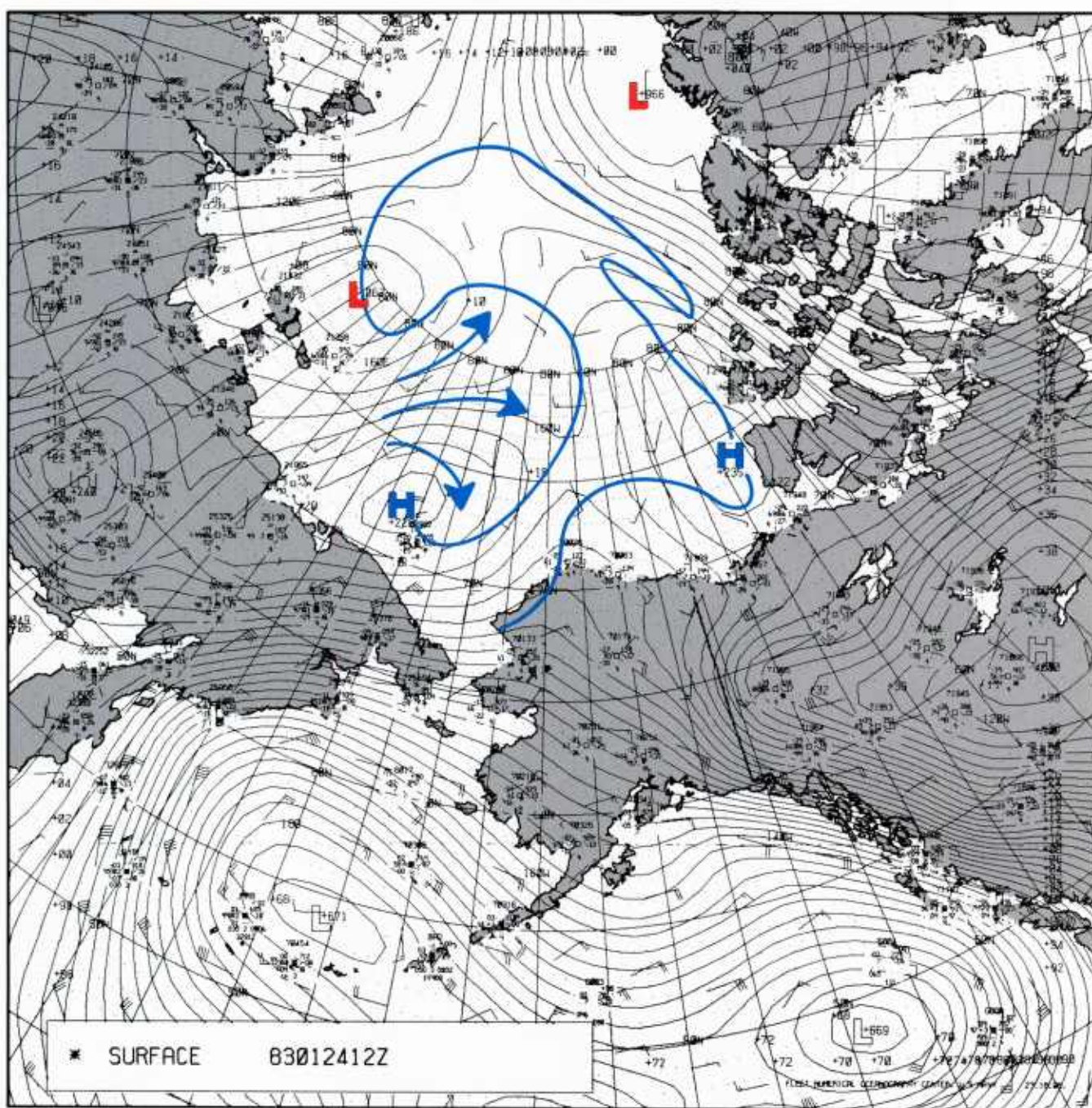
The terrain over Alaska is remarkably cloud free (note the number of perfectly clear observations on the FNOG surface analysis, Fig. 3A-17a). Nevertheless, a wide variation of temperatures is shown ranging from very cold to relatively warm. These temperature variations are largely the result of elevation differences, with low-lying terrain appearing very cold and higher elevations reflecting warming effects of the low-level temperature inversion. As an example, the low elevation areas surrounding the Mackenzie River Delta southwest of Banks Island appear quite cold, while the Richardson Mountain Range to the west (Fig. 3A-14a) is delineated as a warm temperature strip, merging into the equally warm mountain area of the Brooks Range. Cold dendritic patterns in the region are frozen river valleys flowing largely southward toward the cold Yukon River Valley, especially noticeable near 66°N 145°–150°W. To the south the snow-capped summit of Mt. McKinley is visible with a cold ridge line stretching to the southeastward flowing Kahiltna Glacier. Other cold low-lying areas such as the North Slope in the Point Barrow region are indicated in Fig. 3A-14a. One interesting feature in this region is the delineation of the White Hills, south-southeast of Deadhorse, as warm dots rising from the plains of the North Slope tundra. These hills have maximum elevation of 1,317 ft (401 m). However, the northeasternmost hill tops out at 961 ft (293 m), an indication that the inversion is strong below this altitude, a feature well illustrated by the Barrow sounding (Fig. 3A-16a).

The skilled satellite meteorologist can make excellent use of such details not only to assist meteorological interpretation but to assist in pinpoint gridding of satellite data for maximum utility in precision assessment and short-term forecasts of local weather.

### **Important Conclusions**

1. The strong low level Arctic inversion, characteristic of winter conditions, creates warming effects on terrain and low-level cloudiness, which must be understood for proper interpretation of satellite infrared data.
2. Satellite infrared data can yield useful clues relative to location of geographical features for precision gridding of such data.





3A-17a FNOC surface analysis (with cloud pattern and streamline analysis superimposed). 1200 GMT 24 January 1983.

#### *Case 4 Opening and Closing of Flaw Leads Along the Siberian and Alaskan Coastlines*

*7-14 April 1991*

The term "flaw lead" is used to describe the lead that often develops more or less parallel to the coastline and at a location that separates drift ice (or pack ice) from fast ice (sea ice that has formed along and become attached to the shore). The flaw lead has a tendency to develop when winds of moderate speed blow offshore over a period of several hours. The flaw lead closes or fails to develop when winds blow onshore. The opening and closing of flaw leads is of great importance to Eskimos and predators who regularly exploit such features as prolific hunting grounds (Nelson, 1969) and to sea mammals who use such features as conduits to the open ocean water. Development of such leads is also of more than casual interest to oil rigs, often located in vulnerable areas where they become exposed to the crushing effects of ice movement. In some regions flaw leads are often located adjacent to facilities of strategic or economic importance. From a meteorological standpoint development of such leads can promote significant heat and moisture flux leading to the development of dense, low overcast cloudiness as a result of air-sea interaction effects. Nelson (1969) notes that steam fog over a lead develops when the air temperature is 14°F or more colder than the sea surface temperature. During the winter months when the air temperature is 30° to 40° below zero, visibility may be reduced to only 50 to 100 ft over the lead. This study concerns flaw lead development in the Alaskan and Siberian coastal region during the pilot Leads Experiment (LEADEx) in April 1991, when an ice camp was occupied during much of that time in the Beaufort Sea and the opportunity existed to photograph and document the appearance of some of the flaw lead features.



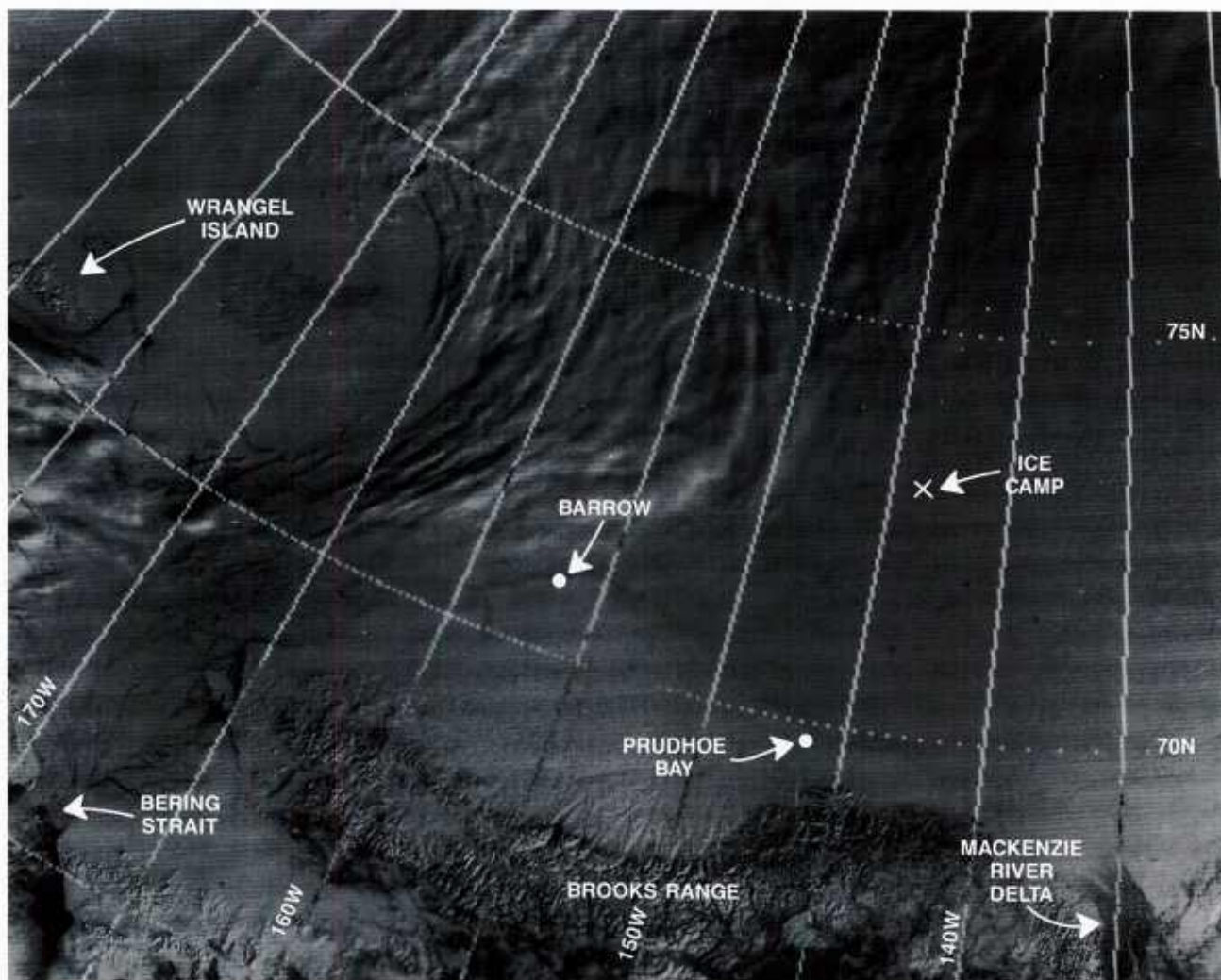
*7 April 1991*

The DMSP visual (LF) data received at 1756 GMT (Fig. 3A-20a) show the North Slope region of Alaska stretching westward toward Wrangel Island. An Arctic front and cloud vortex are apparent in this image with the front approaching Barrow, Alaska. It is difficult but not impossible to discern the North Slope coastline, which is made subtly apparent by a slight change in surface albedo, in a comparison of the ice of the Beaufort Sea to the snow-covered tundra of the North Slope. Different roughness characteristics are responsible for the surface albedo change, an example of which can be seen in the aircraft photo of Prudhoe Bay (Fig. 3A-20b).

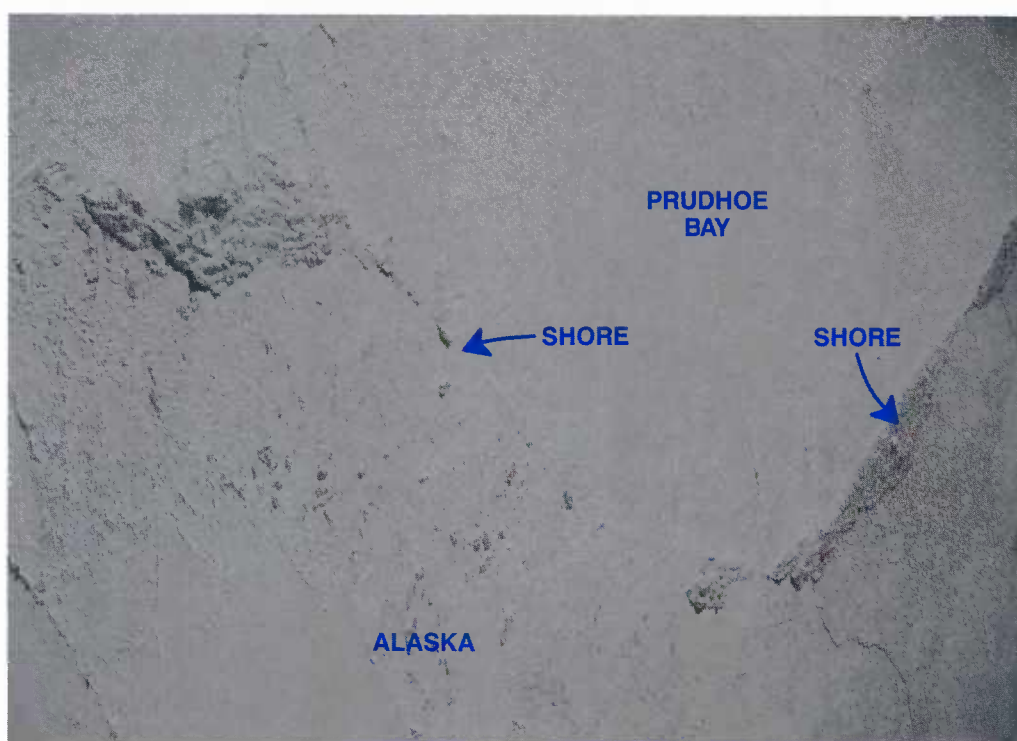
In the satellite image (Fig. 3A-20a) the albedo of the ice is slightly less than that of the snow and ice-covered terrain. At low sun angles, the flatter surface of the ice reflects more of the Sun's rays away from the satellite sensor, causing the reduction in reflectivity as sensed by the satellite. Crushed ice visible along the shoreline in the aircraft photo (Fig. 3A-20b) and other terrain roughness features apparent over the land act to scatter more light back to the spacecraft sensor. The effect is similar to that noted over a water area. When seas are perfectly calm (flat) away from the Primary Specular Point (PSP) (see NTAG Vol. 1, Section 2: Fett and Mitchell, 1977), so that the Sun's rays are reflected away from the satellite, the area appears dark or black in satellite visible imagery. Rough seas in the same region have the effect of making the area appear brighter due to reflection of some of the Sun's rays back to the satellite from facets of capillary waves in the region. This difference (ice darker than snow-covered land) is not so apparent from the aircraft photo. In fact the effect seems to be reversed, with the ice over Prudhoe Bay appearing slightly lighter than the snow-covered terrain of northern Alaska. The reason for this apparent contradiction is that for an observer in an aircraft in the lower atmosphere, the sensed albedo of a surface is not strictly a function of the intensity of direct reflected solar reflection from the surface. The roughness features responsible for reflecting more light to the satellite than to a flat surface divert light from the perspective of the aircraft observer and cause shadow effects, which makes the rough area appear darker. At the same time diffuse scattering effects from the atmosphere back to the surface of the Earth serve to highlight the brightness of the flat snow-covered region.

Some faint signs of leads are evident over the Beaufort Sea in the satellite image (Fig. 3A-20a), but none are pronounced except the flaw lead extending northeast and southwest of Barrow. The lead southwest of Barrow is hunted extensively by the Eskimos residing near Wainwright (Nelson, 1969).

The National Weather Service (NWS) surface analysis prepared at Fairbanks for 7 April 1991 at 1800 GMT is shown in Fig. 3A-21a. The analysis captures the Arctic front very well and indicates southerly winds at Barrow, in advance of the system. It is these winds that may have led to the short flaw lead segment evident northeast of Barrow. Onshore flow southwest of Barrow behind the front would tend to close the flaw lead in that region (Fig. 3A-20a).

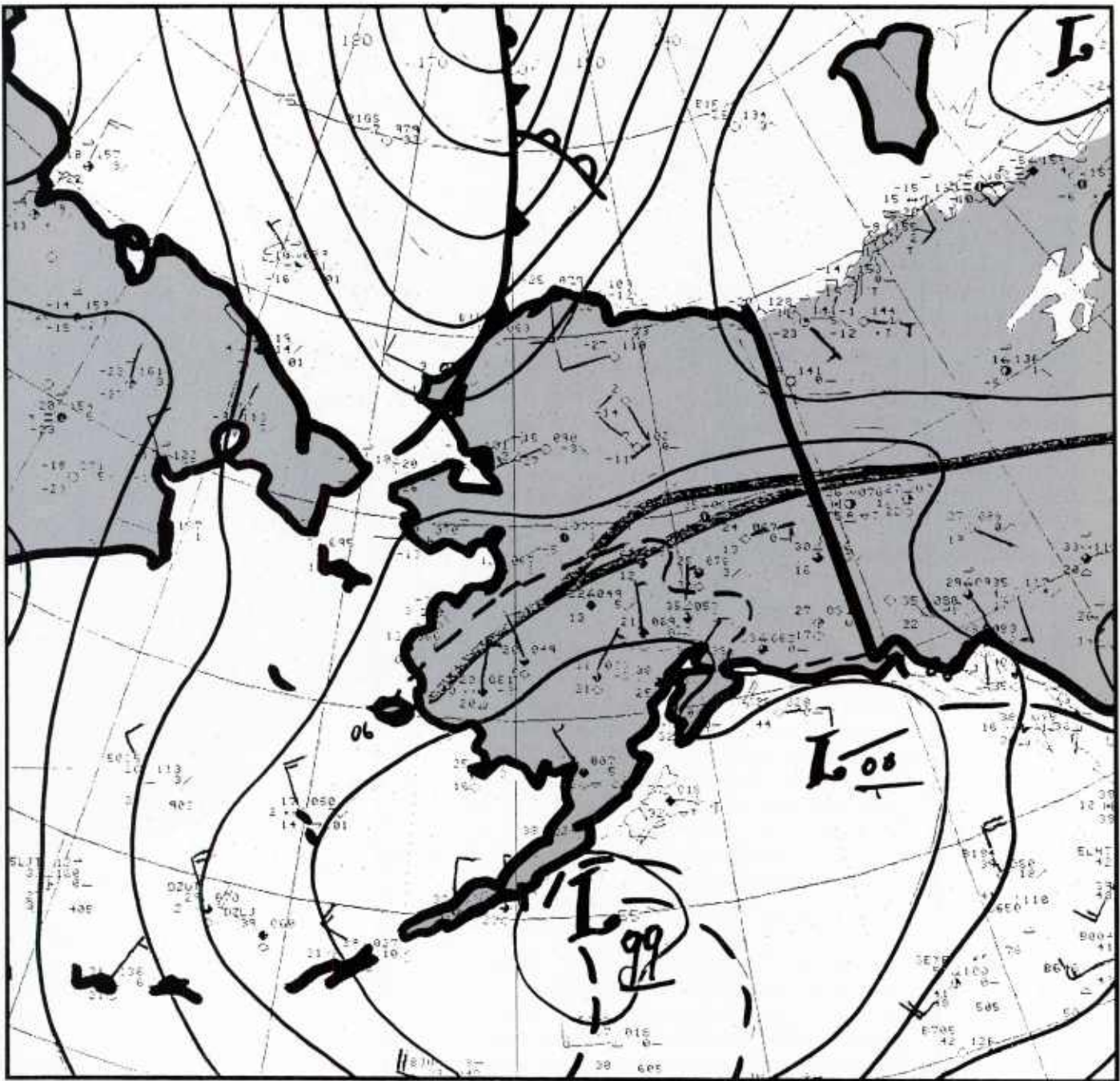


3A-20a DMSP visible (LF) data. 1756 GMT, 7 April 1991.



3A-20b A 35-mm color image of the Prudhoe Bay area. 13 April 1991.





3A-21a Fairbanks, Alaska NWS surface analysis. 1800 GMT, 7 April 1991.

*8 April 1991*

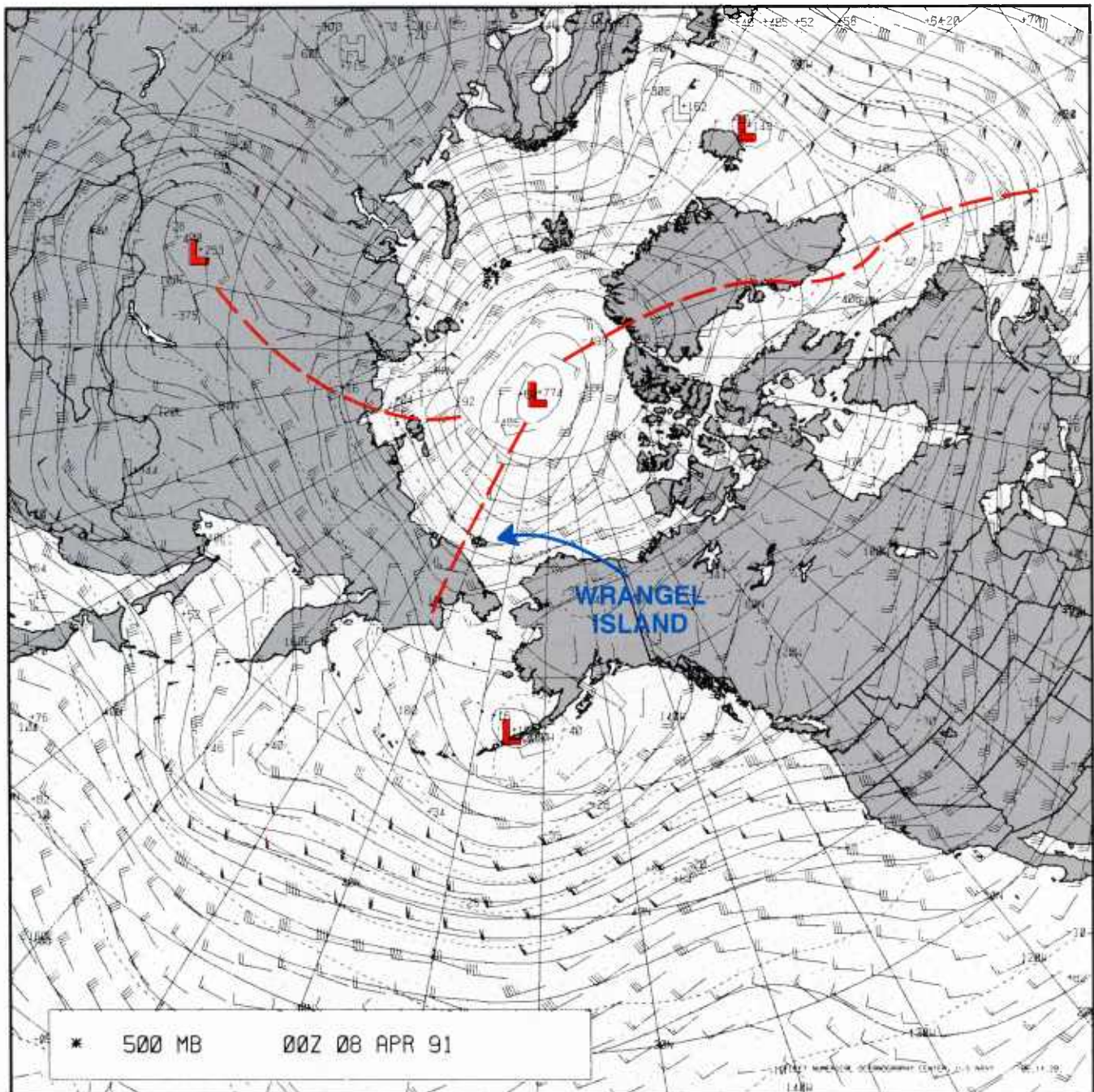
The 500-mb analysis for 8 April 1991 at 0000 GMT (Fig. 3A-22a) shows the circumpolar vortex over the central Arctic Ocean at this time. Major troughs extend from the vortex in association with frontal systems near those locations. For example the trough located near Wrangel Island is associated with the Arctic front shown in Fig. 3A-20a. The DMSP visible (LF) data on 8 April at 1734 GMT are shown in Fig. 3A-23a. The front at this time (roughly 24 hr after the preceding view) has moved westward toward Banks Island and is out of the view of this image. A narrow flaw lead is apparent paralleling the Siberian coastline southeast of Wrangel Island. The lead near Barrow is still evident with no obvious major change. Some evidence of leads over the Beaufort Sea are apparent as are some minor indications of the Barrow flaw lead extending eastward. Note again in this visible image the contrast between the darker appearing ice and the lighter appearing snow-covered North Slope.

Some additional Arctic Ocean features in the satellite image are of special interest. Katie's floeberg (named after the University of Alaska's librarian, Mrs. Katherine [Katie] Martz, who brought the feature to the attention of the university's scientific staff) (Kovacs, Gow, and Dehn, 1975), is evident as are Ostrov Herald and Herald's Reef. Each of these features, as well as Wrangel Island, shows evidence of the eastward movement of the Arctic drift ice through the development of areas of open water (polynya) on their sides. The flow of ice indicated by these data is counter to the normal anticyclonic westward drift of ice normally found (Sechrist et al., 1989) and is an indication of the anomalous prevailing westerly winds blowing over much of the region. An enlarged enhancement of simultaneous infrared (TS) data (Fig. 3A-24a) provides a more detailed view of the Alaskan area. The view shows clearly the polynya on the east side of Katie's floeberg and the sharp delineation of the flaw lead near Barrow and Wainwright. Many small leads extend from the region of Katie's floeberg, which acts as a "stress concentration," causing fractures in the ice east and west of its location (Stringer and Barrett, 1975). This infrared view also demonstrates clearly how the colder frozen land in wintertime can be distinguished from the warmer temperature of shorefast ice, permitting the delineation of such features as Dease Inlet, Teshekpuk Lake, Harrison Bay, and the Kuk River near Wainwright.

A larger scale view of the DMSP infrared (TS) data of Fig. 3A-24a is shown in Fig. 3A-25a. The image confirms open (warm) regions on the east side of the small features (described above) of the Chukchi and Beaufort Seas with perhaps greater clarity than the visible image (Fig. 3A-23a). Many of the valley features in mountainous terrain are evident in this image. Tracking of these features from image to image improved the accuracy of the geographical gridding of data. The Fairbanks NWS analysis for 8 April at 1800 GMT (Fig. 3A-26a) shows the frontal location, with ridging and light westerly winds evident over the North Slope. A high pressure cell has developed behind the front near Wrangel Island, producing northerly onshore flow over the Siberian or Chukotskiy Peninsula and the northwest coast of Alaska.

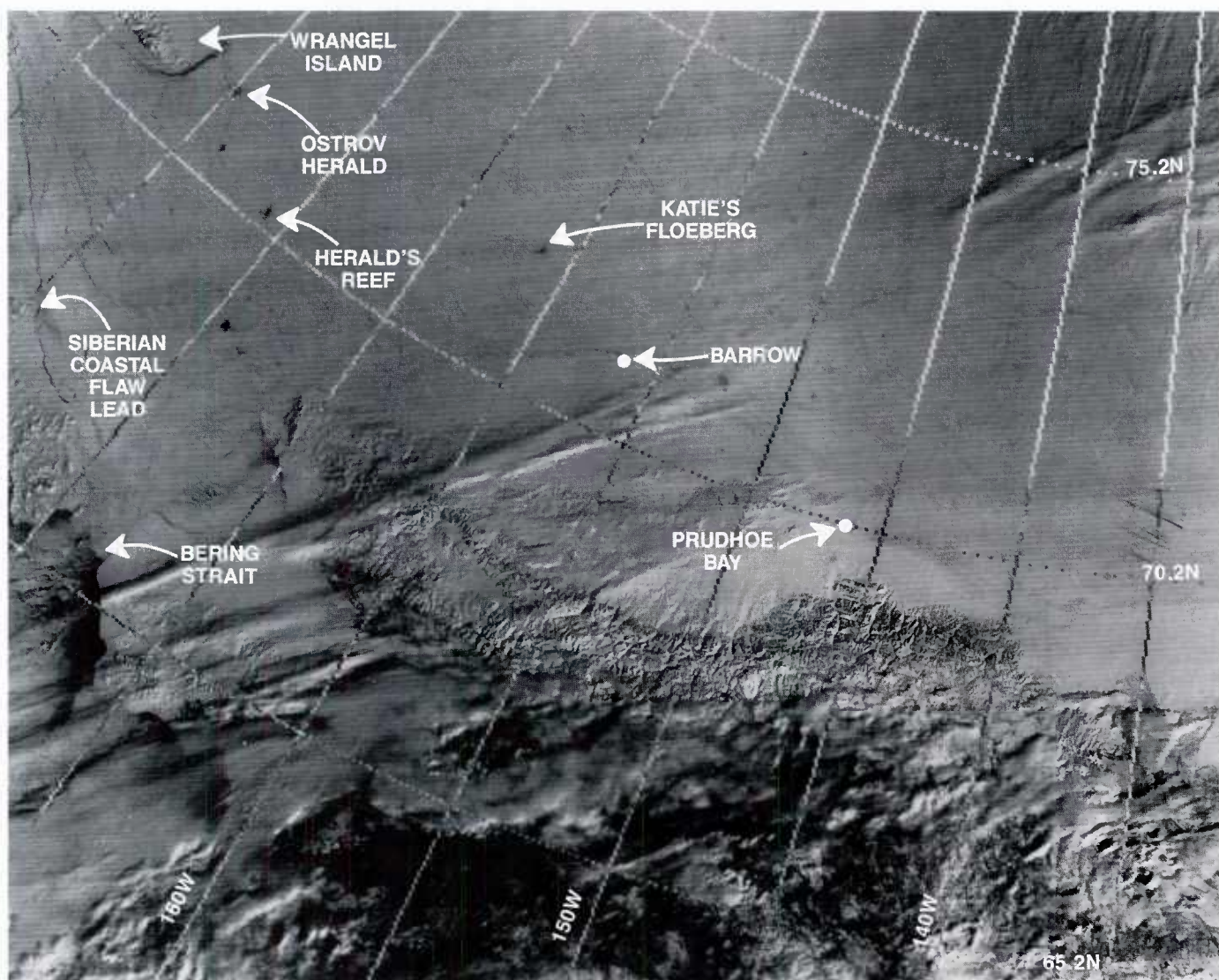
Aloft at the 500-mb level (Fig. 3A-27a), progressive eastward movement of the troughs over the East Siberian and Chukchi Seas can be noted. Strong southwesterly winds over Barrow align with the high and low cloud striations visible in the DMSP view (Fig. 3A-23a), indicating that the upper level trough lags well west of the surface frontal position.





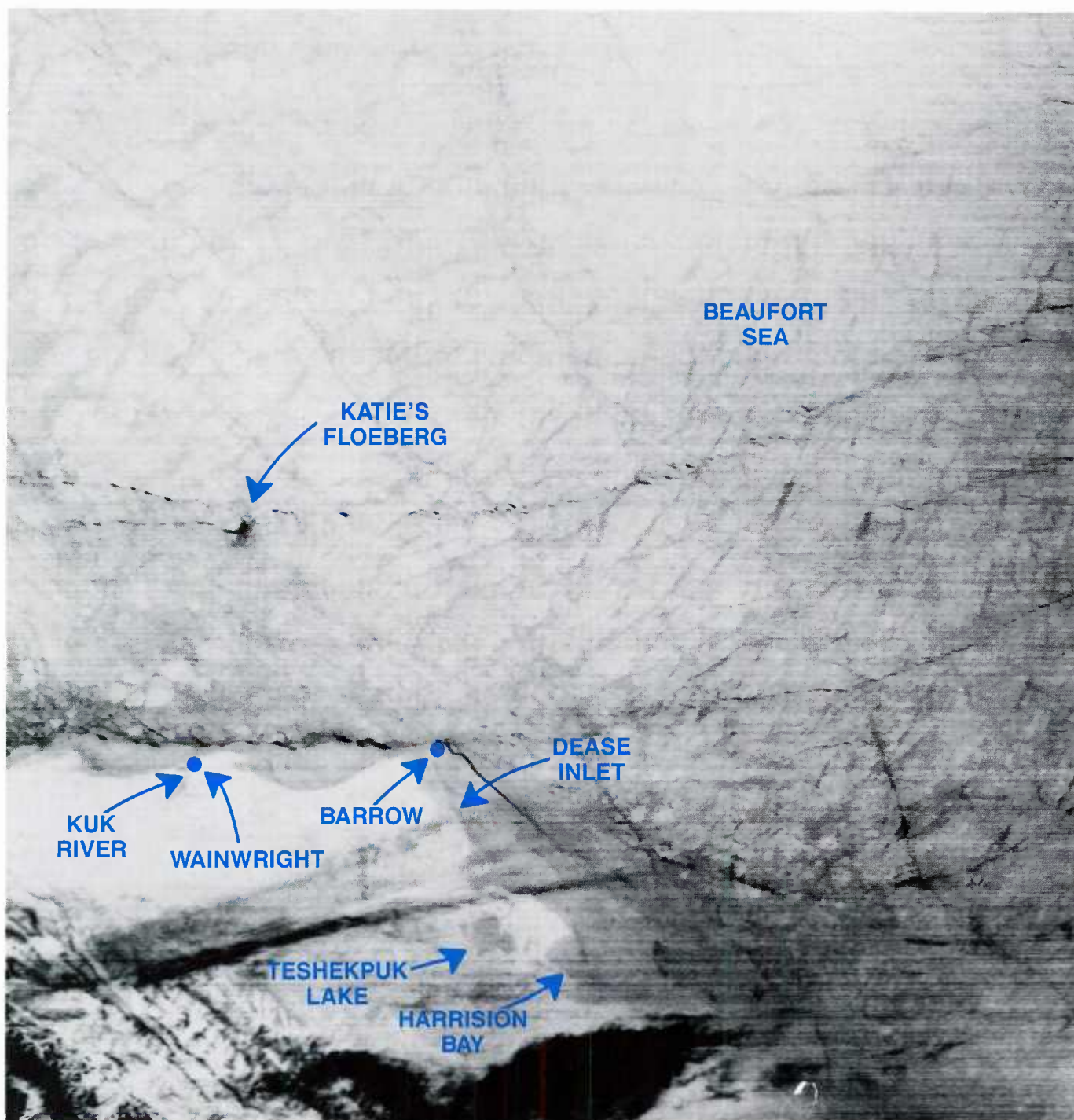
3A-22a FNOC 500-mb analysis. 0000 GMT, 8 April 1991.



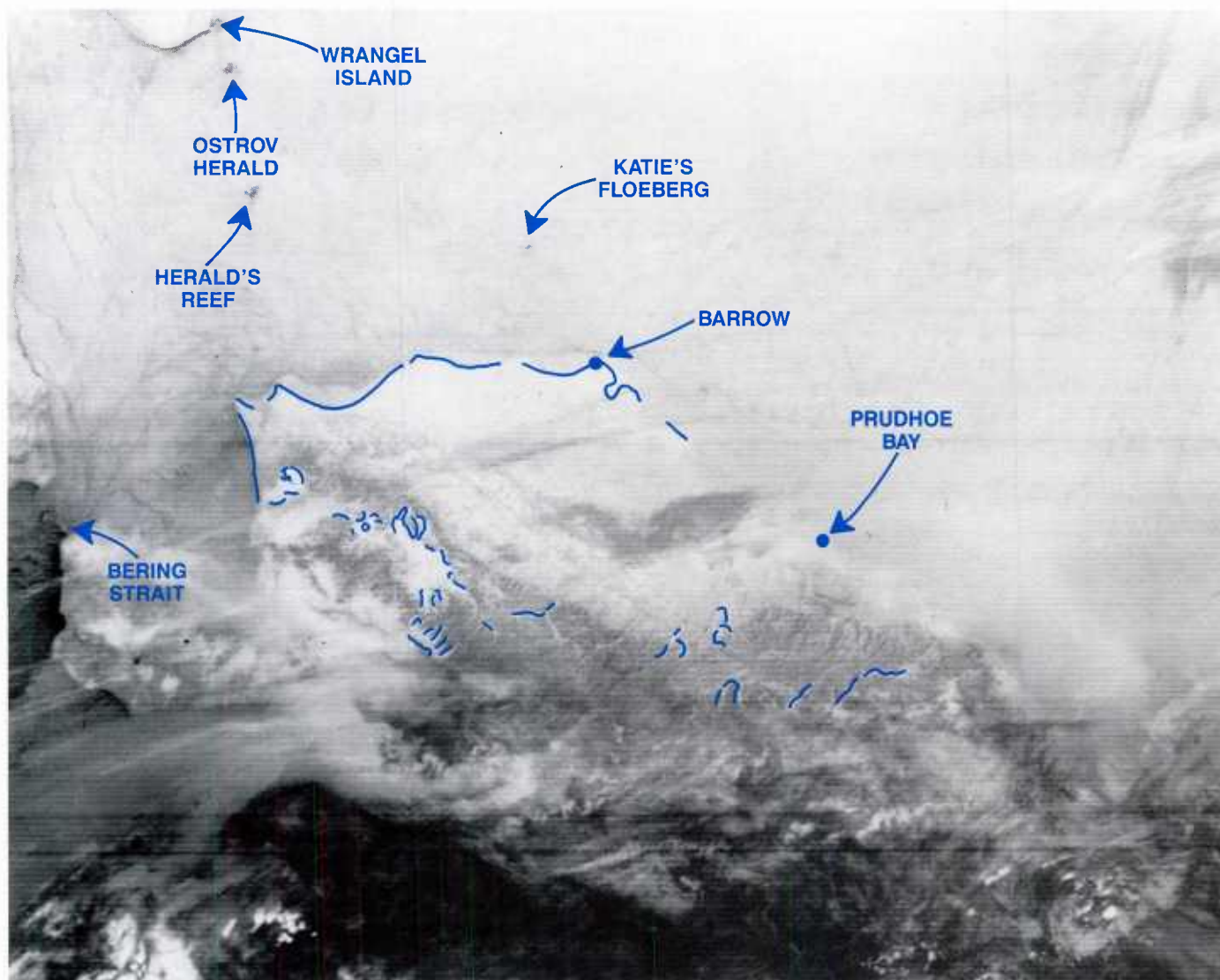


3A-23a DMSP visible (LF) data. 1734 GMT, 8 April 1991.



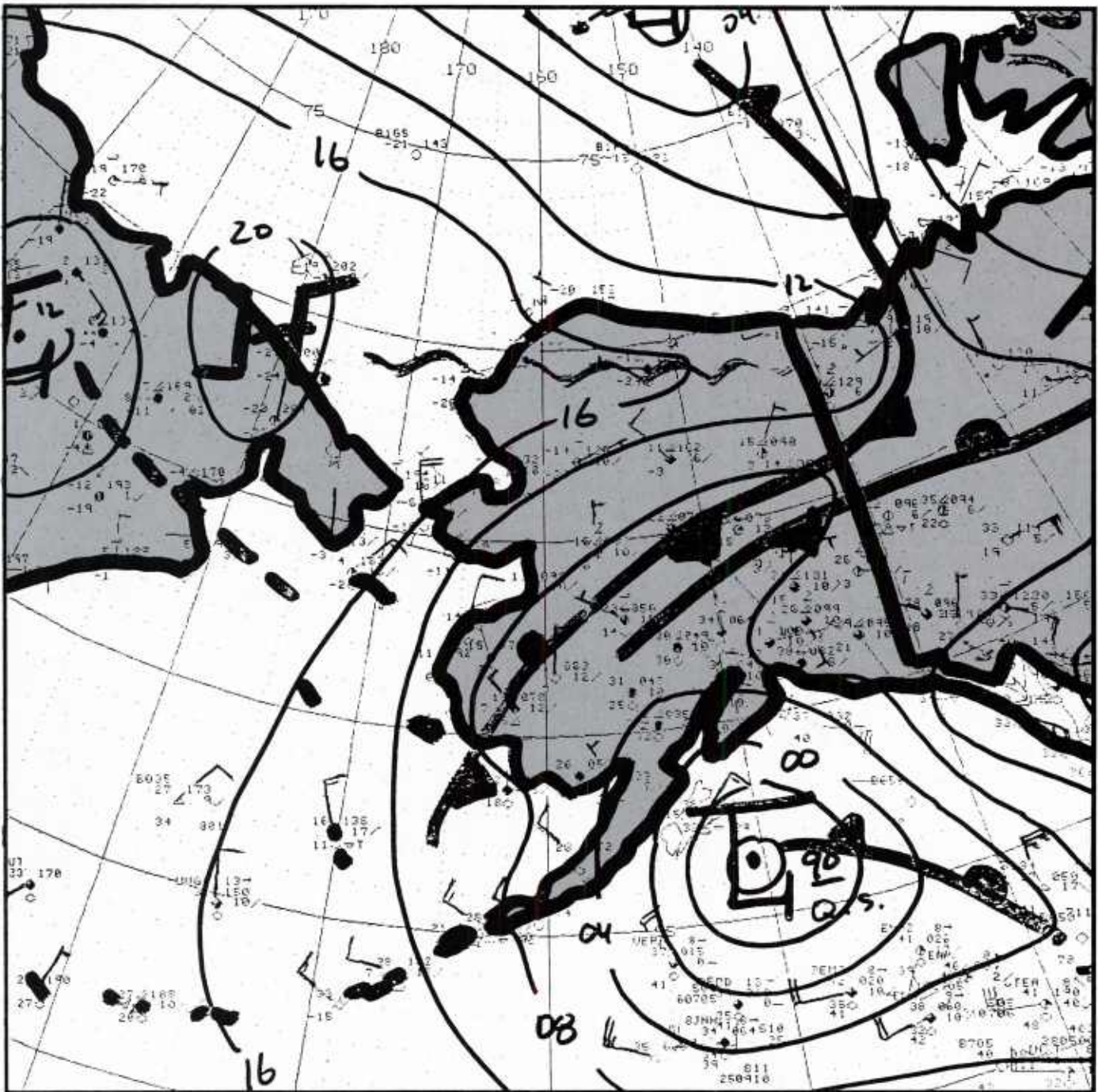


3A-24a Enlarged (X4) DMSP infrared (TS) data. 1734 GMT, 8 April 1991.



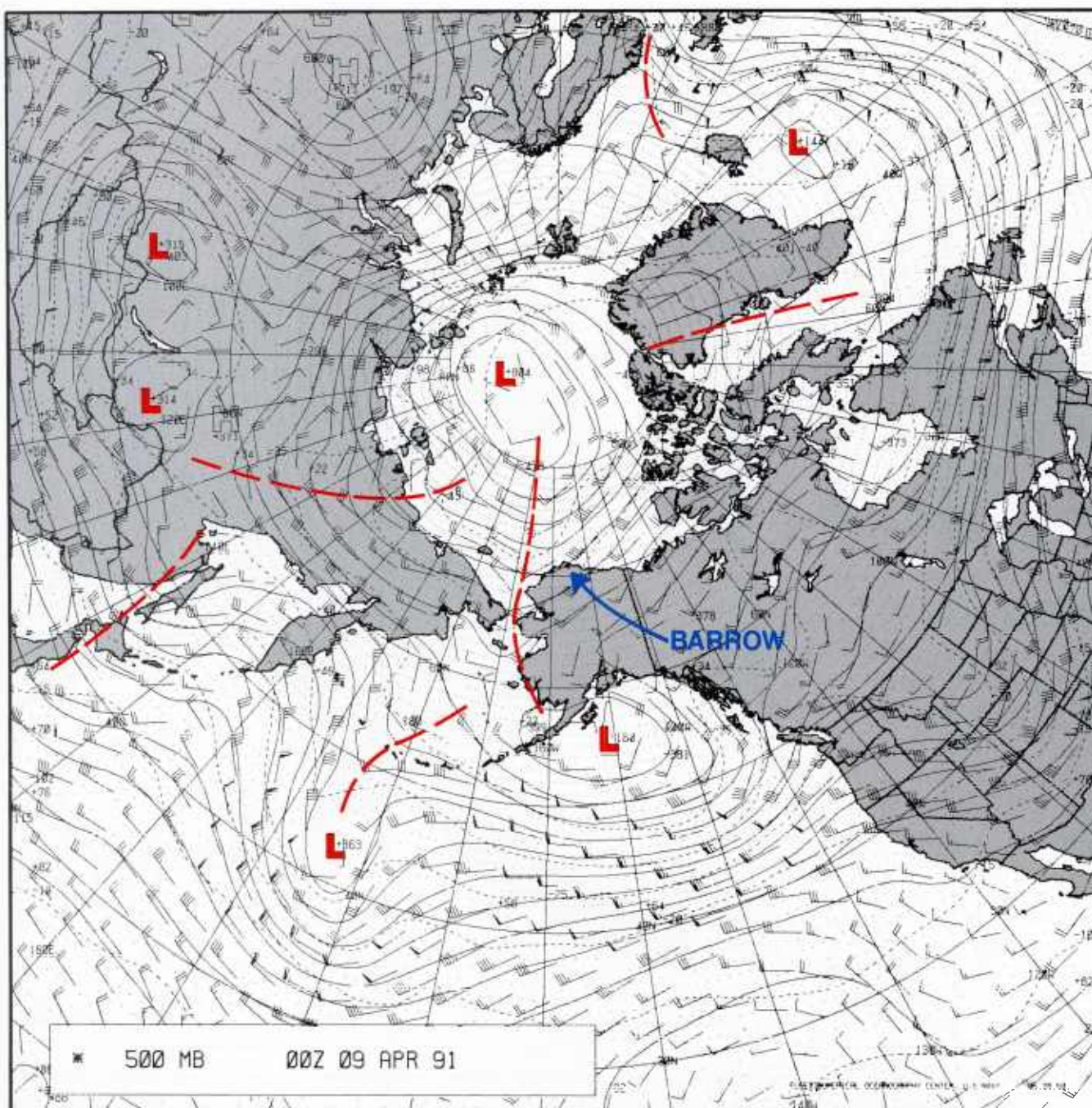
3A-25a DMSP infrared (TS) data. 1734 GMT, 8 April 1991.





3A-26a Fairbanks, Alaska NWS surface analysis. 1800 GMT, 8 April 1991.





3A-27a FNO 500-mb analysis. 0000 GMT, 9 April 1991.



*9 April 1991*

The Fairbanks NWS surface analysis on this date at 1800 GMT is shown in Fig. 3A-28a. The high pressure cell that had been located near Wrangel Island (Fig. 3A-26a) has now moved to a position east of Barrow. At the same time another Arctic front has progressed to the East Siberian Sea. At this time the north coast of Siberia is exposed to southerly flow that extends to Barrow. The offshore flow should tend to widen the flaw lead seen earlier in the Siberian region (Fig. 3A-23a) and also act to widen and/or lengthen the flaw lead near Barrow and Wainwright.

The DMSP infrared (TS) data at 1804 GMT (Fig. 3A-29a) tend to support at least the lengthening of the flaw lead southwest of Barrow and an extension of this lead northeast of Barrow. Figure 3A-30a duplicates the DMSP data in an overlay defining some of the features.

*10 April 1991*

The FNOC 500-mb 0000 GMT analysis (Fig. 3A-31a) shows a minor trough approaching Wrangel and a major low center near the New Siberian Islands (75°N, 140°E). The Fairbanks NWS surface analysis for 10 April at 0600 GMT is shown in Fig. 3A-32a. The Fairbanks analysis shows new Arctic warm and cold fronts passing to the east of the New Siberian Islands. The pressure gradient between the high over the Beaufort Sea and the low near the New Siberian Islands has intensified, so that moderate southerly offshore flow extends from near the frontal system all along the north Siberian coastline to Barrow. Southerly offshore winds of 30 kt are reported at Cape Lisburne (68.9°N, 166.1°W) and 15 kt at Barrow.

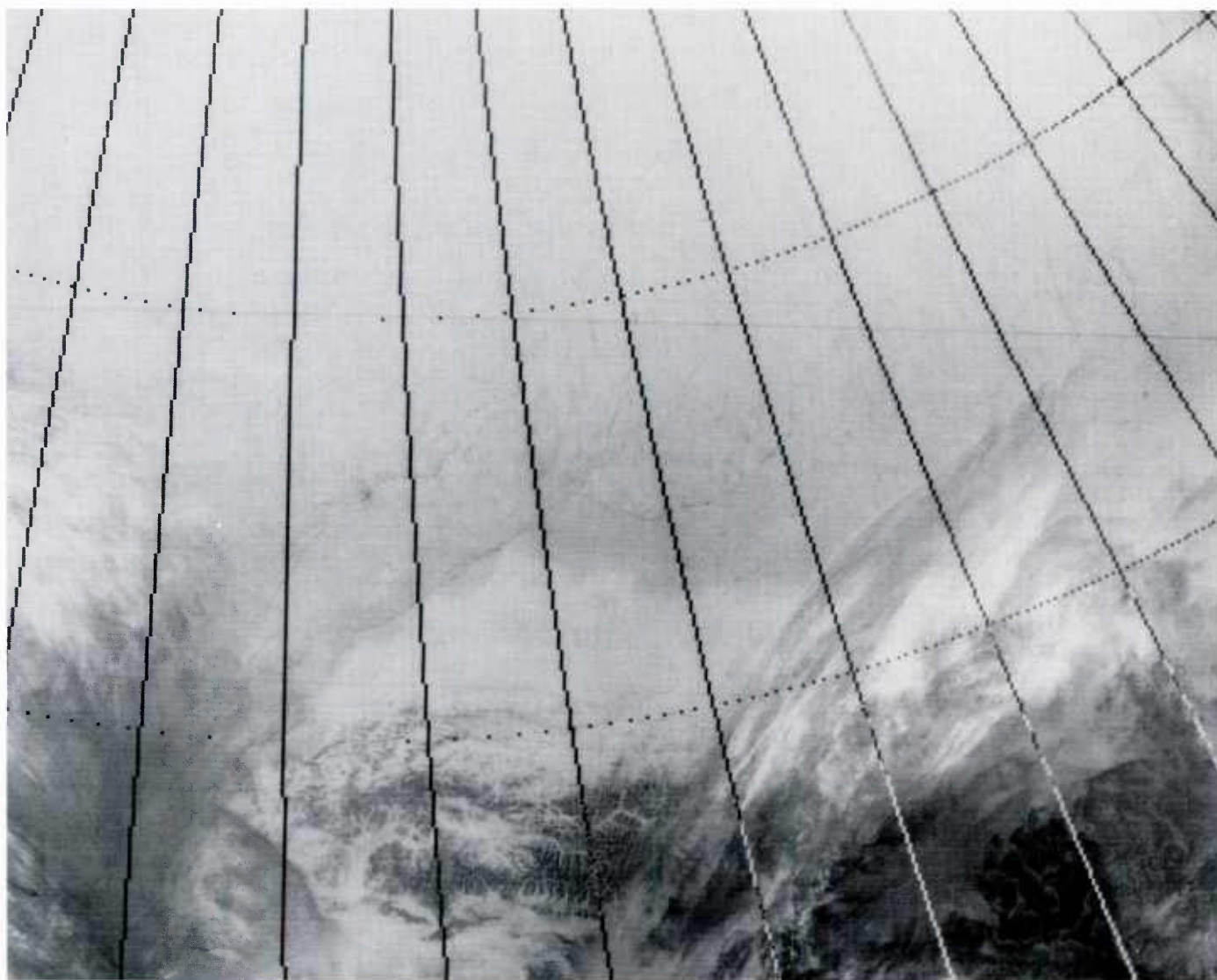
A DMSP infrared (TS) image at 0408 GMT on this date (Fig. 3A-33a) shows an immediate widening of the flaw lead southwest of Barrow. An overlay (Fig. 3A-34a) shows some details of lead location and geography. Cold striated cloudiness turns anticyclonically over the Chukchi Sea east of Wrangel Island flowing northward from the Bering Sea, suggesting the approach of the short-wave trough noted earlier at 500 mb (Fig. 3A-31a). A FNOC update to the 500-mb analysis on 10 April at 1200 GMT is shown in Fig. 3A-35a. The figure shows the short-wave trough progressing eastward past Wrangel Island. Judging from the striations in the DMSP infrared data, anticyclonic curvature of flow west of the trough axis is more pronounced than the analysis indicates. The more probable 500-mb flow pattern is indicated on the figure.

The southerly winds blowing through the Bering Strait resulted in the beginning of a surge of warm, moist air into the Arctic that was destined to produce profound changes, not only in flaw lead development but in lower atmospheric structure over a vast portion of the Arctic Ocean. Figure 3A-36a shows the FNOC surface analysis on 10 April at 1200 GMT. The bulging of isotherms through the Bering Strait and into the Chukchi Sea shows evidence of this surge, which is associated with the cloudiness seen in the DMSP data of Figs. 3A-33a and 3A-34a.

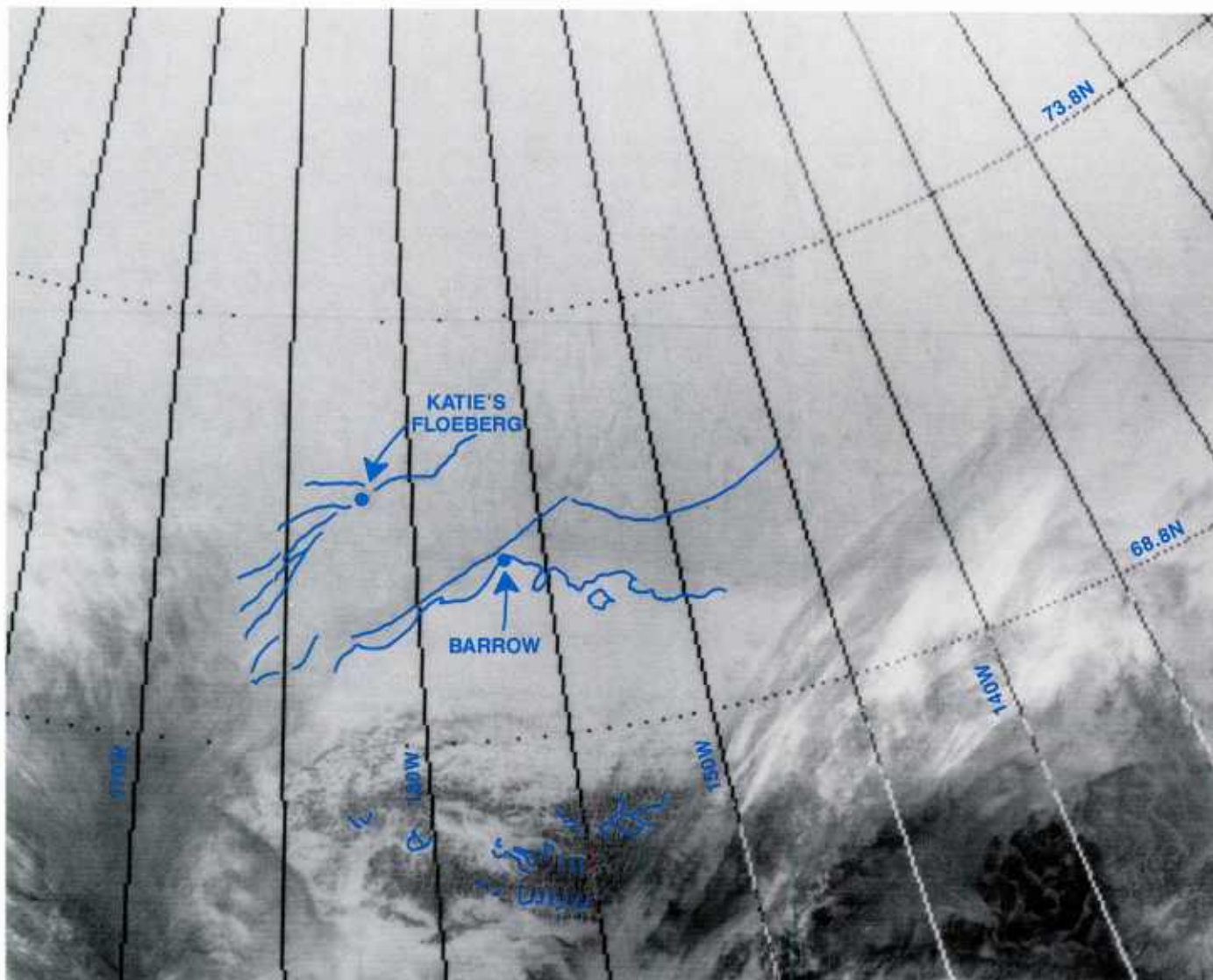
The DMSP visual (LF) data at 2055 GMT (Fig. 3A-37a) and with overlay (Fig. 3A-38a) show further evidence of this cloudiness and of the widening of leads along the Siberian and northern Alaskan coastlines. The Alaskan leads continued to widen dramatically during the next few hours as shown in an enlarged DMSP infrared (TS) view at 2310 GMT (Fig. 3A-39a).





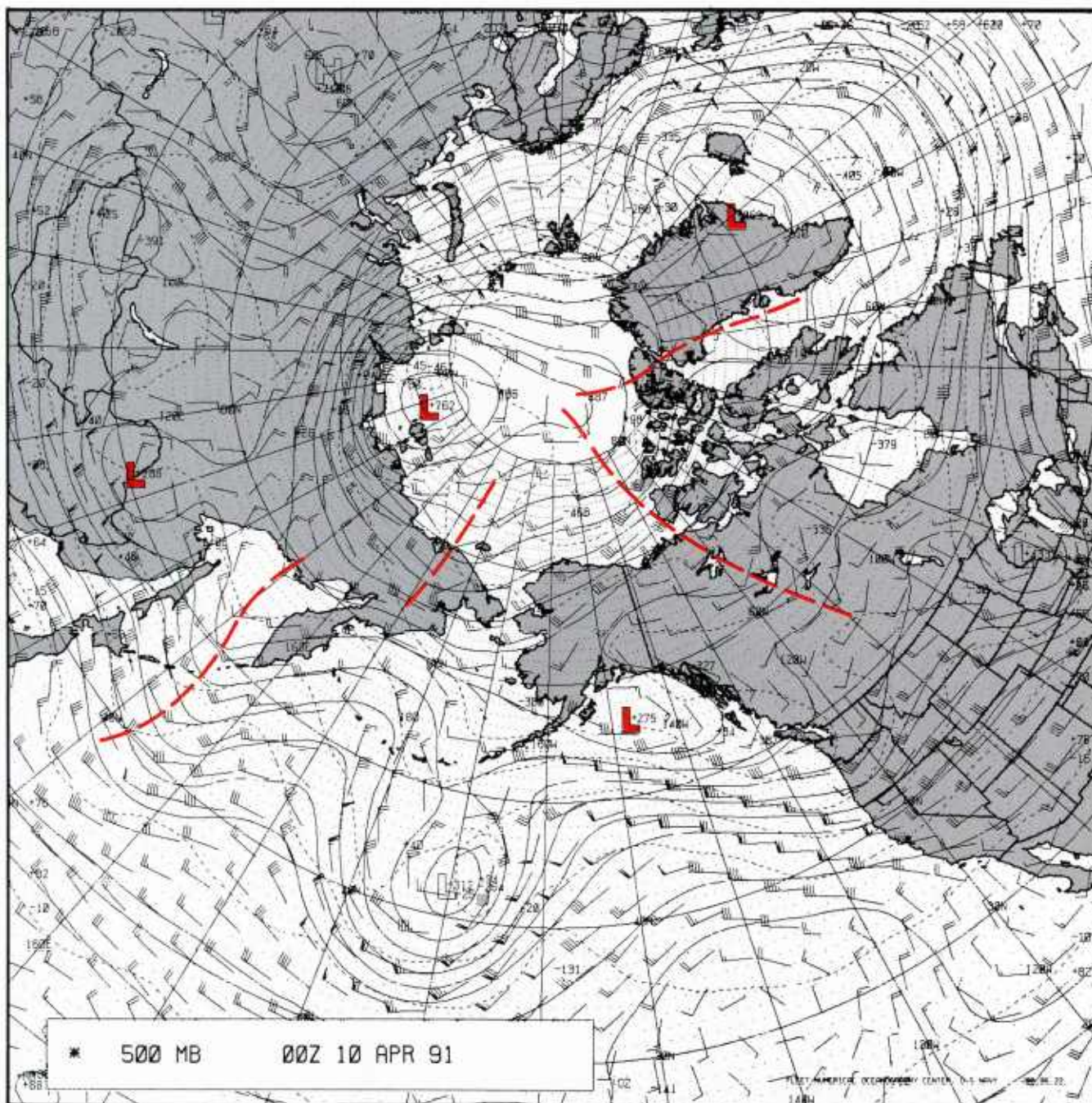


3A-29a DMSP infrared (TS) data. 1804 GMT, 9 April 1991.



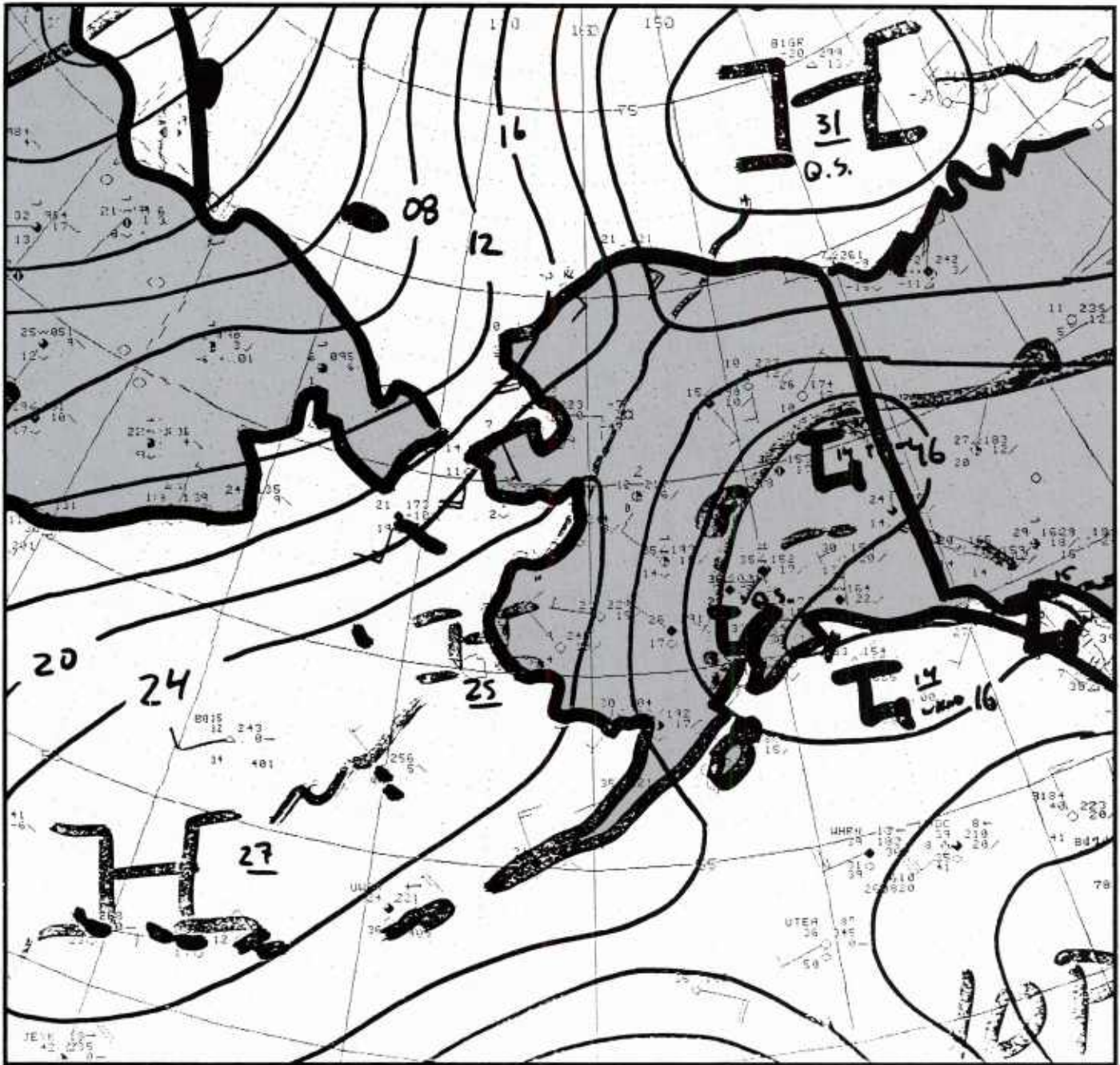
3A-30a DMSP infrared (TS) data (with overlay). 1804 GMT, 9 April 1991.





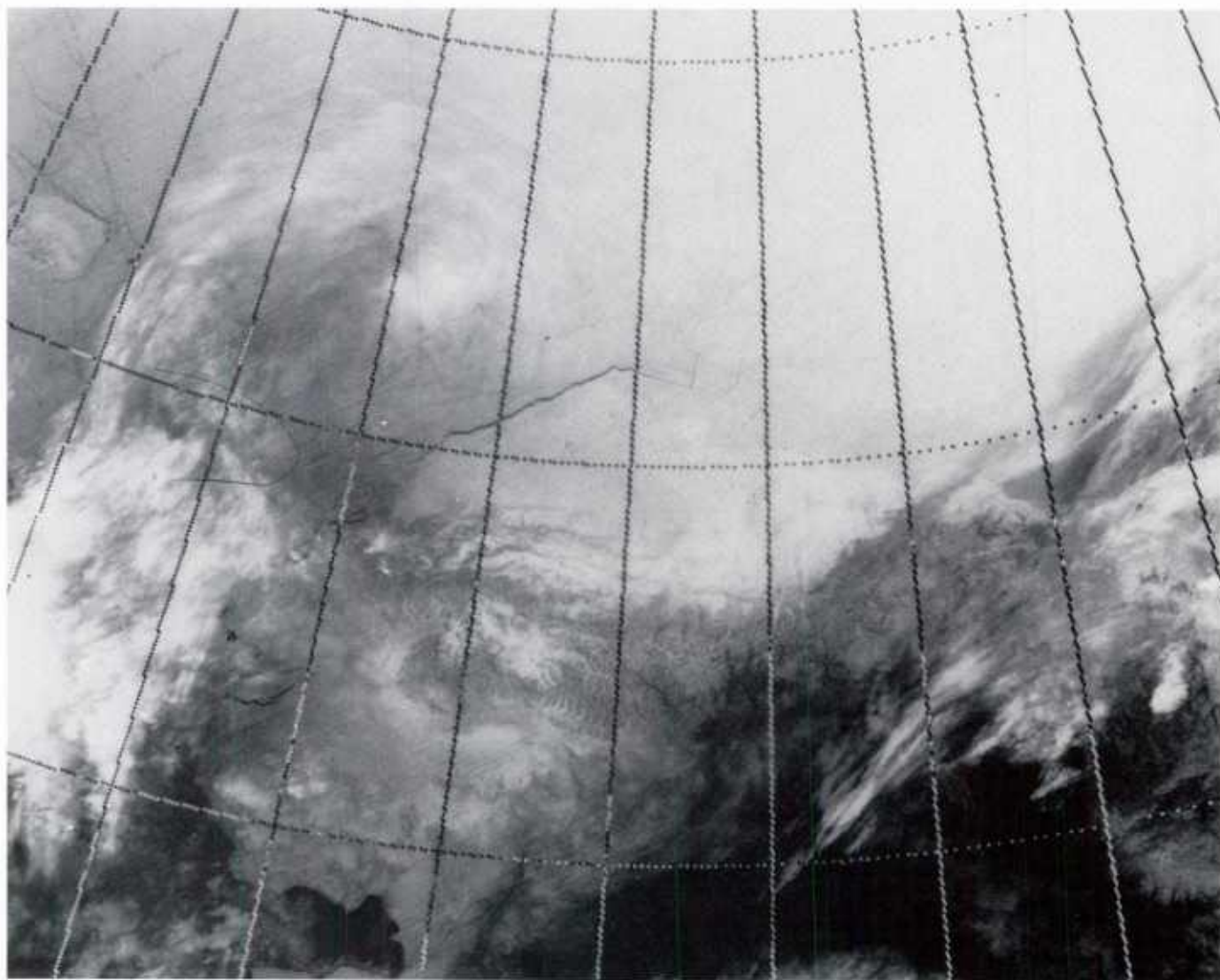
3A-31a FNOC 500-mb analysis. 0000 GMT, 10 April 1991.



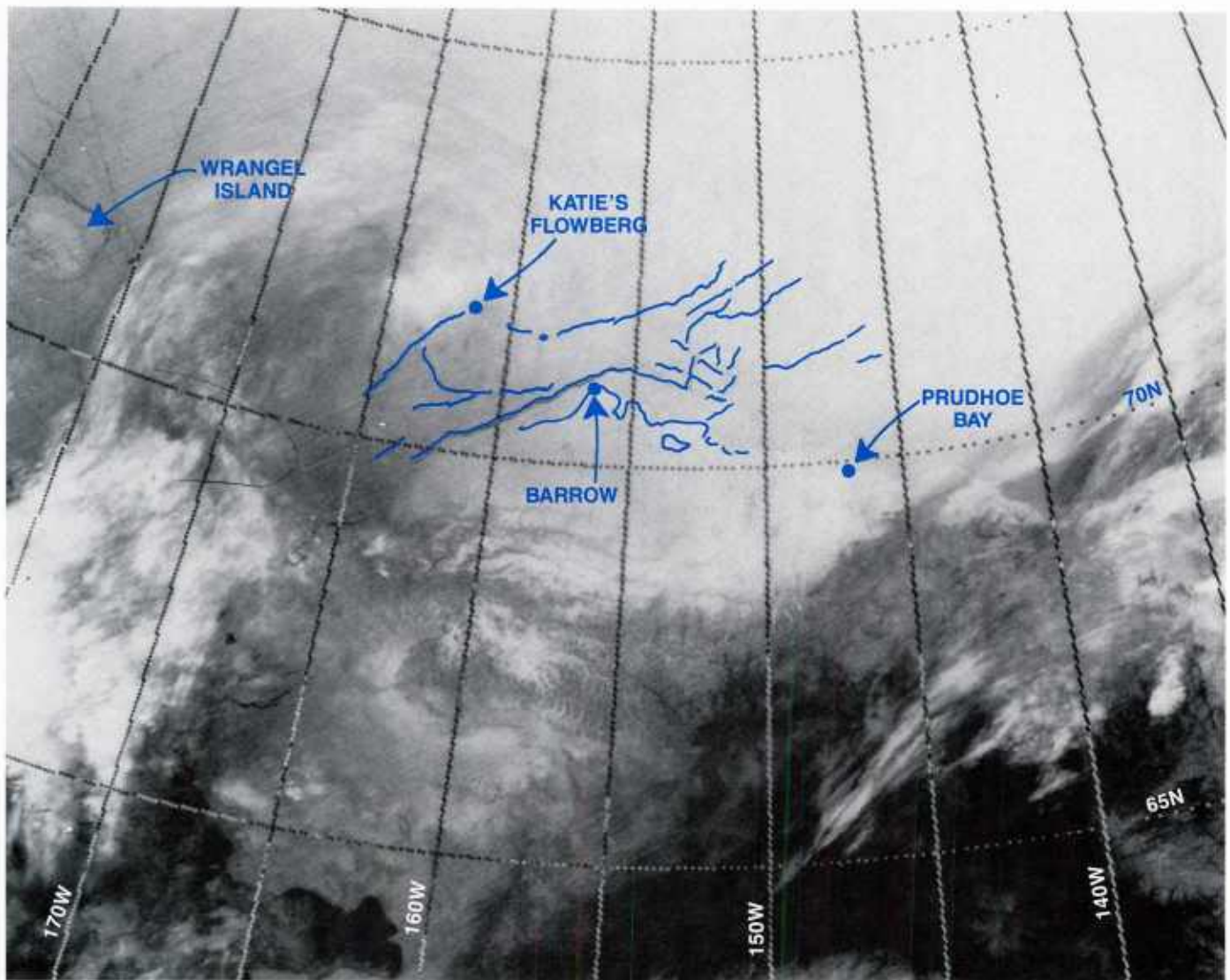


3A-32a Fairbanks, Alaska NWS surface analysis. 0600 GMT, 10 April 1991.



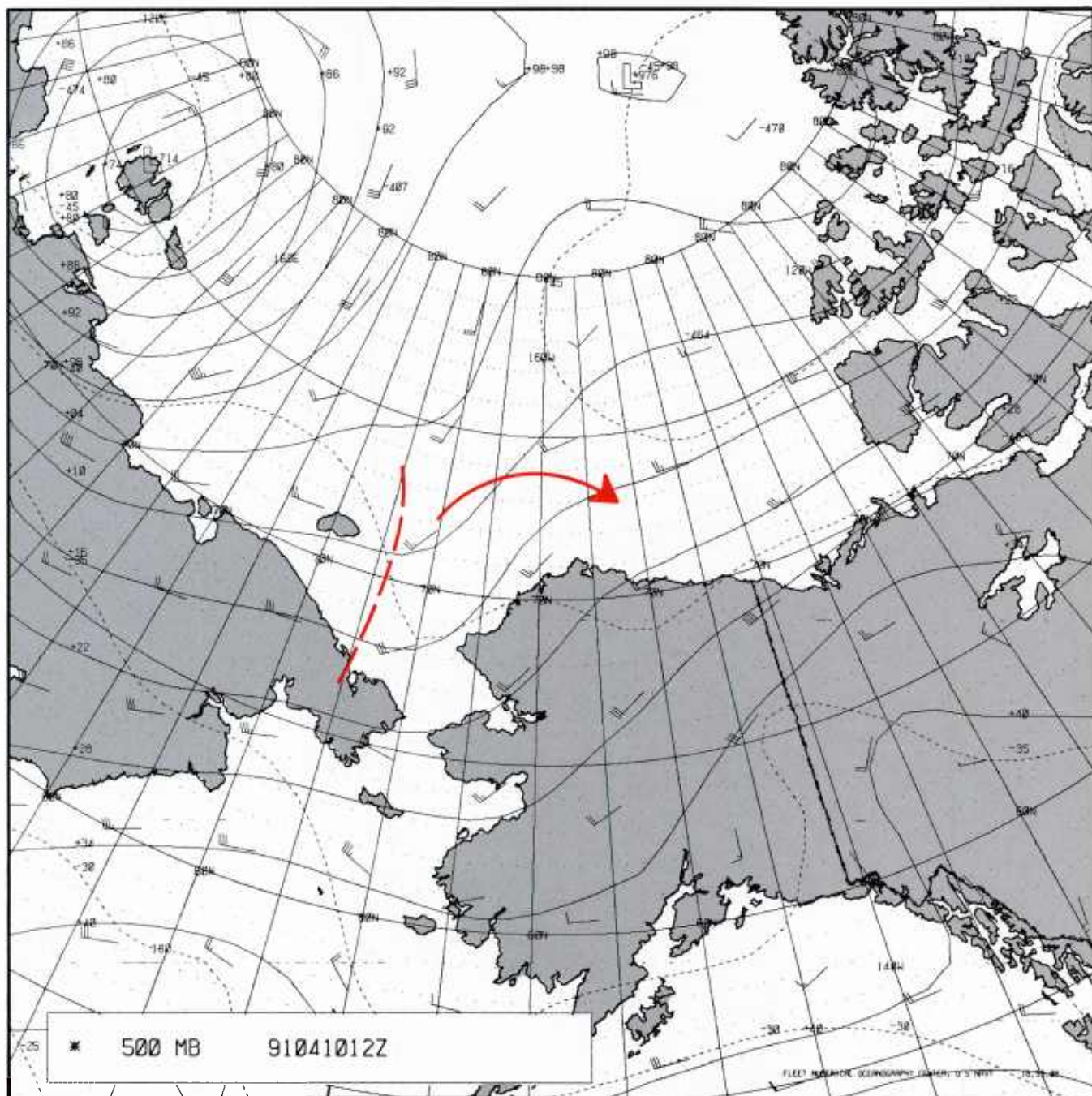


3A-33a DMSP infrared (TS) data. 0408 GMT, 10 April 1991.

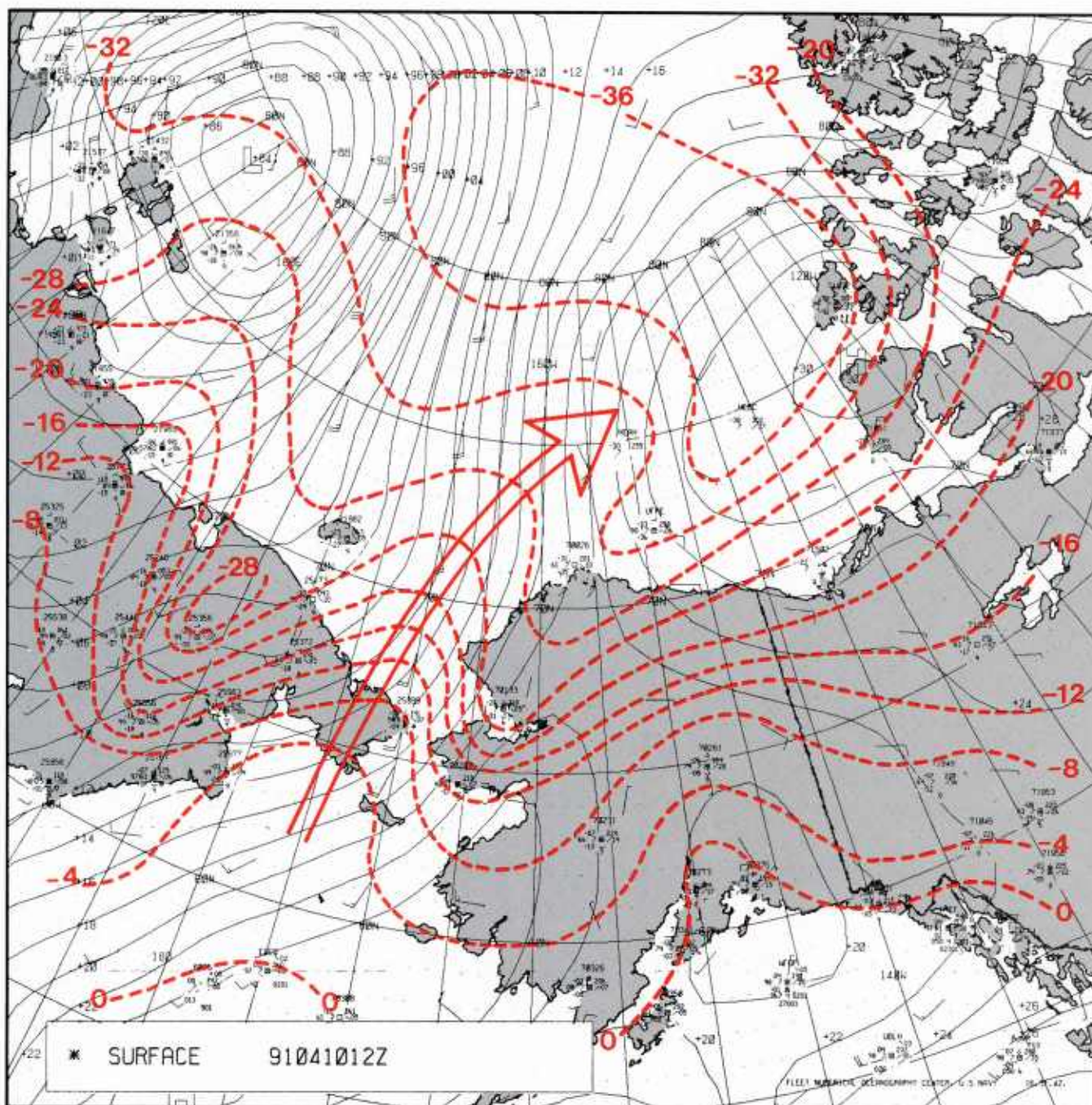


3A-34a DMSP infrared (TS) data (with overlay). 0408 GMT, 10 April 1991.



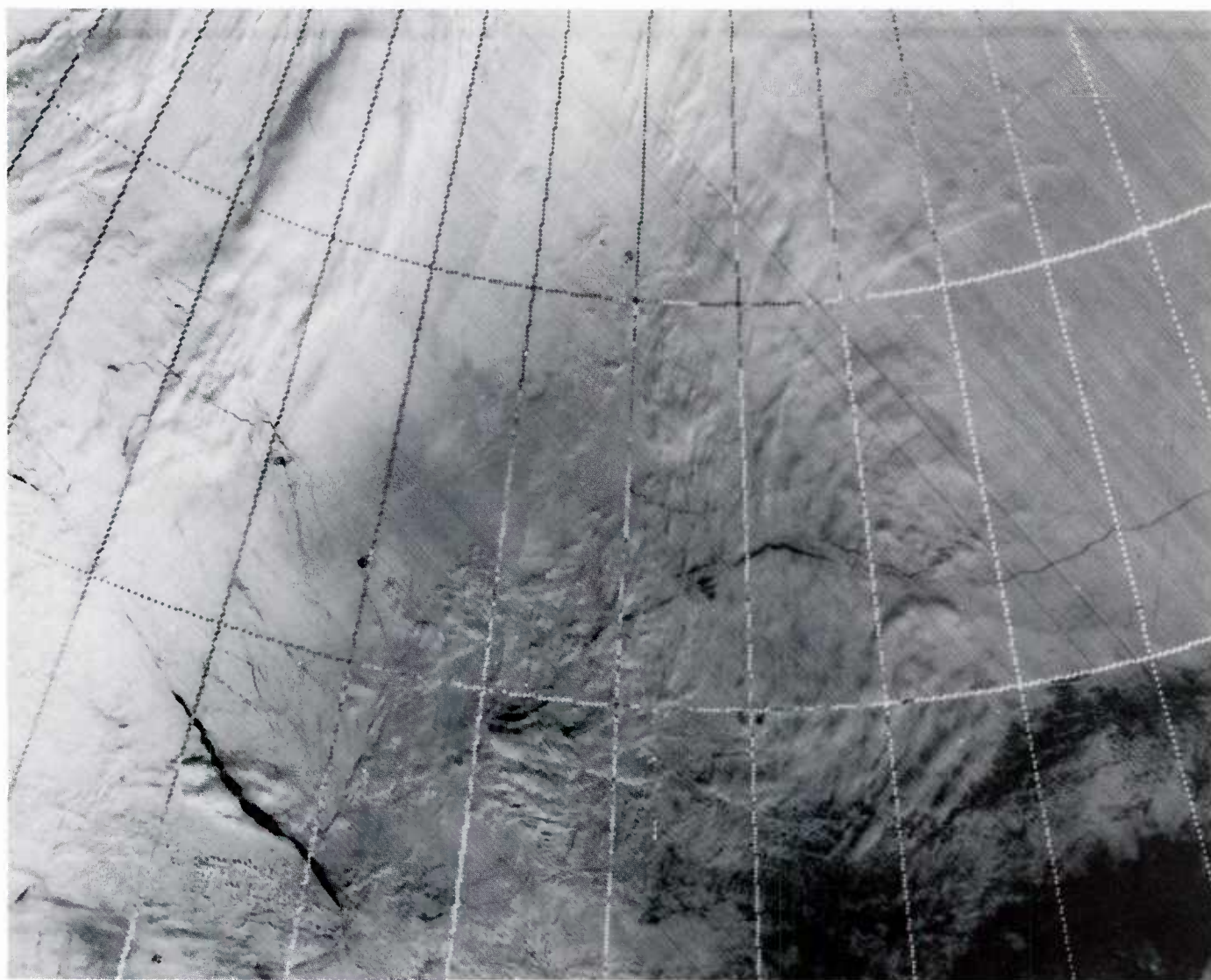




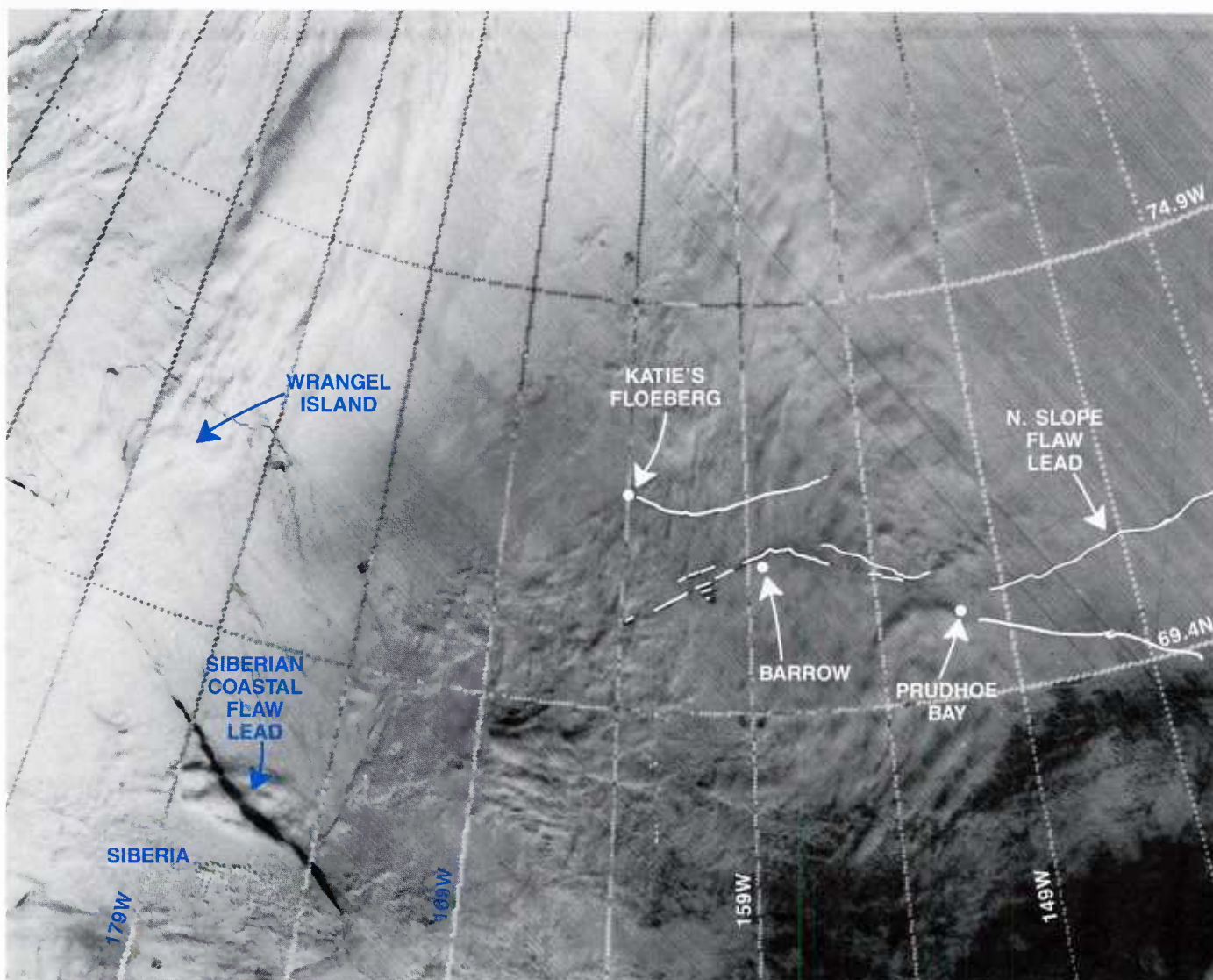


3A-36a FNOc surface analysis. 1200 GMT, 10 April 1991. (Isotherm analysis in degrees Celsius shown in red as an overlay. Warm surge is indicated by an arrow.)



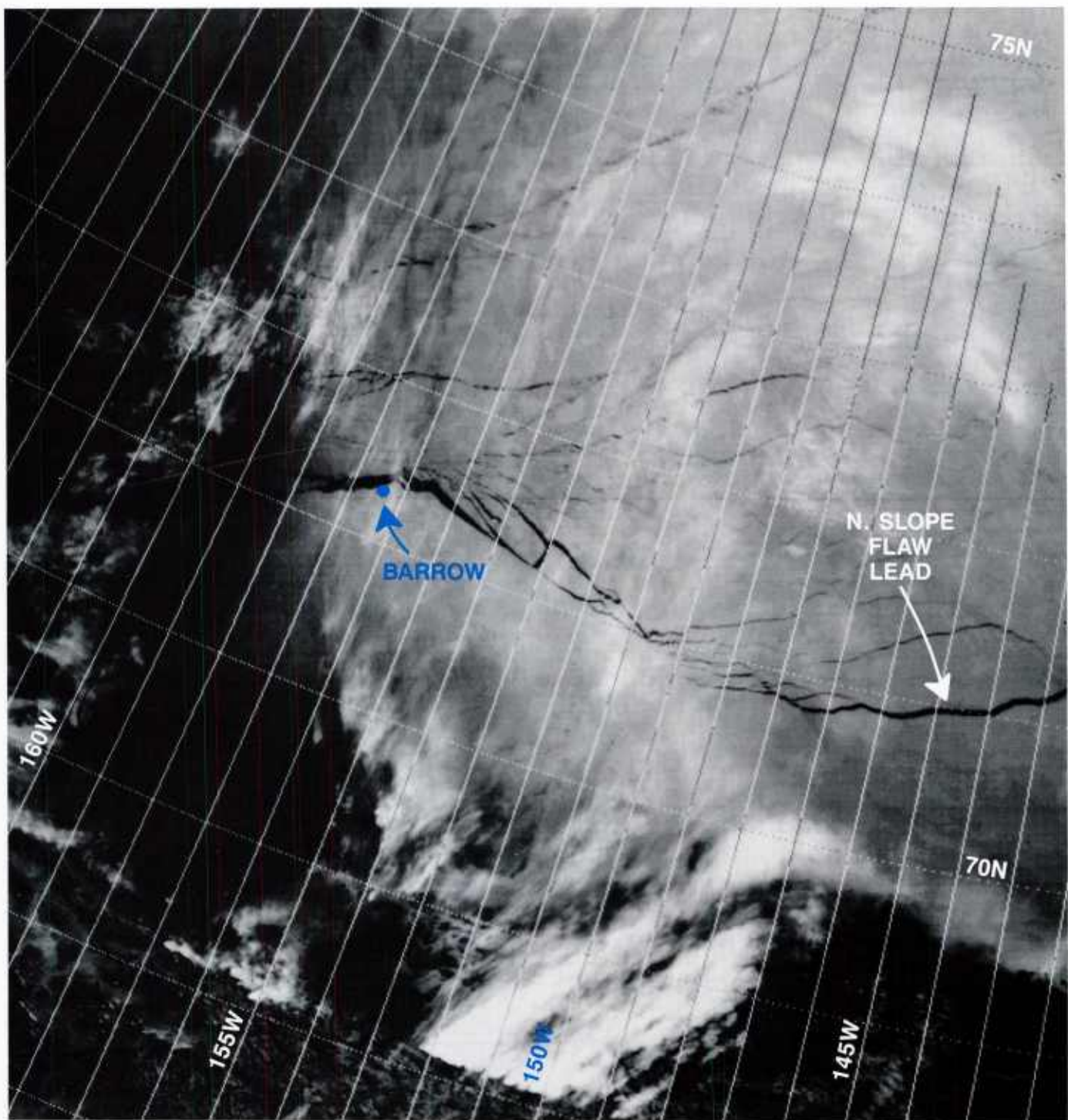


3A-37a DMSP visible (LF) data. 2055 GMT, 10 April 1991.



3A-38a DMSP visible (LF) data (with overlay). 2055 GMT, 10 April 1991.





3A-39a Enlarged (X4) DMSP infrared (TS) data (with overlay). 2310 GMT, 10 April 1991.

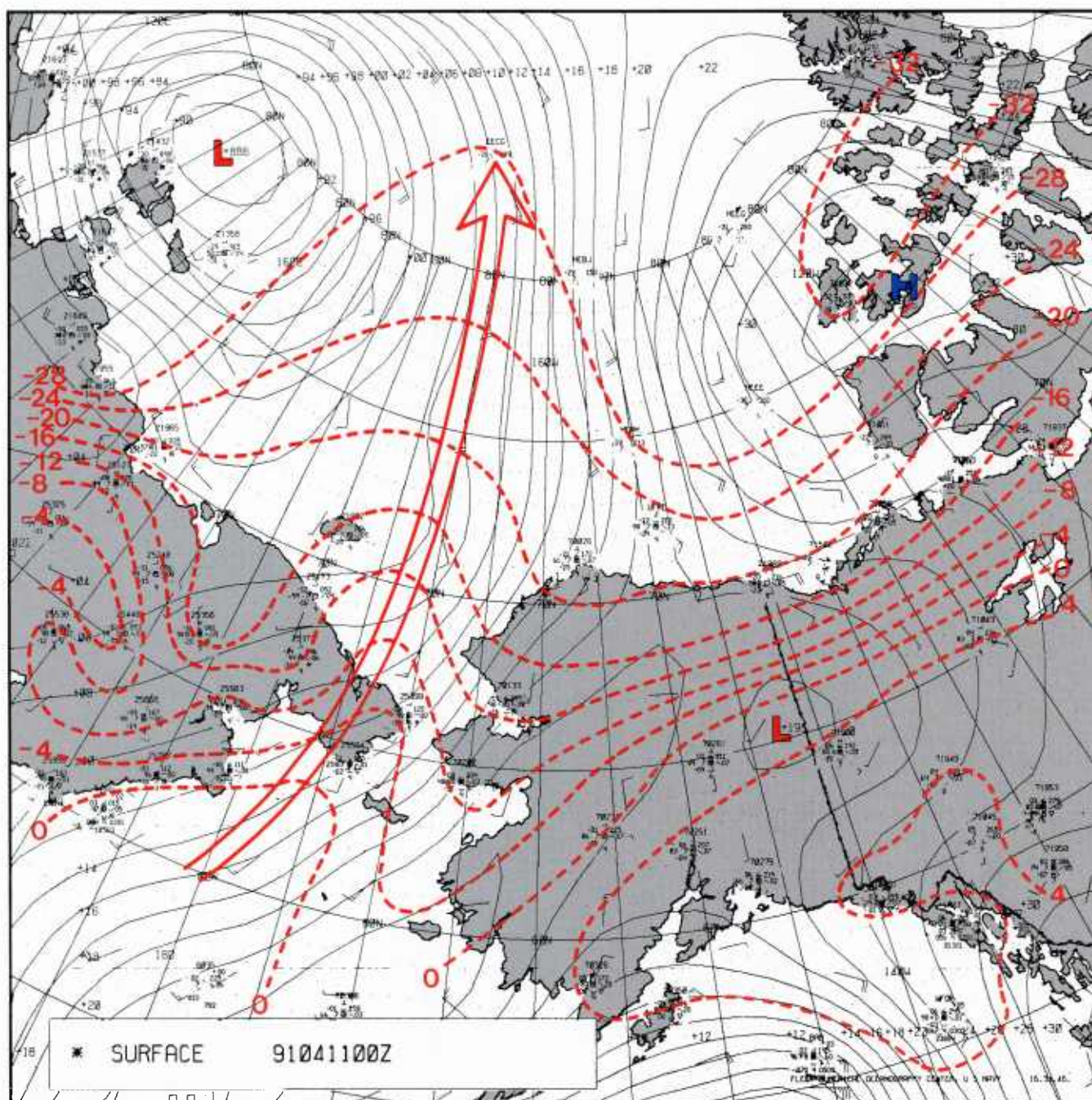
*11 April 1991*

Effects of the warm surge into the Arctic Ocean are dramatically shown by the isotherm analyses of the FNOC surface charts at 0000 GMT and 1200 GMT (Figs. 3A-40a and 3A-41a, respectively). Surface temperature at Barrow increased from  $-31^{\circ}\text{C}$  on 10 April at 1200 GMT (Fig. 3A-36a) to  $-21^{\circ}\text{C}$  on 11 April at 0000 GMT (Fig. 3A-40a) and to  $-17^{\circ}\text{C}$  on 11 April at 1200 GMT (Fig. 3A-41a). Meanwhile, the Fairbanks surface analysis for 11 April at 1200 GMT (Fig. 3A-42a) showed the Arctic front moving in from the west, approaching Wrangel Island.

The DMSP visible (LF) data at 1112 GMT are shown in Fig. 3A-43a. An overlay to this figure is shown in Fig. 3A-44a. The image shows the wide lead extending east of Barrow; the continued existence of the large flaw lead along the Siberian coast; and the development of several smaller width leads oriented southwest-northeast in the central Beaufort Sea and northwest-southeast in the East Siberian Sea. The contrast in the gray shade between ice and land continues to be evident in this visible image. The region extending northward and westward from Barrow, where leads cannot be seen, is covered by a dense low overcast and some higher level clouds casting shadows on the lower deck. This cloudiness has apparently resulted because of cooling to saturation of the warm, moist southerly current of air that was sweeping into the region, as shown in the surface analyses (Figs. 3A-36a, 3A-40a, and 3A-41a).

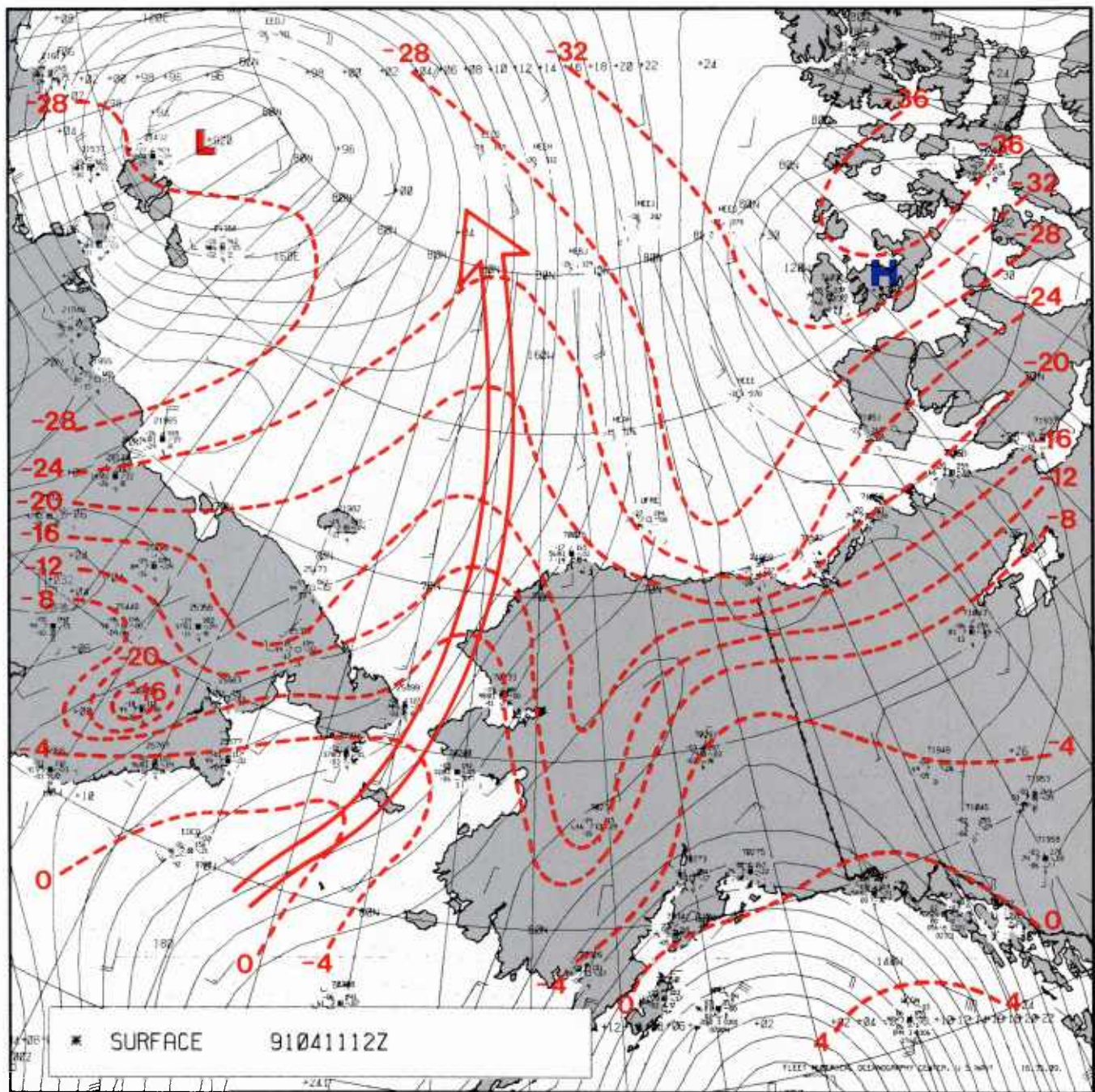
The warm (low) nature of the overcast region is shown very clearly in DMSP infrared (TS) data received on 11 April at 1630 GMT (Fig. 3A-45a) and an overlay to this figure (Fig. 3A-46a). The cloudiness is seen to extend from near the Bering Strait north-northeastward into the central Arctic Ocean. Faint indications of curvature suggest cyclonic shear along the western side of the warm cloudiness. Such an effect would be induced by a higher speed current of warm air being introduced into a lower wind speed environment. This area is very near the position of a warm front drawn on the 11 April 1800 GMT Fairbanks surface analysis (Fig. 3A-47a). However, the warm surge of air and resulting cloudiness occurred independently of the cold frontal system and any associated warm front. A comparison of Barrow's sounding on 10 April at 0000 GMT, before the warm surge, and its later sounding on 11 April at 1200 GMT, after the warm surge had commenced (Fig. 3A-48a), shows the extreme warming and moistening of the lower atmosphere that occurred well in advance of the classical warm front shown on the Fairbanks NWS analysis (Fig. 3A-47a).





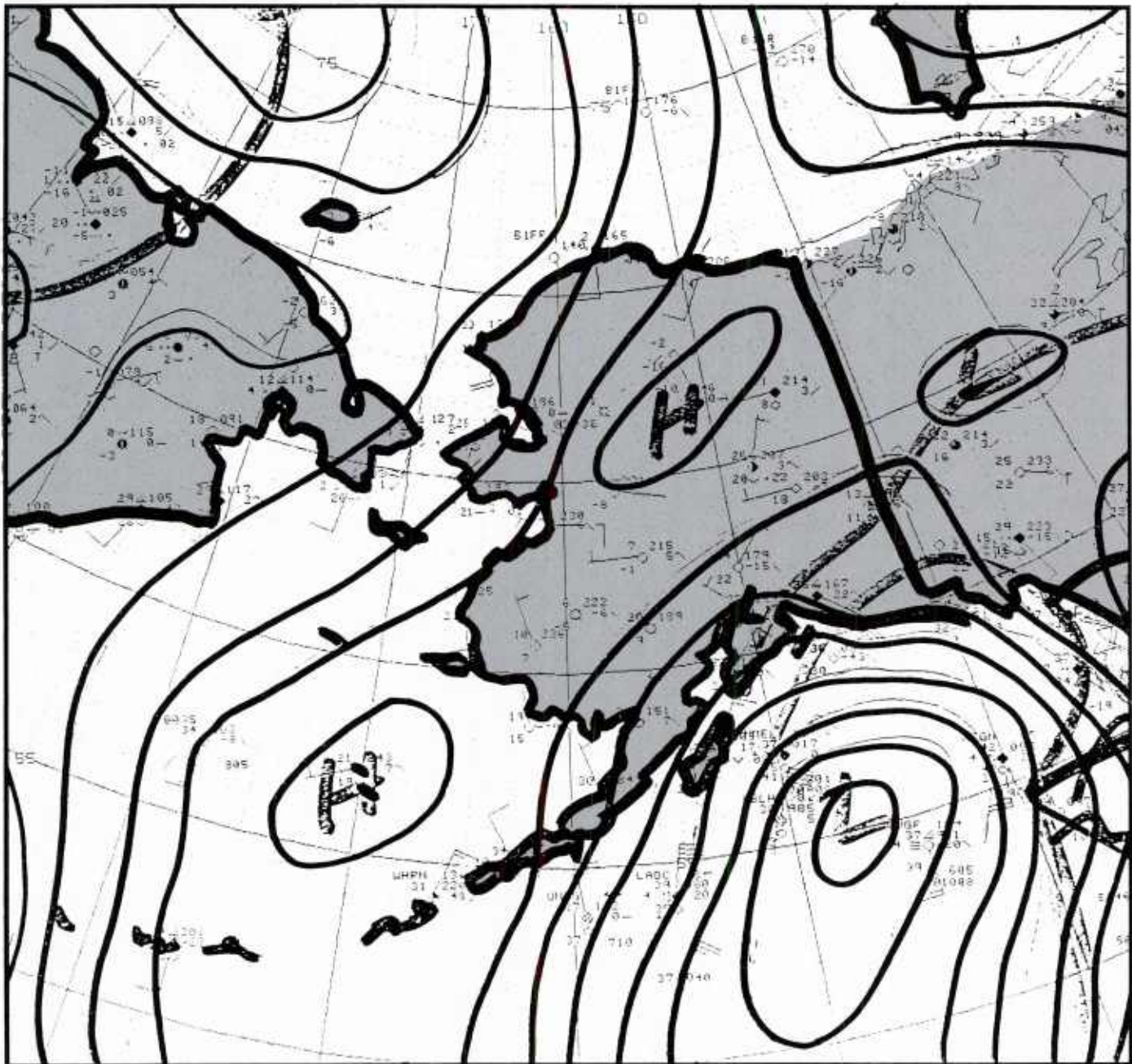
3A-40a FNOC surface analysis. 0000 GMT, 11 April 1991. (Isotherm analysis in degrees Celsius shown in red as an overlay. Warm surge is indicated by an arrow.)



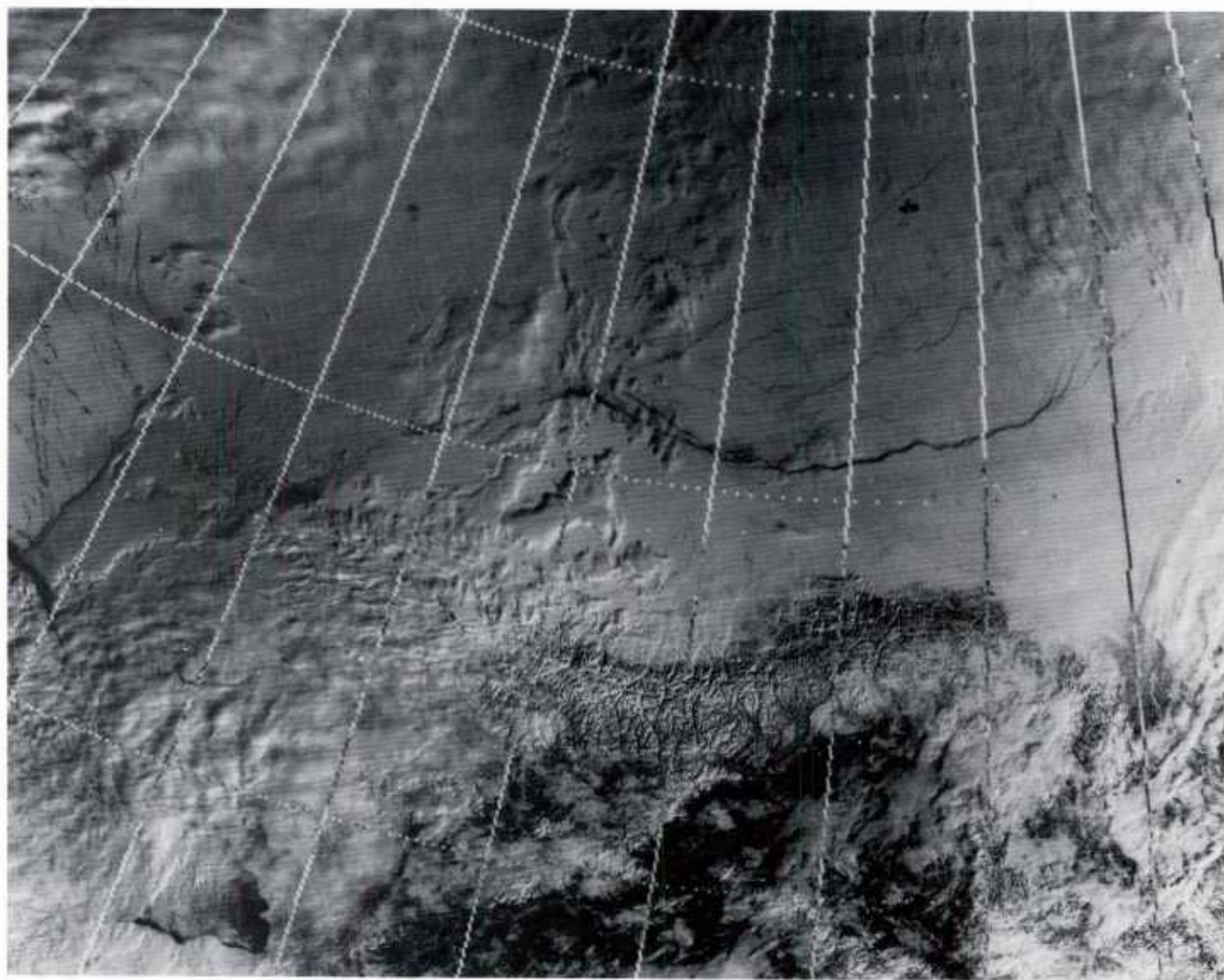


3A-41a FNOC surface analysis. 1200 GMT, 11 April 1991. (Isotherm analysis in degrees Celsius shown in red as an overlay. Warm surge is indicated by an arrow.)



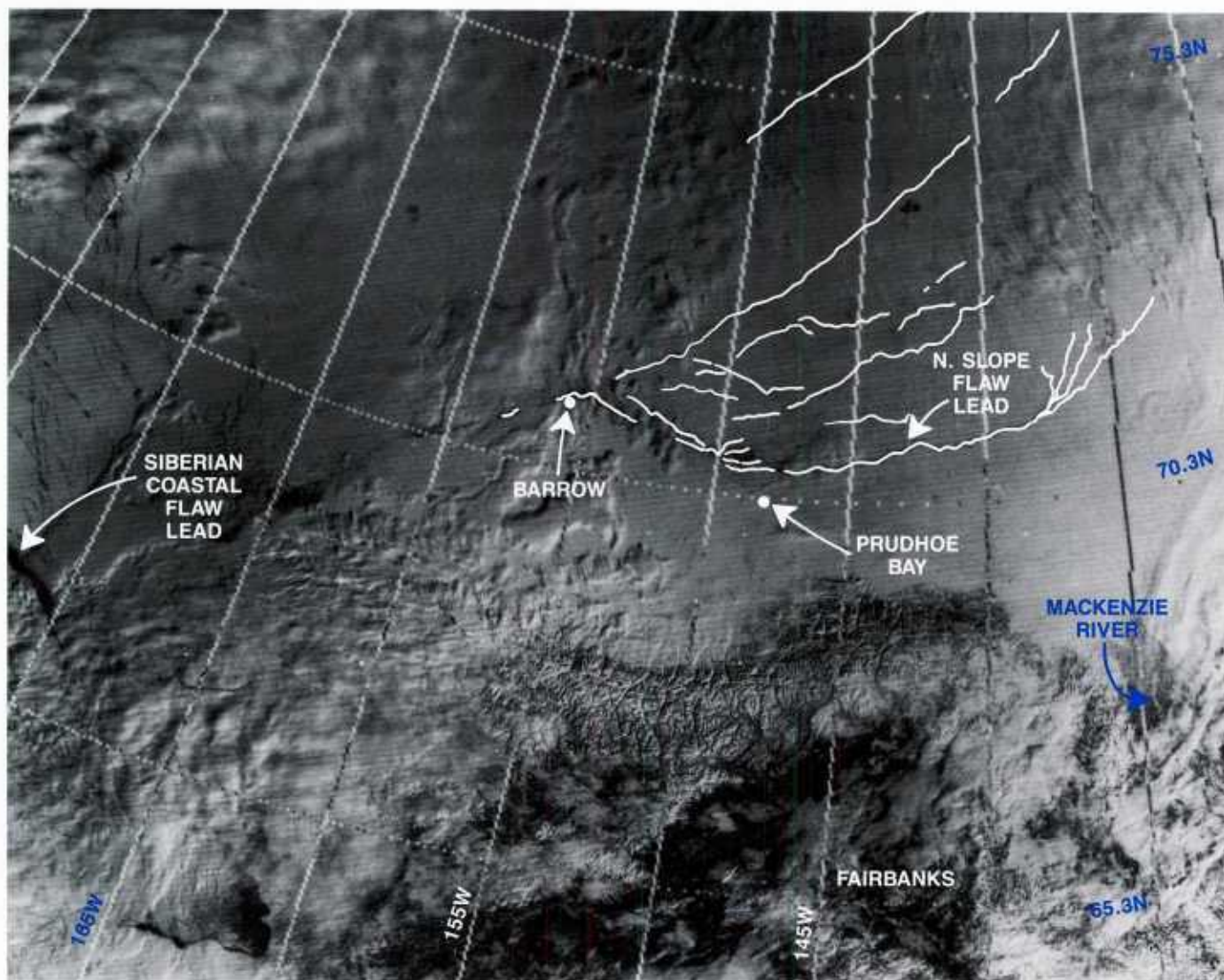


3A-42a Fairbanks, Alaska NWS surface analysis. 1200 GMT, 11 April 1991.

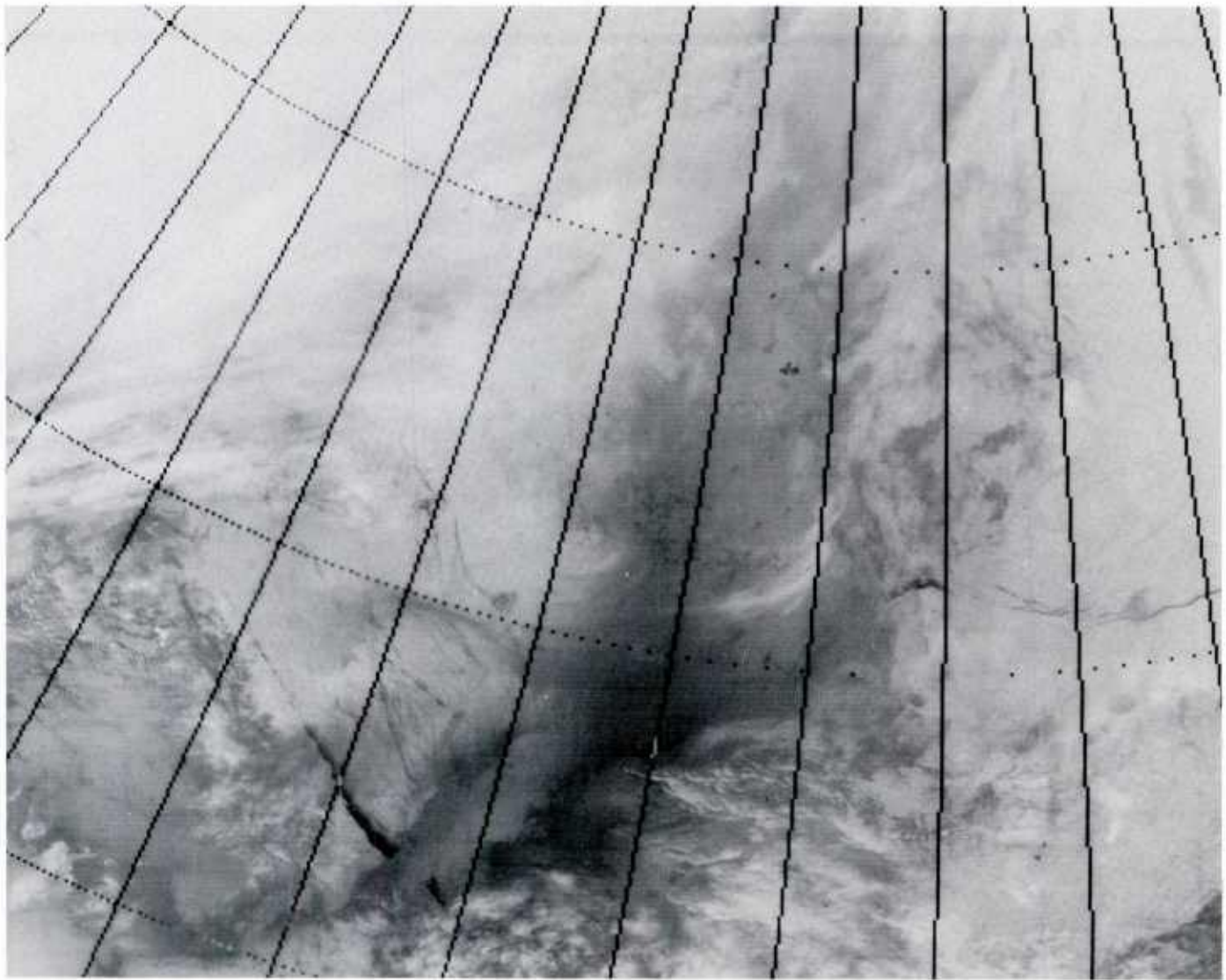


3A-43a DMSP visible (LF) data. 1112 GMT, 11 April 1991.



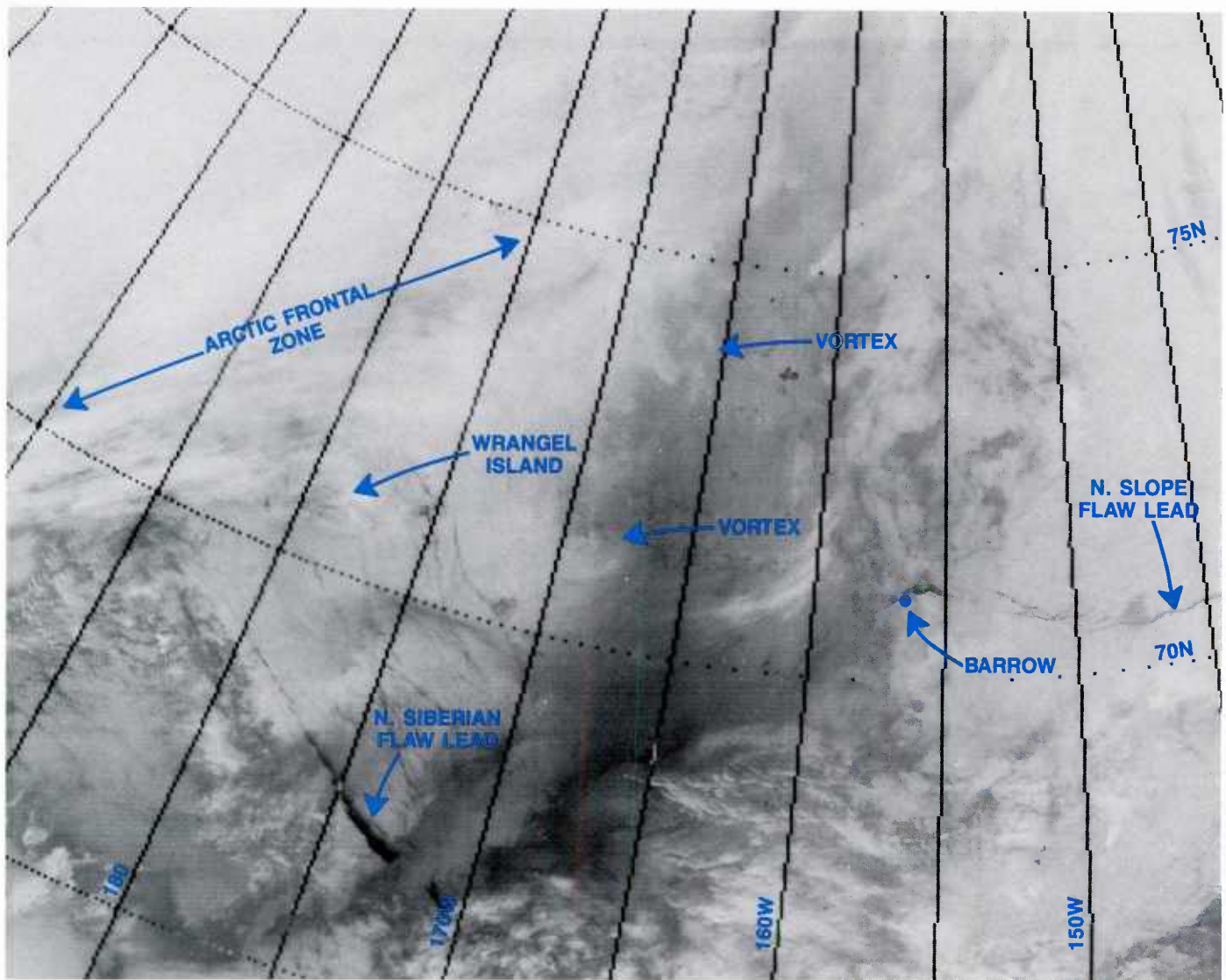


3A-44a DMSP visible (LF) data (with overlay). 1112 GMT, 11 April 1991.

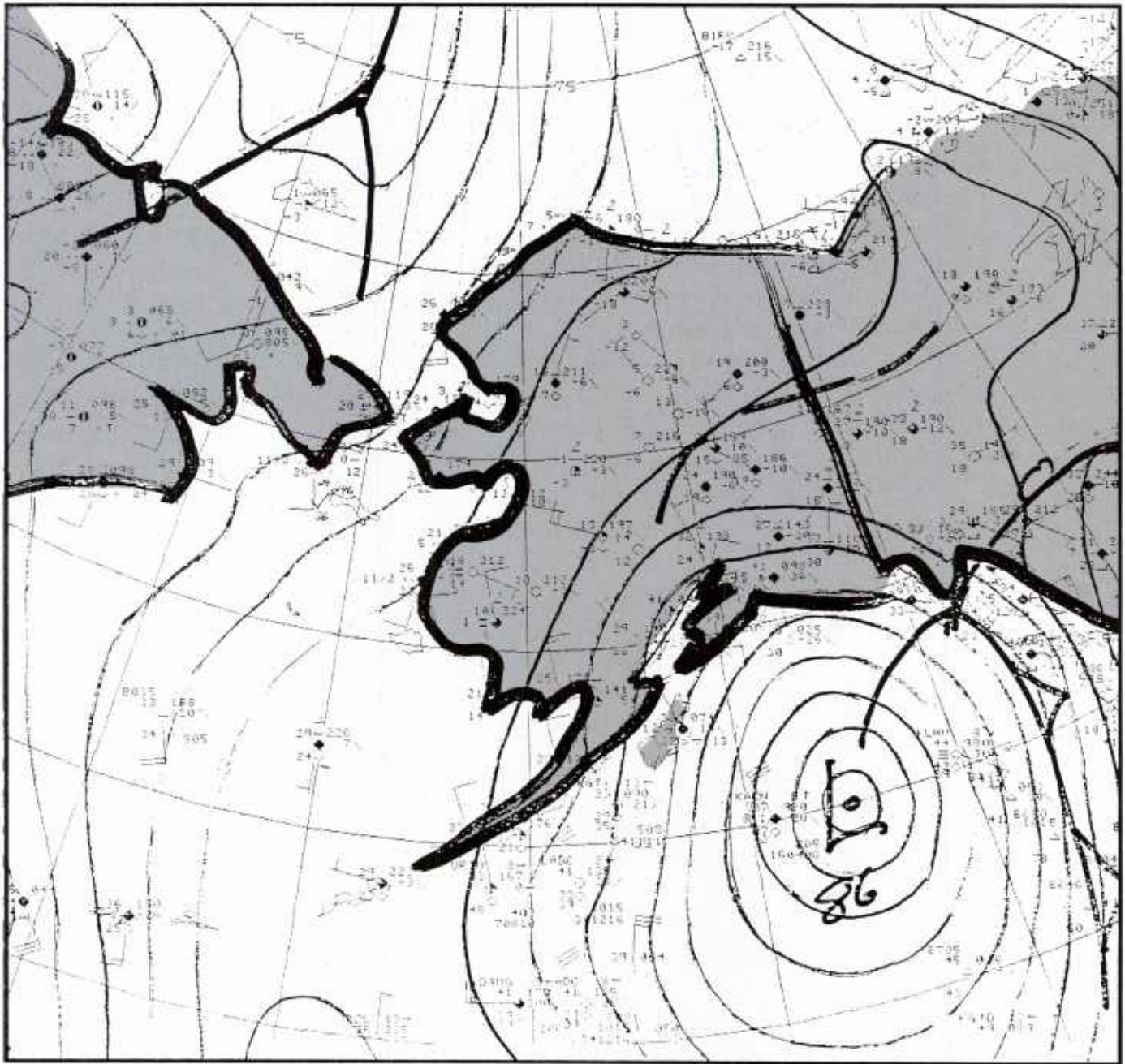


3A-45a DMSP infrared (TS) data. 1630 GMT, 11 April 1991.





3A-46a DMSP infrared (TS) data (with overlay). 1630 GMT, 11 April 1991.



3A-47a Fairbanks, Alaska NWS surface analysis. 1800 GMT, 11 April 1991.

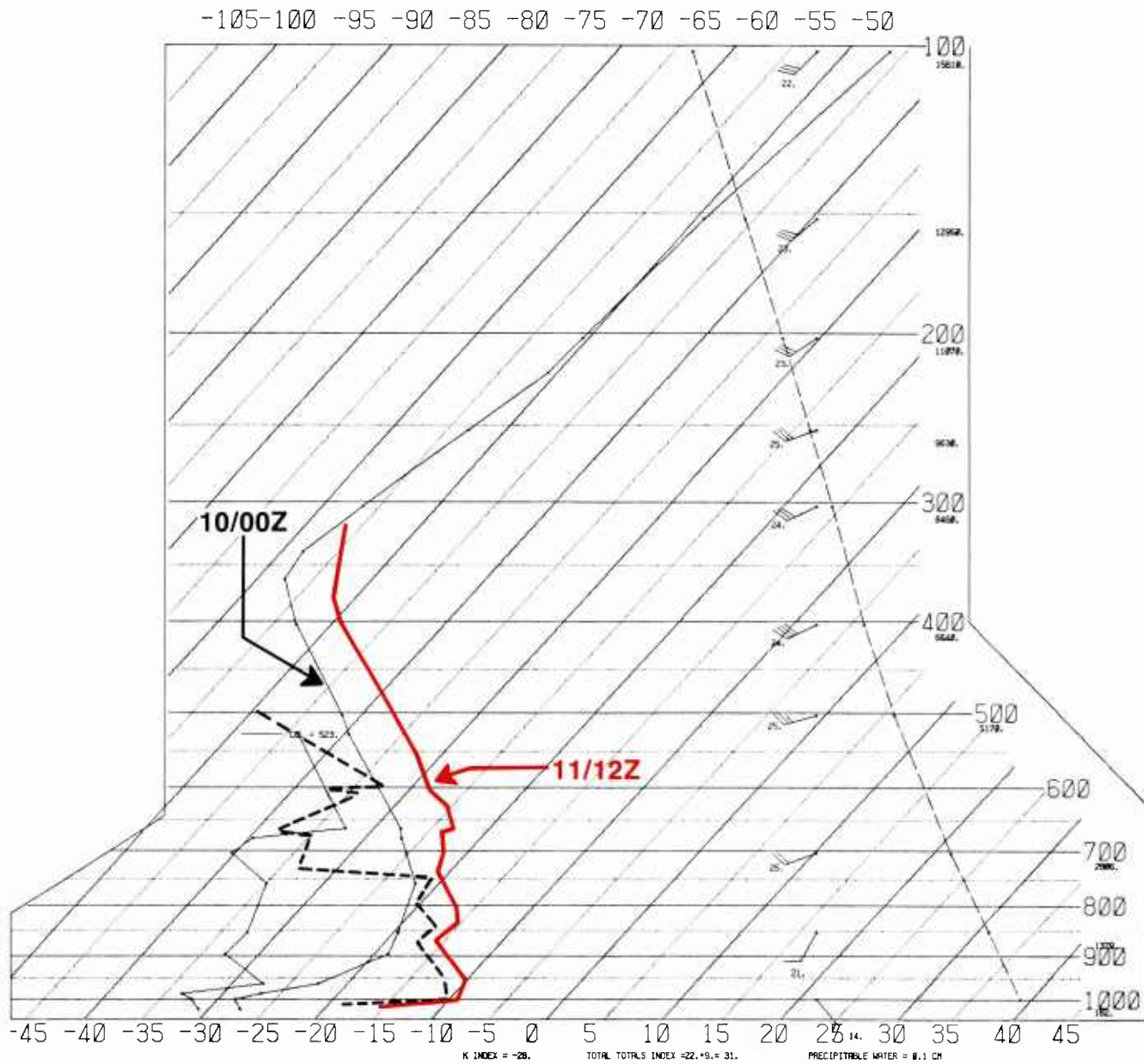


# SKEW T, LOG P DIAGRAM

910410

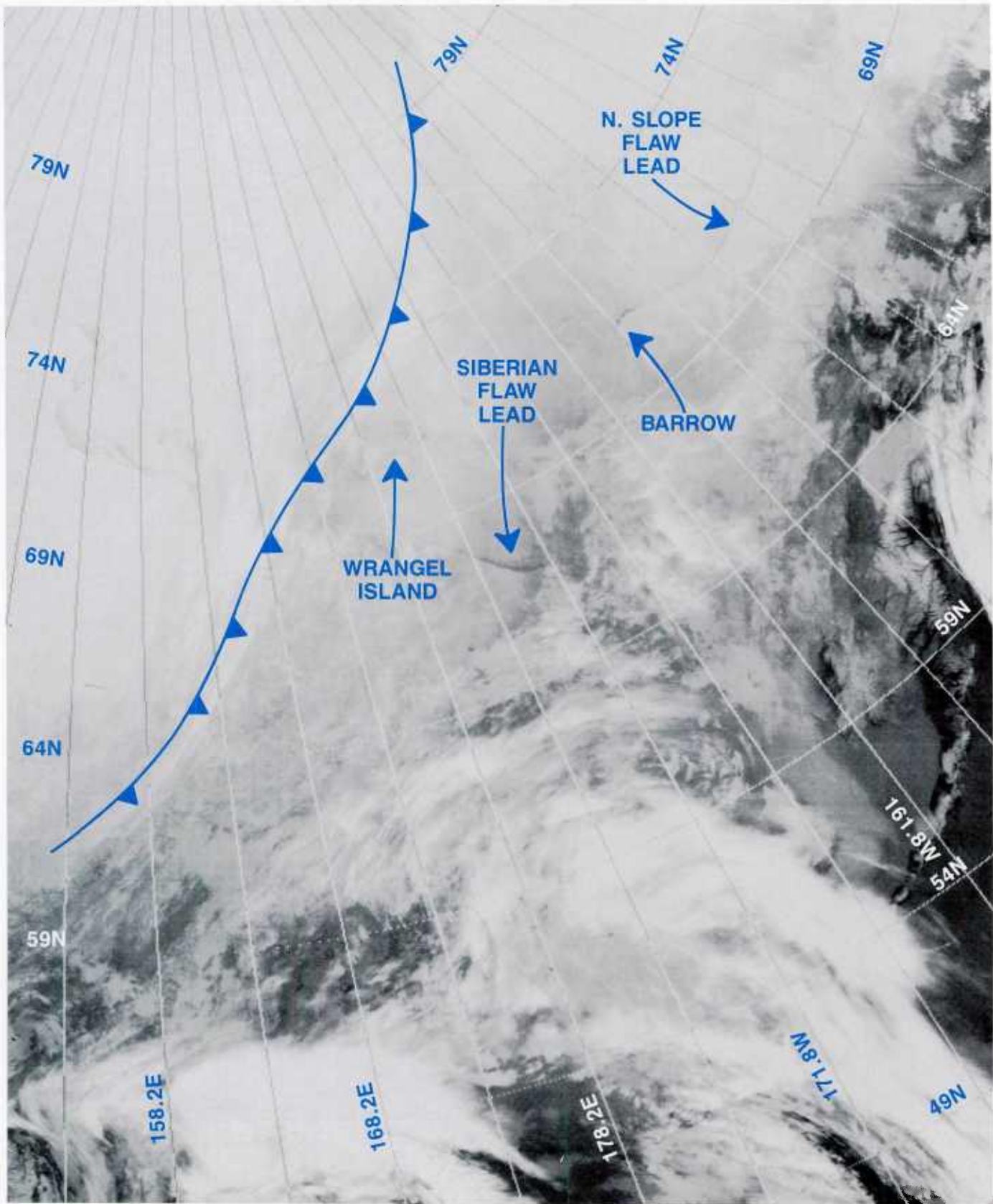
0000Z

70026



3A-48a Radiosonde data for Barrow, Alaska. 0000 GMT, 10 April 1991. (1200 GMT, 11 April 1991, data shown in red as an overlay.)

A larger scale later view of the region on 11 April with an overlay to show important features is shown in a DMSP infrared (TS) image acquired at 2024 GMT (Fig. 3A-49a). The Siberian and North Slope flow leads are easily identifiable on this image. The cold front is seen to be an extensive feature passing close to Wrangel Island deep into the Arctic Basin.

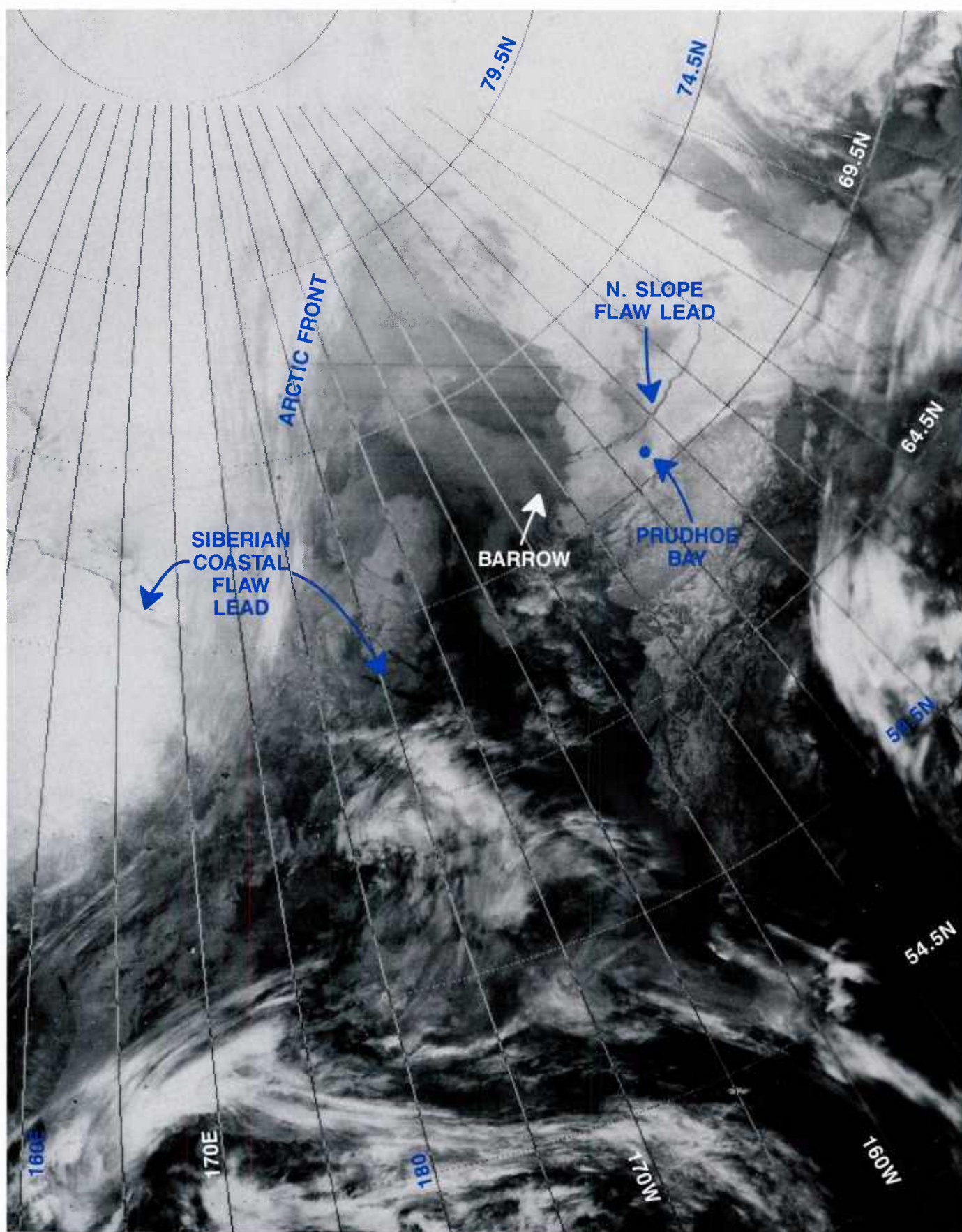


3A-49a DMSP infrared (TS) data (with overlay). 2024 GMT, 11 April 1991.



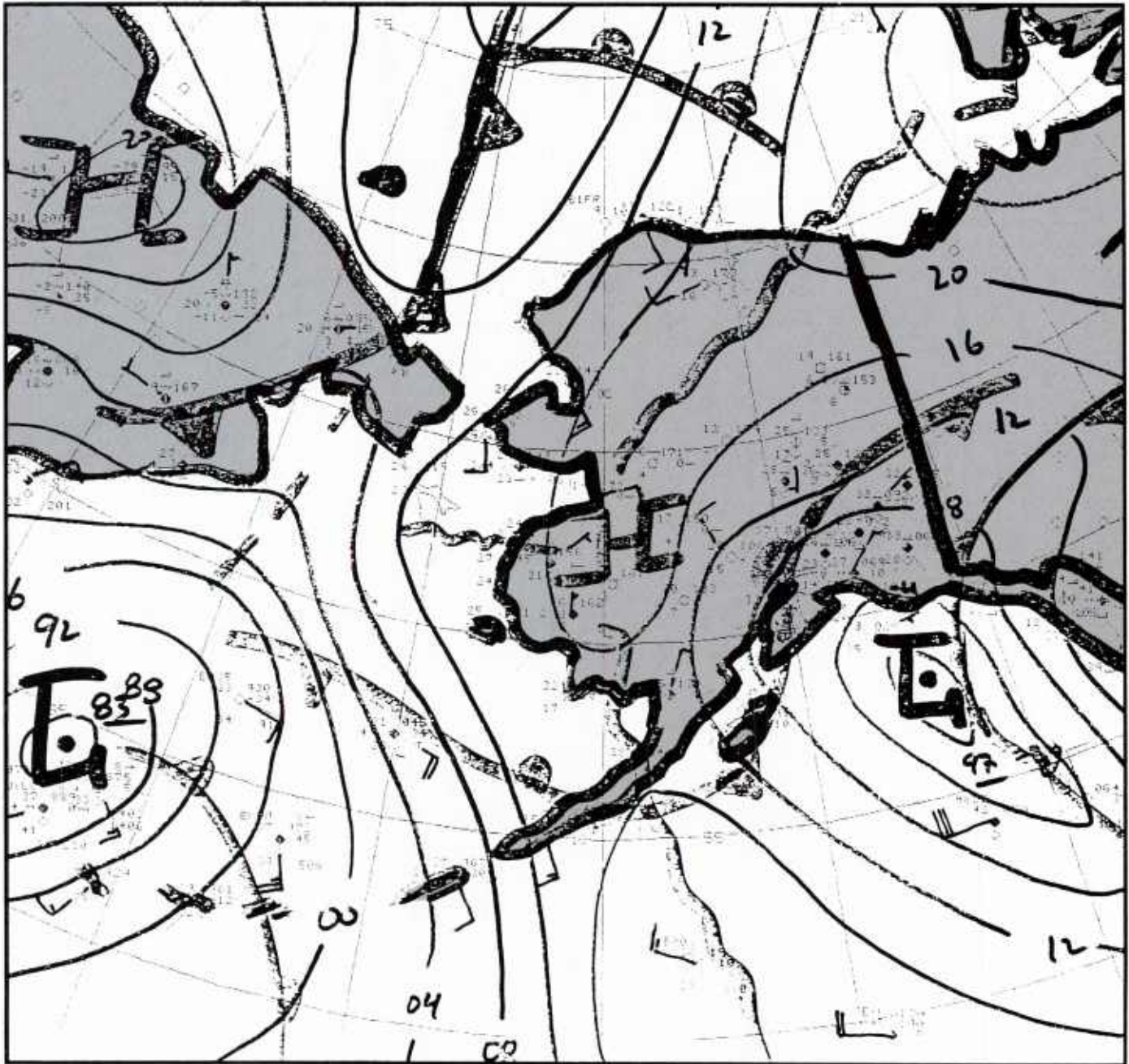
*12 April 1991*

A DMSP infrared (TS) view of the region on 12 April at 0923 GMT is shown in Fig. 3A-50a. This remarkable image shows further coalescence of the warm, moist surge of air into an extensive low cloud area in advance of the Arctic front. This flow was becoming cut-off, however, as a low pressure system with a cloud vortex near 63.5°N, 180° moved eastward through the Bering Sea. Evidence of "cutting-off" of the warm surge is the sudden appearance of a perfectly clear area over the Chukchi Sea just east of the Arctic front near 71°N, 170°W. The Siberian coastal lead and additional leads within the drift ice are visible within the clear area. Figure 3A-51a is the Fairbanks NWS surface analysis for 1800 GMT. The analysis shows the cold front east of Wrangel Island and a warm front segment north of Barrow. Again, the depiction of the classic warm front in this example does not seem appropriate. By 11 April at 1200 GMT (Fig. 3A-41a and Fig. 3A-42a) the temperature at Barrow warmed from -31° (10 April) to -17°C. On 12 April at 1200 GMT (Fig. 3A-52a) a further warming to -10°C is indicated. The warming at Barrow and at locations over the drift ice to the north occurred long before a warm front was indicated passing over the region. Effects of the warming extended at the surface almost to the North Pole. In this analysis Barrow is reporting overcast skies with stratocumulus cloudiness having a base from 600-999 m (2,000-3,299 ft). As seen from the DMSP data on 12 April at 0923 GMT (Fig. 3A-50a), Barrow lies under the induced cloud shield of the warm surge. Conditions at Barrow are probably representative of conditions for a large area under the warm, low cloud shield.

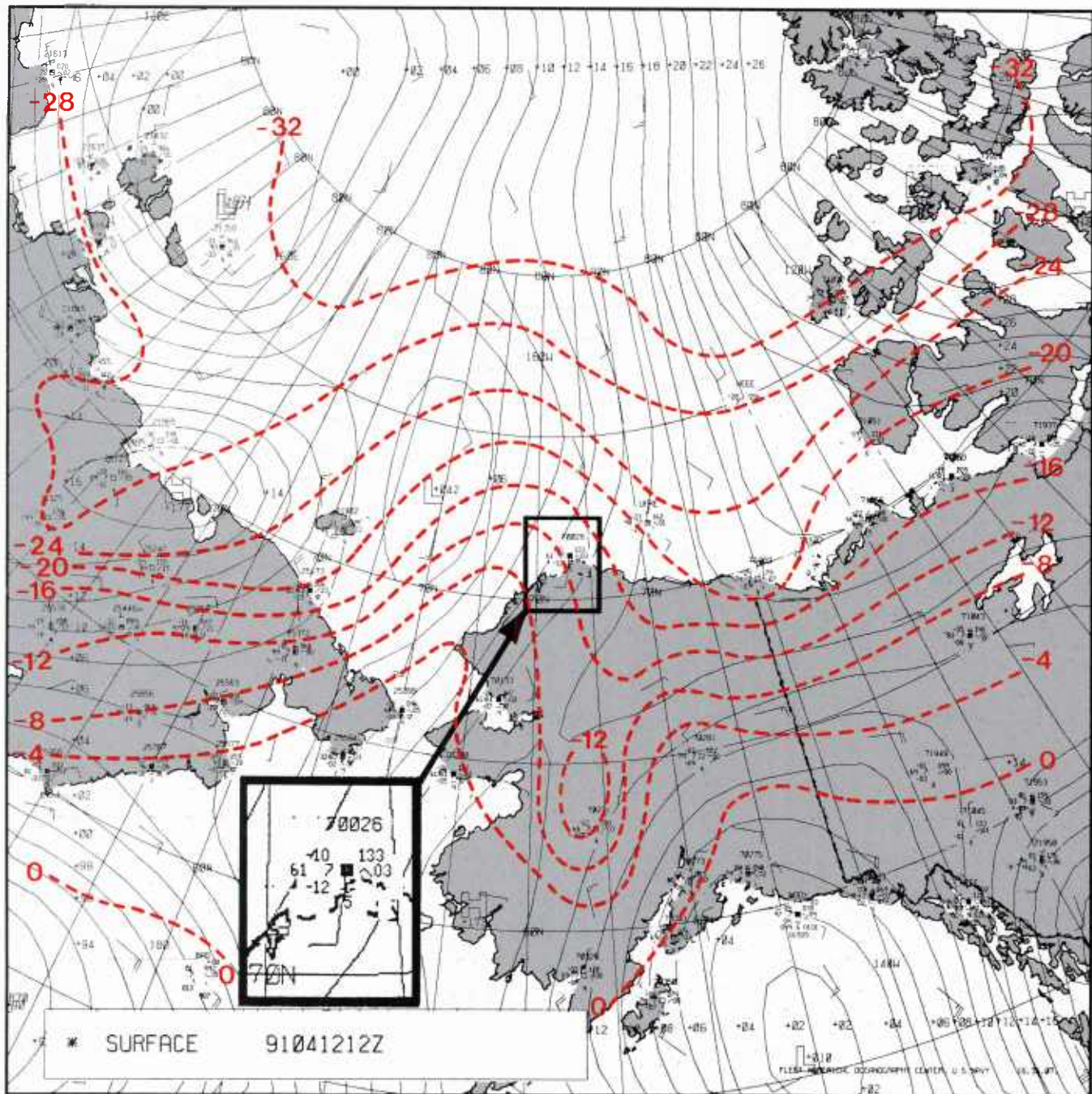


3A-50a DMSP infrared (TS) data (with overlay). 0923 GMT, 12 April 1991.





3A-51a Fairbanks, Alaska NWS surface analysis. 1800 GMT, 12 April 1991.



3A-52a FNOC surface analysis. 1200 GMT, 12 April 1991. (Isotherm analysis in degrees Celsius shown in red as an overlay. Weather observation for Barrow, Alaska is shown in enlarged format.)



13 April 1991

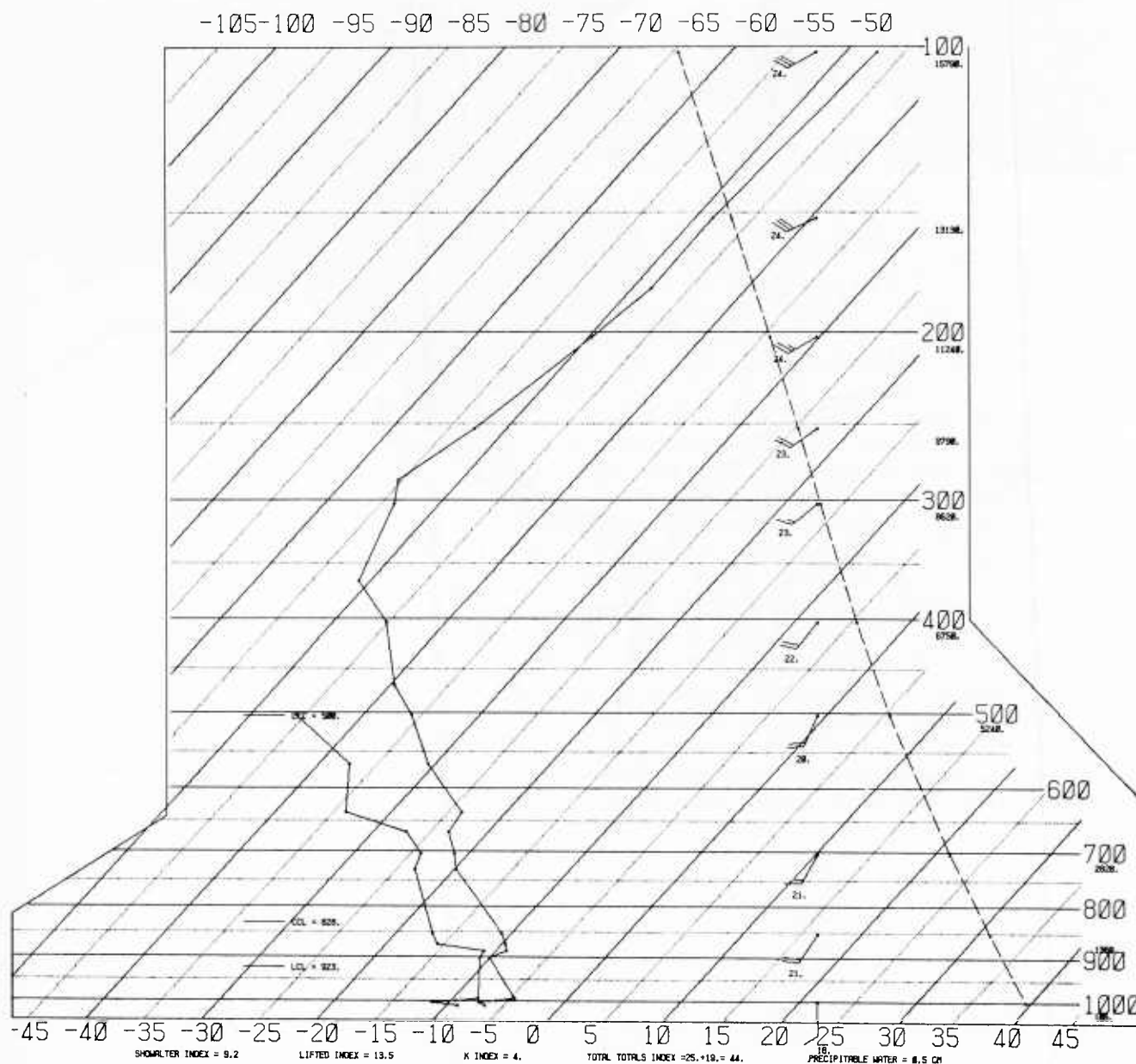
The Barrow sounding for 0000 GMT (Fig. 3A-53a) suggests a thin deck of clouds forming near the 900-mb level (near 1,000 m or 3,200 ft) in excellent agreement with the surface data report (Fig. 3A-52a). Note that the surface temperature in this analysis shows a further warming to  $-7^{\circ}\text{C}$ .

# SKEW T, LOG P DIAGRAM

910413

0000Z

70026



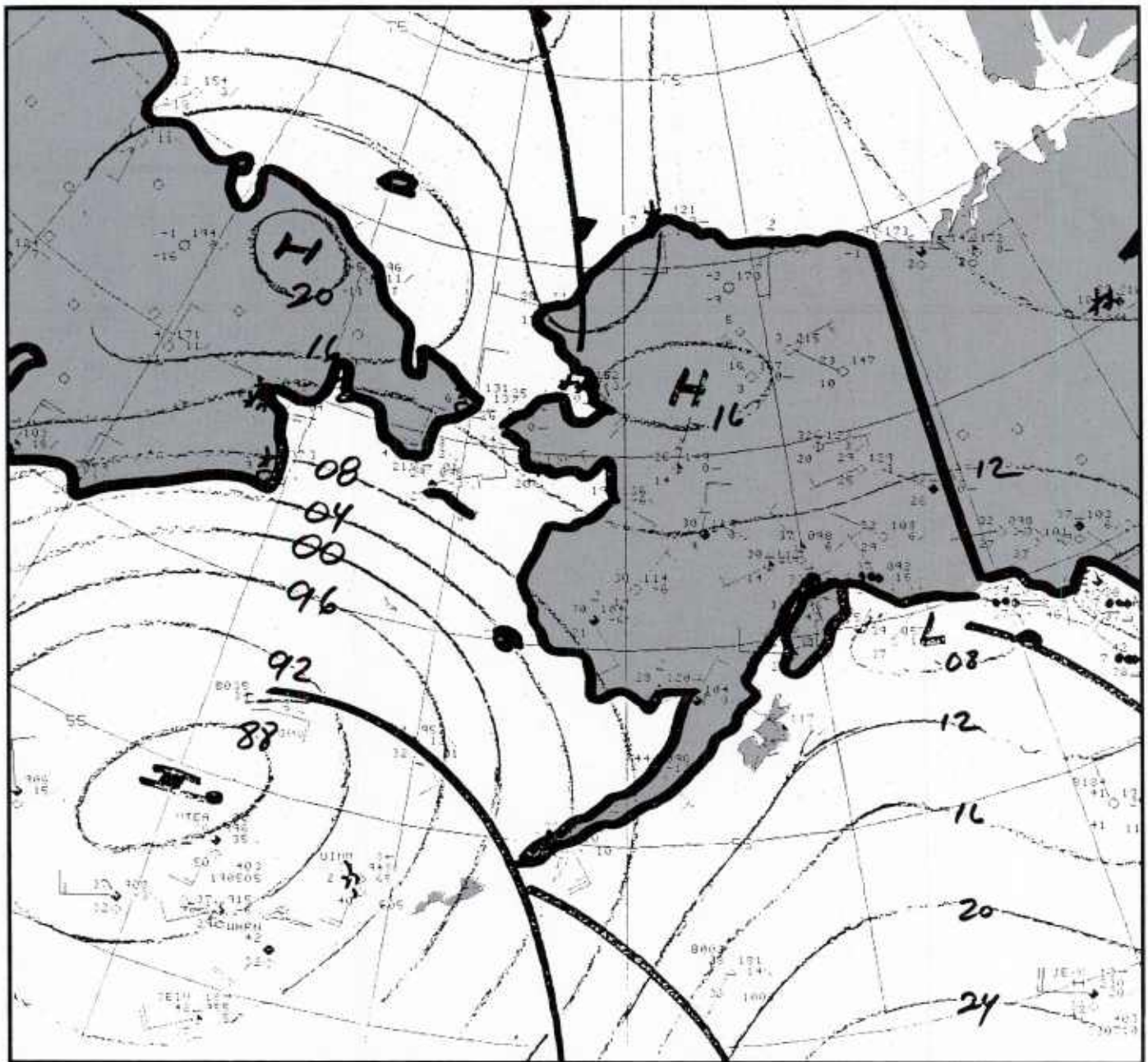
3A-53a Radiosonde data for Barrow, Alaska. 0000 GMT, 13 April 1991.

By 0600 GMT the cold front was still approaching Barrow as shown in the Fairbanks NWS surface analysis (Fig. 3A-54a). High pressure moved in behind the front over coastal Siberia, producing onshore flow in the area where a wide flaw lead was previously observed (Figs. 3A-37a and 3A-38a). The front was very close to Barrow by 1200 GMT, as indicated by the appearance of the isotherm field on the FNOC surface analysis for that time (Fig. 3A-55a). Apparent from this analysis, the surge of warm air from the Bering Sea still noticeable 24 hours earlier (Fig. 3A-52a), has now been cut off, as a vigorous low pressure system moved into the Bering Sea. Moderate northeasterly flow is indicated pushing the ice toward the coast of northern Siberia in the region southeast of Wrangel Island. Easterly flow south of the Bering Strait has prevented any further extension of the warm surge from that area.

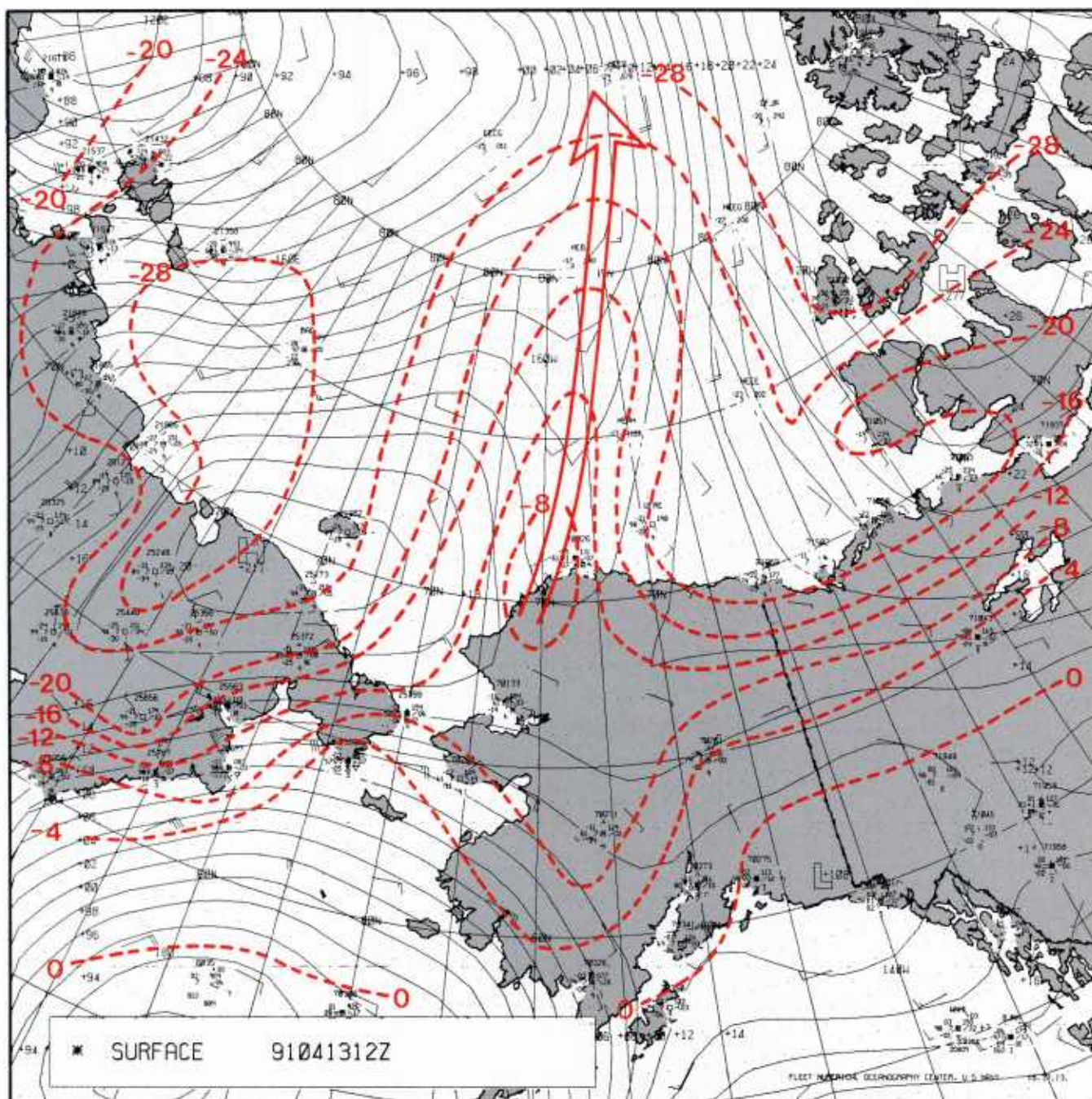
A flight was made on 13 April from Prudhoe Bay to the LEADDEX ice camp (73.25°N, 145°W) in the morning, with a return flight near midnight (GMT). Figure 3A-56a is a DMSP visible image near the time of takeoff (1729 GMT). As seen, the route was largely clear of clouds at this time but closing in as the Arctic front approached the region. Figure 3A-57a is a 35-mm color image of the flaw lead just north of Prudhoe Bay looking to the west. A view to the east is shown in Fig. 3A-58a. The effect of southerly flow has caused the lead to develop with open water on the south side of each image. The different conditions have been numbered in Fig. 3A-57a: (1) open water, (2) grease ice, (3) dark nilas, (4) light nilas, (5) gray ice, and (6) first year ice. Figure 3A-58a shows conditions observed east of the aircraft: (1) open water, (2) grease ice, (3) light nilas, (4) gray ice, and (5) first year ice. The dark nilas category noted in Fig. 3A-57a cannot be detected in Fig. 3A-58a.

Other smaller leads north of the flaw lead were encountered enroute to the ice camp. Figure 3A-59a shows a lead extending to the northeast over the Beaufort Sea. This is one of the smaller leads evident north of the flaw lead in the DMSP data of Fig. 3A-56a. Again six conditions appear evident: (1) a small area of open water, (2) grease ice, (3) dark nilas, not broken up, however, as in Fig. 3A-57a, (4) light nilas, (5) gray ice, and (6) first year ice. A final aircraft example is shown in Fig. 3A-60a. This lead exhibited only a small and not continuous line of open water. The rest of the lead shows only gray ice and then first year ice. None of the leads showed any visual evidence of air-sea interaction in the form of steam fog or condensation plumes, despite the fact that the surface temperature was around  $-23^{\circ}\text{C}$  ( $-9.4^{\circ}\text{F}$ ). This example may relate to Nelson's (1969) observation that steam fog is first noticeable only when the air temperature is approximately  $-26.6^{\circ}\text{C}$  ( $-14^{\circ}\text{F}$ ).



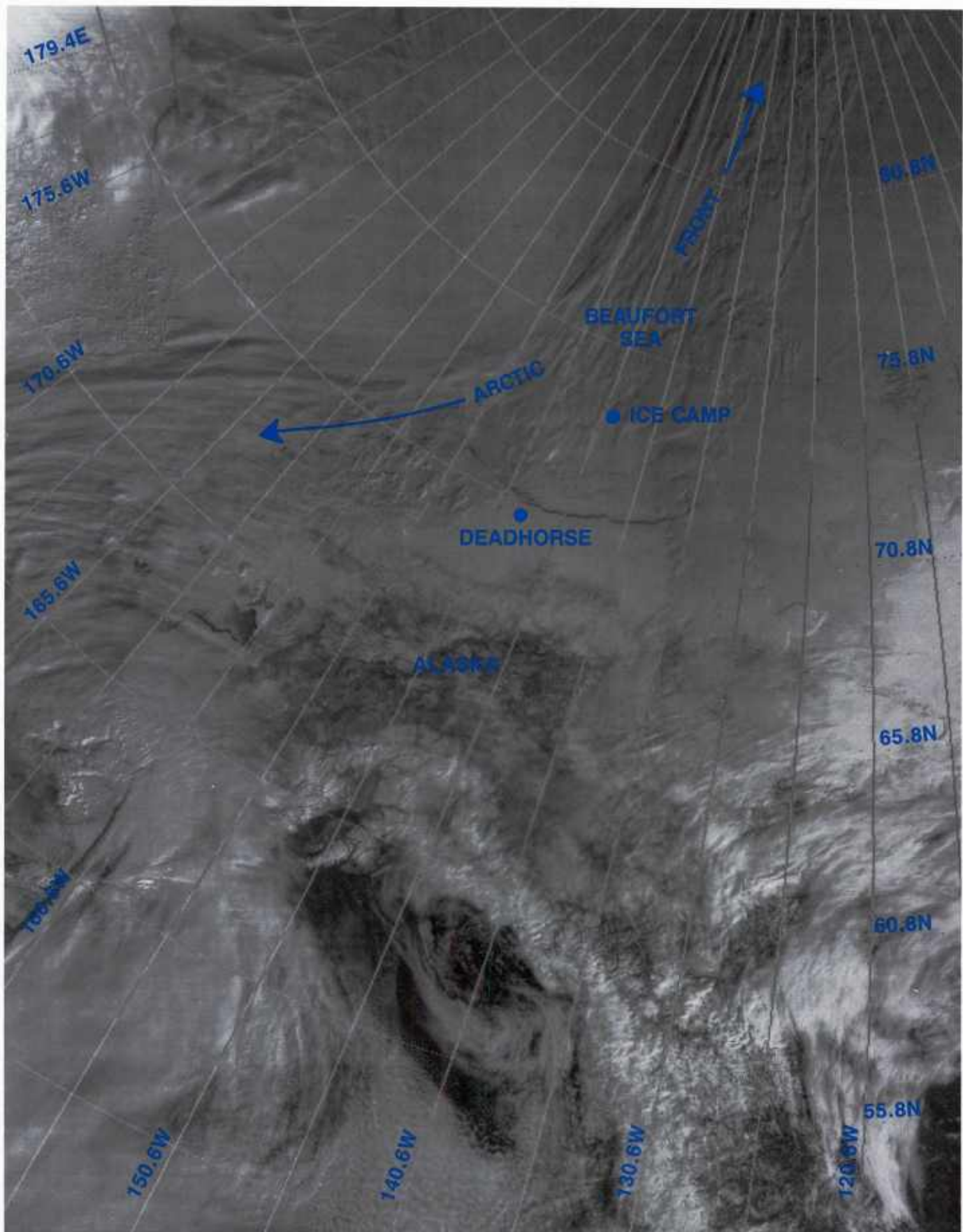


3A-54a Fairbanks, Alaska NWS surface analysis. 0600 GMT, 13 April 1991.

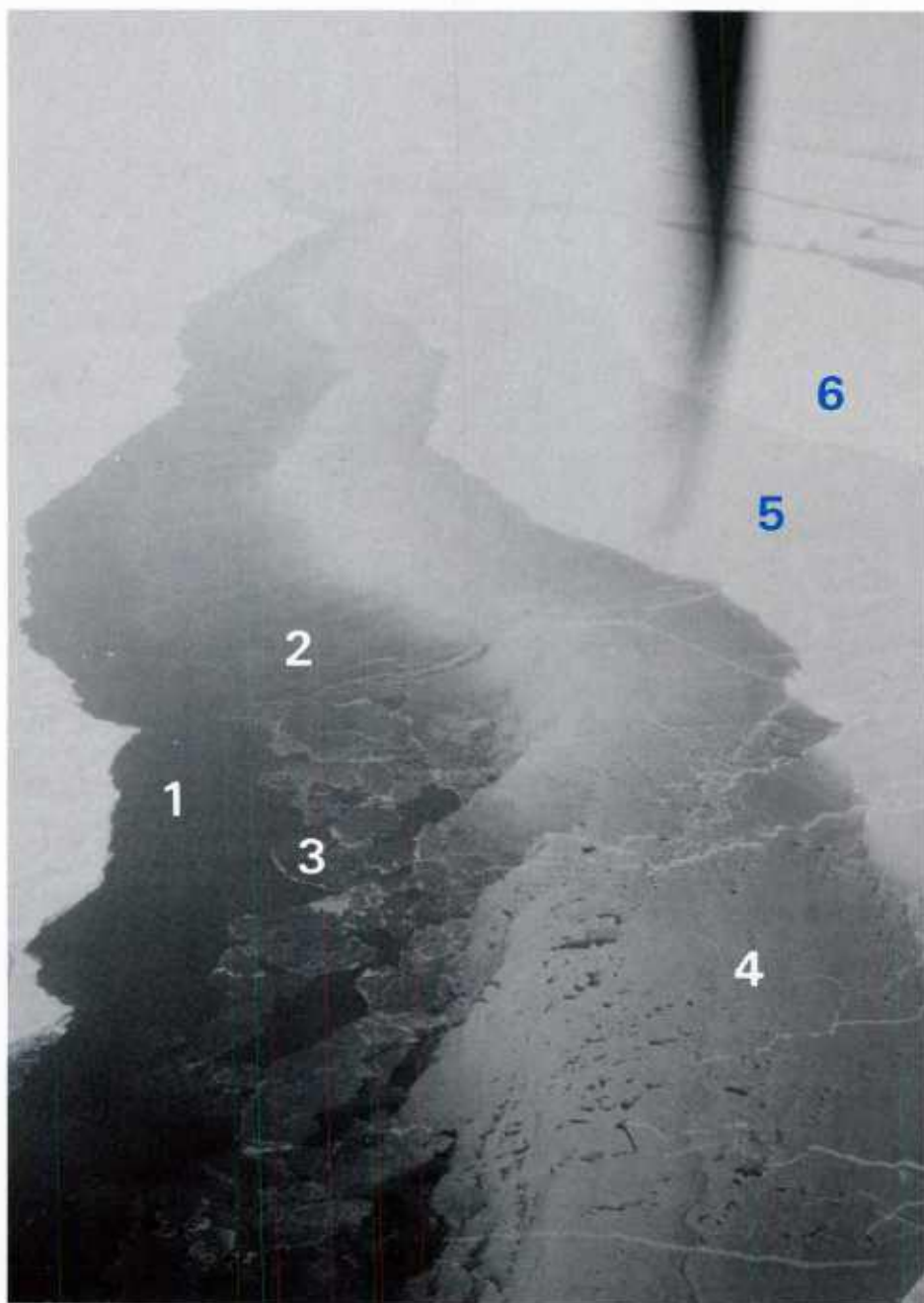


3A-55a FNOC surface analysis. 1200 GMT, 13 April 1991. (Isotherm analysis in degrees Celsius shown in red as an overlay. Warm surge is indicated by an arrow.)



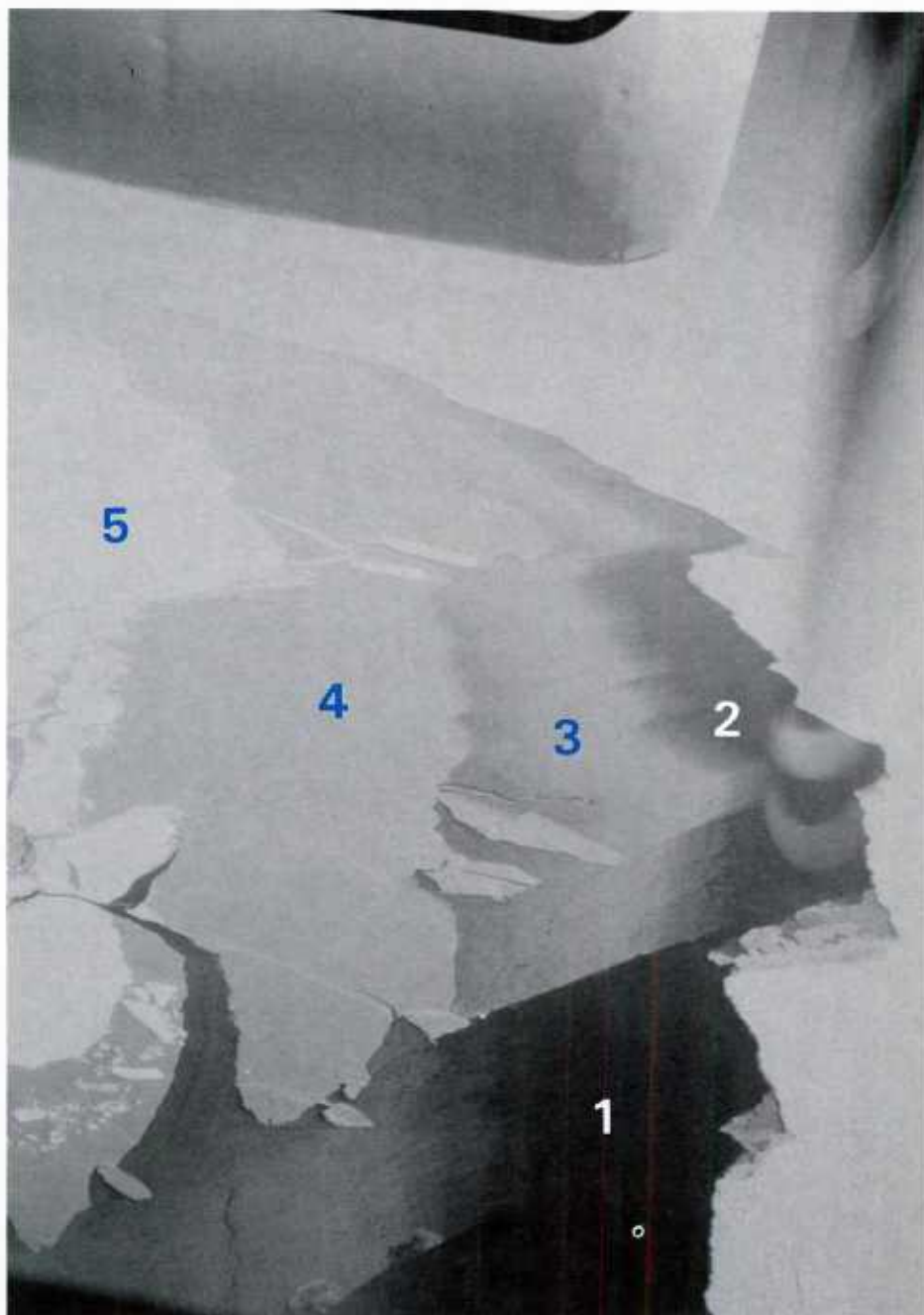


3A-56a DMSP visible (LF) data (with overlay). 1729 GMT, 13 April 1991.

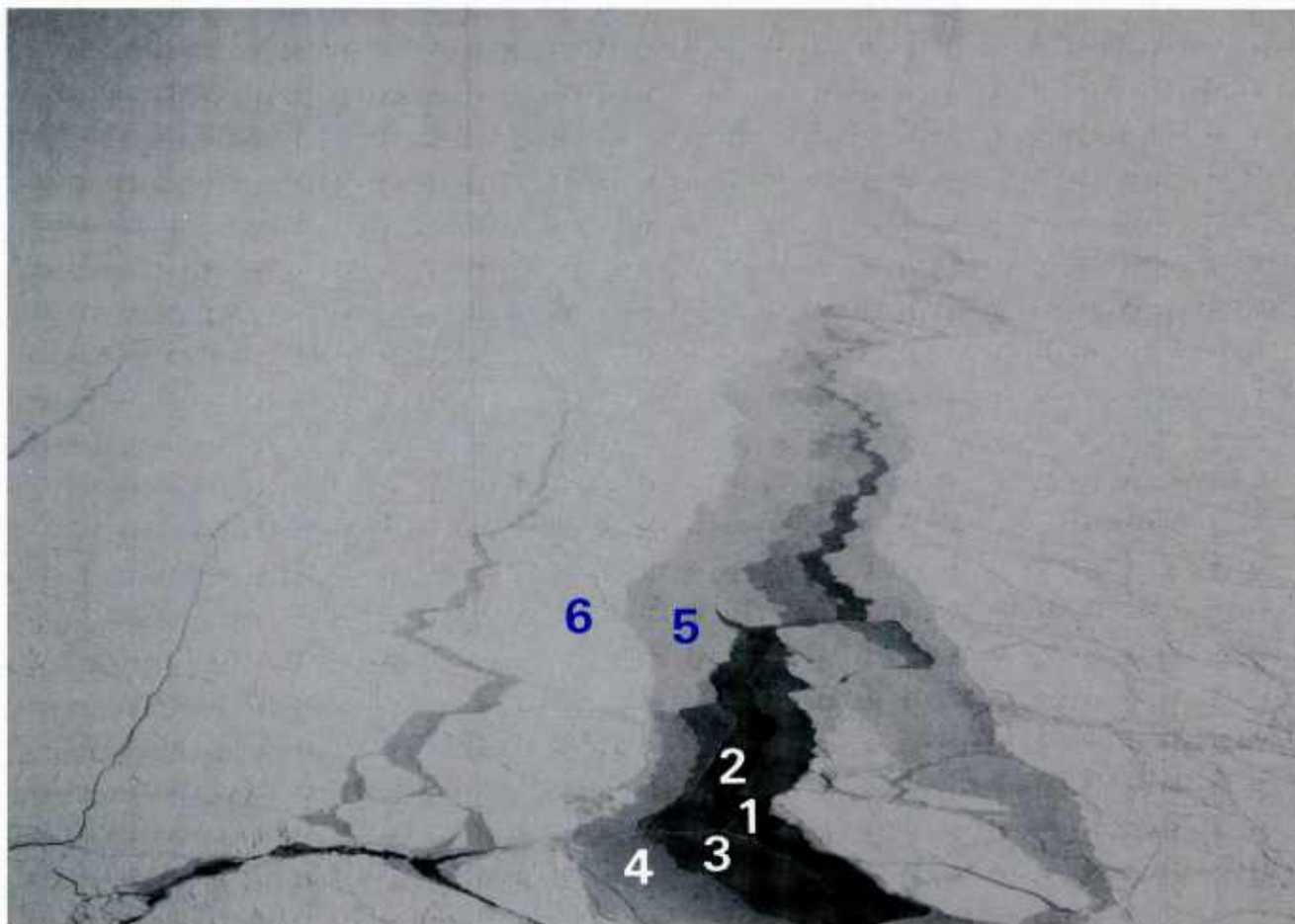


3A-57a A 35-mm color image of Beaufort flaw lead looking west: 1 = open water; 2 = grease ice; 3 = dark nilas; 4 = light nilas; 5 = gray ice; and 6 = first year ice.



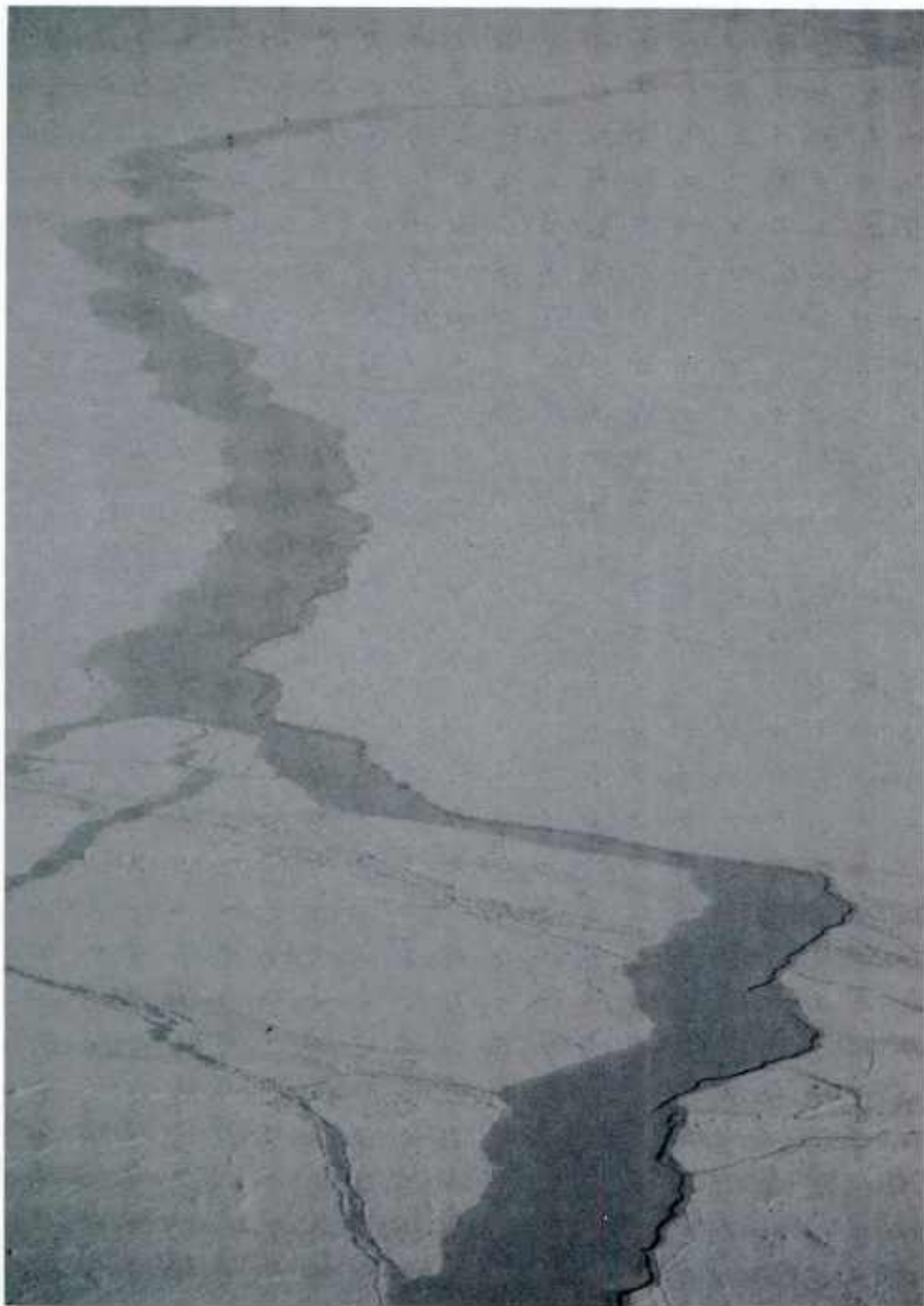


3A-58a A 35-mm color image of a Beaufort flaw lead looking east: 1 = open water; 2 = grease ice; 3 = light nilas; 4 = gray ice; 5 = first year ice.



3A-59a A 35-mm color image of a Beaufort flaw lead extending to the northeast: 1 = open water; 2 = grease ice; 3 = dark nilas; 4 = light nilas; 5 = gray ice; and 6 = first year ice.

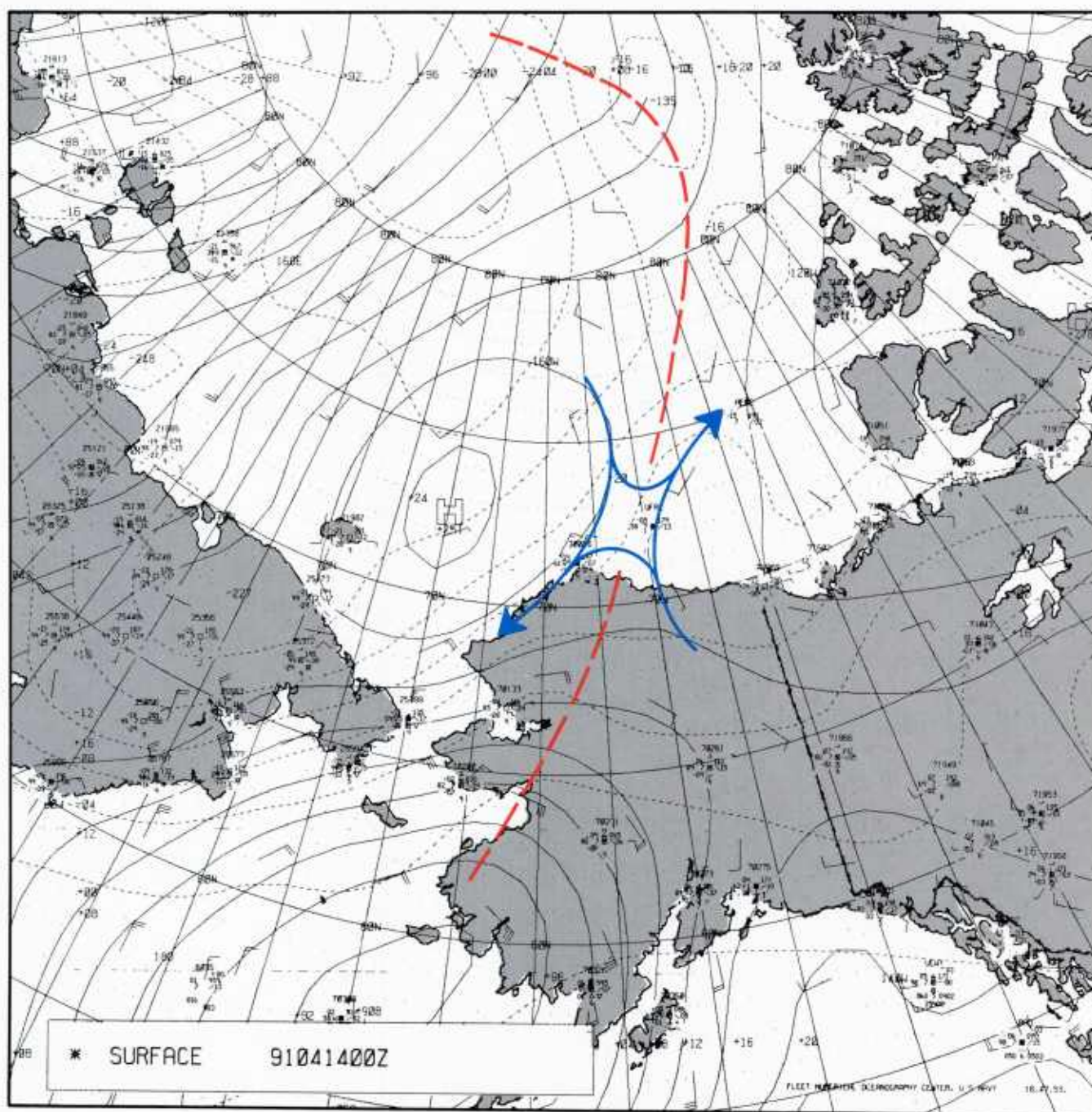




3A-60a A 35-mm color image of a Beaufort flaw lead extending to the northeast.

14 April 1991

The front had moved past Barrow on 13 April by 1800 GMT as winds at Barrow shifted from southerly to northerly. Figure 3A-61a is the FNOC surface map for 14 April at 0000 GMT. The analysis shows Barrow reporting north-easterly winds at 15 kt, and northerly flow blowing against the north Siberian coastline. The trough associated with the front is shown east of Barrow extending southward to a low in the Bering Sea. The trough extends over the Arctic Ocean well to the north, curving back toward low pressure west of the New Siberian Islands. A col region is shown just northeast of Barrow.

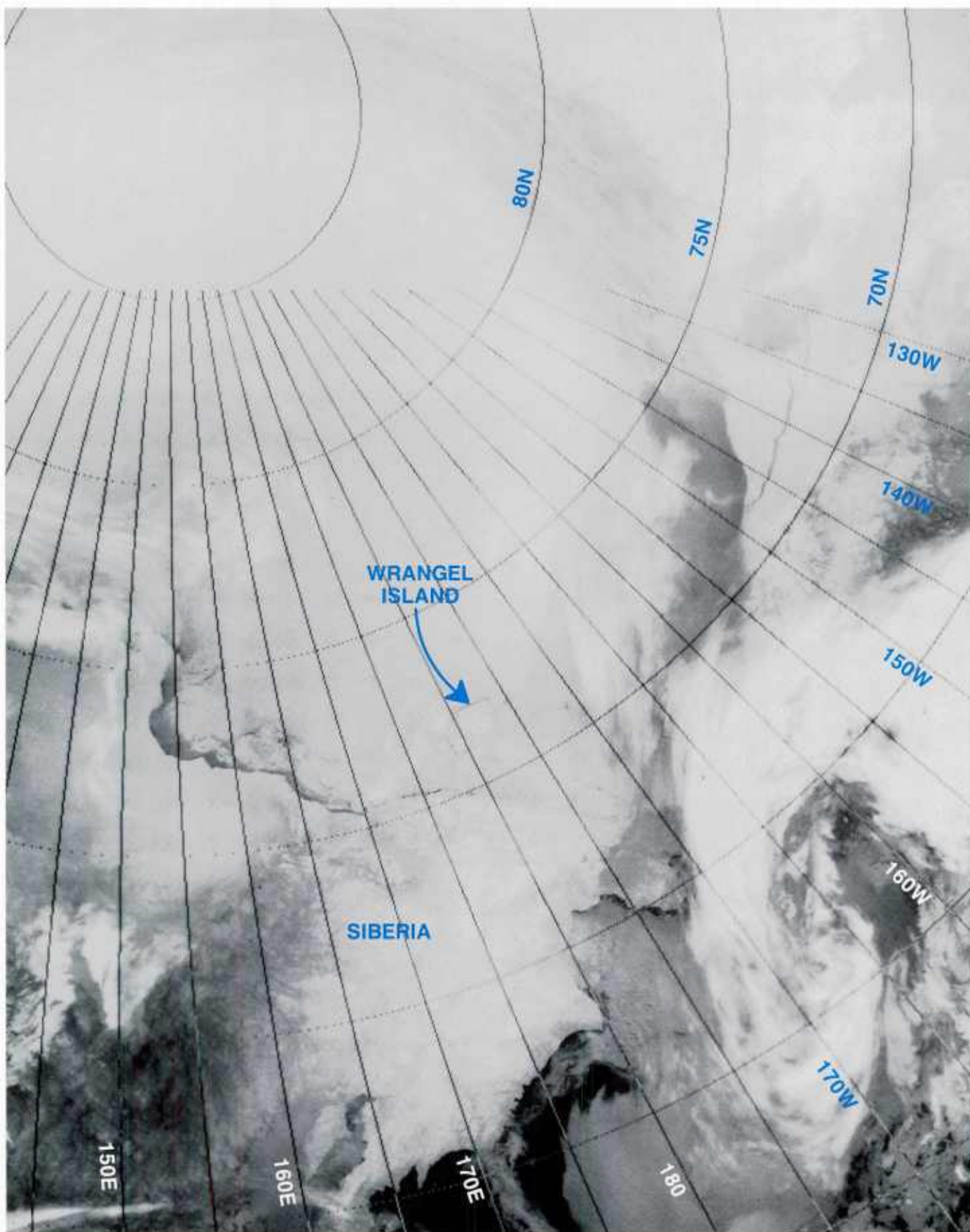


3A-61a FNO surface analysis. 0000 GMT, 14 April 1991. Col area and trough are shown as an overlay.



The DMSP infrared (TS) data at 0719 GMT (Fig. 3A-62a) reveal the Arctic front positioned close to the region of the trough shown in the FNOC data (Fig. 3A-61a). The warm nature of overcast cloudiness northeast of Barrow is suggestive of col cloud cloudiness as discussed in Section 1B, Cases 2 and 3. The region does in fact lie within a col as analyzed on the FNOC surface chart (Fig. 3A-61a). At Barrow the surface observation at 0000 GMT indicated overcast stratus conditions with a cloud base of 1 to 2,000 ft in snowshowers and a visibility reduced to 11 km. Such conditions are typical of col cloud systems.

Note in the DMSP data (Fig. 3A-62a) that the flaw lead along the north Siberian coast southeast of Wrangel has essentially closed. Previous views on 10, 11, and 12 April (Figs. 3A-37a, 3A-38a, 3A-43a, 3A-44a, 3A-45a, 3A-46a, 3A-49a and 3A-50a), prior to frontal passage when winds were blowing offshore, showed the lead open and as much as 20 nm in width. An additional item of interest is that both Wrangel Island and Herald's Reef show polynyi developing on their western sides, indicating a reversal of drift ice flow from easterly (as shown in Figs. 3A-23a and 3A-24a) back to westerly in that region. This development is consistent with easterly winds over the area shown in the FNOC surface analysis (Fig. 3A-61a). The rapidity of change in ice direction of movement despite winds of only 10–15 kt in a few hours is noteworthy.



3A-62a DMSP infrared (TS) data (with overlay). 0719 GMT, 14 April 1991.



### Important Conclusions

1. Arctic fronts and associated winds play a major role in the opening and closing of flaw leads along the Siberian and Alaskan coastlines.
2. Surge effects of southerly flow bringing heat and moisture into the Arctic Basin are responsible for much of the low overcast cloudiness found at times over the region.
3. The classical warm frontal model is inappropriate for use in describing attributes of a warm surge.
4. Roughness differences between ocean ice and snow and ice-covered land create albedo differences that can be sensed by satellite and aircraft in the visible portion of the spectrum.
5. Properly enhanced, satellite infrared data can be used to discriminate snow and ice-covered land from shore fast ice, which appears warmer as the result of radiation through the ice from the underlying warmer water. Inland rivers and lakes not frozen to the bottom are similarly revealed.
6. Grounded islands of ice or floebergs that have grounded act as stress coordinators causing formation of leads upwind and downwind of the grounded feature.
7. Direction of ice movement can be determined by noting the presence of polynyi on the lee side of grounded ice islands and other islands and reefs in the Arctic Ocean.
8. Drift ice reverses direction rapidly after wind direction reverses.
9. Flaw leads have a tendency to form when the wind flow is offshore. Similarly, such leads rapidly close with onshore flow.
10. Infrared views of mountain valleys are useful in monitoring satellite imagery and assisting in gridding satellite imagery accurately.
11. Leads apparent in satellite visible and infrared images are often frozen over to a large extent.

### References

- Fett, R.W., and W.F. Mitchell, 1977: Navy Tactical Applications Guide, Vol. 1, *Techniques and Applications of Image Analysis*. NEPRF Technical Report 77-03, Naval Environmental Prediction Research Facility (now Naval Research Laboratory-NRL), Monterey, CA 93943-5006, 176 pp.
- Kovacs, A., A.J. Gow, and W.F. Dehn, 1976: *Islands of Grounded Sea Ice*. CRREL Report 76-4, United States Cold Regions Research and Engineering Lab, Hanover, NH, 24 pp.
- Nelson, R.K., 1969: *Hunters of the Northern Ice*. Univ. of Chicago Press, Chicago, IL 60637, 429 pp.
- Sechrist, F.S., R.W. Fett, and D.C. Perryman, 1989: *Forecasters Handbook for the Arctic*. NEPRF Technical Report 89-12, Naval Environmental Prediction Research Facility (now Naval Research Laboratory-NRL), Monterey, CA 93943-5006, 364 pp.
- Stringer, W.J., and S.A. Barrett, 1975: Ice motion in the vicinity of a grounded floeberg. *Proceedings of the Third International Conference on Port and Ocean Engineering Under Arctic Conditions*, Univ. of Alaska, Institute of Marine Science, Fairbanks, Alaska, 527-551.





## 3B Mountain-Gap Winds

### *Features Associated with the Development of Mountain-Gap Winds*

Mountain-gap winds have previously been described in the NTAG series (Fett and Bohan 1977, NTAG Vol. 1, Sec. 2A, Case 7). Such winds are caused by a component of the low-level pressure gradient directed through the channel or gap in the mountain range (Lackmann and Overland, 1989). Mountain-gap winds frequently develop when colder air and higher pressure build up on one side of a mountain range under stable conditions. When this occurs, air will eventually surge through any gap in the range and accelerate toward lower pressure.

The effect of a mountain-gap wind can be intensified with the approach of a synoptic-scale system that imposes a strong pressure gradient whose major component is essentially parallel to the gap axis (isobars nearly perpendicular to the gap axis). Winds of 100 kts or more have been experienced within mountain gaps and, not infrequently, several hundred kms to the lee. The strongest winds appear to occur during the period in which the sea level pressure gradient is increasing most rapidly (Mass and Albright, 1985).

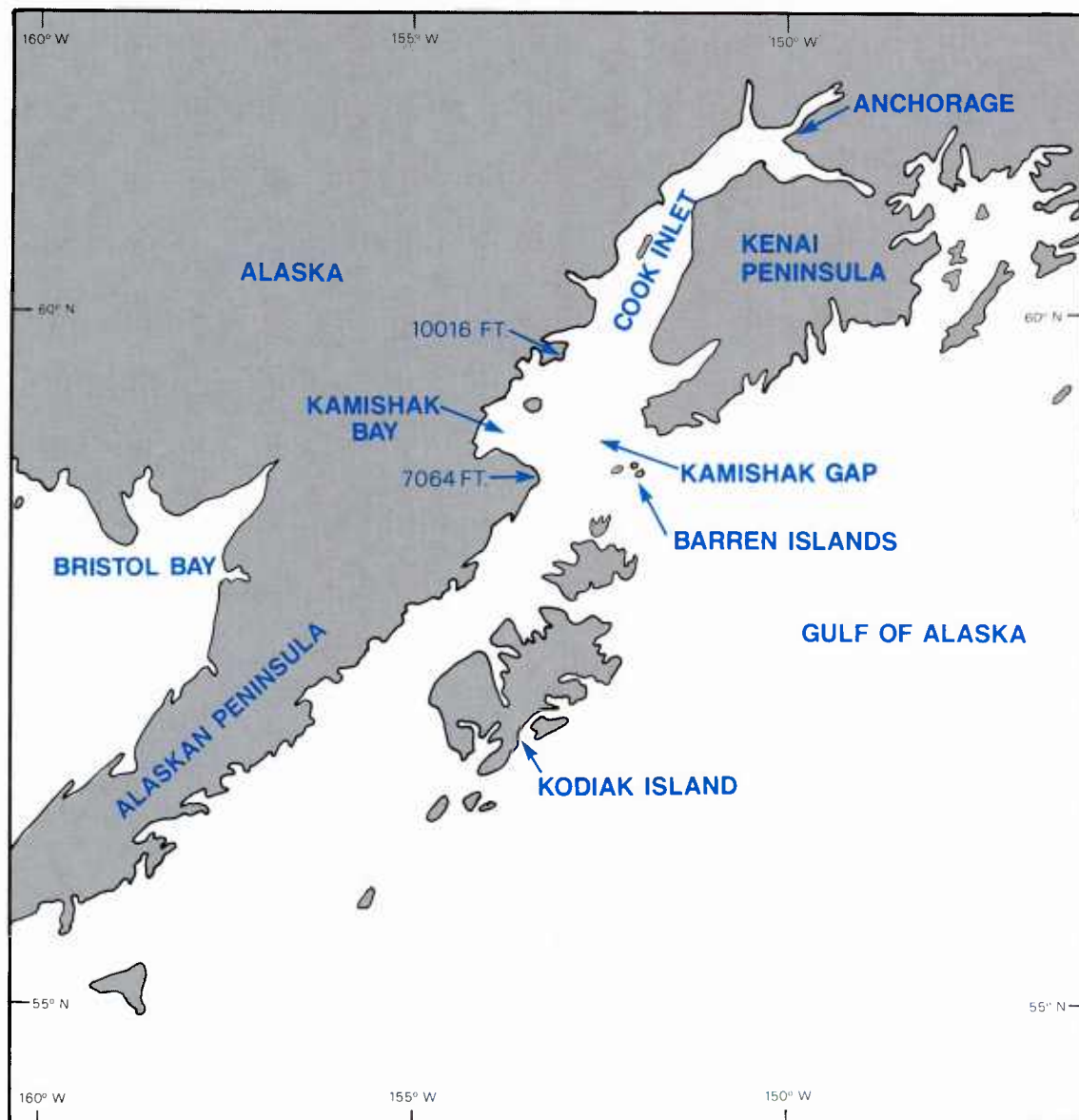
Mesoscale boundary layer effects include a ridging tendency and higher boundary layer heights along the right side of the flow within the gap, and troughing with lower boundary layer heights to the left (Lackmann and Overland, 1989).

### References

- Fett, R.W., and W.A. Bohan, 1977: Navy Tactical Applications Guide, Vol 1, Techniques and Applications of Image Analysis, NEPRF TR 77-03, Naval Environmental Prediction Research Facility, Monterey, CA, 93943-5006, pp 176.
- Lackmann, G.M., and J.E. Overland, 1989: Atmospheric Structure and Momentum Balance during a Gap-Wind Event in Shelikof Strait, Alaska, Mon. Wea. Rev., Vol 117, pp 1817-1833.
- Mass, C.F., and M.D. Albright, 1985: A Severe Windstorm in the Lee of the Cascade Mountains of Washington State, Mon. Wea. Rev., Vol 13, pp 1261-1281.

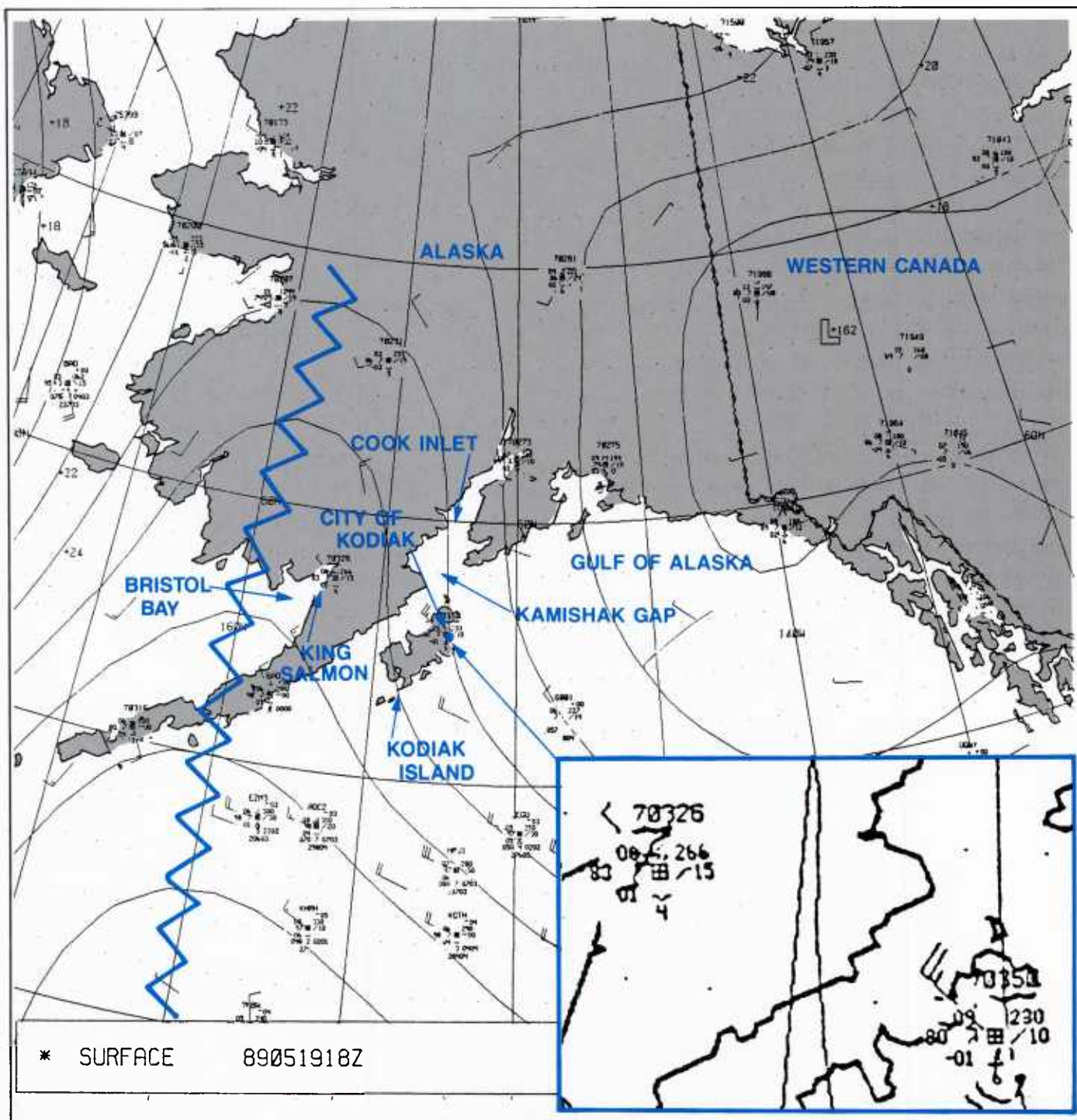
## Case 1 The Kamishak Gap Wind

Kamishak Bay lies at the extreme southwest portion of Cook Inlet, which stretches from Anchorage, on the northeast end of the Inlet, southwestward to the northeast end of the Alaskan Peninsula. The Bay lies between two high mountain peaks as shown in Figure 3B-2. Several smaller peaks with intervening valleys lie between the two higher peaks. Marshland then extends from the mountainous coastal region of Cook Inlet west-southwestward to Bristol Bay. When high pressure builds over the lowlands west of Cook Inlet and low pressure exists over the northern portion of the Gulf of Alaska or southeastern Alaska, a pressure gradient is developed which will cause an acceleration of the wind from the lowland and high pressure region through the Kamishak Gap, past the Barren Islands, between Kodiak and the Kenai Peninsula, and further out to sea. These winds are much stronger than the winds on either side of the gap and, in extreme conditions, can reach speeds in excess of 70 kts. Obviously, a sudden, unexpected encounter, especially by smaller vessels, of winds of this magnitude with commensurate sea state, depending on fetch, poses a significant and often life-threatening hazard. In wintertime, in particular, the additional problem of ice accretion on ships due to high seas and wind-driven spray, in sub-zero conditions, can spell disaster (see Sec 1A, Case 2 of this NTAG volume).



3B-2 Locator map for southern coast of Alaska.





3B-3 FNO surface analysis. 19 May 1989, at 1800 GMT.

19 April 1989

The FNO surface analysis for 1800 GMT (Fig. 3B-3) shows a ridge extending northward past the Alaskan Peninsula, over Bristol Bay, and into western Alaska, just west of Cook Inlet. Low pressure (1016.2 mb) is shown to exist over Canada in the Northwest Territories with cyclonic flow extending into the Gulf of Alaska. The isobaric pattern produces a pressure gradient that could accelerate winds through the Kamishak Gap. In this latter respect, it is of interest to note that King Salmon (Station 70326), west of the Gap, is reporting only a light northwesterly wind, while Kodiak (Station 70350), east of the Gap, reports northwesterly winds of 25 kts.

A DMSP visible (LF) image of the region at 1630 GMT (Fig. 3B-4) shows the overall area to be mainly cloud covered. However, the eastern portion of the image is illuminated by sunglint, and the Kamishak Gap region is relatively clear of cloudiness. Sunglint also extends northward and has illuminated a portion of the Yukon River.

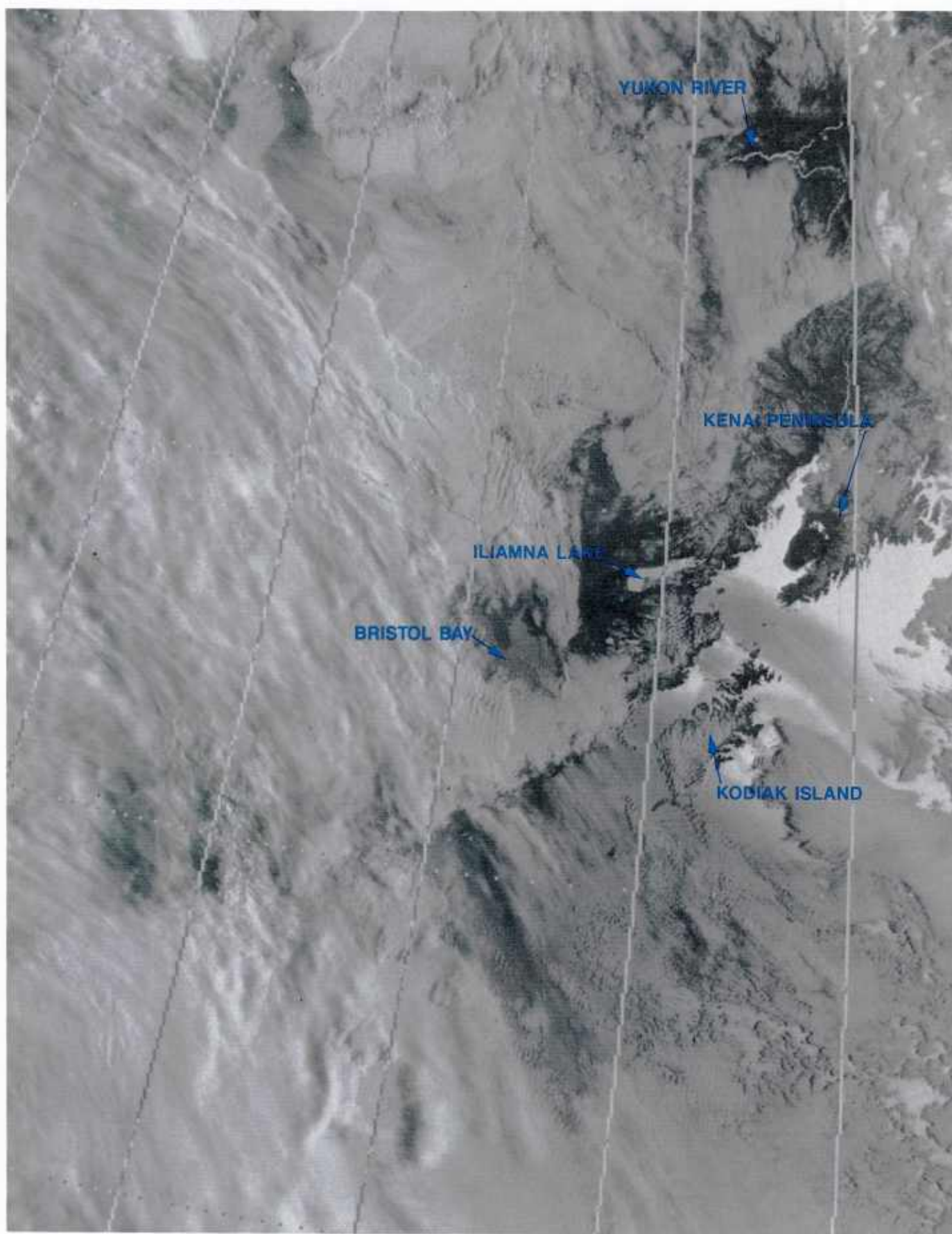
An additional enlargement of the Kamishak Gap area is shown in Figure 3B-5. This figure clearly reveals the dark swath of wind-roughened seas caused by the jet-like Kamishak wind blowing past the Barren Islands into the Gulf of Alaska. The roughened seas appear darker because many of the capillary wave facets in this region are diverting sunglint reflection away from the spacecraft sensor. In the brighter areas, seas are calmer, and spacecraft/sun geometry is such that the sun's rays in those areas are reflected directly into the spacecraft sensor. These differences in reflectivity enable one to locate the exact areas of rough versus relatively calm seas.

The long, thin, streaks in the lee of the Barren Islands indicate the topographic sheltering influence of the island barriers. Terrain height on these islands ranges from 980 to 1986 ft. The fact that the calm streaks extend many miles downstream of the islands indicates very stable conditions of smooth, almost laminar flow. Turbulence is found only at the air/sea boundary interface. In this region, spray can severely limit surface visibility, while at mast level the visibility can be unlimited.

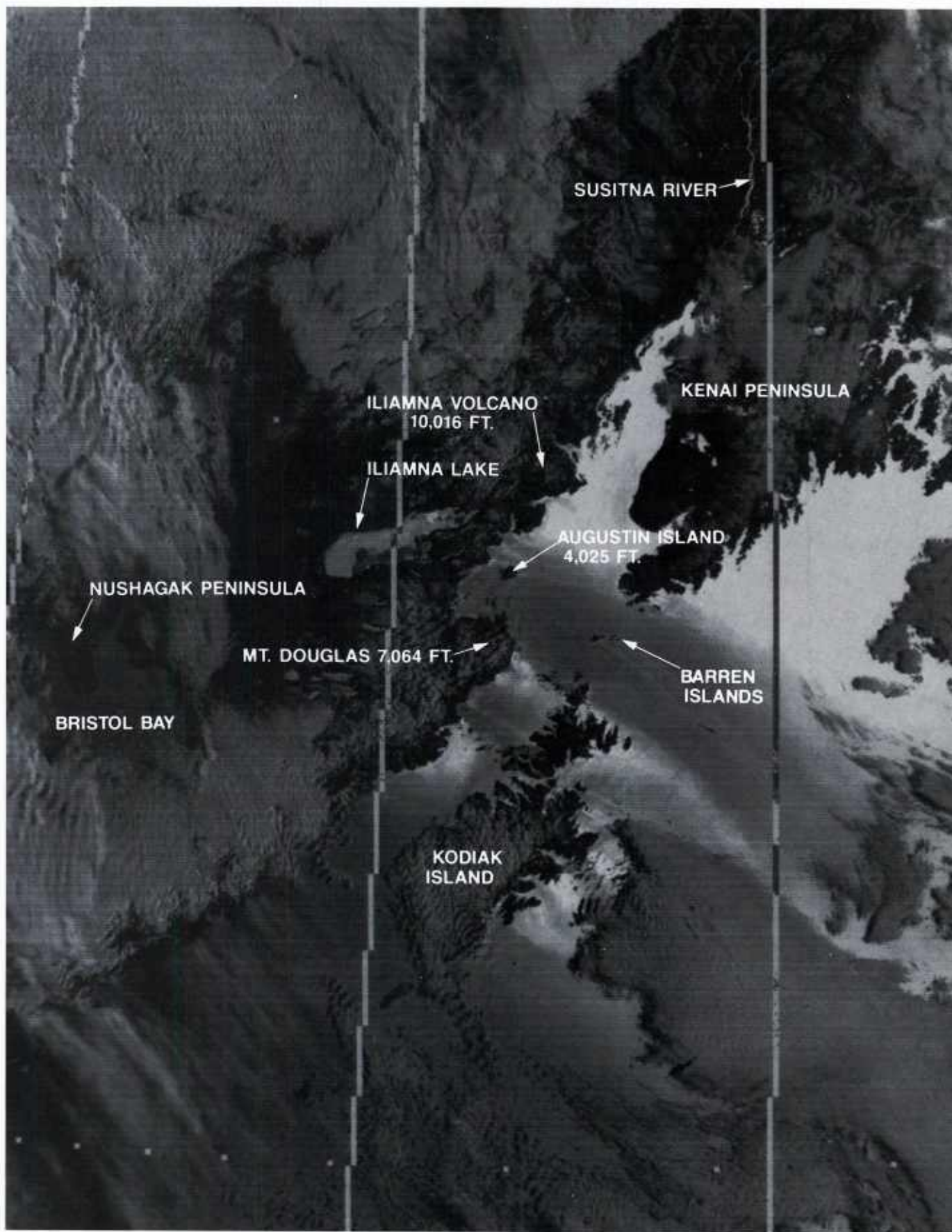
### **Important Conclusions**

1. When high pressure is forecast west of the Cook Inlet, and low pressure in or near the Gulf of Alaska, conditions favor strong northwest winds through the Kamishak Gap.
2. The Kamishak Gap wind can be dangerous, particularly in winter, when ship icing due to wind-driven spray can be severe.
3. Protection from the Kamishak wind can sometimes be found in restricted swaths in the lee of the Barren Islands, or by sailing northeast or southwest.



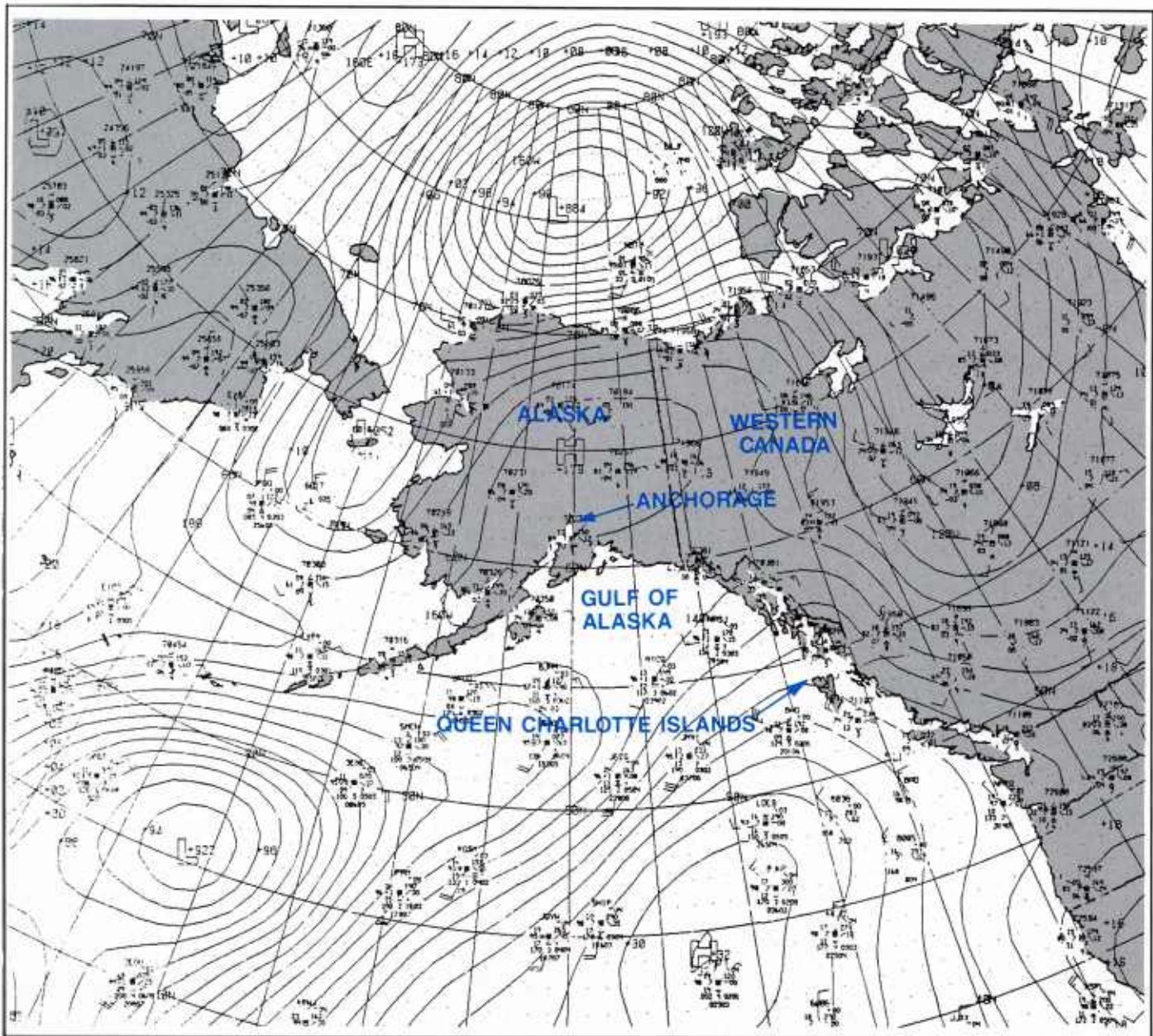


3B-4 DMSP visible (LF) image. 19 May 1989, at 1630 GMT.



3B-5 Enlargement of Fig. 3B-4 showing roughened sea swath through the Kamishak Gap.





3B-6 FNOC surface analysis. 22 September 1986, 0000 GMT.

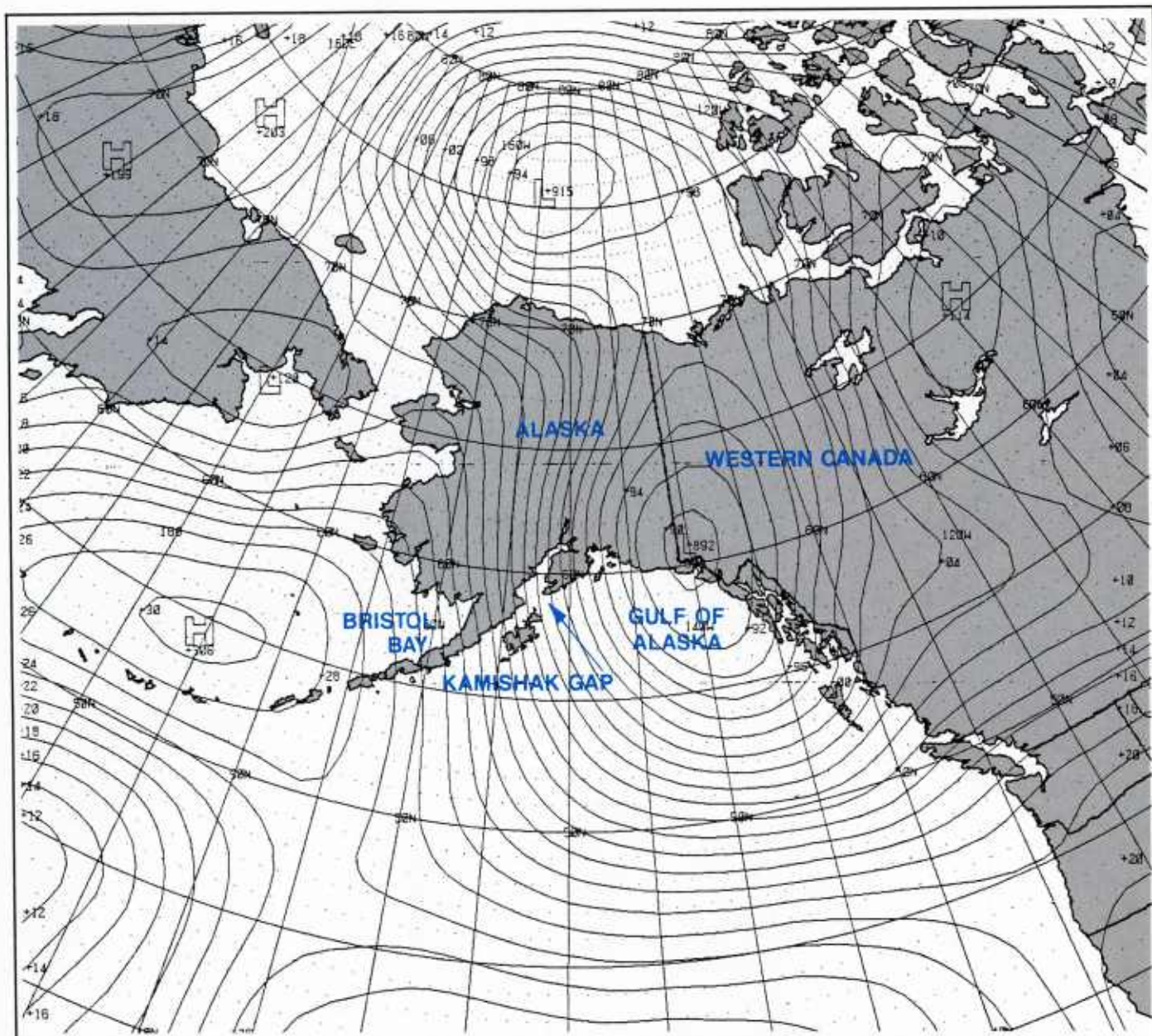
## Case 2 *A Synoptic Intensification of the Kamishak Gap Wind*

22 September 1986

On 22 September 1986 (Local Time), aircraft carrier U.S.S. Constellation was en route from near the Queen Charlotte Islands to Anchorage, Alaska, in an exercise that included a scheduled meeting and ceremony on 23 September with the mayor of Anchorage.

At 0000 GMT, the FNOC surface analysis (Fig. 3B-6) showed high pressure over central Alaska and a col, indicative of light winds, over the Gulf of Alaska. This type of weather would pose no hazard to entering Cook Inlet on the following day.



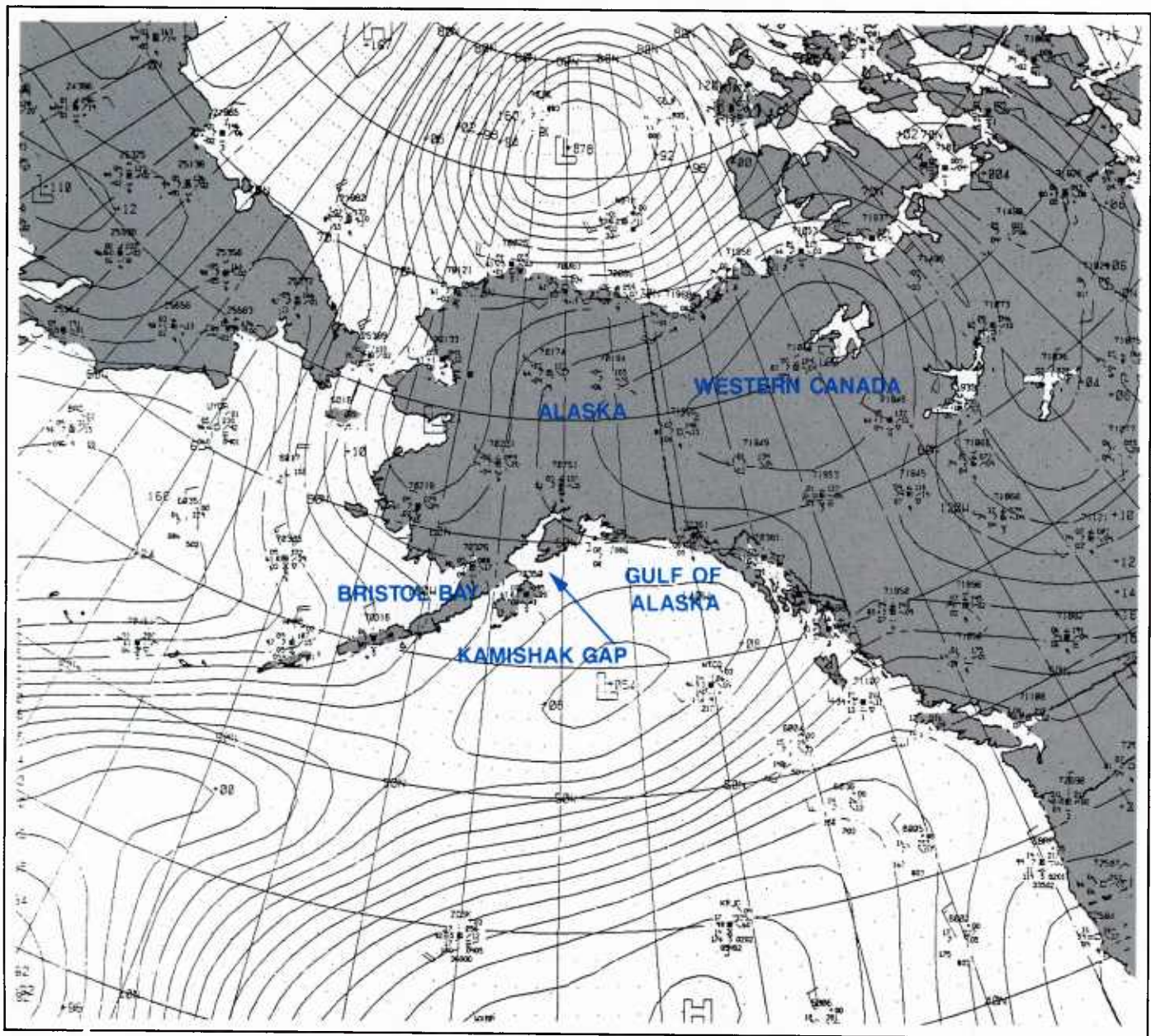


3B-7 FNOC 36 hour surface prog. Valid 23 September 1986, 1200 GMT.

The 36-hr FNOC surface prog, valid for 1200 GMT on the 23rd (Fig. 3B-7), however, showed a significant change by indicating a deep, low-pressure system over SE Alaska, with high pressure building behind, over Bristol Bay. If this scenario unfolded as the prog indicated, very strong winds would be expected to be encountered, especially in the lee of the Kamishak Gap. Unfortunately, this chart was not received aboard Constellation. Failure to receive Fleet products often occurs at sea when communications problems prevent reception of charts or the charts received are blurred and unreadable.

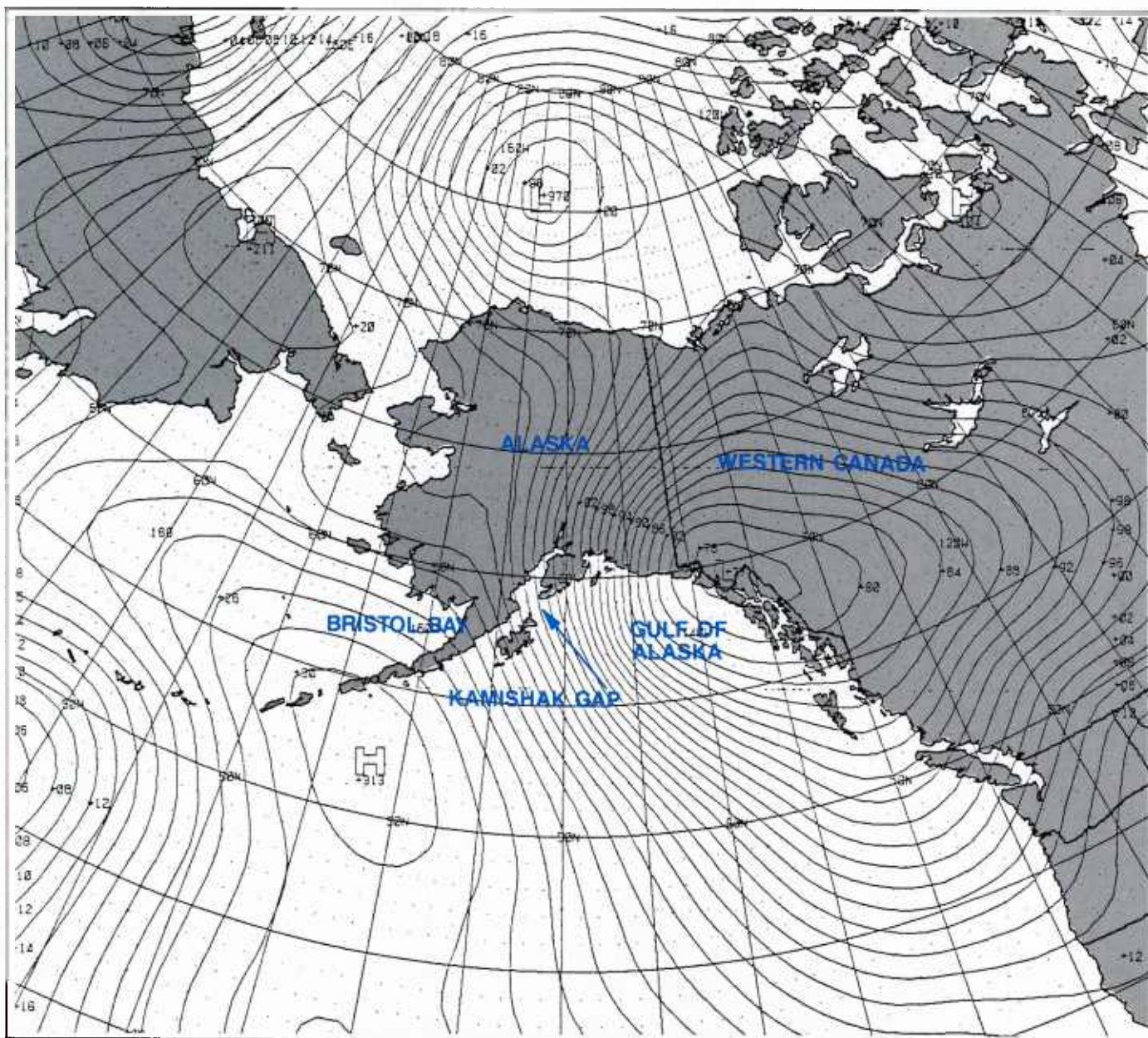


The FNOC surface analysis for 1200 GMT, 22 September (Fig. 3B-8), showed a low-pressure center moving into the Gulf, with no strong winds yet evident in the Kamishak Gap region. However, the 36-hr FNOC prog, based on this analysis, valid for 0000 GMT on 24 September (Fig. 3B-9), continued to support the previous prog in showing strong evidence of continued deepening, as the low was forecast to remain nearly stationary over SE Alaska, with high pressure building up over Bristol Bay. This, again, would cause very high winds in the lee of the Kamishak Gap (and still strong, but lesser winds, in the circulation of the low itself). The FNOC surface analysis for 1800 GMT (Fig. 3B-10) began to support the prog by showing the low moving into the Gulf of Alaska and deepening from 1005.4 mb (Fig. 3B-8) to 999.4 mb (Fig. 3B-10).



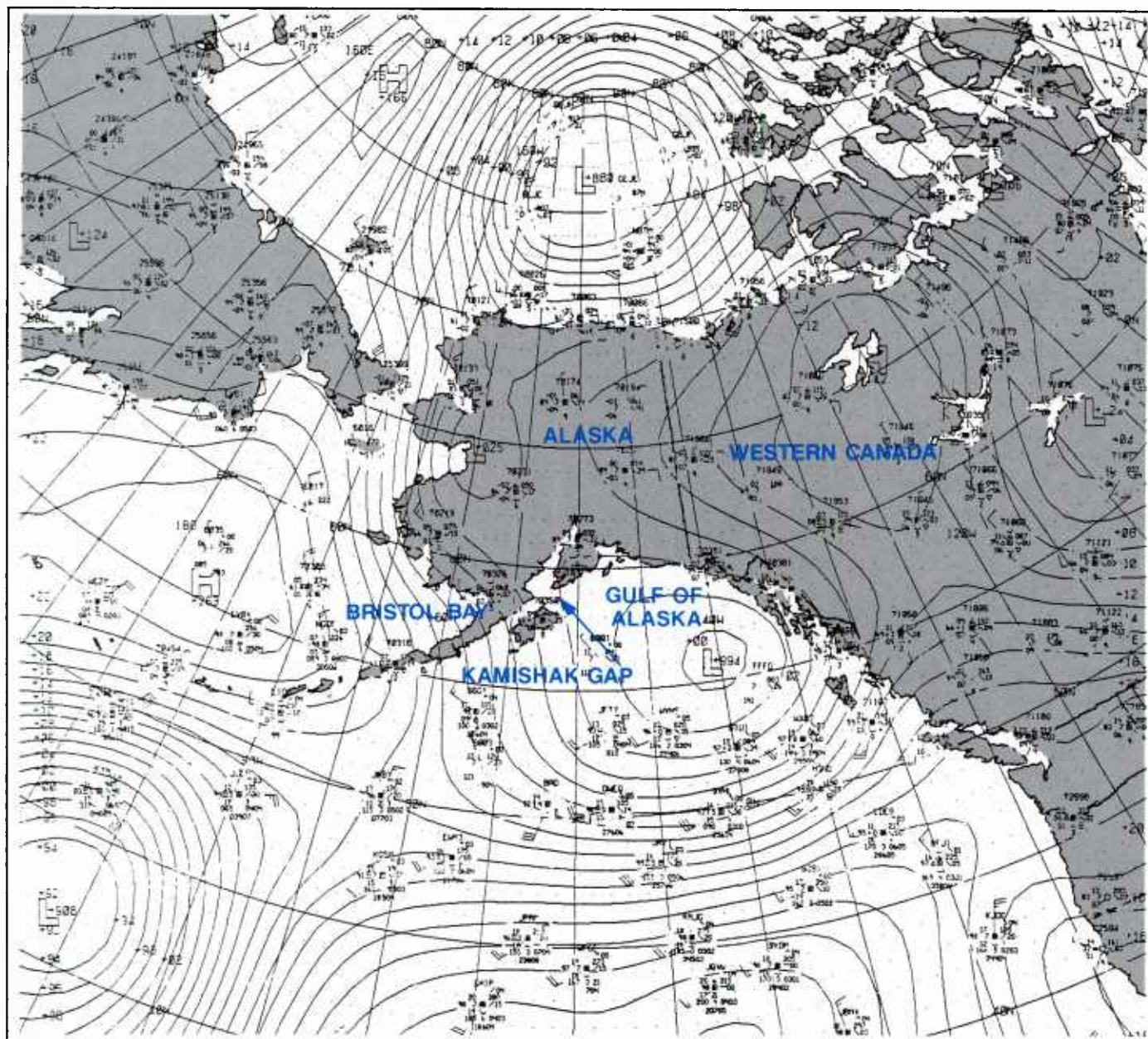
3B-8 FNOC surface analysis. 22 September 1986, 1200 GMT.





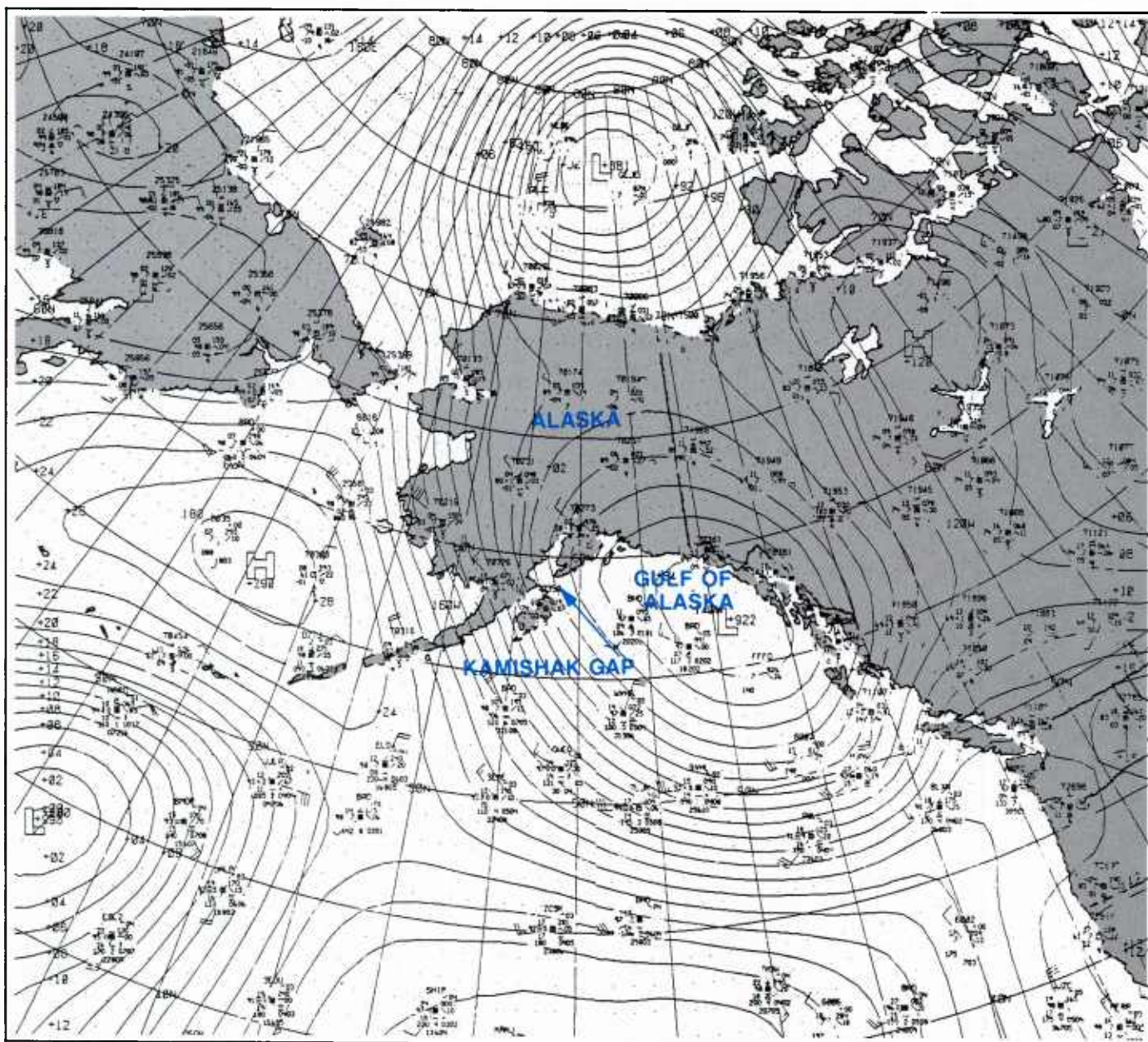
3B-9 FNOC 36 hour surface prog. Valid 24 September 1986, 0000 GMT.





3B-10 FNOC surface analysis, 22 September 1986, 1800 GMT.



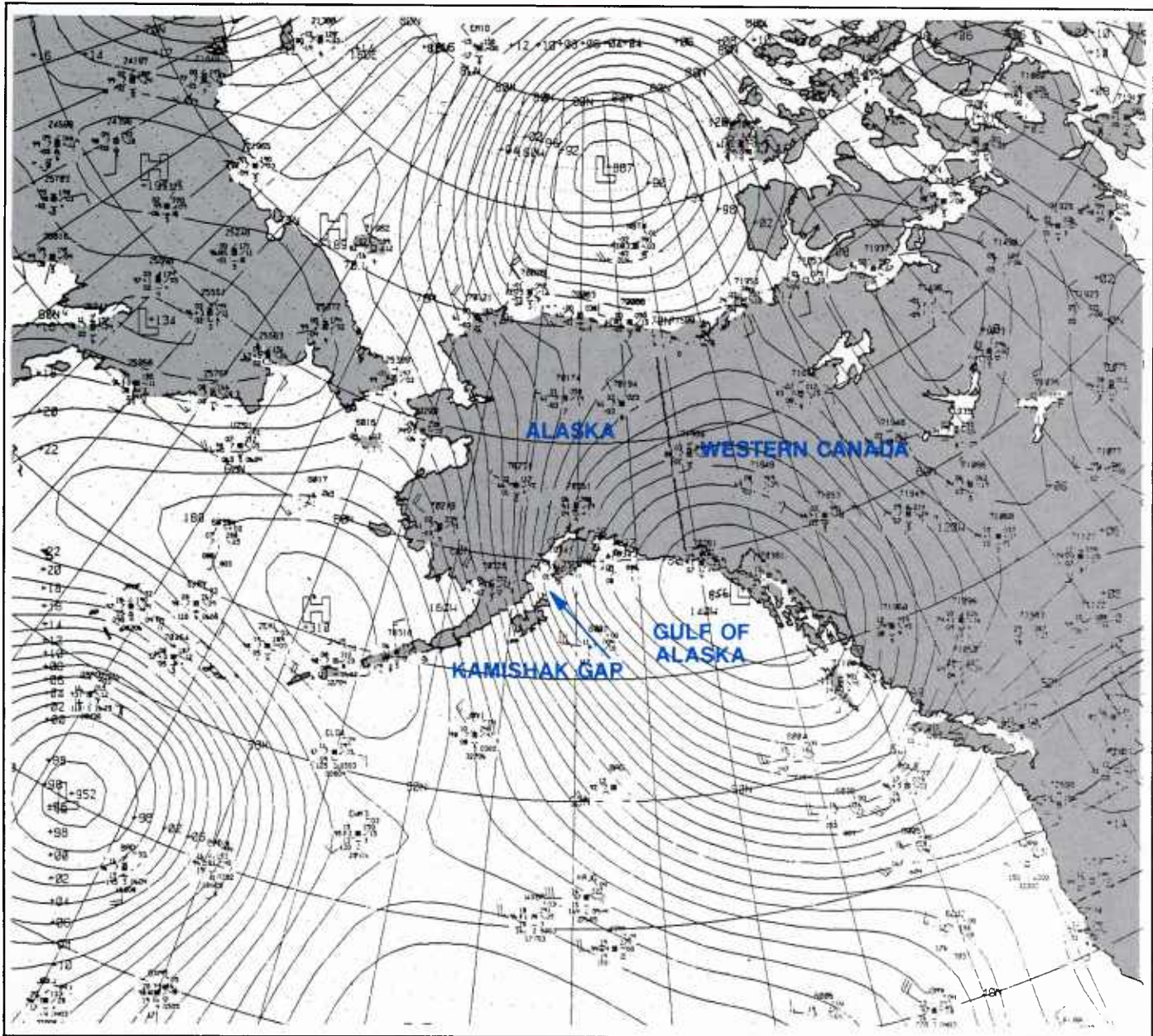


3B-11 FNOC surface analysis. 23 September 1986, 0000 GMT.

*23 September 1986*

Deepening continued from 999.4 mb to 992.4 mb, as indicated by the FNOC surface analysis on this date for 0000 GMT (Fig. 3B-11). Based on a similar analysis prepared aboard Constellation, and, noting a shift to northwesterly winds at 30 kts by 0200 GMT, the ship's weather officer, who was familiar with "gap" winds in the Kodiak region, briefed the Captain on the possibility of increasing northwesterly winds that could conceivably reach hurricane force or higher. This warning enabled the ship to tie down and prepare for the event.

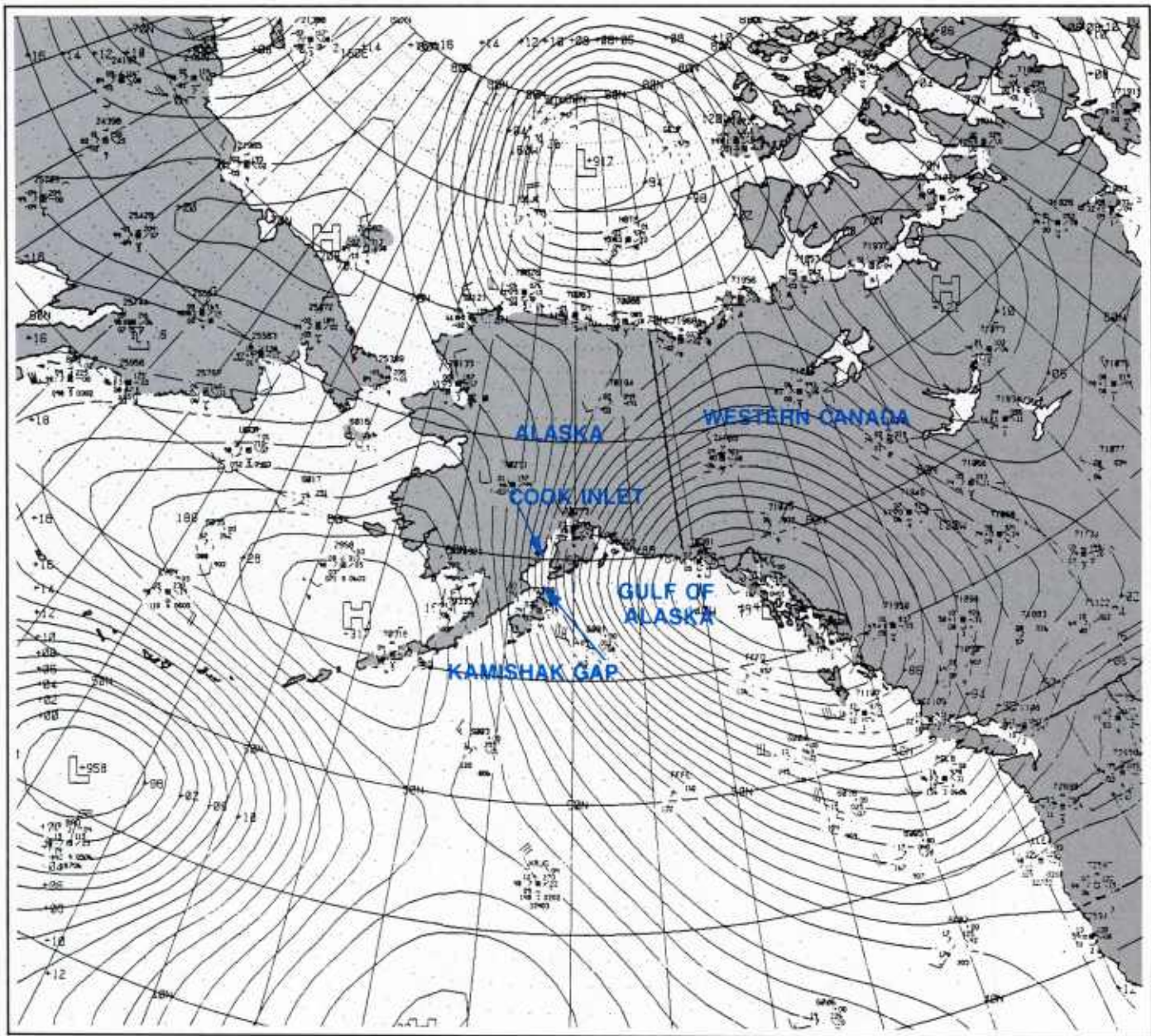




3B-12 FNOC surface analysis. 23 September 1986. 0600 GMT.

By 0600 GMT it became obvious that the low was intensifying in significant fashion. The FNOC surface analysis for that time (Fig. 3B-12) shows a central pressure that dropped to 985.6 mb, and by 0800 GMT, Constellation was facing northwesterly winds at 50 kts.





3B-13 FNO surface analysis. 23 September 1986, 1200 GMT.

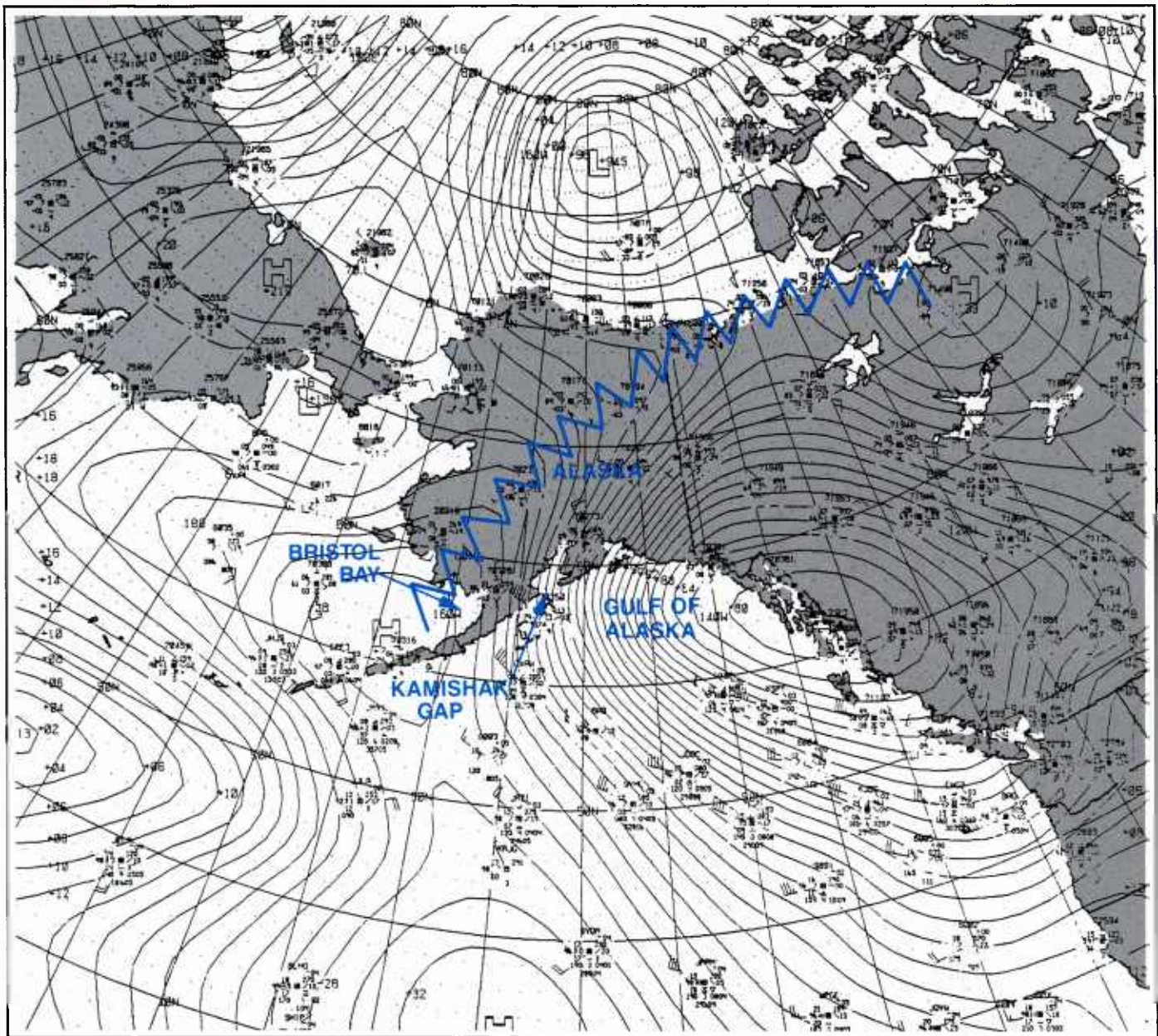
The low deepened further to 979.4 mb, as shown on the FNO surface analysis for 1200 GMT (Fig. 3B-13). Winds continued building as Constellation slowed its approach to the Cook Inlet, trying to reduce the relative wind across the flight deck. Maximum winds of 75 kts were recorded at 1600 GMT with numerous gusts to 85 kts. Two blades from a helicopter, stationed on the flight deck as the only ready Search and Rescue aircraft, were snapped and blown overboard by the hurricane-force winds. By this time, Constellation was only able to make 2-3 kts, while continuing its northwest heading in the face of the Kamishak Gap winds.

The FNOC 1800 GMT surface analysis (Fig. 3B-14) shows the ultimate expression of the event. Note, in particular, the prominent ridge building into western Alaska from a high centered over Bristol Bay, and the strong pressure gradient over the Gap region with axis nearly perpendicular to the Gap.

Constellation acquired a DMSP visible (LF) image near this time (1931 GMT) (Fig. 3B-15), and itself was positioned just south of the Barren Islands—in a position where it received the full blast of the extreme event. Due to the limited fetch, Constellation did not experience high seas; however, sea spray was lifted in the strong winds and was blown horizontally past the ship, severely reducing visibility. It is the sea spray effect that causes the gray shade extending from the Gap region southeastward, where clouds are eventually generated. (For a similar effect in a mistral condition, see NTAG Vol. 3, Sec 2B, Case 3.)

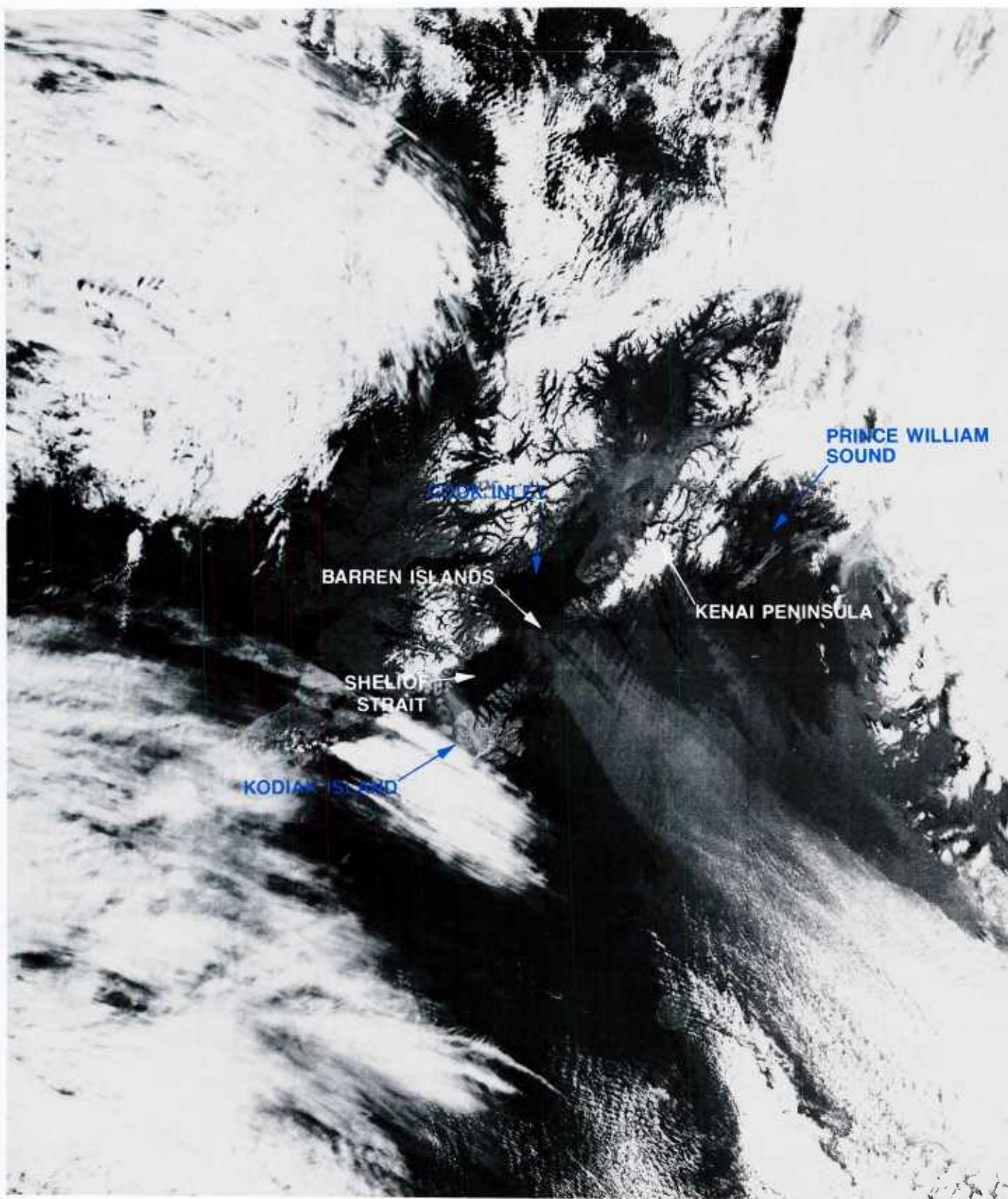
Note that spray is retarded from development in the lee of the Barren Islands, which form topographic blocks to the strong winds. A similar blocking effect can be noted in the lee of the Kenai Peninsula except for one narrow swath which also suggests some spray or haze effects due to strong winds. The pressure gradient (Fig. 3B-14) is also very strong over that area. Combined evidence suggests that winds, lifted over the mountains, were still colder than the surrounding environment, and hence descended immediately on the lee side as katabatic or fall winds of moderate to strong intensity.





3B-14 FNOG surface analysis. 23 September 1986, 1800 GMT.





3B-15 DMSP visible (LF) data. 23 September 1986, 1931 GMT.



*24 September 1986*

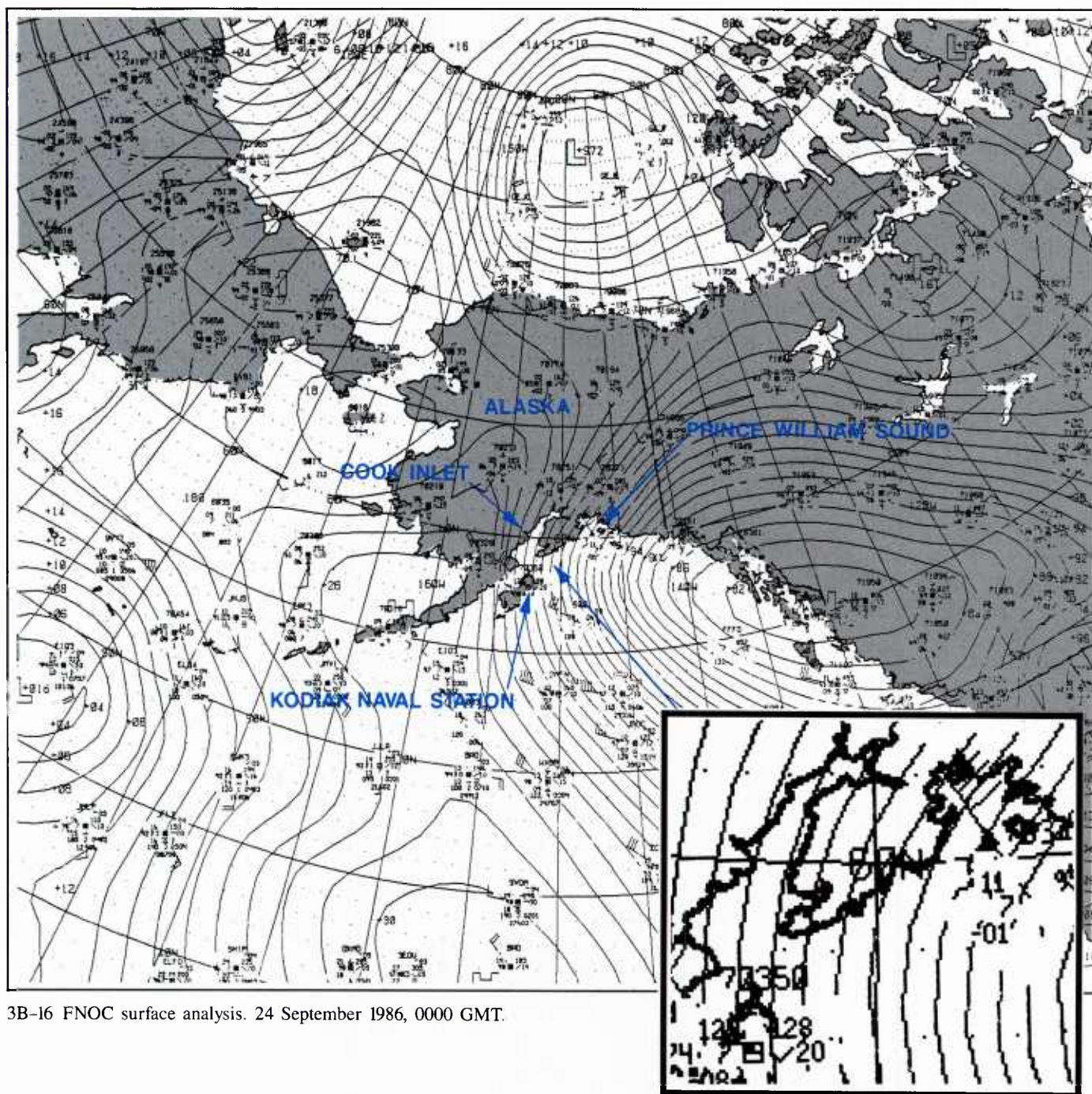
The interpretation of katabatic winds in lee mountain regions is supported by wind observations in Figure 3B-16. (FNOG surface analysis, 0000 GMT), which indicate speeds of 40 kts at Kodiak Naval Station, on the SW side of the island, and another observation of 40 kts near Prince William Sound.

Prominent havens from such strong winds in the region appear to be primarily in the lee of the Barren Islands, Shelikof Strait, and Cook Inlet.

By 1200 GMT (Fig. 3B-17), winds had slackened to the extent that Constellation was able to make progress into Cook Inlet. On entry, as the ship turned toward Anchorage one day late, winds immediately dropped to less than 35 kts.

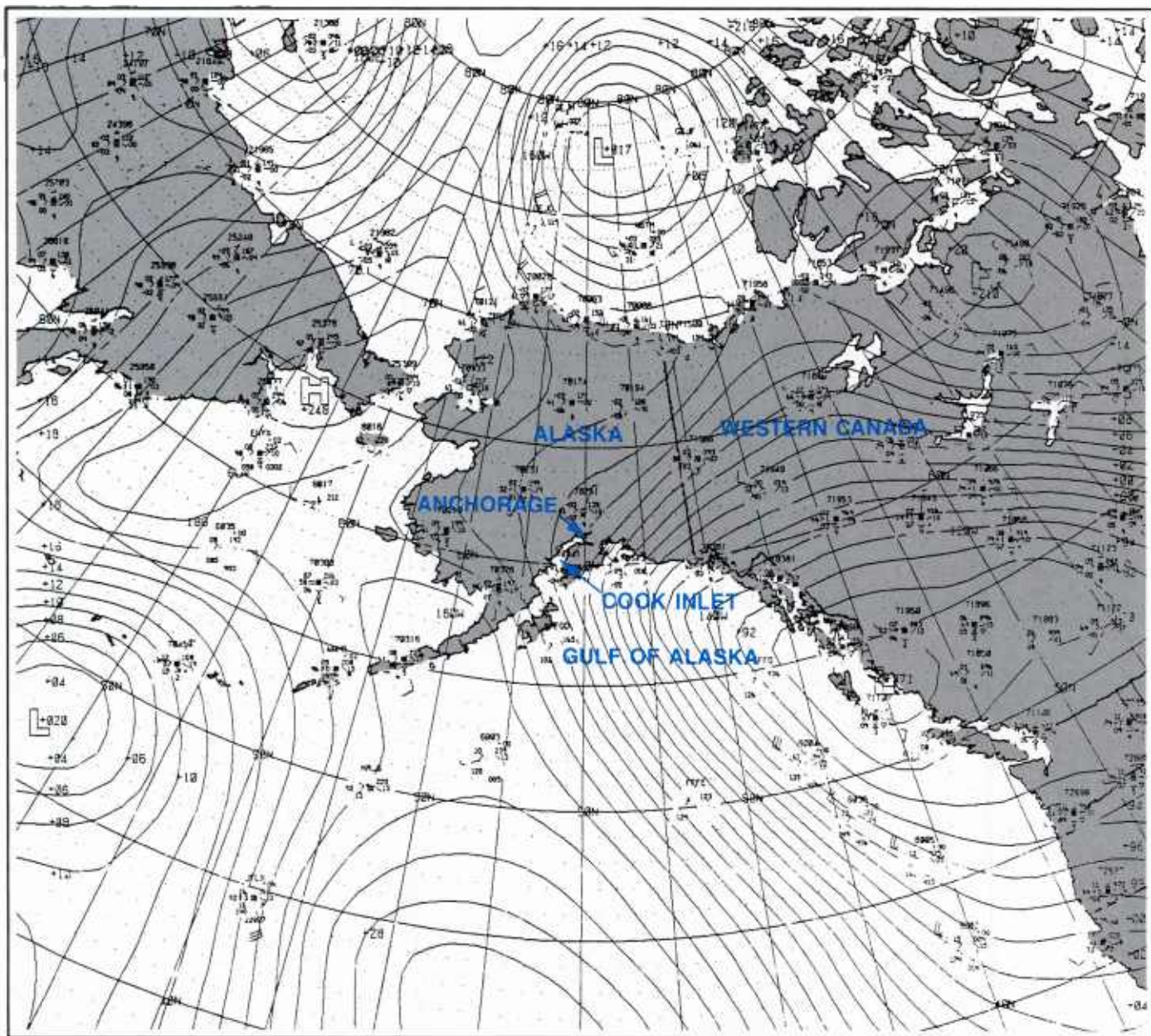
### **Important Conclusions**

1. Northwest winds of hurricane or typhoon force and higher can develop very rapidly and be sustained over many hours in the region of the Kamishak Gap.
2. When the pressure gradient is strong over the Kenai Peninsula and Kodiak, due to low pressure to the SE, strong winds may still be experienced in the immediate lee of these barriers, due to katabatic or fall wind effects.
3. Ships transiting from the south to Anchorage should be alert for rapid 24-hr changes that can lead to strong winds through the Kamishak Gap.



3B-16 FNOC surface analysis. 24 September 1986, 0000 GMT.





3B-17 FNOC surface analysis. 24 September 1986, 1200 GMT.





### *3C Islands of Grounded Sea Ice: Their Use in Detecting Changes in Direction of Ice Motion and Their Role in Lead Formation*

The movement of ice is generally attributed to the combined effect of wind, ocean current, and coriolis acceleration. Internal forces within the ice also have an effect on ice motion, but, for floating ice, are disregarded in most forecast methods.

Over a short period of time, when winds are moderate or strong, the wind force completely dominates, and the ice generally moves in a direction determined by the stress of the wind. Typical ice motion, factoring in the coriolis effect, is 30–40° to the right of the surface wind (northern hemisphere). This converts to about 5° to the right of the geostrophic wind for wind speeds of about 12 kts, and 18° to the right for lower wind speeds of about 5 kts (Stringer, et al., 1984).

Floebergs are massive pieces of floating ice in the form of broken hummocks or ridge systems that have frozen together. They often have freeboards of 5 m or higher and keels that can result in grounding at water depths of over 30 m (Stringer, et al., op cit). When floebergs become grounded on shoals in the Arctic Ocean, they may incorporate other forms of sea ice and, with time, undergo more massive changes in response to the pressure of the surrounding ice fields. The surface of these larger areas of grounded ice typically contains “shear ridges and fields of brecciated ice averaging 5 to 6 m high with many peaks on the order of 15 m” (Kovacs, et al., 1975). These large, massive features of permanent or semi-permanent grounded ice are referred to as “Islands of Grounded Sea Ice” (Kovacs, et al., op cit).

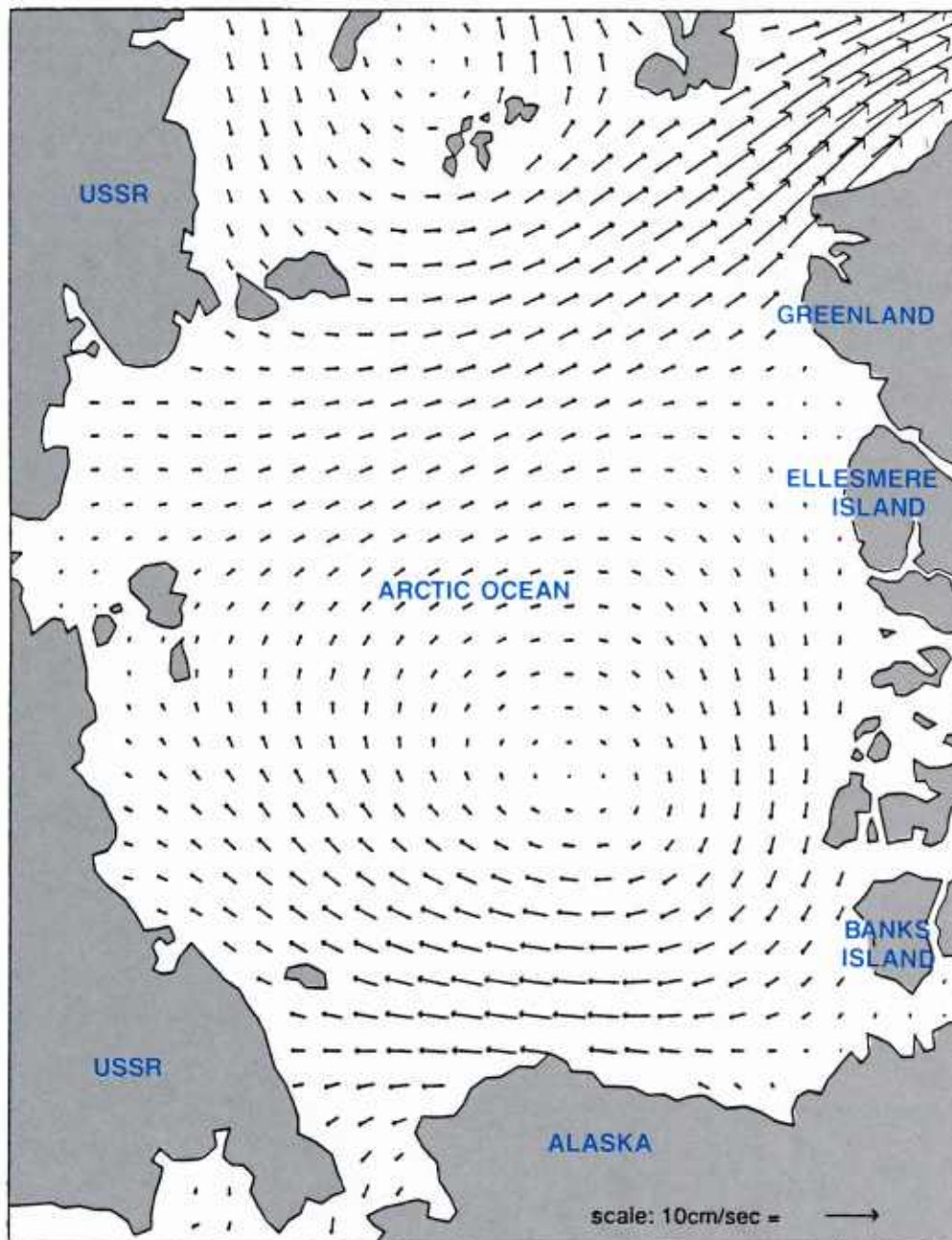
Islands surrounded by ice and islands of grounded ice create obstacles to ice movement, forcing the floating ice field to move around the edges of the barrier. The movement of the floating ice around the barrier edges creates lee wake effects, apparent as warmer regions in satellite infrared imagery. The lee wake effects are areas where the ice is thinner than surrounding areas, emitting thermal radiation at a higher temperature because of heat conduction through the ice from the water below, or from open water in the same region. The wakes are formed as ice in the lee of the barrier is pushed and entrained in the direction of prevailing ice flow, creating an open water polynya in the obstacle's lee. Depending on the strength, direction, and duration of the flow, the polynya may enlarge, change relative position, or refreeze with time. Since ice movement is largely governed by surface wind flow, any change in wind direction, in a moderate wind speed condition, will be rapidly followed by a change in alignment of the obstacle's lee wake pattern.

Another important feature concerning islands of grounded ice is their role as “stress concentrators.” It has been found that an island of grounded ice influences the motion of a “column of ice approximately 20 km wide upstream and downstream of its position” (Stringer and Barrett, 1975). The island, in fact, slows the motion of this ice in comparison to the surrounding ice field, resulting in the development of appreciable stress. Couple this factor with additional wind stress imposed by passing weather systems, and it becomes obvious that a single such feature could play a major role in significant lead development. Stringer and Barrett (op cit.) felt that the influence could result in a lead formation several hundreds of kilometers in length.

Case 1 of this section shows such an example in the East Siberian Sea. The study documents several new, previously undocumented, islands of grounded sea ice, where ice drift reversal was noted, followed by a dramatic example of significant lead formation.

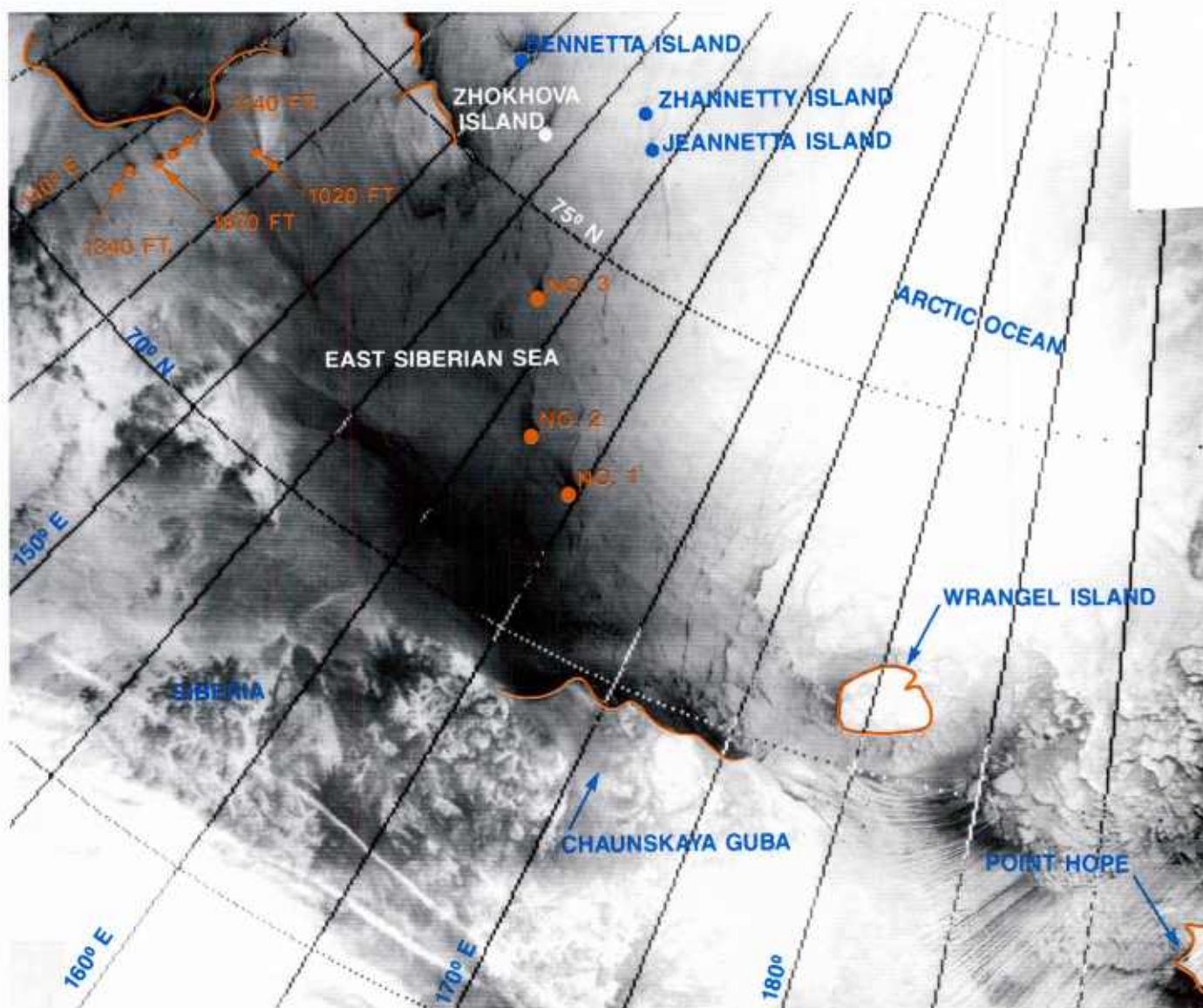
### *CASE 1 Ice Drift Reversal and Lead Formation in the Chukchi and East Siberian Seas*

The mean ice motion in the central Arctic Ocean during November, December, and January is anticyclonic, moving about a center west of the Canadian archipelago in the Canada Basin (Fig. 3C-2). The motion reflects the existence of an anticyclonic oceanic gyre, centered near that location, and the dominating presence of high pressure, generally over that area during that period.



3C-2 Mean ice motion in the Arctic Basin during Nov., Dec., and Jan. (Based on 7 years of buoy data, courtesy R. Colony, Polar Science Center, Univ. of Washington)

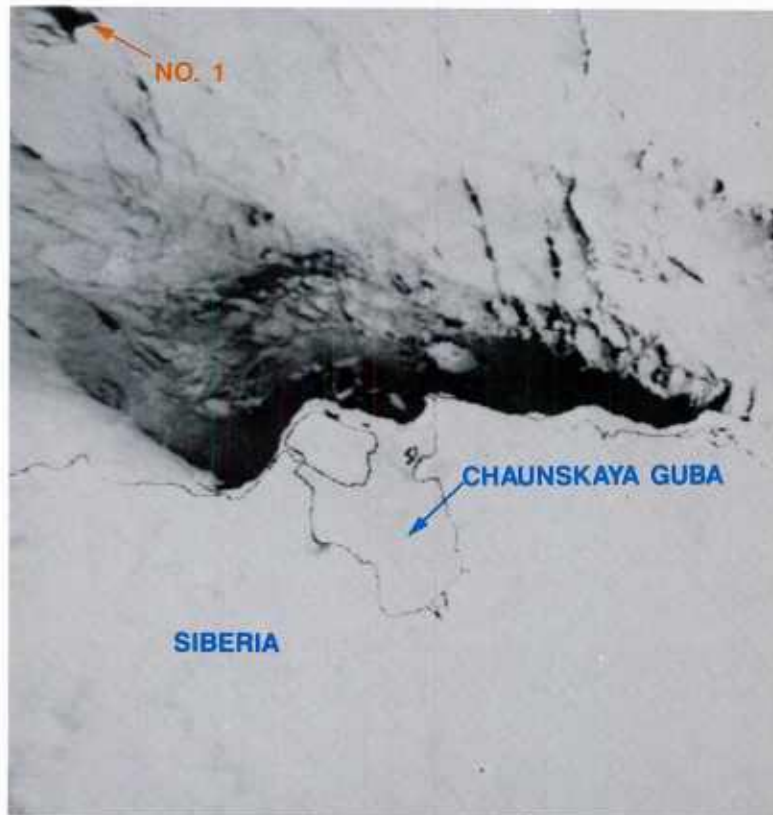




3C-3a DMSP infrared (TS) data. 12 November 1988, 1704 GMT.

Figure 3C-3a is a DMSP infrared depiction of the area on 12 November 1988. Apparent in the image are several islands of grounded ice in the East Siberian Sea and land islands of the New Siberian group. The island features show lee wake effects on the northwest side, indicating a flow of ice from the SE to the NW, in general agreement with the expected ice movement pattern, shown in Figure 3C-2. Figure 3C-3b is a NOAA AVHRR infrared view, enlarged and enhanced to more clearly delineate conditions near grounded ice island #1.

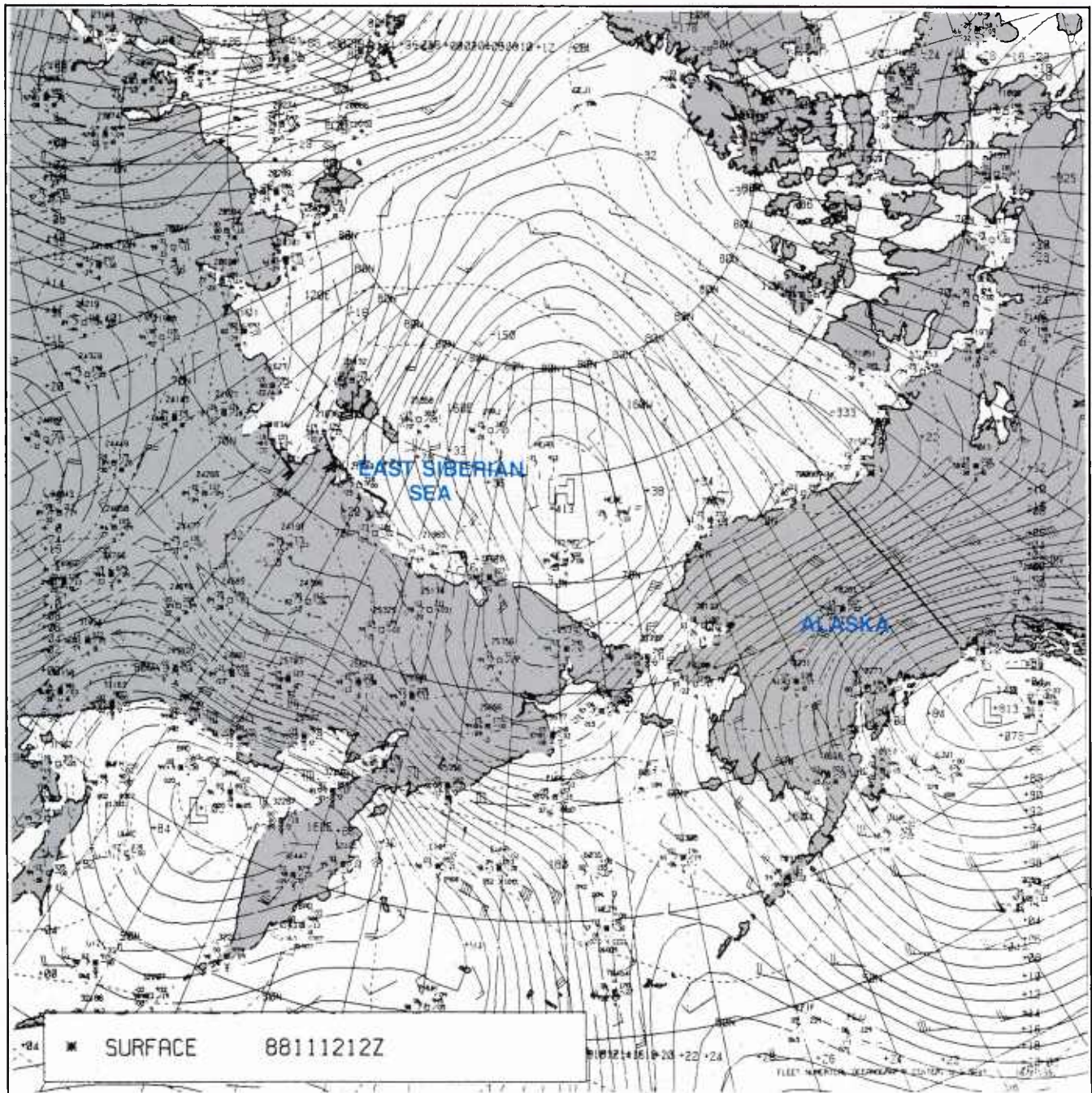
Effects of strong northeasterly flow can be seen in the Chukchi Sea region SE of Wrangel Island (Fig. 3C-3a). Here, cloud streets are formed as cold, dry, air flowing off the ice, suddenly encounters the southern limit of ice in an open water region extending southeastward past Point Hope into the Bering Strait. Assuming a surface wind closely aligned in direction with the cloud plumes, ice should have a tendency to move 30–40° to the right or roughly from the east or east-southeast in the Chukchi Sea region.



3C-3b NOAA AVHRR infrared (channel 4) data. 12 November 1988, 2046 GMT.



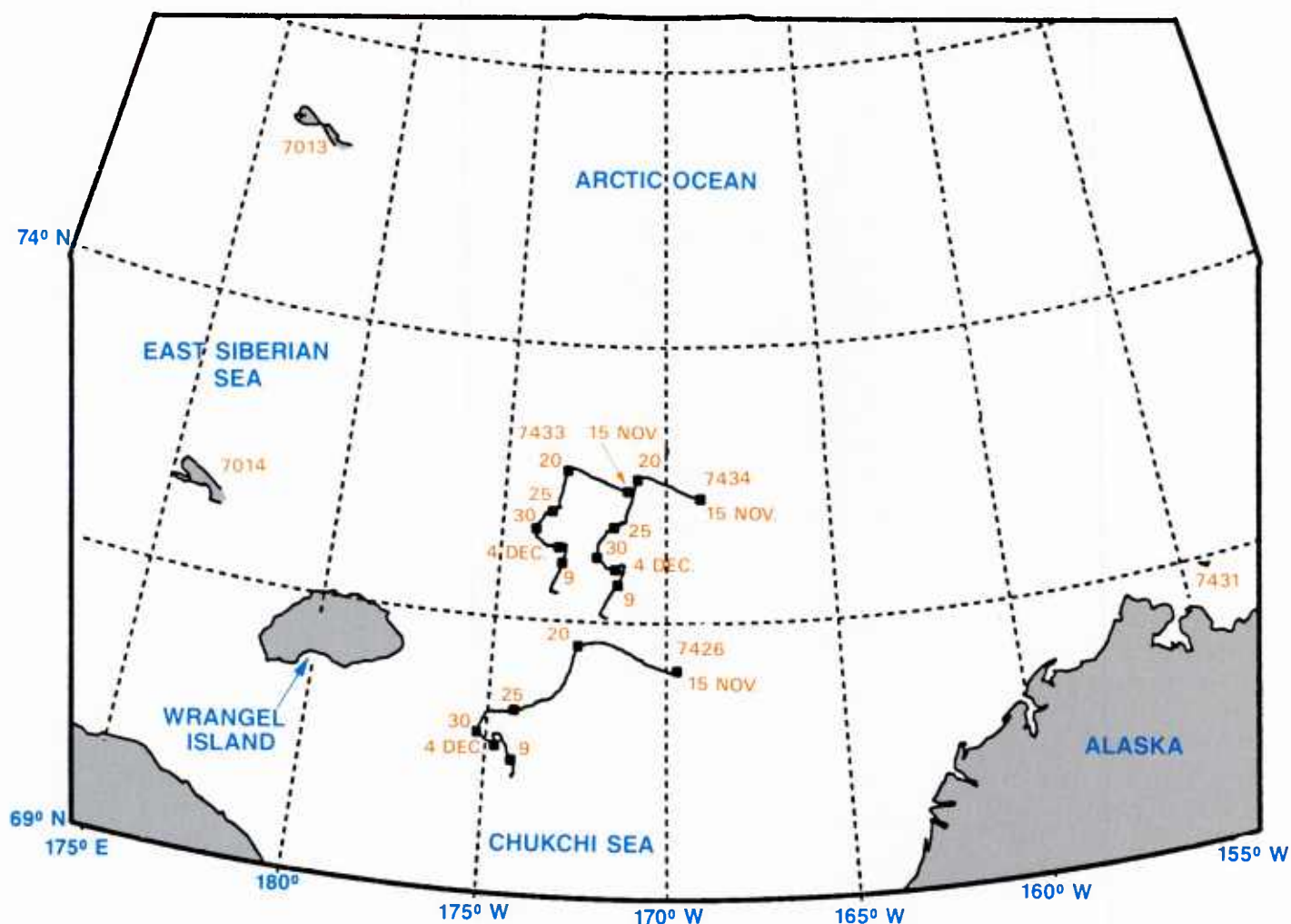
Figure 3C-4 is the FNOC surface analysis for 12 November 1988 at 1200 GMT. The analysis shows a huge high pressure cell covering the Beaufort, Chukchi, and East Siberian Seas, with center near 73.5° N on the 180° meridian line. The pattern would tend to promote the anticyclonic movement of ice shown in the DMSP data (Fig. 3C-3a). An interesting side-effect shown in Figure 3C-3a is the warm wake effect over land in the lee of mountains having heights of 1020, 1140, 1870, and 1340 feet, respectively. The mountains, apparent in the left-hand corner of the image near 140-145° E, were subject to strong 20-30 kt surface winds from the east-southeast. The flow pattern apparently produced a katabatic warming effect extending many kilometers to the mountains' lee.



3C-4 FNOC surface analysis, 12 November 1988, 1200 GMT.

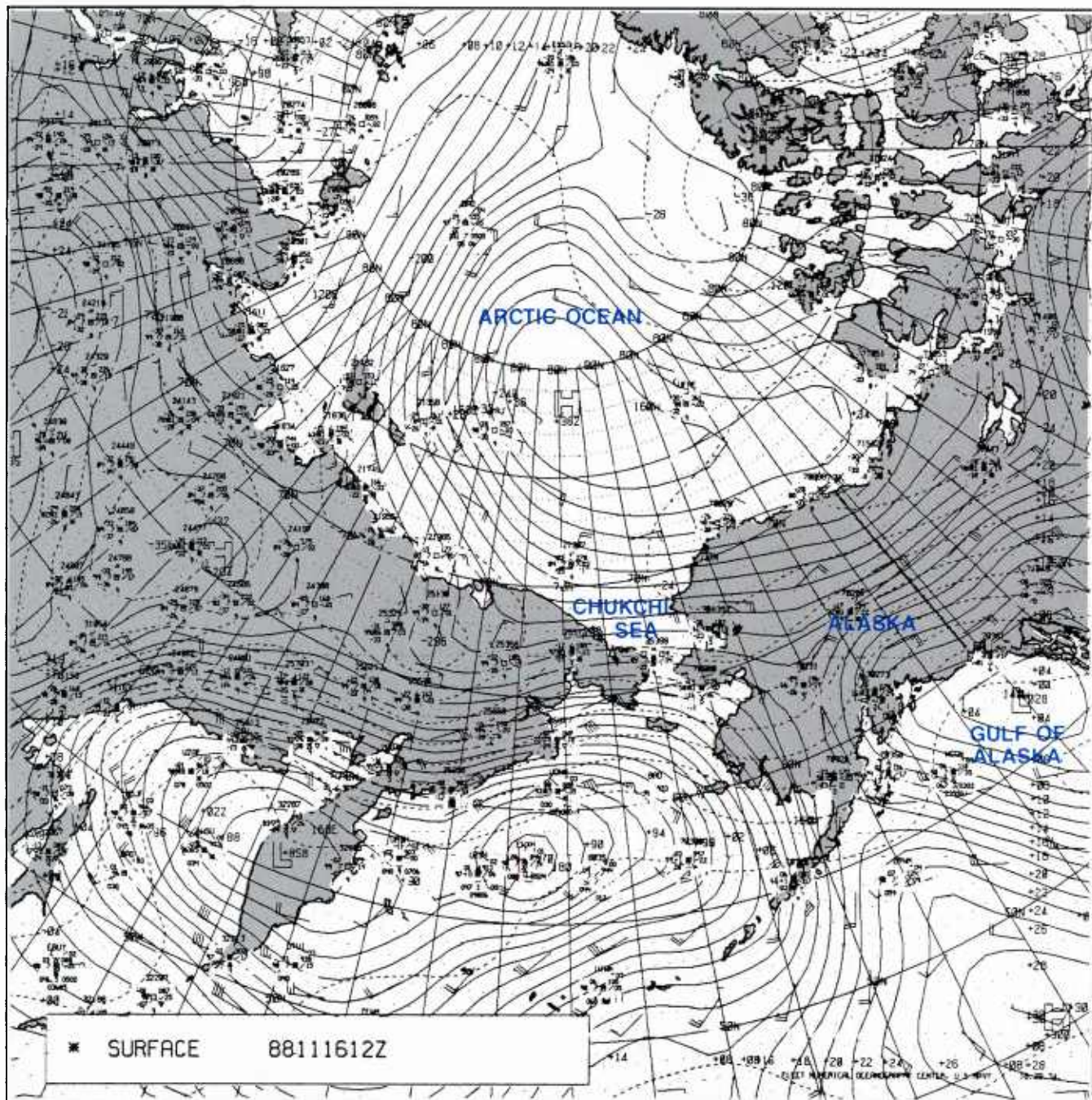
Buoy tracks for the region during the period 15 November to 15 December 1988 are shown in Figure 3C-5 (Courtesy C. Pease, PMEL/NOAA, 1990). Squares shown on the buoy trajectories for buoys 7433, 7434, and 7426 correspond to dates of 15 Nov, 20 Nov, 25 Nov, 30 Nov, 4 Dec, and 9 Dec 1988. Movement of ice was too slow to indicate such dates on the East Siberian buoys, 7013 and 7014.

The trajectories show a general westerly drift except for a reversal in flow to easterly starting 30 November to 15 December for the East Siberian buoys, and from 30 November to 5 December for the Chukchi Sea buoys. The Chukchi buoys also show a pronounced southward movement starting on 20 November, not shown by the East Siberian buoys.



3C-5 Ice buoy trajectories in the Arctic Ocean, 15 November 1988 to 15 December 1988 (Courtesy Carol Pease, NOAA/PMEL).

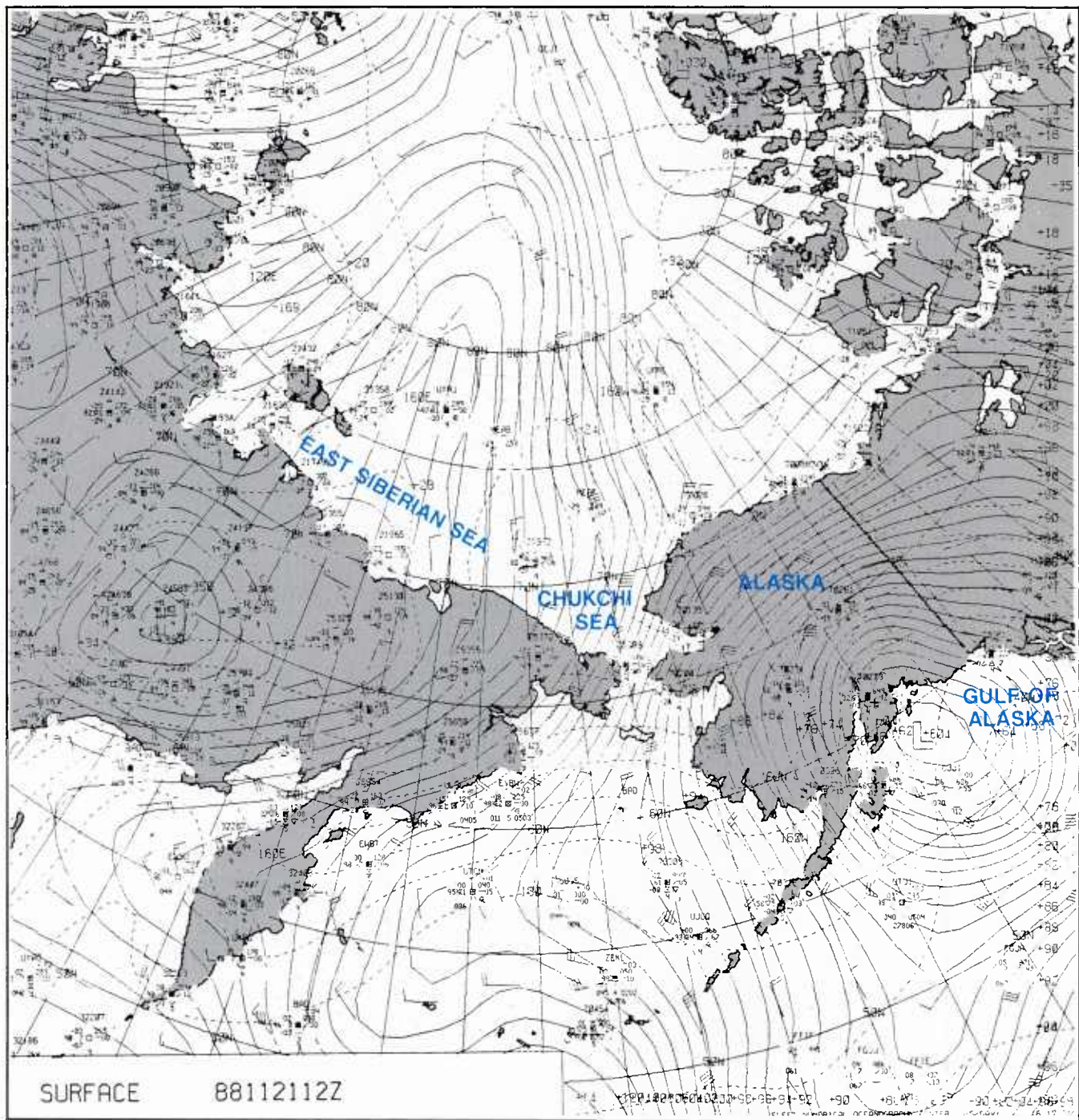




3C-6 FNOC surface analysis. 16 November 1988, 1200 GMT.

The FNOC surface analysis for 16 November 1988, at 1200 GMT (Fig. 3C-6), shows the large high pressure system which continued to promote ice movement in an anticyclonic fashion toward the northwest, typical of the period 15-20 November. However, this system moved rapidly northeastward, while low pressure began to develop and strengthen in the Gulf of Alaska.

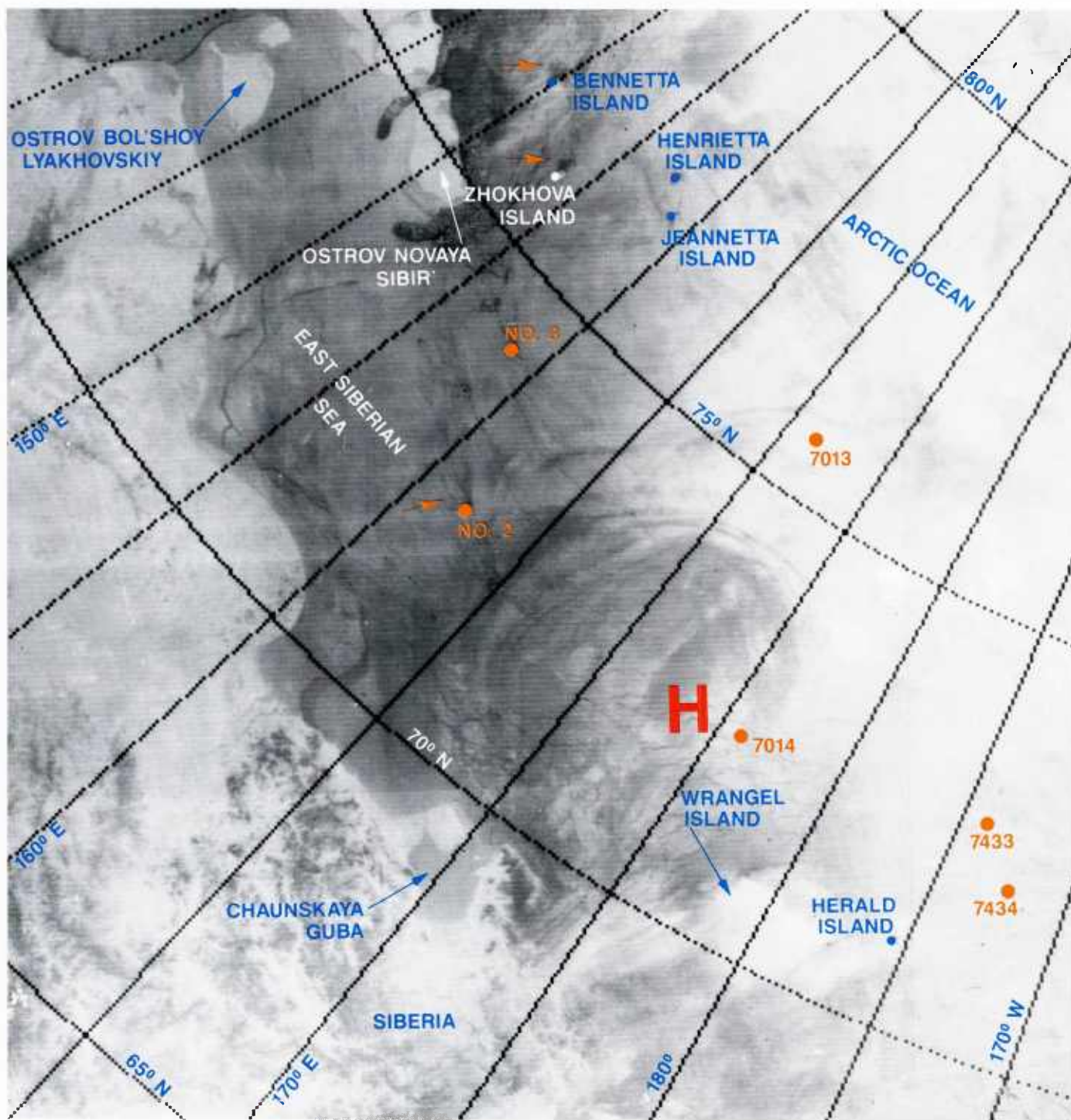








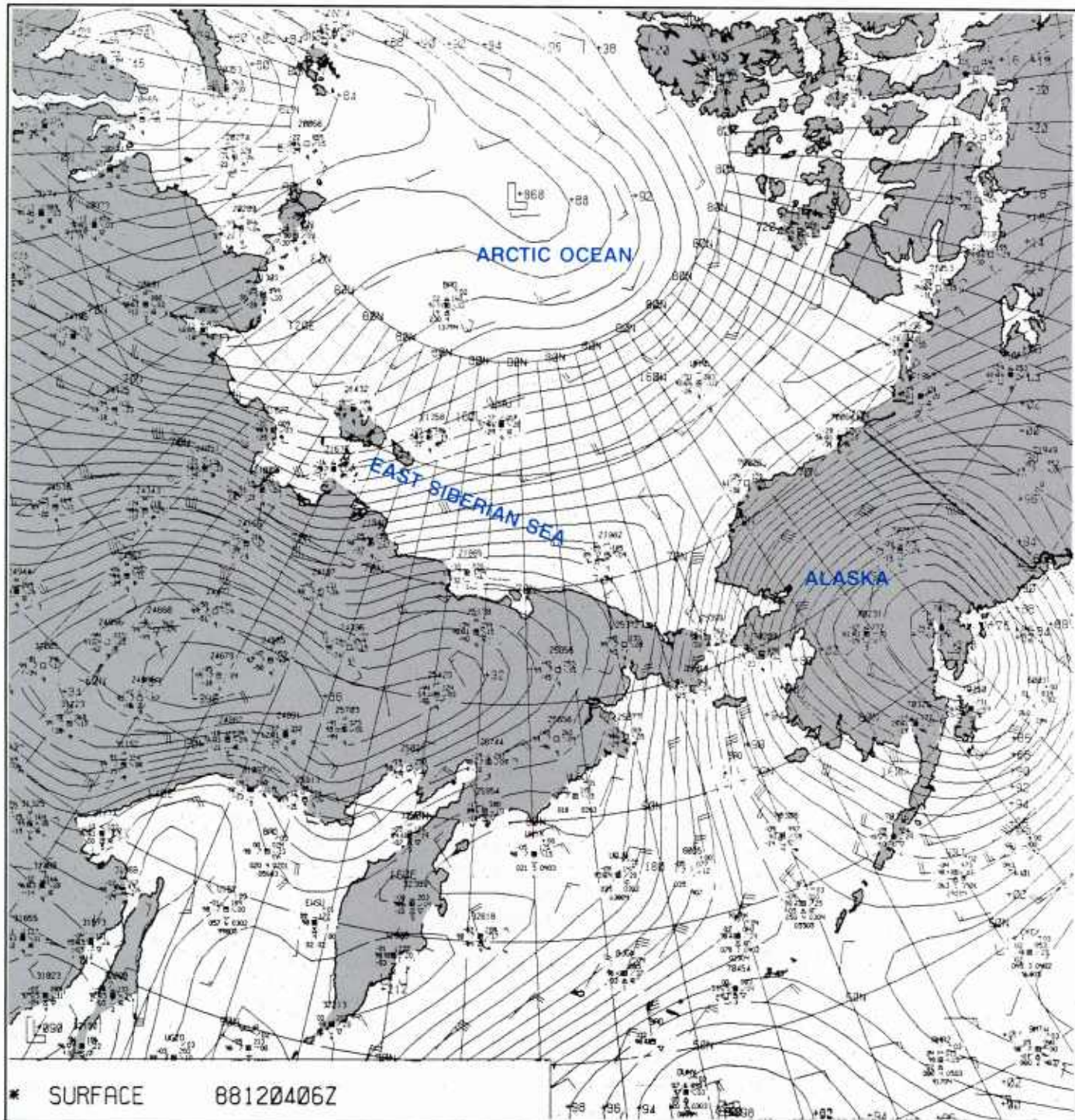




3C-9 DMSP infrared (TS) data. 30 November 1988, 1919 GMT.

Figure 3C-9 is a DMSP infrared (TS) image of the area on 30 November 1988, at 1919 GMT. Low inversion-dominated cloudiness, radiating at a warm (dark) temperature, defines the region of the high pressure system over the East Siberian Sea. A careful scrutiny of the image reveals that visible islands of grounded ice and land islands are still exhibiting wake effects on their northwest side, indicating a continuation of the anticyclonic movement taking place.

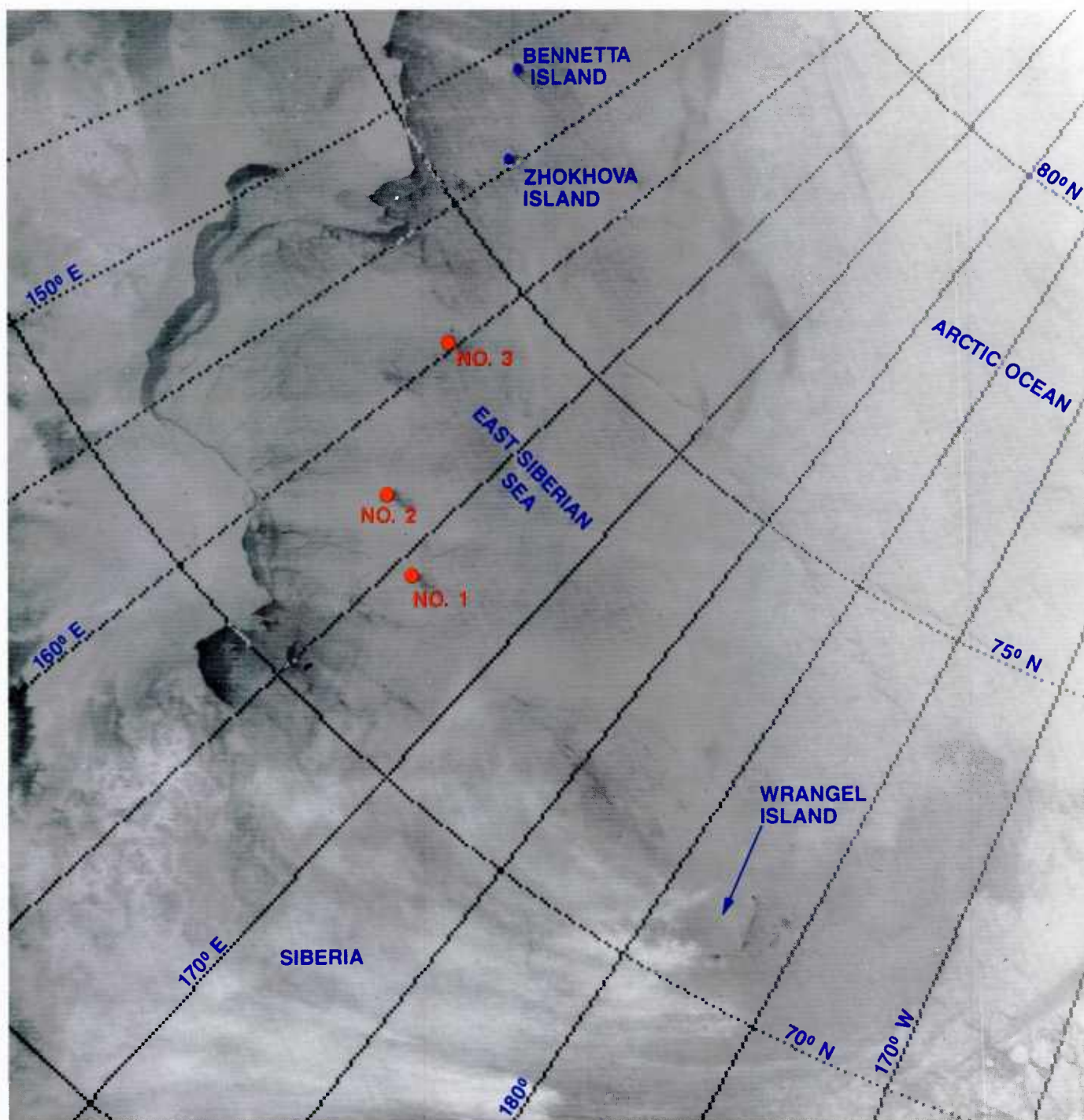




3C-10 FNOc surface analysis. 4 December 1988, 0600 GMT.

From this point on, the weather situation changed quite rapidly, as the high pressure over the East Siberian Sea moved southward into northern Siberia on 1 December 1988. At the same time, the retreat of the high permitted westerly winds to begin flowing over a large portion of the Arctic Ocean. By 4 December 1988, 20–30 kt westerly winds covered the East Siberian Sea as shown in the FNOc surface analysis for that date at 0600 GMT (Fig. 3C-10).

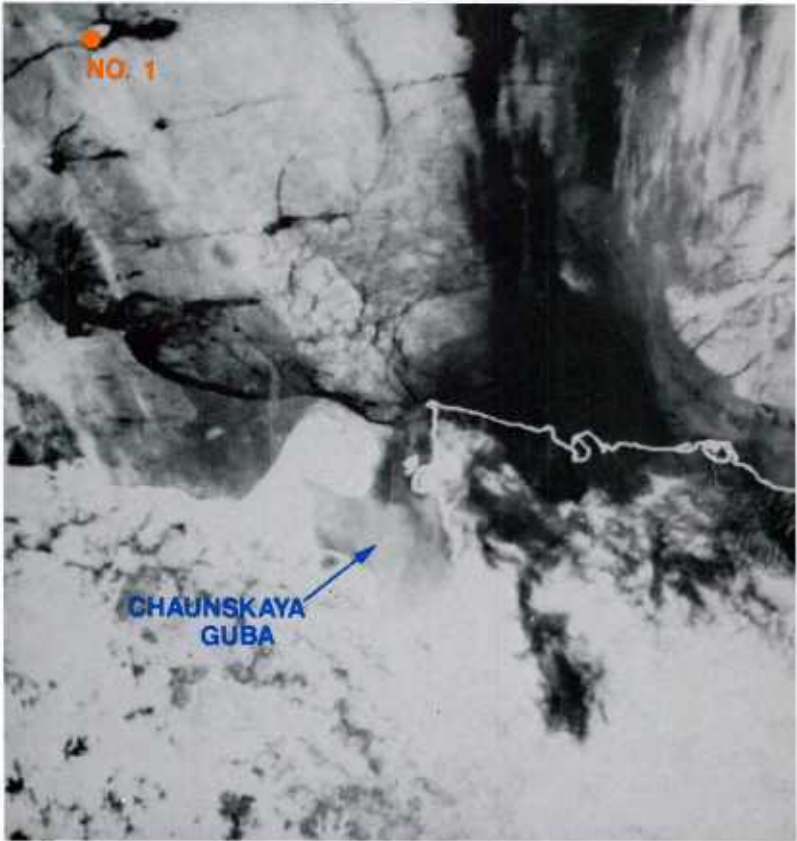




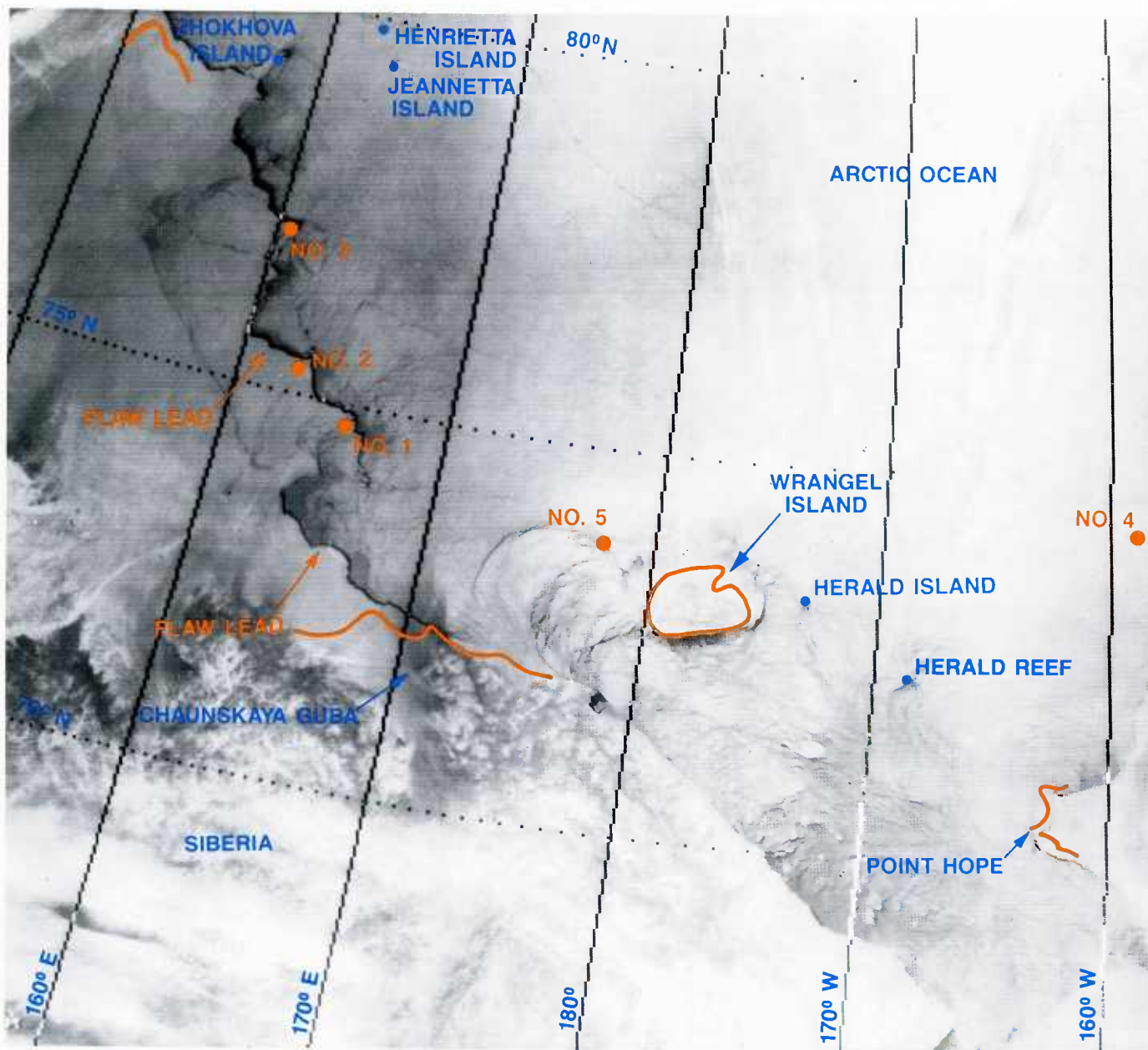
3C-11a DMSP infrared (TS) data. 5 December 1988, 1541 GMT.



The effect on direction of ice movement was dramatic. Figure 3C-11a is a DMSP infrared (TS) image of the region on 5 December at 1541 GMT. Wake effects from the land islands and ice islands now show a reversal in movement of the entire ice pack in that region to an easterly direction as opposed to the former westerly and northwesterly flow direction. The shift in direction had occurred during the course of only a few days as a result of the changed meteorological conditions. Figure 3C-11b is an enlarged and enhanced NOAA AVHRR infrared image showing the effect on the island of grounded sea ice labeled #1, as it appeared on 7 December 1988 at 2140 GMT.



3C-11b NOAA AVHRR infrared (channel 4) data. 7 December 1988, 2140 GMT.



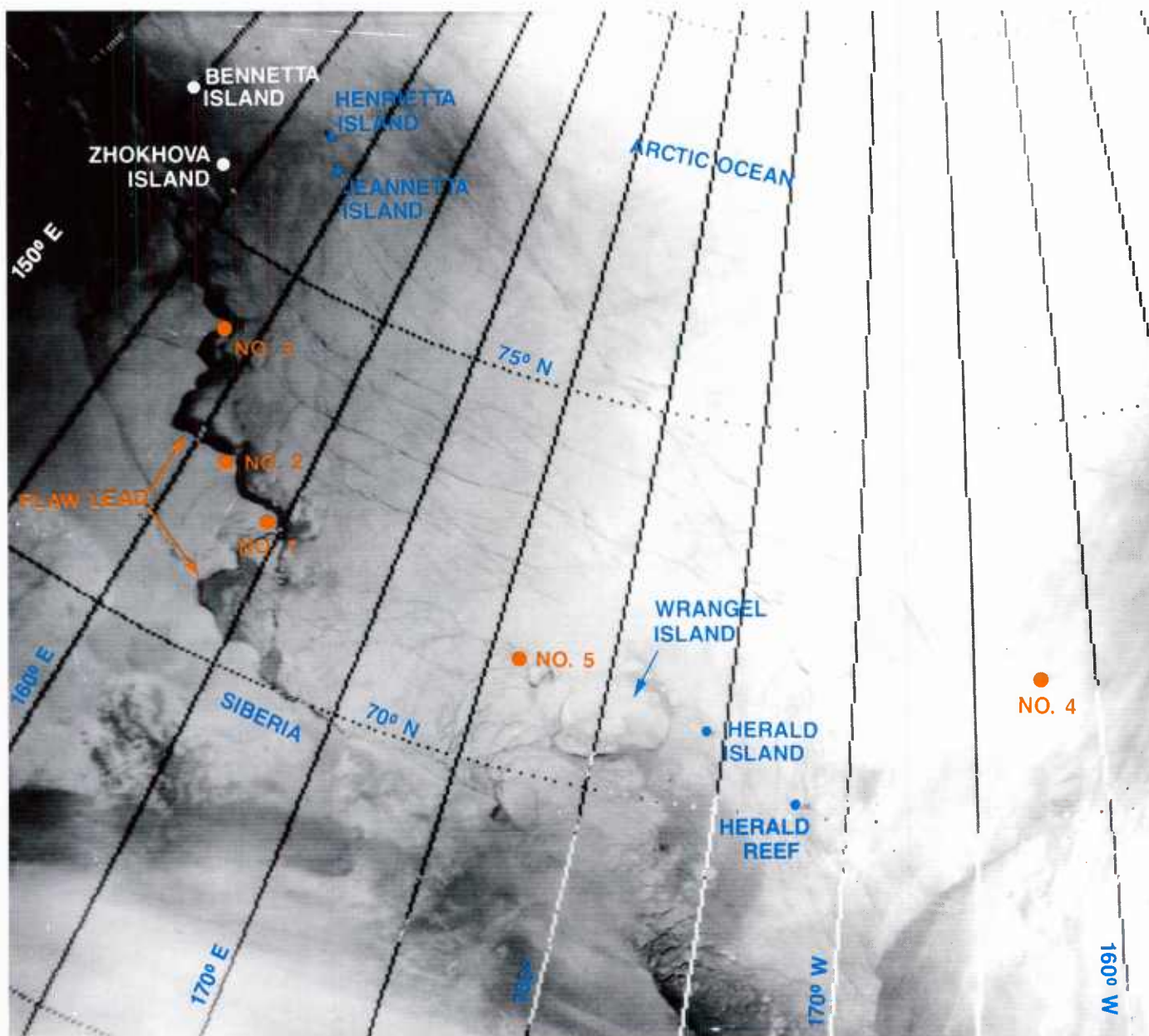
3C-12 DMSP infrared (TS) data. 2 March 1989, 2051 GMT.



### *Flaw Lead Development*

It is of great additional interest that a major flaw lead developed, connecting the immediate vicinity of ice islands #1, #2, and #3 with the island of Zhokhova, very apparent in DMSP infrared imagery acquired on 2 March 1989, at 2051 GMT (Fig. 3C-12). The lead widened to massive proportions only two days later, as revealed in DMSP infrared (TS) imagery acquired on 5 March 1989, at 1710 GMT (Fig. 3C-13). The islands of grounded ice, #1, #2, and #3, were located in water having depths ranging from roughly 14 to 16 fathoms. Such depths are not unrealistic for islands of grounded ice; however, it is also possible that the bathymetry is not contoured carefully enough in the East Siberian Sea and that these island locations may overlie appreciably shallower water. Herald Reef, in the Chukchi Sea, east-southeast of Wrangel Island, and Herald Island (Figs. 3C-12 and 3C-13) show wake effects on their southern extremities. In these same figures, two additional islands of grounded ice (#4 and #5) have also become apparent, both located in water having depths indicated as about 20 fathoms. Ice Island #4 is possibly a remnant of the famous ice island T3, which grounded near that location in 1960 (Shindler, 1968), after having been repeatedly utilized as an Arctic research station in earlier times.

Having located these islands of grounded ice as they appeared in 1989, it was of some interest to determine whether the features were also apparent in the adjoining years of 1988 and 1990.



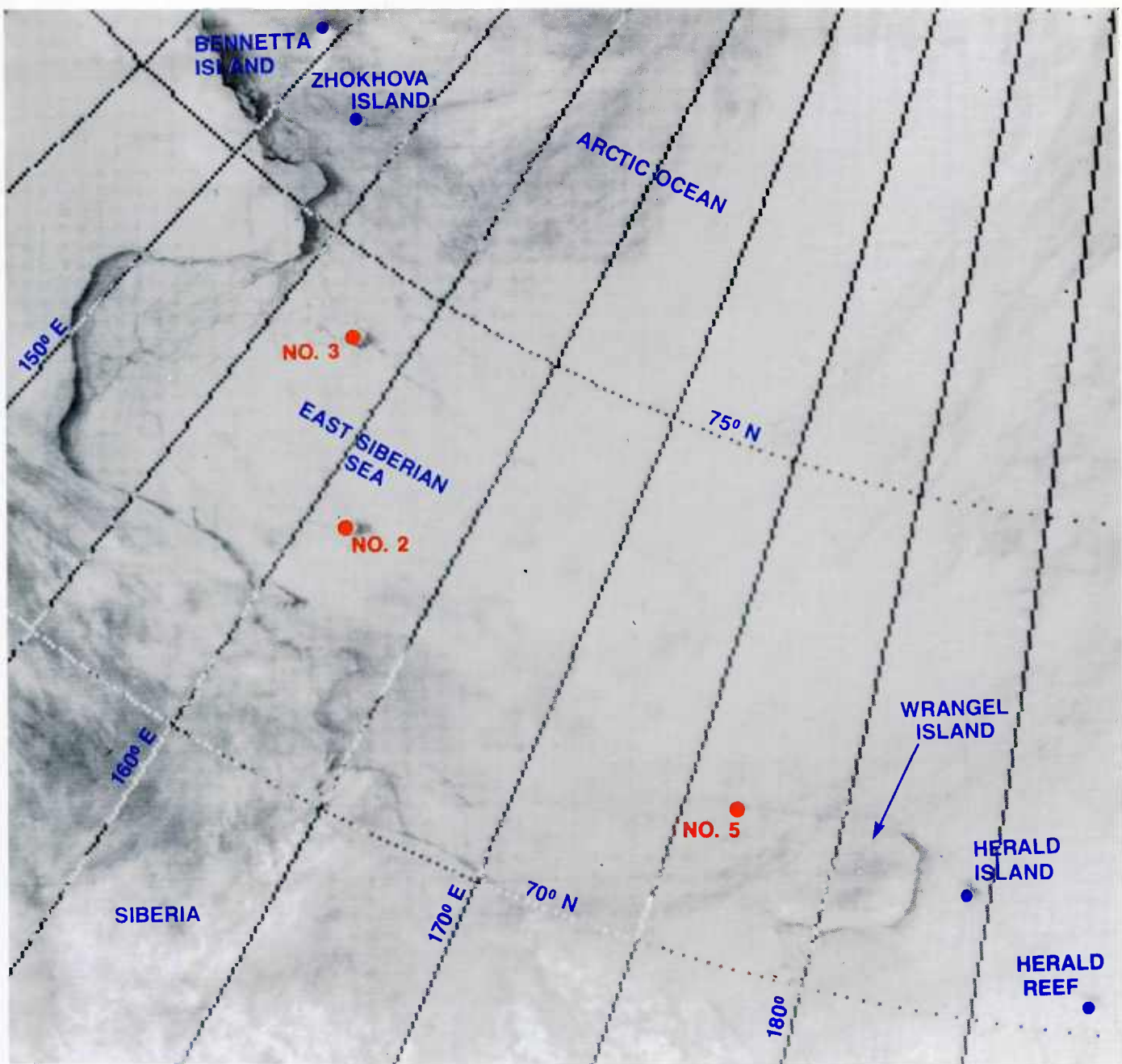
3C-13 DMSP infrared (TS) data, 5 March 1989, 1710 GMT.





3C-14 DMSP infrared (TS) data. 10 March 1988, 1948 GMT.

Figure 3C-14 is a DMSP infrared (TS) view of the region on 10 March 1988.



3C-15 DMSP infrared (TS) data. 10 March 1988, 1848 GMT (with overlay).

The position of the ice islands from 1989 are superimposed as an overlay in Figure 3C-15. It is apparent that the positions of the features from 1989 are identical to the preceding year. Additionally, of major importance are the obvious lead effects associated with each of the ice islands.



Figure 3C-16 shows the area on 1 March 1990, and Figure 3C-17 on 26 March 1990. The features are still evident in the identical locations! The major lead associated with their positions has not occurred at this time. However, minor leads appear adjacent to the islands in each instance.

### **Important Conclusions**

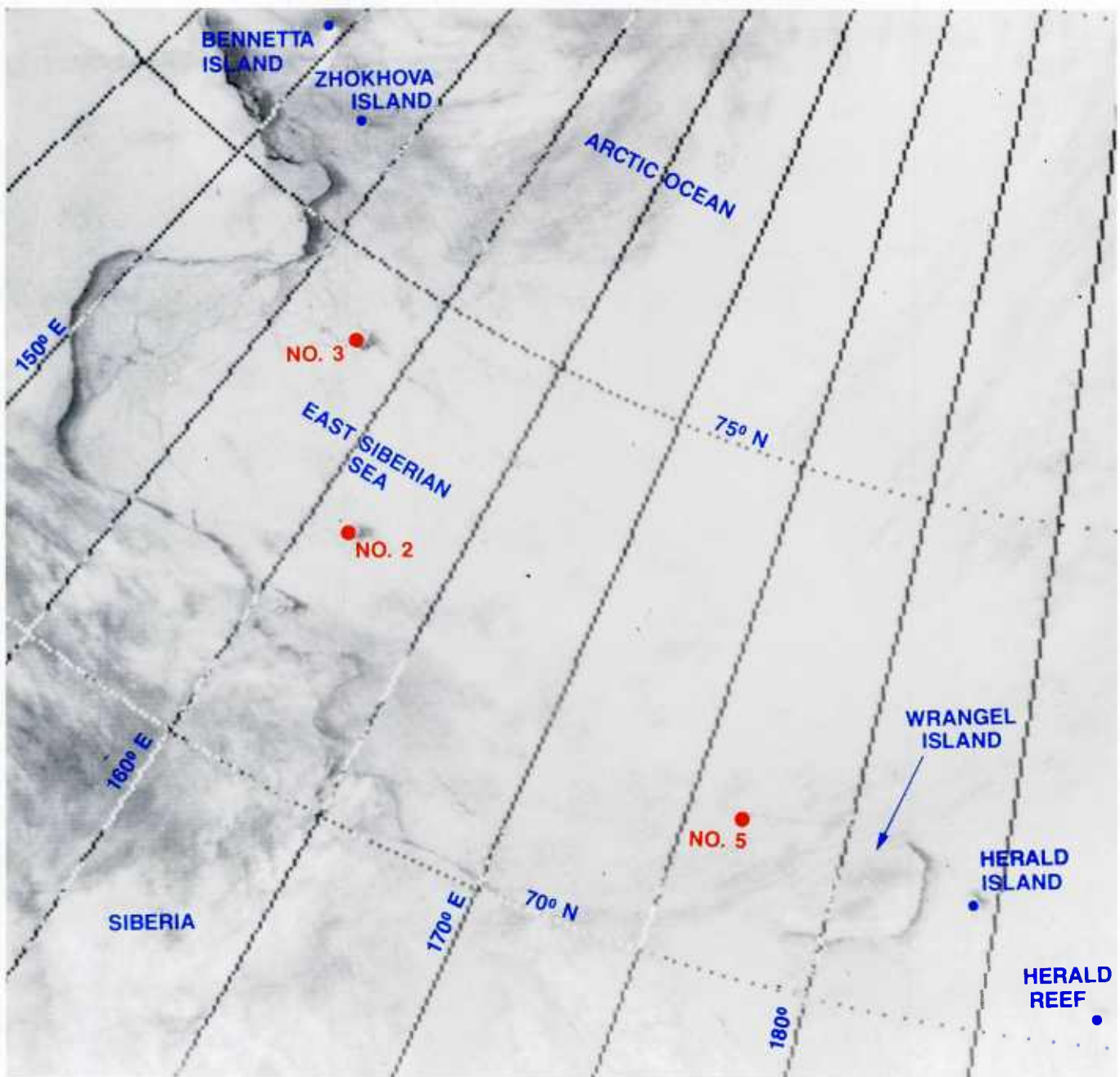
1. Ice movement is very responsive to changes in wind direction and speed. A single storm can be sufficient to reverse ice drift direction in a matter of only 2-3 days.
2. Land islands and islands of grounded sea ice reveal telltale signs of ice drift direction and changes in ice drift direction. It is important to identify such features for optimum ice analysis.
3. Ice islands create stress that often forces the formation of significant lead patterns that can extend over hundreds of kilometers.
4. Islands of grounded ice may indicate the position of shoals not revealed in available bathymetric charts.

### **References**

Kovacs, A., A. Gow, and W.F. Dehn, 1975: Islands of grounded sea ice. Proceedings of the Third International Conf. on Port and Ocean Engineering under Arctic Conditions, 11-15 Aug 1975, Univ. of Alaska, Inst. of Marine Science, pp 333-348.

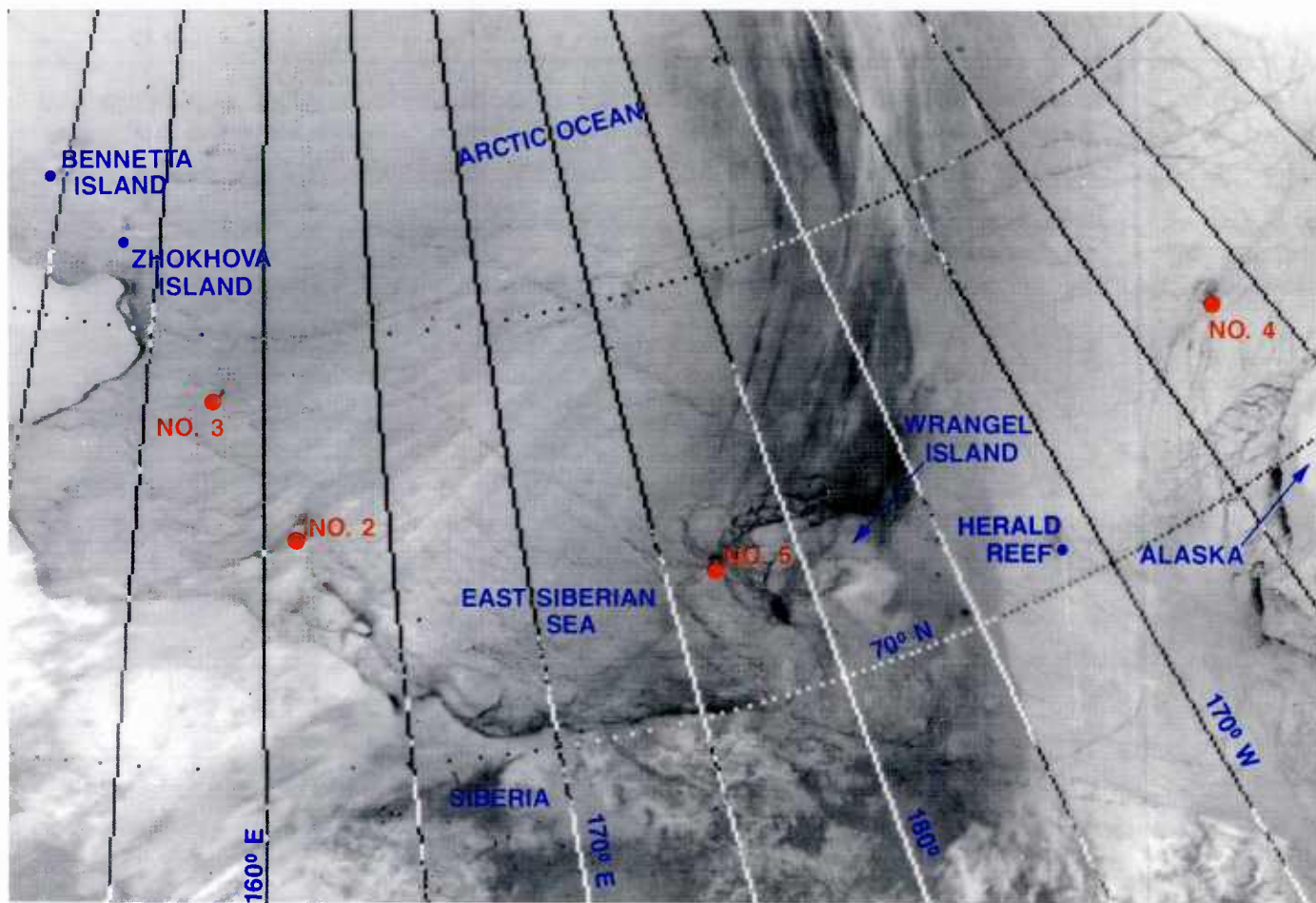
Stringer, W.J., D.G. Barnett, and R.H. Godin, 1984: Handbook for sea ice analysis and forecasting. NEPRF Contractor Report CR84-03, Monterey, CA 93943-5006, p 324.

Stringer, W.J., and S.A. Barrett, 1975: Ice motion in the vicinity of a grounded floeberg. Proceedings of the Third International Conf. on Port and Ocean Engineering under Arctic Conditions, 11-15 Aug 1975, Univ. of Alaska, Inst. of Marine Science, pp 527-551.



3C-16 DMSP infrared (TS) data. 1 March 1990, 1799 GMT.





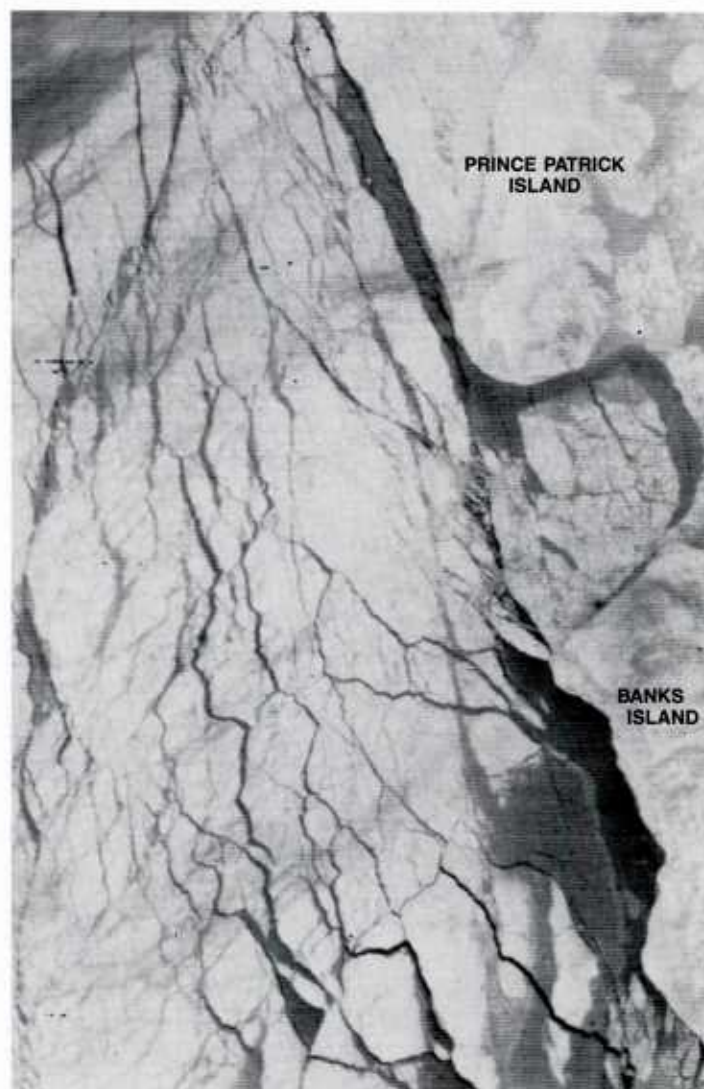
3C-17 DMSP infrared (TS) data. 26 March 1990, 1005 GMT.





### *3D Characteristic Structure and Seasonal Changes in Arctic Sea Ice*

Arctic sea ice undergoes profound seasonal changes in terms of size of ice floe and rigidity, which change due to melting effects as the summer season progresses. Figure 3D-1a is a DMSP infrared image of 550 m (0.3 n mi) resolution showing the ice patterns in the Beaufort Sea just west of Banks and Prince Patrick Islands on 12 January 1986. Open water areas in leads and polynya have led to air-sea interaction effects that can be detected as dark gray shades especially apparent on or near the west coasts of Banks and Prince Patrick Islands.



3D-1a DMSP infrared (TF) imagery. 12 January 1986.

The dark (warm) gray shades indicate the presence of fog or low stratus trapped under the strong low-level inversion, characteristic of Arctic regions during winter. Numerous leads are apparent in this image; however, not all appear to have fog or stratus strongly evidenced resulting from cold air – warm water interaction. No interaction occurs where the leads are frozen over with thin ice; the lead still radiates at a warmer temperature than the surrounding thicker multiyear ice. Additionally, many of the leads have only thin strips of open water that cannot be distinguished from adjacent regions of thinly ice-covered water.

By way of contrast, a NOAA AVHRR visible channel image with a resolution of 927 m (0.5 n mi) acquired during summer conditions (13 July 1985) over the same region is shown in Fig. 3D-2a. The breaking up or shattering of the large ice floes of winter are clearly obvious in this image.

Changes in ice structure and condition can be monitored by satellite in visual, infrared, and microwave channels. The SSM/I data of DMSP are particularly valuable for this purpose in differentiating first year ice from multiyear ice, and in detecting areas of flooded ice resulting from the annual springtime melt (Goroch and Fett, 1991). The first indication of a springtime melt resulting in areas of flooded sea ice can often be seen in DMSP visual data as a result of sunglint effects off the melted surface, contrasting with normal reflection from adjacent regions where the ice is still frozen.

#### References

Goroch, A.K., and R.W. Fett, 1991: Observation of flooded ice in Arctic regions. *Int. J. Remote Sensing*, in press.



3D-2a NOAA AVHRR visible (channel 2) imagery. 13 July 1985.



### *Case 1 Satellite Detection of Flooded Sea Ice*

During the spring melt, pools of water commonly form on the ice surface, which appears as a mottled region of snowy or icy humps and shallow basins of open water. Figure 3D-3a is an example of such a condition over a large region in far-northern latitudes (World Meteorological Organization, 1970). The region where melting first occurs over a large body of water, such as the Beaufort Sea, is dependent upon many factors including time of year, latitude, air temperature, humidity, wind speed, atmospheric stability, ice type, color, age, salinity, ocean currents, ocean depth, and sea temperature. Therefore, exact prediction of such an event is a complex task; observing its occurrence, even from space, is much easier.



3D-3a Representative flooded ice region in the Arctic (World Meteorological Organization, 1970).

Figure 3D-4a is a DMSP visible image over the Beaufort Sea at 1820 GMT on 8 June 1989. The region west of Banks Island appears almost totally ice-covered except for a large lead or polynya immediately west of Banks Island, some openings to the south of the island, and for a large strip of water extending along the coast of Canada, north of the Mackenzie River Delta.

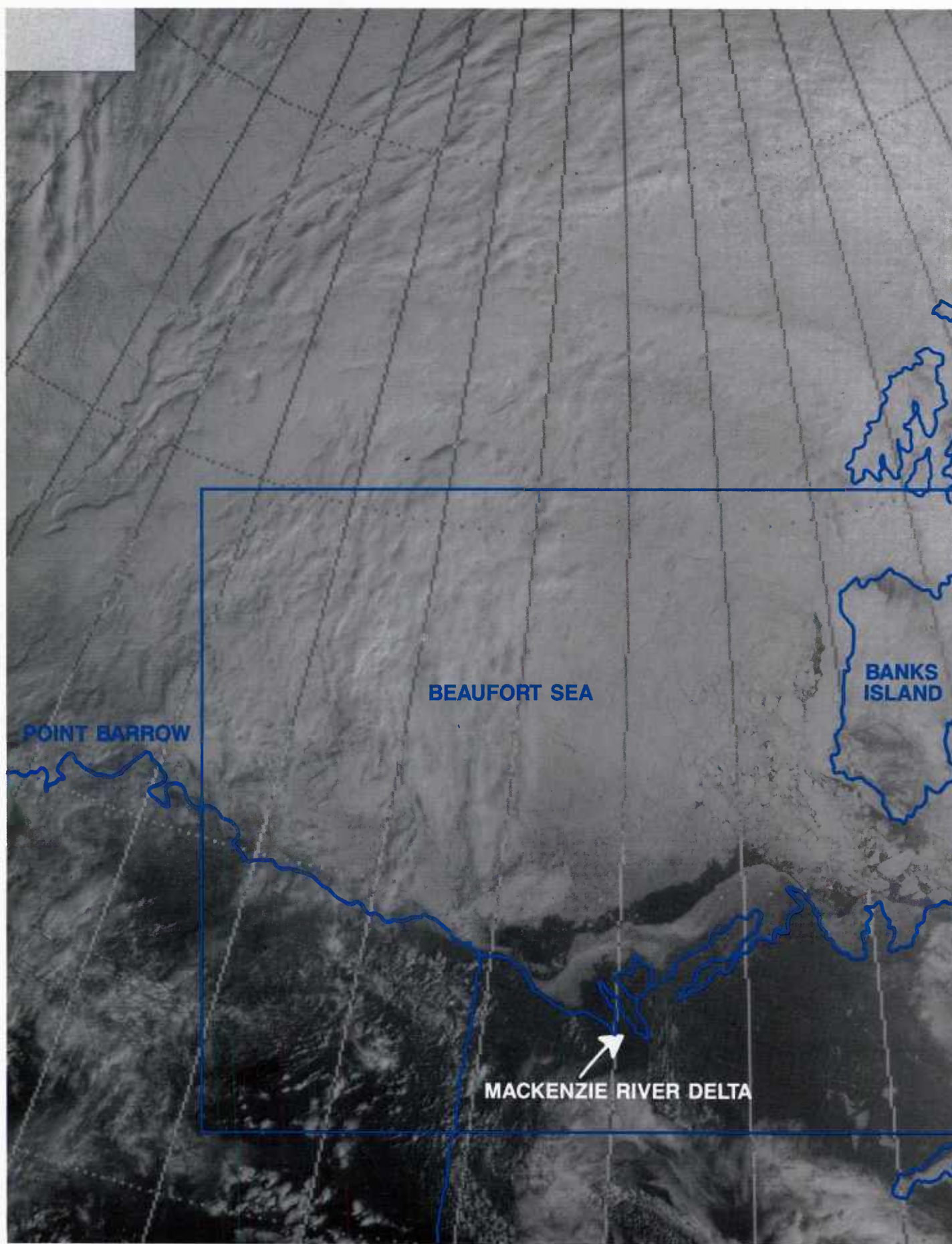
It is of great interest, therefore, to observe an earlier view of the region on the same day, at 1536 GMT (Fig. 3D-5a), under conditions of sunglint. This view shows the area slightly west of the preceding view, so that Banks Island does not appear in the image. However, the Mackenzie River Delta is evident, in this case illuminated in sunglint, and it can be seen that the sunglint appears not only over the open water areas but well to the north, over what appeared on the previous image to be an area of solid ice cover (Fig. 3D-4a). The fact that sunglint is continuous over much of the region does not mean that this area is totally flooded. A flooded ice field, as in Fig. 3D-3a, would show continuous sunglint in satellite data having the appropriate perspective, since the small elements of ice would not be resolved in the poorer resolution of the satellite data. The reflectivity of the ice would be averaged, within a given pixel, as part of the more brilliant reflection from the surrounding water. Figure 3D-5b shows the outline of the sunglint area, superimposed over the preceding view for comparison.

Some additional important points should be made relative to the images. These are described briefly in the remainder of the case study.

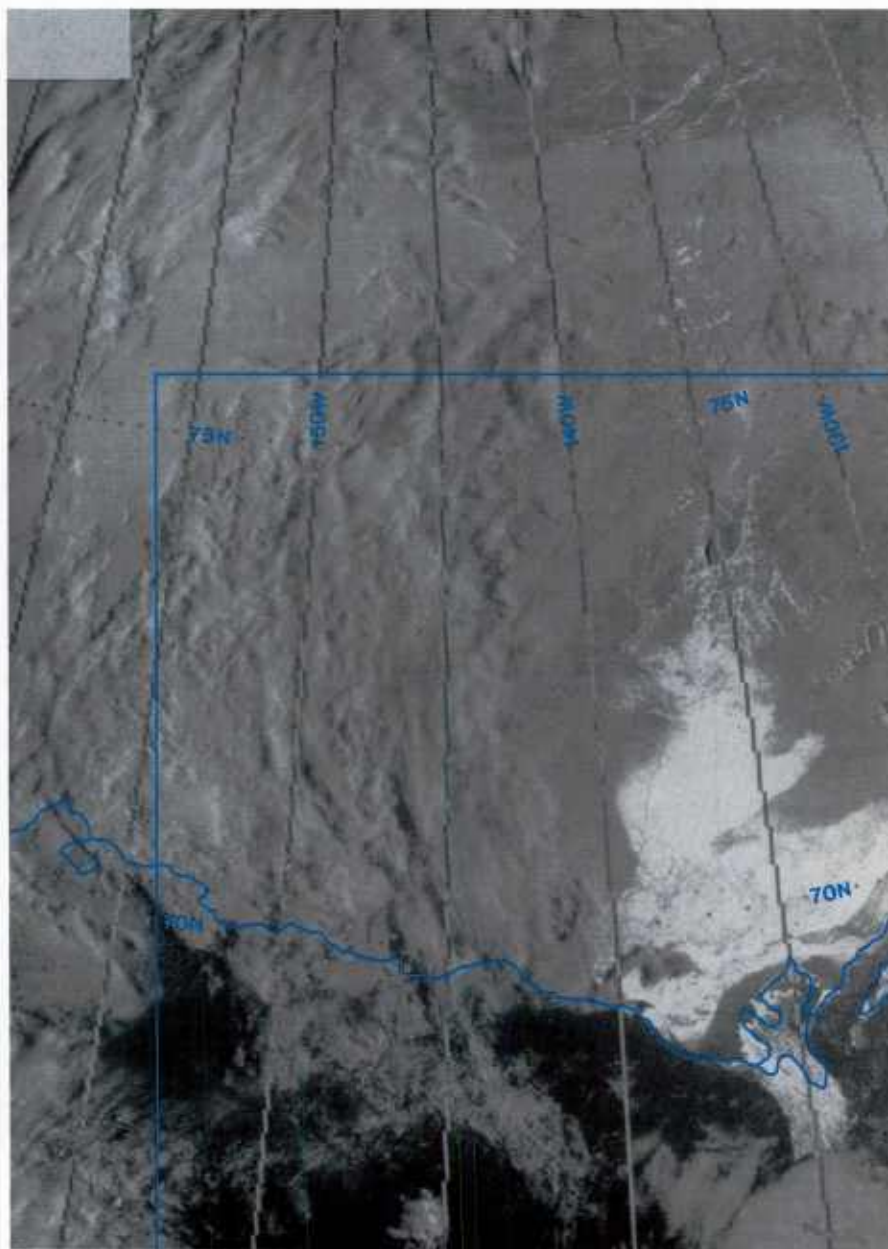
The first is that although the ice region west of Banks Island, out to about 140°W, appears largely free of clouds in Fig. 3D-4a, clouds are apparent in Fig. 3D-5a, actually blocking the sunglint pattern and effectively forming the outline of the sunglint. Individual ice floes can be seen through some of the breaks in the cloudiness, where their outline is etched by surrounding sunglint from the open water. It is highly probable that these same clouds existed in the Fig. 3D-4a data, but because of the thinness of the layer, the angle of view, and the poor contrast of the clouds with the ice covered sea surface, they could not be seen. (This point will be verified in the discussion and description of the near simultaneous AVHRR data that follow).

Another item of interest is the frozen band of ice lying along the Canadian coast, south of the open water region, apparent in Fig. 3D-4a. Note that this band of ice and many of the floes of ice in Fig. 3D-5a do not reflect brilliantly and, therefore, by implication remain frozen in contrast to most of the ice pack in that region, which is apparently flooded. A possible explanation for the band of ice in Mackenzie Bay remaining frozen is that this ice consists mainly of fresh water, which melts at 0°C, as opposed to sea water, which has a lower melting point of about -2.2°C. Similarly the ice floes, which appear frozen, may consist of far less saline multiyear ice and also, therefore, require warmer temperatures before melting.

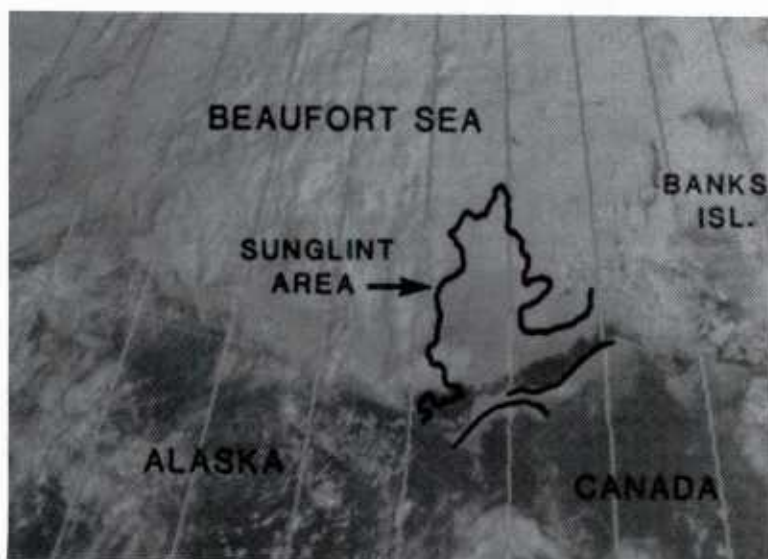




3D-4a DMSP high resolution visible image. 1820 GMT 8 June 1989.



3D-5a DMSP visible image showing sunglint. 1536 GMT 8 June 1989.

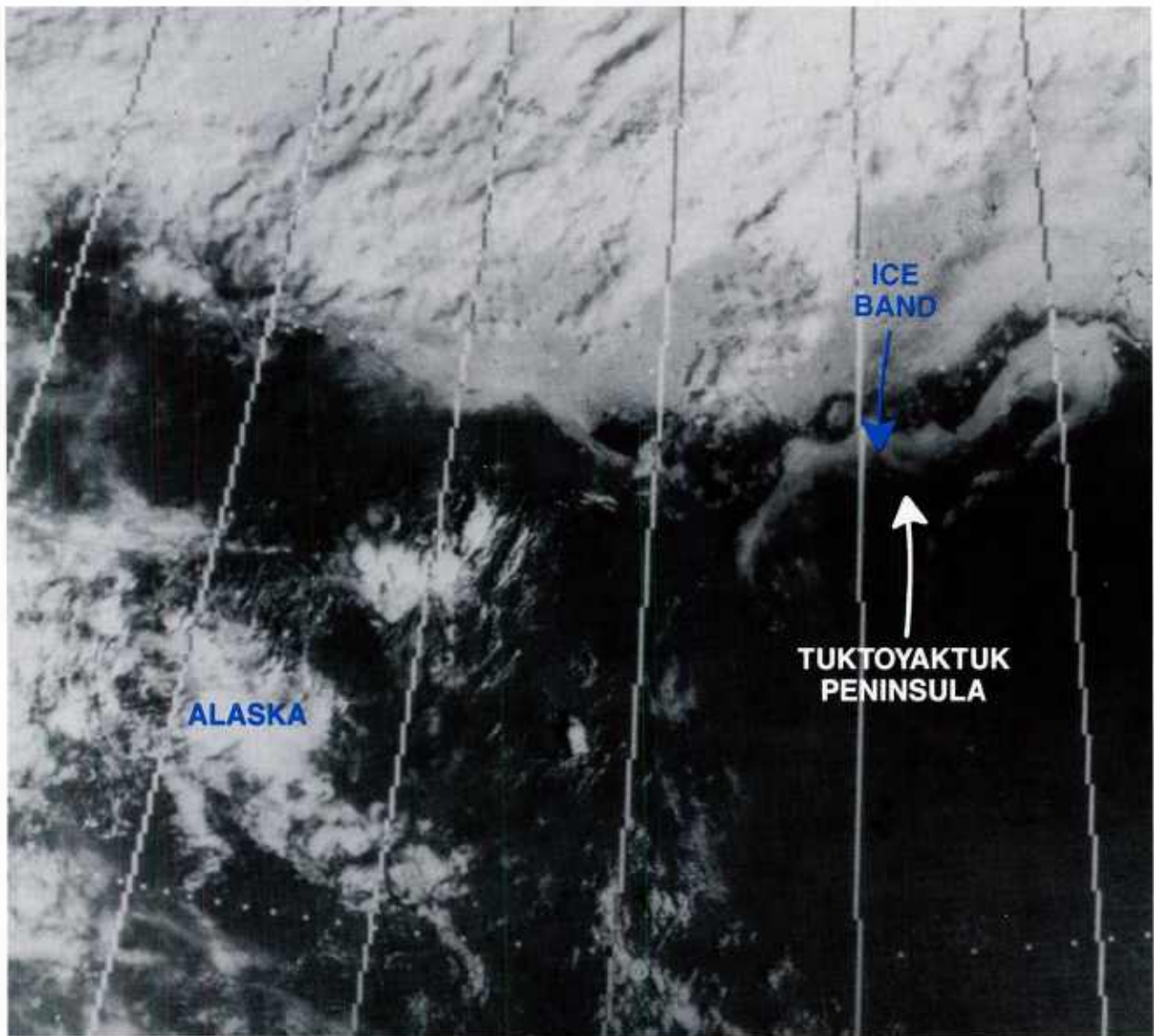


3D-5b Overlay of sunglint pattern determined from Fig 3D-5a, overlaid on Fig 3D-4a.



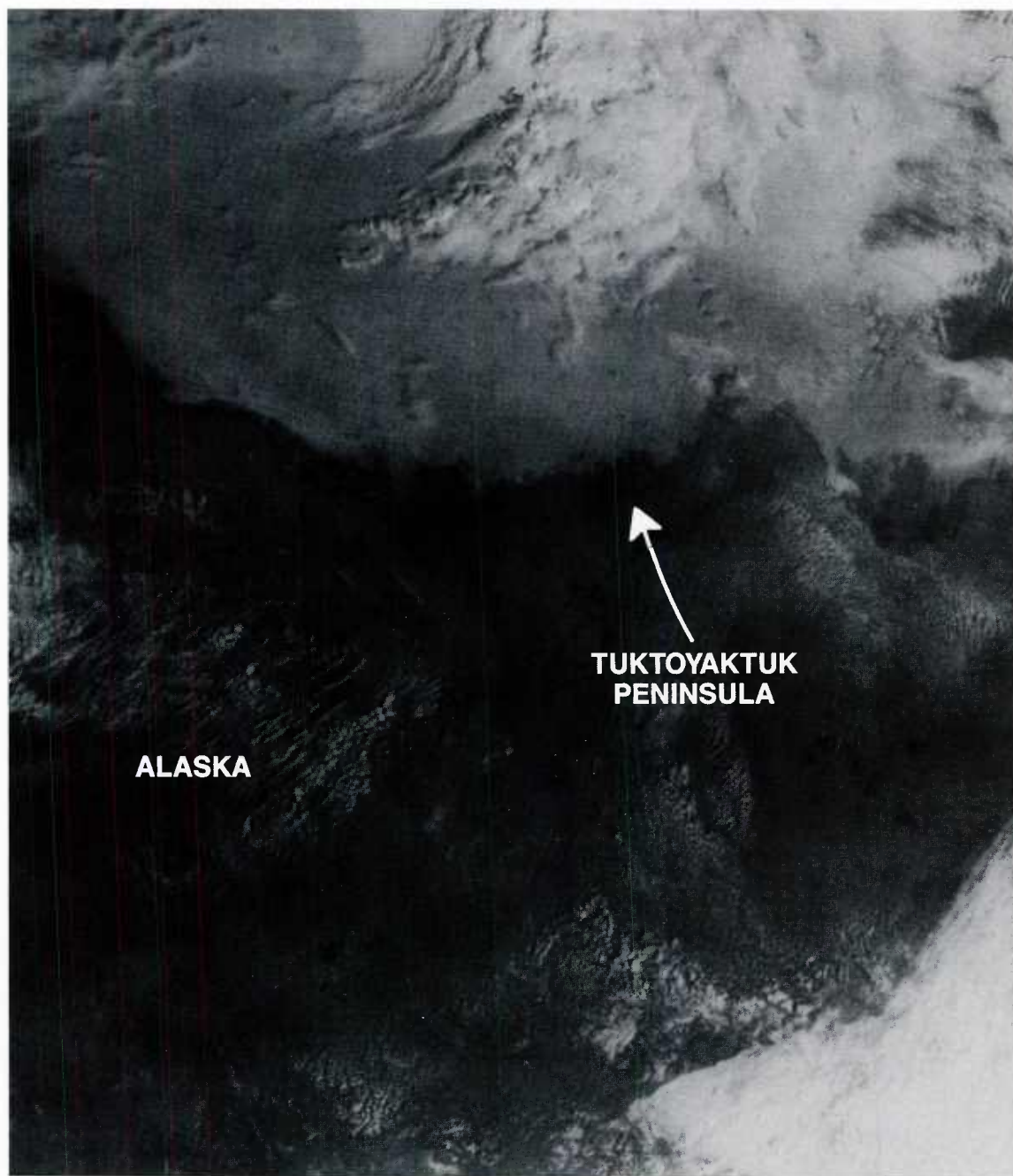
Extensive summertime cloudiness restricted frequent monitoring of the ice condition in the region in this example; however, a visible view on 22 June 1989 at 1841 GMT (Fig. 3D-6a) shows a band of ice still intact surrounding the Tuktoyaktuk Peninsula. By 18 July 1989 in another visible view at 1820 GMT (Fig. 3D-7a) this ice appears to have largely melted. However, the edge of the pack ice remains in the same relative position in both views. An additional view in sunglint on 19 August (Fig. 3D-8a) confirms that although the pack ice may still exist, its surface is flooded since brilliant sunglint covers the area. Note however that some giant floes, faintly discernible just west of Banks Island, remain frozen and are made discernible by reflective open water that etches their outline.

Additional insight concerning interpretation of effects in the area can be gleaned from an examination of the multichannel AVHRR data of NOAA 10. Figure 3D-9a shows the channel 4 (10.3–11.3  $\mu$ m) infrared imagery, obtained less than an hour before the visible DMSP data of Fig. 3D-4a. The land surfaces of Alaska and Canada are dark gray, or black, indicating temperatures warmer than that of the ice to the north. The land surface of Banks Island and Parry Peninsula are slightly colder than land temperatures further south and west. An area of snow southeast of the Parry Peninsula appears cold, emitting radiation at a temperature very similar to the temperature over the Beaufort Sea. The snow area can also be seen in Fig. 3D-4a. The open water area or thin-covered ice region, apparent in the visible data in Fig. 3D-4a, appears in the infrared as a warmer band, extending northeastward from Herschel Island.

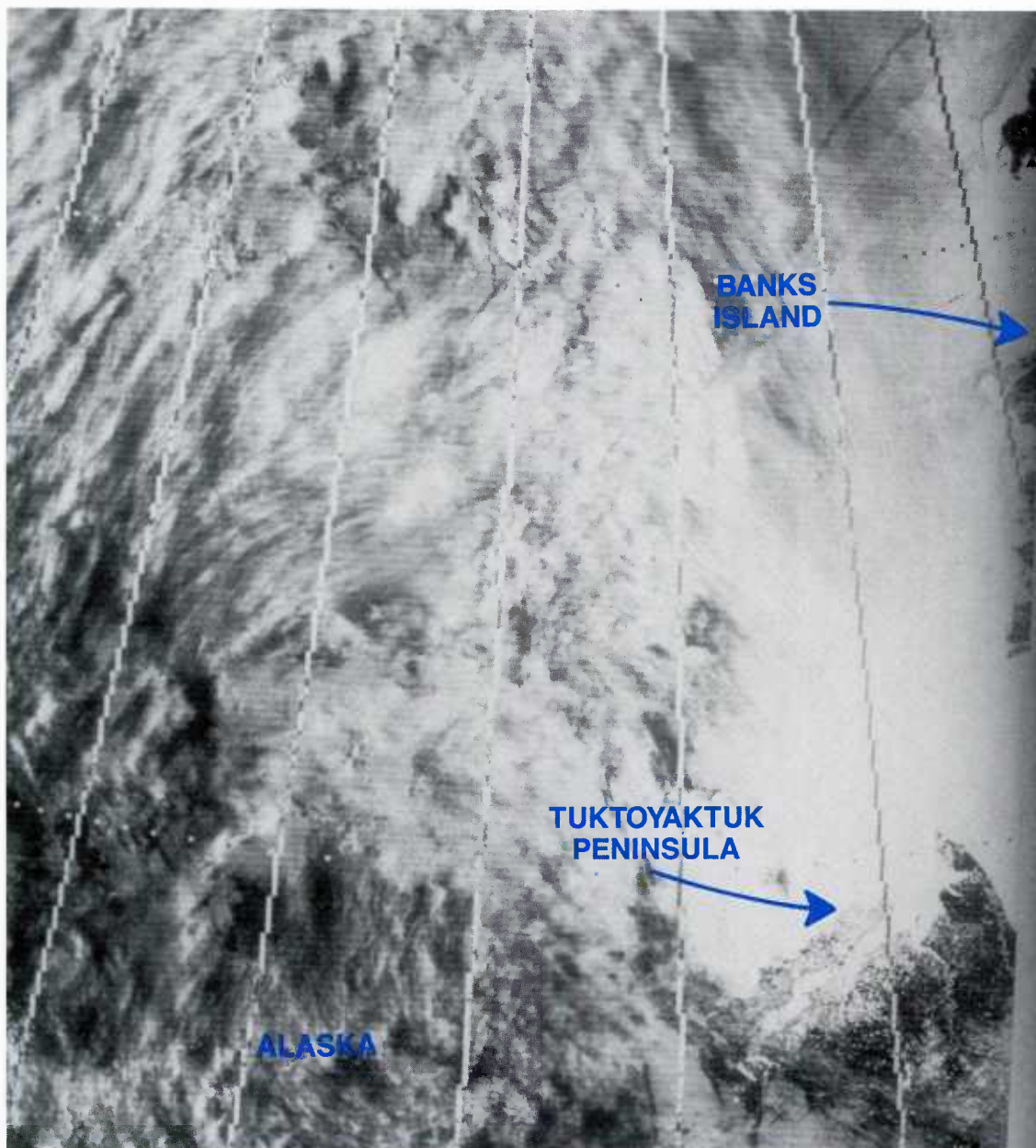


3D-6a DMSP visible image, 1841 GMT 22 June 1989.



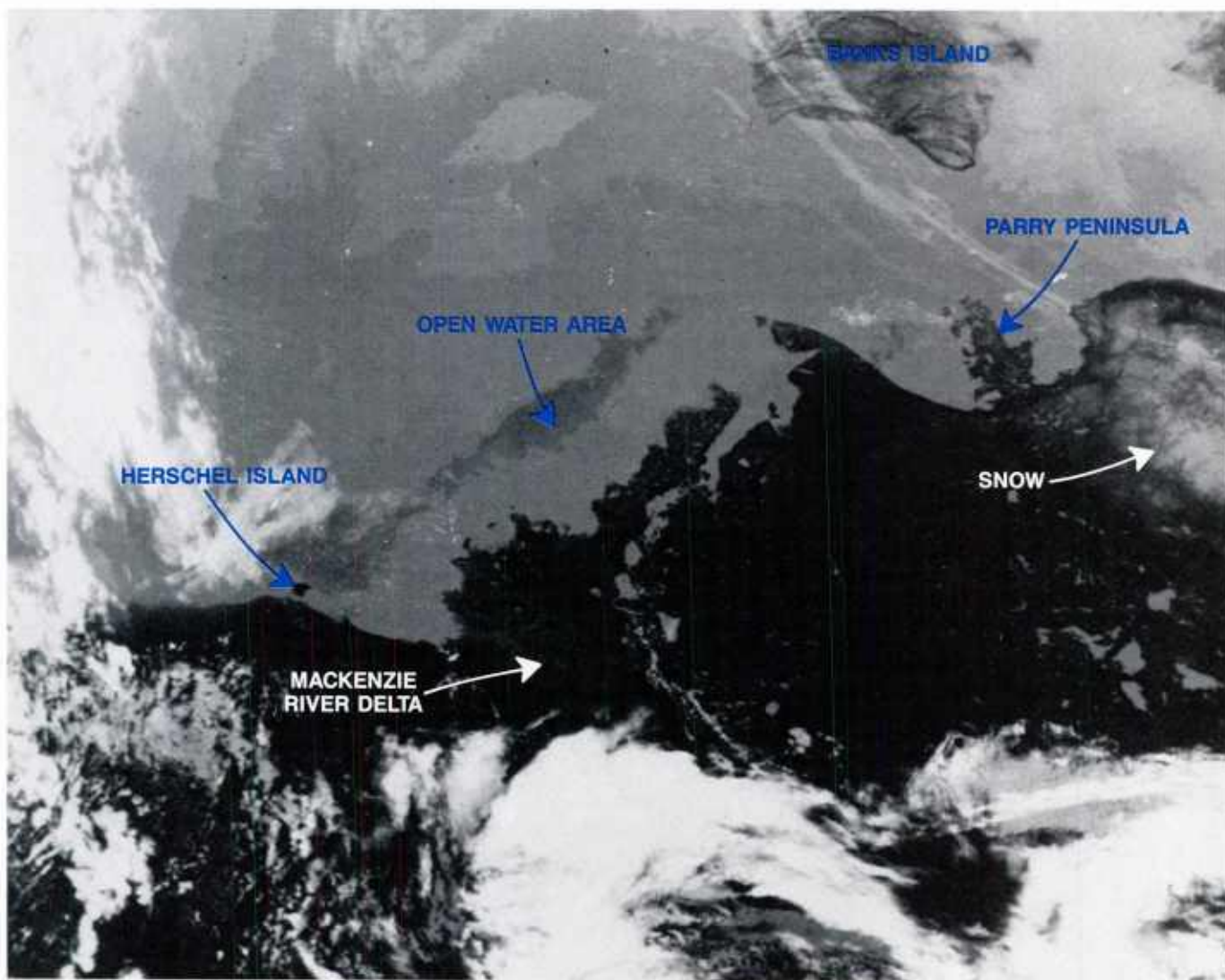


3D-7a DMSP visible image, 1820 GMT 18 July 1989.



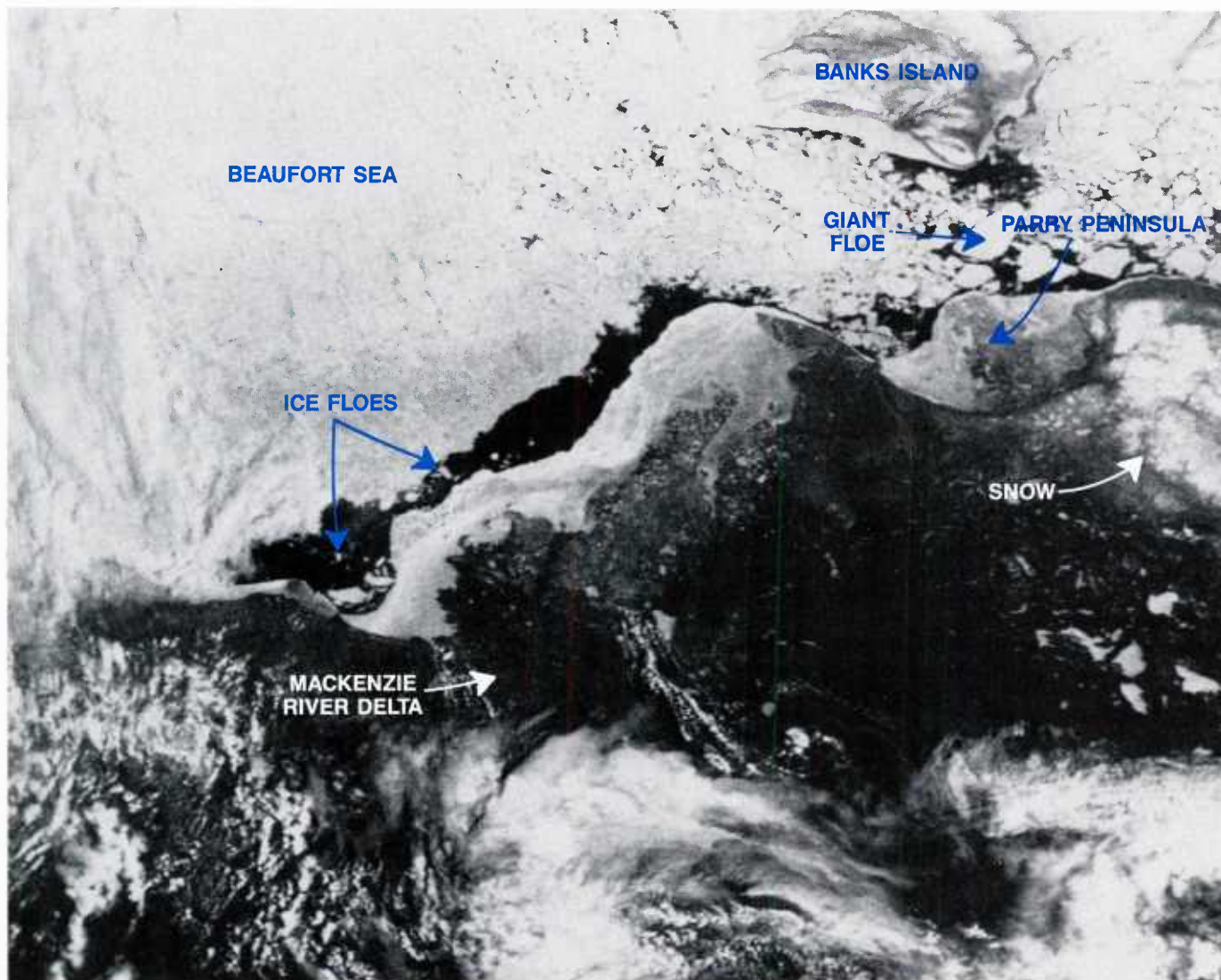
3D-8a DMSP visible image showing sunglint. 1523 GMT 19 August 1989.





3D-9a Channel 4 NOAA 10 image. 1730 GMT 8 June 1989.

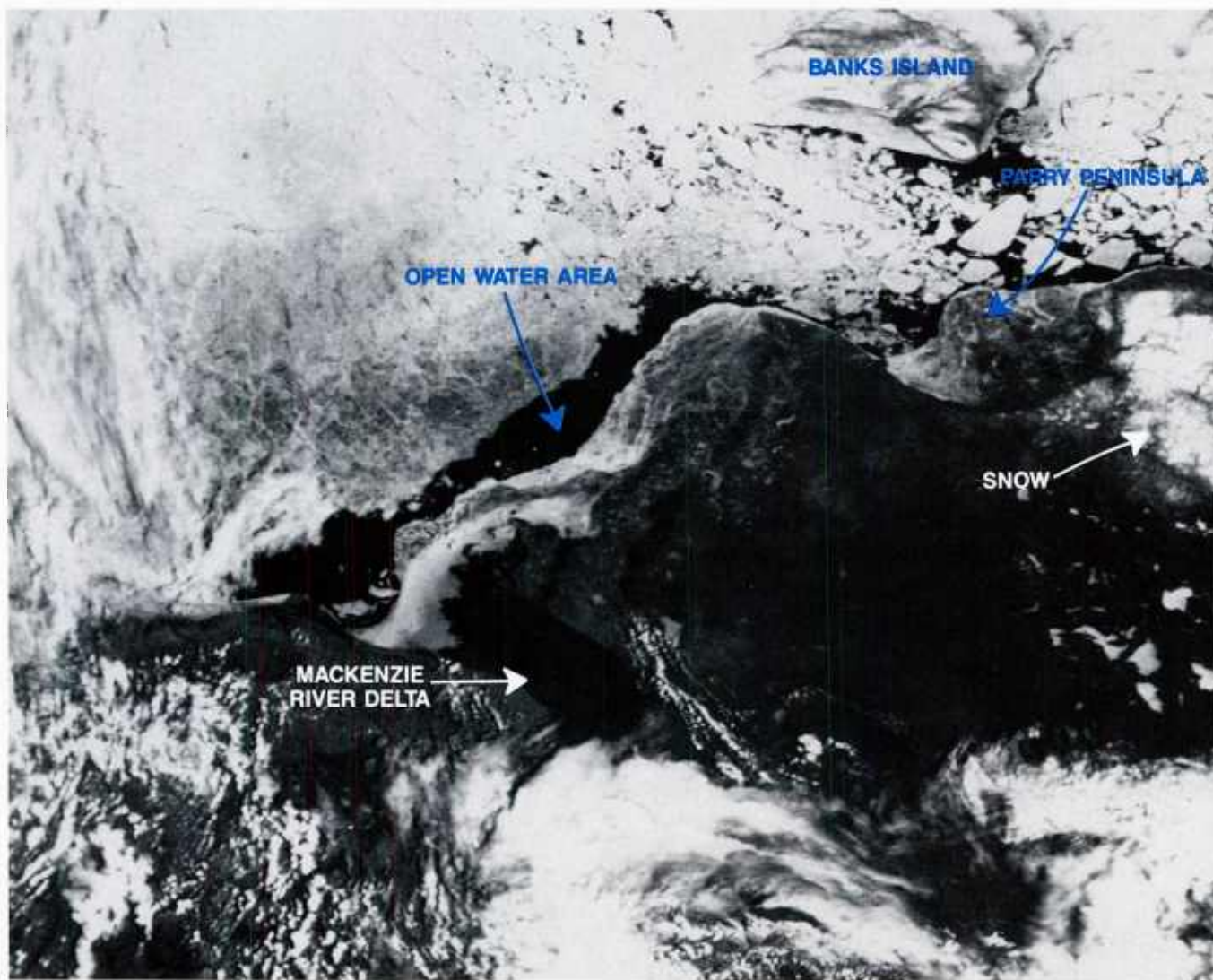
The NOAA 10 channel 1 (0.58–0.68 n mi) visible data are shown in Fig. 3D-10a. These data show, especially well, large ice floes within the apparent open water area and a giant floe south of Banks Island. Note that the southern edge of the Beaufort Sea ice has a darker tone, indicative of a thinner ice condition.



3D-10a Channel 1 NOAA 10 image. 1730 GMT 8 June 1989.



The channel 2 (0.725–1.10  $\mu\text{m}$ ) data of NOAA 10 (Fig. 3D-11a) are of special interest since the channel is limited to the near infrared. Liquid water absorbs near infrared radiation more strongly than visible radiation, with the result that a darkening of the ice surface where melting has occurred is immediately apparent. This coincides almost perfectly with the sunglint region shown in Fig. 3D-5a.



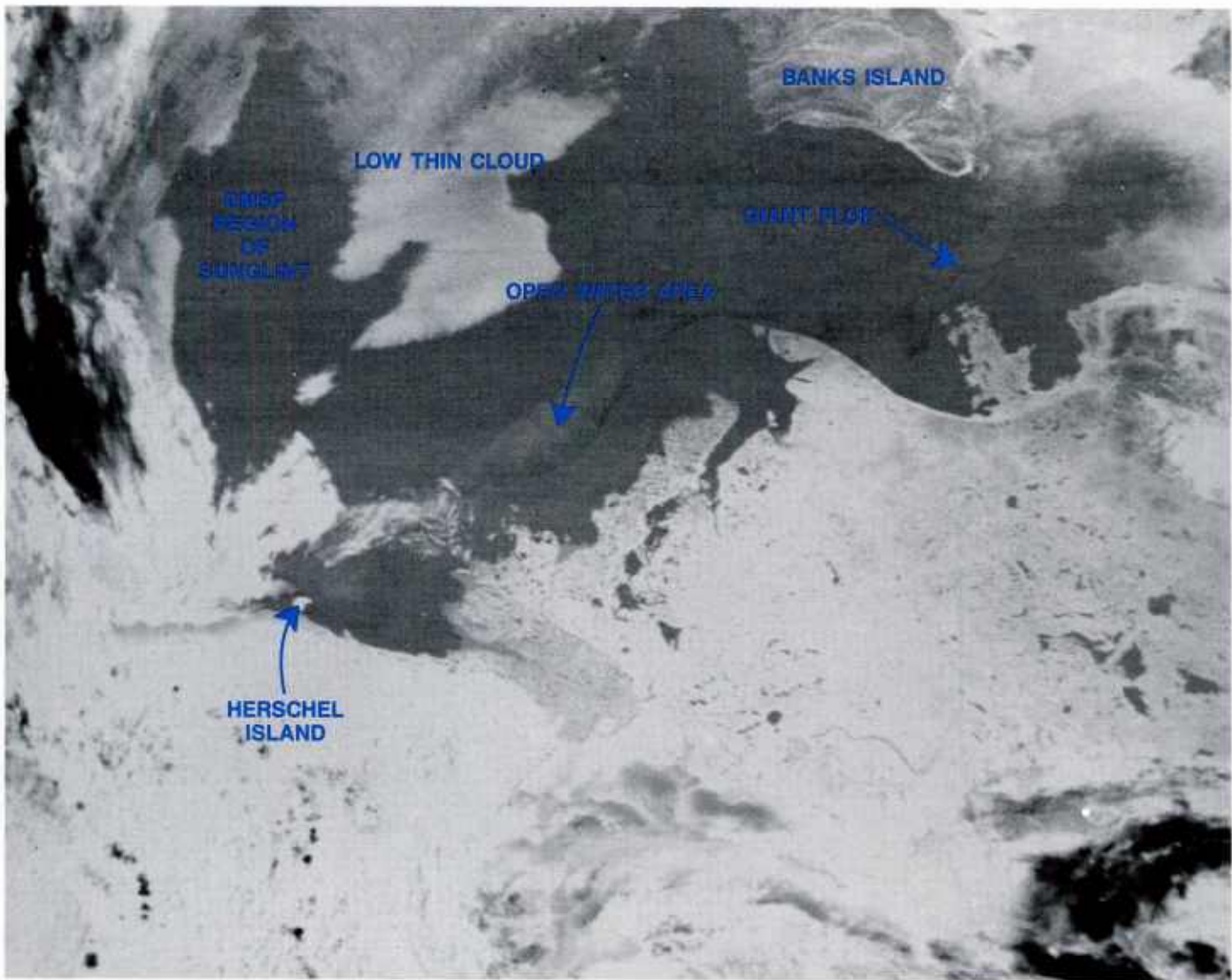
3D-11a Channel 2 NOAA 10 image. 1730 GMT 8 June 1989.

The mid-infrared (3.55–3.93  $\mu\text{m}$ ) channel of NOAA 10 is of additional interest. Figure 3D-12a shows this channel 3 image of the region inverted to show higher radiance (warmer) values as white. Figure 3D-13a is an enhancement of this image used to bring out detail in the ice and cloud cover. Channel 3 daytime imagery senses both scattered visible radiation and infrared emittance. Snow and ice surfaces and ice crystal clouds absorb strongly at this wavelength and appear black in the channel 3 image. Ice crystal clouds are apparent in both the upper left and the lower right corners of Fig. 3D-11a. Note that the ice floes and band of shore fast ice apparent in channel 4 data (Fig. 3D-9a) are almost invisible in channel 2 (Fig. 3D-11a). In the channel 3 image (Fig. 3D-12a), the open water area shows as a warmer (lighter gray shade) region, and the outline of the giant floe south of Banks Island can be faintly discerned because of heightened solar reflection.

Water areas outside of sunglint regions are essentially nonreflective and also appear dark when the water is cold. Hence, most of the frozen ice, the water-covered ice, and the other cold, open water areas, appear as darker shades of gray, with little discrimination of differences. However, a low, thin cloud appears in the top center of the image southwest of Banks Island (Figs. 3D-12a and 3D-13a), and a patch of clouds occurs just northeast of Herschel Island (Fig. 3D-12a), which is not particularly noticeable in either of the visible NOAA channels, or in Fig. 3D-4a, the first DMSP image.

Only when the second DMSP image (Fig. 3D-5a) is carefully examined can one see that the gray shade intrusions into the sunglint to the west and east are, in fact, clouds obscuring underlying features of ice. The pattern of the cloud in the NOAA channel 3 data exactly replicates the pattern of the gray shade intrusion from the east into the sunglint region of Fig. 3D-5a. The fact that this cloud and the cloudy patch northeast of Herschel Island cannot be seen with any distinction in any of the other visible depictions indicates that the cloudiness is quite thin and essentially transparent at other viewing angles. Cloudiness extending over a sunglint area, however, immediately reduces the reflectivity of the region, making it easy to detect in satellite visible imagery (Fett and Bohan, 1977). The cloudiness is apparently very low, and perhaps surface based, since the temperature of the clouds are virtually indistinguishable from the temperature of the surrounding ice as shown by the infrared data (Fig. 3D-9a).





3D-12a Channel 3 NOAA 10 image. 1730 GMT 8 June 1989.

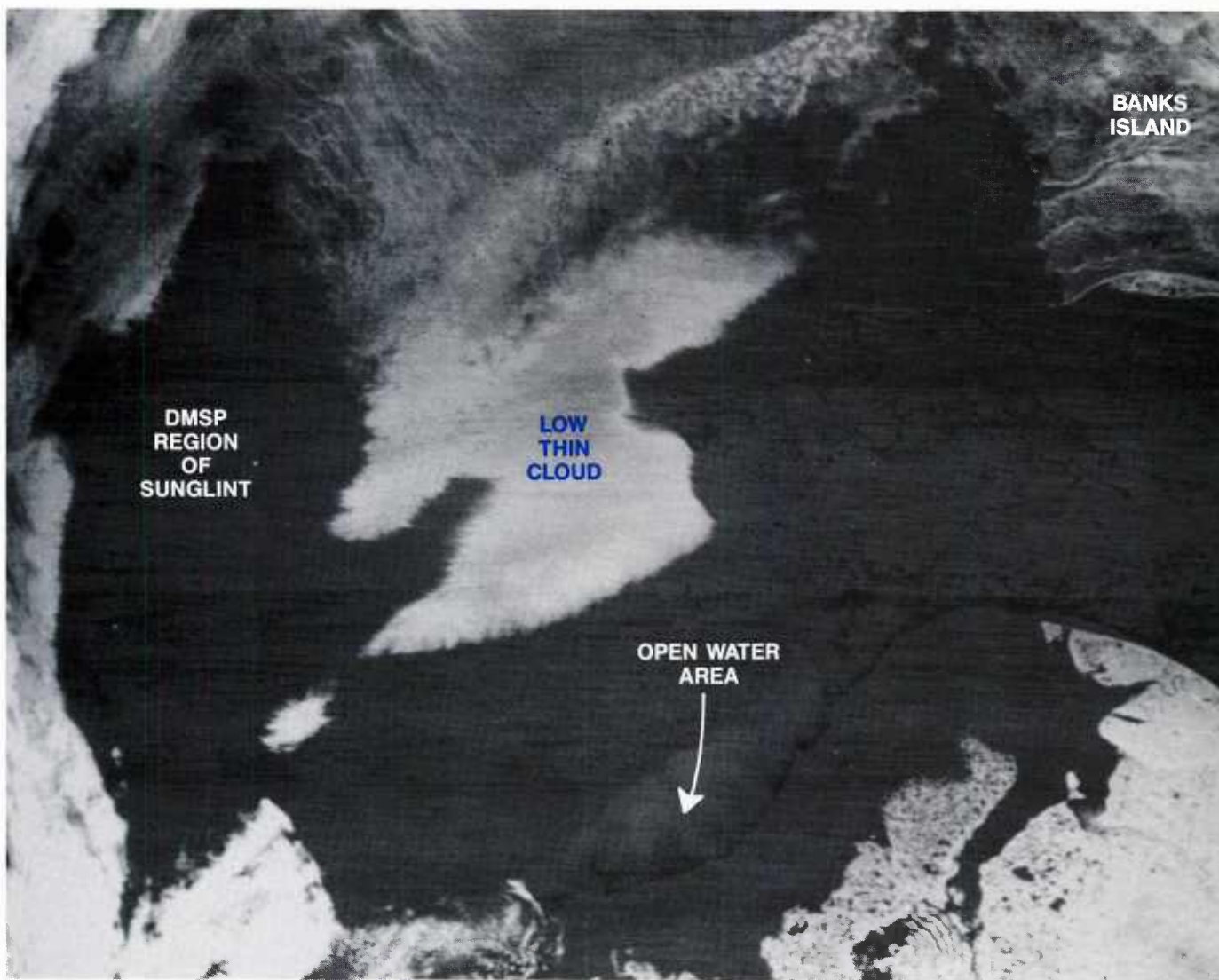
### **Important Conclusions**

1. Areas of flooded ice in the Arctic can be detected in DMSP visible imagery as a result of reflection from the water covered surface.
2. First year sea ice melts at a lower temperature than fresh water ice or multi-year ice, which has a lower salinity. Therefore, sunglint will first be observed during the spring melt over the first year ice. This makes it possible to delineate multiyear floes from first year ice.
3. Low, thin cloudiness may be very difficult to detect over the ice pack in DMSP visible data; conversely, NOAA AVHRR channel 3 data during daylight hours resolve such cloudiness with excellent contrast.
4. NOAA and DMSP infrared data are limited in their usefulness in detecting extremely low clouds or fog over the ice pack when cloud or fog top temperature may be very close in value to the temperature of the ice surface.
5. NOAA AVHRR channel 2 data reveal flooded ice surfaces as darker regions due to absorption by water and limited scattering of light back to the spacecraft sensor from water regions at this wavelength frequency (0.725–1.1  $\mu$ m).

### **References**

- Fett, R.W., and W.A. Bohan, 1977: Navy Tactical Applications Guide, Vol. 1, *Techniques and Applications of Image Analysis*. NEPRF TR 77-03, Naval Environmental Prediction Research Facility, Monterey, CA, 93943–5006, 176 pp.
- World Meteorological Organization, 1970: *Sea Ice and Nomenclature*. Technical publication No. 259, WMO, Geneva, Switzerland.





3D-13a Enhancement of Fig. 3D-12a to improve ice and cloud detail.

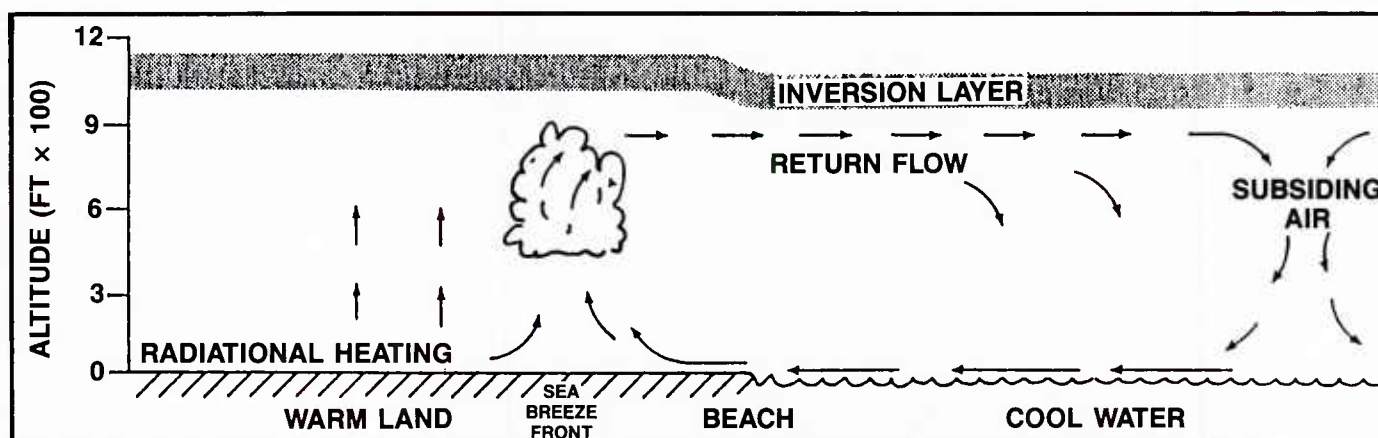




### 3E Land and Sea Breezes

Sea breezes are common mesoscale features in coastal areas around the world. Although not commonly associated with the Arctic, Kozo (1982) provided direct evidence of their existence at 70°N latitude. The intensity, duration, and extent of the sea breeze circulation is determined by horizontal gradients in the amount of heat supplied by the Earth's surface to the atmosphere (Fig. 3E-1a) by large scale synoptic conditions and by topography. The main factor, the horizontal gradient of surface heating, is caused by a difference in the response to solar radiation of land, water, and in Arctic regions, sea ice.

Equal amounts of incoming radiation over water and land will not raise the water surface temperature as much as the land surface temperature. Over water, more energy is used for evaporation, and the remainder of the energy reaches greater depths due to water turbulence and water transparency. Warmer air heated from below by the land rises and is replaced by cooler denser air from over the water (Fig. 3E-1a). Convective cloud lines can develop in areas of convergence along the sea breeze frontal boundary inshore. Convective cloudiness is absent along and off the coastline in areas of subsiding return flow.



3E-1a Major features of the sea breeze circulation cell including the capping inversion (from Fett et al., 1979).

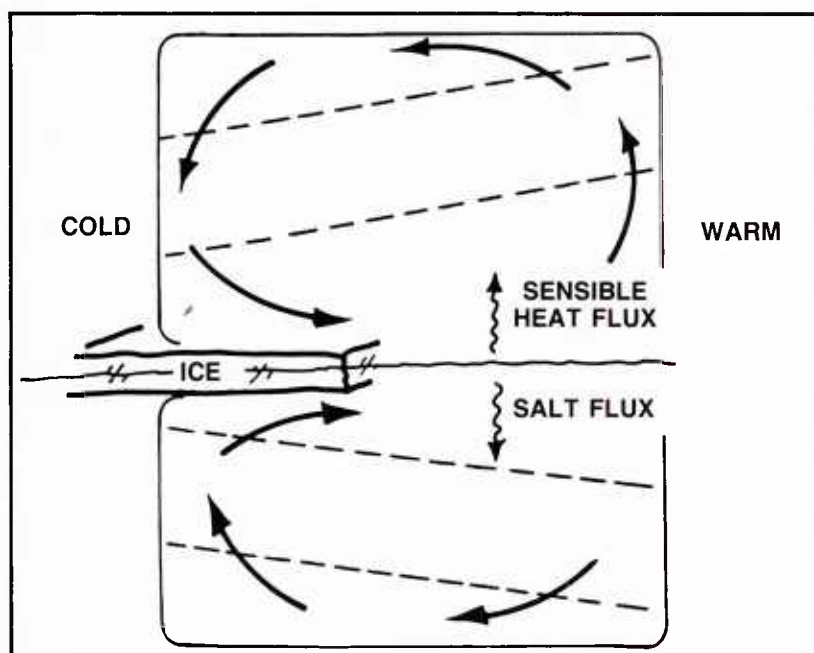
In the cases of water and sea ice (Fig. 3E-2a), a separate "ice breeze" can occur (McPhee, 1980; Chu, 1987). The sea ice will never have a temperature greater than adjacent ocean water. A positive temperature gradient (ice to water) in the surface layer of the atmosphere will cause surface winds to blow from the ice to water.

In summer, Arctic coastal areas generally have a more stable boundary layer (shallower and inversion-capped) than the middle latitude coastal areas (Fig. 3E-1a). Seaward flow aloft during sea breeze events can occur at elevations of less than 1,000 ft or about one third of the elevation in temperate regions. The land-sea temperature differential is often twice that of temperate or tropical regions. This differential makes the Arctic sea breeze possible, despite the high atmospheric stability. Some effects of sea breezes are

1. Movement of oceanic contaminants onshore
2. Promotion of stable atmospheric lapse rates, which are favorable for propagation of radio and radar signals (Meyer, 1971)
3. Diurnal fluctuation of ambient noise (summer) as landfast ice responds to breeze-imposed stresses (Waddell and Farmer, 1988)
4. Creation of vertical wind shear, which can be hazardous to landing aircraft

#### References

- Chu, P.C., 1987: Generation of unstable modes of the iceward-attenuating swell by ice breeze. *J. Geophys. Res.*, 17, 828-832.
- Fett, R.W., P.E. LaViolette, M. Nestor, J.W. Nickerson, and K. Rabe, 1979: Navy Tactical Applications Guide, Vol. 2, *Environmental Phenomena and Effects*. NEPRF TR 77-04, Naval Environmental Prediction Research Facility, Monterey, CA, 93943-5006, 161 pp.
- Kozo, T.L., 1982: An observational study of sea breezes along the Alaska Beaufort Sea Coast: Part I. *J. App. Meteor.*, 12, 891-905.
- McPhee, M.G., 1980: Physical oceanography of the seasonal sea ice zone. *Cold Regions Sci. Technol.*, 2, 93-118.
- Meyer, J.H., 1971: Radar observations of land breeze fronts. *J. App. Meteor.*, 10, 1224-1232.
- Waddell, S.R., and D.M. Farmer, 1988: Ice breakup: Observations of the acoustic signal. *J. Geophys. Res.*, 93, 2333-2342.



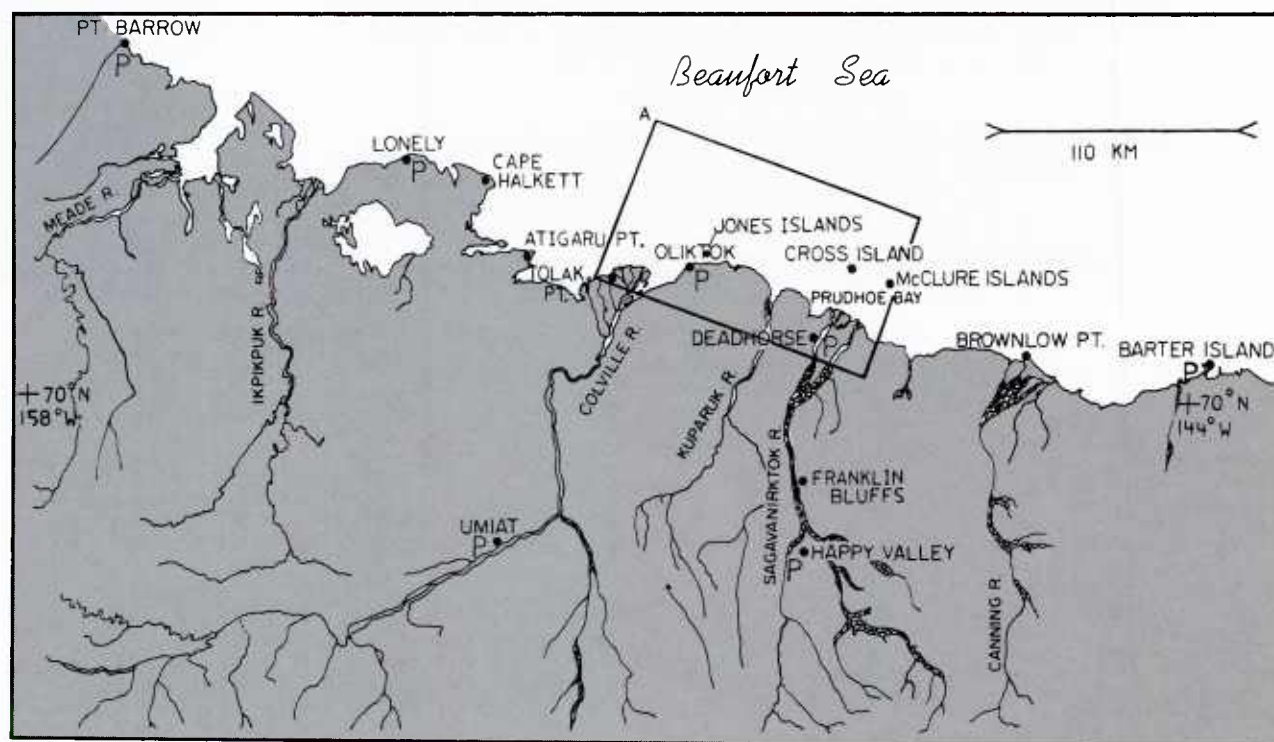
3E-2a Schematic of the ice breeze cell in the atmosphere and simultaneous oceanic circulation cell created by new ice growth (from McPhee, 1980).



### *Case 1 Sea Breezes Along the Alaskan Beaufort Seacoast*

Moritz (1977), after investigating historical surface wind data from the Beaufort Seacoast of Alaska (Fig. 3E-3a), found that measured surface winds with easterly components have greater magnitudes and frequency than westerly winds. He suggested that contrasts in surface temperatures across the boundary along Alaska's north coast produce an added pressure gradient component not resolved by existing synoptic observation networks. Moritz conjectured that this pressure gradient produces a sea breeze circulation with a large alongshore component (from the east) due to the almost continuous solar irradiance, larger Coriolis force ( $70^{\circ}\text{N}$  versus  $45^{\circ}\text{N}$ ), and large horizontal extent and orientation of the coastlines.

A study by Kozo (1982) took place at two field locations: Prudhoe Bay and the Jones Islands (Pingok Island) (Fig. 3E-3a, rectangle A). Those coastal locations exist in an area where the summer tundra - ocean thermal contrast remains positive (land always warmer than the water) despite  $15^{\circ}\text{C}$  drops in land temperatures over short Arctic summer nights (Moritz, 1977). This unique feature of the Alaskan Beaufort Seacoast ensures that a summer sea breeze will never be followed by a land breeze.



3E-3a Alaskan Beaufort Seacoast with the major data sites enclosed by rectangle (A). Atmospheric pressure stations (P) are also shown (from Kozo, 1982).

Profiles (Fig. 3E-4a) of wind speed, wind direction, and temperature are shown from Pingok Island. The land-sea temperature difference was 12.8 °C. The directional difference between the lower level wind (onshore) and the upper level wind (offshore) was greater than 100° for each profile. The direction reversal indicating a sea breeze cell generally was complete at the altitude of the inversion layer top. Figure 3E-4b provides evidence from atmospheric acoustic soundings of the height of the inversion layer (main horizontal echo pattern) on an August sea-breeze day. The vertically oriented echo patterns that become prominent around 0900 local time are thermal plumes that “push” the capping inversion upward (from 110 m to 450 m) and try to eliminate it.

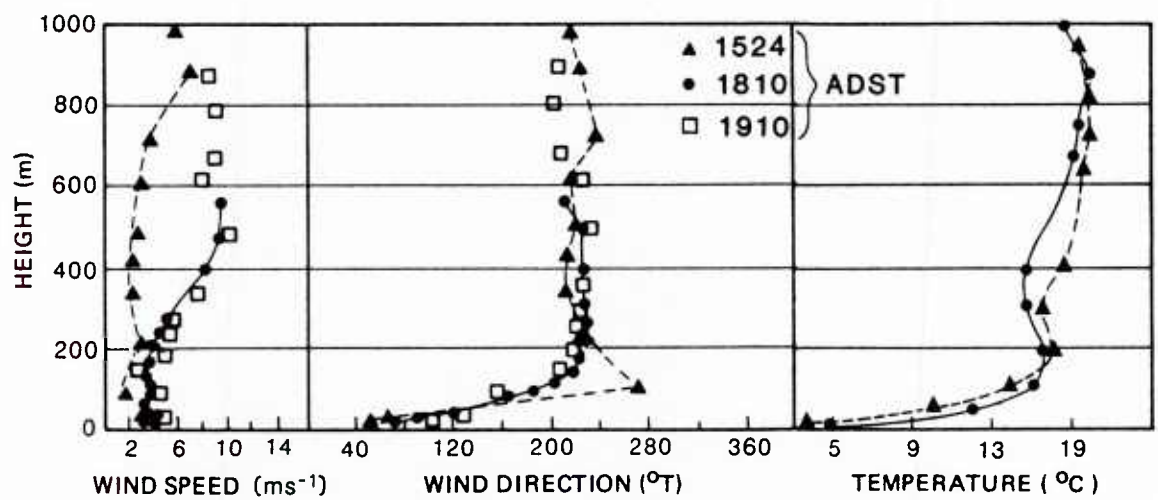
Figure 3E-5a, which is a histogram of surface wind speed and direction for the Augusts of 1976, 1977, and 1978, provides evidence of imbalance in the frequency of easterly and northeasterly winds along the Alaskan Beaufort Seacoast such as that observed by Moritz (1977).

Satellite evidence of the presence of a sea breeze is the “sea breeze front” (Fett et al., 1979), which is associated with a convective cloud line. This cloud line is inland and generally parallel to a relatively straight coastline. When the coastline is curved so as to form bays and peninsulas, convective intensity is modulated due to varying effects of convergence and divergence induced by the curvature.

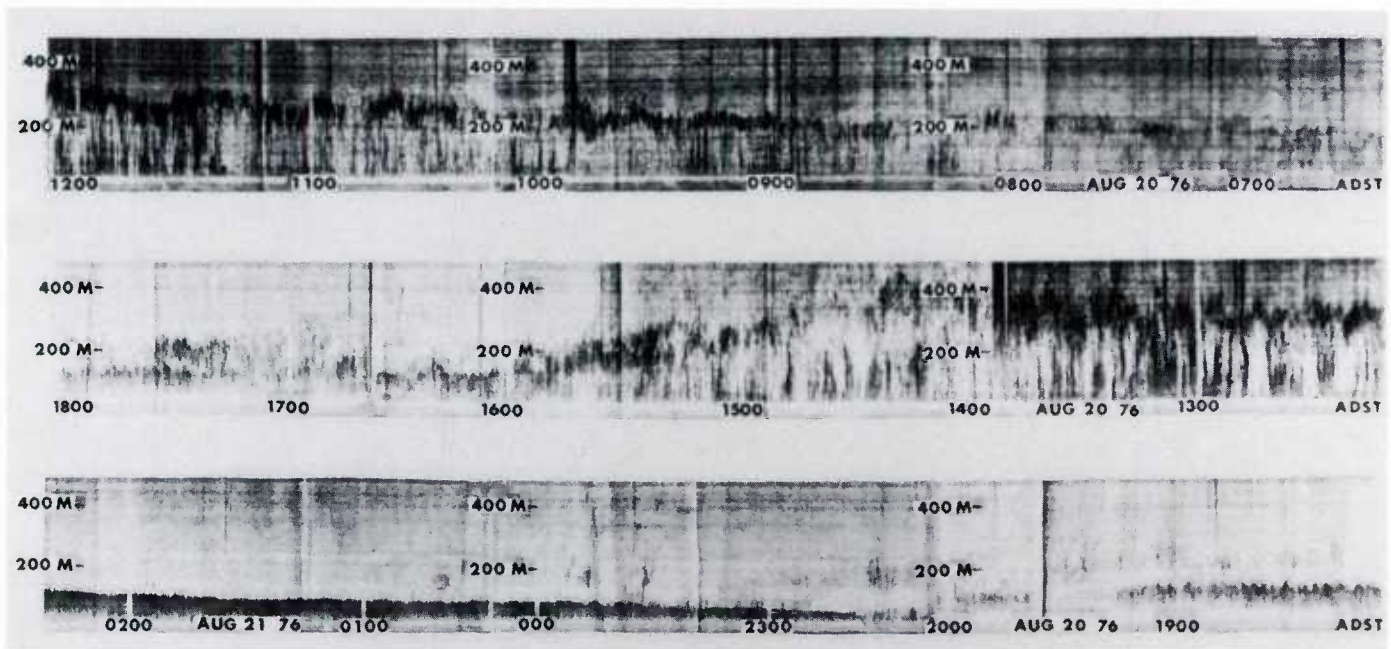
### *3–7 July 1990*

In particular, as shown in Fig. 3E-5b, peninsulas are favored areas for development of vigorous convection because of winds converging from each side of the peninsula. Barrow is located at the northwest tip of a peninsula formed by the Dease Inlet on the east side and the Beaufort Sea on the north and west sides (Fig. 3E-6a). Figure 3E-6b is a DMSP visible (LF) image of the area on 3 July 1990 at 1931 GMT showing appreciable heavy convective activity over the peninsula. The FNOC surface analysis for this date at 1800 GMT (Fig. 3E-7a) shows onshore northerly winds reported at Barrow, consistent with a sea breeze effect. However, a small low-pressure center just southeast of Barrow may be influencing the wind circulation and weather at this time. The low is not intense enough to show obvious features or signs of circulation in the satellite data (Fig. 3E-6b).

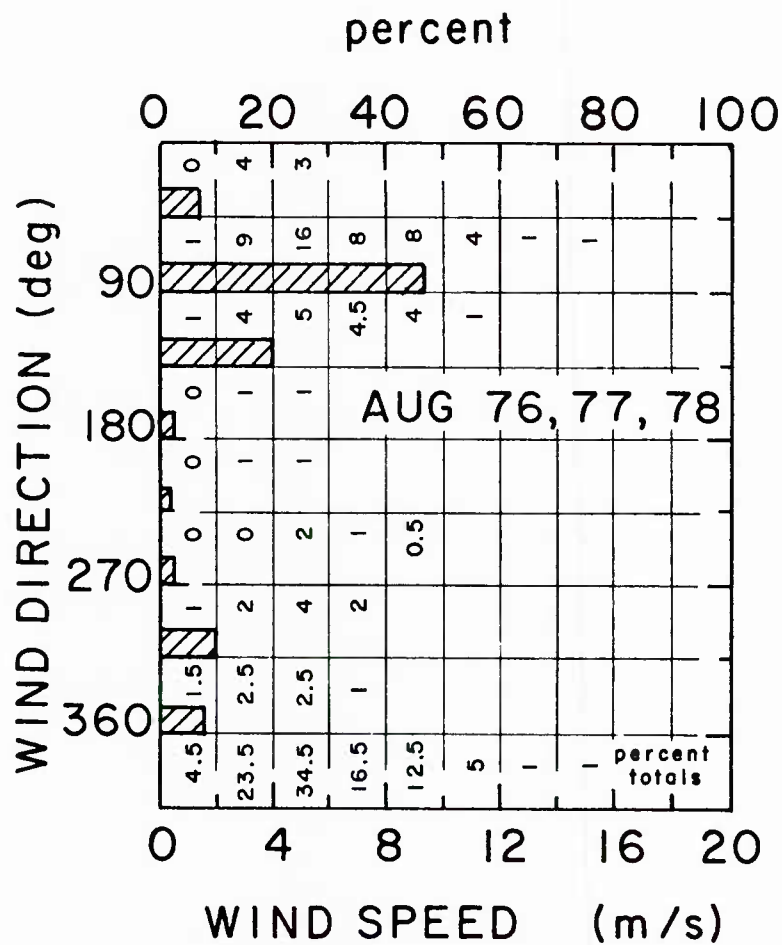




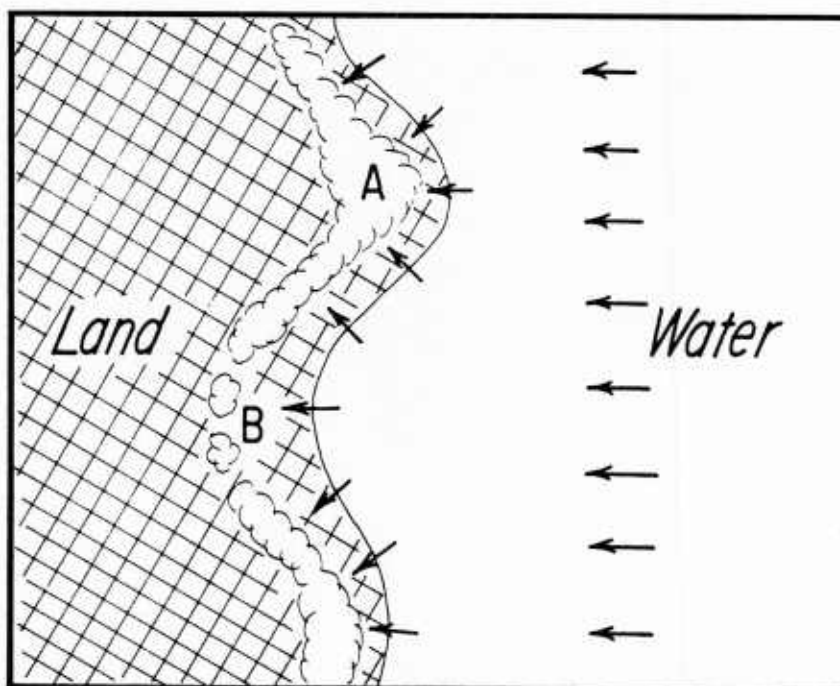
3E-4a Profiles of wind speed, wind direction, and temperature for 1524, 1810, and 1910 (ADST) on 15 August 1977 (from Kozo, 1982). The data were taken on Pingok Island (Jones Islands).



3E-4b Facsimile record of acoustic sounding from 0700 ADST on 20 August 1976 to 0200 ADST on 21 August 1976 (a sea-breeze day) recorded 15 km inland near Deadhorse, Alaska (from Kozo, 1982).



3E-5a Histogram of surface wind speed and direction for August 1976, 1977, and 1978 combined from the Jones Islands (from Kozo, 1982).

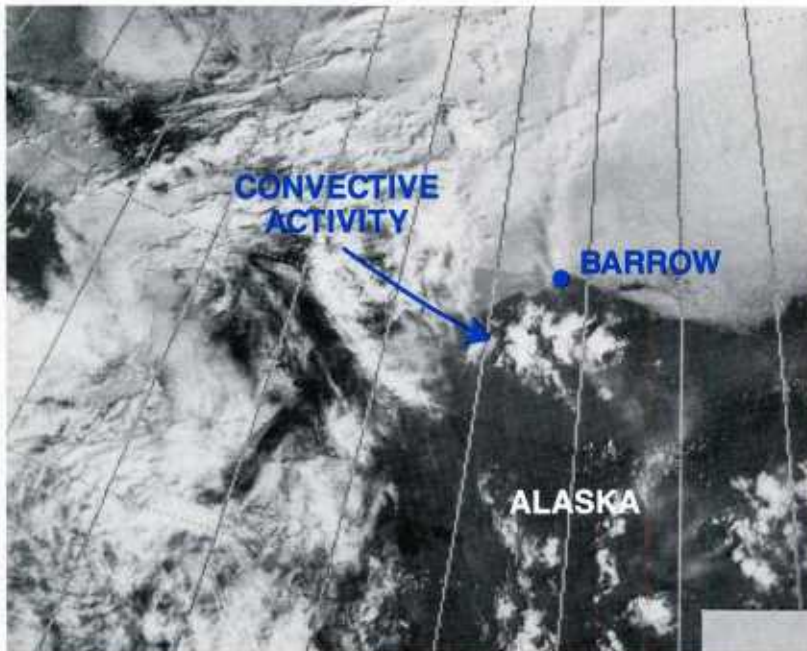


3E-5b Schematic showing the relationships between coastline curvature and sea breeze frontal cloud lines.

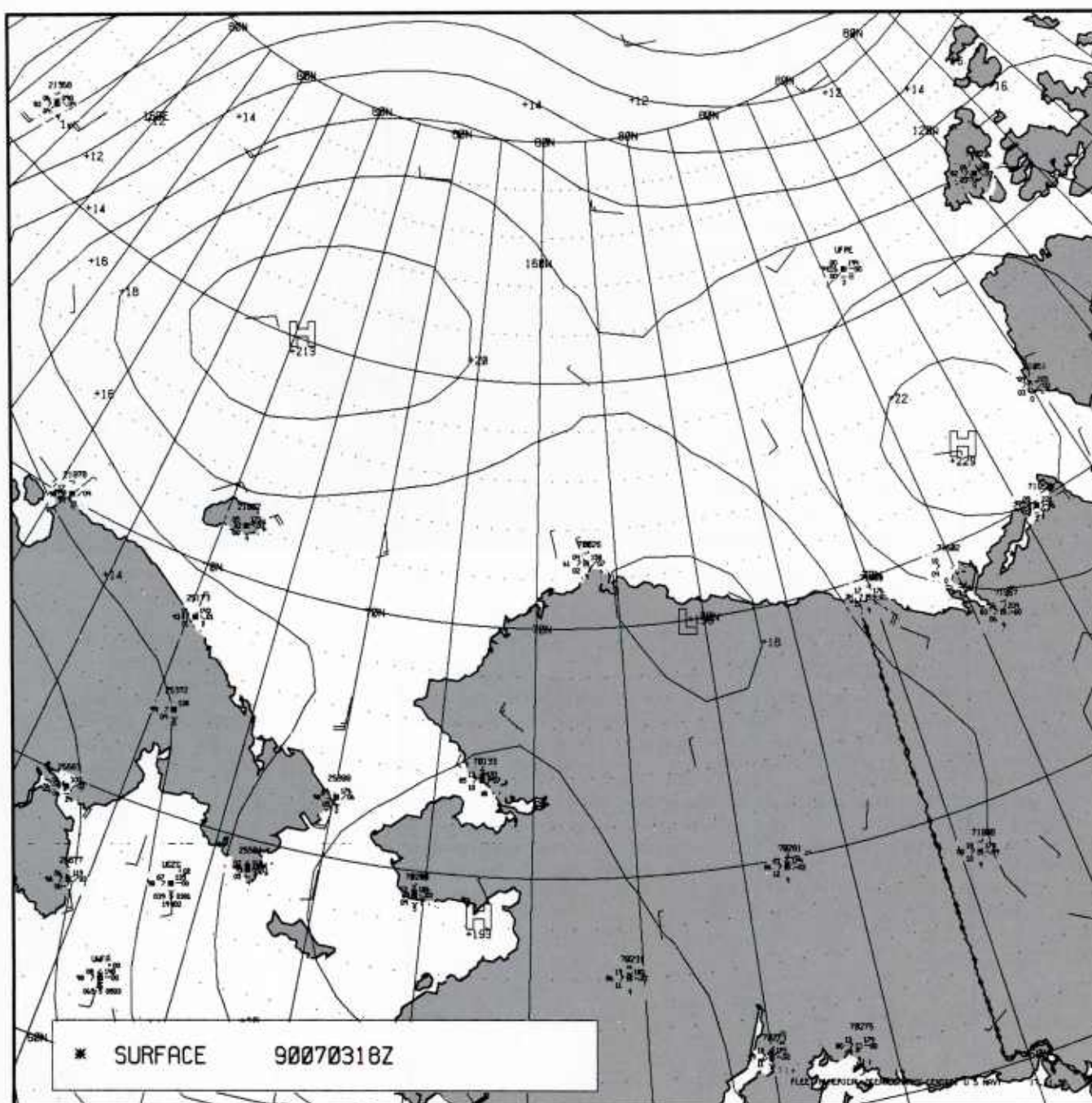




3E-6a Map showing region near Barrow, Alaska.



3E-6b DMSP visible (LF) image. 1931 GMT 3 July 1990.



3E-7a FNOC surface analysis. 1800 GMT 3 July 1990.



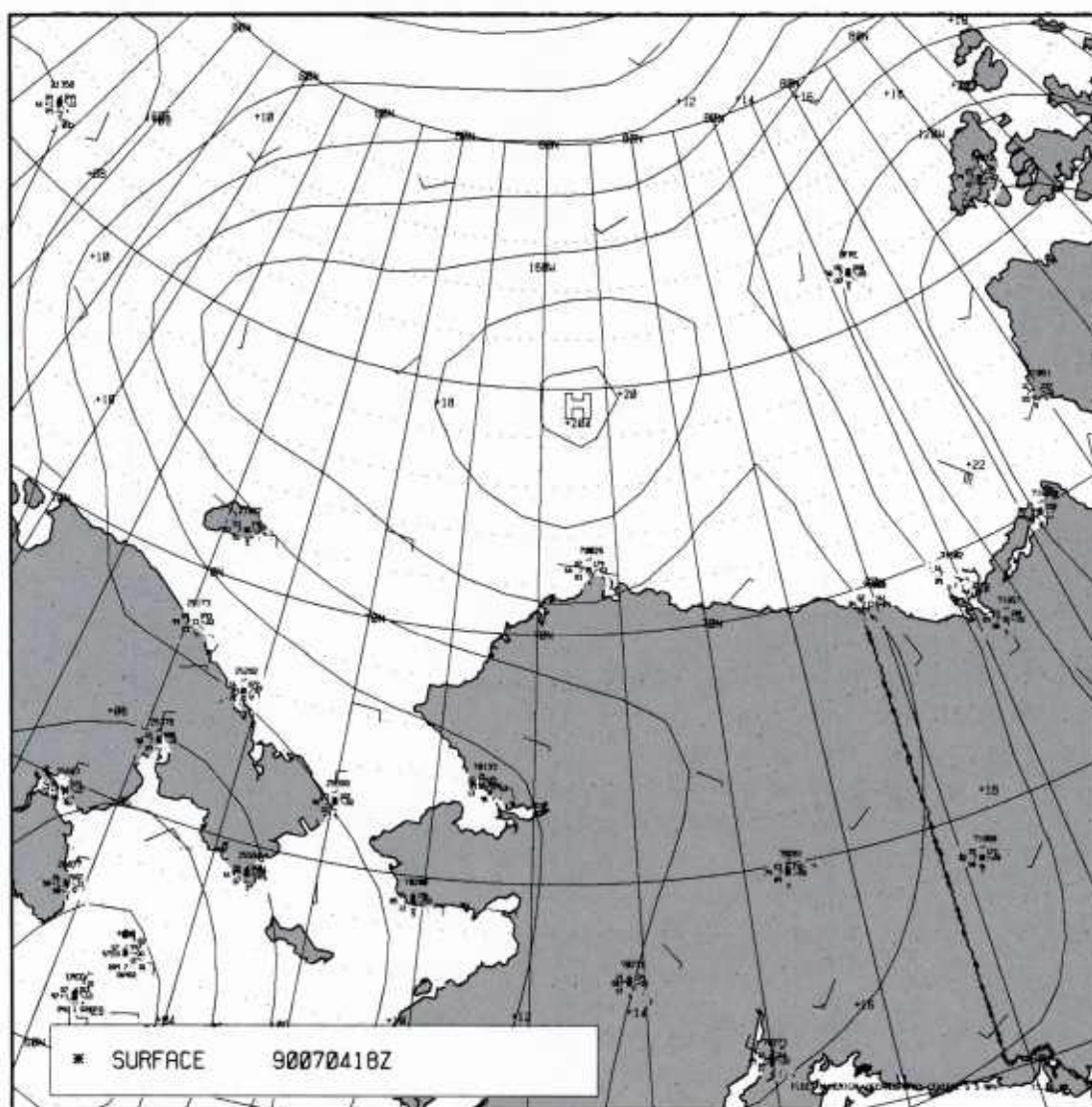
A view of the region on the following day, 4 July at 1910 GMT (Fig. 3E-8a), again reveals a convective cloud cluster over the peninsula apparently induced by sea breeze convergence. The FNOC surface analysis on this date, at 1800 GMT (Fig. 3E-8b), shows ridging extending over the peninsula. The wind at Barrow is light and variable, not inconsistent with a sea breeze condition. The RAOB for Barrow at 1200 GMT (Fig. 3E-9a) shows light onshore northerly winds, suggestive of a sea breeze effect, under a very pronounced and shallow low-level inversion. The sounding implies that the sea breeze circulation was contained within the lower 500 m of the atmosphere. Convergence adequate to break through the inversion in a moist adiabatic ascent would release considerable potential energy. In this respect it is of interest that Barrow reported rain showers on its 0000 GMT 5 July observation with cumulonimbus in the area.

At 1555 GMT 5 July, DMSP visible (LF) data (Fig. 3E-10a) again revealed a convective cloud cluster over the peninsula implying a sea breeze effect. The image is additionally interesting in that sunglint to the east over the Beaufort Sea has etched the outlines of broken floes of pack ice and some of the islands in and near Mackenzie Bay. The Mackenzie River Delta also is outlined because of sunglint off of its flooded surface. The FNOC surface analysis for 1800 GMT (Fig. 3E-10b) reveals northeasterly flow at Barrow with a minor trough over the area.

A final DMSP visible (LF) view at 1828 GMT 6 July (Fig. 3E-11a) is shown to reveal the remarkable persistence of convective activity over the peninsula south of Barrow resulting from the sea breeze circulation. A cloud shadow from the northernmost cell near Barrow falls to the west, over the ice, indicating the vertical extent of the convective activity. To the east the broken floes of ice west of Banks Island are now revealed in their normal appearance, unaffected by sunglint. The approaching intense cold front from the northwest signals the end of the sea breeze regime as stronger pressure gradients become established to move into the area. The FNOC 1800 GMT surface analysis for 6 July (Fig. 3E-11b) reveals the situation with light northwesterly winds reported at Barrow.



3E-8a DMSP visible (LF) image. 1910 GMT 4 July 1990.



3E-8b FNOC surface analysis. 1800 GMT 4 July 1990.

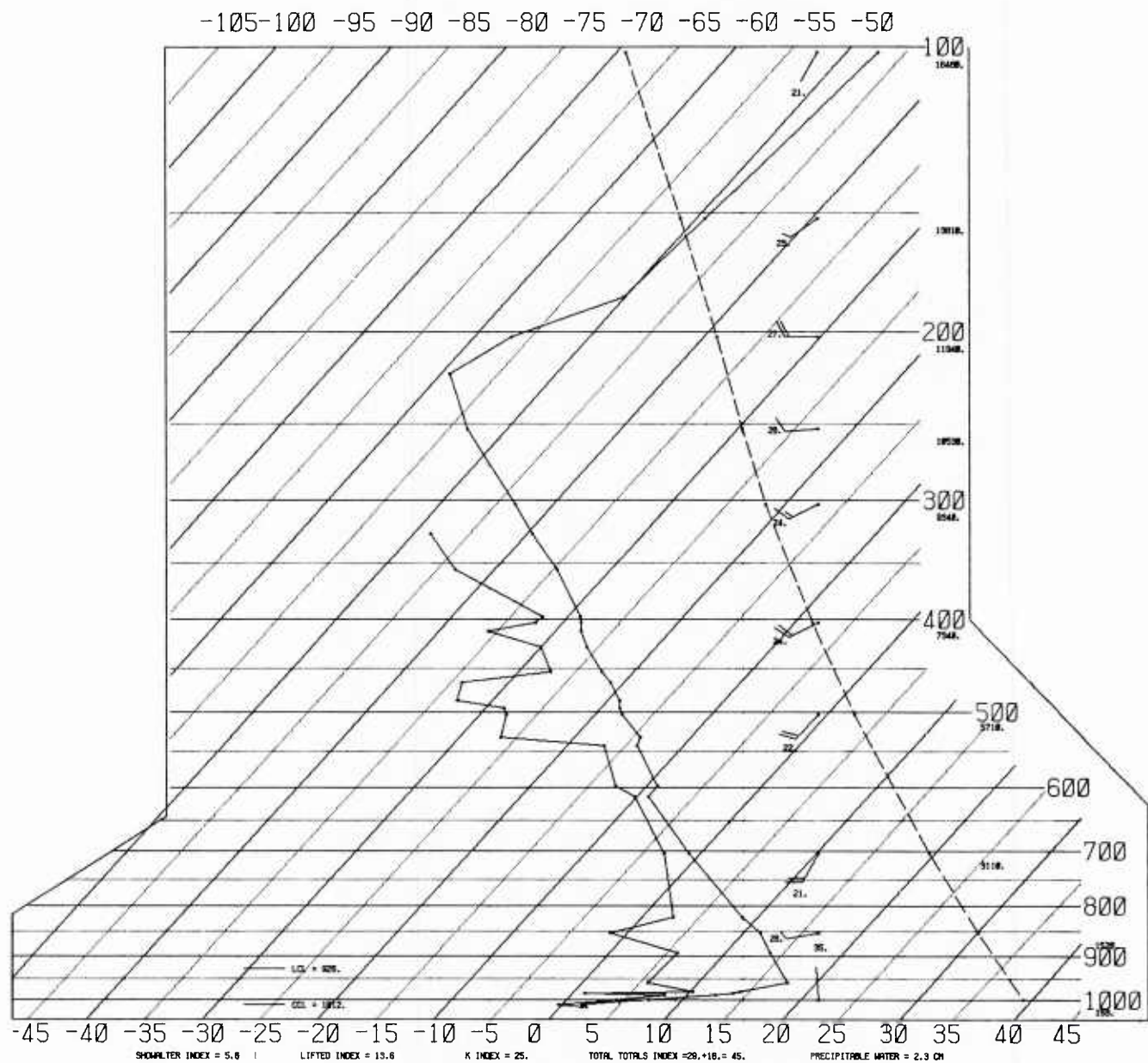


# SKEW T, LOG P DIAGRAM

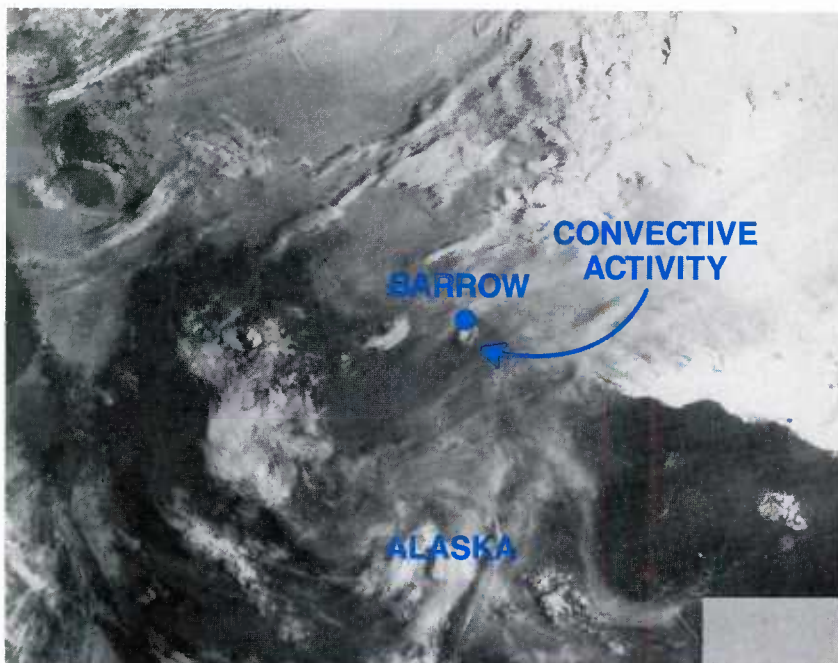
900704

1200Z

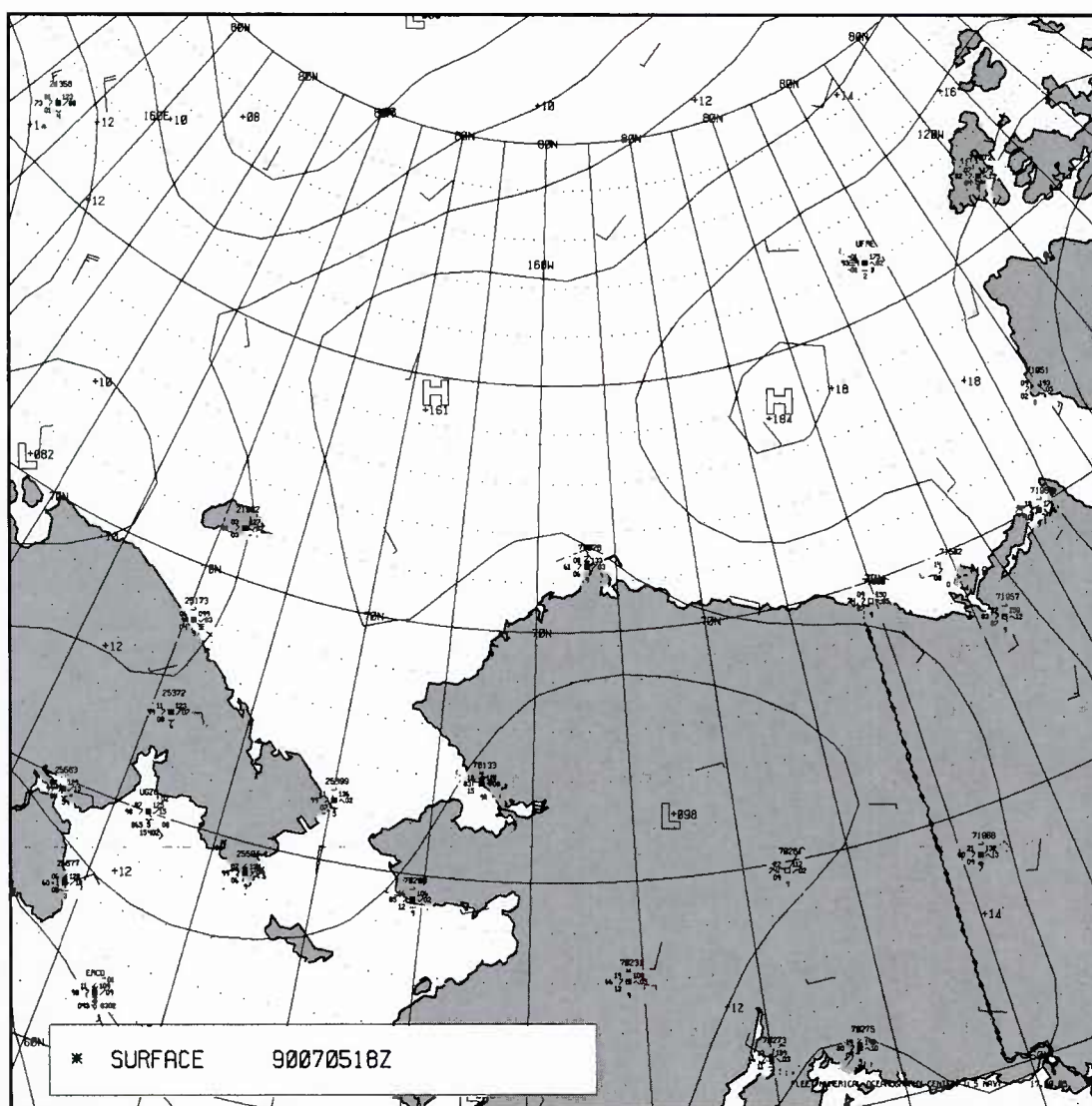
70026



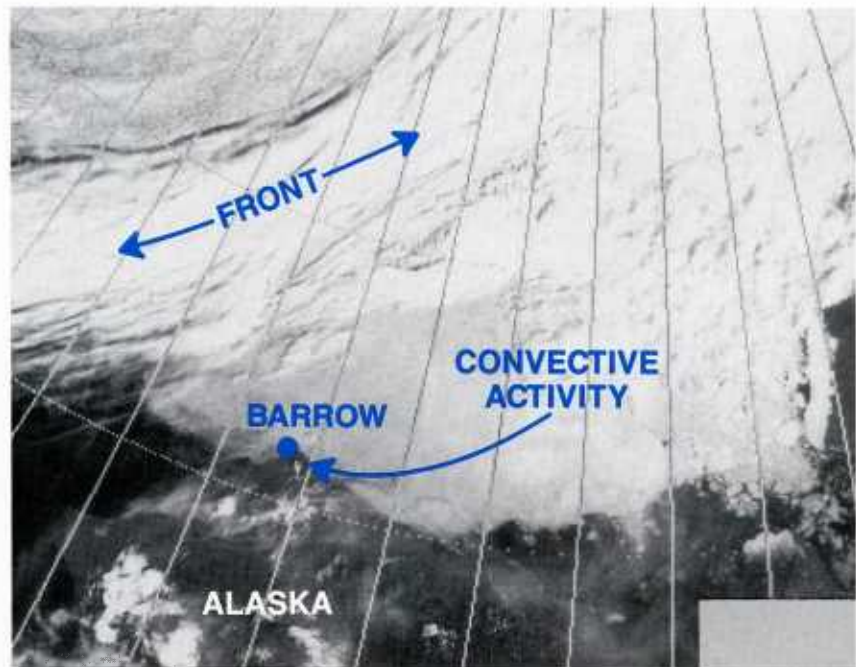
3E-9a RAOB for Barrow, Alaska. 1200 GMT 4 July 1990.



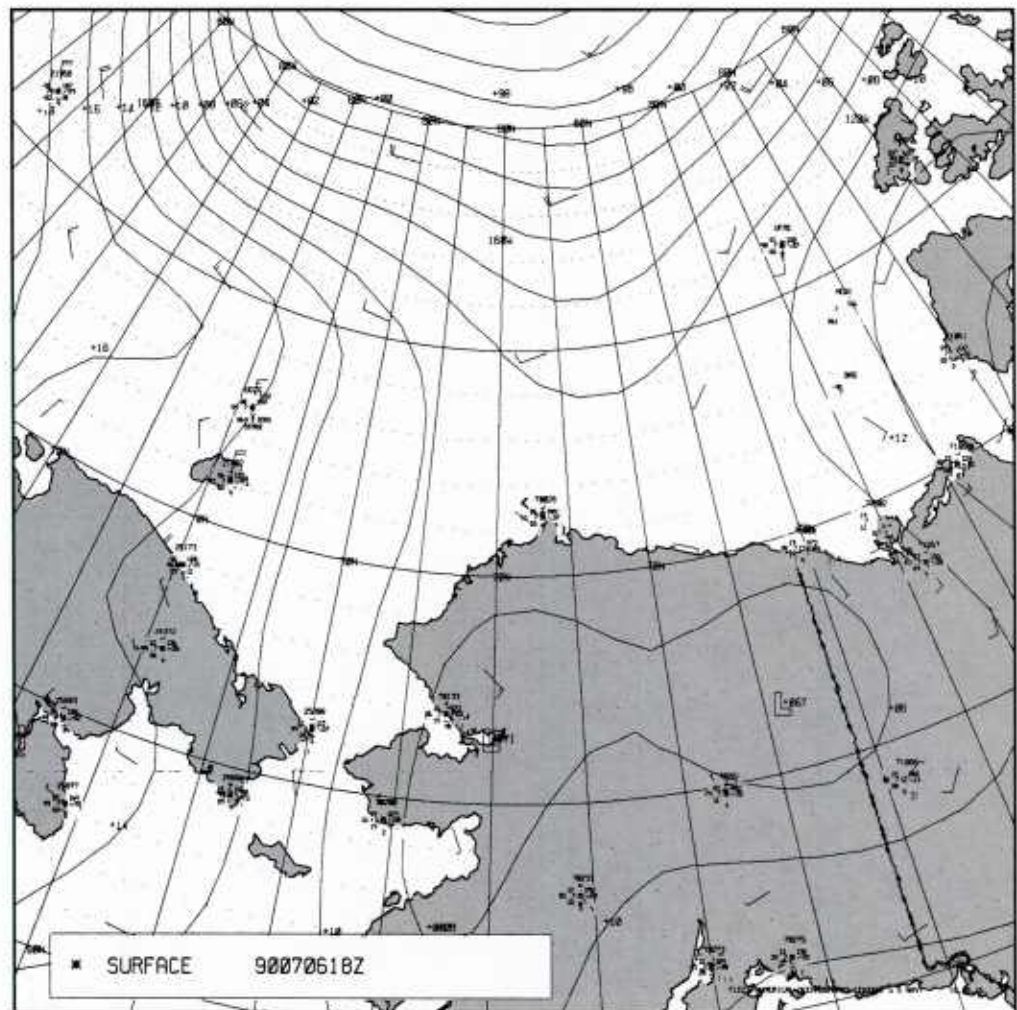
3E-10a DMSP visible (LF) image. 1555 GMT 5 July 1990.







3E-11a DMSP visible (LF) image. 1828 GMT 6 July 1990.



3E-11b FNO surface analysis. 1800 GMT 6 July 1990.

### Important Conclusions

1. The sea breeze along the Alaskan Beaufort Seacoast is not followed by an evening land breeze because the land-sea temperature difference is always positive.
2. The tendency for low level, surface-based inversions over water in the Arctic summer limits the vertical extent of sea breeze cells and weakens fronts.
3. The increased frequency of northeasterly and easterly surface winds on the Alaskan Beaufort Seacoast during the summer months is due to the sea breeze.
4. Bays and peninsulas modulate sea breeze effects tending to promote vigorous convective activity over peninsulas and reducing convection inland from bays.
5. The peninsula surrounding Barrow, Alaska, is notable for sustained sea breeze convection during summer in the absence of pronounced pressure gradients over the area.

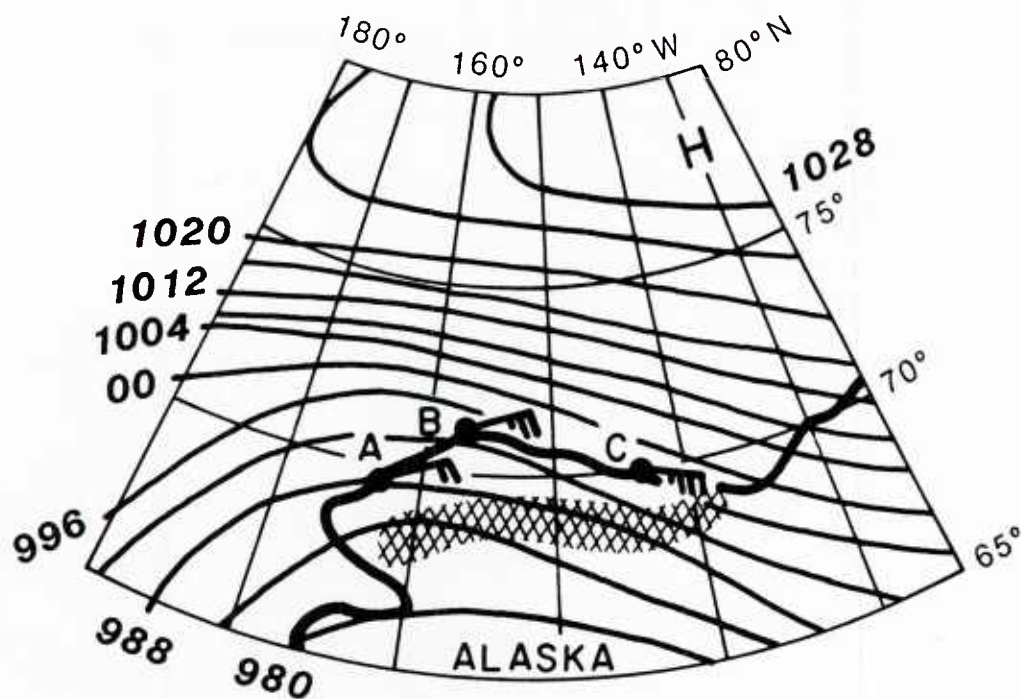
### References

- Fett, R.W., P.E. La Violette, M. Nestor, J. Nickerson, and K. Rabe, 1979: Navy Tactical Applications Guide, Vol. 2, *Environmental Phenomena and Effects*. NEPRF TR 77-04, Naval Environmental Prediction Research Facility, Monterey, CA, 93943-5006, 161 pp.
- Kozo, T.L. 1982: An observational study of sea breezes along the Alaska Beaufort Sea Coast: Part I. *J. App. Meteor.*, 12, 891-905.
- Moritz, R.E., 1977: On a possible sea breeze circulation near Barrow, Alaska. *Arctic Alp. Res.*, 9, 427-431.



### Case 2 *Land Breezes Along the Alaskan Beaufort Seacoast*

Although the summer sea breeze does not have an associated land breeze, a late autumn land breeze (without a sea breeze) was recorded in this region (Kozo, 1984). The initiating event was a November gale class wind system (Fig. 3E-13a).



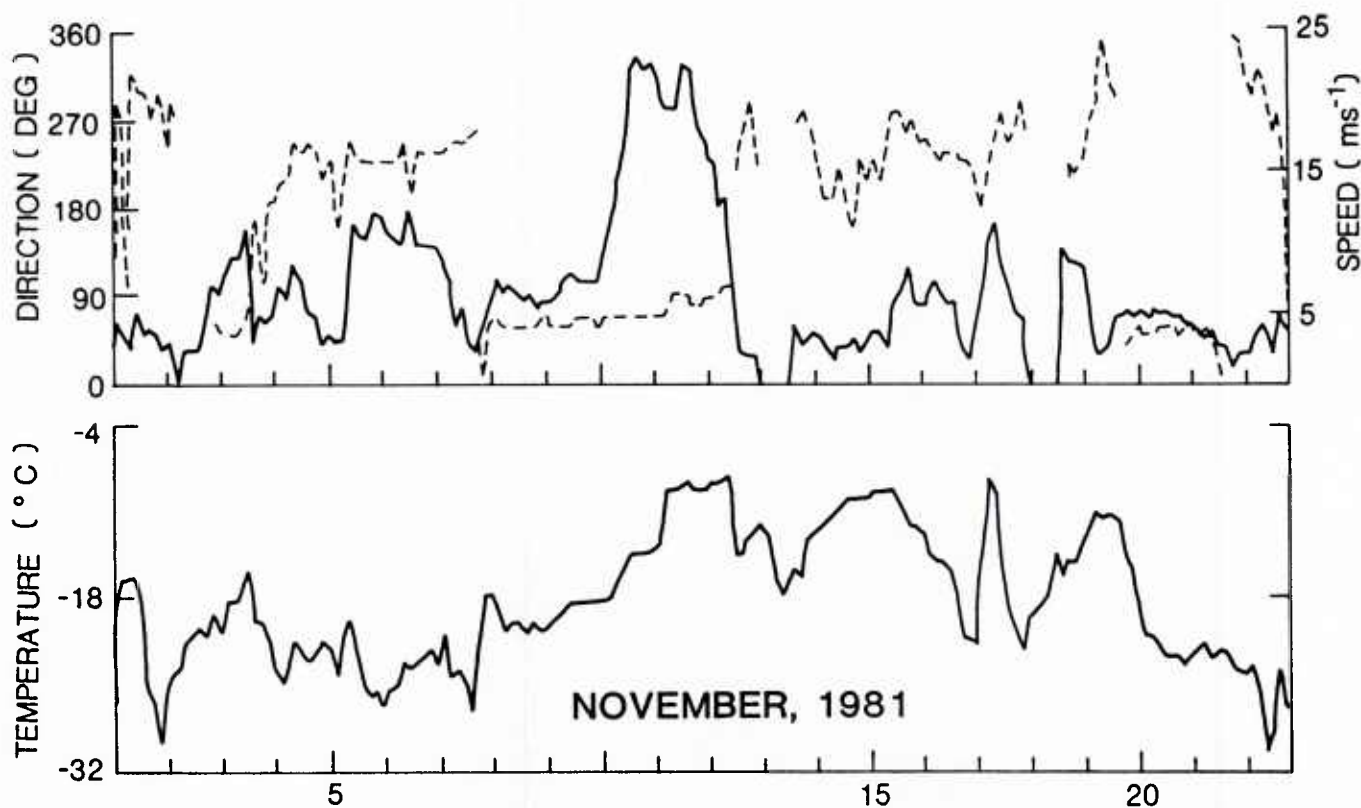
3E-13a Section of a NWS synoptic chart for 12 November 1981 (0000 GMT). The Brooks Range is crosshatched. The wind speeds at A (Point Lay), B (Barrow), and C (Barter Island) are  $10 \text{ ms}^{-1}$ ,  $12.5 \text{ ms}^{-1}$ , and  $17.5 \text{ ms}^{-1}$ , respectively (from Kozo, 1984).

Strong easterly surface winds lasting 3 days were recorded at Deadhorse, Alaska (Fig. 3E-13a). The sea ice canopy was fractured north of the fast ice zone in the Beaufort Sea, opening a 32 n mi (60 km) wide lead parallel to the coast (Fig. 3E-14a). After the ice fracture event, weak surface winds existed for several days (Fig. 3E-14b), during which the total daylight dropped to 1 hr (70°N in mid-November). The large lead represented a source of moisture and heat 20 °C above typical ambient air temperatures (see Fig. 3E-14a, bottom graph). Solar radiation was a negligible factor in supplying heat to the Earth's surface at this time of year.

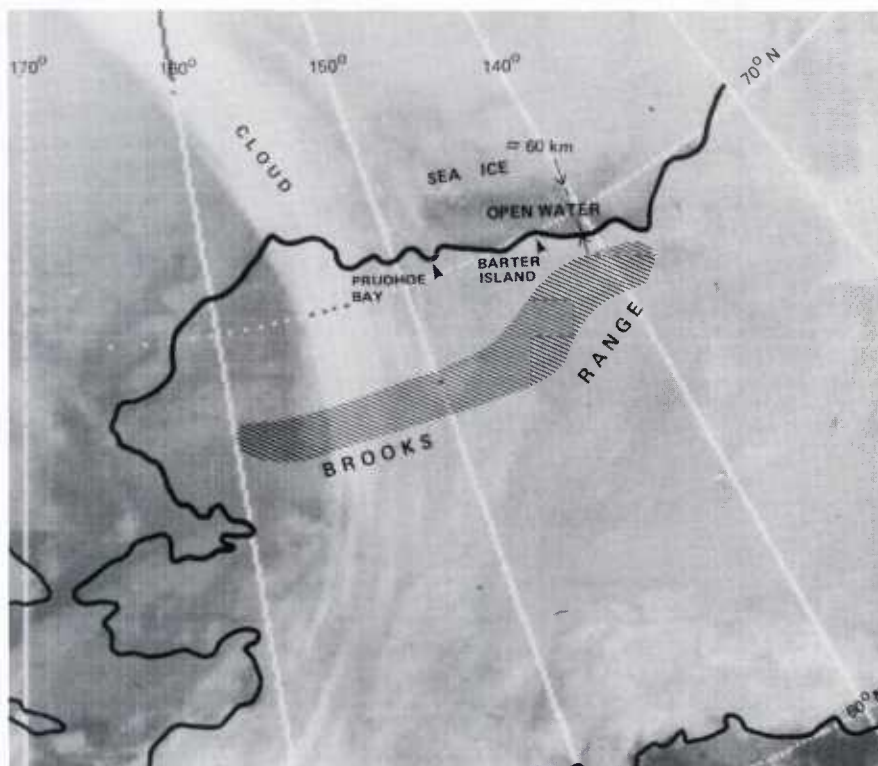
After moving from the area, the initiating synoptic scale weather system created an unstable boundary layer, in which the visibility was greatly reduced due to steam fog. This system also produced a mesoscale land breeze circulation (offshore winds, see Fig. 3E-15a) by inducing a horizontal temperature gradient between the land and the open lead. The thermal contrast between the snow-covered land, sea ice, and the open-water lead led to southwesterly surface winds on 13–14 November. This subsynoptic event was not included in the National Weather Service (NWS) forecasts for the area. During this period the visibility was very poor and icing conditions were prevalent. An inshore self-contained weather station had sufficient ice accumulation to stop its anemometer cups from rotating (Fig. 3E-15b). Air temperatures and wind directions returned to seasonal values in one week (by 20 November, Fig. 3E-14a – bottom) as the large lead froze and visibility conditions improved.

Kozo (1988) has also shown that “false” summer land breezes can occur in mountainous Arctic coastal regions with river valleys perpendicular to the coast. The Norton Sound region of Alaska (Fig. 3E-16a) fits this description, but the Alaskan Beaufort region does not. The towns of Nome and Unalakleet are subject to mountain and valley wind systems that exhibit cold air drainage in the evenings. These drainage winds, on reaching the coast and moving offshore, can be mistaken for land breezes. Fett et al. (1979) also have observed that normal land breezes are intensified by downslope winds in coastal regions.

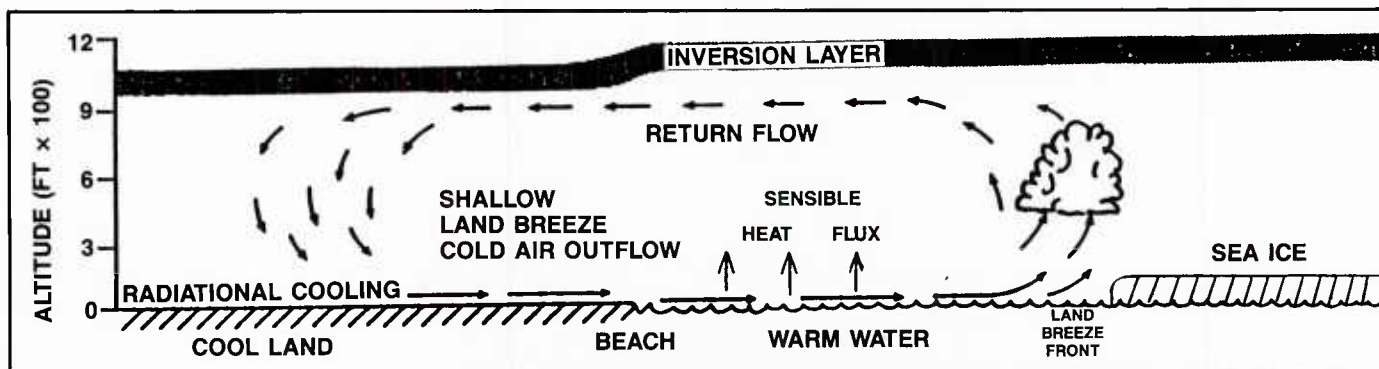




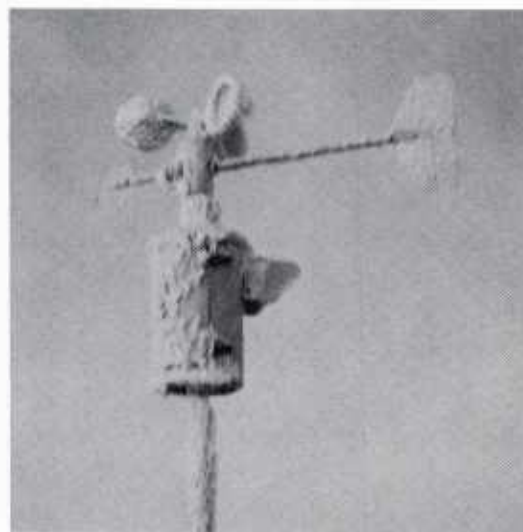
3E-14a Wind speed (solid) and direction (dashed) and air temperature at Deadhorse, Alaska, for 1–22 November 1981 (from Kozo, 1984).



3E-14b Satellite infrared image of Alaska on 17 November 1981. The ice in the Beaufort Sea was fractured by gale-force winds (Fig. 3E-13a) producing a 60 km wide lead north of the coast. Dark tones north of the coast represent warmer areas (from Kozo, 1984).

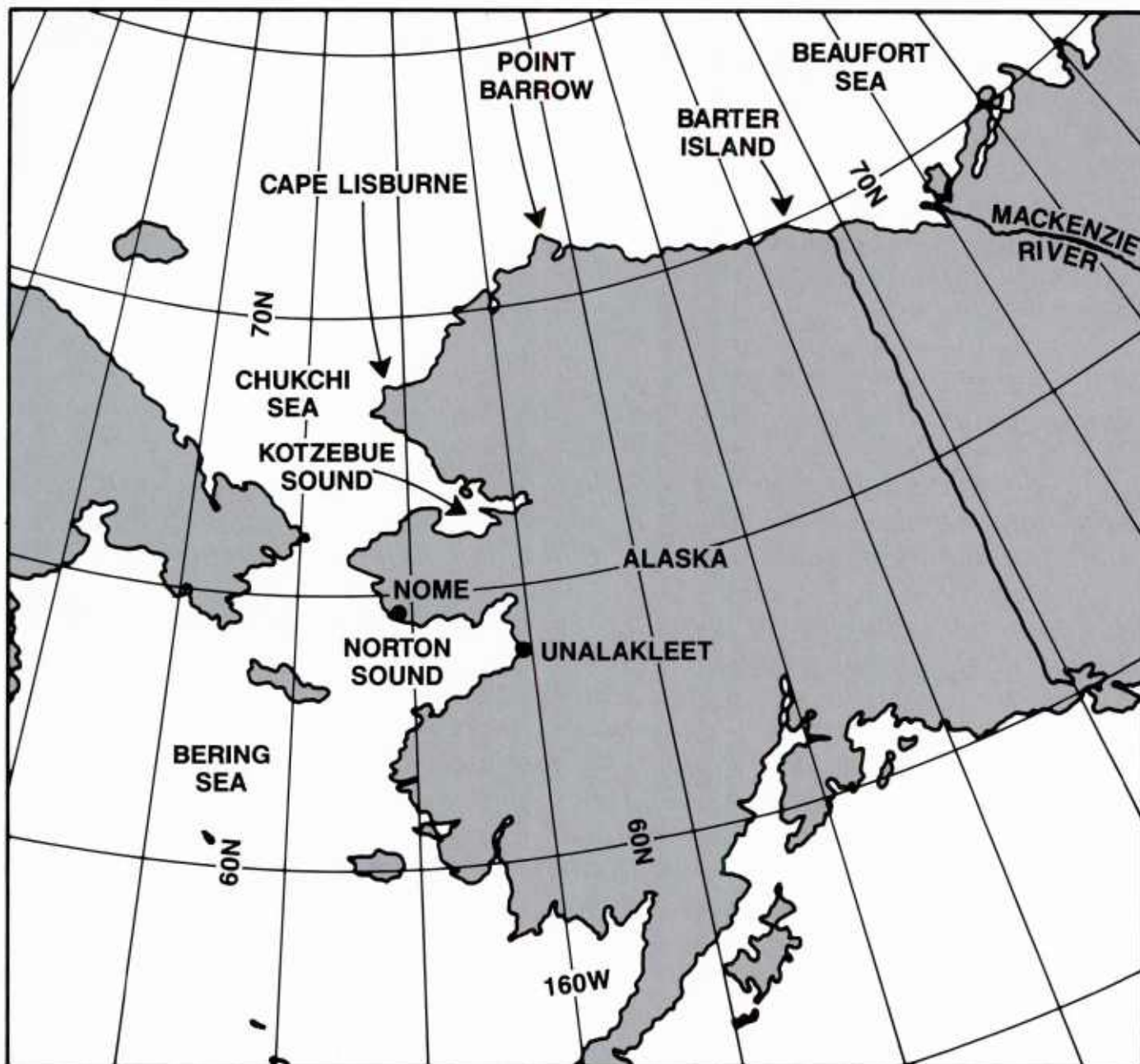


3E-15a Major features of the Arctic land breeze circulation cell including the capping inversion (from Fett et al., 1979).



3E-15b Inshore automated weather station with sufficient ice accumulation to stop its anemometer cups from rotating.





3E-16a Locator map showing Norton Sound, Nome, and Unalakleet.

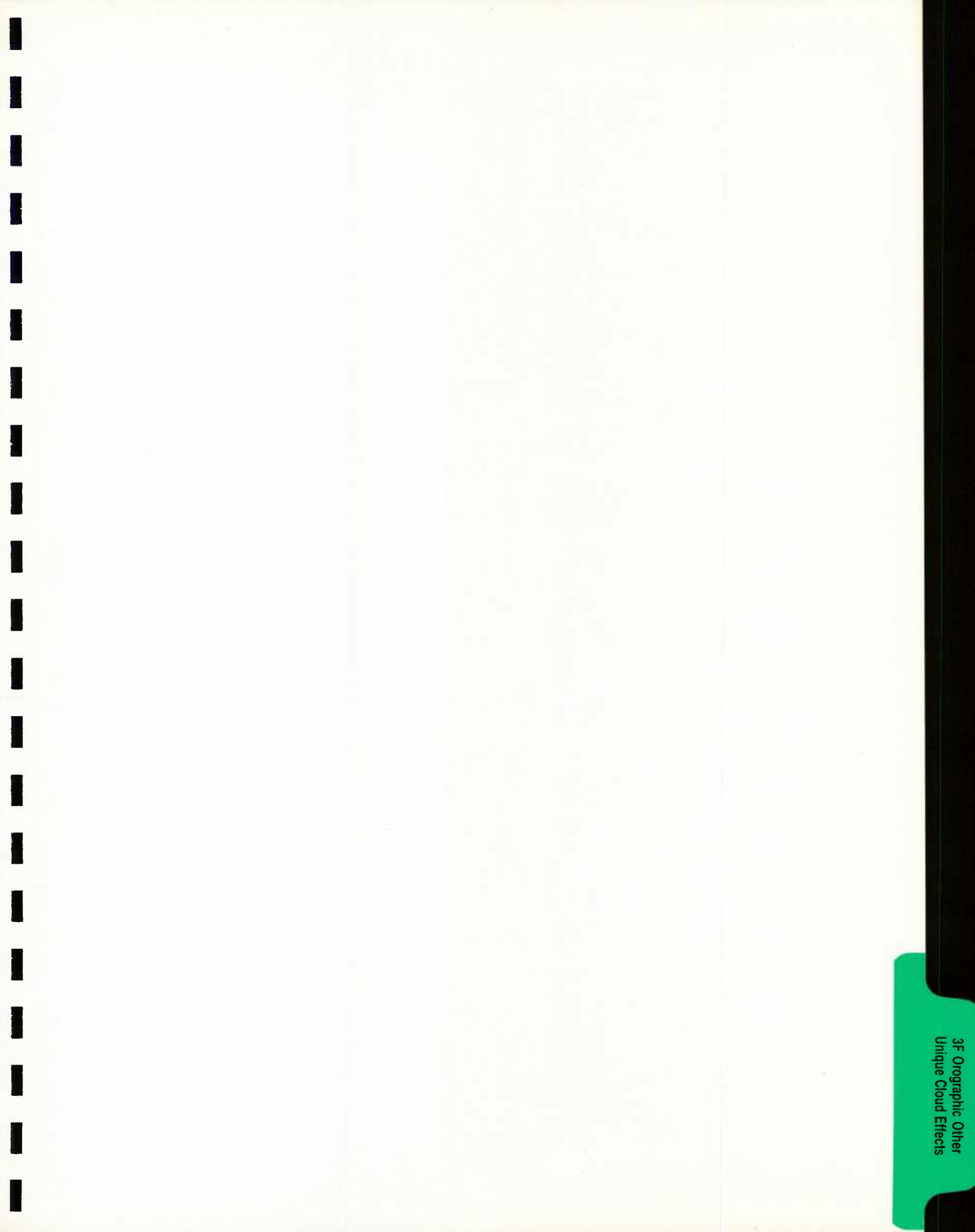
### Important Conclusions

1. Land breezes do not occur along the Alaskan Beaufort Seacoast during the summer.
2. They can occur in seasons when the land temperature falls below freezing and sudden fractures occur in the nearshore sea ice canopy.
3. Mountainous Arctic coastlines can have evening drainage winds that can be mistaken for land breezes as they move offshore.

### References

- Kozo, T.L., 1984: Mesoscale wind phenomena along the Alaska Beaufort Seacoast. *In the Alaska Beaufort Sea: Ecosystems and Environment*, P.W. Barnes, D.M. Schell, and E. Reimnitz (Eds.), Academic Press, Orlando, FL, 23-45 pp.
- Kozo, T.L., 1988: Mesoscale meteorology of the Norton Sound region. *Proc. of Ninth Int. Conf. on Port and Ocean Engineering under Arctic Conditions*, University of Alaska, Fairbanks, AL, Vol. 3, 163-181.
- Fett, R.W., P.E. LaViolette, M. Nestor, J.W. Nickerson, and K. Rabe, 1979: Naval Tactical Applications Guide, Vol. 2, *Environmental Phenomena and Effects*. NEPRF TR 80-07, Naval Environmental Prediction Research Facility, Monterey, CA, 93943-5006, 200 pp.





### *3F Orographic Cloud Formations and Other Unique Cloud Effects*

A perusal of satellite data over the Arctic will quickly reveal a number of unusual cloud formations and other special cloud effects. Many of the cloud formations can be seen only through use of special enhancement techniques. As an example, low clouds, difficult to discern over ice in the usual visible and infrared data, are often sharply delineated in the NOAA AVHRR channel 3 data. Cloud plumes emanating from leads and polynyï have already been described (Section 3A). Gravity wave clouds, well-known under inversion conditions in midlatitudes, are also abundantly found in the Arctic over mountainous terrain.

More recently the existence of cloud plumes emanating from selected islands have attracted attention since an article appeared suggesting possible volcanic origin with respect to plume development near Bennett Island (Ostrov Bennetta) in the East Siberian Sea (Kienle et al., 1983). Another article followed in 1986, regarding a plume emanating from the vicinity of Novaya Zemlya, an island which separates the Kara Sea from the Barents Sea, also suggesting a geomorphic or anthropomorphic origin for the plume (Matson, 1986). This suggestion gains additional credibility since Novaya Zemlya has been used by the Russians for some time as an atomic bomb testing range. Parmenter-Holt (1987), however, argued rather convincingly that the latter plume was not geomorphic or anthropogenic but, rather, a naturally occurring, orographically induced event, which signaled cloud formation as a result of lee mountain wave activity.



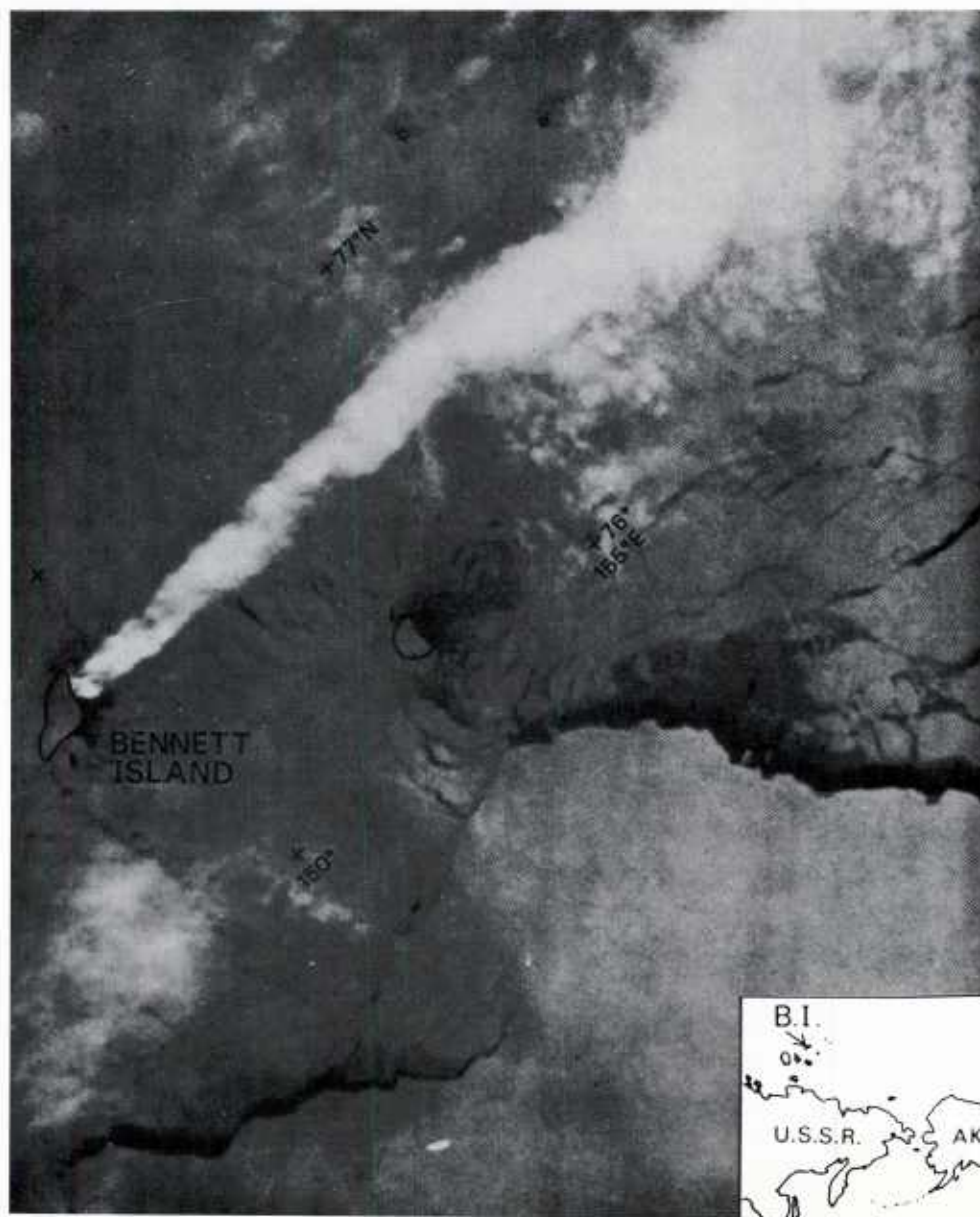
Research in developing this publication (without disallowing the potential for an atomic bomb explosion to produce a plume) substantiates Parmenter-Holt's conclusion as generally valid for both of the preceding examples and distinguishes differences between orographic plumes and lower level polynya-produced plumes, also often noted during the cold months over the Arctic region. It is further suggested that the orographic plumes are often excellent indicators of Arctic frontal location and associated jetstream activity. This section will attempt to document the variety of Arctic cloud events and illustrate their use in the analysis and forecast process.

#### References

- Fett, R.W., 1990: Navy Tactical Applications Guide, Vol. 8, Part 1, *Arctic: Greenland/Norwegian/Barents Seas Weather Analysis and Forecast Applications*. NEPRF TR 80-07, Naval Environmental Prediction Research Facility, Monterey, CA, 93943-5006, 200 pp.
- Kienle, J., J.G. Roederer, and G.E. Shaw, 1983: Volcanic event in the Arctic? *EOS Trans. AGU*, 64, 377.
- Matson, M., 1986: Large plume events in the Soviet Arctic, *EOS Trans. AGU*, 67, 1372.
- Parmenter-Holt, F., 1987: The large plumes of Novaya Zemlya, *EOS Trans., AGU*, 68, 1129/1142.

*Case 1 Use of Orographic Cloud Plumes in Defining Arctic Frontal Location*

Figure 3F-3a is a NOAA-6 infrared view of an area near the New Siberian Islands at 0615 GMT on 18 February 1983. The image shows the plume referred to in the introduction that attracted so much early attention. The plume is colder than the surrounding environment and radiating at a temperature of about  $-45^{\circ}\text{C}$ . Zhokhova is the small island outlined in the figure to the east-southeast of Bennett.



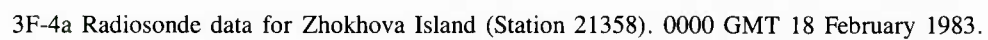
3F-3a NOAA-6 infrared imagery. 0615 GMT 18 February 1983.



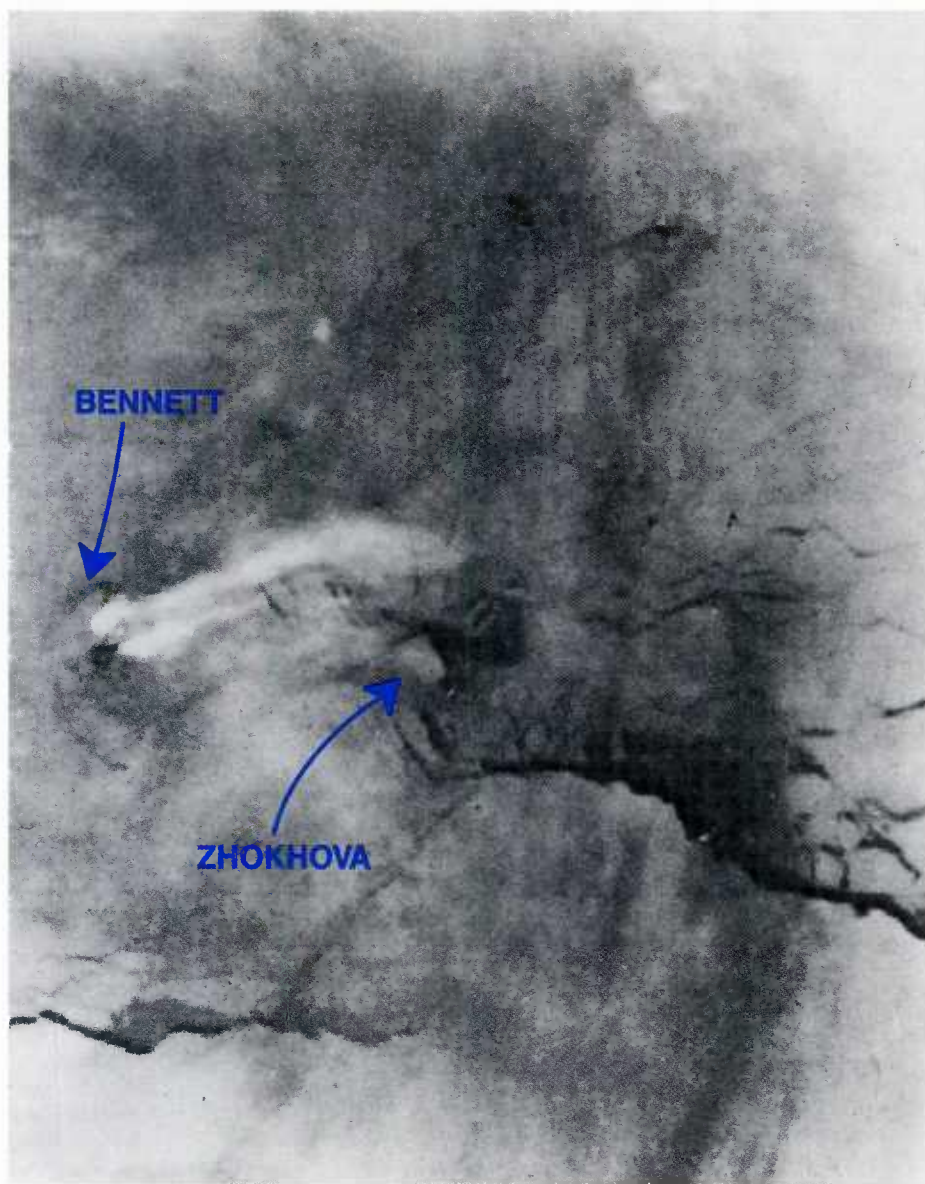
The 0000 GMT sounding for Zhokhova on 18 February is shown in Fig. 3F-4a. Using the above temperature assessment the sounding implies that the plume top was located below the tropopause near the 450 mb level. From Fig. 3F-3a it appears that the plume has its source over the polynya, apparent as a warm region on the east side of Bennett Island, however, this theory is ruled out for two reasons: (1) the low-level inversion shown on the Zhokhova sounding would have been a strong influence tending to prevent the cloud from extending to altitudes above the lowest levels; and (2) data from NOAA-7 at 0047 GMT (Fig. 3F-5a) reveal that the northernmost plume extended inland, over the island, at that time. A second plume appeared slightly southeast of the first plume. It is unfortunate that the outline of Bennett Island was rather crudely drawn on the original image used in the 1983 article (Fig. 3F-3a). A more exact outline of the island, showing topographical features is shown in Fig. 3F-6a. This outline is superimposed over the NOAA-7 image and shown in Fig. 3F-7a. It reveals that the first plume had developed somewhat downstream but in the lee of a 1,398 ft (425 m) mountain; the second southernmost plume also developed in the lee of higher terrain (exact height not specified) near the southeast tip of the island. Thus, it is likely that both plumes are effects of vertically propagating mountain waves of the type commonly seen in the lee of mountainous terrain over other islands in the Arctic and other regions of the world. The turbulent appearance of the particular plume in this example is different from the more stratified and striated appearance of many plumes more commonly seen. The difference may be attributed to the fact that this particular plume was generated as the result of airflow over an isolated mountain peak, rather than the more commonly seen flow over the crest of a lengthy ridge oriented perpendicular to the prevailing flow.

It is important to bear in mind that the apparent plume source region can appear to shift with time, probably depending upon a sudden relaxation, or conversely, intensification, in the strength of the wind flowing over the obstacle. A good example is shown by plume cloud development in the lee of the island of Kvitoya, just east of Svalbard, on 28 March 1987. The image for this example (Fig. 3F-8a) shows the region as observed by NOAA-10 in channel 4 infrared data at 1114 GMT. From this image one might judge that the plume's source is the polynya on the south lee of the island. However, a later NOAA-10 channel 4 view at 1515 GMT (Fig. 3F-9a) shows the main plume formation very near or even slightly over the southern shore of the island. A second thinner plume also emanates from the shoreline near the southeast tip of the island. Figure 3F-10a is a map of the island showing that a ridge line exists between two peaks aligned east-west on the island. The width of the ridge line correlates well with the width of the larger plume. The contours indicate an additional separate peak near the southeast end of the island, which aligns quite well with the thinner cloud plume extending from the shore of the island.

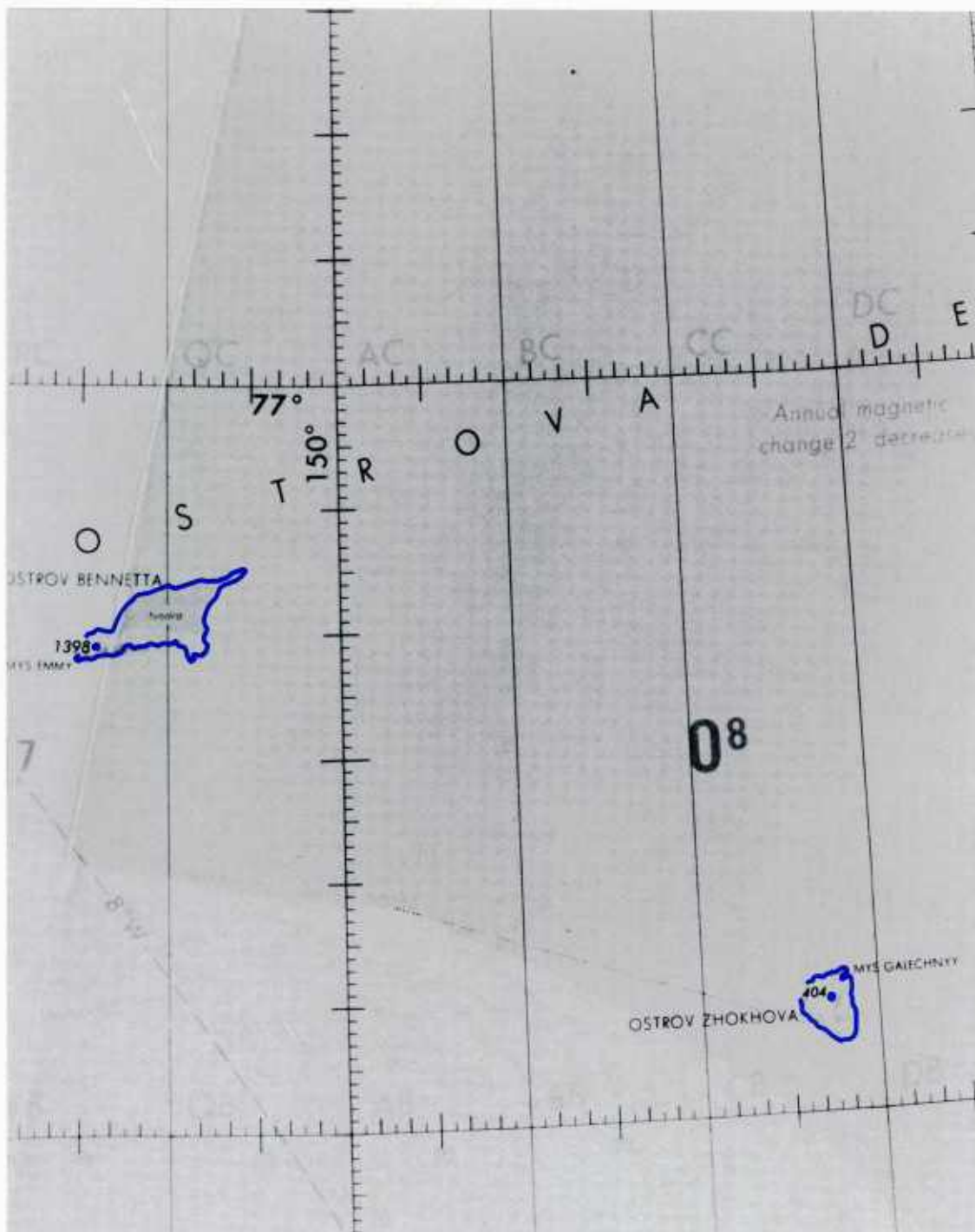
## 21358





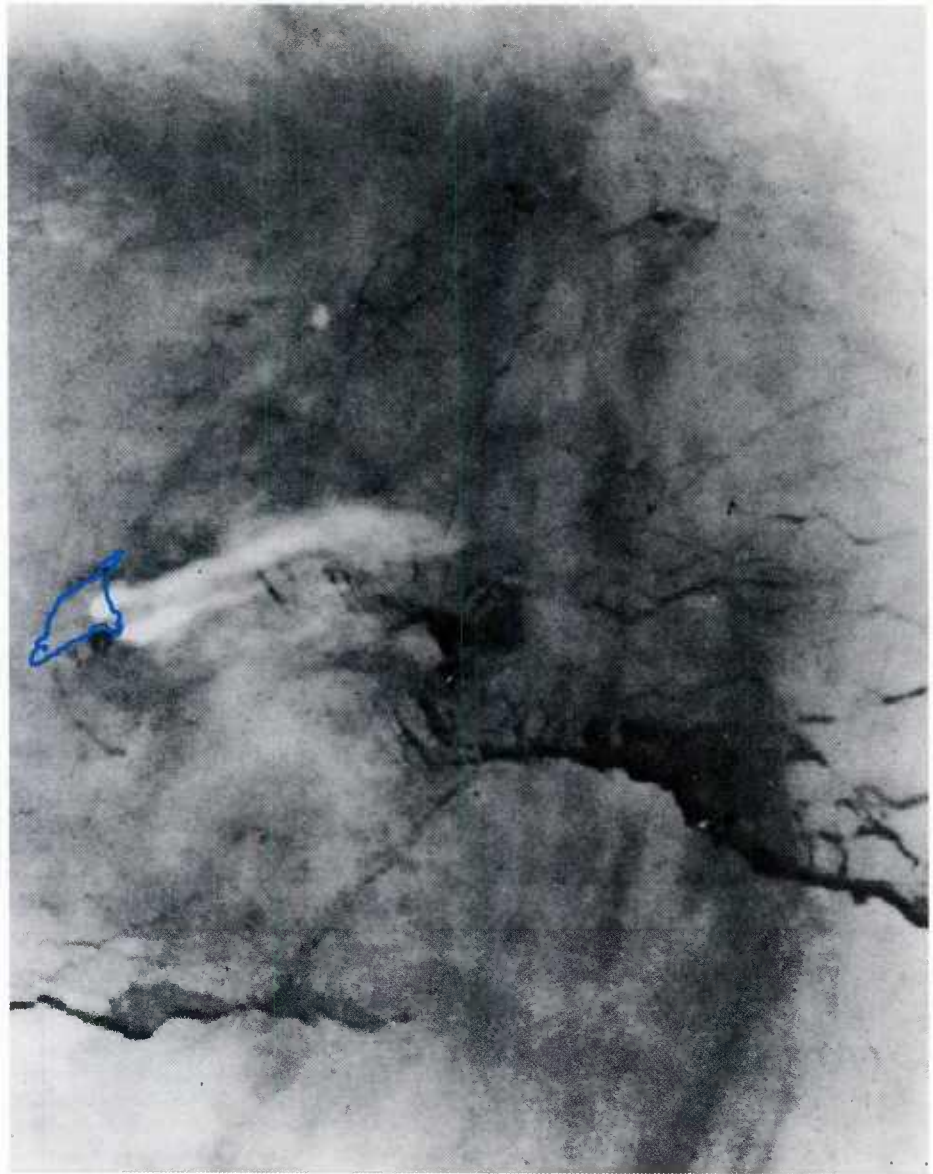


3F-5a NOAA-7 infrared imagery. 0047 GMT 18 February 1983.

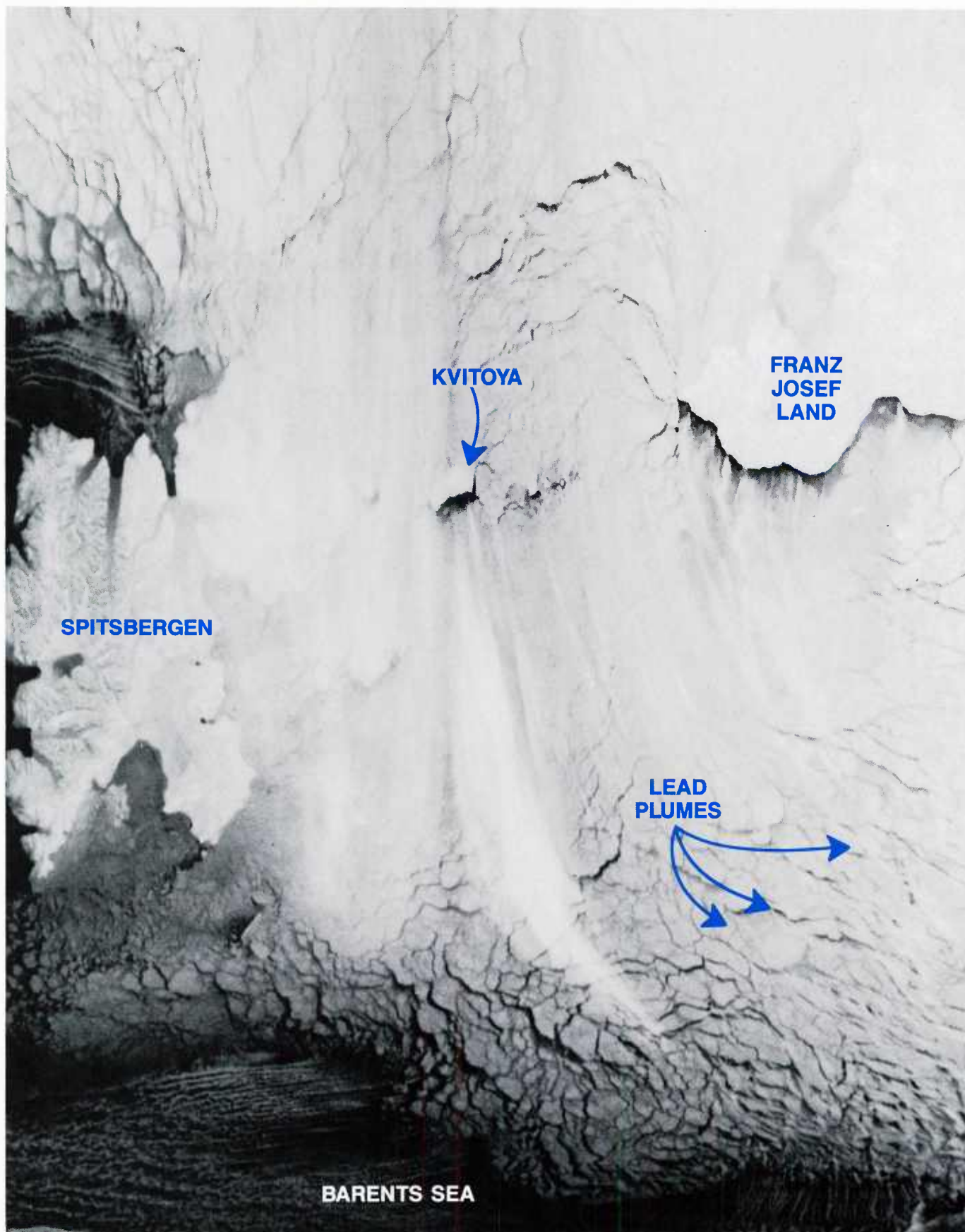


3F-6a Map of Bennett Island.





3F-7a NOAA-7 infrared imagery with outline of Bennett Island superimposed.  
0047 GMT 18 February 1983.

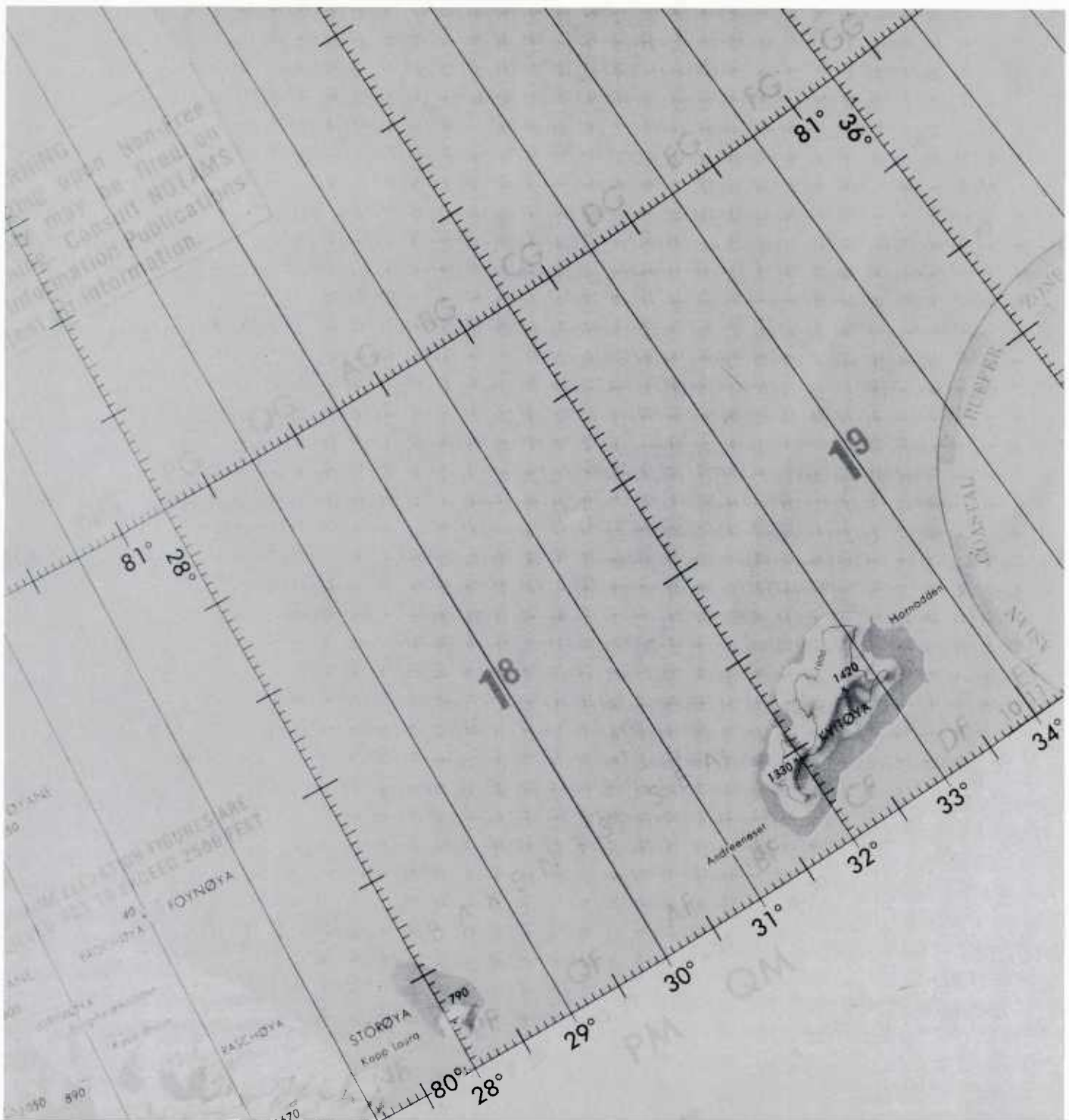


3F-8a NOAA-10 infrared (channel 4) imagery. 1114 GMT 28 March 1987.





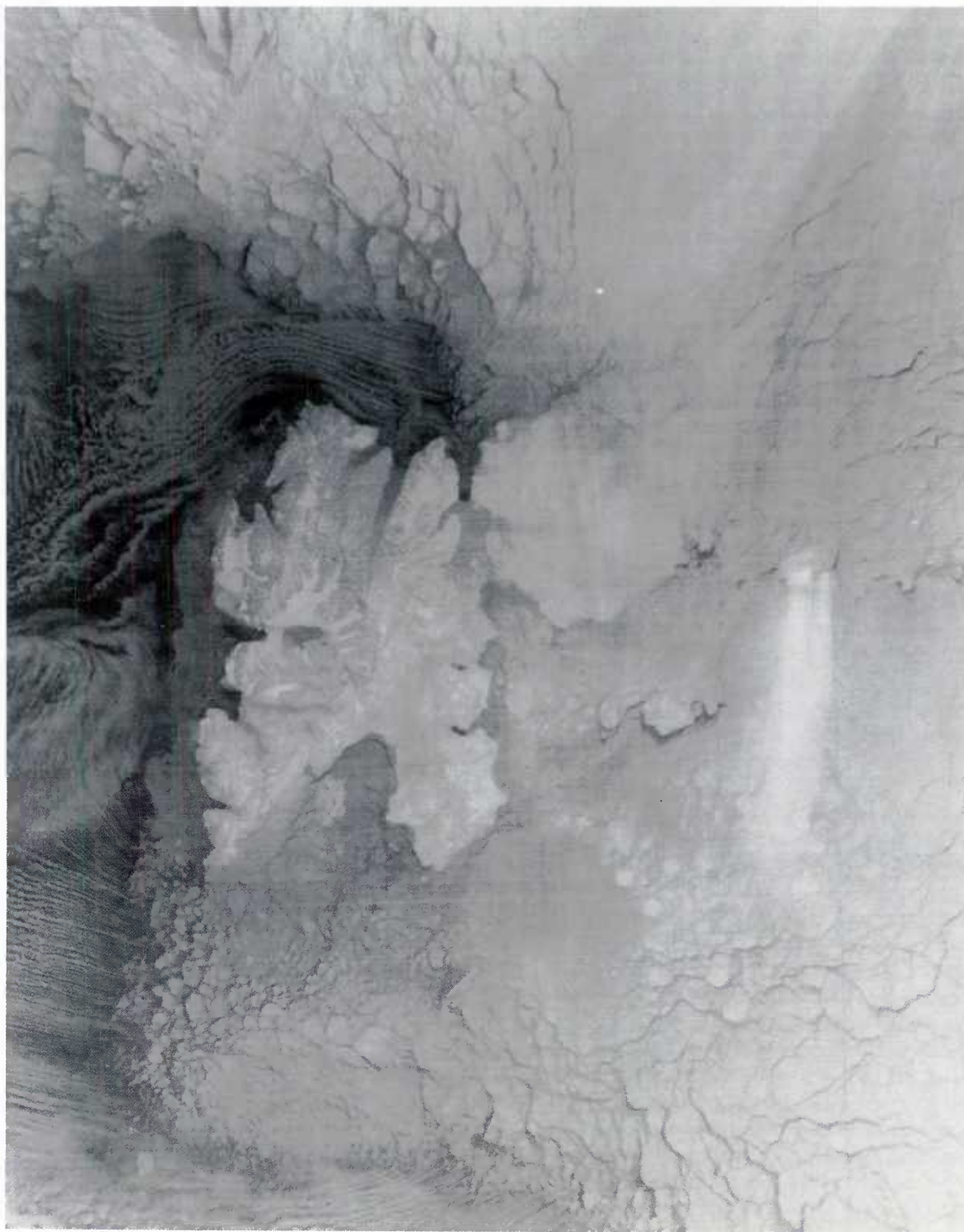
3F-9a NOAA-10 infrared (channel 4) imagery. 1515 GMT 28 March 1987.



3F-10a Map of Kvitoya Island.



Conclusive proof of formation as a result of island topography is provided much earlier in the day by DMSP (2 n mi resolution) infrared imagery (Fig. 3F-11a). These data acquired at 0254 GMT on 28 March 1987 show plume formation clearly over the edge of the island on the lee slope of the ridge line and the smaller southeastern peak. Note that cloud top temperatures are colder at the plume source, immediately adjacent to the higher terrain, an indication of greater wave amplitude and highest cloud top altitude in that region. If the plume were polynya-produced, its lowest altitude would be at the point source of generation, similar to cloud plume formation at the ice edge (Figs. 3F-8a and 3F-11a).



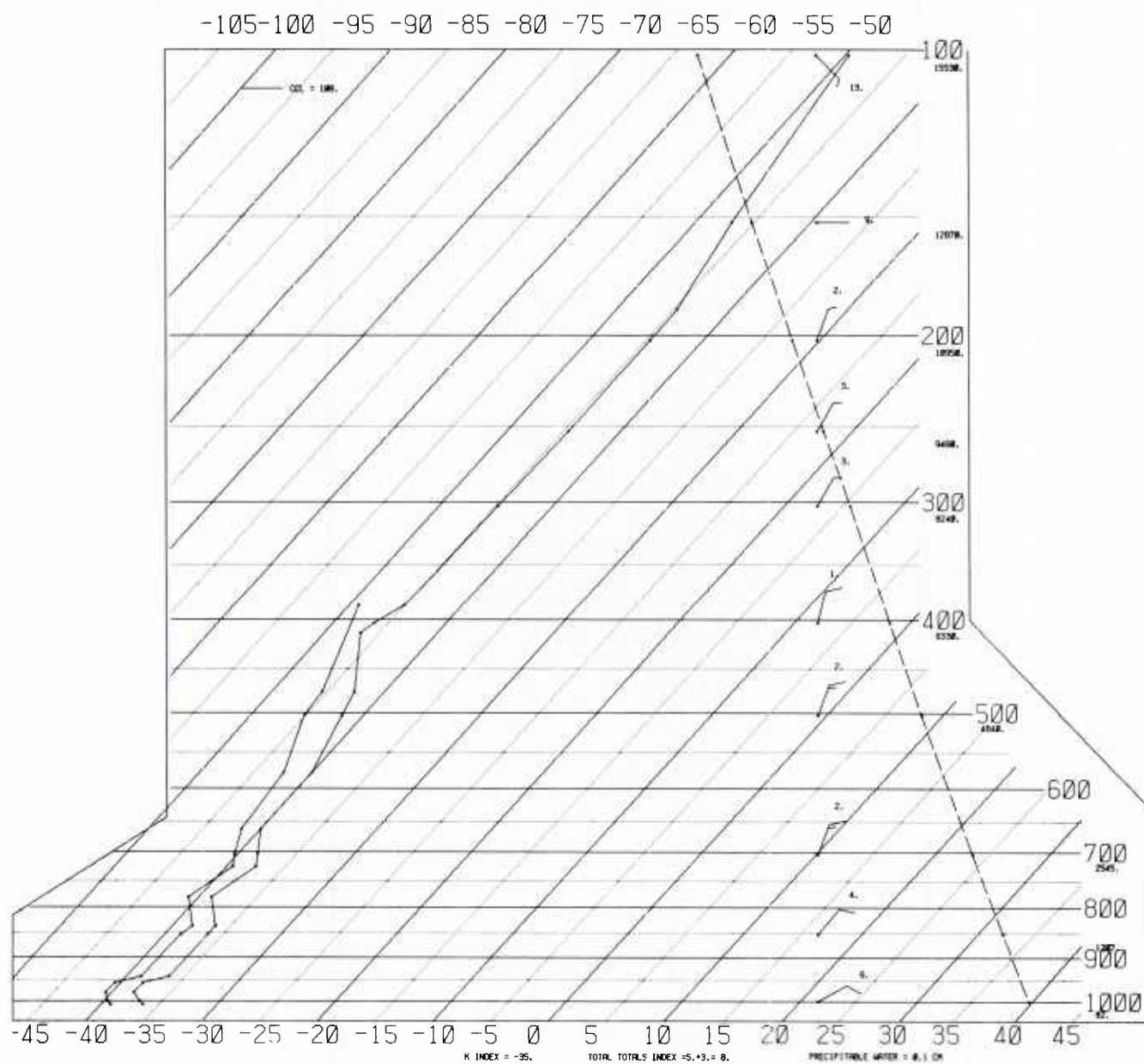
3F-11a DMSP infrared (TS) data. 0254 GMT 28 March 1987.

# SKEW T, LOG P DIAGRAM

870328

0000Z

20046



3F-12a Radiosonde data for Heysa (Station 20046). 0000 GMT 28 March 1987.



### *Polynya Plume Examples*

In the NOAA-10 satellite image of Fig. 3F-8a, some obvious small plumes emanating from lead features in the southeastern portion of the figure can be seen. Polynya and lead plumes in cold Arctic regions generally appear warmer than the surrounding ice covered sea surface over which they lie (see Section 3A), due to normal formation under a pronounced surface based low-level inversion. The lead plumes in Fig. 3F-8a appear colder than the surrounding region. This observation suggests that the air was more unstable than normal at lower levels and that the plumes were forming under an inversion base whose temperature was colder than the surface temperature.

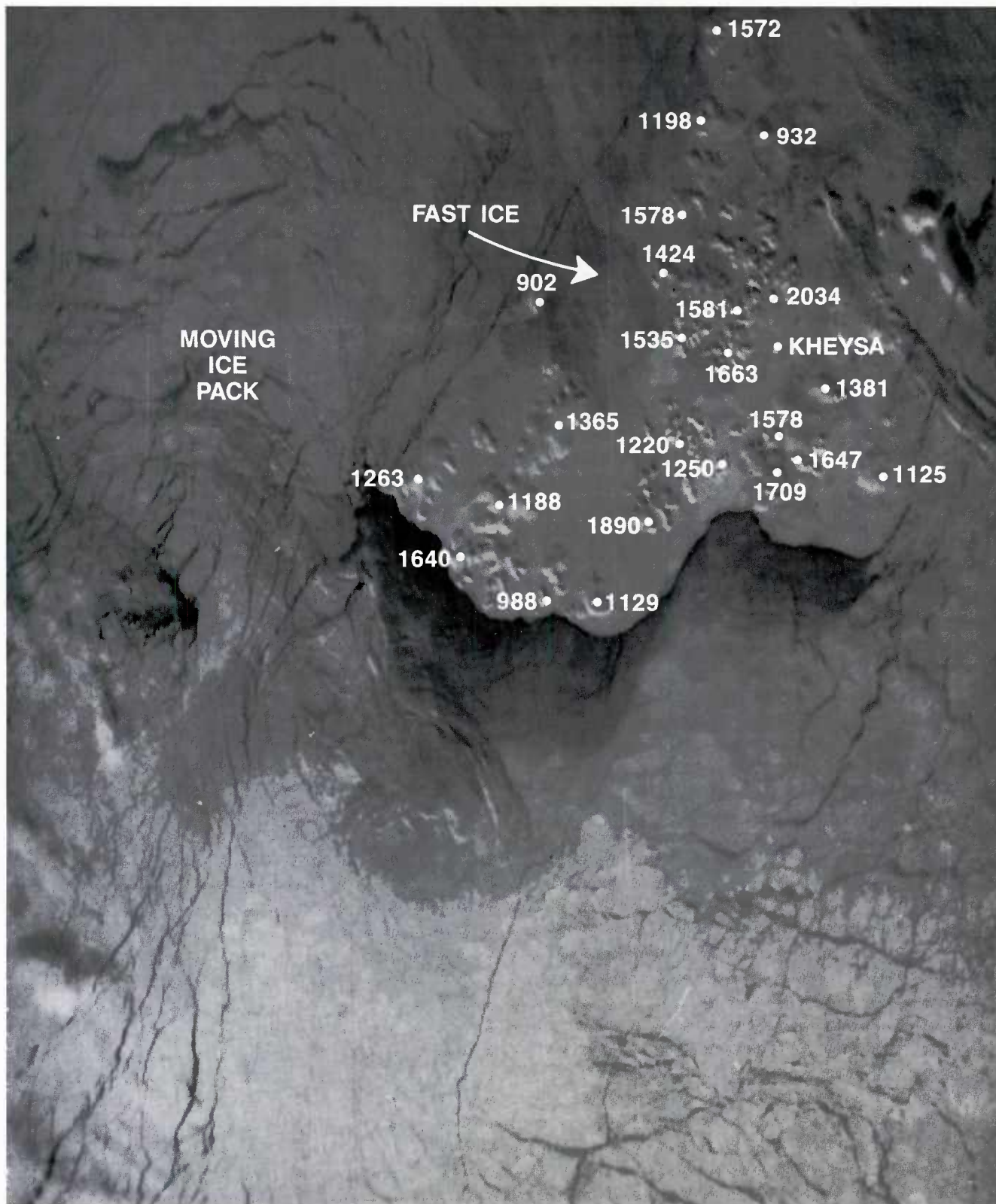
A sounding from Heysa (Kheysa) (Fig. 3F-12a), located at 80.6°N 58.0°E on Franz Josef Land north of the polynya region, confirms this potential. At first glance the higher and colder inversion base would also appear to explain the colder temperature of plumes forming over what appears to be a polynya region in the lee of Franz Josef Land (Fig. 3F-8a). However, a NOAA-10, channel 1 visible depiction of Franz Josef Land on 2 April 1989 (Fig. 3F-13a) shows topographic features of the island group with maximum elevations (in feet) of some of the islands indicated. The islands rise as "lumpy" snow-covered features above the flat and snow-covered ice, which appears to link the group as a solid non-moving entity. This ice sheet appears distinct from the surrounding ice pack, which contains many fractures, leads, and larger open areas, reflecting the stress and strain of wind and ocean currents that move and change its appearance. Note that each of the plumes in the polynya area of Franz Josef Land in Fig. 3F-8a have also largely formed in the lee of elevated terrain shown in Fig. 3F-13a. Because of the unstable nature of the low-level air on this date, polynya production cannot be positively ruled out, but it appears equally likely that the plumes may have originated as a result of the local orography.

### *Association of Arctic Plumes and Arctic or Polar Frontal and Jetstream Location*

An examination of Arctic plume formation over the Svalbard/Barents Sea region (Fett, 1990) showed that the plumes could often be used as indicators of Arctic frontal position and co-existing jetstream location. Plume generation requires strong winds aloft and sufficient moisture, characteristic of frontal zones. Since Arctic fronts are often ill-defined over the relatively flat ice surface, the sudden generation of a plume over mountainous island terrain may be an early unambiguous signal of Arctic frontal position.

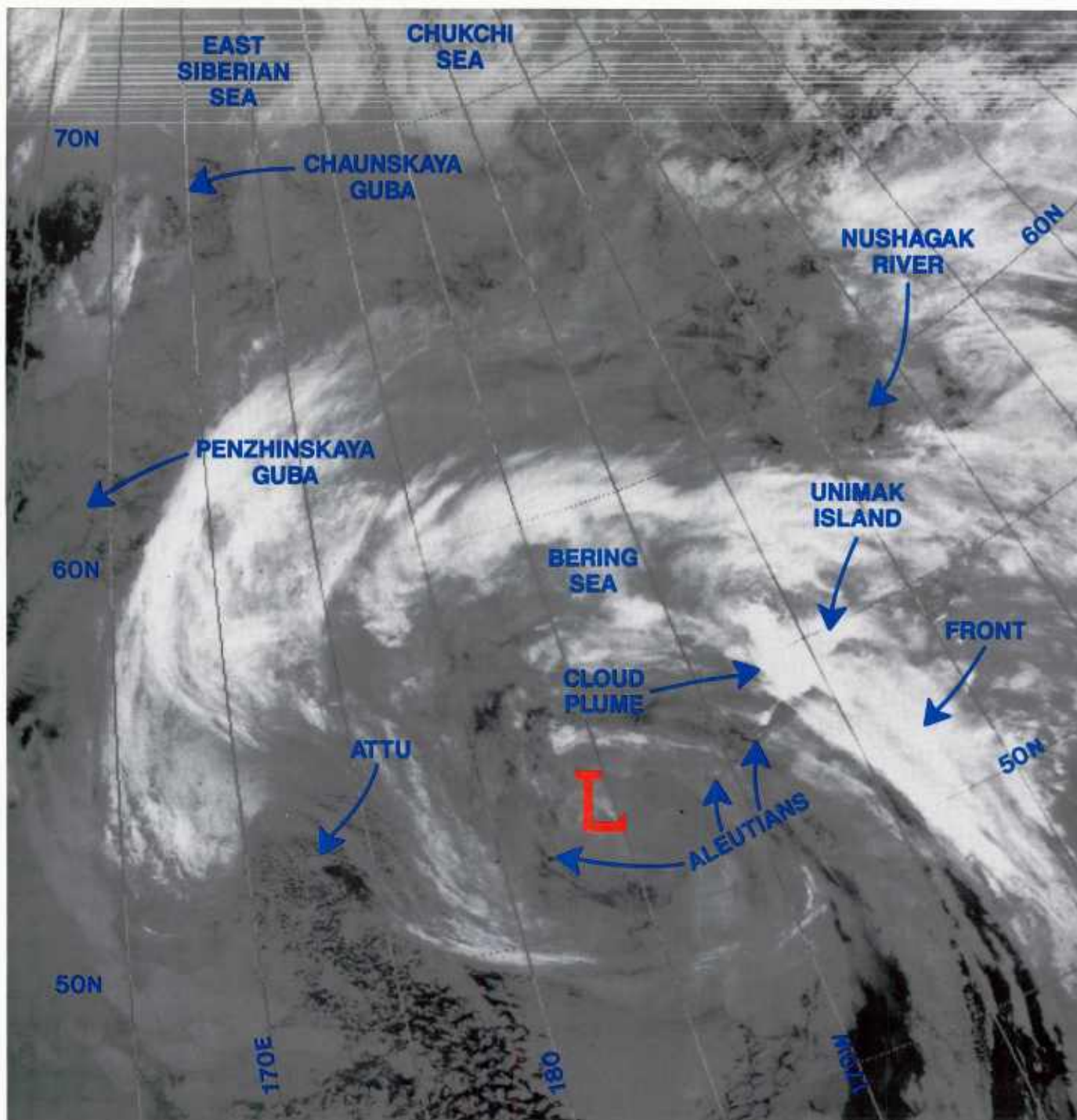
Figure 3F-14a illustrates the concept for a polar front, slightly south of Arctic latitudes, over the Aleutian Islands area. The image is from DMSP infrared TS (thermal smooth) data received at Elmendorf AFB on 5 November 1990. Plume generation is apparent near Unimak Island in obvious close association with a polar front position and accompanying low pressure center or cloud vortex. Note that plume formation at this time is restricted to Unimak Island, where the front is located, and not over equally mountainous terrain to the east-northeast or west-southwest. It is this fact that makes the use of island plumes so valuable in meteorological analysis. An additional excellent example of lee wave formation (29 October 1985), in this case south of the Brooks Range in association with an Arctic front, is shown in Fig. 3F-15a. For this example the southern slope of the Brooks Range is clear because of strong downward vertical motion with strong northerly winds aloft. The vertically propagating lee wave cloud is formed by equally strong upward vertical motion a little further to the south. In this example, again, the connecting Arctic front is very apparent lying over the Beaufort Sea. A small vortex associated with the front is evident near the North Slope.

It should be noted that vertical motions induced by this type of wave formation can be very hazardous to aircraft, particularly to those flying under visual flight conditions at lower levels trying to clear the range by only 500 ft or so. Many aircraft have been forced into the sides of mountains by waves similar to those described in this example, succumbing to the powerful downward force of the mountain wave.

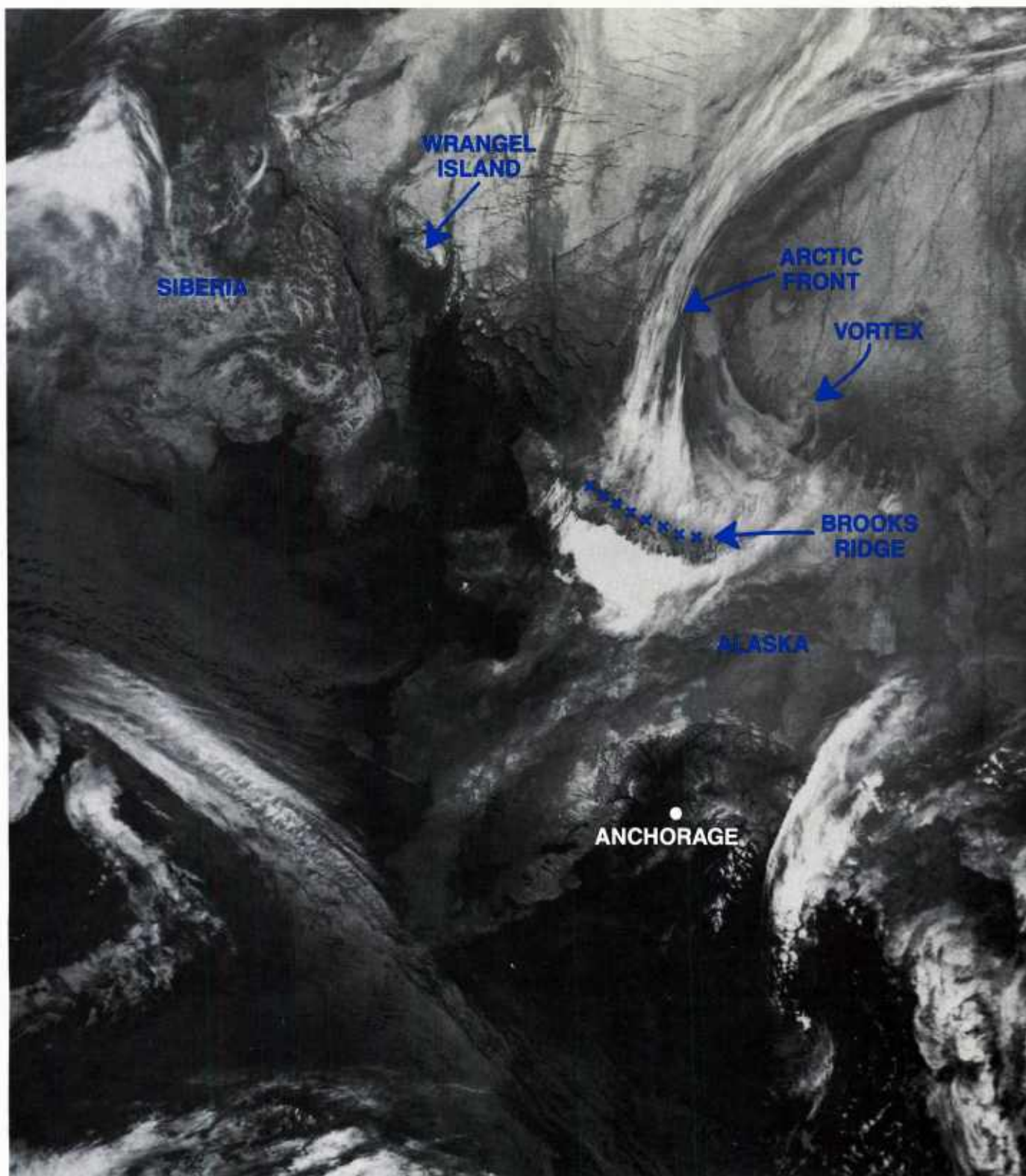


3F-13a NOAA-10 visible (channel 1) imagery. 1105 GMT 2 April 1989.





3F-14a DMSP infrared (TS) imagery. 0613 GMT 5 November 1990.



3F-15a DMSP infrared (TS) imagery. 2344 GMT 29 October 1985.



### **Important Conclusions**

1. Orographic cloud plumes are commonly observed over elevated regions, mountain peaks, and ridges of the Arctic.
2. The orographic plume observed in the Arctic is an excellent indicator of an Arctic or polar front near that location.
3. Orographic cloud plumes are always colder than the surrounding ice or snow-covered area, unlike low-level plumes from leads or polynyi that normally appear warmer than the surrounding ice or snow-covered region.
4. Orographic cloud plumes often appear to originate several kilometers downwind from the barrier that caused their formation, at times falsely suggesting that their source was a lower level water feature.